Physics and Chemistry of Fission 1979

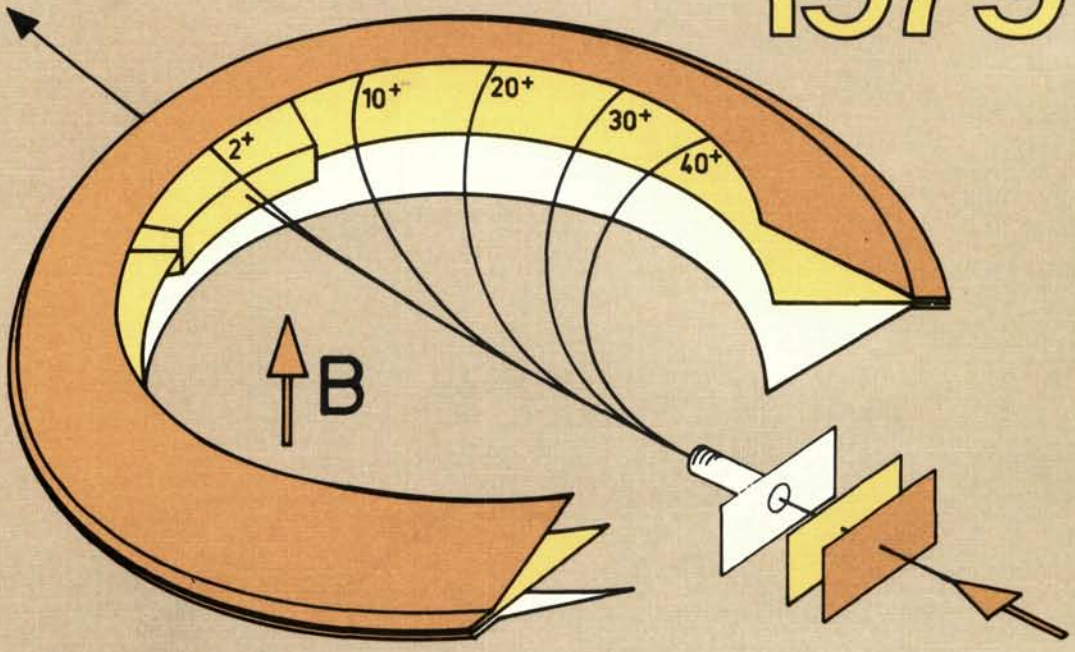

Proceedings of a Symposium, Jülich, 14-18 May 1979

Vol. II

INTERNATIONAL ATOMIC ENERGY AGENCY, VIENNA, 1980

PHYSICS AND CHEMISTRY OF FISSION 1979

VOL. II

The following States are Members of the International Atomic Energy Agency:

AFGHANISTAN
ALBANIA
ALGERIA
ARGENTINA
AUSTRALIA
AUSTRIA
BANGLADESH
BELGIUM
BOLIVIA
BRAZIL
BULGARIA
BURMA
BYELORUSSIAN SOVIET SOCIALIST REPUBLIC
CANADA
CHILE
COLOMBIA
COSTA RICA
CUBA
CYPRUS
CZECHOSLOVAKIA
DEMOCRATIC KAMPUCHEA
DEMOCRATIC PEOPLE'S REPUBLIC OF KOREA
DENMARK
DOMINICAN REPUBLIC
ECUADOR
EGYPT
EL SALVADOR
ETHIOPIA
FINLAND
FRANCE
GABON
GERMAN DEMOCRATIC REPUBLIC
GERMANY, FEDERAL REPUBLIC OF
GHANA
GREECE
GUATEMALA
HAITI
HOLY SEE
HUNGARY
ICELAND
INDIA
INDONESIA
IRAN
IRAQ
IRELAND
ISRAEL
ITALY
IVORY COAST
JAMAICA
JAPAN
JORDAN
KENYA
KOREA, REPUBLIC OF
KUWAIT
LEBANON
LIBERIA
LIBYAN ARAB JAMAHIRIYA
LIECHTENSTEIN
LUXEMBOURG
MADAGASCAR
MALAYSIA
MALI
MAURITIUS
MEXICO
MONACO
MONGOLIA
MOROCCO
NETHERLANDS
NEW ZEALAND
NICARAGUA
NIGER
NIGERIA
NORWAY
PAKISTAN
PANAMA
PARAGUAY
PERU
PHILIPPINES
POLAND
PORTUGAL
QATAR
ROMANIA
SAUDI ARABIA
SENEGAL
SIERRA LEONE
SINGAPORE
SOUTH AFRICA
SPAIN
SRI LANKA
SUDAN
SWEDEN
SWITZERLAND
SYRIAN ARAB REPUBLIC
THAILAND
TUNISIA
TURKEY
UGANDA
UKRAINIAN SOVIET SOCIALIST REPUBLIC
UNION OF SOVIET SOCIALIST REPUBLICS
UNITED ARAB EMIRATES
UNITED KINGDOM OF GREAT BRITAIN AND NORTHERN IRELAND
UNITED REPUBLIC OF CAMEROON
UNITED REPUBLIC OF TANZANIA
UNITED STATES OF AMERICA
URUGUAY
VENEZUELA
VIET NAM
YUGOSLAVIA
ZAIRE
ZAMBIA

The Agency's Statute was approved on 23 October 1956 by the Conference on the Statute of the IAEA held at United Nations Headquarters, New York; it entered into force on 29 July 1957. The Headquarters of the Agency are situated in Vienna. Its principal objective is "to accelerate and enlarge the contribution of atomic energy to peace, health and prosperity throughout the world".

Printed by the IAEA in Austria
June 1980

PROCEEDINGS SERIES

PHYSICS AND CHEMISTRY OF FISSION 1979

PROCEEDINGS OF AN INTERNATIONAL SYMPOSIUM
ON PHYSICS AND CHEMISTRY OF FISSION
ORGANIZED BY THE
INTERNATIONAL ATOMIC ENERGY AGENCY
AND HELD AT
JÜLICH, 14–18 MAY 1979

In two volumes

VOL.II

INTERNATIONAL ATOMIC ENERGY AGENCY
VIENNA, 1980

PHYSICS AND CHEMISTRY OF FISSION 1979, VOL. II
IAEA, VIENNA, 1980
STI/PUB/526
ISBN 92–0–030180–0

FOREWORD

The Kernforschungsanlage Jülich is among the leading nuclear research centres in the world. It provided a suitable and hospitable meeting-place for the Fourth International Symposium on the Physics and Chemistry of Fission, held from 14 to 18 May 1979.

Previous symposia in this series (Salzburg 1965, Vienna 1969, and Rochester 1973) had set the pace for these IAEA-organized meetings, which summarize the important advances in the field during the last twenty years. From one symposium to the next the scientific emphasis is shifted, new ideas and new experimental approaches being assimilated from year to year, such that it has become difficult to accommodate all the different lines of research under the roof of one meeting. To make the working hours at the Fourth Symposium acceptable, approximately two-thirds of the submitted papers could not be accepted for oral presentation; they were made available at the Symposium in the form of extended summaries. These are included in the Book of Extended Synopses made available to all the participants. Further copies can be obtained from the Physics Section, Department of Research and Laboratories, IAEA.

Many pages in the present Proceedings are taken up with review papers, on the assumption that in this way a more complete and unbiased coverage of many different orientations in fission research could be obtained. The contributed papers have been selected to illustrate or complement the extensive reviews.

The interest in the 1979 Symposium, the number of excellent contributions and the lively discussions during the meeting demonstrate the vitality of fission research. Both theoretical and experimental studies reported at the symposium indicate that fission studies have provided many valuable solutions to problems, but clearly other problems are still open and much work remains to be done.

EDITORIAL NOTE

The papers and discussions have been edited by the editorial staff of the International Atomic Energy Agency to the extent considered necessary for the reader's assistance. The views expressed and the general style adopted remain, however, the responsibility of the named authors or participants. In addition, the views are not necessarily those of the governments of the nominating Member States or of the nominating organizations.

Where papers have been incorporated into these Proceedings without resetting by the Agency, this has been done with the knowledge of the authors and their government authorities, and their cooperation is gratefully acknowledged. The Proceedings have been printed by composition typing and photo-offset lithography. Within the limitations imposed by this method, every effort has been made to maintain a high editorial standard, in particular to achieve, wherever practicable, consistency of units and symbols and conformity to the standards recommended by competent international bodies.

The use in these Proceedings of particular designations of countries or territories does not imply any judgement by the publisher, the IAEA, as to the legal status of such countries or territories, of their authorities and institutions or of the delimitation of their boundaries.

The mention of specific companies or of their products or brand names does not imply any endorsement or recommendation on the part of the IAEA.

Authors are themselves responsible for obtaining the necessary permission to reproduce copyright material from other sources.

CONTENTS OF VOL. II

MUON-INDUCED FISSION (Session E)

FRAGMENT PROPERTIES AND PARTICLE EMISSION (EXPERIMENTS) (Session F)

FRAGMENT PROPERTIES AND PARTICLE EMISSION (THEORY) (Session G)

DYNAMICAL THEORIES OF FISSION (Session H)

SUMMARY OF THE SYMPOSIUM

MUON-INDUCED FISSION
(Session E)

Chairman

E. CHEIFETZ
Israel

MUON-INDUCED FISSION

S. POLIKANOV
The Niels Bohr Institute,
University of Copenhagen,
Copenhagen, Denmark

Abstract

MUON-INDUCED FISSION.

A review of recent experimental results on negative-muon-induced fission, both of ^{238}U and ^{232}Th, is given. Some conclusions drawn by the author are concerned with muonic atoms of fission fragments and muonic atoms of the shape isomer of ^{238}U.

Since the family of elementary particles was discovered, a study of many exotic phenomena appeared to be possible. Some of the elementary particles (μ^-, π^-, κ^-, $\bar{p}$, Σ^-, Ξ^-, Ω^-) are stable enough to be slowed down by ionization to the velocity $\sim \alpha c$ and from the continuous spectrum to enter into the discrete one replacing an electron. After that atomic transitions with the emission of Auger electrons and x-rays occur, and finally hydrogen-like atoms are formed. Because of the larger masses in comparison with that for the electron, the atomic orbits for the particles mentioned are placed much closer to the nucleus than electron orbits. But only in the case of a negatively charged muon which we can call a "heavy electron", a rather stable atom is formed living hundreds of nanoseconds. Due to the strong interaction, all other elementary particles are absorbed by nuclei in a short time. For heavy elements they cannot even enter the orbit 1S being captured from orbits with higher n.

In heavy muonic atoms the muon disappears mainly in the process

$$p + \mu^- \rightarrow n + \nu$$

Most of the energy released is taken away by the neutrino. However, the residual nucleus is excited up to an energy of about 20 MeV. As a result, neutron emission or fission will take place. The muon absorption by a nucleus goes through the weak interaction and the typical lifetimes for fissile elements are close to 80 nsec.

It can happen, however, that during the atomic de-excitation the energy of a transition will be transferred into the nucleus without X-ray emission. The possibility of such a radiationless transition was pointed out firstly by Wheeler [1]. The theory was later developed by Zaretsky et al [2]. Until now radiationless transitions are not explored with good accuracy. Balatz et al [3] observed that the probability of a 2P-1S radiationless transition is close to 20% for Th and U.

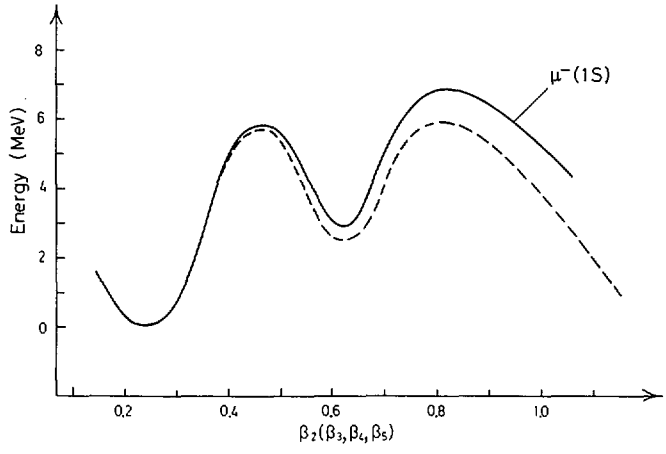

FIG.1. Fission barrier rise in the presence of a negative muon.

In this work the decrease of the intensity for X-rays was determined by comparison with lead. The energy for the 2P-1S transition is about 6 MeV for fissile nuclei and fission can take place. In fact, we can consider that as photofission in the presence of a negative muon. In the early experiments of Diaz et al [4] fission induced by radiationless transitions was observed.

Since then not too many physicists have been interested in studying muon-induced fission. In the 60's the main attention was paid to the investigation of the effects connected with the two-humped fission barrier [5,6]. Charged particles (p,d,α) beams of high quality available at the electrostatic tandem-generators as well as γ-rays were used in many laboratories. A lot of information was accumulated and the Strutinsky theory was strongly supported by many experimental facts. It is hard now to doubt the role of shell effects at large deformation of nuclei. There are still some groups working in this field and the results obtained so far are concerned with the spectroscopy of the states in the second well.

The improvement of old accelerators as well as the appearance of "mesic factories" with higher intensities of negative muons made it possible to perform some new experiments on muon-induced fission.

In my further considerations I shall follow the lines which were of main interest in the last few years:

1) Muonic shape isomers

2) Muonic fission fragments.

The investigations mentioned stimulated the consideration for the possibility of fission due to nuclear excitation in the β-decay of the muon in the 1S orbit. Rather poor experimental date on these subjects are available now and I would like to start with the Dubna group experiment on the search for muonic

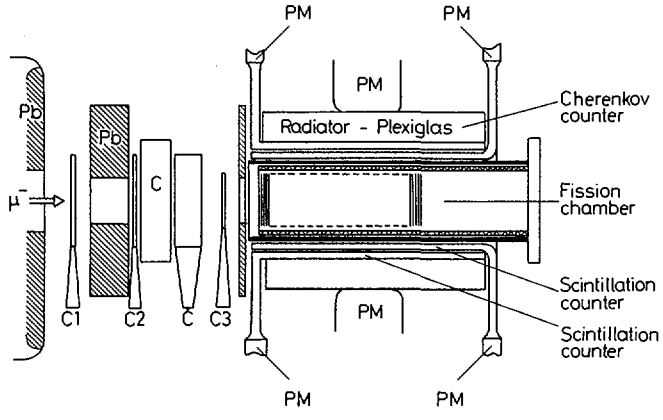

FIG. 2. Simplified scheme of experimental layout.

atoms of ^{238m}U [7]. These experiments were initiated by the work of Bloom [8] who suggested that a muonic shape isomer of ^{238}U can be formed with a rather high probability. The main idea was based on the difference in the measured half-lives for electrons from muon β-decay and fission mode. Later, more precise measurements have shown the difference to be not so large.

Before talking about the experiments it is useful to refer to the theoretical work done by Leander and Möller [9] where the influence of a negative muon sitting in the 1S orbit on the fission barrier was analysed.

Fig. 1 shows how the fission barrier is changed by the presence of a negative muon. It is necessary to remind oneself that the whole change is explained as due to the electromagnetic interaction of the muon with the nucleus. Some conclusions can be drawn from a study of Fig. 1.

First of all the height of the fission barrier is increased. A comparison of the known date on muon-induced fission with those for photofission [10] supports this conclusion. The fission probability is suppressed in the presence of the muon. Especially strong suppression takes place for ^{232}Th. One can understand that because of the large height for the outer barrier in this case.

One can also see that the properties of the shape isomer should be changed enormously in the presence of a muon in the 1S orbit:

1) The isomeric shift is expected to be about 0.5 MeV.
2) The probability for γ-decay will be increased.
3) The probability for spontaneous fission will be decreased.

In the experiments carried out by the Dubna group a target of ^{238}U was irradiated by negative muons. Both X-rays and nuclear

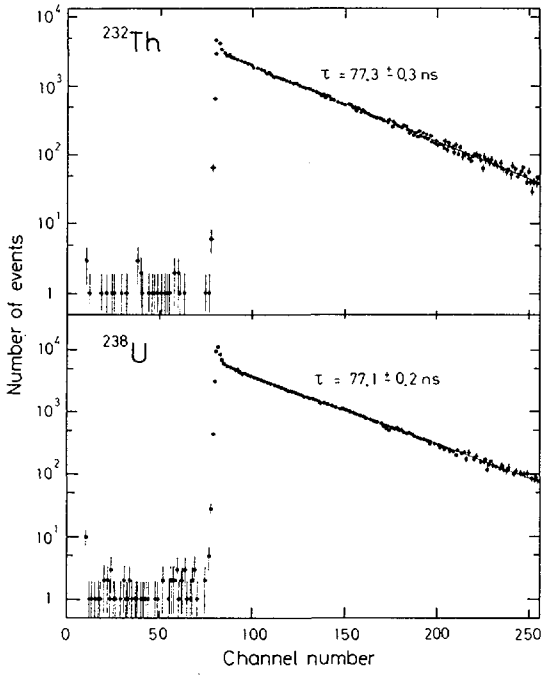

FIG. 3. μ-stop-fission time distribution.

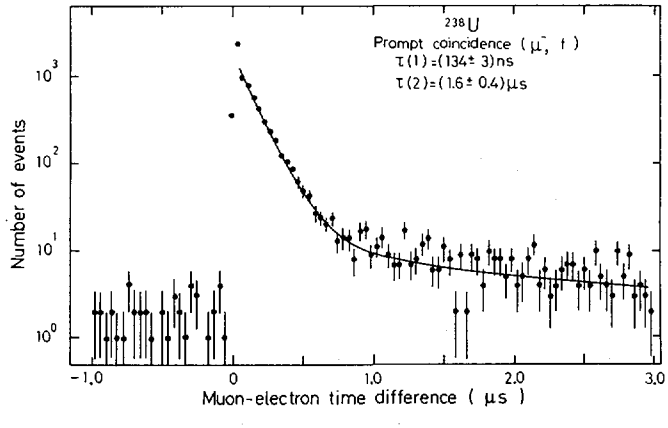

FIG. 4. μ-stop electron time distribution for prompt μ-stop-fission events.

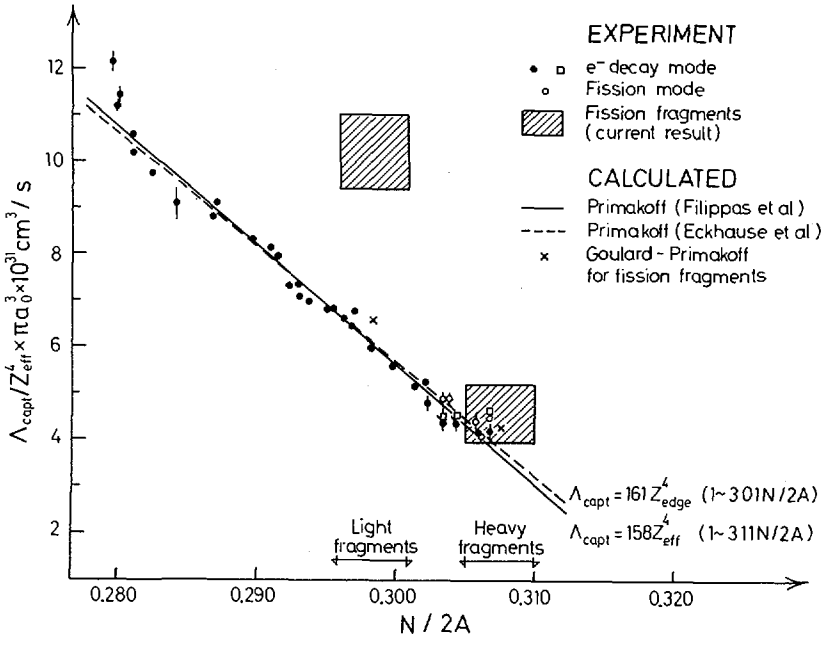

FIG. 5. The Primakoff plot.

γ-rays were registered by a 60 cm^3 Ge-Li detector. The experiments have shown the presence of delayed γ-rays of very low intensity. The half-life was estimated to be about 12 nsec. In similar conditions for ^{232}Th target only γ-rays due to nuclear muon capture were observed. The results obtained gave rise to a suggestion for possible evidence of muonic atom for ^{238}U shape isomer. Because of the extremely poor statistics, that statement is not very strong. The energy of the isomeric level was estimated to be 3.1 MeV. It is about 0,6 MeV higher than that for the well known ^{238}U shape isomer [11]. The half-life measured in the Dubna experiments is 20 times shorter than the one known for ^{238}U. That fits nicely with what one can expect for γ-decay of muonic ^{238}U shape isomer. Similar experiments were done earlier by Kaplan et al [12] but only an upper limit for the effect was established. To some extent confusing is the high probability for the population of the state identified. It is close to 1% per μ^--stop in the target. If the conclusion concerning the existence of a muonic atom for ^{238m}U is right, one has to think about quite a special mechanism for isomeric state population.

A further development of the experiments on muonic atoms of ^{238}U took place at the CERN synchrocyclotron. There some experiments with the equipment produced partially in JINR (Dubna) were done. Fig. 2 shows schematically the last version of the equipment which was used.

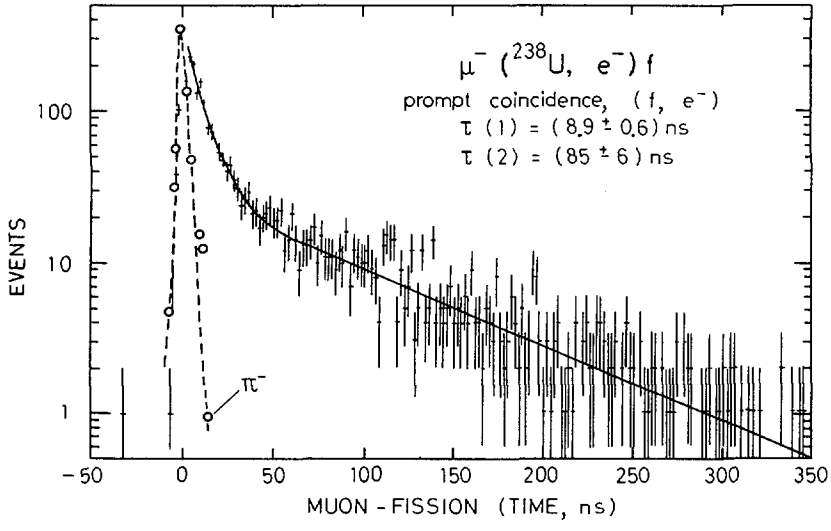

FIG.6. μ-stop-fission time distribution for prompt fission-electron events.

As a target the multiplate ionisation chamber was used. About 20g of ^{238}U were put on 100 electrodes. The fission fragments were detected by using this chamber. For muon detection a conventional telescope was used. To eliminate the electrons in the muon beam a plexiglas Cerenkov counter was incorporated into the telescope. By a moderator the admixture of pions was minimised. The resolution time (FWHM) was about 4 nsec.

The ionisation chamber was surrounded by two plastic detectors and a plexiglas Cerenkov counter to detect the electrons emitted by the β-decay of a muon.

Fig. 3 shows the μ⁻-stop-fission time distribution measured by the equipment described [13] . One can see clearly both the prompt fission due to radiationless excitation and the exponent due to nuclear capture of a muon.

As a first step of the CERN experiment the β-decay of muonic atoms of fission fragment was studied. One can expect that in the scission process the muon will be transferred to the 1S orbit of one of the fission fragments. Later this muonic atom will decay by nuclear capture or by muon β-decay. In the experiments prompt fission induced by radiationless transitions was detected and the time distribution for the electrons emitted by β-decay of the muon was measured [14] . Both ^{238}U and ^{232}Th targets were used. Fig. 4 shows the time distribution observed. It is necessary to mention here that the amount of material between the targets and Cerenkov counter implied a threshold for electron registration of about 10 MeV. The decay curve presented in Fig. 4 was measured by using one plastic detector in combination with a water Cerenkov counter. By adding a second plastic detector the efficiency for electron detection was decreased by not more than about 10%.

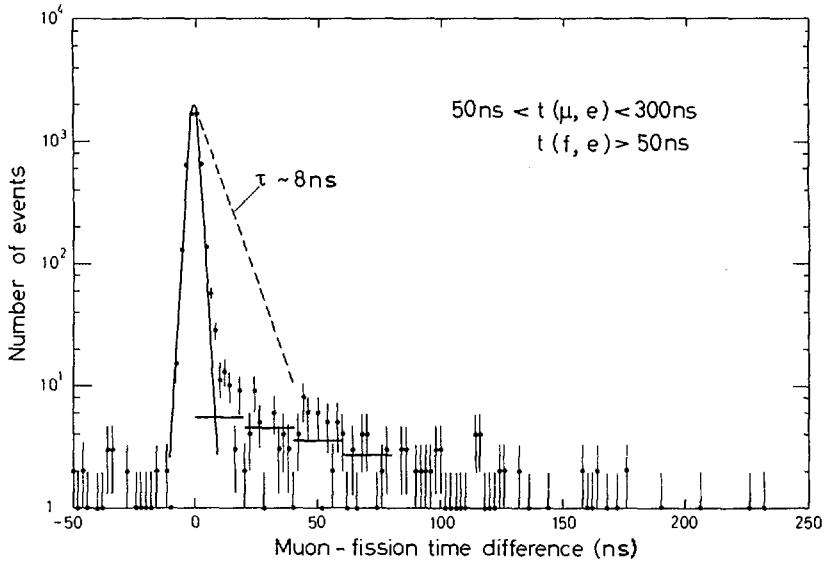

FIG. 7. μ-stop-fission time distribution for delayed fission-electron events.

There is seen clearly from Fig. 4 the presence of two components. The same was observed for the ^{232}Th target where the lifetime of the short-lived components was found equal to 132 ± 7 nsec. The short-lived components both for ^{238}U and ^{232}Th can be explained as due to β-decay of a muon sitting in the 1S orbit of one of the fragments. At the separation of the two fragments the muon can be bound either to heavy or light fragments. The experiments do not allow to answer in a direct way how the process proceeds. However, by using the so-called Primakoff plot one can draw some conclusions. The Primakoff plot presenting the dependence of muon capture rate on the value N/2A is shown in Fig. 5. The shaded areas correspond to heavy and light fragments. It shows certainly that the muon appears mainly attached to the heavy fragments. The long component indicates that muon conversion takes place, because fission fragments are highly excited. The muon converted is absorbed by light elements (Al, C, H) forming muonic atoms with rather long lifetime. The long-lived component contains about 1% of all prompt fission when the measured number of events is corrected for the large difference in muon absorbtion rate.

When discussing the properties of muonic atoms of fission fragments one also has to refer to the results of the Rochester group [15] on neutron emission from actinide muonic atoms. They indicate clearly that the main mode of the decay is nuclear capture of the muon. For the neutrons at the irradiation of ^{238}U by negative muons the exponential corresponding to the lifetime 78.3 nsec is due to nuclear capture of muons by ^{238}U. At the same time the presence of a

longer lifetime is evident. It apparently corresponds to nuclear capture of negative muons by fission fragments.

As mentioned earlier the Dubna group indicated the possible evidence of muonic shape isomer for ^{238}U. Some attempts to observe the fission branch for such an isomer were done at CERN. By doing these experiments one has to keep in mind that this branch should be very weak. The signature of this process has to be as following. After delayed fission a muonic atom of fission fragment will be formed. This atom will decay partially by electron emission with the lifetime 134 nsec.

The results obtained at CERN make it possible to estimate only an upper limit which is equal to 10^{-4} per muon stop.

At the same time delayed fission with a lifetime of about 10 nsec (Fig. 6) was observed when the electron detector was triggered in prompt coincidence with fission [16]. Both 10 nsec and 80 nsec components are seen. For comparison also the results obtained by using negative pions are shown in Fig. 6. Here only a clearly defined peak was observed with a FWHM equal to about 4 nsec. Fig. 7 represents the prompt fission peak (with the same FWHM) due to radiationless transitions. In this case again no indication for the 10 nsec component was obtained.

To understand better the origin of the events presented in Fig. 6 an ionisation chamber containing a ^{252}Cf source was used. The prompt coincidences fission-"electron" were detected here with an efficiency $\sim 10^{-3}$. That shows that the "electron" detector is sensitive to some extent to γ-rays and probably neutrons accompanying fission. The 80 nsec component as well as the prompt peak for pions are to be explained in the same way.

By the addition of a second plastic detector the efficiency of the "electron" detector to γ-rays and neutrons emitted in spontaneous fission of ^{252}Cf is suppressed by a factor ~ 5. Both the 10 and the 80 nsec components were also suppressed but less efficiently than for ^{252}Cf. It follows that delayed fission is not accompanied by high energy electron emission in muon β-decay. An excess of events for the 80 nsec component as compared to that for ^{252}Cf might be explained as due to the difference in the multiplicity and energy spectra for γ-rays and neutrons.

It might also be treated as an indication for the possibility of fission induced by the "shake-off" effect (the sudden change of the Coulomb field following the β-decay of a muon). However, at this moment it is more safe to talk only about an upper limit for this effect. In accordance with very rough estimates it is close to 3×10^{-3} fission/μ-decay. The experiments carried out indicate certainly the presence of a short-lived ($\sim$ 10 nsec) component for fission which is not seen in Fig. 3. That means it is accompanied by some radiation which triggers the "electron" detector with a higher efficiency than by muon nuclear capture. It is surprising that the half-life coincides with that measured in Dubna for delayed γ-rays.

To understand the origin of the 10 nsec component some additional experiments are needed. One cannot exclude completely that it might be connected with the formation of muonic atoms of hydrogen in the ionisation chamber filled by CH_4, and the subsequent transfer of the muon to ^{238}U.

References

[1] J. A. Wheeler, Rev. Mod. Phys. 21 (1949) 133
[2] D. F. Zaretsky et al., Nucl. Phys. 28 (1961) 177
[3] M. A. Balats et al., Sov. Phys., JETP 38 (1960) 1715
[4] J. A. Diaz et al., Nucl. Phys. 40 (1963) 54
[5] V. M. Strutinsky, Nucl. Phys. A95 (1967) 420
[6] S. Bjørnholm et al., Nucl. Phys. A139 (1969) 1
[7] W. D. Fromm et al., Nucl. Phys. A278 (1977) 387
[8] S. D. Bloom, Phys. Lett. 48B (1974) 420
[9] G. Leander and P. Möller, Nucl. Phys. 57B (1975) 245
[10] B. M. Alexandrov et al., Phys. Lett. 57B (1975) 238
[11] P. L. Russo et al., Nucl. Phys. A240 (1975) 3
[12] S. N. Kaplan et al., 6th Int. Conf. on High Energy Physics and Nuclear Structure, Santa-Fe, 1975
[13] Dz. Ganzorig et al., Phys. Lett. 78B (1978) 41
[14] Dz. Ganzorig et al., Phys. Lett. 77B (1978) 257
[15] W. W. Wilcke et al., Phys. Rev. C18 (1978) 1452
[16] Dz. Ganzorig et al., to be published

DISCUSSION

D. HOFFMAN: What is the intensity of the muons in the latest experiment you have carried out?

S. POLIKANOV: I cannot quite remember the number of muon stops in the target. I can tell you, though, that by using the new meson producers one can attain much higher muon stop density. So the fission due to transfer from (μH) molecules or atoms could be studied for highly exotic radioactive fissile isotopes.

K.M. DIETRICH: First, a comment on your suggestions that the fission of a hypernucleus, such as hyperuranium, should be investigated. In this connection, I have come to the conclusion that the main advantage of this process would be that the Λ particle would be located in the heavy fragment only if the passage from saddle to scission were slow, compared with the period of a bound Λ particle; in the opposite case we would find it in both fragments with heights proportional to the nuclear volumes. To ensure a clear-cut situation we would need to be sure that the Λ particle was in its lowest possible state. This could be done by looking only at events where the initially-formed hypernucleus had an excitation energy close to the fission threshold. It would be possible to attain this by measuring the energy of the pion that is emitted in the formation process ($N + K \rightarrow \Lambda + \pi$). Hence my question is, are the present-day kaon beans sufficiently intensive for an experiment of this kind?

S. POLIKANOV: Yes, I think they are adequate for the study of K-induced fission.

FISSION PROBABILITIES AND TIME DISTRIBUTIONS IN μ^--INDUCED FISSION OF ^{232}Th, ^{233}U, ^{235}U, AND ^{238}U

H.W. REIST, A. GRÜTTER, H.R. VON GUNTEN
Eidgenössisches Institut für Reaktorforschung,
Würenlingen

D. JOST
Anorganisch-Chemisches Institut,
Universität Bern,
Bern,
Switzerland

Abstract

FISSION PROBABILITIES AND TIME DISTRIBUTIONS IN μ^--INDUCED FISSION OF ^{232}Th, ^{233}U, ^{235}U, AND ^{238}U.

In a counter experiment, the probabilities of μ^--induced fission of ^{232}Th, ^{233}U and ^{235}U were measured relative to that of ^{238}U, and the time distributions of the muon fission were determined for ^{232}Th, ^{233}U, ^{235}U and ^{238}U. Using the previously measured absolute fission probability per muon capture for ^{238}U the prompt and delayed fission probabilities were derived. The delayed-muon-fission probabilities follow the Γ_n/Γ_f systematics. The prompt-muon-fission yields per radiationless transition probability suggest a contribution of fissions induced by higher-order radiationless transitions. The relatively small amount of fissions due to radiationless K_α-transitions can be explained by an increase of the fission barrier.

Introduction

The interest in μ^--induced fission was stimulated by the possibility to improve the understanding of the fission process of heavy nuclei. When a muon is captured by an atom it cascades down through the atomic orbitals, hereby emitting X-rays or exciting the nucleus by inverse internal conversion.

The muon may be captured by a nucleus from the 1s orbital with a mean life of $\sim$ 75 ns. Thus, the nucleus is excited to 15 - 20 MeV and may undergo fission. In actinide nuclei the 2p - 1s muonic transition energies are of the order of 6 MeV, and higher order transition energies approximately 10 MeV.

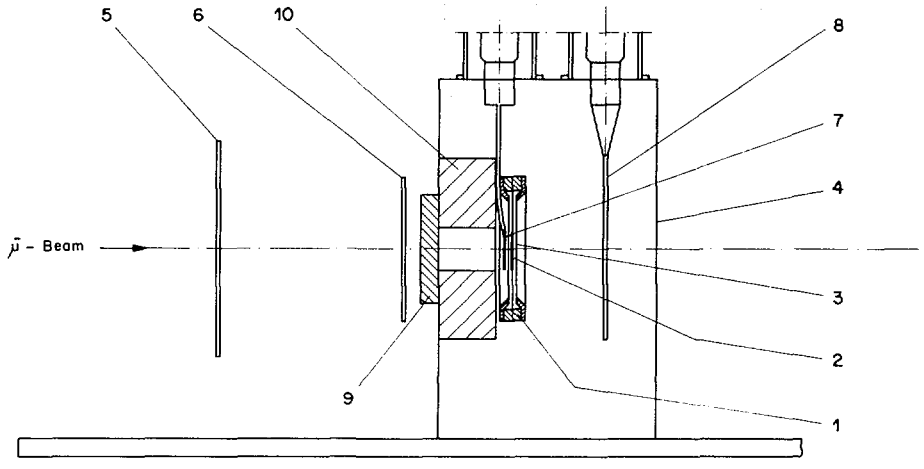

FIG.1. Detection system:
1) Double-parallel-plate fission chamber; 2) targets; 3) mylar window; 4) Faraday cage; 5–8) scintillation counters 1, 2, 3, 4 (μ^- stop signal: $1 \cdot 2 \cdot 3 \cdot \bar{4}$); 9) Be-degrader; 10) polyethylene collimator.

Hence, in muon-induced fission, besides the delayed a prompt fission mode occurs as a result of a radiationless energy transfer of a muonic transition to the nucleus. During the prompt fission process the muon remains in the ground state orbital. Leander and Möller (1) calculated the decrease of the binding energy of a muon in its 1s orbit with nuclear deformation. This can be interpreted as an increase of the fission barrier. Thus, by comparing the prompt muon fission probability to the photofissility, one may learn about the deformation of the fissioning nucleus.

The present investigation was motivated by the considerable scatter of the available data on the fission probability of the μ^--induced fission (2 - 7). The most recent results differ by more than a factor of 4 for ^{238}U and by more than a factor of 6 for ^{235}U. In a radiochemical experiment (6) the mass distribution and the fission probability of ^{238}U were determined. Here we report on a counter experiment performed at SIN, Villigen, Switzerland, in which the muon fission probabilities of ^{232}Th, ^{233}U and ^{235}U were measured relative to that of ^{238}U. Also measured were the time distributions of the muon fission for ^{232}Th, ^{233}U, ^{235}U and ^{238}U.

Experimental

The detection system consisting of a fission chamber and a counter telescope is shown in figure 1. The fission chamber was a fast, double parallel plate ionisation chamber with aluminized mylar windows (1 mg·cm^{-2}) and a polystyrene frame. In order to keep the number of false muon stops and the neutron background as small as possible the target materials (0.1 to 0.5 mg·cm^{-2}) were electroplated back-to-back onto aluminium foils of 6 mg·cm^{-2} thickness. The investigated isotopes were deposited on one side and as reference ^{238}U on the other. The deposits were converted to oxides at 500 ^{o}C. Fission counter, targets and telescope-counter # 3 amounted to totally 61 mg·cm^{-2}. A faraday cage reduced the electronic noise to a negligible amount and served also as a light sight protection for the counters #3 and #4.
Negative muons with a momentum of 85 MeV/c were further degraded with beryllium to maximize the muon stop rate in the targets. The width of the stopping distribution (FWHM) was 1.1 g·cm^{-2} of beryllium. Behind the degrader a polyethylene collimator limited the beam spot to the size of the targets (6 cm dia). The fission chamber was turned a couple of times during each measurement in order to diminish systematic errors. Equal amounts of data were accumulated for each target in both positions. The π^- contamination at the target position was below the 10^{-4} level for the investigations with the uranium isotopes. The high contamination of electrons ($\sim$ 10 times the μ^--intensity) in the beam had no effect on the measurements as was shown by varying the thickness of the degrader. The measurement with $^{232}Th/^{238}U$ was performed under different beam conditions with a pion contamination of $< 10^{-5}$.

The fission fragments were registered with an efficiency of at least 97 %. This was deduced from discriminator curves which were measured for each target under experimental in-beam conditions.

Table I presents the isotopic composition of the uranium targets. Several targets were prepared for each uranium isotope. Thorium was measured only once. After the irradiation the uranium- and thorium-oxyde targets were dissolved in nitric and sulfuric acid, respectively. The amount of uranium was determined by isotope dilution techniques, thorium was assayed by colorimetry.

TABLE I . ISOTOPIC COMPOSITION OF THE U-TARGETS (%)

	^{233}U	^{234}U	^{235}U	^{236}U	^{238}U
^{233}U	97.06	1.91	0.3	0.04	0.7
^{235}U	0.004	1.6	97.48	0.08	0.84
^{238}U	0.003	0.005	0.24	0.01	99.74

As the yields of prompt fission events are only 5 to 20 % compared to the delayed fission yields, a good time resolution was essential. The muon stops were counted with a four element telescope ($1.2.3.\bar{4}$) using conventional fast electronics. The signal of the counter # 3, fed into a constant fraction discriminator, determined the time of a muon stop. Two identical fast systems, also working in the constant fraction regime, were used to develop the fission chamber signals. A fission pulse started a time-to-amplitude converter (TAC). The muon stop signal provided the stop pulse after passing a low attenuation delay line of 750 ns. A pile-up generator rejected events with more than one muon stop during the acceptance time.

The specified integral linearity of the TAC was < 0.1 % and its differential linearity was < 2 %. The TAC/ADC-system was calibrated with a time calibrator. The 680 ns interval of the TAC enabled a simultaneous measurement of the time distribution and the random event background. The channel contents of the ADC's were read out on magnetic tape in intervals of 10^3 seconds.

Several times during each run data were also collected for a short time on π^--induced fission. The measurements with the π^--beam gave the possibility to control the stability of the timing system and to analyse independently the response curve of prompt coincidences for every run.

Analysis of the data

The measured time distributions were analysed by a least squares method. The procedure was split up into four steps:

a) An exponential curve of the form
$y = A_1 \exp(-\lambda t) + B$
was fitted to the delayed fission part of the time spectrum to get the muon-disappearance rate. The constant background was taken from the 125 ns-wide negative part of the time spectrum.

b) The time spectra of the π^--induced fission were fitted with an asymmetric Gaussian function
$y = A_0 \exp\left[-(t-t_0)^2 / (2(\sigma \pm \Delta\sigma)^2)\right]$; $\sigma \pm \Delta\sigma$ for $(t-t_0) \gtrless 0$
The dispersion σ, the asymmetry parameter $\Delta\sigma$ and the peak position t_0 were treated as free parameters.

c) The fit function was the sum of an asymmetric Gaussian function and its convolution with an exponential function.

$$y = A_0 \exp\left[-(t-t_0)^2 / (2(\sigma+\Delta\sigma)^2)\right] + A_1 \int_{t_0}^{\infty} \exp(-\lambda(u-t_0)) \cdot \exp\left[-(t-u)^2 / (2(\sigma+\Delta\sigma)^2)\right] du + B$$

The parameters obtained in steps a) and b) were used to determine the ratios of the areas under the prompt and delayed parts of the spectra.

d) All the parameters were optimized by a least squares fit with the function given in step c).

Care was taken to obtain a linear convergence of the least squares procedure in order to have reliable values in the diagonal elements of the coefficient matrix for the variances of the fitted parameters.

The $\chi^2/2$-probabilities with respect to the number of degrees of freedom were normally higher than 0.6 for all the fits. The asymmetry parameter $\Delta\sigma$ was usually negligibly small compared to σ.

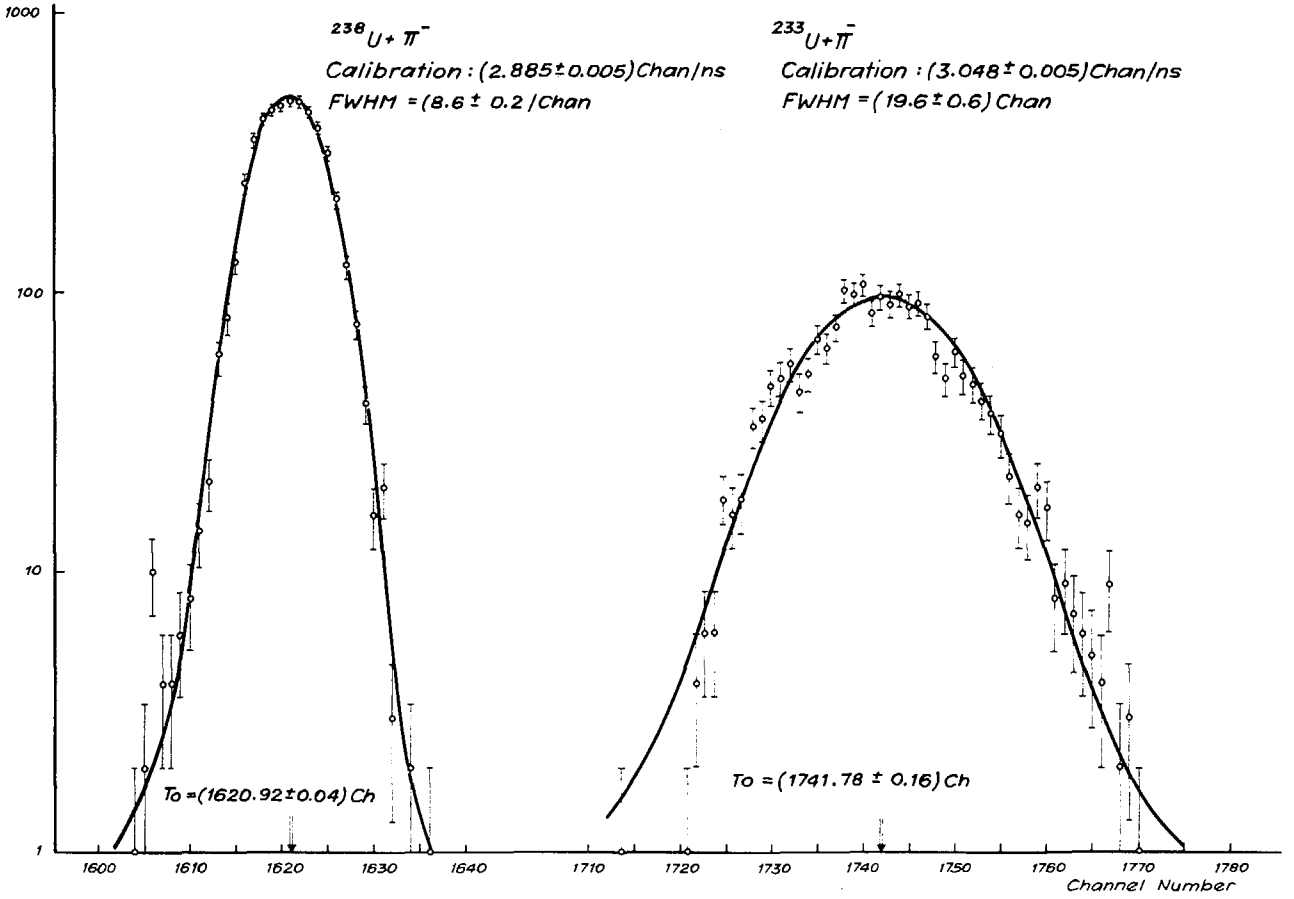

FIG. 2. Time distributions of the π^--induced fission of ^{238}U and ^{233}U.

This fitting procedure gave the life-times $\tau = \lambda^{-1}$ of the muon in the 1 s orbit for ^{232}Th and the three uranium isotopes and the ratios of the spontaneous to the delayed muon induced fission as well. The results represent the weighted means of the different measurements. The μ^- fission probabilities of ^{232}Th, ^{233}U and ^{235}U relative to that of ^{238}U were obtained by summing up the simultaneously measured spectra, correcting for the detection efficiencies and the weights of the targets.

Results

Two examples for measured time distributions of the π^--induced fission are given in fig. 2. The stability of the prompt peak was usually better than 0.5 ns. The dispersions of the symmetric Gaussian time distributions amounted to $\sim$ 1.2 ns for ^{238}U, $\sim$ 1.4 ns for ^{235}U and $\sim$ 2.5 ns for ^{233}U. The latter reflects the influence of the more than 10^4 times higher alpha activity of ^{233}U.

Fig. 3 and 4 show two representative time spectra of the μ^--fission of ^{238}U and ^{233}U, respectively. The spectra of ^{235}U are similar to those of ^{238}U. In order to present the distributions of the prompt fission clearly only the first part of the spectra is shown. The investigation of the spectra up to 450 ns after the prompt peak did not indicate different background values than those found for the negative parts of the spectra.
The events on the left hand side of the prompt peak in fig.4 are again a consequence of the high alpha activity of ^{233}U which caused some pile-up effects of alpha pulses with prompt and delayed fission pulses. These events were evaluated by a fit function which described the sum of two shiftet fit functions of the form given above. The amount of these shifted events was about 1 % of the total.

The results for the muon capture mean lives and the ratios of the prompt-to-delayed fission probabilities are presented in tables II and III together with the results of other authors. The agreement for the reported muon lifetimes is considerably better than for the prompt-to-delayed ratios. The latter scatter by more than a factor of 2.

The quoted uncertainties include statistical errors and errors due to the instability of the detector system, the calibration and the differential and

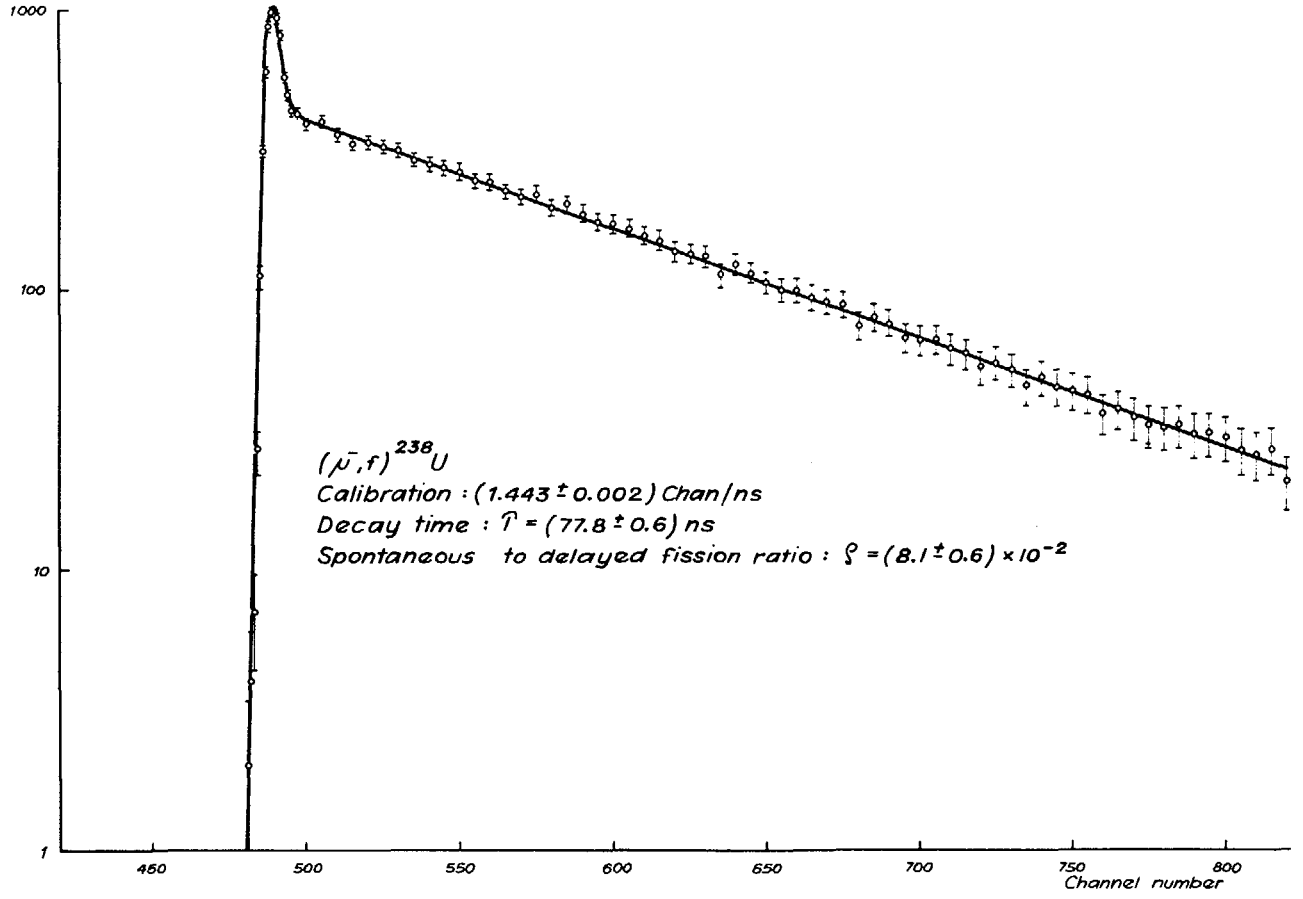

FIG. 3. Representative time spectrum of the μ^--induced fission of ^{238}U.

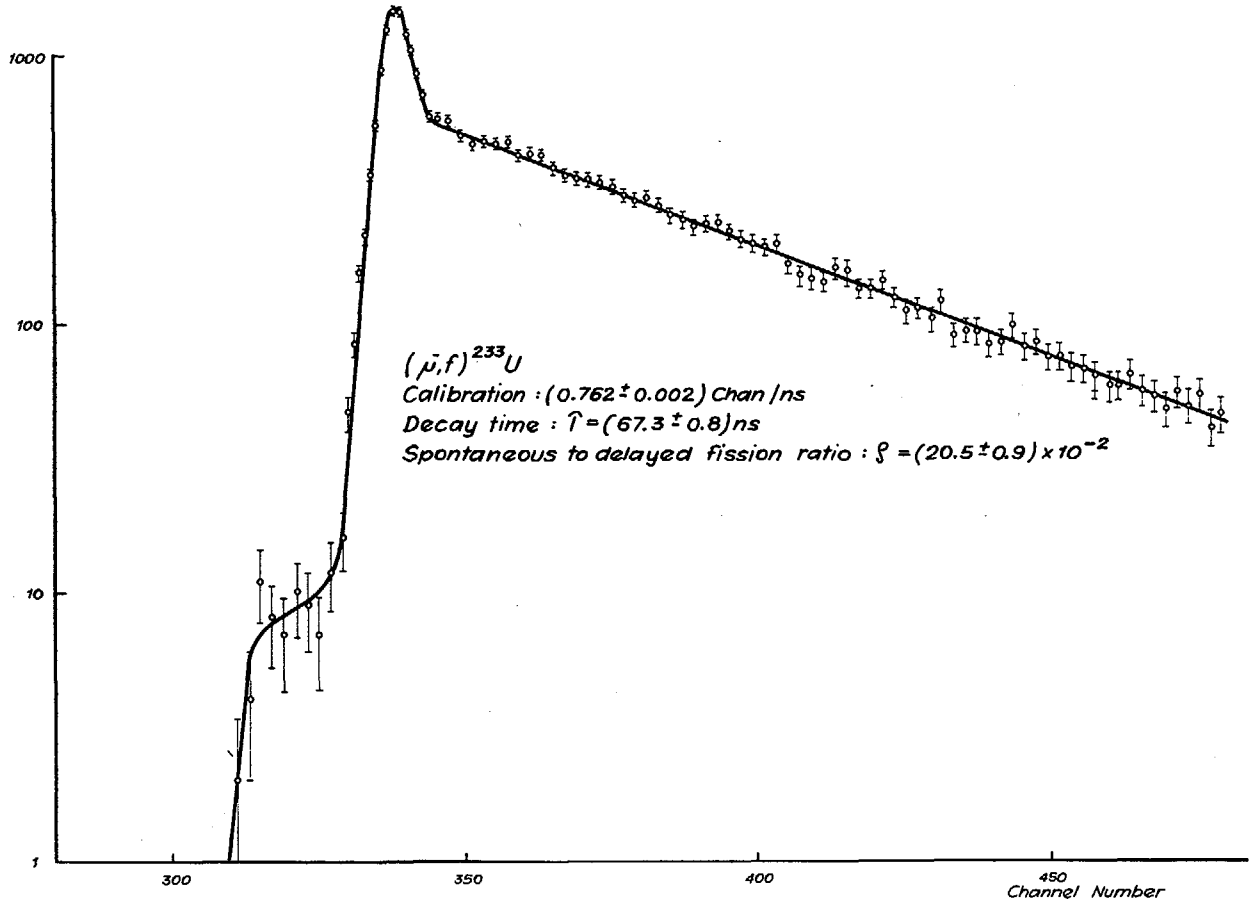

FIG.4. Representative time spectrum of the μ^--induced fission of ^{233}U. Pile-up effects of alpha with fission pulses cause a shift to the left for about 1% of all the fission events.

TABLE II . μ^- - CAPTURE TIMES IN ^{232}TH, ^{233}U, ^{235}U AND ^{238}U

^{232}Th	^{233}U	^{235}U	^{238}U	Mode of Detection	Ref.
78.5±2.0	68.5±0.7	72.8±0.6	77.7±0.6	f	present work
74.2±5.6	-	66.5±4.2	75.6±2.9	f	(8)
-	61.7	65.3±2.8	74.1±2.8	f	(9)
87 ±4	-	75.6±2.3	76.0±1.0	f	(5)
84.0±4.5	-	-	-	f	(10)
77.3±0.3	-	-	77.1±0.2	f	(11)
-	-	-	88.0±4.0	e	(12)
80.4±2.0	-	78.0±4.0	81.5±2.0	e	(13)
79.2±2.0	-	75.4±1.9	73.5±2.0	e	(14)
-	-	-	79.1±0.5	γ	(15)
-	-	-	78.6±1.5	γ	(16)
80.1±0.6	-	75.0±0.7	78.3±1.0	n	(17)

f: Fission fragments, e: Decay electrons, γ: Fission gamma rays, n: Fission neutrons.

integral non-linearity of the TAC/ADC. An additional uncertainty caused by a small asymmetry in the prompt muon fission peak was taken into account for the ratio for ^{238}U. A pion contamination corresponding to the upper limits of 10^{-4} and 10^{-5} for the measurements with the uranium- and thorium targets, respectively, would influence the prompt-to-delayed fission ratio for all the targets by less than 0.7 %. The contribution to the capture times of ^{233}U and ^{235}U by ^{234}U with its unknown muon capture time was estimated to be ± 0.1 %. The constant background did not affect the errors.

TABLE III . PROMPT-TO-DELAYED FISSION YIELD RATIOS

^{232}Th	^{233}U	^{235}U	^{238}U	Ref.
$(5.1\pm0.8)\times10^{-2}$	$(20.5\pm0.8)\times10^{-2}$	$(11.5\pm0.5)\times10^{-2}$	$(7.9\pm0.6)\times10^{-2}$	This work
$(6.4\pm2.2)\times10^{-2}$		$(11.1\pm2.1)\times10^{-2}$	$(7.2\pm1.4)\times10^{-2}$	(8)
	4.6×10^{-2}	$(6.3\pm2.5)\times10^{-2}$	$(4.8\pm2.5)\times10^{-2}$	(9)
$(13.0\pm1.2)\times10^{-2}$		$(17\pm1)\times10^{-2}$	$(7.1\pm0.3)\times10^{-2}$	(5)
13×10^{-2}				(7)
4.9×10^{-2}		11×10^{-2}	8×10^{-2}	a)

a) For comparison: prompt-to-delayed neutron emission yield ratios of Ref (17).

TABLE IV . μ^- -FISSION PROBABILITIES RELATIVE TO ^{238}U

^{232}Th	^{233}U	^{235}U	Ref.
$.16\pm0.02$	2.69 ± 0.16	2.07 ± 0.08	This work
$.139\pm0.003$		1.19 ± 0.03	(5)
.375 a)		1.667 a)	(7)

a) Delayed μ^- -fission only.

The μ^--fission probabilities of the investigated nuclides relative to that of ^{238}U are listed in table IV. Test measurements were also performed with ^{238}U against ^{238}U resulting in a ratio of 1.0 ± 0.04. This shows the absence of an asymmetry between the two detection systems.

The relative fission probability for ^{232}Th agrees with the one reported in (5) whereas a clear discrepancy is observed for the values of ^{235}U. As the uranium isotopes were all in the form of U_3O_8 with possibly a small amount of UO_3 mesochemical effects did not influence the relative muon capture rates. Thorium was in the chemical form of ThO_2. A recent investigation (19) gave as capture probabilities per atom relative to oxygen 3.57 ± 0.5 for ThO_2 and 4.99 ± 0.64 for U_3O_8.
Zinov (20) reported for UO_3 a value of 6.0 ± 0.5. Thus, mesochemical effects implied differences in the relative muon capture rates of $\sim 10^{-2}$. The errors quoted in table IV include uncertainties in the target thicknesses (2×10^{-2}) and registrations efficiencies (2×10^{-2}) and the statistical errors.

Discussion of the fission probabilities

Prompt and delayed fission probabilities per muon capture were calculated for the investigated nuclides using the fission probability per muon capture for ^{238}U of 0.15 ± 0.03 as determined in our previous work (6). They are presented in table V together with published muon fission yields. The large differences in the published muon fission probabilities are noticeable. However, ignoring the results of (5) the scattering is smaller. With the exception of ^{232}Th the muon fission probabilities of this work are compatible with those of (7).

a) Delayed muon fission

Fig. 5 presents the delayed fission probabilities per captured muon, the fission probabilities taken from the Γ_n/Γ_f systematics (21, 22) and calculated muon fission probabilities (23). The fissility parameter was taken from Nix (24).

The delayed muon fission can be described in terms of the Γ_n/Γ_f systematics as a first approximation.

TABLE V . FISSION PROBABILITIES PER CAPTURED μ^-

Nuclide	prompt	delayed	total	Ref.
^{232}Th	$(1.2\pm0.3)\times10^{-3}$	$(2.3\pm0.6)\times10^{-2}$	$(2.4\pm0.5)\times10^{-2}$	This work
			$(1.8\pm1.2)\times10^{-2}$	(18)
	$(5.0\pm1.2)\times10^{-4}$	$(3.8\pm0.9)\times10^{-3}$	$(4.3\pm1.0)\times10^{-3}$	(5)
	5.9×10^{-3}	4.5×10^{-2}	5.1×10^{-2}	(7)
^{233}U	$(6.9\pm1.4)\times10^{-2}$	$(3.3\pm0.7)\times10^{-1}$	$(4.0\pm0.8)\times10^{-1}$	This work
^{235}U	$(3.2\pm0.6)\times10^{-2}$	$(2.8\pm0.6)\times10^{-1}$	$(3.1\pm0.6)\times10^{-1}$	This work
	$(5.1\pm1.2)\times10^{-3}$	$(3.2\pm0.8)\times10^{-2}$	$(3.7\pm0.9)\times10^{-2}$	(5)
		2×10^{-1}		(7)
^{238}U	$(1.1\pm0.2)\times10^{-2}$	$(1.4\pm0.3)\times10^{-1}$	$(1.5\pm0.3)\times10^{-1}$ a)	This work
			$(1.5\pm0.6)\times10^{-1}$ }	(3)
			$(7\pm3)\times10^{-2}$ }	
			$(7.0\pm0.8)\times10^{-2}$	(4)
	$(2.03\pm0.45)\times10^{-3}$	$(2.90\pm0.65)\times10^{-2}$	$(3.1\pm0.7)\times10^{-2}$	(5)
		1.2×10^{-1}		(7)

a) Fission probability for ^{238}U from Ref. (6).

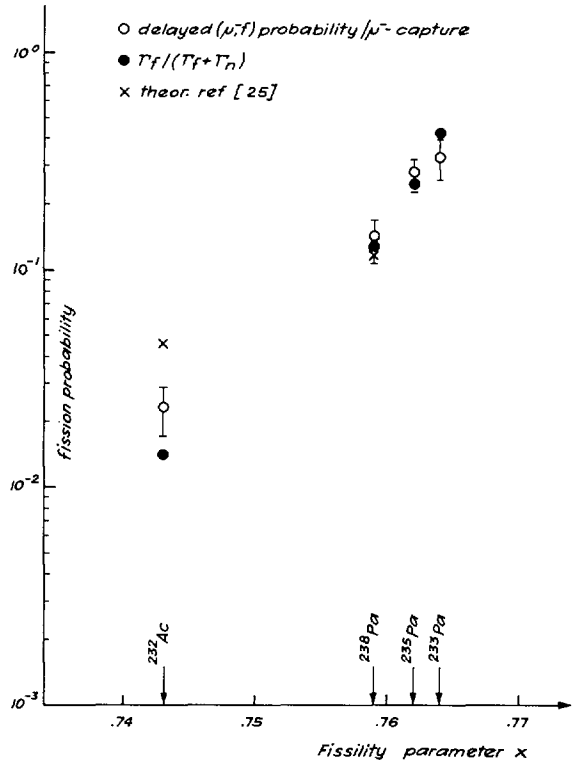

FIG. 5. Comparison of measured delayed muon fission probabilities and fission probabilities deduced from the Γ_n/Γ_f systematics. The $\Gamma_f/(\Gamma_f+\Gamma_n)$ values are based on an excitation energy of 18 MeV. The fissility parameter is taken from Ref. [24].

The excitation energy of heavy nuclei amounts characteristically to 15 - 20 MeV after a muon capture. Some neutrons are emitted directly, before the nucleus reaches an equilibrium state carrying away, on the average, an energy > 5 MeV. About 85 - 90 % of the neutrons are evaporated from the equilibrium state. The Γ_n/Γ_f systematics can be applied to this part of the emitted neutrons. The fission probabilities taken form the Γ_n/Γ_f systematics are based on an excitation energy of 18 MeV and include first and second chance fission. Due to the uncertainties in the extrapolations only a rough agreement between the systematics and muon fission can be expected. Nevertheless the agreement between our measurements and the fission probabilities deduced from the Γ_n/Γ_f systematics is remarkably good.

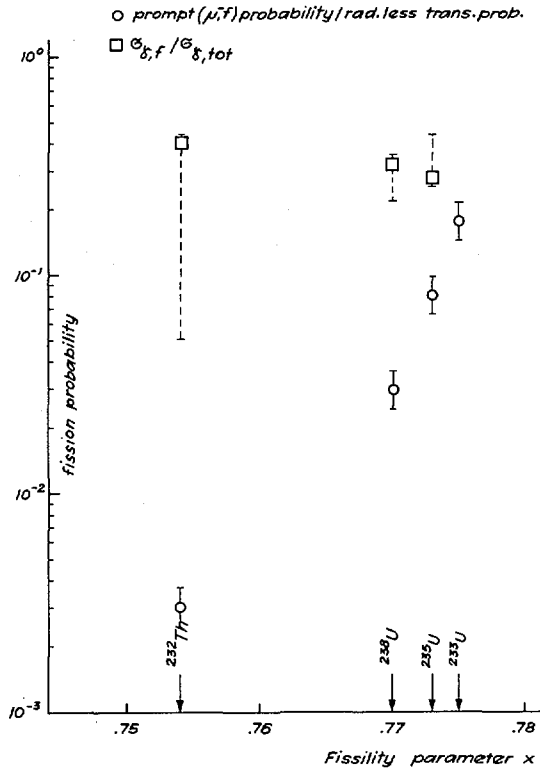

FIG. 6. Measured prompt muon fission yields per radiationless transition probability and photofissilities for the weighted K_α- and higher-order transition energies. The fissility parameter is taken from Ref. [24]. The given ranges for the weighted photofissilities mark the fissilities with all the radiationless transitions being either K_α-transitions (upper limit for ^{232}Th, ^{238}U and lower limit for ^{235}U) or higher-order transitions (lower limit for ^{232}Th, ^{238}U and upper limit for ^{235}U).

b) Prompt μ^- fission yields per radiationless transition probability

The prompt muon fission yields per radiationless transition probability and photofission probabilities are plotted in fig. 6 as function of the fissility parameter. The radiationless transition probabilities per muon capture were derived from experiments (25-28) and from theory (29-31). Butsev et al. (25) measured absolute muonic X-ray intensities in ^{232}Th and ^{238}U, but could not settle the populations of the 2p levels. Cascade calculations are unreliable because they do not

reproduce the different measured transition intensities in ^{232}Th and ^{238}U with a single starting condition. Thus the fraction of missing X-rays can only be estimated by assuming that the populations of the 2 p levels in ^{232}Th and ^{238}U equal the known populations in Pb or Bi. With a population of 0.92 and a 2 p - 1 s X-ray emission probability of 0.55 the radiationless transition probability for K_α - transitions is 0.37 per muon capture. Theoretical calculations (29 - 31) on the radiationless conversion coefficient for E 1 transitions ended up with Γ_{rl}/Γ_x = 0.6 - 0.9. Based on measured relative intensities of muonic X-rays (28) Γ_{rl}/Γ_x values have been estimated for E 1 and E 2 transitions as 0.5 and 0.17, respectively. With 0.6 and 0.17 and a population of .87 for the 3 d level (29) the probability of higher order radiationless transitions is $\sim$ 0.02 per muon capture. Hence, the total probability for radiationless transitions in ^{232}Th and in ^{238}U amounts to 0.39 per muon capture. This value agrees with the one in ^{232}Th reported by Zglinski (7).

In the following the prompt muon fission is compared with photofission assuming that the nuclear excitation in radiationless muonic transitions proceeds by the same interaction as the photoabsorption. With the photofission and photoabsorption cross sections taken from (32 - 35) the weighted photofission probabilities (W_0) at energies corresponding to the muonic transition energies were calculated and are included in fig. 6. The weights are the relative intensities of the radiationless transitions. The relative intensities of the $K_{\alpha 1}$- and $K_{\alpha 2}$-transitions were taken from (25, 27). As the photofissilities for ^{232}Th, ^{235}U and ^{238}U are energy-independent in the range of 9- to 12 MeV the relative intensities of the higher-order radiationless transitions are insignificant.

The given ranges for the weighted photofissilities mark the fissilities with all the radiationless transitions being either K_α-transitions (upper limit for ^{232}Th, ^{238}U and lower limit for ^{235}U) or higher-order transitions (lower limit for ^{232}Th, ^{238}U and upper limit for ^{235}U).

Since no cross-section data could be found for ^{233}U, the discussion is restricted to ^{232}Th, ^{235}U and ^{238}U. The striking feature of fig. 6 is the

steep dependence of the prompt muon fission yield (W_μ) on the fissility parameter X, while the photofission yield (W_o) is almost independent of it. This indicates a contribution of higher order radiationless transitions due to a reduced fission yield of the K_α radiationless transitions. The photofissilities at higher-order transition energies (lower limit given for ^{232}Th, ^{238}U and upper limit given for ^{235}U) also show a strong dependence on the fissility parameter, while the photofissilities at K_α-energies are almost independent on it. Because the higher-order transition energies are far above the fission barriers they contribute fully to W_μ. On the other hand the energies of the K_α-transitions are close to the fission barrier heights. Hence only a small increase of the fission barrier by the muon [1, 31] reduces the potential contribution of the K_α radiationless transitions to W_μ considerably.

With a photofissility of 0.05 for ^{232}Th at 9 - 12 MeV [34] the fission yield due to higher-order radiationless transitions (W_{oh}) amounts to 2.5×10^{-3}. Thus the prompt muon fission yield for ^{232}Th is almost completely due to higher-order transitions.

The relation between W_μ and W_o can be written as

$$W_\mu = \delta \cdot W_{o\alpha} + W_{oh}$$

By comparing W_μ to W_o the diminution factor δ was determined to be $\leq 1.6 \times 10^{-3}$, 5.4×10^{-2} and 2.4×10^{-1} for ^{232}Th, ^{238}U and ^{235}U, respectively.

In the following the observed diminution factor is explained by an increase in the fission barrier due to the presence of the muon in the 1s-orbital. Fission barrier parameters deduced from photofission measurements [32, 36] of ^{232}Th and ^{238}U were used. ^{235}U has been omitted since no such barrier parameters could be found for it. The fission barrier was increased by steps and the ratios of the penetrabilities of the increased and undisturbed barriers were calculated. Based on [1] the increase of the inner barrier, the valley and the outer barrier was chosen to 7.5×10^{-3} MeV, 2×10^{-2} MeV and 5×10^{-2} MeV, respectively, for each step. The penetrability of a double humped fission barrier was calculated according to [37]. Several sets of barrier parameters resulted in an increase of $\sim$ 0.6 MeV for

^{238}U. Both, the relative and absolute intensities of the radiationless muonic transitions are not well known. For ^{238}U an uncertainty in the relative intensities of the radiationless transitions is not critical (fig. 6). A change of $\pm$ 50 % in the absolute radiationless transition probability per captured muon implies a change of $\pm$ 0.1 MeV for the barrier increase. For ^{232}Th only an upper limit for the diminution factor can be given. The corresponding lower limit for an increase of the fission barrier is (0.6 $\pm$ 0.2) MeV.

Conclusions

The measured delayed muon fission probabilities follow roughly the Γ_n/Γ_f systematics. The dependence of the prompt muon fission yields per radiationless transition probability on the fissility parameter indicates a contribution of higher-order radiationless transitions. The fission yields obtained by muonic radiationless K_α-transitions are lower than the photofissilities at equal energies. For ^{238}U, this can be explained by an increase of $\sim$ 0.6 MeV of the fission barrier. Theory predicts a comparable increase due to the deformation of the fissioning nucleus with a muon in the 1s orbit. Muon-induced fission could improve the understanding of the fission process further if a better knowledge of the relative and absolute radiationless transition intensities were available.

Acknowledgement

The authors are indebted to C. Petitjean, H.S. Pruys, P.G. Seiler and H.U. Zwicky for their assistance and valuable discussions, and to R. Keil, D. Orciuolo and E. Rössler for the performance of the analyses. The interest of P. Baertschi is highly appreciated. Part of the work was supported by the Swiss National Science Foundation.

References

(1) Leander, G., Möller, P., Phys. Lett. 57B (1975) 245.

(2) Galbraith, W., Whitehouse, W.J., Phil. Mag. 44 (1953) 77.

(3) John, W., Fry, W.F., Phys. Rev. 91 (1953) 1234.

(4) Belovitsky, G.E. et al., JETP 38 (1960) 404.

(5) Chultem, D. et al., Nucl. Phys. A 247 (1975) 452.

(6) Baertschi, P. et al., Nucl. Phys. A 294 (1978) 369.

(7) Zglinski, A. et al., Nucl. Phys. A 305 (1978) 381.

(8) Diaz, J.A. et al., Nucl. Phys. 40 (1963) 54.

(9) Budick, B. et al., Phys. Rev. Lett. 24 (1970) 604.

(10) Gavrilov Yu.K. et al., Yad. Fiz. 24 (1976) 241.

(11) Ganzorig, Dz. et al., Phys. Lett. 78B (1978) 41.

(12) Sens, J.C., Phys. Rev. 113 (1959) 679.

(13) Hashimoto, O. et al., Phys. Lett. 62B (1976) 233.

(14) Johnson, M.W. et al., Phys. Rev. C 15 (1977) 2169.

(15) Kaplan, S.N. et al., Phys. Lett. 64B (1976) 217.

(16) From, W.D. et al., Nucl. Phys. A 278 (1977) 2169.

(17) Wilcke, W.W. et al., Phys. Rev. C 18 (1978) 1452.

(18) Petrascu, M.G., Mihul, A.K., Dokl. Akad. Nauk 126 (1959) 752.

(19) Hartmann, F.J., private communication.

(20) Zinov, V.G. et al., Sov. Jour. Nucl. Phys. 2 (1966) 613.

(21) Gavron, A. et al., Phys. Rev. Lett. 34 (1975) 827,
Phys. Rev. C 13 (1976) 2374.

(22) Vandenbosch, R., Huizenga, J.R., Phys. Rev. C 13 (1976) 2374,
"Nuclear Fission", Acad. Press, New York (1973).

(23) Hadermann, J., Junker, K., Nucl. Phys. A 256 (1976) 521.

(24) Nix, J.R., Nucl. Phys. A 130 (1969) 241.

(25) Butsev, V.S. et al., Dubna report E 1-9580, JINR (1976).

(26) McKee, R.J., Phys. Rev. 180 (1969) 1139.

(27) De Wit, S.A. et al., Nucl. Phys. 87 (1967) 657.

(28) Schneuwly, H. et al., Nucl. Phys. A 196 (1972) 452.

(29) Lohs, K.P. et al., Nucl. Phys. A 236 (1974) 457.

(30) Srinivasan, V., Sundaresan, M.K., Can. Jour. of Phys. 49 (1971) 621.

(31) Zaretsky, D.F., Novikov, V.M., Nucl. Phys. 14 (1960) 540.
Nucl. Phys. 28 (1961) 177; JETP 14 (1962) 157.

(32) Dickey, P.A., Axel, P., Phys. Rev. Lett. 35 (1975) 501.

(33) Zhuchko, V.E. et al., Nucl. Instr. Meth. 136 (1976) 373.

(34) Veyssière, A. et al., Nucl. Phys. A 199 (1973) 45.

(35) Caldwell, J.T. et al., Los Alamos Scient. Lab-Report No. LA-UR 76-1615 (1976)

(36) Alm, A. et al., IAEA, Vienna (1974) 55.

(37) Martinelli, T. et al., CNEN-RT/F 1 (1978) 7.

FRAGMENT PROPERTIES AND PARTICLE EMISSION (EXPERIMENTS)

(Session F)

Chairmen

P. ARMBRUSTER
FRG

B.G. YANKOV
USSR

G.F. HERRMANN
FRG

EXPERIMENTAL APPROACH TO THE DYNAMICS OF FISSION

H.A. NIFENECKER, J. BLACHOT, J.P. BOCQUET*,
R. BRISSOT*, J. CRANÇON, C. HAMELIN*,
G. MARIOLOPOULOS, C. RISTORI
Centre d'études nucléaires,
Grenoble Cedex, France

Abstract

EXPERIMENTAL APPROACH TO THE DYNAMICS OF FISSION.

It is shown that the preference for the formation of even-Z fragments in low-energy fission implies that the fission mode is weakly coupled to quasi-particle excitation. This contradicts the statistical model. Existence of even-odd effects on the kinetic energy of the fragments also implies that the number of time-even quasi-particle excitations is vanishing or small. However, the variations of the kinetic energy of the fragments with excitation energy and the analysis of light-charged-particle-accompanied fission show that fission is a slow process, in contrast to what the liquid-drop theory of fission stipulates. The thermodynamical model of fission is compatible with the existing experimental evidence. It is, however, possible that the different distributions are determined at different times during the process. A minimal duration for the process of 10^{-20} s is derived from the widths of the isobaric distributions.

The dynamical properties of nuclear matter have come to the foreground with the multiplication of heavy-ion accelerators. Meanwhile spontaneous or light particle induced fission remains, and is more and more, a rich source of information on these properties. This is due to some unique features of the fission process.

In spontaneous or low energy fission the nuclear system goes past a definite quasi-stationary saddle point which may be used as a well defined starting point for dynamical computations. In particular the excitation energy of the nucleus at the saddle point can be precisely controlled and, for instance, the system may be prepared in a superfluid state. Therefore only fission allows a study of large amplitude motions of superfluid nuclear matter as well as the transition between superfluid and normal dynamics.

In the following we shall try to review some of the fission related experimental results which may tell us something about nuclear dynamics. Doing so, we want to be as free as possible of nuclear models. It is clear, however, that some frame is necessary to interpret the experimental results. As a compromise we have chosen to make qualitative comparisons between experiment and some basic features of the most current models of nuclear fission. It will appear in the following that a satisfactory quantitative

* Also U.S.M. Grenoble.

theory of fission does not exist at the moment. It is even questionable that a satisfactory qualitative theory exists. It is our hope that nature herself may tell us what basic ingredients should be put in such a theory. The clarity of the message obviously depends on the completeness of the experimental results. We shall therefore try to pin-point the holes in our experimental knowledge of fission in so far as they are relevant to the understanding of the dynamics of fission.

The fission process may be divided into three phases. In the first one the nucleus proceeds to the first saddle point. The second phase corresponds to the transition between the first and second saddle. The last is the descent to scission. Although some information on the dynamics of fission can be and has been [1] obtained from the widths of the vibrational states in the second well we shall concentrate on the third phase of the fission process. This is by far the shortest. This circunstance means that it is there that damping or frictional effects may be best studied if they are strong. There is also a chance that, on such short time-scale, a hierarchy of characteristic times similar to that introduced in H.I. reactions may be established.

In section 1 we shall examine the fission fragments charge distributions. We hope to show that these distributions give a very direct clue on the extent to which nuclei remain superfluid during the fission process.

In section 2 we shall examine the variations of the fragments' kinetic energies as a function of the excitation energy of the fissioning nucleus. Such results have implications on the amount of damping of the fission mode.

In section 3 we discuss the possible use of L.R.A. fission to obtain a description of the scission configuration.

Finally in section 4 we examine if it possible to say at what stage the different mass and energy distributions are determined.

1. FRAGMENTS'CHARGE AND CHARGE-RELATED DISTRIBUTIONS

Here we shall concentrate on the so-called even-odd effect observed in certain fragments' charge distributions. We shall come back in section 4 on some aspects of charge distributions like the value of the widths of the isobaric distributions.

1.1. Even-odd effects in elemental yields

1.1.1. Experimental status

The enhancement of even Z fragments has first been suspected from the observation of fine structures in the mass distribution of U^{235} slow neutron induced fission [2,3,4]. It was then confirmed by evaluation of radiochemical data [5,6]. J.P. Unik et al.[7] made a systematic survey of fine structures in mass distributions observed both in slow neutron induced and spontaneous fission for a wide range of nuclei between Th^{229} and Fm^{256}. Here again, when present, the fine structures were nicely correlated with a probable enhancement in the production of even-Z fragments. From this survey it appears that the relative intensity of the fine structures depends markedly on the nature of the fissioning system. Two main trends show up for even-Z fissioning nuclei.

The fine structures are usually more apparent in spontaneous than in induced fission.

They tend to vanish when the mass of the fissioning nucleus increases.

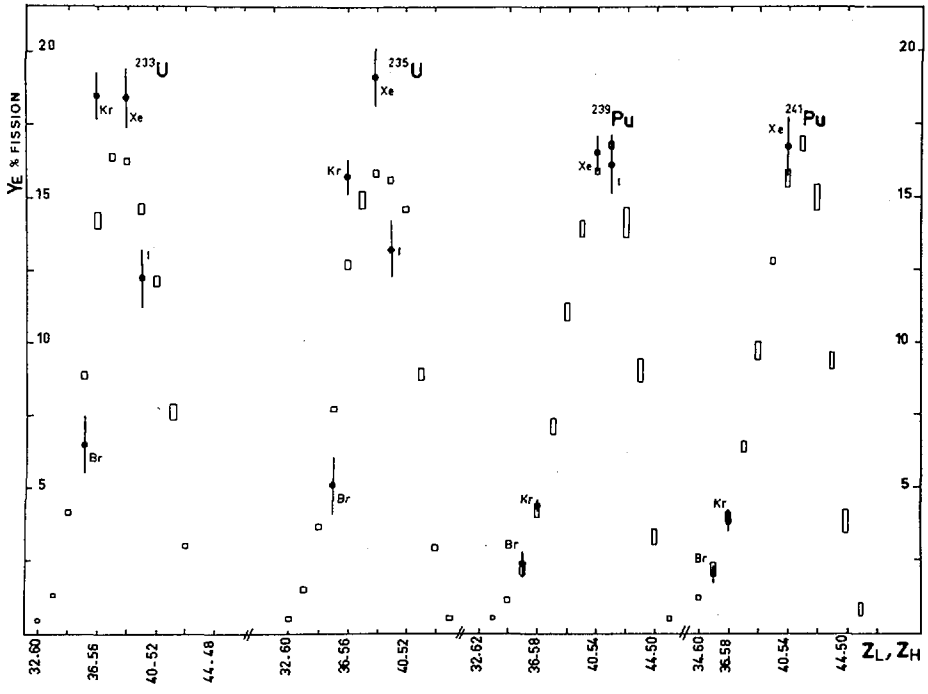

FIG.1. Selected elemental yields from $^{233,235}U$ and $^{239,241}Pu$ thermal-neutron-induced fission. The rectangles are estimates of the yields from the mass distributions on the assumption of no even-odd effect. The dots and error bars correspond to the measured values. The measured element is indicated. Owing to the binary character of fission, measurement on one element is equivalent to the measurement on the complementary element.

It should be pointed out,at that point that J.P. Unik et al. used the double-energy method to obtain pre-neutron emission fragments'masses. This method suffers from a rather modest mass resolution which worsens when the number of neutrons emitted by the fragments increases. To some extent the two trends mentioned above might have reflected a mass resolution effect since, as a rule, the number of emitted neutrons is larger for induced than for spontaneous fission and for heavy than for light fissioning nuclei. Therefore, a direct confirmation of J.P. Unik et al. results where nuclear charges of the fission fragments would be directly measured was needed. It has been partly obtained in the recent years. Along the lines of Wahl [5] and Amiel [6] radiochemical methods have been used to obtain elemental yields in a number of fissioning systems. Fig.1 shows an example of the data which have been obtained [64]. It is clear, on the figure, that the even-odd effects which are prominent for the two Uranium isotopes are barely visible for the two Plutoniums. These findings are in agreement with what can be deduced from the mass distributions presented by J.P. Unik et al. From Fig.1 the authors deduced an average amplitude of the even-odd effect as shown in Table I. Similar values have

TABLE I. AMPLITUDE OF THE EVEN-ODD EFFECTS (ENHANCEMENT OF THE EVEN ELEMENTS WITH RESPECT TO THE 'NORMAL' ONES) (from Brissot et al. [64])

Fission process	$^{235}U(n_{th})$	$^{233}U(n_{th})$	$^{239}Pu(n_{th})$	$^{241}Pu(n_{th})$
Even-odd effect	1.25 ± 0.05	1.23 ± 0.05	1.034 ± 0.05	1.04 ± 0.05

TABLE II. AMPLITUDE OF THE EVEN-ODD EFFECT FROM WAHL [9]

Fission process	$^{235}U(n_{th})$	$^{233}U(n_{th})$	$^{239}Pu(n_{th})$	$^{252}Cf(sf)$
Even-odd effect on charge yields	1.26 ± 0.02	1.30 ± 0.05	1.07 ± 0.03	1.00 ± 0.05

been obtained for U^{235} and U^{233} by Amiel [8] from an evaluation of radiochemically determined independent yields of fission fragments. More recently Wahl [9] obtained the results shown on Table II.

Here again the results agree with the trends found by J.P. Unik et al.

It is only recently that direct physical methods have become available for obtaining fission fragments' charge distributions. These methods take advantage of the variation of the specific energy loss of fission fragments with their charges. A charge resolution better than one unit has only been obtained on mass and velocity selected fission fragments [10,11]. This limitation is related to the fact that solid mediums seem to have better charge resolution capabilities than gases. In the first case charge resolution as good as 1/55 [12], have recently been reported while the best results obtained with gas ionization energy loss chamber range around 1/38 [13,14,15]. Because of the necessity of preselection of the fragments in mass and velocity only the slow neutron induced fission of U^{235} has been studied at the moment [16,17]. The elemental and isotonic distributions obtained by Clerc [17] are shown on Fig.2 and 3.

Even-odd effects are clearly visible in both distributions but are much more pronounced in the elemental distribution. It is worth noting, here, that this distribution is not modified by the deexcitation of the fission fragments while the isotopic distribution is. It may even be that the neutron evaporation alone explains the even-odd effect on the isotonic distribution. For this matter we shall only discuss the charge distributions from now on.

Even if ΔE-E systems using ionization chambers cannot provide a clear charge separation in the fission fragments domain they may be used in conjunction with an unfolding technique to obtain charge distributions. For unfolding the ΔE-E arrays it is necessary to know the arrays which correspond to each individual charge. We have recently been able to apply this

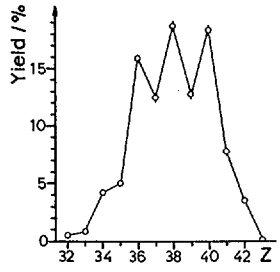

FIG. 2. Elemental yields from the thermal-neutron-induced fission of ^{235}U from Clerc et al. [17].

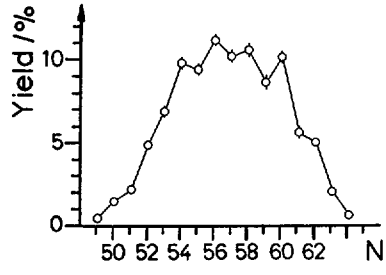

FIG. 3. Isotonic yields for the light-fragment group from the thermal-neutron-induced fission of ^{235}U from Clerc et al. [17].

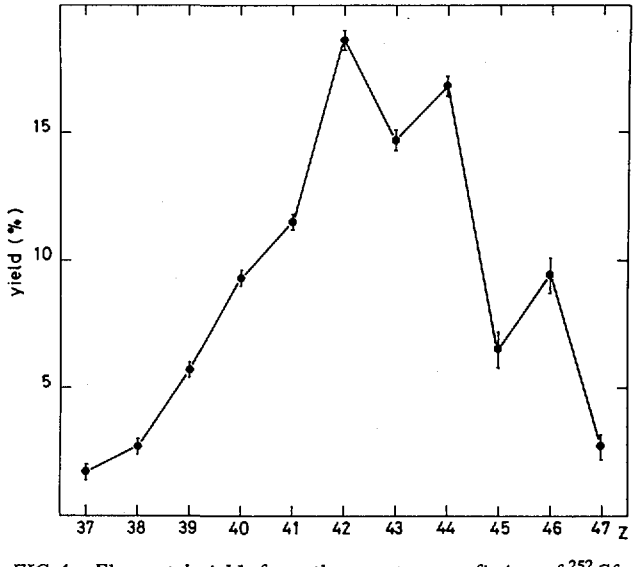

FIG. 4. Elemental yields from the spontaneous fission of ^{252}Cf.

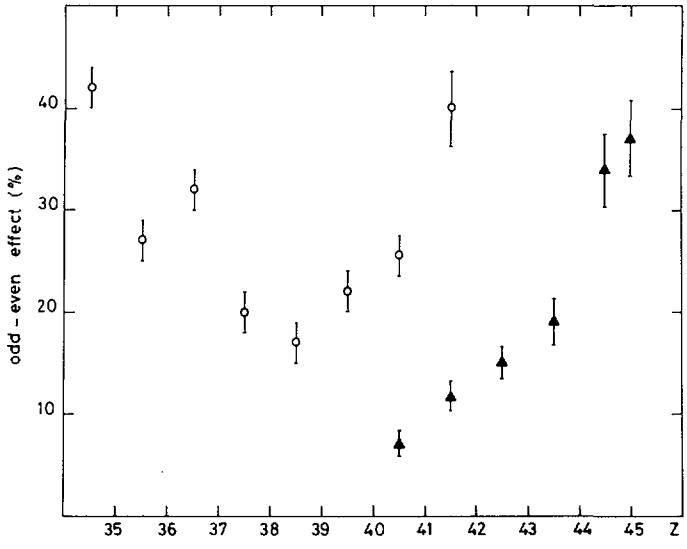

FIG. 5. Even-odd as a function of charge for ^{235}U (n_{th},f) (○) and ^{252}Cf (▲). The even-odd amplitude is defined as:

$$\delta_{Z+1.5} = (-1)^{Z+1} \left\{ \begin{matrix} \mathrm{Log}(Z+3) - \mathrm{Log}(Z) \\ -3\,[\mathrm{Log}(Z+2) - \mathrm{Log}(Z+1)] \end{matrix} \right\} \quad [8].$$

technique to the spontaneous fission of Cf^{252} [18]. The individual response functions were determined by means of a complementary experiment where the X-rays emitted by the fission fragments were detected in coincidence with the fragments entering the E-ΔE counters. The X-rays were used to select the fragments'charges. The E-ΔE array obtained without the X-ray coincidence requirement was then unfolded providing a new Z-E array where the energy bins were 1 MeV wide. Summing over the energies the elemental yields in Cf^{252} fission were obtained as shown on Fig.4. Although still present the even-odd effect is reduced to a value of approximately 8%. It is also possible to compute an even-odd parameter for each even charge from third order difference in the logarithms of the yields [19]. The result of such a computation is shown on Fig.5 both for Cf^{252}(sf) and U^{235} (nf).

The charge yields of Cf^{250}(s,f) and Cf^{249}(nf) have been obtained from those of Cf^{252}(s,f). This was done by comparing the X-ray yields observed in the three cases. The ratios of the X-ray yields of Cf^{250} spontaneous fission and of Cf^{249} thermal neutron induced fission to those of Cf^{252} spontaneous fission are shown an Fig.6. Due to the possible selectivity of the X-ray emission process it may be misleading to use the values of Fig.6 quantitatively. However the qualitative picture suggested by the figure is clear. The even-odd effects are similar in both spontaneous fission of Cf^{252} and Cf^{250}. The odd Z fission fragments increase in yield significantly in the neutron induced fission of Cf^{249}.

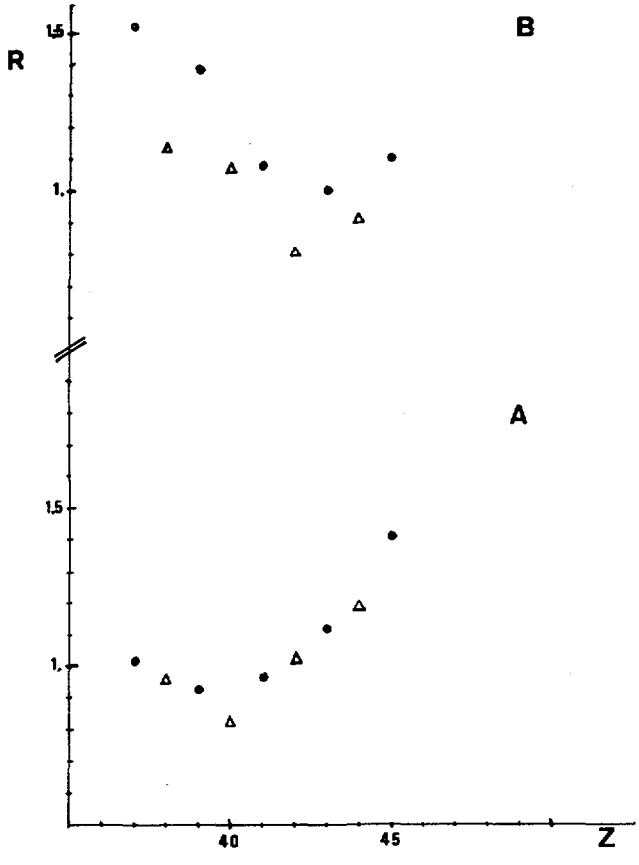

FIG. 6. Ratio of X-ray yields as a function of charge:
● *Odd charges*
△ *Even charges*
A) $R = Y_x(^{249}Cf)/Y_x(^{250}Cf)$
B) $R = Y_x(^{252}Cf)/Y_x(^{250}Cf)$.

Studies of the variation of even-odd effects in charge yields of fission fragments as a function of the excitation energy of the fissionning nucleus are very scarce. Amiel [20], from an evaluation of existing data, found an 8% even-odd effect when the fission of U^{235} was induced by fission neutrons. This figure shows a sharp decrease as compared to the 25% effect observed for slow neutron induced fission. We have measured independent yields obtained [21] in U^{235} fission induced by 3 MeV monochromatic neutrons. Fig.7 shows a number of isobaric distributions obtained for slow and 3 MeV neutrons induced fission. It is clearly visible that the even-odd effects are drastically reduced at 3 MeV. On the figure curves corresponding to Wahl's assumptions for Z_p and $\sigma^2(Z)$ are also reported. They correspond to the distributions without even-odd effects. They seem to agree closely with the 3 MeV distributions.

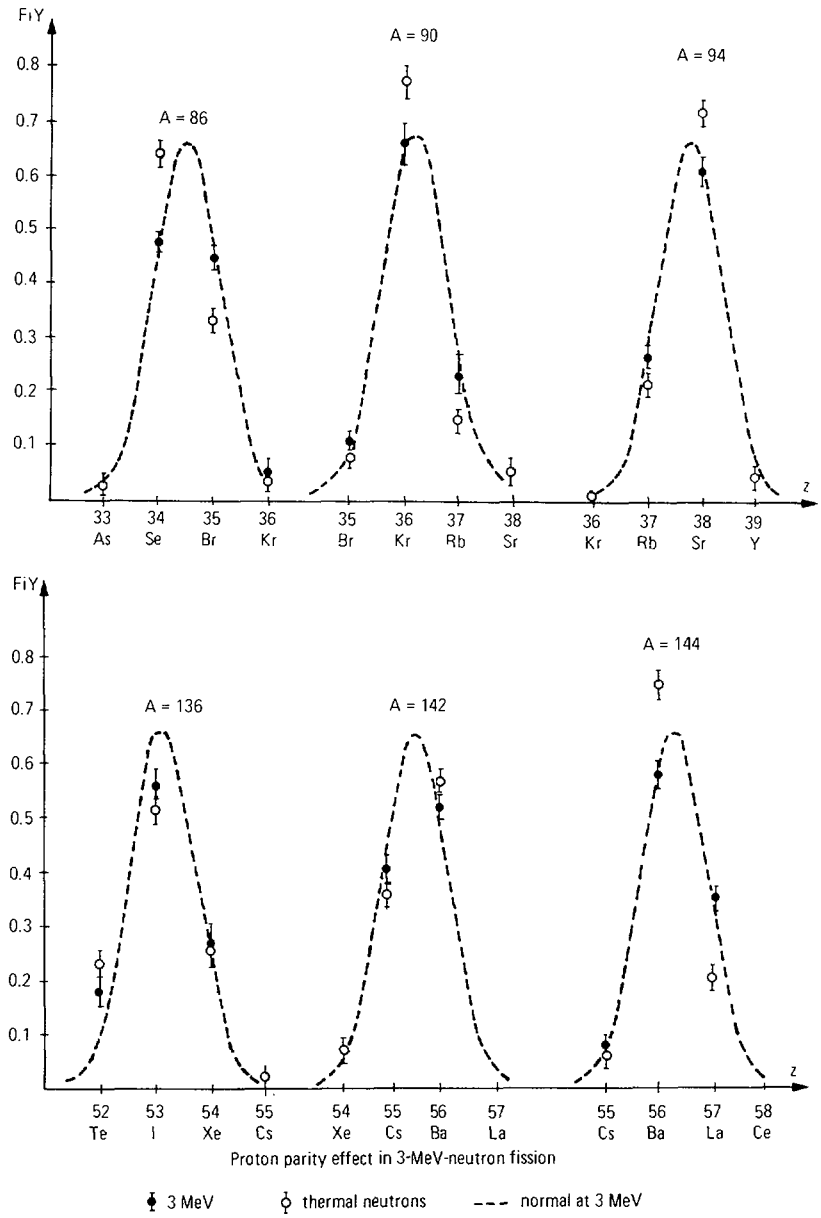

FIG. 7. Selected isobaric distributions for: ● 3-MeV-neutron-induced fission of ^{235}U; ○ Thermal-neutron-induced fission of ^{235}U. The dashed curve is an estimate of the isobaric distributions for 3-MeV neutron energy from the mass distributions, assuming no even-odd effect and using Wahl's universal charge distribution curve.

Summarizing this section we find that the production of even-charge fragments is favored in low energy fission. This enhancement is the origin of the fine structures observed on the mass distributions. The magnitude of this so called even-odd effect depends sensitively both on fissility parameter and the excitation energy of the fissionning nuceus. In particular an increase of the excitation energy by two to three MeV above the fission barrier decreases the effect by a factor of 3 to 5.

1.1.2. Significance of the even-odd effects

Even-odd effects and fine structures were first related [2] to energy balance considerations. On the average fissions of even Z nuclei which give a split into two even-Z fragments are 2 Δ_p (2.7 MeV approximately) more energetic than those which give a split into two odd-Z fragments. However although energy considerations may be useful they are unable to account for the fast variations of the even-odd effects with the excitation energy and nature of the fissionning system. As seen above, an increase of 3 MeV in the total excitation energy of the fission fragments suffices to destroy the even-odd effects. Such a limited variation is certainly unable to make energy balance considerations lose their relevance, if they have some.

It is possible to make this point more quantitative in the frame of the statistical model introduced by P. Fong [22]. In this model a scission configuration may be defined by the neutron number N, the charge Z of one of the fragments and a set of deformation coordinates $\{\alpha\}$. Each scission configuration is characterized by a potential energy

$$V(Z, N, \{\alpha\})$$

The free energy of the configuration may be defined as

$$X(Z, N, \{\alpha\}) = Q(Z, N) - V(Z, N, \{\alpha\})$$

where $Q(Z,N)$ is the Q value of the reaction and is calculated as :

$$Q(Z,N) = M(Z_T, N_T) - M(Z,N) - M(Z_T - Z, N_T - N)$$

M(Z,N) beeing the masses of the nucleus Z,N.

The probability to observe a given scission configuration is then equal to

$$W(Z, N, \{\alpha\}) = \int_0^X \rho_1(\varepsilon)\, \rho_2(X - \varepsilon)\, d\varepsilon$$

ρ_1 and ρ_2 beeing the level densities of the two nascent fission fragments. In Fong's theory ρ is taken as a standard level density namely.

$$\rho = \exp\sqrt{a(\varepsilon - \Delta(N) - \Delta(Z))}$$

Here $\Delta(N)$ and $\Delta(Z)$ are the neutron and proton pairing energies when N or Z are even and 0 when they are odd. In the following we only consider the effect of a change in the parity of Z and therefore omit N. When Z_1 (and Z_2) are odd we write

$$X_o = Q_o - V$$

and

$$W_o(Z, \{\alpha\}) = \int_0^{X_o} \exp\sqrt{a_1 \varepsilon}\, \exp\sqrt{a_2 (X - \varepsilon)}\, d\varepsilon$$

if Z_1(and Z_2) are even then

$$x_e = x_o + \Delta_1 + \Delta_2 \qquad \text{with}$$

$$\Delta_1 = \Delta(Z_1) \qquad \Delta_2 = \Delta(Z_2)$$

and

$$W_e(Z,\{\alpha\}) = \int_0^{x_e} \exp\sqrt{a_1(\varepsilon-\Delta_1)}\,\exp\sqrt{a_2(x_o+\Delta_1-\varepsilon)}\,d\varepsilon$$

if we write $u = \varepsilon - \Delta_1$

then

$$W_e(Z,\{\alpha\}) = \int_{-\Delta_1}^{x_o+\Delta_2} \exp\sqrt{a_1 u_1}\,\exp\sqrt{a_2(x_o-u_1)}\,du_1$$

it is known [22] that the integrand has a sharp maximum around

$$\sqrt{\frac{a_1}{u_1}} = \sqrt{\frac{a_2}{(x_o-u_1)}} = \frac{1}{T}$$

and the contributions to the integrals of regions close to the limit of integration are small. Thus if one restricts oneself to u > o

$$W_e(Z) \# \int_0^{x_o} \exp\sqrt{a_1 u_1}\,\exp\sqrt{a_2(x_o-u_1)}\,du_1 = W_o(Z)$$

Therefore the statistical theory does not predict any significant even-odd effect as long as there is no even-odd effect on V(Z,N, $\{\alpha\}$).

This result comes from the introduction of the effective excitation energies

$$u = \varepsilon - \Delta$$

which compensate the increase in the Q of the reaction for even-even splits.

Let us lift the constraint that

$$u = \varepsilon - \Delta$$

and assume that the effective excitation energy is

$$u = \varepsilon - k\Delta$$

then

$$W_o(x) = \int_0^{x} \exp\sqrt{a_1\varepsilon}\,\exp\sqrt{a_2(x-\varepsilon)}\,d\varepsilon$$

$$W_e(x) = \int_0^{x+\Delta_1+\Delta_2} \exp\sqrt{a_1(\varepsilon-k\Delta_1)}\,\exp\sqrt{a_2(x+\Delta_1+\Delta_2-k\Delta_2-\varepsilon)}\,d\varepsilon$$

Here again the maximum of the integrand for $w_e(Z)$ is obtained for :

$$\frac{a_1}{\varepsilon-k\Delta_1} = \frac{a_2}{x+\Delta_1+\Delta_2-k\Delta_2-\varepsilon}$$

The maximum of the integrand is the n equal to

$$\exp\sqrt{(a_1+a_2)x\left(1+(\Delta_1+\Delta_2)\frac{(1-k)}{x}\right)}$$

Then assuming that the ratio of the integrals is equal to that of the maximum of the integrands

$$\frac{W_e(Z)}{W_o(Z)} = \exp\left[\sqrt{(a_1+a_2)x\left(1+(\Delta_1+\Delta_2)\frac{(1-k)}{x}\right)} - \sqrt{(a_1+a_2)x}\right]$$

Let us first assume that $(1-k)\left(\frac{\Delta_1+\Delta_2}{X}\right) \ll 1$

then

$$\frac{W_e(Z)}{W_o(Z)} \# \exp\left[\sqrt{\frac{a_1+a_2}{X}}\ \frac{(\Delta_1+\Delta_2)}{2}(1-k)\right]$$

or

$$\left[\log \frac{W_e(Z)}{W_o(Z)}\right]^2 = \frac{(a_1+a_2)}{X}\frac{(\Delta_1+\Delta_2)^2}{4}(1-k)^2$$

For slow neutron induced fission the experiment gives

$$\frac{W_e(Z)}{W_o(Z)} \# 1.8$$

while at 3 MeV excitation energy

$$\frac{W_e(Z)}{W_o(Z)} < 1.2$$

With these values one obtains

X = 0.32 MeV

k = 0.95

The condition that $(\Delta_1+\Delta_2)(1-k)/X \ll 1$ is barely fulfilled. However we do not need an exact solution. It can be seen that the total excitation energy X obtained is very small and would certainly not justify the statistical model approach.

The values obtained for k and X can be understood qualitatively as the result of a competition between two effects.

The small values of the even-odd effect for 3 MeV neutrons shows that the "effective energy" approach for level densities is valid to a large extent.

If the effective energy approach is approximately valid the only possibility to obtain the strong even-odd effects observed in slow neutron induced fission is that the excitation energies of the fragments be close to the pairing gap.

The alternative explanation of the even-odd effects and of their variations is provided by the consideration of pair-breaking.

We consider an even-Z nucleus at saddle. Let us assume in first approximation that no pair is broken during the fission process. If the nucleus is completely paired (ground state band) at saddle only fragments with even Z will be produced. If, on the other hand, one pair at least is broken in the fissionning nucleus at the saddle point, the celibatary nucleons will behave independently during the fission process. Odd Z and even Z splits will be equally probable and no even-odd effect will be left. This very simple model therefore explains qualitatively the very fast variation of the magnitude of the even-odd effect with neutron energy. Il also may explain, in part, the variations of the even-odd effect with the charge (mass) of the fissionning species. It is known that the energy of the second saddle point, which is probably relevant here, decreases with A(or Z). Therefore even-odd effects in slow neutron induced fission are expected to decrease with A, as observed experimentally. Along the line of the model it is also clear that the very existence of important even-odd effects implies that the probability of pair breaking during the fission process is small. In itself, this fact is far reaching with respect to the dynamics of the fission process. It should be pointed out, however, at this point, that a small probability for pair breaking is not equivalent to a small probability for quasi-particle excitations.

The possible importance for fission of 2 quasi-particles excitations in time reserved states has been noted several times [23,24,25]. In the BCS formalism such states are defined as

$$\alpha_k^+ \alpha_{-k}^+ |BCS\rangle$$

Such excitations lead to the localization of the two quasi particles in the same fragment. However a small perturbation is, in principle, sufficient to break this pair.

The small probability for pair breaking is also related to the microscopic conservation of the k quantum number as well as of the axial symetry during fission.

The production of odd-Z elements in spontaneous fission shows evidently that the assumption that no pair-breaking occurs during the fission process is oversimplifiing. Do these pair breakings occur at an early stage during the descent from saddle point or at the very late scission stage ?

Effects such as even-odd effects on the kinetic energy of the fragments, or the variations of the magnitude of the even-odd effects on fragment yields as a function of the charges of the fragments, may give a clue to it.

1.2.Additional aspects of the even-odd effects

1.2.1 Experimental status

Using the X-ray charge assignment technique [26] even-odd Z effects were found on the fragments'total kinetic energies and excitation energies. The effect on the kinetic energies was estimated to be

$$\overline{\Delta E}_K = 1.6 \text{ MeV}$$

and that on the excitation energy was almost entirely related to γ-ray emission and amounted to 0.7 MeV. No effect was found, at that time, on the neutron emission.

The selectivity of the X-ray emission process might have biased these results. We have therefore used the ΔE-E shape analysis described above to study even-odd effects on kinetic energy distributions. The E-ΔE array was subdivided in 1 MeV wide kinetic energy bins. Each bin was then analyzed in terms of charge yields. Fig. 8 shows the yields so obtained for some energy bins.

It may be seen on the figure that the even-odd effects increase with increasing kinetic energy. Also seen on the figure is the dramatic change of behavior of the yield-curves around Z = 42. From these spectra one obtains the average kinetic energies as a function of charge. These are shown on Fig.9(a) where the values obtained with the X-ray technique have also been reported. The agreement between the two types of measurements is very good. However, the derivation of the magnitude of the kinetic energy even-odd effect suffers from some ambiguity. The sudden change of behavior of the kinetic energy around Z = 42 which may be related to closure of the neutron deformed shell N = 60,62 does influence the calculated values of the even-odd effect. This is shown on Fig.9(b) where the even-odd effect was computed from the second order difference of the kinetic energy curve. The discontinuity of the curve around Z = 42 produces an exceptionally high even-odd difference for Z = 42,43 [17] of more than 2 MeV. For the other charges the effect lies around 1 MeV. At this point it is worth noticing that the magnitudes of the even-odd effect on the kinetic energies does not appear to be correlated

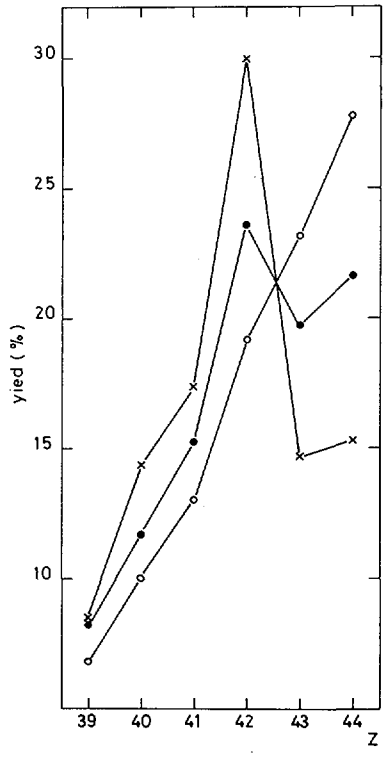

FIG. 8. Charge yields from the spontaneous fission of ^{252}Cf for several kinetic energy bins:
x 114 ± 3 MeV
• 106 ± 3 MeV
o 99 ± 3 MeV.

with those of the charge yields as they appear on Fig.5 for Cf^{252}. The even-odd effect is also apparent on the variances of the kinetic energies as shown on Fig. 10. This observation agrees with the hypothesis made in Ref.26.

Summarizing we find that kinetic energies do show an even-odd effect in Cf^{252}(s,f) the magnitude of which, however is difficult to define precisely . In any case it is at least of order 1 MeV.

In their very detailed study of U^{235}(n,f) Clerc et al. [27] have also found an even-odd effect on the kinetic energy of the fission fragments. Their results is shown an Fig. 11(a). On Fig. 11(b) we have calculated, as in the Cf^{252}, the magnitude of the even-odd effect on E_K as a function of fragment charge. It can be seen that $U^{235}(n_{th},f)$ is very similar to Cf^{252}(s,f) as far as the even-odd effect on kinetic energies is concerned.

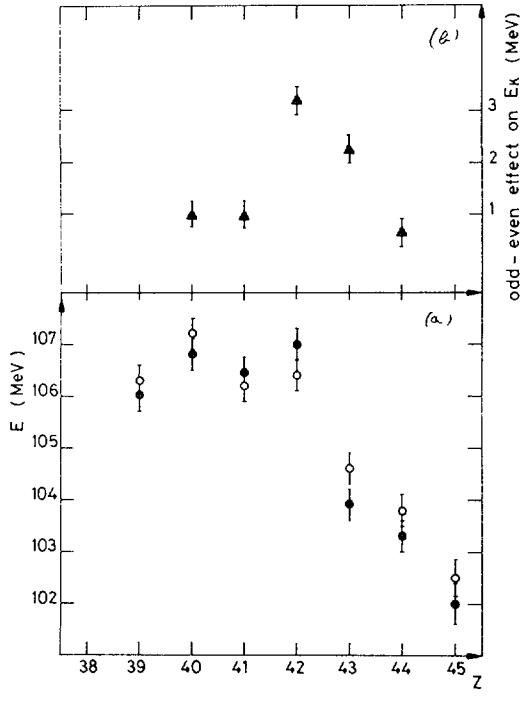

FIG. 9. $^{252}Cf\,(s,f)$

(a) Lower part: Average fragment kinetic energies as a function of charge:

● *from the* ΔE–E *measurement;*

○ *from the X-ray measurement* [26].

(b) Upper part: Even-odd effect on the total kinetic energies. The total kinetic energy was computed from the fragment kinetic energy by

$$E^K(Z) = E^F(Z) \times \frac{98}{98-Z}$$

and the even-odd effect from the second-order difference:

$$\delta_Z^{E^K} = \frac{1}{2}(-)^{Z+1}\,[E^K(Z-1) - 2E^K(Z) + E^K(Z+1)]$$

1.2.2 Implications for the dynamics of fission

We now examine the origin of the even-odd effect on the kinetic energies. Any such effect is accompanied by a complementary effect on the excitations energies

$$\Delta E^{ex}_{e-o} = \Delta Q_{e-o} - \Delta E^K_{e-o}$$

The difference ΔQ_{e-o} being approximately 2.7 MeV [26]. This difference is related to the condensation energy of the ground state of even-Z nuclei.

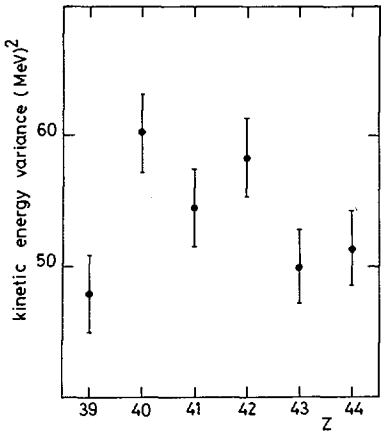

FIG.10. Kinetic energy variance (^{252}Cf sf) as a function of fragment charges.

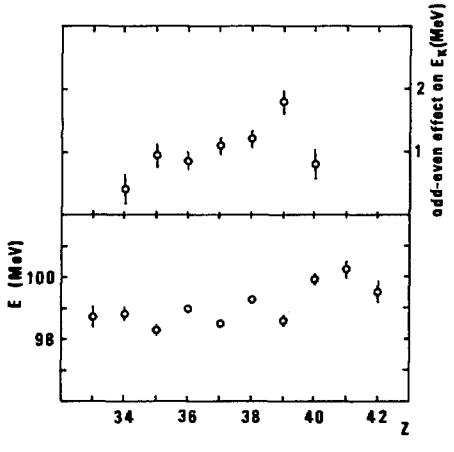

FIG.11. Same as Fig.9, for ^{235}U slow-neutron-induced fission, from Clerc et al. [17].

Let us first consider an even fissioning nucleus, highly excited at the saddle point. Many pairs are broken under these conditions. This is also true for the two fragments, just after scission. It is clear that, on the average, during the deexcitation process, even-Z splits will gain the condensation energy of one pair more than odd-Z splits. Therefore, for high energy fission one expects even-Z fragments to have a total excitation energy 2.7 MeV approximately higher than odd-Z fragments. Consequently, no even-odd effect should appear on the total kinetic energy.

A similar conclusion can be reached if a pair is broken long before scission. By this we mean a time long enough for each member of the pair to behave independently at scission. The probability that both members of the former pair end in the same fragment is then equal to that they end up in different fragments. Even and odd splits have the same probability

$$Y_e = Y_o$$

and the even-odd effect is only apparent on the excitation energy

$$\Delta E^{ex}_{e-o} = \Delta Q_{e-o}$$

$$\Delta E^{K}_{e-o} = 0$$

Unfortunately we have no experimental data to test the validity of these considerations. Such data on the even-odd effects on kinetic energies and/or excitation energies for moderate energy fission would be extremely interesting. In the following we shall assume, in the absence of such data, that the considerations just presented are valid. Along this line the existence of an even-odd effect on the kinetic energies both in Cf^{252} spontaneous and in U^{235} slow neutron induced fissions implies that the number of broken pairs at scission is small. In that respect time even two quasi particle states $\alpha^{+}_{K} \alpha^{+-}_{K} | BCS >$ such as those considered by Schütte and Wilets [24] are similar to other two quasi particle states since it requires no energy to break the time-even pair. Such states may give even-odd effects on the fragments yields but not on the kinetic energies.

The even-odd effects on the kinetic energies have received two different explanations. In the first, due to S. Bjornholm [1], the fully correlated fissioning ground state band has different dynamical properties from bands where pairs are broken. More pre-scission kinetic energy is gained in the first case, thus giving rise to the observed difference in fragments kinetic energies. Clerc et al. [27] have used a similar idea for analysing their data together with the assumption that the energy necessary to break the pair comes entirely from the pre-scission kinetic energy. Assuming that only one pair at most is broken one may, then, derive a relationship between the even-odd effects on the fragments' yields and on their kinetic energies. Let p the probabily for pair breaking and 1-p the probability for the system to remain in the ground state band. Then

$$P_{odd} = \frac{Y_{odd}}{Y_{even} + Y_{odd}} = \frac{p}{2}$$

$$P_{even} = \frac{Y_{even}}{Y_{even} + Y_{odd}} = 1 - \frac{p}{2}$$

$$E^{K}_{even} = \left[E^{K}_{odd} \frac{p}{2} + (1-p)(E^{K}_{odd} + \Delta)/(1 - \frac{p}{2}) \right]$$

$$= E^{K}_{odd} + \Delta (1-p)/(1 - \frac{p}{2})$$

Let

$$\delta = \frac{P_{even} - P_{odd}}{P_{even} + P_{odd}} = 1 - p$$

$$\Delta E^{K}_{e-o} = \Delta \frac{2\delta}{1+\delta}$$

For example, for an even-odd effect of 25% on the elemental yields one obtains

$$\delta = \frac{1.25 - 0.75}{2} = 0.25$$

and $\Delta E^{K}_{e-o} = 0.4 \Delta \# 1.08$ MeV in close agreement with the results of Clerc [27]. The agreement is much worse in the $Cf^{252}(s,f)$ case where one finds that the calculated value of less than 0.5 MeV for ΔE^{K}_{e-o} is, at least, a factor of two less than the experimental one.

It is worth noting that S. Bjornholn [1] and J.B. Clerc hypothesis [27] may lead to two different behaviors when the excitation energy of the fissioning nucleus above saddle increases. If the even-odd effect on the kinetic energies is related to different dynamical behavior of the ground state band and of 2-q particle states one expects a strong decrease of pre-scission kinetic energy as a function of excitation energy since states with 4-q particle or more should have an increased viscosity. We shall see that experiment does not show such a behavior. On the other hand, along Clerc's hypothesis, the probability of pair breaking during the descent from saddle to scission is directly connected to the viscosity of the fission process. As said above this viscosity leads to a decrease of pre-scission kinetic energy which is entirely converted into 2 q-p excitation. The increase of excitation energy of the fissioning system would not necessarily imply an increase of viscosity. Clerc's hypothesis, therefore, is not in contradiction with the results on kinetic energy we shall examine in the next section.

The failure of Clerc's approach to account for the even-odd effect on kinetic energies in the $Cf^{252}(s,f)$ case leads to an alternative hypothesis. It was suggested [26] that pairs may be broken at scission in a highly correlated way such that, in first approximation, only odd splits would be accompanied by pair breaking. In such case, part or all the energy necessary to break the pair would be provided by the potential energy of the dinuclear system prior to scission. Part of the potential energy is of Coulomb origin and appears as ultimate kinetic energy of the fragments. One would, then, expect the magnitude of the even-odd on kinetic energy to be independent of the pair breaking probability. The comparison between the $Cf^{252}(s,f)$ and the $U^{235}(n_{th},f)$ seems to favor this assumption. The hypothesis that, at least, a significant fraction of the pair breakings occur at scission has the additional advantage to leave room for the observed strong variation of the elemental-yields even-odd effect with fragments' charges. In effect, if the pairs are broken long before scission one would not expect any correlation between the probability of that breaking and the charge of the fragments. If, on the other hand, the pair breaking occurs at scission its probability should depend, to some extent, on such properties of the preformed fragments as their deformability, deformation, level density etc. From the $U^{235}(n,f)$ and $Cf^{252}(s,f)$ results its seems that the probability for pair breaking decreases close to magic nuclei with N = 50, 82 or Z = 50. This may be attributed to a level density effect.

Summarizing this section we conclude that the existence and variation of even-odd effects on fragments elemental yields and kinetic energies show that the probability for pair breaking during fission is small. It may even be that most of these breakings occur at scission. The superfluidity of nuclear matter is thus conserved during the fission process.

2. VARIATIONS OF FRAGMENTS' KINETIC ENERGY WITH INITIAL EXCITATION ENERGY

Since the work of R. Nix and W. Swiatecki [28] it has become usual to associate a fission degree of freedom to the pre-scission kinetic energy.

The total final kinetic energy of the fragments is then equal to the sum of the pre-scission kinetic energy and of the Coulombic repulsion between the two fragments, at scission. According to Nix and Swiatecki the fission degree of freedom is the only unstable degree of freedom in the saddle configuration. In the frame of the hydrodynamical model, and in the absence of viscosity, most of the potential energy gain between saddle and scission should appear as pre-scission kinetic energy. For instance, one expects low energy induced fission to yield a total kinetic energy larger than that of spontaneous fission by approximately the height of the fission barrier. On the other hand, the increase of excitation energy above the barrier is expected to increase the viscosity. According to the hydrodynamical model [29] the increase of viscosity leads to a decrease of the fragments' total kinetic energy due to :
a) the increase coupling of the fission mode to other modes,
b) more elongated scission shapes. As we have shown in the preceding section that, at low energy, the fissioning nucleus remains basically superfluid one expects the above predictions of the low viscosity hydrodynamical model to be at least, qualitatively valid. We now review some relevant experimental results.

2.1. Spontaneous versus induced fission

Very few new results have been obtained since the Rochester Conference concerning the comparison of fragments' kinetic or excitation energies in spontaneous and induced fission. At that time well documented results were presented for the cases of Pu^{240} [30], Cm^{246} [7], Cf^{250} [7]. The kinetic energies observed in induced fission were larger than in spontaneous fission by quantities ranging between 0.3 MeV (Cm^{246}) and 2.1 MeV (Cf^{250}). In all cases these excesses were smaller than the second fission barriers height. The increase, when it existed, was mass dependent. For instance, in the case of Cf^{250}, the increase in total kinetic energy for the induced over spontaneous fission was limited to the heavy fragment masses lighter than 140. Such an increase, as will be discussed below, may be related to the influence of shell effects in the fragments' deformabilities. The case of Cm^{246} is especially interesting since fine structures in the mass distribution are present both in spontaneous and induced fission. We have shown above that these structures were probably caused by even-odd effects on the charge yields and were evidence for a small probability for pair-breaking during the fission process. The fissioning Cm^{246} is therefore in the same ground state band at scission in the spontaneous and induced cases. It is interesting to note that, it is precisely for Cm^{246} that the difference in kinetic energy between the two cases is smallest (0.3 MeV). From these data it seems reasonable to conclude that less than one quarter to one fifth of the fission barrier height appears in extra kinetic energy of the fragments in the case of induced fission.

A strong coupling of the fission mode to other modes in the first part of the descent from saddle to scission is therefore suggested by the experimental results just recalled.

Isomeric fission has also been studied [31,32,33]. Both in Am^{242} and Pu^{240} it was found that isomeric fission is more energetic by about 2-3 MeV than low energy induced fission. The sign of the difference is contrary to what could be expected from the simple potential energy considerations. Here again the differences observed depend markedly upon the mass of the fragments pointing to possible shell effects.

Finally only one experimental result appears to be in clear contradiction with the assumption of a strong coupling between the fission degree of freedom and other modes. This result has been reported by

Lashkar et al. [34]. These authors found that at 4.63 MeV excitation in Pu^{240} the total kinetic energy of the fragments was about 5 MeV higher than in spontaneous and slow neutron induced fission for all mass splits. This result led [35] to the hypothesis of two possible dynamical modes of fission, one superfluid and the other normal. This distinction seems difficult to maintain in view of the analysis given in the preceding section about even-odd effects.

One must, therefore, admit that Lashkar et al. result remains unexplained. The confirmation of this result as well as the search of similar cases in other nuclei would be of great interest.

2.2. Variations of total kinetic energy with excitation energy above saddle point

In their study of the Pu^{239}(dpf) reaction Specht et al. [36] first found that

- The kinetic energy of the fission fragments decreased with increasing excitation energy.
- This decrease of the kinetic energy was only significant in a mass range between around 125 and 140.

Similar behavior was found in the proton induced fission of Uranium isotopes [37]. The decrease of the kinetic energy in a limited mass range was associated with a selective increase of the excitation energy of the heavy fragment [38]. For systems lighter than Uranium such as Th^{232}(n,f) [39] the variation of kinetic energy with excitation energy is reversed at least for neutron energies varying between 2 and 5 MeV. However, here again, the variations are localized in the mass range 125-140. Although the difference between the Thorium case and the other is not completely understood it seems clear that the above-mentioned behaviors of the fragments' kinetic and excitation energies reflect the washing out of shell effects with increasing excitation energy [40]. These effects seem to be small for masses of the heavy fragment larger than 140. Here the kinetic energies of the fragments is remarkably insensitive to the excitation energy of the fissioning nucleus.

It follows that, apart from shell effects, both the scission configurations and pre-scission kinetic energies are almost independent upon the excitation energy of the fissioning system. Since one would expect a fast increase of normal two-body viscosity with this increase of excitation these results appear to be in complete disagreement with the expectations of the viscous liquid-drop model [29].

At this point we may temporarily conclude that experiment suggest that the fission mode is weakly coupled to quasi-particle excitations but strongly coupled, to other, probably collective, modes and thus strongly damped.

The thermodynamical model of W.Nörenberg [40] alone incorporates such features. The one-body friction model of W.S. Swiatecki et al. [41] could also incorporate them if it were extended to the consideration of superfluidity. The question wether strong coupling may lead to statistical equilibrium between the collective modes as suggested by N. Noremberg remains to be examined. Before doing so we very briefly come back to the question of the magnitude of the pre-scission kinetic energy by reviewing some recent results and analysis on LRA fission.

3. LIGHT CHARGED PARTICLE ACCOMPANIED FISSION (LRA FISSION)

LRA fission was firs invoked [42] as a proof for large pre-scission kinetic energies, in agreement with the liquid-drop calculations. More specifically, the width of the angular distribution of the α particles and

the anti-correlation between the energy of these α and that of the fragments appeared as the main arguments favoring a large (around 40 MeV) pre-scission kinetic energy. Since the first experiments and analysis progresses have been made on both sides. Better angular resolution have shown that the angular widths had been largely overestimated. The latest of the FWHM of the angular distributions fall around 18° both for Cf^{252}(s,f) and U^{235}(n,f). The experimental results have gained in precision and completeness. Of special interest is the finding that the angular width is a decreasing function of the fragments kinetic energy [43].

This result has been interpreted as showing that the variations of fragments' kinetic energy reflects variations of the fragments' interdistance at scission rather than fluctuations of the pre-scission kinetic energy.

The analysis of LRA fission has become more refined by incorporating two basic features.

- The finite dimensions of the two fragments which allow α reabsorption [44].
- The distribution of the interfragment distance [45].

With these improvements C. Guet et al. [40] have analysed a large body of data on α and He^5 accompanied fission.They obtain excellent fits with a fragment kinetic energy of around 8-10 MeV in agreement with that derived by Rajajopalan et al. [47], Katase et al. [48].

This value is an upper value for the pre-scission kinetic energy since the α particle may be emitted some time after scission. Such result seems to be compatible with the strong coupling hypothesis. Furthermore, the very great similarity of the results for Cf^{252}(s,f) and U^{235}(n,f) also shows that the scission configurations are similar in both cases, at variance with the liquid-drop model which predicts higher pre-scission kinetic energy in the Californium case.

We may therefore conclude this section in agreeing with P. Fong et al. [45] who claim that LRA fission results do not exclude compact scission configurations and small pre-scission kinetic energies.

4. ENERGY, MASS AND CHARGE DISTRIBUTIONS

In the following section we shall briefly adress ourself to the question of when, in the fission process, are the energy, mass and charge distributions determined. We shall not try to be complete and refer to the work of Wilkins et al. [49] for very thorough discussion of experimental results and predictions of the thermodynamical model which, as stated above, appears to be one of the best existing approach to fission.

The different types of distributions we want to consider need not be determined at the same time during the process. It is clear that, for example, the characteristic time associated with the mass degree of freedom becomes very large just before scission, since the possibility of mass exchange between the two nascent fragments becomes very small. The system will therefore not have time to adjust to possible rapid change in the potential energy along the mass degree of freedom.

Such consideration do not apply to the deformation modes (stretching and distorsion assymetry) whose characteristic frequency is not directly connected to the nucleonic exchange between the fragments. Indeed,the liquid drop calculations of R. Nix [28] show that the phonon energy of the mass assymetry mode vanishes at scission while the stretching and distortion assymetry modes phonon energies converge to approximately 1 MeV. The charge equilibration mode is of special interest since its characteristic frequency spans the largest range of values during the fission process.

4.1. Isobaric distributions

The charge to mass equilibration degree of freedom for fixed mass asymmetry of the fission fragments was first considered by Updegraff and Onley [50]. This mode has the desirable feature that the relevant potential energy is dominated by the liquid-drop isospin-dependent term so that single-particle effects have only limited influence.

Close to scission the potential energy may be approximated by that of two spheroids in contact. Near the equilibrium charge the potential energy may be approximated by a harmonic function of Z where Z is, for example, the charge of the light fragment for fixed mass. Using Green and Engler [51] mass formula, Berlanger et al. [52] obtain a stiffness coefficient K_Z for the charge to mass equilibration mode

$$K_Z \text{ MeV/(charge unit)}^2 = 1.39\left(A_1^{-1/3} + A_2^{-1/3}\right) + 186.28\left(\frac{1}{A_1} + \frac{1}{A_2}\right) - \frac{2.88}{1.24\left(A_1^{1/3} + A_2^{1/3}\right)}$$

which for symetric fission of U^{235} yields

$$K_Z = 3.49 \text{ MeV/(charge Unit)}^2$$

In other words the potential energy may be written as

$$\frac{1}{2} K_Z (Z - Z_p)^2 = 1.75 (Z - Z_p)^2$$

wher Z_p is the most probable charge.

The width of the charge distribution must be equal to or larger than the minimum width allowed by the uncertainty principle or alternatively the energy in the charge equilibration mode must be higher than $1/2\,\hbar\omega$ where ω is the characteristic frequency of the mode.

One obtains the condition that

$$\sigma^2(Z:A) \geq \hbar\omega_Z / 2K_Z$$

or

$$\hbar\omega_Z \leq 7\,\sigma^2(Z:A)$$

According to Wahl [9] a good value for $\sigma(Z : A)$ is $\sigma(Z : A) = 0.54$ then $\hbar\omega_Z \leq 2.04$ MeV

The width of the charge distribution has been interpreted [48] in terms of a temperature

$$T = K_Z \times \sigma^2(Z : A) = 1.02 \text{ MeV}$$

This interpretation is only valid if $T >> \frac{\hbar\omega_Z}{2}$. It is doubtful that this condition is fulfilled.

The condition that $\hbar\omega_Z < 2.04$ MeV is not as straight forward to understand as it first seems. The characteristic frequency ω_Z is in fact a function of time during the fission process. If B_Z is the inertia corresponding to the charge equilibration mode then

$$\omega_Z = \sqrt{K_Z / B_Z}$$

While the value of K_Z does not depend very much upon the shape of the fissioning nucleus, that of B_Z does. In particular B_Z increases indefinitely near scission. From the work of Brosa and Krappe [53] one can extract a value for

$$B_Z = \frac{2n}{3} Z_0^3 m \frac{A^2}{ZN} \frac{1}{c}$$

where c is the radius of the neck joining the two nascent fragments A, Z,

N are the mass, charge and neutron number of the fissioning nucleus r_0 = 1.16 Fm and m the average nucleonic mass

For U^{235} one obtains

$$B_Z \# \frac{13}{c}$$ where c is expressed in Fermi and the time unit is 1.10^{-22} sec.

Therefore

$$\omega_Z \# \sqrt{c} \times 0.5$$

If we assume that, near scission, c goes linearly to zero then

$$\omega_z \# \sqrt{v_c (t_{sc}-t)} \times 0.5$$

The change of ω_Z in one period $2\pi/\omega_z$ is then

$$\frac{2\pi}{\omega_z} \left| \frac{d\omega_z}{dt} \right| = \frac{\pi}{(t_{sc}-t)}$$

This change should at most be equal to ω_Z itself for the width of the charge distribution to adjust to the motion so that

$$\frac{\pi}{t_{sc}-t} \lesssim \omega_z = 0.5 \sqrt{v_c (t_{sc}-t)}$$

which yields finally

$$c \geq 3.4 \left(\frac{dc}{dt}\right)^{2/3} \quad \text{with } v_c = \frac{dc}{dt}$$

For smaller values of c the charge distribution cannot adjust itself any more.

The limit on $\hbar\omega_Z$ obtained from the width of the charge distribution reads

$$\hbar\omega_Z = h\ 0.52 \sqrt{c} \leq 2.04 \text{ MeV}$$

or

$$c \leq 0.36 \text{ Fermi}$$

a very small value, even less than the nucleonic radius. It is, therefore, doubtful that the condition

$$T >> \frac{\hbar\omega_Z}{2}$$

is fulfilled since this condition would lead to even smaller values of c.

One also obtains

$$\frac{dc}{dt} \leq \left(\frac{c}{3.4}\right)^{3/2} \leq 0.034$$

meaning that the rate of change of the neck radius should be less than 0.3 Fermi/10^{-21} sec. This means that, even in its final phase, the fission process is slow. If one assumes that the necking starts at c # 4 Fermis one obtains a time for the fission process of order 10^{-20} sec. and even more. The above considerations are very approximate. The time dependent equations for the charge equilibration degree of freedom should be solved to improve this crude analysis. However the basic result that fission is a slow process is not expected to be affected by a more exact treatment. It is not surprising that, in course of such a slow process, the probability for pair breaking remains small.

4.2. Energy distributions

The characteristic frequencies of the two main deformation modes, stretching and distorsion asymmetry, are comparable to that of the charge equilibration mode close to scission. It is, therefore, plausible that the fragments' deformations may adjust to the potential energy variations almost down to scission. The sawtooth shape of the average excitation energy

of the fragments as well as the dip in the total kinetic energy near symetric masses were first related to the deformabilities of the nascent fragments in the two spheroïd model of Vandenbosh [54]. Dickmann and Dietrich [55] showed that the Strutinsky shell correction applied to the scission geometry provided a justification to Vandenbosh's approach. More systematically, Wilkins et al. [48] have obtained a very striking correlation between the calculated deformations of the fragments and their measured excitation energy. Mass and charge distributions [56,57] have been obtained at very high kinetic energies. These measurements show without ambiguity that the spherical shells with Z = 50 and N = 82 are responsible for the maximum in the kinetic energy curve. In this conference [58] it is shown that as soon as the Z = 50 shell is broken the kinetic energy decreases abrubtly. These new results confirm that the fragments' deformations are determined at the very late stage of the process.

4.3 Mass distributions

The stiffness coefficient of the mass degree of freedom is approximately 500 times smaller than that of the charge equilibration mode while its moment of inertia is only two times smaller. This last result is obtained simply by considering that, in the charge equilibration mode, for each proton going from fragment 1 to fragment 2 a neutron goes from fragment 2 to fragment 1. The mass associated with one charge unit change is therefore two nucleonic masses while that associated with a change of one mass is obviously one mass.

It follows that the characteristic frequency associated with the mass degree of freedom, for the same value c of the neck radius is approximately 15 times smaller than that of the charge equilibration mode. One can therefore write the condition

$$\frac{\pi}{t_{sc}-t} \leq \omega_M \approx 3.3 \cdot 10^{-2}\sqrt{c}$$

and

$$c \geq 20 \left(\frac{dc}{dt}\right)^{2/3}$$

if we take the maximum value of $\frac{dc}{dt} = 0.03$ found in section 4.1

We find a minimum value of $c = 2$ Fermis

This corresponds to a rather compact shape. Of course, if the velocity of the necking is decreased the mass distribution may be determined later in the fission process ; however it is plausible that the mass distribution is determined at rather early stage in the descent from saddle point. In fact the question wether mass distributions are determined at the saddle point or close to scission remains open. Both approaches [48, 49] have success in predicting qualitatively the features of mass distributions. Both explain, for instance, the behavior of the Radium and Actinium isotopes with their transition from assymetric to symetric fission through the intermediate stage of the triple humped mass distribution. It is possible that the mass distributions of the Polonium and Fermium isotopes favor the hypothesis of a late determination of the mass distributions. This is suggested by the calculations of Mosel et al. [60] in the first case and of Mustafa [61] in the second.

5. SUMMARY AND CONCLUSION

The existence of even-odd effects on the charge distributions of fission fragments as well as their variations led us to the conclusion that the fission mode(s) is(are) weakly coupled to the quasi-particle degrees of freedom. This agrees with the thermodynamical model [39] assumption.

Similarly the study of the variations of the total kinetic energy with the excitation energy of the fissioning nucleus leads to the conclusion that the fission degree of freedom is probably strongly damped. It should be noted, here, that this conclusion is based on the old parameterization of R. Nix [28] which defined a center of mass motion identified to the fission mode. Furthermore the kinetic energy associated with this mode was equalized to the pre-scission kinetic energy. It would be useful to reexamine these two assumptions. The justification of the strong coupling hypothesis made in the thermodynamical model may depend on this reexamination. Finally it is not clear if the statistical equilibrium between collective degrees of freedom is achieved. The zero-point oscillations and quantization of the collective modes should certainly be taken into account as have done Mahrun et al. [63] for the bending mode.

Many of the conclusions we have reached are based on too weak experimental grounds. Systematic experimental work on charge distribution and kinetic energy variations should be actively pursued.

REFERENCES

[1] BJORNHOLM, S., Phys. Scripta 10A (1974) 110.
[2] THOMAS, T.D. and VANDENBOSCH, R., Phys. Rev. 133 B (1964) 976.
[3] SCHMITT, H.W., NEILER, J.H and WALTER, F.J., Phys. Rev. 141 (1966) 1146.
[4] FRASER, J.S., MILTON, J.C.D., BOWMAN, H., THOMPSON, S.G., Can. Journ. Phys. 41 (1963) 2080.
[5] WAHL, A.C., NORRIS, A.E., ROUSE, R.A., WILLIAMS, J.C., Proc. Second Symposium on Physics and Chemistry of Fission, Vienna 1969 (813).
[6] AMIEL, S. and FELDSTEIN, H., Proc. 3rd Symposium on Physics and Chemistry of Fission, Rochester (1973), Vol.II, p.65
[7] UNIK, J.P., GINDLER, J.E., GLENDENIN, L.E., FLYNN, K.F., GORSKI, A., and SJOBLOM, R.D., Proc. 3rd Symposium on Physics and Chemistry of Fission, Rochester (1973) Vol.2, p.19.
[8] AMIEL, S. and FELDSTEIN, H., Phys. Rev. CII (1975) 845.
[9] WAHL, A.C., Contribution to paper n° 11 Proceedings 2nd advisory group meeting on Fission Product Nuclear Data, IAEA Petten (1977).
[10] CLERC, H.G., SCHMIDT, K.H., WOHLFARTH, H., LANG, W., SCHRADER, H., PFERDEKAMPER, K.E., JUNGMANN, R., ASHGAR, M., BOCQUET, J.P., SIEGERT, G., Nucl. Inst. Meth. 124, 607 (1975).
[11] SIEGERT, G., WOLLNIK, H., GREIF, J., FIEDLER, G., ASHGAR, M., BAILLEUL, G., BOCQUET, J.P., GAUTHERON, J.P., SCHRADER, H., EWALD, H., ARMBRUSTER, P., Phys. Lett. B53, 45 (1974).
[12] QUADE, J., and SIEGERT, G., ILL Internal Report 1979.
[13] BOCQUET, J.P., BRISSOT, R., MARIOLOPOULOS, G., NIFENECKER, H., RISTORI, Ch., Unpublished.
[14] STRITTMATTER, R.B. and WEHRING, B.W., Internal Report, University of Illinois.
[15] SIEGERT, G., ILL, Internal Report 1979.
[16] SIEGERT, G., GREIF, J., WOLLNIK, H., FIEDLER, G., DECKER, R., ASHGAR, M., BAILLEUL, G., BOCQUET, J.P., GAUTHERON, J.P., SCHRADER, H., ARMBRUSTER, P., EWALD, H., Phys. Rev. Lett. 34, 1036 (1975).
[17] CLERC, H.G., LANG, W., WOHLFARTH, H., SCHIDT, K.H., SCHRADER, H., PFERDE KAMPER, K.E., JUNGMANN, R., Z. Physik A 274 (1975) 203.
[18] MARIOLOPOULOS, G., BOCQUET, J.P., BRISSOT, R., RISTORI, Ch., NIFENECKER, H., GIRARD, J., PECQUET, A., This Conference, paper SM 241/F30.
[19] See Ref. 17.
[20] AMIEL, S., FELDSTEIN, H., Phys. Rev . C11 (1975) 845.

[21] BLACHOT, J., CRANÇON, J., HAMELIN, Ch., MOUSSA, A., This Conference paper SM/241 F29.
[22] FONG, P., Phys. Rev. 102 (1956) 434.
[23] SCHÜTTE, G., and WILETS L., Proceedings 3rd Symposium on Physics and Chemistry of Fission, Rochester 1973 (Vol. I, p. 503).
[24] SCHUTTE, G., Z. Physik A283 (1977) 183.
[25] STRUTINSKY, V.M., Z. Physik A280 (1977) 99.
[26] NIFENECKER, H., SIGNARBIEUX, C., BABINET, R. and POITOU, J., Proceedings 3-rd Symposium on Physics and Chemistry of Fission, Rochester 1973 (Vol.II, p.117)
[27] CLERC, H.G., LANG, W., WOHLFARTH, H., SCHRADER, H. and SCHMIDT, K.H. This Conference paper SM 241/F2.
[28] NIX, J.R. and SWIATECKI, W.J. , Nucl. Phys. 71 (1965)1.
[29] DAVIES, K.T.R., SIERK, A.J. and NIX, J.R., Phys. Rev. C13 (1976) 2385.
[30] DERUYTTER, A.J. and WEGEWER-PENNING, G., Proc. 3rd Symp. on Phys. and Chem. of Fission, Rochester 1973 (Vol.II, p.51).
[31] FERGUSON, R.L., PLASIL, F., ALAM, G.D. and SCHMITT, H.W., Nucl. Phys. A172 (1971) 33.
[32] WEBER, J., SPECHT, H.J., KONECNY, E. and HEUNEMANN, D., Nucl. Phys. A221 (1974) 414.
[33] WEBER, J., ERDAL, B.R. and WILHELMY, J.B., Phys. Rev. 13C (1976) 189.
[34] LASHKAR, J.C., SIGAUD, J., PATIN, Y., CHARDINE, J. and HUMEAU, C. Rapport CEA-R-4715 (1975).
[35] NIFENECKER, H., LASHKAR, J.C., SIGAUD, J., PATIN, Y., Journées d'Etudes sur la Fission, Aussois (May 1976).
[36] MILTON, J.C.D., FRASER, J.S. and SPECHT H.J., Conf. Aix-en-Provence Compte rendu, Vol.II (1972) 17.
[37] FERGUSON, R.L., PLASIL, F., PLEASONTON, F., BURNETT, S.C., SCHMITT, H.W., Phys. Rev.C7 (1973) 2510.
[38] BURNETT, S.C., FERGUSON, R.L., PLASIL, F. and SCHMITT, H.W., Phys Rev. C3 (1971) 2034.
[39] GONNEN WEIN, F., Private communication.
[40] NÖRENBERG, W., Proc. 2nd Symp on Phys. and Chem. of Fission, Vienna (1969) p.51.
[41] BLOCKI, J., BONEH, Y., NIX, J.R., RANDRUP, J., ROBEL, M., SIERK, A.J and SWIATECKI, W.J., Annal of Physics (1979).
[42] FRAENKEL, Z., Phys. Rev 156 (1967) 1283.
[43] GUET, C., SIGNARBIEUX, C., PERRIN, P., NIFENECKER, H., ASHGAR, M., CAITUCOLI, F. and LEROUX, B., Nucl. Phys. A324 (1979) 1.
[44] DAKOWSKI, M., PIASECKI, E. and NOWICKI, L., Nucl.Phys.A315(1979)370.
[45] FONG, P., Phys. Rev. C2 (1970) 735.
[46] GUET, C., NIFENECKER, H., SIGNARBIEUX, C. and ASHGAR, M., This Conference paper SM.241 F13.
[47] RAJAGOPALAN, M., and THOMAS, T.D., Phys. Rev. C5 (1972) 2064.
[48] TSUJI, K., KATASE, A., YOSHIDA, Y., KATAYAMA, T., TOYOFUKU, F., and YAMAMOTO, Y., Proc. 3 rd Symp. Phys. Chem. Fission Rochester 1973, Vol. II p. 405.
[49] WILKING, B.D., STEINBERG, E.P., and CHASMAN, R.R., Phys. Rev. C14 (1976) 1832.
[50] UPDEGRAFF, W.E., and ONLEY, D.S., Nucl. Phys. A161 (1971) 191.
[51] GREEN, A.E.S. and EWGLER, N.A., Phys. Rev . 91 (1953) 40.
[52] BERLANGER, M., GOBBI, A., HANAPPE, F., LYNEN, U., NGO, C., OLMI, A., SANN, H., STELZER, H., RICHEL, H. and RIVET, M.F., To be published.
[53] BROSA, U. and KRAPPE, H.J., To be published in Z. Phys.
[54] VANDENBOSCH, R., Nucl. Phys. 46 (1963) 129 .
[55] DICKMANN, F., DIETRICH, K., Nucl. Phys. A129 (1969) 24.
[56] WOHLFARTH, H., LANG, W., CLERC, H.G., SCHRADER, H., SCHMIDT, K.H. and DANN, H., Phys. Lett. 63B (1976) 275.

[57] GUET, C., ASHGAR, M., PERRIN, P. and SIGNARBIEUX, C., Nucl. Inst. and Meth. 150 (1978) 189.
[58] BOCQUET, J.P., BRISSOT, R., RISTORI, Ch., CRANÇON, J., NIFENECKER, H., MONTOYA, M., DAKOWSKI, M., GUET, C., PERRIN, P., This Conference, paper SM.241-F4.
[59] BRITT, H.C., This Conference, paper SM/241-A1
[60] MUSTAFA, M.G., MOSEL, U. and SCHMITT, H.W., Phys. Rev. C7 (2973) 1519.
[61] MUSTAFA, M.G., FERGUSON, R.L., Phys. Rev. C18(1978) 301.
[62] MAHRUN, J.A. and GREINER, W., Z. Physik 251 (1972) 431.
[63] DIETRICH, K., ZIELINSKA-PFABE, M., 6 th Hirshegg Meeting on gross Properties of Nuclear Excitations (1978) p. 98.
[64] BRISSOT, R., CRANÇON, J., RISTORI, Ch., BOCQUET, J.P., and MOUSSA, A., Nucl. Phys. A282 (1977) 109.

DISCUSSION

H.O. DENSCHLAG: I should like to make some comments with regard to your finding that the exchange of the nuclear charge between the fragments formed occurs even when mass exchange has stopped. Fischbach, Weis and myself have studied this problem using the independent yield distribution for ^{235}U (n_{th}, f) and have reached the same conclusion.

To demonstrate the point, we have plotted the parameter $\Delta A'_p$ ($= A'_p - A_{UCD}$) against the nuclear charge (Z) for heavy (s) or light (ℓ) fragments, as can be seen in the lower part of Fig. A. The way we obtained $\Delta A'_p$ from A'_p, the most probable (fragment) mass of each element, and from A_{UCD}, the mass calculated on the assumption of unchanged charge density, is shown at the top of Fig. A.

When $\Delta A'_p$ is obtained as the maximum of a plot of the (experimental) absolute independent yields, the points shown on the left-hand side of the figure at the bottom are the result. The marked variation in the $\Delta A'_p$ values with Z is difficult to understand.

However, when $\Delta A'_p$ is obtained by plotting fractional independent yields, the points shown at the bottom of Fig. A on the right are the result. Here the fractional yields are calculated by dividing each independent element yield by the corresponding mass yield.

Figure B is intended to show that the $\Delta A'_p$ values based on absolute independent yields are biased by the decreasing chain yields of both sides of the mass yield curves. For this purpose, we show a contour diagram of the absolute independent fission yields within a display of the nuclear charge (Z) against the neutron number (N), in a manner similar to a nuclide chart. In addition, Z_{UCD}, the nuclear charge calculated on the assumption of 'unchanged charge density' and Z_p ($= Z_{UCD} - 0.5$) are shown for the heavy mass peak.

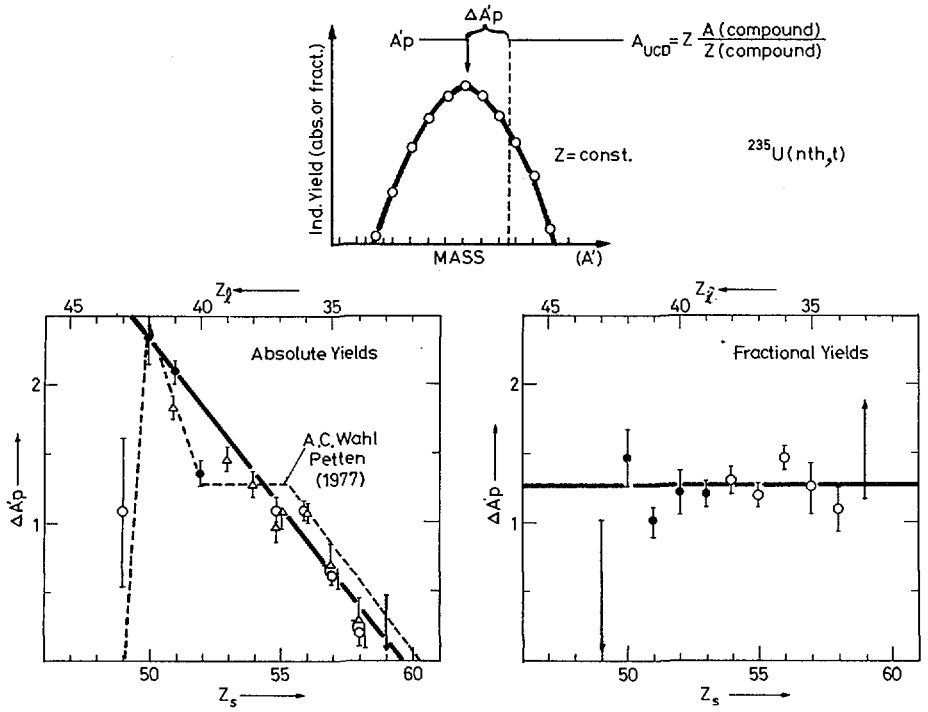

FIG.A. Experimental $\Delta A'_p$ values as obtained from absolute (left) and fractional (right) independent yields by fitting a Gaussian curve to the corresponding yield values and by subtracting A_{UCD}, as shown at the top of the figure.

Two cuts through the contour diagram are shown:

(1) A cut along a constant mass axis ('A = const' in Fig. B) enables us to read off Z_p;

(2) A cut along an axis of constant nuclear charge ('Z = const' in Fig. B) enables us to obtain A'_p.

It is clear from the figure that the cut 'Z = const', as opposed to the cut 'A = const', becomes asymmetric on the wings of the mass yield curve, and that its maximum shifts towards Z_{UCD} (the heavy side), or away from Z_{UCD} (the valley side of the mass yield curve). This bias would evidently disappear if we applied the cut to a contour diagram of fractional yields. The fact that the use of fractional yields (decoupling mass and charge distribution) gives a better description than the use of absolute yields indicates, in our opinion, that mass and charge distribution in the scission process must also be decoupled under natural conditions.

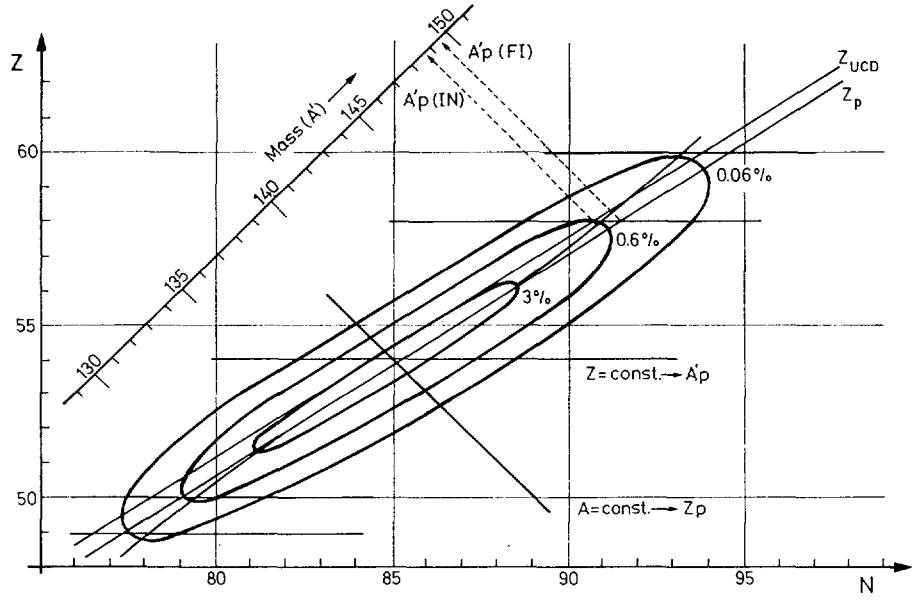

FIG. B. Schematic representation of absolute independent fission yields in a contour diagram and cuts through the diagram along the lines of constant nuclear charge (Z = const) so as to illustrate the bias of A'_p values on the basis of absolute yields ($A'_p(IN)$) with respect to the values based on fractional yields ($A'_p(FI)$).

Consequently, we interpret this result as an indication that the final charge distribution is decided at another – and presumably later – time than the mass distribution.

This finding is in full agreement with your conclusions and also with the result that the charge exchange takes place 'faster', i.e. over longer distances, than mass exchange in heavy-ion collisions.

P. FONG: With regard to the statistical-theory prediction of the even-odd effect, there are, in my opinion, two issues involved. First, we must ask ourselves whether the statistical principle is correct. And second, we must ask whether the method of calculation is correct. That the previous statistical theory failed to predict the even-odd effect is not a feature of the statistical theory itself, but rather of the particular level density formula used for the calculation. That formula was designed to eliminate the even-odd effect completely. It seemed appropriate at that time to use a formula of this kind following the Bethe and Fermi discussions. A more sophisticated formula would enable the even-odd effect to survive a few MeV of excitation, after which, for higher excitation, it would be washed out.

This formula, applied to the statistical theory would predict the observed even-odd effect and its absence at higher excitation. One conclusion that follows from this is that the existence of the even-odd effect in fission distribution does not preclude the possibility of energy dissipation, since the statistical theory, based on energy dissipation, *can* predict an even-odd effect.

H.A. NIFENECKER: I am interested to hear your view, but to me, personally, the main difficulty presented by the even-odd effects within the framework of the statistical theory is their rapid variation with excitation energy. If we estimate that the total intrinsic excitation energy of the fragments at scission is of the order of 10 MeV for thermal-neutron-induced fission, then for 3-MeV-neutron-induced scission it would be around 13 MeV. I doubt whether this 30% increase in excitation energy (15% increase in temperature) would suffice to explain the washing out of the even-odd effect with any realistic level density.

G. SCHÜTTE: You have shown us that the passage from saddle to scission is slow, with the result that excitation energy is high, while the viscosity is low since statistical equilibrium is not attained. The question is, therefore, how is the excitation energy introduced into the system without inducing statistical equilibrium?

You have linked the gap parameter Δ with the kinetic energy difference between even and odd fragmentation. But the only place where the gap parameter comes into play is in the energy difference between the ground state and the lowest excited state at each deformation, which is always a pair excitation and not a broken pair state. Since the fissioning nucleus is excited during the fission process, I do not see any relationship between Δ and the odd-even effect in the excitation energy from a theoretical standpoint.

H.A. NIFENECKER: Regarding your first point, I would agree that we have to try to understand why a selective excitation of collective states at the expense of 2-qp states occurs in fission. The even-odd effect by itself does not exclude the occurrence of pair excitation in time-even states.

In order to understand the link between the even-odd effect and the kinetic energy it is easier to think of the excitation energies. After scission the same state in terms of the number of qp excitations will give rise to even splits that are more excited than odd splits by the additional condensation energy of one pair, namely 2Δ.

J.R.T. GALIN: It strikes me that there is something of a contradiction between fission and heavy-ion-induced reactions as far as the degrees of freedom of mass and charge are concerned. If I have understood you correctly, in the case of fission the mass asymmetry degree is equilibrated more rapidly than the charge asymmetry degree of freedom, whereas the opposite is observed in the deep inelastic collision of heavy ions.

H.A. NIFENECKER: No, I do not think there is any contradiction here. In fission one starts with an equilibrium situation at saddle point. The potential

energy then changes during the descent from saddle to scission. The faster modes are the ones which follow the potential for a longer time. The charge-to-mass degree of freedom is faster than the mass degree of freedom, which is why the isobaric distribution may be determined later than the mass distribution.

P. DAVID: First let me say that I agree with your statement that fission is a weakly dissipative process. As regards the pairing gap, in the paper I presented (see SM-241/C6 of these Proceedings) I showed a consistent set of total kinetic energy $\overline{\text{TKE}}$ data which indicate that the behaviour of $\overline{\text{TKE}}$ when plotted against E_x is different when excitation energy in the interval of $\sim$ 1.5 MeV above the highest barrier (B_f, B_f + 1.5) is compared with the one in the interval (B_f + 1.5, B_{nf}). We do not know the exact location of the E_x points where the pairing gap at the saddle is to be found, but the slopes $\partial \text{TKE}\,(A_H, E_x)/\partial E_x$ indicate such behaviour quite clearly. It is best expressed in the case of the light nucleus ^{232}Th and is less pronounced for heavier nuclei. Since deformation also plays a role, the separation of the effects seems hardly possible in practice.

H.A. NIFENECKER: What you observe may be due to change in the deformation potential surface caused by 2-qp excitations. An interpretation in terms of change in pre-scission kinetic energy through change in the dynamic behaviour of the fissioning nucleus creates two difficulties:

First, how is it that the spontaneous-fission kinetic energies are not significantly lower than induced-fission energies, just above the barrier, and second, what is special about 2-qp excitations at the saddle, compared with more 4-qp excitations? One would expect the decrease in TKE to continue above the 2-qp threshold. So I have no explanation to offer for the effect observed.

DETAILED STUDY OF THE NUCLIDE YIELDS IN $^{235}U(n_{th}, f)$ AND THEIR RELATION TO THE DYNAMICS OF THE FISSION PROCESS*

H.-G. CLERC, W. LANG, H. WOHLFARTH
Institut für Kernphysik,
Technische Hochschule Darmstadt,
Federal Republic of Germany

H. SCHRADER
Institut Max von Laue-Paul Langevin, Grenoble,
France

K.-H. SCHMIDT
Gesellschaft für Schwerionenforschung (GSI),
Darmstadt,
Federal Republic of Germany

Abstract

DETAILED STUDY OF THE NUCLIDE YIELDS IN $^{235}U(n_{th}, f)$ AND THEIR RELATION TO THE DYNAMICS OF THE FISSION PROCESS.

The fission product mass spectrometer 'Lohengrin' of the Institut Laue-Langevin in Grenoble was used to determine yields of light fission products as a function of A, Z, the kinetic energy E and the ionic charge state q. The nuclide yields summed over all ionic charge states are given for five kinetic energies between 88.5 and 108.0 MeV. – From the measured isobaric nuclear charge distribution the pre-neutron emission variance σ_z^2 of the isobaric Z-distributions was determined to be independent of the total excitation energy. This may be an indication for quantum-mechanical zero-point motion. The kinetic-energy distributions for odd-Z elements are shifted towards lower kinetic energies by 0.4 MeV with respect to even-Z elements. The weak dependence of the proton odd-even effect on the kinetic energy of the fragments leads to the conclusion that the energy dissipation between saddle and scission is almost independent of the asymptotic kinetic energy. Furthermore, it can be estimated that in about 25% of all fission events all protons remain in a paired state.

* Supported by GSI.

1. INTRODUCTION

The distribution of the nucleons between the two fragments and the kinetic energy of the fragments are observable quantities which permit conclusions about the fission process in its late stage beyond the saddle point. Particularly in the case of low energy fission quantummechanical phenomena such as shell effects or the superfluidity of nuclei or zero-point oscillations, are expected to have a strong influence on the fission process.

In the present investigation of the thermal-neutron-induced fission of ^{235}U a report on yield measurements in the light fission product group is given. In particular with regard to the dependence of the yields on the fission product kinetic energy, these measurements are more comprehensive than the data available for any other fissioning nucleus let alone those for deep inelastic heavy ion reactions. Part of the results were published previously [1,2,3]. In the present paper the discussion of the data is extended to some aspects not considered in our previous publications.

The widths of the isobaric element distributions in deep inelastic reactions have recently aroused considerable interest [4]. In the case of low energy fission this problem may be investigated at very low temperatures.

Another point of interest has been the question of single particle excitations of the system between saddle and scission and their dependency on the kinetic energy of the fragments. In the fission of nuclei with almost zero excitation energy at the saddle point this problem is experimentally accessible.

2. EXPERIMENTAL PROCEDURE

The measurements were performed at the mass spectrometer "Lohengrin" [5] of the Institut Laue-Langevin in Grenoble. The absolut mass yields were measured in the mass range $80 \leq A \leq 110$ [3,6]. The relative nuclear charge distributions for a given mass number A were determined by measuring the fission product energy loss in a carbon absorber by a time-of-flight technique [7,8]. The isobaric nuclear charge distributions were measured at five different kinetic energies between 88.5 and 108.0 MeV .

It should be noted that Lohengrin separates the fission products according to their A/q- and E/q-values, with A being the mass number, q the ionic charge state and E the kinetic energy of the fission products. The ionic charge distributions of several nuclides are strongly influenced by the internal conversion of excited nuclear state [9]. Therefore the dependence of the yields on q was determined, and the A- and Z-yields summed over q could be obtained. Finally the A- and Z-yields were combined to give the nuclide yields for the light group of the fission products as a function of the kinetic energy as listed in table I. Because of the short analyzing time ($\approx$ 2 μs) of Lohengrin the yields in table 1 are those before the emission of delayed neutrons and before β-decay.

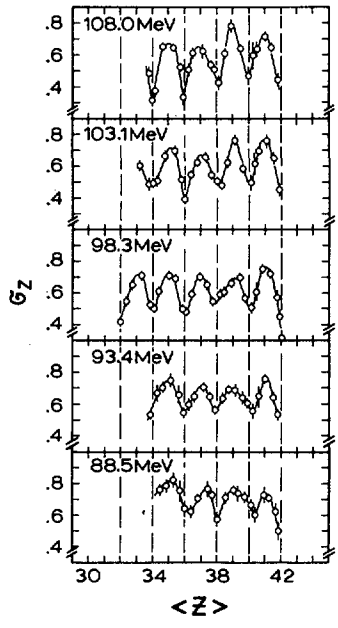

FIG.1. rms-widths σ_z of the post-neutron emission Z-distributions at fixed post-neutron mass number as a function of the average nuclear charge number <Z> at different kinetic energies of the light fission products.

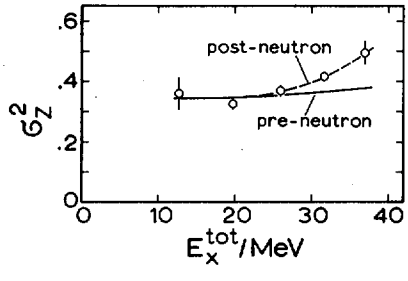

FIG.2. Variance σ_z^2 of the isobaric element distribution as a function of the total excitation energy E_x^{tot} of the two fragments.
Open points connected by dashed line: Measured post-neutron emission values at constant post-neutron mass number A, averaged over the mass range $94 \leqslant A \leqslant 97$, and corrected for the proton odd-even effect.
Solid line: Corresponding variance of the pre-neutron emission Z-distribution at constant pre-neutron emission mass number A', averaged over the mass range $95 \leqslant A \leqslant 98$.

TABLE I. INDEPENDENT YIELDS FOR THE THERMAL NEUTRON INDUCED FISSION OF ^{235}U AS A FUNCTION OF THE KINETIC ENERGY OF THE FISSION PRODUCTS[a]

A	Z	E = 88.5 MeV	93.4 MeV	98.3 MeV	103.1 MeV	108.0 MeV	$\sum$ E [b]
80 [c]	31			.010 ± .003			.010 ± .004
	32			.099 ± .015			.090 ± .013
	33			.011 ± .003			.015 ± .004
81 [c]	31			.004 ± .002			.005 ± .003
	32			.133 ± .023			.121 ± .014
	33			.069 ± .013			.069 ± .008
	34			.004 ± .003			.008 ± .002
82 [c]	31						.002 ± .001
	32			.146 ± .011			.127 ± .013
	33			.181 ± .012			.161 ± .011
	34			.039 ± .009			.043 ± .008
83 [c]	32			.062 ± .012	.064 ± .014		.053 ± .007
	33			.363 ± .024	.353 ± .037		.314 ± .024
	34			.225 ± .021	.166 ± .024		.241 ± .023
	35			.033 ± .015			.025 ± .010
84 [c]	32		.003 ± .003	.005 ± .005	.005 ± .005	.003 ± .003	.005 ± .003
	33		.202 ± .045	.223 ± .025	.218 ± .035	.094 ± .016	.205 ± .017
	34		.784 ± .083	.755 ± .035	.657 ± .056	.358 ± .048	.703 ± .029
	35		.110 ± .028	.067 ± .026	.019 ± .019	.021 ± .016	.065 ± .013
85	33	.097 ± .027	.106 ± .037	.119 ± .022	.140 ± .026	.054 ± .015	.116 ± .014
	34	.797 ± .064	1.036 ± .093	1.125 ± .044	.930 ± .072	.725 ± .082	1.003 ± .035
	35	.441 ± .063	.474 ± .060	.286 ± .034	.160 ± .037	.027 ± .017	.281 ± .022
	36	.155 ± .042	.094 ± .042				.029 ± .010
86	33	.020 ± .020	.017 ± .017	.028 ± .023	.016 ± .016	.005 ± .005	.020 ± .010
	34	.70 ± .10	.989 ± .094	1.336 ± .091	1.25 ± .11	.98 ± .11	1.175 ± .052
	35	.80 ± .12	.838 ± .089	.656 ± .090	.461 ± .081	.185 ± .066	.613 ± .046
	36	.48 ± .12	.256 ± .055	.111 ± .030	.032 ± .018		.131 ± .018
87	34	.454 ± .062	.576 ± .099	.627 ± .062	.664 ± .066	.509 ± .059	.609 ± .038
	35	1.085 ± .097	1.51 ± .14	1.507 ± .077	1.017 ± .085	.524 ± .061	1.273 ± .050
	36	.943 ± .098	.83 ± .12	.580 ± .064	.278 ± .065	.116 ± .026	.533 ± .041
	37	.158 ± .098	.081 ± .045	.047 ± .030			.043 ± .016

88	34	.22 ± .12	.21 ± .12	.323 ± .073	.279 ± .048	.176 ± .028	.269 ± .041
	35	1.17 ± .12	1.29 ± .14	1.57 ± .11	1.248 ± .092	.857 ± .083	1.341 ± .058
	36	1.84 ± .14	2.39 ± .18	1.84 ± .12	1.307 ± .098	.657 ± .068	1.724 ± .067
	37	.44 ± .11	.21 ± .10	.116 ± .081	.076 ± .050		.133 ± .040
89	34	.029 ± .029	.033 ± .033	.027 ± .027	.016 ± .016	.012 ± .012	.024 ± .013
	35	.71 ± .13	.89 ± .11	.98 ± .12	1.03 ± .10	.902 ± .092	.955 ± .059
	36	3.14 ± .20	3.97 ± .23	3.99 ± .16	2.88 ± .16	2.06 ± .16	3.481 ± .094
	37	.78 ± .16	.55 ± .11	.34 ± .12	.168 ± .058	.108 ± .065	.342 ± .054
	38	.090 ± .090	.022 ± .022				.009 ± .007
90	35	.082 ± .082	.35 ± .11	.42 ± .14	.41 ± .11	.29 ± .14	.375 ± .066
	36	3.01 ± .20	4.12 ± .25	4.76 ± .21	4.83 ± .23	3.88 ± .26	4.49 ± .12
	37	1.73 ± .18	1.68 ± .16	1.13 ± .16	.46 ± .11	.19 ± .11	1.021 ± .076
	38	.29 ± .12	.164 ± .082				.051 ± .020
91	35	.017 ± .017	.037 ± .037	.046 ± .046	.076 ± .033	.099 ± .036	.055 ± .021
	36	1.86 ± .15	2.85 ± .21	3.55 ± .19	3.49 ± .19	3.42 ± .22	3.28 ± .10
	37	2.68 ± .17	2.83 ± .21	2.66 ± .19	1.77 ± .14	.89 ± .15	2.312 ± .095
	38	.98 ± .11	.52 ± .10	.274 ± .098	.115 ± .055	.099 ± .063	.305 ± .046
92	36	.61 ± .23	1.01 ± .11	1.53 ± .14	2.06 ± .14	2.25 ± .18	1.573 ± .072
	37	2.75 ± .22	3.48 ± .19	3.36 ± .15	2.97 ± .16	1.70 ± .16	3.123 ± .086
	38	2.39 ± .21	2.03 ± .15	1.17 ± .11	.503 ± .059	.265 ± .081	1.165 ± .057
	39	.43 ± .15	.126 ± .087	.080 ± .055			.078 ± .029
93	36	.37 ± .10	.340 ± .098	.42 ± .10	.602 ± .068	.399 ± .063	.450 ± .047
	37	2.11 ± .17	2.67 ± .20	3.17 ± .18	3.40 ± .19	2.12 ± .16	2.994 ± .099
	38	3.73 ± .21	3.68 ± .24	2.89 ± .18	1.66 ± .14	.72 ± .12	2.595 ± .096
	39	.72 ± .19	.25 ± .10	.193 ± .093	.127 ± .070	.063 ± .060	.203 ± .046
94	36	.054 ± .054	.065 ± .036	.091 ± .035	.106 ± .040	.066 ± .030	.086 ± .019
	37	.849 ± .090	1.31 ± .13	1.79 ± .19	2.11 ± .21	1.19 ± .14	1.684 ± .091
	38	4.94 ± .20	5.11 ± .27	4.84 ± .22	4.26 ± .26	2.36 ± .18	4.56 ± .13
	39	.86 ± .14	.77 ± .12	.31 ± .12	.14 ± .11	.048 ± .048	.373 ± .061
	40	.082 ± .082					.004 ± .004

TABLE I (cont.)

A	Z	E = 88.5 MeV	93.4 MeV	98.3 MeV	103.1 MeV	108.0 MeV	$\sum E$ [b]
95	37	.25 ± .15	.327 ± .071	.524 ± .088	.717 ± .089	.807 ± .087	.543 ± .045
	38	3.15 ± .27	4.01 ± .25	4.46 ± .18	4.92 ± .23	3.77 ± .22	4.38 ± .11
	39	2.63 ± .26	2.35 ± .20	1.61 ± .14	.94 ± .13	.537 ± .081	1.555 ± .079
	40	.60 ± .14	.278 ± .091	.128 ± .061			.138 ± .031
96	37	.013 ± .013	.025 ± .025	.087 ± .044	.109 ± .077	.12 ± .11	.078 ± .029
	38	1.48 ± .22	2.29 ± .19	3.24 ± .19	4.81 ± .23	5.25 ± .28	3.54 ± .11
	39	3.33 ± .26	3.19 ± .21	2.64 ± .18	1.44 ± .13	.78 ± .10	2.315 ± .091
	40	1.66 ± .21	.800 ± .089	.275 ± .087	.058 ± .058	.087 ± .056	.385 ± .042
	41	.160 ± .087	.045 ± .045				.018 ± .011
97	38	.77 ± .16	.84 ± .16	1.47 ± .19	2.28 ± .22	2.68 ± .21	1.62 ± .10
	39	3.09 ± .23	3.38 ± .23	3.24 ± .20	2.87 ± .22	1.91 ± .17	3.06 ± .11
	40	2.30 ± .21	1.81 ± .17	1.11 ± .15	.47 ± .14	.298 ± .089	1.082 ± .079
	41	.28 ± .19	.12 ± .12				.041 ± .029
98	38	.277 ± .087	.276 ± .085	.55 ± .12	1.15 ± .22	1.83 ± .32	.742 ± .083
	39	1.74 ± .18	1.73 ± .17	2.10 ± .17	2.54 ± .26	2.41 ± .28	2.15 ± .11
	40	3.74 ± .24	3.40 ± .24	2.92 ± .18	1.98 ± .21	1.21 ± .17	2.67 ± .11
	41	.84 ± .22	.23 ± .16	.119 ± .080	.116 ± .070	.100 ± .072	.177 ± .052
99	38	.037 ± .037	.027 ± .027	.059 ± .030	.154 ± .059	.335 ± .093	.098 ± .022
	39	.82 ± .10	1.03 ± .11	1.54 ± .14	2.77 ± .24	3.43 ± .29	1.884 ± .093
	40	3.78 ± .20	3.66 ± .21	3.96 ± .18	4.18 ± .28	3.60 ± .31	3.92 ± .12
	41	1.51 ± .16	.704 ± .088	.374 ± .089	.227 ± .096	.26 ± .11	.453 ± .048
	42	.094 ± .094	.044 ± .044				.015 ± .011
100	38				.021 ± .021	.045 ± .045	.009 ± .007
	39	.131 ± .079	.165 ± .072	.243 ± .085	.43 ± .11	.73 ± .14	.310 ± .048
	40	3.13 ± .36	3.55 ± .36	4.16 ± .37	5.38 ± .44	7.32 ± .57	4.56 ± .21
	41	1.78 ± .38	1.31 ± .33	1.20 ± .38	1.04 ± .41	.77 ± .53	1.18 ± .20
	42	.19 ± .12	.118 ± .082	.045 ± .045	.055 ± .055	.063 ± .063	.073 ± .030
101	39	.046 ± .046	.048 ± .037	.093 ± .044	.188 ± .052	.403 ± .082	.131 ± .024
	40	1.14 ± .18	1.59 ± .17	2.24 ± .15	3.30 ± .24	6.27 ± .40	2.64 ± .10
	41	2.26 ± .33	1.76 ± .18	1.93 ± .14	2.00 ± .20	1.94 ± .22	1.928 ± .091
	42	1.11 ± .47	.28 ± .20	.15 ± .15	.21 ± .21	.34 ± .33	.257 ± .099

102	40	.598 ± .092	.84 ± .11	1.255 ± .092	2.57 ± .17	6.15 ± .36	1.870 ± .071
	41	1.68 ± .13	1.37 ± .13	1.444 ± .086	2.08 ± .16	4.35 ± .31	1.836 ± .068
	42	1.47 ± .12	.95 ± .11	.717 ± .070	.583 ± .092	.55 ± .19	.755 ± .047
	43	.011 ± .011	.010 ± .010	.014 ± .014	.021 ± .021	.10 ± .10	.021 ± .011
103	40	.127 ± .056	.120 ± .038	.297 ± .044	.625 ± .093	1.45 ± .22	.428 ± .036
	41	.747 ± .081	.858 ± .085	1.124 ± .075	1.57 ± .13	3.32 ± .27	1.336 ± .055
	42	1.59 ± .10	1.31 ± .11	1.068 ± .075	.98 ± .11	1.59 ± .22	1.161 ± .052
	43	.076 ± .043	.066 ± .040	.072 ± .044	.095 ± .062	.064 ± .064	.077 ± .026
104	40	.025 ± .025	.036 ± .016	.056 ± .023	.131 ± .038	.256 ± .046	.086 ± .015
	41	.274 ± .081	.260 ± .049	.330 ± .047	.704 ± .071	1.52 ± .13	.507 ± .031
	42	1.30 ± .10	1.096 ± .099	1.164 ± .062	1.319 ± .099	1.56 ± .14	1.229 ± .045
	43	.079 ± .045	.058 ± .039	.060 ± .042	.067 ± .051	.037 ± .034	.061 ± .023
105 [c]	41			.116 ± .023	.221 ± .039	.400 ± .072	.156 ± .021
	42			.600 ± .034	.975 ± .089	1.52 ± .14	.753 ± .044
	43			.044 ± .024	.054 ± .030	.051 ± .051	.050 ± .017
106 [c]	41			.013 ± .007			.017 ± .007
	42			.306 ± .032			.386 ± .030
	43			.019 ± .011			.029 ± .013
107 [d]	41						.002 ± .001
	42						.089 ± .013
	43						.016 ± .006

a) The independent yields are normalized to 100% for each energy. To obtain the energy distributions for the nuclides, the yields must be multiplied by the following factors: .04815 ± .00022 (E = 88.5 MeV); .2280 ± .0029 (E = 93.4 MeV); .3610 ± .0011 (E = 98.3 MeV); .2891 ± .0039 (E = 103.1 MeV); .0737 ± .0010 (E = 108 MeV) .

b) The independent yields summed over the kinetic energy ($\sum$ E) have been obtained by summing the independent yields at the different kinetic energies multiplied by the normalizing factors given in footnote a).

c) The nuclear charge distributions of the masses A = 80, 81, 82, 83, 84, 105 and 106 have not been measured at all kinetic energies. To obtain the independent yields summed over E the missing charge distributions have been estimated and combined with the corresponding mass yields.

d) The independent yields for A = 107 have been estimated from a measurement of the nuclear charge distribution at a kinetic energy of 104.5 MeV .

3. RESULTS AND DISCUSSION

3.1 Widths of the isobaric Z-distributions

Fig. 1 shows the rms-widths σ_Z as a function of the average nuclear charge number $\langle Z \rangle$ of the corresponding isobar. The most prominent feature of fig. 1 is the strong modulation of σ_Z at all kinetic energies. The maxima and minima in σ_Z are located at odd and even $\langle Z \rangle$-values, respectively.

This modulation is a consequence of the odd-even effect in the element yields which is discussed in section 3.2. Apart from this modulation, the general trend in σ_Z before neutron evaporation as a function of the fragment excitation energy is of particular interest. Therefore, the influence of the proton odd-even effect on σ_Z was eliminated by correcting the measured yields in such a way as to obtain zero odd-even effect. Furthermore, a neutron evaporation calculation was performed [10] by which the known number of neutrons evaporated per fragment [11] was reproduced, and primary nuclide yields were fitted to the measured nuclide yields after neutron evaporation. The resulting dependence of the pre-neutron emission variance σ_Z^2 on the total fragment excitation energy is shown in fig. 2. The measured variances for the corresponding post-neutron emission isobaric Z-distributions are shown for comparison. These results refer to a selected mass range centred at the most probable mass split. Evaporation calculations for other mass splits are in progress. The striking result of this analysis is the fact that the pre-neutron emission variance has a constant value of about $\sigma_Z^2 = 0.35$ even at the lowest total fragment excitation energy of only 12 MeV investigated here. In the range of lower excitation energies where neutron evaporation is only of minor importance, already the post-neutron emission values show this tendency. It may therefore be concluded that the details of the assumptions entering the evaporation calculations do not influence this result.

In the framework of the semi-quilibrium model as proposed by Nörenberg [12,13], the isobaric nuclear charge distribution is determined by the collective temperature T_{coll} as follows: $\sigma_Z^2 = T_{coll}/c$. The collective temperature characterizes the thermal equilibrium between the collective degrees of freedom of the fissioning nucleus. The constant c is given by the dependency of the liquid drop potential energy at scission on the deviation of the nuclear charge number Z from its most probable value Z_p at fixed mass split: $V = c/2\ (Z-Z_p)^2$. For ^{236}U different mass formulae give a value of about $c = 3.2$ MeV . The collective temperature may thus be determined from the pre-neutron emission variance σ_Z^2 to be $T_{coll} = 1.1$ MeV . With about 10 collective degrees of freedom or more [13] this temperature corresponds to a collective excitation energy of at least 11 MeV . In the case of a total excitation energy of 12 MeV this seems to be an unrealistically high value. It must thereby be taken into consideration that a few MeV of excitation energy are bound in single particle excitations as

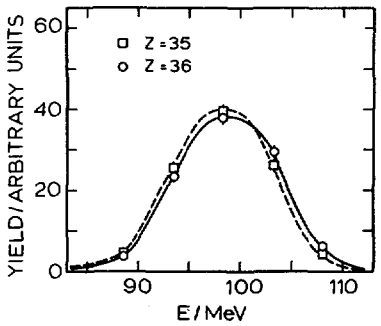

FIG.3. Kinetic energy distributions of the elements bromine (Z = 35) and krypton (Z = 36). The measured yields were normalized to 100% in both cases.

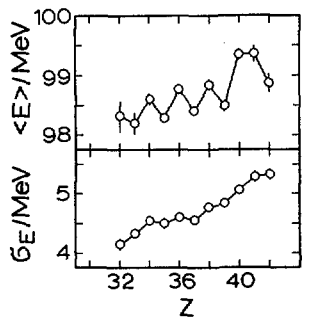

FIG.4. Moments of the kinetic energy distributions of the elements as a function of the nuclear charge number Z.
Upper part: average kinetic energies ⟨E⟩ ;
Lower part: rms-widths σ_E.

may be taken from the appearance of fragments with an odd proton number even at high kinetic energies. Furthermore, some energy may also be bound in fragment deformation. We therefore conclude that the isobaric element distributions can not be explained by the semi-equilibrium model [12].

It was stated [4,14,15] that quantummechanical zeropoint motion should put a lower limit on σ_Z^2 which is given by the relation $\sigma_Z^2 = \hbar\omega/2c$. Here $\hbar\omega$ is the phonon energy of the degree of freedom which determines the charge to mass ratio. For nuclear temperatures with $T << \hbar\omega$ the variance σ_Z^2 is thus expected to have a constant value independent of the excitation energy. Since experimentally it was found that σ_Z^2 is independent of the excitation energy, it may be possible that the effect of zeropoint motion is indeed observed here.

From the experimental value for σ_Z^2 a phonon energy of $\hbar\omega \approx 2.2$ MeV is determined. At present there is no theoretical value for $\hbar\omega$ for a fissioning nucleus at scission available for comparison. The calculation of the variance of the isobaric nuclear charge distribution on the basis of zeropoint motion should thus be considered as a task of future theoretical work.

3.2 The proton odd-even effect in the kinetic energy and in the yields

The kinetic energy distributions of even-Z elements are shifted by about 0.4 MeV to higher kinetic energies with respect to their odd-Z neighbours, see figs. 3 and 4. This shift corresponds to a shift of about $\delta E = 0.7$ MeV in the total kinetic energy. In addition to the odd-even effect, the average kinetic energy is generally enhanced by shell effects in the region $40 \leq Z \leq 42$. We shall now concentrate on the region which is not influenced by shell effects and propose the following very simple picture for explaining the observed energy shift between even-Z and odd-Z elements: We assume that it is due to the breaking of a proton pair, and that this energy for breaking a pair is taken from the prescission kinetic energy. Experimental estimates [16] of the pairing gap at the saddle point indicate that the energy necessary to break a pair should amount to about $\Delta E = 1.7$ MeV. In order to explain the observed energy shift, we assume that two components contribute to the even-Z yield, see fig. 5: One component which contains one broken proton pair, and the other, a superfluid component, where not a single proton pair is broken. If one proton pair is broken anywhere between the saddle and the scission point, we assume that the two unpaired protons will be distributed statistically on the two fragments. Therefore the even-Z yield component with one broken pair is equal in amplitude to the odd-Z yield, and the energy distributions are expected to be the same, too. In contrast, the superfluid component of the even-Z yield is shifted to higher kinetic energies by the pairing energy. For simplicity the shape of the energy distributions of the two components of the even-Z yield are assumed to be equal. Now the amplitude of the superfluid component is adjusted to reproduce the observed energy shift of 0.7 MeV between the total even-Z yield (dotted curve in fig. 5) and the odd-Z yield. In the following we shall examine the consequence of this simple model.

According to fig. 5, the proton odd-even effect in the yields, which is defined as the difference between the yields of even-Z and odd-Z elements, is given by the superfluid component which has to be equal to $\delta E/\Delta E/(2-\delta E/\Delta E) = 26\%$ in order to reproduce the observed odd-even effect in the kinetic energy. This value is in good agreement with the measured energy integrated proton odd-even effect of $(23.7 \pm 0.7)\%$.

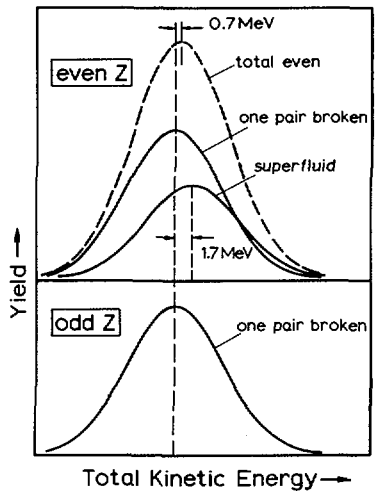

FIG.5. Schematic model (not drawn to scale) for explaining the proton odd-even effect in the kinetic energy and in the fission product yield. The even-Z yield is assumed to consist of two components which are shifted against one another by the pairing energy.

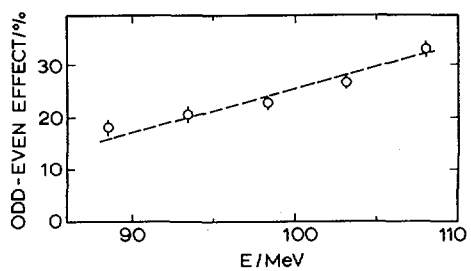

FIG.6. Proton odd-even effect in the light-fission-product yields as a function of the fission product kinetic energy. The proton odd-even effect is defined as the difference between the yields of even-Z and odd-Z elements in percent. The dotted curve is the energy dependence of the proton odd-even effect as predicted by the simple model sketched in Fig.5.

Fig. 6 shows the dependence of the proton odd-even effect on the kinetic energy. The odd-even effect is significant (18%) even at the lowest investigated kinetic energy of 88.5 MeV which corresponds to a total fragment excitation energy of about 38 MeV . The energy dependence as predicted by our model is seen to be in good agreement with the data.

The even-Z kinetic energy distributions are expected to be slightly broader than the odd-Z energy distributions,

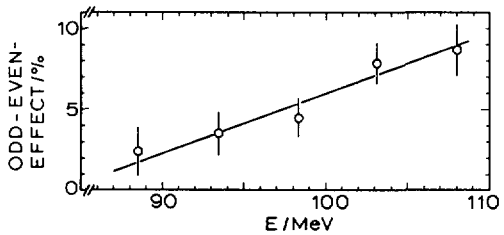

FIG. 7. Neutron odd-even effect in the light-fission-product yields as a function of the fission product kinetic energy.

since the even-Z yield is made up of two components of different kinetic energy. This effect seems to be born out by the data in fig. 4, which show an odd-even effect in the rms-widths of the kinetic energy distributions of the elements.

Thus it seems that the simple model explained in fig. 5 allows a consistent interpretation of our data. It may be concluded that in fact in about 25% of all fission events all protons remain in a paired state. Furthermore, the probability for the pair breaking processes does not strongly depend on the kinetic energy.

In the case of the fission of ^{230}Th, the odd-even effect in the total kinetic energy may be estimated from the experimental data in ref. [17] to be about $\delta E = 1$ MeV . If this value is used to calculate the proton odd-even effect in the yields in the same way as for ^{236}U, a value of 42% will be obtained. For the fission of ^{233}Th, a proton odd-even effect of (38±13)% was determined for the yields [18]. Since the odd-even effect in ^{230}Th and ^{233}Th may not be expected to be very different, the agreement with the odd-even effect in the kinetic energy is good.

Nifenecker et al. [15] reported an energy shift between even-Z and odd-Z elements of about $\delta E \approx 1$ MeV for the spontaneous fission of ^{252}Cf. If the above reasoning is applied to ^{252}Cf, the expected proton odd-even effect in the yields will be 42%, and this value is in sharp contradiction to the measured small odd-even effect for ^{252}Cf of only (5±4)% according to ref. [19] or (0±5)% according to ref. [20]. Further measurements are necessary to clear up the contradiction between the measurements for ^{236}U and ^{230,233}Th on the one hand and for ^{252}Cf on the other hand.

3.3 Neutron odd-even effect in the yields

The neutron odd-even effect in the energy-integrated yields was measured to be (5.4±.7)% . The neutron odd-even effect increases almost linearly with the kinetic energy, see fig. 7. Unfortunately it seems impossible at present to

draw any definite conclusion on the primary neutron odd-even effect from these measurements. Neutron evaporation calculations have shown that a possible primary neutron odd-even effect will be masked completely by the neutron evaporation process, and the extraction of a primary neutron odd-even effect will, therefore, depend on the details of the assumptions that have to be made in the evaporation calculations.

4. CONCLUSIONS

a) The widths of the pre-neutron emission isobaric Z-distributions are independent of the total fragment excitation energy even at very low fragment excitation energies. This seems to be an indication of zeropoint motion.

b) The single-particle excitation energy of the fragments at the scission point seems to be almost independent of the fragment kinetic energy. Furthermore the fraction of the fission events in which no proton pair is broken is estimated independently both from the odd-even effect in the kinetc energy and from the odd-even effect in the yields, to be about 25%. This supports the view that low energy fission is a weakly dissipative process.

ACKNOWLEDGEMENT

Fruitful discussions with P. Armbruster are gratefully acknowledged.

REFERENCES

[1] CLERC, H.-G., LANG, W., WOHLFARTH, H., SCHMIDT, K.-H., SCHRADER, H., PFERDEKÄMPER, K.E., JUNGMANN, R., Z. Physik A 274 (1975) 203

[2] CLERC, H.-G., LANG, W., WOHLFARTH, H., SCHMIDT, K.-H., SCHRADER, H., Proceed. of the 3rd Intern. Conf. on nuclei far from stability, Cargèse, Corsica May 1976, CERN 76-13, Genf (1976) p. 509

[3] WOHLFARTH, H., LANG, W., CLERC, H.-G., SCHRADER, H., SCHMIDT, K.-H., DANN, H., Phys. Lett. 63B (1976) 275

[4] MORETTO, L.G., SVENTEK, J., MANTZOURANIS, G., Phys. Rev. Lett. 42 (1979) 563

[5] MOLL, E., SCHRADER, H., SIEGERT, G., HAMMERS, H., ASGHAR, M., BOCQUET, J.P., ARMBRUSTER, P., EWALD, H., WOLLNIK, H., Kerntechnik 19 (1977) 374

[6] WOHLFARTH, H., Thesis, Technische Hochschule Darmstadt (1976)

[7] LANG, W., CLERC, H.-G., Nucl. Instrum. Methods 126 (1975) 535

[8] CLERC, H.-G., SCHMIDT, K.-H., WOHLFARTH, H., LANG, W., SCHRADER, H., PFERDEKÄMPER, K.E., JUNGMANN, R., ASGHAR, M., BOCQUET, J.P., SIEGERT, G., Nucl. Instrum. Methods 124 (1975) 607

[9] WOHLFARTH, H., LANG, W., DANN, H., CLERC, H.-G., SCHMIDT, K.-H., SCHRADER, H., Z. Physik A 287 (1978) 153

[10] LANG, W., Thesis, Technische Hochschule Darmstadt (1979)

[11] WOLFSBERG, K., Report LA-5553-MS (1974)

[12] NÖRENBERG, W., Habilitationsschrift, Universität Heidelberg (1970)

[13] NÖRENBERG, W., in Proceed. of the 3rd IAEA Symp. on physics and chemistry of fission, Rochester 1973, Vol. 1 (IAEA, Vienna, 1974) p. 547

[14] VANDENBOSCH, R., HUIZENGA, J.R., "Nuclear Fission", Academic Press, New York (1973)

[15] NIFENECKER, H., BLACHOT, J., BOCQUET, J.P., BRISSOT, R., CRANCON, J., HAMELIN, C., MARIOLOPOULOS, G., RISTORI, CH., This conference, paper SM-241/F1

[16] BRITT, H.C., HUIZENGA, J.R., Phys. Rev. C 9 (1974) 435

[17] UNIK, J.P., GINDLER, J.E., GLENDENIN, L.E., FLYNN, K.F., GORSKI, A., SJOBLOM, R.K., in Proceed. of the 3rd IAEA Symp. on physics and chemistry of fission, Rochester 1973, Vol. 2 (IAEA, Vienna, 1974) p. 19

[18] IZAK-BIRAN, T., AMIEL, S., Phys. Rev. C 16 (1977) 266

[19] LIPINSKI, R.J., WEHRING, B.W., Phys. Lett. 66 B (1977) 326

[20] WAHL, A.C., contribution to review paper 11 in Proc. of the 2nd Adv. Group Meeting on fission product nuclear data, Petten 1977, to be published by IAEA, Vienna

DISCUSSION

W. REISDORF: You have measured σ_Z^2 as a function of the excitation energy at infinity. On the basis of the statistical model one would have to know the excitation energy before scission in order to establish a possible non-dependence of σ_Z^2 on temperature. I, therefore, feel that your conclusion regarding the predominance of zero point motion may be somewhat premature.

H:G. CLERC: We find $\sigma_Z^2 = 0.35$ even at the lowest total asymptotic fragment excitation energy, which is only 12 MeV. This energy therefore constitutes an upper limit for the excitation energy of the system at scission. The variance σ_Z^2 observed in our experiments is too high to be explained by a statistical model without taking zero-point motion into account, even if the excitation energy at the scission point were to reach this limiting value of 12 MeV.

K. SISTEMICH: Could not the odd-even effect in the most probable kinetic energies that you observe also be explained by different deformability of odd-mass and even-mass nuclei?

H:G. CLERC: Yes, we cannot rule out that explanation, which would certainly lead to very similar conclusions, namely that there are two components in the even Z yield, one of which is superfluid, indicating low damping, and that the rms widths of the kinetic energy distributions of the elements could be expected to show an odd-even effect, as is found experimentally.

However, the magnitude of the energy shift between the two components would be unknown and the consistency of the observed energy shift with the magnitude of the superfluid component could not be checked.

K.M. DIETRICH: I do not understand why you excluded a statistical explanation for the observed magnitude of σ_Z and the constancy of this quantity as a function of the excitation energy. If the temperature (k_B) T is small compared to the photon energy corresponding to the (N–Z) degree, then the Boltzmann distribution would predict that only the zero point mode of this degree of freedom can be occupied. Thus, as long as the temperature remains low, as compared to the photon energy, σ_Z^2 is only given by the zero point mode and is not therefore dependent on the excitation energy. The magnitude of σ_Z^2, too, is determined only by the zero point wave function.

H:G. CLERC: I would agree that an interpretation of σ_Z as determined by zero point motion still lies within the framework of a statistical model. What I wanted to say, however, was that the experimental result whereby a high σ_Z is not dependent on the excitation energy seems to indicate that σ_Z may, in fact, be determined by zero-point motion. So the procedure usually adopted in theoretical calculations based on some kind of statistical model, namely calculation of temperature from the observed variation using the relationship $T = c\sigma_Z^2$, c being determined by the liquid-drop asymmetry energy ($c \approx 3.2$ MeV), is no longer justified in low-energy fission; it yields unreasonably high temperatures and therefore unreasonably high excitation energies.

FISSION FRAGMENT ENERGY CORRELATION MEASUREMENTS FOR $^{241}Am(n_{th},f)$, AND SHELL EFFECTS IN THERMAL-NEUTRON-INDUCED FISSION

M. ASGHAR*, F. CAÏTUCOLI**, P. PERRIN**, G. BARREAU,
C.R. GUET, B. LEROUX†, C. SIGNARBIEUX††
Institut Laue-Langevin,
Grenoble Cedex, France

Abstract

FISSION FRAGMENT ENERGY CORRELATION MEASUREMENTS FOR $^{241}Am(n_{th},f)$, AND SHELL EFFECTS IN THERMAL-NEUTRON-INDUCED FISSION.

Fission fragment mass and kinetic-energy distributions and mass-versus-energy correlations were measured for the sub-barrier ^{241}Am (n_{th},f) using the strong thermal neutron beam available at the Grenoble high-flux reactor. The results are compared with the even-even and the other odd-odd fissioning systems to have, among other things, some information on the saddle-point-to-scission-point dynamics. This comparison shows that in an even-even fissioning nucleus most of the pairs are broken somewhere after the freezing of the structure of the nascent fragments and most probably just before and/or in the act of scission. As to the shell effects in the thermal-neutron-induced fission fragment global-mass distributions and the distributions for high-kinetic-energy events, it is found that, up to ^{241}Am at least, the neutron spherical shells at $N = 82$ and $N = 50$, and the neutron deformed shells at $N \geqslant 60$ and $N \approx 88$ play an important role in determining these distributions.

1. INTRODUCTION

We have been studying systematically the fragment mass and kinetic energy distributions and mass-versus-energy correlations of odd-odd sub-barrier fissioning systems resulting from thermal neutron capture [1,2]. Generally, these nuclei have very low fission cross sections compared with the neighbouring even-even fissioning systems. However, the strong thermal neutron flux available at the Grenoble high-flux reactor makes such measurements quite feasible.

In this paper we present our results on ^{241}Am (σ_f = 3.15 b). Furthermore, we join our results on the different odd-odd fissioning systems with those for the even-even nuclei resulting from thermal neutron capture,

---

* At present at CEC Joint Research Centre, Ispra-Establishment, Italy.
** Département de recherche fondamentale, CEN-Grenoble, France.
† Centre d'études nucléaires de Bordeaux-Gradignan, Université de Bordeaux, France.
†† Centre d'études nucléaires de Saclay, France.

either measured by us or taken from the literature. Here the aim was to look for shell effects either in the global mass distributions or in the mass distributions resulting from high fragment kinetic energies.

2. EXPERIMENTAL SET-UP, DATA PROCESSING AND RESULTS

The experiment was carried out at the inclined cold neutron beam hole (IHI) of the Grenoble high-flux reactor. The circular neutron beam was collimated to 1 cm diameter a few cm before the fission target with an enriched ^{6}Li collimator placed inside the vacuum chamber evacuated to $\approx 10^{-4}$ Torr. The equivalent thermal neutron flux at the target position was $\phi_{th} \approx 5 \times 10^{9}$ n/cm^2.s with $\phi_{th}/\phi_{fast} \approx 5 \times 10^{4}$ (calc.). A 3.23 μg/cm^2 $^{241}AmO_2$ target and a 4.04 μg/cm^2 U_3O_8 (93% enrichment in ^{235}U) calibration target were used. Each of these targets was evaporated onto a 110 μg/cm^2 nickle backing.

The coincidence complementary fragment pulse heights were measured with two ORTEC π cm^2 gold-silicon surface-barrier detectors. These detectors were collimated with appropriate diaphragms to avoid edge effects. They were placed symmetrically on both sides of the fission target with $\approx$ 3 cm between the centre of the target and each detector. Fast and slow coincidence gates of $\approx$ 16 ns and $\simeq$ 2 μs respectively were used.

In addition to the two complementary fragment pulse heights, the time-of-flight difference ΔT (ΔT_{meas}) was also recorded between the two fission fragments, when they reach their respective detectors.

This three-parameter information was recorded event by event on a magnetic tape with a Multi-8 data recording system and 2048 channels were allocated for each of the three parameters. Altogether $\approx 1.56 \times 10^{5}$ fission events were recorded and analysed for ^{241}Am. The data were analysed with a PDP-10 computer. The fragment pulse heights were converted into fragment kinetic energies and provisional (pseudo-) masses through an iterative procedure using the mass-dependent energy calibration method of Schmitt et al. [3], the mass and momentum conservation relations and the ^{235}U calibration data. Furthermore, the difference δT between ΔT_{meas} and ΔT calculated (ΔT_{calc}) from the experimental fragment kinetic energies and the flight paths corresponding to the two fission detectors has a normal distribution about $\delta T = 0$ [4], as shown in Fig. 1. The FWHM of the δT distribution of 280 ps reflects the effective time resolution of the set-up. This good time resolution helps us to use effectively this coherence condition (between ΔT_{meas} and ΔT_{calc}) for our compact geometry. A window is put on this distribution (see Fig. 1) such that the events within this window are accepted as being good with a high probability. This coherence test leads to the elimination of a relatively high proportion of events in the symmetric and the far-out asymmetric regions which are, in fact, predominantly contaminated by scattered and poorly measured high yield events. Thus this method of selecting data helps one to obtain significant results in the low yield regions.

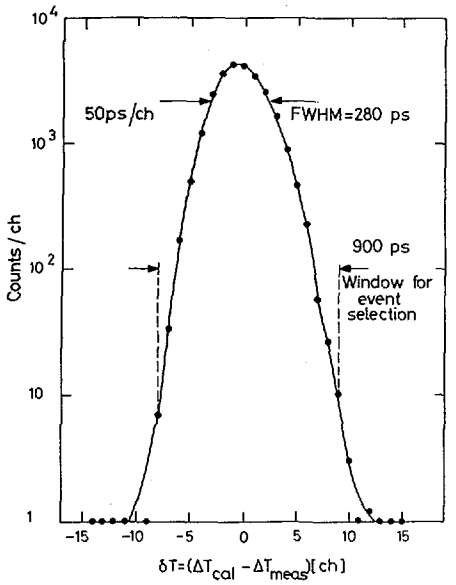

FIG.1. The $\delta T = [\Delta T_{cal} - \Delta T_{meas}]$ *distribution. Also shown is the window around the* δT *peak to eliminate the events that do not satisfy the coherence test.*

Figs. 2, 3, 4, 6 and 7 show the results on the various distributions for ^{241}Am and compare them with the corresponding ^{235}U data. These distributions have not been corrected for neutron emission and are presented as a function of provisional (μ) masses. Furthermore, the energy distributions $<E_K>(\mu_H)$ and $<E>(\mu)$ have not been corrected for the loss due to neutron emission. Moreover, the data have not been corrected for resolution effects. Table I summarises and compares the results on ^{241}Am with those on ^{235}U.

3. DISCUSSION OF RESULTS: MASS DISTRIBUTIONS AND MASS-ENERGY CORRELATIONS

Fig. 2 shows the mass distributions for the odd-odd sub-barrier fissioning ^{242}Am nucleus and for ^{235}U. As far as we know, our results are the first on the thermal neutron-induced fission of ^{241}Am. The global mass distribution for ^{241}Am is rather smooth and structureless and quite similar to the mass distribution for ^{239}Pu (Fig. 13). The experimental peak/valley (P/V) ratio of mass distribution is 117 $\pm$ 10 against 554 $\pm$ 31 for ^{235}U. When corrected for the mass resolution effects, one gets a value of 137 $\pm$ 12. This value should be compared with 151 for both ^{239}Pu and ^{237}Np, and 155 for ^{245}Cm [16] . It is interesting to see a decrease in P/V of a factor of $\approx$ 4 as one moves up from ^{235}U and, thereafter, a plateau with P/V $\approx$ 150 up to ^{245}Cm. In fact, this constancy of P/V for these nuclei, whether even-even or odd-odd fissioning systems, reflects the similarity of their mass distributions (Fig. 13).

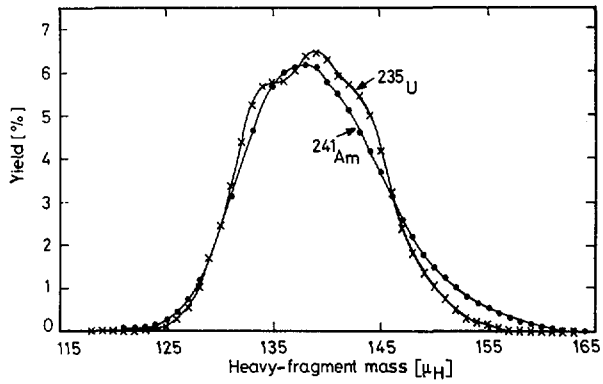

FIG. 2. Provisional mass distributions for ^{241}Am and ^{235}U. The data have not been corrected for resolution effects.

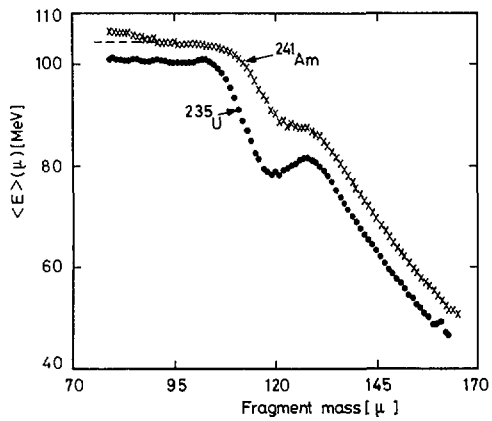

FIG. 3. The single-fragment kinetic energy as a function of the fragment provisional mass for ^{241}Am and ^{235}U.

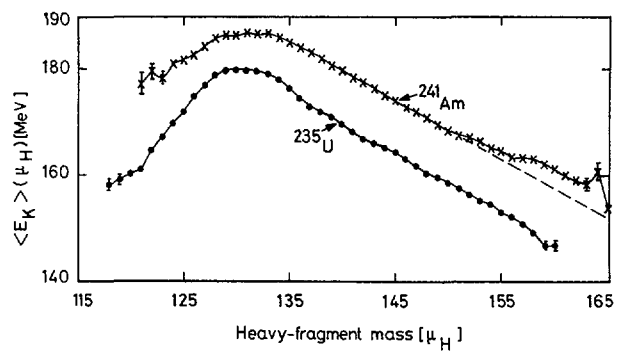

FIG. 4. The total fragment kinetic-energy distributions for ^{241}Am and ^{235}U as a function of the heavy-fragment provisional mass.

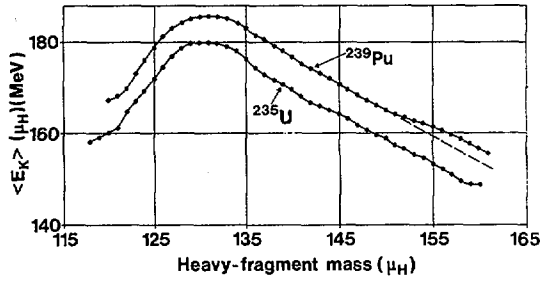

FIG.5. The total fission fragment kinetic-energy distributions for ^{239}Pu and ^{235}U as a function of the heavy-fragment mass.

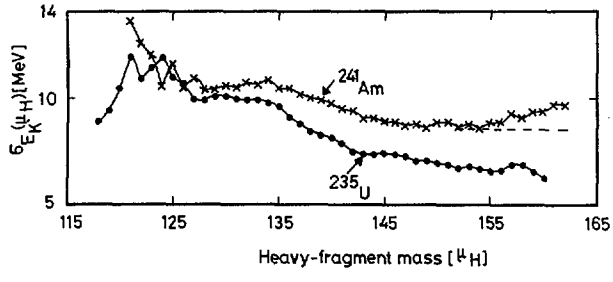

FIG.6. The rms widths of the total fission fragment kinetic energy for ^{241}Am and ^{235}U as a function of the heavy-fragment provisional mass.

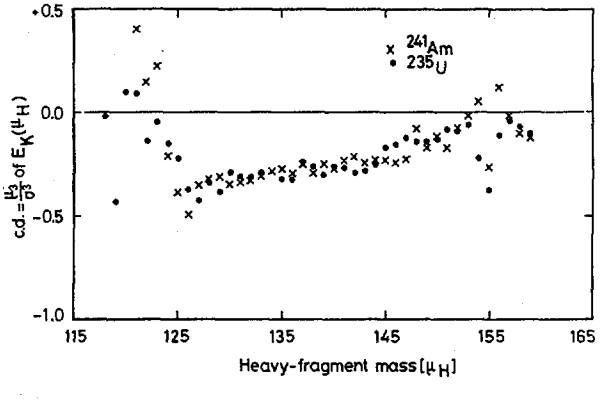

FIG.7. The coefficients of dissymmetry (c.d. = μ_3/σ^3, where μ_3 and σ are the third and second moments, respectively) for ^{241}Am and ^{235}U as a function of the heavy-fragment provisional mass.

TABLE I. MEAN VALUES, ROOT-MEAN-SQUARE WIDTHS AND OTHER RELEVANT QUANTITIES FOR THE THERMAL NEUTRON FISSION OF ^{241}Am AND ^{235}U

	$^{241}Am(n_{th}, f)$ (provisional mass quantities)	$^{235}U(n_{th}, f)$
$\langle E_K \rangle$ (MeV)	179.7 ± 0.4 181.6 ± 0.4 a)	171.0 ± 0.4 172.7 ± 0.4 a)
σ_{E_K} (MeV)	11.7	10.7
$\langle E_L \rangle$ (MeV)	103.4	100.4
σ_{E_L} (MeV)	5.9	5.1
$\langle E_H \rangle$ (MeV)	76.4	70.6
σ_{E_H} (MeV)	8.5	7.6
$\langle \mu_L \rangle$ (amu)	102.6	97.2
σ_{μ_L} (amu)	6.5	5.7
$\langle \mu_H \rangle$ (amu)	139.4	138.8
σ_{μ_H} (amu)	6.5	5.7
P/V	117 ± 10 137 ± 12 c)	554 ± 31
$\Delta E_K = \langle E_K \rangle_{max} - \langle E_K \rangle_{sym.\ fission}$ (MeV)	9.6 ± 2.1 8.6 ± 2.1 a)	21.8 ± 1.1 20.6 ± 1.1 a)
neutron binding energy B_n (MeV)	5.54	6.536 b)
barrier heights (MeV) V_A	6.5	5.63 b)
barrier heights (MeV) V_B	5.7	5.53 b)

a) corrected for neutron emission with $\langle \nu_T \rangle$ for ^{241}Am taken to be the same as for ^{235}U: $\langle \nu_T \rangle = 2.44$;

b) [22]; c) normalised to the radiochemical value (650) through the present P/V results for ^{235}U.

4. KINETIC ENERGIES

The various quantities of interest for ^{241}Am and ^{235}U are presented in Table I. The rms widths σ_{E_K}, σ_{E_L} and σ_{E_H} for ^{241}Am are higher than the corresponding values for ^{235}U. The dip ΔE_K in the average total kinetic energy, defined as the difference between the maximum value and the value at symmetry, is 8.6 ± 2.1 MeV for ^{241}Am compared with 20.6 ± 1.1 MeV for ^{235}U. Our previous work on the other odd-odd fissioning such as ^{231}Pa and ^{237}Np, and ^{239}Pu gave 14.8 ± 4.2 MeV, 14.1 ± 3.5 MeV and 18.6 ± 0.4 MeV, respectively [1, 2, 5]. As discussed below, these low values of ΔE_K for the odd-odd fissioning nuclei compared with the neighbouring even-even fissioning systems seem to result partly from the flattening off of the $\langle E_K \rangle (\mu_H)$ distributions in the $\mu_H \approx 125 - 135$ mass region. However, in the case of ^{241}Am a major part of this decrease in ΔE_K comes from an important increase in $\langle E_K \rangle$ in the symmetry region, where it is ≈ 19 MeV higher than the corresponding value for ^{235}U. The calculations of Wilkins et al. [12] foresee such an increase in the Am and Cm region.

In Figs. 3, 4 and 6 we compare the $\langle E \rangle (\mu)$, $\langle E_K \rangle (\mu_H)$ and $\sigma_{E_K}(\mu_H)$ distributions for ^{241}Am and ^{235}U. We notice that the $\langle E_K \rangle (\mu_H)$ distribution (Fig. 4) for ^{241}Am in the mass region of $u_H \approx 125 - 135$ is flatter than for ^{235}U and it is shifted upwards by only ≈ 6.5 MeV; however, for $\mu_H \geq 135$ this shift is ≈ 10 MeV. Similar behaviour was observed in the case of ^{231}Pa and ^{237}Np [1, 2]. We believe that, to a large extent, this difference is a consequence of the presence of two unpaired particles (one proton and one neutron) right from the beginning and at the saddle point in the odd-odd fissioning systems such as ^{241}Am, ^{237}Np and ^{231}Pa [1, 2]. Similar flattening off of $\langle E_K \rangle (\mu_H)$ in the $\mu_H \approx 125 - 135$ region is observed for the even-even fissioning systems such as ^{239}Pu, when the excitation energy of the fissioning system is increased [6]. One can understand at least qualitatively this flattening off in the $\mu_H = 125 - 135$ mass region with the help of the Nörenberg model based on the molecular model of fission [7]. In this model the dependence of the different features of fission on the compound nucleus excitation energy comes through the number of quasi-particle excitations (qp) at the saddle point. Moreover, the scission point distance depends strongly on the deformability of fragments which, in turn, is a function of the number of quasi-particle excitations; this effect will entail a change in the fragment mean kinetic energies which are mainly determined by the Coulomb energy at the scission point. According to this model, the quasi-particles will strongly perturb the fragments with masses in the magic region around mass 132 and render them less stiff and more deformable. However, the fragments with masses outside this region will be much less disturbed (see also [12]).

One can go farther and try to understand something about the fission dynamics in the saddle-point-to-scission-point region. For example, we know that in the case of ^{239}Pu(n_{th}, f) (an even-even fissioning system), one observes a very low preference for proton and neutron pairing in the mass distribution - only (11 + 9)% [8, 9], compared to an average value of ≈ 22%

for $^{235}U(n_{th}, f)$ [10, 11] . We want to know as to where along the saddle-to-scission path are most of the proton and neutron pairs broken and qp excited? Furthermore, where and when along this path are the qp excited with respect to the formation of nascent fragments? We have seen just above that if the qp are present at the saddle point as in an odd-odd fissioning nucleus or in the MeV neutron-induced fission of an even-even fissioning system, such as ^{235}U and ^{239}Pu, there is a strong interaction between these qp and the formation of the fragments, which manifests itself in the flattening off of the $<E_K>(\mu_H)$ distributions in the $\mu_H \approx 125 - 135$ mass region. However, the $<E_K>(\mu_H)$ distribution shown in Fig. 5 for $^{239}Pu(n_{th}, f)$ does not seem to show this flattening off. Hence these results on odd-odd and even-even fissioning nuclei lead us to the conclusion that most of the pairs are broken in ^{240}Pu and probably in other even-even nuclei, too, somewhere after the freezing of the structure of the nascent fragments and there is not much interplay between them and the qp before their separation. This is possible only if these pairs are broken just before and/or in the act of scission [12, 13] .

In Fig. 4 we also see that the $<E_K>(\mu_H)$ for ^{241}Am increases rather suddenly by ≈ 2 MeV for $\mu_H \gtrsim 153$. Most of this increase goes to the complementary light fragments (Fig. 3). This feature is common for the fissioning systems heavier than ^{235}U that we studied and is probably related to the relatively stable but deformed heavy fragments with masses in the rare earth region. The $\sigma_{E_K}(\mu_H)$ for ^{241}Am, shown in Fig. 6, diverges from and is higher than for ^{235}U for $\mu_H \gtrsim 125$. However, unlike ^{235}U, the $\sigma_{E_K}(\mu_H < 125)$ for ^{241}Am has a tendency to go up; the data on $^{245}Cm(n_{th}, f)$ show a similar behaviour [14] . Wilkins et al. [12] explained this behaviour in terms of deformed shells which cause the presense of more than one configurations with different deformations but comparable contributions for mass ratios in this region. However, since the mass yield, the neutron emission and the $<E_K>(\mu_H)$ change quite rapidly in this region, this, compounded with the resolution effects, might lead to some singularities in $\sigma_{E_K}(\mu_H)$ behaviour in this part. But why should these resolution effects on the $\sigma_{E_K}(u_H)$ distributions in this region be different for nuclei up to ^{239}Pu - where one observes a sort of a peak around $\mu_H \approx 123$ - from the nuclei such as ^{241}Am and ^{245}Cm which seem to show a different behaviour? Hence, these experimental effects alone might not be sufficient to explain this behaviour in this mass region. Furthermore, the increase in $\sigma_{E_K}(\mu_H \gtrsim 153)$ might be partly due to the above effects and partly to the rather sudden increase in $<E_K>(\mu_H \gtrsim 153)$.

In Fig. 7 we give the coefficients of dissymmetry (c. d.) or skewness of $E_K(\mu_H)$ and $E(\mu)$ defined as c. d. $= u_3/\sigma^3$, where u_3 is the third moment and σ, the dispersion of E_K and E. Since we eliminate effectively the poorly measured events which manifest as low energy tails of fragment energy distributions, we think that the c. d. (μ_H) distributions are significant. These distributions for ^{241}Am and ^{235}U are quite identical. Furthermore, one observes that the dissymmetry is low for the symmetric and the far-out asymmetric fission. The c. d. is the highest for

$\mu_H \approx 130$, which roughly corresponds to the highest value of $E_K(\mu_H)$ and it decreases smoothly as μ_H goes up. However, as discussed above, the rapid changes in mass yields, fragment energies and neutron emission (close to symmetry) convoluted with an experimental mass resolution of ≈ 4 amu (FWHM) may result in a rapid change in the values of c.d. in this region as observed. These effects may also have some influence on the far-out asymmetric region. However, we feel that $E_K(\mu_H)$, $E_L(\mu_L)$ and $E_H(\mu_H)$ in the high yield regions have low energy tails produced in the fission process itself. These data are consistent with the results of Wohlfarth [15] for ^{235}U. He used the Lohengrin mass separator to measure the energy distributions of light fragments in a limited mass range of 96 to 106. These low energy tails may result from a simultaneous contribution, for a given mass ratio, from (at least) two different configurations for which the nascent complementary fragments have different deformations resulting in different final E_K values [12].

5. SHELL EFFECTS

It seems that the structure of potential energy surface determines mostly the profiles of mass distributions for different fissioning systems in low energy fission. This structure results from shell effects for different fragment masses and for different fragment deformations [12]. We have investigated these shell effects by studying the systematics of global mass distributions and the mass distributions resulting from high kinetic energy events in thermal neutron-induced fission of odd-odd and even-even fissioning nuclei.

5.1 N ≈ 88 deformed shell and N = 50 spherical shell

In Fig. 8 are shown the mass distributions for ^{229}Th, ^{231}Pa, ^{233}U and ^{235}U [16, 2, 5]. One observes that the higher edge of all these distributions remains stable and fixed at $\mu_H \approx 145$. Although the neutron number in the complementary light fragments is close to the N = 50 neutron spherical shell, the stability of this edge over this range of nuclei is most probably due to a combination of some influence of this shell and the deformed N ≈ 88 neutron shell in the heavy fragment with $\mu_H \approx 145$ as predicted by the static scission-point model calculations [12]. Furthermore, the strong structure at $\mu_H \approx 145$ for ^{229}Th is possibly due to the closeness of the N = 50 spherical and N ≈ 88 deformed shells in the light and the heavy fragments respectively and proton pairing [16].
Further evidence for this shell comes from the mass distributions derived from the high kinetic energy events for ^{235}U and ^{231}Pa shown in Figs. 9 and 10. In both the cases one notices an enhancement of yield for the $\mu_H \approx 144$-146 mass region. The ^{231}Pa data are from the double fragment

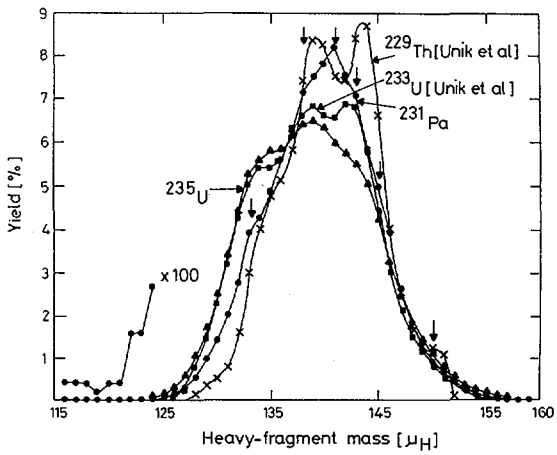

FIG. 8. The global mass distributions for ^{229}Th, ^{231}Pa, ^{233}U and ^{235}U. The data on ^{229}Th and ^{233}U are from Ref. [16].

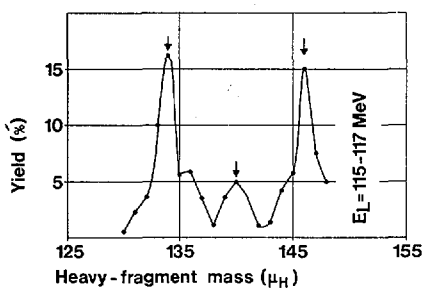

FIG. 9. The mass distribution for ^{235}U as a function of the heavy-fragment mass for high-kinetic-energy events.

energy measurements [2]. However, the ^{235}U results of Fig. 9 were obtained with the time-of-flight difference method [17], which allowed us to separate completely the different fragments in the high fragment kinetic energy region. Notice that for ^{235}U with a window of E_L = 115 - 117 MeV, the yields of masses 134 and 146 are about the same.

It has been thought since a long time that fission becomes asymmetric because of the N = 82 and Z = 50 spherical shells (Section 6.3). These data show, however, that this idea is not correct. The fission becomes asymmetric because of the combined effect of the N ≈ 88 deformed shell and the N = 50 spherical shell.

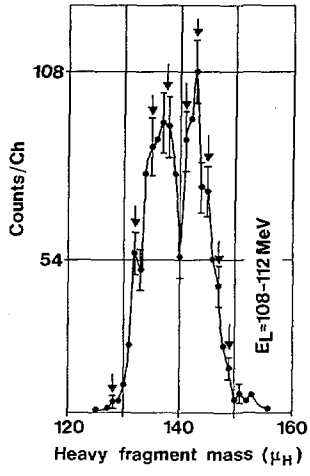

FIG.10. The mass distribution for ^{231}Pa as a function of the heavy-fragment mass for high-kinetic-energy events.

Furthermore, it is interesting to observe that for ^{235}U with this E_L window, the binary fragments 134/102 and 146/90 are produced in fission with less than 2 MeV total excitation energy. These are examples of cold fragmentation in fission (see also Ref.[5]).

5.2 N = 82 spherical shell and N ≥ 60 deformed shells

One observes in Fig. 8 that, as the mass of the fissioning nucleus increases, the mass yield corresponding to the shoulder with $\mu_H \approx 134$ goes up. Furthermore, the mass distribution for ^{235}U for high kinetic energy events show an enhanced yield for $\mu_H = 134$, Figs. 9 and 12 [1, 5, 17-20]. However, no such enhanced yield for high kinetic energy events was observed in the existing data on ^{233}U [18]. This increase in yield for ^{235}U was thought to be due to the N = 82 spherical neutron shell in the $\mu_H = 134$ heavy fragment and the N = 62 deformed neutron shell in the $\mu_L = 102$ light fragment [18]. And the absence of this increase in yield for ^{233}U was explained by assuming that 60 neutrons in the $\mu_L = 100$ light fragment do not show a shell property. However, the recent data show an enhanced yield for high kinetic energy events also for ^{233}U [23]. Does this mean that this enhanced yield is caused only by the N = 82 spherical shell

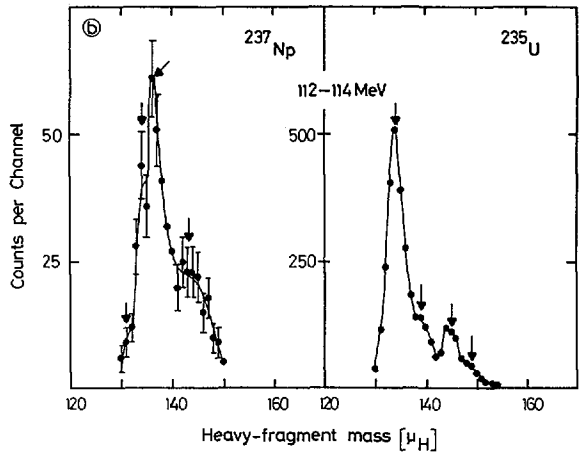

FIG.11. The mass distributions for ^{237}Np and ^{235}U as a function of the heavy-fragment mass for high-kinetic-energy events.

which is common to both these fissioning nuclei? Or does the deformed neutron shell start from and include 60 neutrons? The experimental results on the energies of the first 2^+ state seem to show a sudden onset of deformation in the even-A isotopes of Sr, Zr, Mo and Ru, when the neutrons increase from 58 to 60 [21]. These results might also explain the relatively weak shoulders around $\mu_H \approx 134$ for ^{229}Th and ^{231}Pa in Fig. 8; here the respective light fragments with $\mu_L = 96$ ($^{96}_{38}Sr$) and $\mu_L = 98$ ($^{98}_{39}Y$) with 58 and 59 neutrons, are probably not deformed, because the deformed neutron shell does not reach down to them.

Furthermore, the results on the fragment energy correlations for ^{237}Np (n_{th},f) – an odd-odd fissioning nucleus – provide evidence for the effect of the N = 62 deformed shell [1]. Figure 11 shows the mass distribution for high kinetic energy events for ^{237}Np, where the $\mu_H = 136$ shows an enhanced yield. Here the light fragment with $\mu_L = 102$ has quite probably 62 neutrons. As discussed before, the presence of two unpaired particles (one proton and one neutron) in an odd fissioning system strongly disturbs and reduces the shell properties of the N = 82 spherical shell in the odd-odd fissioning systems. Probably this is the reason here for the lack of enhancement of yield for $\mu_H = 134$. Moreover it is possible that the complementary odd-odd light fragment, $^{104}_{41}Nb_{63}$, may not be deformed. Furthermore, there is some evidence for the influence of the N = 62 deformed shell in the global mass distribution with a relative enhancement of yield for $\mu_H = 136$ as Fig.8 shows [1]. There is also a yield enhancement at $\mu_H = 135$ for ^{239}Pu (Fig.12) for high energy events [5]. This is probably again due to the N = 82 spherical shell and a deformed isotope of ^{105}Mo with N = 63 [21].

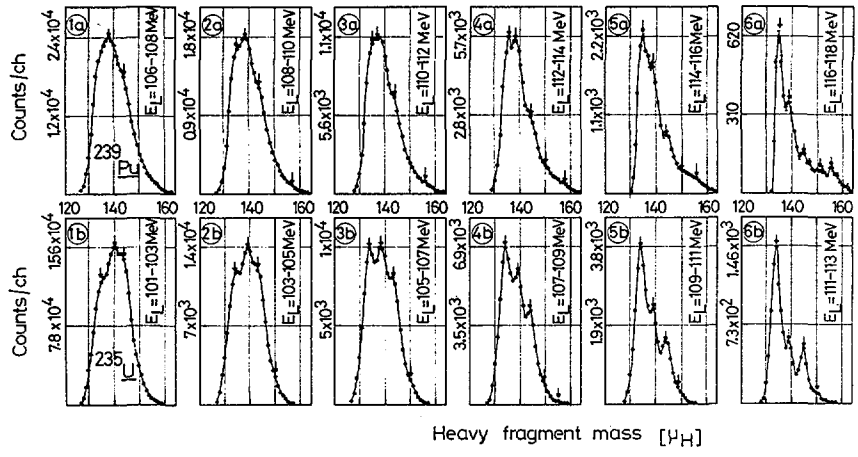

FIG.12. The mass distributions for ^{239}Pu (curves a) and ^{235}U (curves b) as a function of the heavy-fragment mass for six light-fragment kinetic windows. The arrows show the approximate positions of probable fine structures or shoulders. The different but corresponding E_L windows for the two systems were chosen in such a way as to leave about the same excitation energy in each of them.

5.3 N ≈ 88 and N ⩾ 60 deformed shells

We can combine the different shells to create structures in the mass distributions. In Fig. 13, we show, as an example, the mass distributions for ^{243}Am (our recent data), ^{245}Cm (n_{th},f), ^{246}Cm (s,f), ^{248}Cm (s,f). The edge at $\mu_H \approx 145$ in these distributions in a result of the N ≈ 88 and N ⩾ 60 deformed shells in the heavy and the light fragments, respectively.

5.4 Variations of global mass yield distributions

As the mass of the fissioning nucleus increases beyond ^{235}U, the shoulder at $\mu_H = 134$ does not move up very much. Moreover, the stability due to the $\mu_H = 145$ deformed shell does not hold any more and the mass distribution becomes suddenly more asymmetric, Fig. 13, with the heavier fragment masses reaching the deformed nuclei in the rare earth region. The mass distributions for ^{237}Np, ^{239}Pu, ^{241}Pu (not shown) and ^{241}Am in Fig. 14, are quite similar and not much different from one another. Moreover, as we noticed before (section 3), the P/V jumps to ≈ 150 and is the same for all these nuclei. Furthermore, as we noticed in the

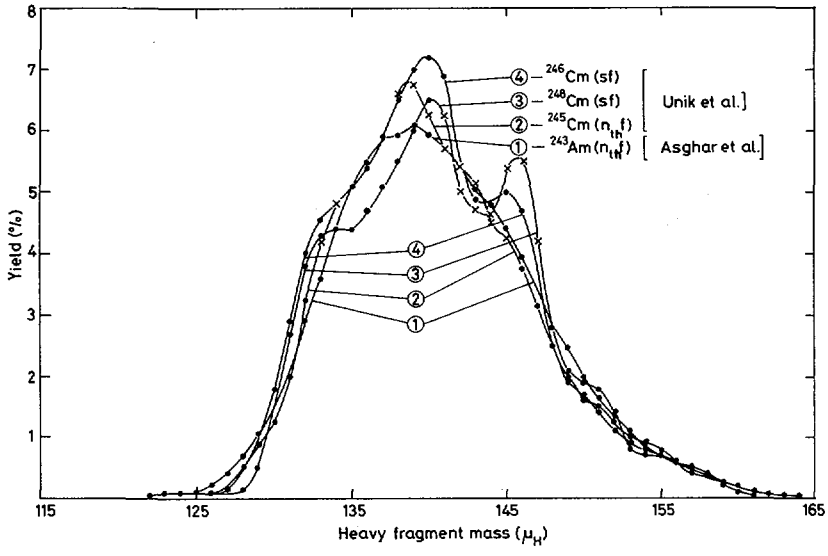

FIG. 13. The global mass distributions for ^{243}Am, ^{245}Cm (n_{th}, f), ^{246}Cm (s,f) and ^{248}Cm (s,f).

case of ^{241}Am, Fig. 4, there is a sudden increase in $E_K(\mu_H)$ of $\approx$ 1.5 - 2 MeV for $\mu_H \geq 153$. This feature seems to be common for the fissioning nuclei heavier than ^{235}U and is probably due to the relatively stable, but deformed heavy fragments with masses in the rare earth region.
This sudden change of 'phase' beyond ^{235}U (as manifested in the change of mass distributions) may have some interesting implications. This could be the reason why the fissioning systems lighter than ^{235}U show relatively weak dissipative effects compared to the systems heavier than ^{235}U (see, e.g. Gindler et al., these Proceedings). This could also explain the presence of the shoulder at $\mu_H - 172 - 177$ seen in the mass distribution yield of ^{238}U(n,f) and its absence in ^{235}U(n,f) (see Iyer et al., these Proceedings).

6. CONCLUSION

The results on the sub-barrier $^{241}Am(n_{th}, f)$ and the systematics of the global mass distributions and those for the high kinetic energy events resulting from the thermal neutron-induced fission show the following principal characteristics:

a) The mass distribution is smooth, structureless, but more asymmetric than for ^{235}U.

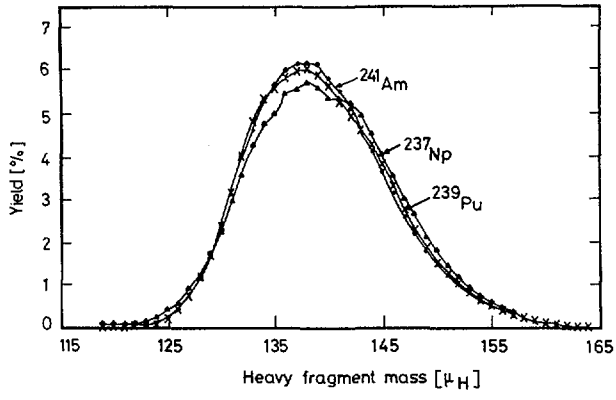

FIG.14. The global mass distributions for ^{237}Np, ^{239}Pu and ^{241}Am.

b) The $<E_K>(\mu_H)$ distribution for $\mu_H \approx 125$-135 is flatter than for ^{235}U and it is shifted upwards by only $\approx$6.5 MeV; however, for $\mu_H > 135$, this shift is $\approx$10 MeV. This difference is mostly due to the presence of two unpaired particles at the saddle point in the odd-odd fissioning system.

c) The $<E_K>(\mu_H)$ increases rather suddenly by $\approx$2 MeV for $\mu_H \gtrsim 153$. Most of this increase goes to the light fragment. This feature is common for the fissioning systems heavier than ^{235}U, and is related to the relatively stable but deformed heavy fragments with masses in the rare earth region.

d) $\sigma_{E_K}(\mu_H)$ also shows an increase for $\mu_H \gtrsim 153$, and unlike ^{235}U, where σ_{E_K} decreases as one approaches the symmetric fission, it seems to go up close to the symmetric fission as in the case of ^{245}Cm [12].

e) The dip ΔE_K at the symmetric fission is 8.6 $\pm$ 2.1 MeV against 20.6 $\pm$ 1.1 MeV for ^{235}U.

f) The peak/valley ratio of mass distribution is 117 $\pm$ 10 against 554 $\pm$ 31 for ^{235}U.

g) The comparison of the even-even and odd-odd fissioning systems shows that in low energy fission of even-even nuclei, the saddle-point-to-scission-point motion is such that most of the pairs are broken somewhere after the freezing of the structure of the nascent fragments and most probably just before and/or in the act of scission.

h) We find that the neutron spherical shells at N = 82 and N = 50 and neutron deformed shells at N $\gtrsim$ 60 and N = 88 play an important role in determining the mass distributions for the fissioning systems discussed in this paper.

REFERENCES

[1] ASGHAR, M., D'HONDT, P., GUET, C., PERRIN, P., WAGEMANS, C., Nucl. Phys. A 292 (1977) 225.

[2] ASGHAR, M., CAÏTUCOLI, F., PERRIN, P., GUET, C., D'HONDT, P., WAGEMANS, C., Nucl. Phys. A 311 (1978) 413.

[3] SCHMITT, H.W., GIBSON, W.M., NEILER, J.H., WALTER, F.J., THOMSON, T.D., Proc. Symp. on Physics and Chemistry of Fission, Salzburg, 1965, vol. 1 (IAEA, Vienna, 1965) 531.

[4] SIGNARBIEUX, C., RIBRAG, M., NIFENECKER, H., Nucl. Phys. A 99 (1967) 41.

[5] ASGHAR, M., CAÏTUCOLI, F., PERRIN, P., WAGEMANS, C., Nucl. Phys. A 311 (1978) 205

[6] LACHKAR, J., PATIN, Y., SIGAUD, J., J. Phys. Lett. 36 (1973) L 79

[7] NÖRENBERG, W., Proc. 2nd Symp. on Physics and Chemistry of Fission, Vienna, 1969, vol. 2 (IAEA, Vienna, 1969) 51.

[8] AMIEL, S., FELDSTEIN, H., IZAK-BRIAN, T., Phys. Rev. C 15 (1977) 109

[9] BRISSOT, R., CRANÇON, J., RISTOR, C., BOCQUET, J.P., MOUSSA, A., Nucl. Phys. A 282 (1977) 109.

[10] AMIEL, S., FELDSTEIN, H., Phys. Rev. C 11 (1975) 845.

[11] CLERC, H.G., LANG, W., WOHLFARTH, H., SCHMIDT, K.H., SCHRADER, H., PFERDEKÄMPER, K.E., JUNGMANN, R., Z. Phys. A 274 (1975) 203.

[12] WILKINS, B.D., STEINBERG, E.P., CHASMAN, R.R., Phys. Rev. C 14 (1976) 1832.

[13] NIFENECKER, H., SIGNARBIEUX, C., BABINET, R., POITOU, J., Proc. 3rd Symp. on Physics and Chemistry of Fission, Rochester, 1973, vol. 2 (IAEA, Vienna, 1974) 117.

[14] UNIK, J.P., private communication, quoted in ref. 12 .

[15] WOHLFARTH, H., Thesis, University of Darmstadt, 1976.

[16] UNIK, J.P., GINDLER, J.E., GLENDENIN, L.E., FLYNN, K.F., GORSKI, A., SJOBLOM, R.K., Proc. 3rd Symp. on Physics and Chemistry of Fission, Rochester, 1973, vol. 2 (IAEA, Vienna, 1974) 19.

[17] GUET, C., ASGHAR, M., PERRIN, P., SIGNARBIEUX, C., Nucl. Instr. and Methods, 150 (1978) 189.

[18] REISDORF, W.N., UNIK, J.P., GLENDENIN, L.E., Nucl. Phys. A 205 (1973) 348.

[19] WOHLFARTH, H., LANG, W., CLERC, H.G., SCHRADER, H., SCHMIDT, K.H., DANN, H., Phys. Lett. 63 B (1976) 275.

[20] ASGHAR, M., GUET, C., PERRIN, P., Nucl. Phys. A 298 (1978) 13.

[21] KHAN, T.A., HORSCH, F., Proc. 3rd Symp. on Physics and Chemistry of Fission, Rochester, 1973, vol. 2 (IAEA, Vienna, 1974) 257.

[22] LYNN, J.E., AERE-R 7468, AERE-Harwell (1974).

[23] SIGNARBIEUX, C. et al. (to be published).

DISCUSSION

M. MONTOYA: At Saclay we have simulated the thermal-neutron-induced fission of ^{235}U, ^{233}U and ^{239}Pu using a Monte-Carlo method. We have shown that $\bar{\nu}(M)$, $\bar{E}_K(M)$ and Y(M) curves produce structures in $\sigma\epsilon_k(\mu)$ curves. We have shown that $\bar{\epsilon}_K(\mu)$ and $Y(\mu)$ are very different from $\bar{E}_K(M)$ and Y(M) curves. Hence I think one should be extremely careful when analysing the quantities obtained by double energy without adequate correction.

D. HOFFMAN: Dr. Asghar, can you see the kinetic energy difference between fragments arising from spherical and from deformed shells? In the deformed case the energy would presumably be lower.

M. ASGHAR: The global mass distributions show structures due to the $N = 82$ (spherical shell) and $N \geqslant 60$ (deformed shell), and $N \approx 88$ (deformed shell) and $N = 50$ (spherical shell) for fissioning systems approximately up to plutonium. These configurations become more visible for fragments with high excitation energies. Furthermore, the $N \approx 88$ (heavy fragment) and $N \geqslant 60$ (light fragment) deformed shells show structures in the Y(M) of ^{243}Am and Cm isotopes, which will not show up at high fragment energies.

KINETIC-ENERGY DISTRIBUTION FOR SYMMETRIC FISSION OF ^{236}U†

R. BRISSOT*, J.P. BOCQUET*, C. RISTORI,
J. CRANÇON, C.R. GUET, H.A. NIFENECKER
Centre d'études nucléaires, Grenoble Cedex

M. MONTOYA
Centre d'études nucléaires,
Gif-sur-Yvette
France

Abstract

KINETIC-ENERGY DISTRIBUTION FOR SYMMETRIC FISSION OF ^{236}U.

Fission fragment kinetic-energy distributions have been measured at the Grenoble high-flux reactor with the Lohengrin facility. Spurious events were eliminated in the symmetric region by a coherence test based on a time-of-flight measurement of fragment velocities. A Monte-Carlo calculation is then performed to correct the experimental data for neutron evaporation. The difference between the most probable kinetic energy in symmetric fission and the fission in which the heavy fragment is 'magic' ($Z_H = 50$) is found to be $\cong$30 MeV. The results suggest that for the symmetric case the total excitation energy available at scission is shared equally among the fragments.

1. INTRODUCTION

A striking feature of the fission process is the fragments mass-asymmetry observed for low-energy fission of nuclei in the Actinides region. The liquid drop model cannot account for this result, which is commonly attributed to shell structure effects favoring, at an appropriate stage of the fission process, deformations deviating from reflection symmetry [1].

It is also well known that for fissioning nuclei close to Uranium, the kinetic energy release shows a pronounced dip near the symmetric mass division together with a greater number of evaporated neutrons. The absolute value of the energy difference between symmetric and asymmetric fission has been measured in several experiments [2,3,4] but the results are in conflict between each other. All these data are obtained by the double fragment kinetic energy method which suffers from a poor mass resolution (f.w.h.m $\gtrsim$ 3 - 4 a.m.u.) and for which the contamination by spurious high yields events is very difficult to overcome.

In the case of fissioning nuclei around the Actinium, the mass distribution shows triple humps and this feature is considered as an evidence for two different fission components : a symmetric fission behaving like a liquid drop and the asymmetric component which is considerably dominant for the Uranium fission.

† Experiments carried out at Institut Laue-Langevin, Grenoble, France.

* And USM/Grenoble, France.

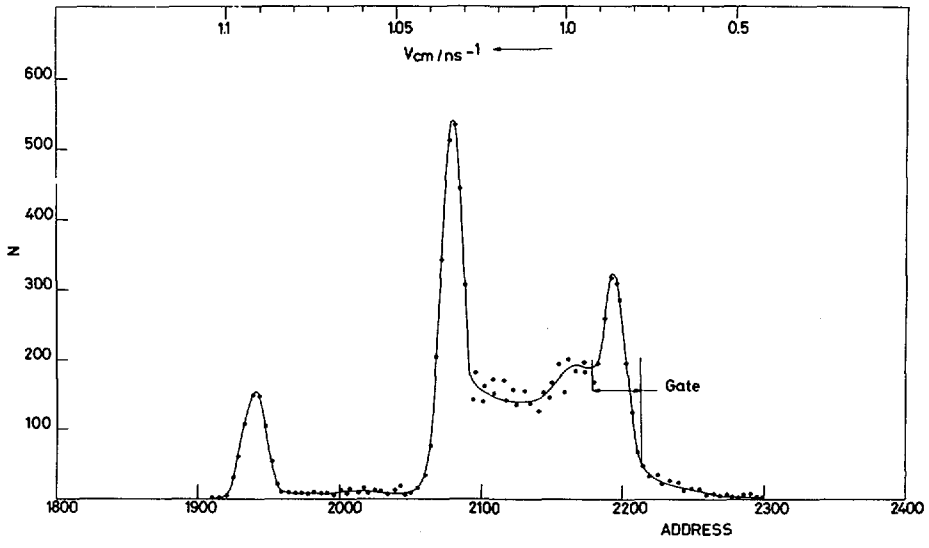

FIG.1. Time-of-flight or velocity spectrum measured for mass 118/19 at Lohengrin. The fragments with the normal speed (corresponding to the field settings) fall inside the gate and represent only a small fraction of the total spectrum.

There is still another open question for Uranium symmetric fission : do the nearly symmetric masses correspond or not to symmetric deformations of the two fragments ? In order to answer to such problems the kinetic energy distribution of masses around symmetry has been studied taking advantage of the high mass and energy resolution provided by the separator Lohengrin. Furthermore the width of the kinetic energy distributions, which is directly correlated to the distribution of the scission shapes, represents a very crucial test of changes in the scission configurations.

2. EXPERIMENTAL METHOD

2.1. Technical details

The separator Lohengrin (installed at the Institute Laue-Langevin) provides fission fragments of a given A/q (mass over ionic charge), at the collector of the instrument. Along the collector the fission fragments are distributed according to their velocity.

Unfortunately, the kinetic energy distribution measurement is not straightforward, when one is interested in low counting rate events, due to the fission fragments background of the instrument. The surroundings of the target are coated with uranium and thus emit fission fragments which are collected with a different velocity. This background becomes critical for the very low counting rates characteristic of symmetric fission in U^{236}.

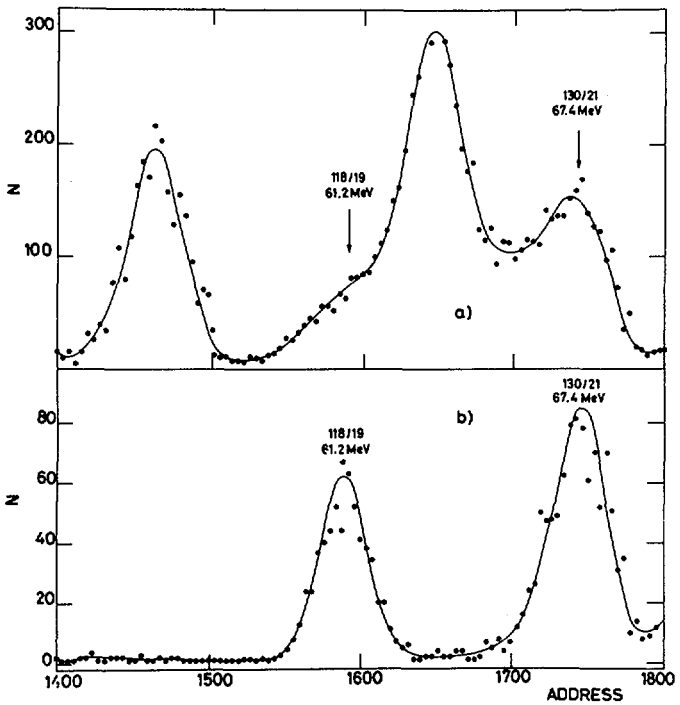

FIG.2. a) Ungated energy spectrum from the solid-state detector showing that the expected peak for mass 118/19 is completely hidden by the background;
b) energy spectrum gated by the time-of-flight (Fig.1) showing the expected peaks for masses 118/19 and 130/21 (nearly the same A/q).

In order to eliminate these spurious events, the speed of the fragments was analysed by a time-of-flight system. The secondary electrons emitted by a carbon-foil, located in the focal plane of the instrument, were collected on channel-plates, thus providing a very fast "start" signal (80 psec.). After a flight path of approximately 30 cm, the ions were stopped into a silicon surface barrier detector, which was giving the "stop" signal and the kinetic energy measurement of the fission fragment. The two parameters (time T and energy E) events are then recorded on a magnetic tape correlated to a M-20 (Intertechnique) data acquisition device. The final resolution of the time-of-flight was around 250 p.s. due to the geometrical arrangement of the carbon foil (45° angle with the beam direction). A typical time-of-flight spectrum is shown in Fig.1, for which the spurious events proportion is very large. The corresponding ungated energy spectrum is shown Fig.2 a) together with the same spectrum, b) gated by a time window. The expected peak for mass 118/19 which is completely hidden by the contamination in the ungated spectrum, shows up very unambiguously in the gated one. Some other peaks are present in the gated spectrum but they correspond to a normal interference from masses for which the A/q ratio is

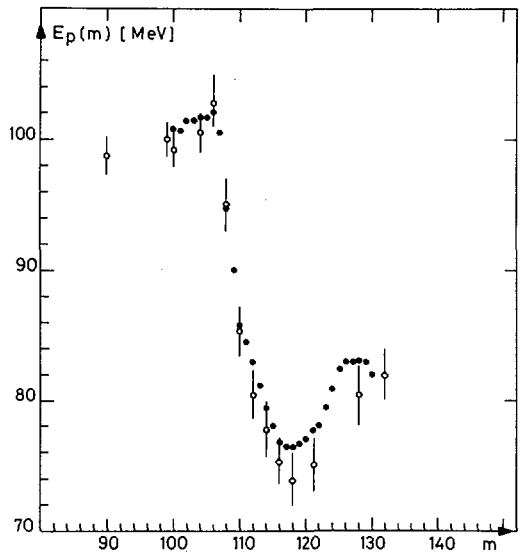

FIG.3. Most probable kinetic energy E_p as a function of the final mass m:
○ experimental data;
● Monte-Carlo simulation.

equal or very close to 118/19 (87/14, 93/15, 130/21). The correct assignment of all peaks present in the gated spectrum, represents a very good crosscheck of the efficiency of the background reduction.

2.2. Target thickness correction

The target thickness was 100 µg/cm² of UO_2, coated with a thin Tantalum film to slow down the burn up of the target. The average energy loss in the target, together with the dispersion of the distribution have been measured for two approximately complementary (90-144) (high yield masses). The energy loss and dispersion corrections can thus be tested with the conservation laws. The measurements of Wohlfarth [5] at Lohengrin have been used to calculate the average energy loss : 4 ± 1 MeV. This result can reasonably [6] be considered as independent of the charge and energy at least for the values characterizing the fission products. The dispersion introduced by this energy loss corresponds to an additional variance of 6 MeV² for mass 144. This variance depends upon the mass and energy according to the law :

$$\sigma^2_{target}(Ai) \approx \sigma^2_{target}(144) \times \frac{E(Ai)}{E(144)}$$

and the true variance σ^2_{th} of a given mass Ai is calculated from the measured one σ^2_{exp} by the relationship :

$$\sigma^2_{th}(Ai) = \sigma^2_{exp}(Ai) - \sigma^2_{target}(Ai)$$

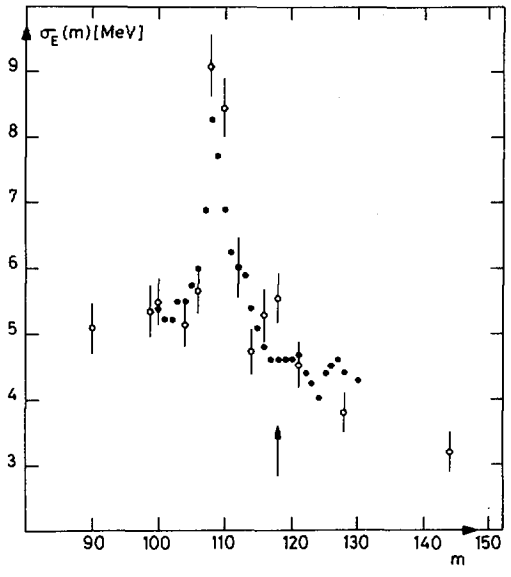

FIG.4. Root-mean-square width of kinetic energy distribution as measured at Lohengrin (m represents the final mass). Notice the strong increase of σ for m = 108.
○ *experimental data;*
● *Monte-Carlo simulation.*

3. EXPERIMENTAL RESULTS

3.1. Most probable kinetic energy and distribution variances

The most probable kinetic energy E_p is plotted in Fig.3 as a function of the mass m of the final fragment (these experimental values are not corrected for the neutrons evaporation). Two striking features emerge from these results :
- the sudden fall of the most probable kinetic energy when going towards symmetry.
- the low energy obtained for symmetric masses.

The root-mean square width σ of the kinetic energy distributions are indicated in Fig.4 as a function of m. The average value of σ for symmetric fission is 5.3 MeV, but very large values have been obtained for masses 108-110, corresponding to fwhm values around 20-22 MeV.

3.2. Monte-Carlo simulation

If one wants to deal with the initial values of the measured quantities (mass, energy, variance), the neutron evaporation must be taken into account. Therefore the neutron evaporation has been simulated using a Monte-Carlo code, in order to compare our results to other measurements (obtained by a double energy method for instance), for which the effect of

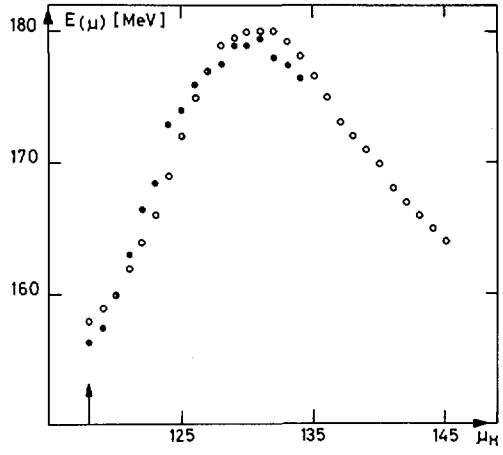

FIG.5. Most probable kinetic energy as a function of the pseudo-mass. The experimental data are taken from Ref.[3].
○ *experimental data;*
● *Monte-Carlo simulation.*

neutron evaporation might be completely different. The data inputs used for the simulation were as follow :
- the total kinetic energy of both fragments as a function of their initial masses : $E_T(M_1,M_2) = E_1 + E_2$
- the dependence of the root-mean square width $\sigma_{E_T}(M_1,M_2)$ with initial mass.
- the average number of evaporated neutrons as a function of initial mass [7]
- the primary yields for the initial masse Y(M).

The results of the procedure was then written on a magnetic tape event by event, each of them beeing characterized by :
- initial masses and total energy : M_1, M_2, E_T
- final masses and energies : m_1, m_2, ε_1, ε_2

In a first step, the simulated events have been selected according to their final masses, in order to check the compatibility of the imput data with the energy distribution of final masses as measured at Lohengrin. During a second step, the data analysis procedure which is commonly used in the double energy method [7] has been applied to the simulated events. Thus for a fission event simulated with masses M_1, M_2 and final energies ε_1, ε_2 the pseudo-masses μ_1 and μ_2 are calculated by : $\varepsilon_1 \mu_1 = \varepsilon_2 \mu_2$ ($\mu_1 + \mu_2 = 236$).

Finally the simulation is considered to be satisfactory when the initial energy distribution $E_T(M_1,M_2)$ reproduces at one and the same time the experimental results obtained at Lohengrin, those resulting from the double energy method and the final masses distribution y(m).

The agreement of the Monte-Carlo simulation with the distribution of energy measured at Lohengrin is shown in Fig.3 and with the recent results of Asghar and al. [8,9] in Fig.5 (double energy method). To perform this last comparison the correction for the resolution of the

detector had to be introduced at the end of the simulation since it was affecting the slope of the experimental curve. The difference between simulation and experience remains in all cases smaller than 2MeV for total energy.

Another interesting point is the peak observed in the final σ_E values obtained at Lohengrin, for masses 108-110 (Fig.4). The simulation reproduces the peak although the initial dependence $\sigma_{ET}(M_1,M_2)$ was a smooth curve. This sudden rise of the final width of the kinetic energy distribution is then originating exclusively from the neutron evaporation process. The region around masses 108-110 is indeed characterized by :
- a sudden fall of the kinetic energy with mass number,
- a large number of evaporated neutrons. Therefore a given final mass m results from several contributions of initial masses M, M+1, M+2, M+3, each of them corresponding to a very different value of the most probable kinetic energy, thus broadening considerably the final distribution.

3.3. Total kinetic energy

For a given mass division the total kinetic energy $E_T(M_1,M_2)$, necessary to calculate the total excitation energy, has been obtained from the simulation, together with the variance σ_{ET}, as described in the preceding section. The dependence of $E_T(M_1,M_2)$ and σ_{ET} with the heavy fragment mass is represented in Fig.6 (full circles). For comparison the total kinetic energy as deduced directly from the measurement of the final energy of the light fragment (open circles) and of the heavy ones (open triangles) are also indicated. As a matter of fact the total energy is commonly calculated by the relationship :

$$E_T(m_H + \nu(m_H)) = \epsilon_H \left(1 + \frac{\nu_H}{m_L}\right) \frac{M_0}{m_0 - m_H - \nu_H} \qquad (1)$$

and a similar one for the light fragment.

As can be seen in Fig.6 these last evaluations do not agree with each other, the main discrepancy arising around mass 129 (about 10 MeV of energy difference). The reason for these differences can be understood easily : the final mass 128 is located in a region where the mass yield is increasing very rapidly, therefore the initial masses 129 and 130 will contribute significantly to the final mass 128. It is necessary that masses 129 and 130 evaporate respectively one and two neutrons, though their most probable excitation correspond to about 0.3 neutron evaporated in the average. Thus the fragments of mass 129 and 130 which contribute to mass 128 will have an excitation energy higher than the average. The kinetic energy measured for the final mass 128 is then lower than the average due to the important contribution of masses 129 and 130. The same effect works in the opposite direction for the final mass 106 to which, due to their very low yields, masses 107 and 108 contribute very little. The events of mass 106 which do not evaporate neutrons correspond, thus, to lower than the average excitation energy or ligher kinetic energy. Therefore, equation (1) cannot be used in those regions where the mass yields vary rapidly; it would lead to an underestimation of the total energy if the heavy mass energy is used and the contrary for the light mass.

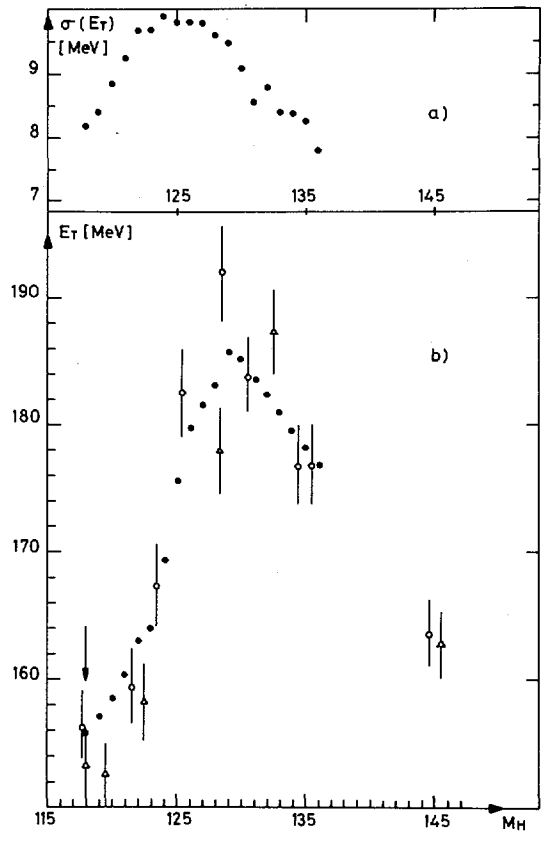

FIG.6. a) The root-mean-square widths of the total kinetic energy introduced into the Monte-Carlo simulation.
b) Total pre-neutron kinetic energy E_T as a function of heavy-fragment mass. The vertical arrow indicates symmetric fission.
○ *E_T calculated from the light fragment kinetic energy measurement (relation (1));*
Δ *E_T calculated from the heavy-fragment kinetic energy;*
● *initial values of the Monte-Carlo simulation.*

4. DISCUSSION

4.1. Evidence for symmetrical shapes in symmetrical fission

The absolute value of the dip in the total kinetic energy was until now estimated to 22 MeV [8,9]. The result of the Monte-Carlo simulation corresponds to a $\Delta E = 30 \pm 4$ MeV difference between the total energy for the mass 129 and for the mass 118. This apparent discrepancy, can be attributed for an important part to mass resolution effects which lower the maximum around mass 129 and raise the minimum at symmetry.

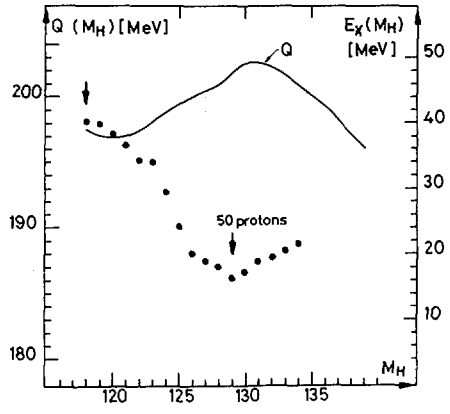

FIG.7. Energy release Q and total excitation energy of the two fragments E_x.

Nevertheless the kinetic energy for asymmetric fission is very low indicating a symmetrical share of the excitation energy among the fragments. This assumption is supported as follows :

The observed kinetic energy corresponds to a distance of 19.5 fm between the fragment centers at scission (assuming punctual charges and a purely Coulombian energy), therefore each fragment should have a deformation corresponding to $\beta \geq 0.8$. As the spherical radius for mass 118 is only around 6.5 fm, thus it seems unrealistic to attribute the whole deformation to one fragment alone.

Another point leads to the same conclusion : the values of σ_{ET} (Fig.6) are maximum around masses 124-125, corresponding to the maximum change of the kinetic energy with mass. This mass region represents then a shape transition from the asymmetric region around mass 129 to the symmetric shapes around mass 118 and the large distribution of shapes explains the maximum of σ_{ET}.

4.2. Excitation energy : influence of the 50 protons shell

The total excitation energy Ex corresponding to a given fission event can be deduced from the total energy release by :

$$Ex = Q - E_T \text{ (kinetic)}$$

The result of this calculation (Fig.7) shows a very large value ($\sim$ 40 MeV) for the excitation energy of symmetric fission, in agreement with the estimated value of Wahl [7] for the number of neutrons evaporated at symetry ($\nu_T(118) \geq 4$).

The minimum value for the excitation energy is obtained at mass 129 rather than mass 132, in coincidence with the 50 protons shell in the heavy fragment (the influence of the 82 neutrons shell would occur around mass 134). The lack of completion of the 50 protons shell is also responsible for the sudden fall in the kinetic energy around mass 106 (Fig.3), since for masses higher than 106 the complementary fragment is no longer spherical.

5. CONCLUSIONS

The kinetic energy distributions for symmetric fission, together with the simulation of the neutron evaporation process lead to the following conclusions.

The kinetic energy dip for symmetric fission is larger than previously measured ($\Delta E \sim 30$ MeV).

The mass dependence of the kinetic energy exhibits a very sharp fall near symmetric fission.

The Monte-Carlo calculation can explain the peak in the widths of the experimental distributions measured at Lohengrin and has shown that it was not possible to calculate in a straightforward manner the initial kinetic energy (see section 3.3.). This work has also shown the strong influence of the 50 protons shell in the kinetic energy distributions.

Finally, the assertion that symmetric fission corresponds to a symmetric share of the excitation energy seems reasonable and could be strongly supported if one could measure an isotopic distribution in the neighbourhood of charge 46.

We are grateful to P. Bisenius, M. Bolore, J. Girard, R. Joly, C. Mazur, M. Ribrag, C. Signarbieux (DPh-N/MF, Saclay), for their help in the initial stage of the experiment.

REFERENCES

[1] MUSTAFA, M.G., MOSEL, U., SCHMITT, H.W., Phys. Rev. C4 (1971) 2185.
[2] UNIK, J.P., GINDLER, J.E., GLENDENIN, L.E., FLYNN, K.F., GORSKI, A., SJOBLOM, R.K., Proc. 3rd Symp. on Physics and Chemistry of Fission; Rochester, 1973, Vol.2 (IAEA, Vienna, 1974) p. 19.
[3] ASGHAR, M., D'HONDT, P., GUET, C., PERRIN, P., WAGEMANS, C., Nucl. Phys. A292 (1977), P. 225.
[4] SCHMITT, H.W., NEILER, J.H., WALTER, F.J., Phys. Rev. 141 (1966) p.1146.
[5] WOHLFARTH, H., Dissertation Darmstadt, 1976.
[6] NORTHCLIFFE, L.C., SCHILLING, R.F., Nucl. Data A7 (1970) 3-4.
[7] WAHL, A.C., NORRIS, A.E., ROUSE, R.A., WILLIAMS, J.C., Vienne 1969, IAEA-SM-122/116.
[8] SIGNARBIEUX, C., RIBRAG, M., NIFENECKER, H., Nucl. Phys. A99(1967) p.41.
[9] ASGHAR, M., CAITUCOLI, F., PERRIN, P., WAGEMANS, C., Nucl. Phys. A311 (1978), p. 205.

DISCUSSION

H.G. CLERC: I am glad to see that, according to your data, the Z = 50 shell produces the largest average total fragment kinetic energy. This tallies well with the data given in the paper which I presented today (see SM-241/F2 of these Proceedings).

My question is, which isobaric Z distribution did you assume in order to be able to calculate the Q value and average fragment excitation energies?

R. BRISSOT: The mass values A_L and A_H result from the superposition of different Z values close to the 2p value of the charge distribution. Hence to obtain the most probable Q value for a given mass split we have to obtain a weighted average of the masses of the different elements on the basis of their estimated independent yields.

M. ASGHAR: Do you consider that E_k around mass 130 can be reduced by more than 5 MeV merely by resolution effects? Furthermore, do you feel that the ^{235}U Monte-Carlo calculations can explain the $\sigma_{E_K}(\mu_H)$ results for other nuclei, such as ^{241}Am, ^{243}Am or ^{245}Cm?

M. MONTOYA: E_k is reduced not only by the energy resolution effect but also by the Y(M), ν(M) and E_K(M) curve effects.

We have carried out Monte-Carlo calculations for ^{233}U, ^{235}U, ^{239}U and ^{252}Cf. For these nuclei the results can explain the $\sigma_{E_K}(\mu_H)$ curves. I feel that we can also explain the $\sigma_{E_k}(\mu)$ results for other nuclei.

H.A. NIFENECKER: Further to this question, I should point out that mass resolution effects not only attenuate peaks in the average kinetic energy curve, but also interfere in events with masses corresponding to low kinetic energy but high yields. This is why the difference in maximum average kinetic energy amounts to 5 MeV in the Monte-Carlo calculation and the double energy measurement.

H.J. SPECHT: The surprising fact that we have come back to a difference of 30 MeV kinetic energy between the symmetric and highly asymmetric fission of ^{236}U should delight Dr. Fraser and Dr. Milton at Chalk River. Their early double-velocity experiments yielded a figure of that order, but it fell into disfavour after the semi-conductor detector groups had discussed the point at great length during the Salzburg Symposium in 1965 and concluded that the figure was an overestimate.

P. ARMBRUSTER *(Chairman)*: Dr. Brissot, what is the accuracy of the procedure used to relate primary and secondary masses?

R. BRISSOT: I think that Dr. Montoya can best answer that question.

M. MONTOYA: The accuracy depends on the number of neutrons emitted and the Y(M) shapes. So it is not the same in all mass regions. In the region of most probable mass the figure is ~ 0.5 mass units.

There is, however, a general comment I would like to make. The Monte-Carlo calculations performed at Saclay (MONTOYA, M., SIGNARBIEUX, C., DAKOWSKI, N., to be published.) and presented by Dr. Brissot require, as the input data, the total energy E_K, mass yield Y, neutron multiplicity $\bar{\nu}$ and assumed energy dispersion σ_{E_K} as functions of the primary mass M. The results of subsequent neutron evaporation are not very sensitive to the details of σ_{E_K}. We have shown that for different fissioning nuclei, even those with a constant σ_{E_K} (M), the interplay of input functions is such that we produce high peaks and valleys in σ_{E_K} selected as a function of pseudo-masses μ or secondary masses m.

These peaks should not be confused, on account of neutron evaporation, with possible peaks indicating shell effects.

M. ASGHAR: In view of the fact that your experimental data show E_k as derived from E_L and E_H to be quite different, I should like to ask Dr. Clerc, who obtained E_K from only the E_L experimental values, how they would be altered by this difference.

H:G. CLERC: The different average TKE values obtained by Dr. Brissot for E_L and E_H may mean that the average neutron numbers $\bar{\nu}_L$ and $\bar{\nu}_H$ emitted per fission product and used to calculate the TKE are not quite correct.

POSSIBLE VISCOSITY EFFECTS IN NEUTRON-INDUCED FISSION OF ^{232}Th AND ^{238}U*

J.E. GINDLER, L.E. GLENDENIN, B.D. WILKINS
Chemistry Division, Argonne National Laboratory,
South Cass Avenue, Argonne, Illinois,
United States of America

Abstract

POSSIBLE VISCOSITY EFFECTS IN NEUTRON-INDUCED FISSION OF ^{232}Th AND ^{238}U.

Fission yields induced in the ^{238}U(n,f) and ^{232}Th(n,f) reactions have been determined as functions of the incident neutron energy (E_n). The ratio of ^{115}Cd-to-^{140}Ba yields as a function of E_n is analysed in the present paper by means of the equation $Y_1/Y_2 = \exp[2\ a_1(E_n + E_1)^{1/2} - 2\ a_2(E_n + E_2)^{1/2}]$ to give values of a_i, the level density parameter, and E_i, the excitation energy for $E_n = 0$. The energies E_i are interpreted on the basis of the liquid-drop model with shell and pairing corrections. Values are deduced for the energy dissipated by viscosity effects in the descent from the saddle point to the point where masses are fixed in the fissioning nucleus. These values are 1.7 MeV for ^{232}Th(n,f) and 4.8 MeV for ^{238}U(n,f). These values are consistent with the experimental observation that $\bar{\nu}_p$ is ~0.6 neutron greater for ^{239}U fission than for ^{233}Th fission and that strong odd-even (nucleon pairing) effects are found in the fragment total-kinetic-energy distribution for ^{230}Th fission but not for ^{234}U fission. The low dissipation energy values together with the low values of pre-scission kinetic energy and compact shapes deduced by Guet et al. [Nucl. Phys. A134(1971) 1] indicate a shorter path from the saddle point of the fissioning nucleus to scission than is generally assumed in theoretical calculations.

1. INTRODUCTION

One of the most perplexing problems in fission today is the degree of adiabaticity in the descent of the nucleus from the saddle point to scission. That is, how much of the potential energy release from saddle to scission appears as nuclear dissipation energy and how much appears as pre-scission kinetic energy? Dynamic calculations [1-3] give a wide range of values for the two energies depending on the initial assumptions made concerning the dissipation mechanism, i.e., two-body viscosity, one-body viscosity, etc. The problem remains since the scission configuration cannot be uniquely determined from experimental measurements of total kinetic energy and excitation energy which are measured at essentially infinite distances between the fragments.

Another experiment that in principle should provide information on the amount of energy dissipated is the measurement of near-symmetric fission yields as a function of incident neutron energy (E_n). Analyses of such yields have been made previously but with different objectives: to measure the effect of angular momentum [4], the effect of excitation

* Work performed under the auspices of the Office of Basic Energy Sciences of the US Department of Energy.

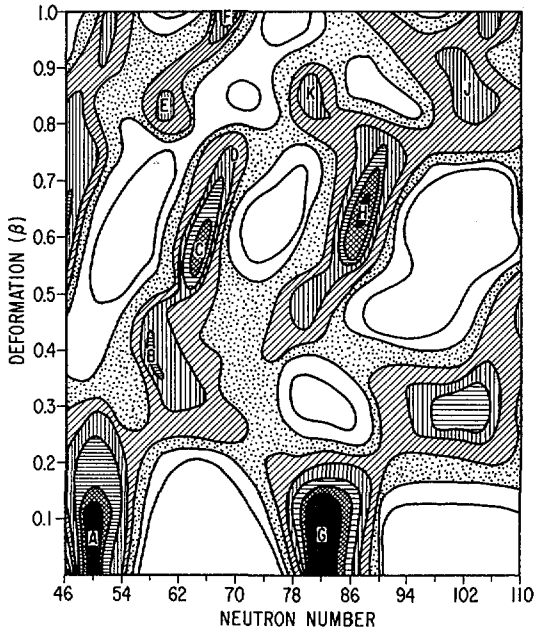

FIG.1. Neutron-shell corrections calculated as a function of β-deformation and neutron number. The β-parameter is defined in terms of the semi-major (c) and semi-minor (a) axes of a prolate spheroid with $c = kr_0A^{1/3}(1+2\beta/3)$ *and* $a = kr_0A^{1/3}(1-\beta/3)$*, where k is a volume conservation factor. The contours are plotted as 1-MeV intervals with the black regions (representing the strongest shells) containing all values less than −4 MeV and the inner white region (representing the weakest shell corrections) containing all values greater than +2 MeV. From Ref.*[10].

energy [5], or the effect of the level density parameter [5,6]. The measurement of such yields is part of a broader program to determine the post-neutron-emission mass distributions for fissile and fertile nuclides as a function of E_n underway at Argonne National Laboratory for the past several years. Experimental results are presently available for ^{238}U(n,f) [7,8] and ^{232}Th(n,f) [9] with neutron energies from 1.5 to 8 MeV.

In view of the success of the quasistatistical scission-point model of fission [10] in interpreting mass and total kinetic energy (TKE) distributions for a wide variety of fissioning systems, it is proposed that the variation of the near-symmetric fission yields for ^{239}U and ^{233}Th compound nuclei be explained in terms of such a model. It is assumed that fission masses are fixed at some point between the saddle and scission points and that a quasistatistical equilibrium is attained at this point. Assuming the level density to be described by a Fermi gas, the density of excited states to which the fission yield is related is given by [11]

$$N = k(E^*)\ \exp(2\sqrt{aE^*}) \qquad (1)$$

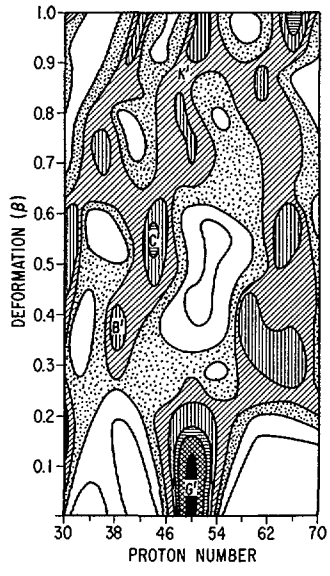

FIG.2. Proton-shell corrections calculated as a function of β-deformation and proton number. Contour strengths are described in the caption for Fig.1. From Ref.[10].

where E* is the excitation energy at the point where masses are fixed and a is the level density parameter. The ratio of two fission yields is then

$$Y_1/Y_2 = (k_1(E_1^*)/k_2(E_2^*))\ \exp(2\sqrt{a_1 E_1^*} - 2\sqrt{a_2 E_2^*}) \qquad (2)$$

The use of Eq. (2), which is also that used by Fong [11] in his statistical approach to nuclear fission, does not necessarily imply a situation of complete damping in the descent of the nucleus from the saddle to the point at which masses are final. Rather, it is assumed that a weak coupling exists between collective and intrinsic states as described by Nörenberg [12].

The excitation energy E_i^* is defined as

$$E_i^* = E_n + B_n - B_f - E_{LDi} + E_{DIS} + \Delta E_{SPi}\ \exp[-(T_i/T_o)^2] \qquad (3)$$

The first three terms are respectively the kinetic energy of the neutron, its binding energy in the compound nucleus, and the fission barrier height of the compound nucleus. All of these terms are known for ^{239}U and ^{233}Th [13]. The liquid drop term E_{LDi} is the energy required to form a pair of fragments other than the symmetric pair since the latter is the favored configuration in the liquid drop model. The value of this term is obtained from liquid drop calculations. The quantity E_{DIS} represents the unknown amount of dissipation energy at the point where masses are determined. The ΔE_{SPi} term includes the microscopic single-particle corrections for shell and pairing effects. The magnitude of the shell correction determined in the scission-point model of fission is shown for neutrons in Fig. 1 and for protons in Fig. 2 [10]. Although these corrections

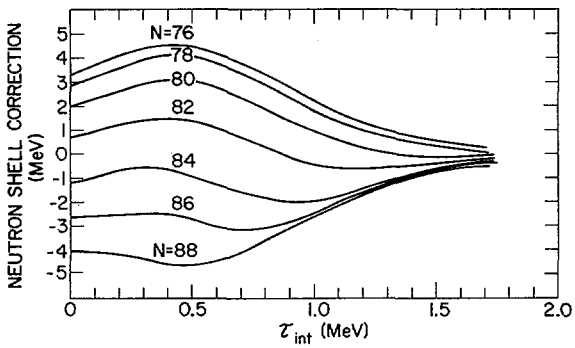

FIG.3. Neutron-shell corrections at fixed deformation ($\beta = 0.65$) calculated as a function of the temperature of the nucleus. From Ref.[10].

are for independent fragments, they are comparable to the single-particle shell corrections obtained with the two-center model [14]. The shell corrections shown in Figs. 1 and 2 are for $E_i^*=0$. The variation of the shell correction with intrinsic temperature of the nucleus is shown in Fig. 3 for neutrons at a fixed (0.65) β-deformation [10]. These functions were calculated with the approximation described by Jensen and Damgaard [15]. The more simplified temperature dependence, $\exp[-(T_i/T_o)^2]$, given in Eq. (3) is one suggested by Ziegenhain, et al., [16]. In this expression $T = (E_i^*/a_i)^{\frac{1}{2}}$ and $T_o = 1.5$ MeV. Although the pairing correction exhibits a different temperature dependence [17] than do the shell corrections, the latter are generally larger in magnitude. Therefore, since one will not be able to distinguish between pairing and shell corrections, the temperature dependence suitable for the latter is applied.

Because of the temperature (or E_i^*) dependence of $\Delta E_{SPi}(T)$ and its unknown relationship with E_n, the excitation energy E_i^* as defined in Eq. (3) is some convoluted function of itself. Therefore, a series of equations of the form of Eq. (2) cannot be solved explicitly for E_i^*. If, however, $\Delta E_{SPi}(T)$ varies slowly over the E_n range of the analysis, then a least-squares fit to the data should yield reasonable values of E_i^* and, consequently, E_{DIS}. In the present paper we have assumed this slow variation and that the values of $\Delta E_{SPi}(T)$ obtained are most relevant to the mid-point of the E_n range or ∿4.5 MeV.

2. EXPERIMENT

The experimental method is described more completely in Ref. [7]. Metallic foils of thorium or uranium were irradiated with essentially monoenergetic neutrons produced by the $^7Li(p,n)^7Be$ or $^2H(d,n)^3He$ reactions. The induced fission product activities were analyzed by means of γ-ray spectrometry or radiochemical techniques. After applying appropriate corrections for chemical yield or γ-ray abundance, detection efficiency, decay, genetic relationships, and degree of saturation, absolute yields were calculated by normalizing the resulting mass distributions to 200% total yield.

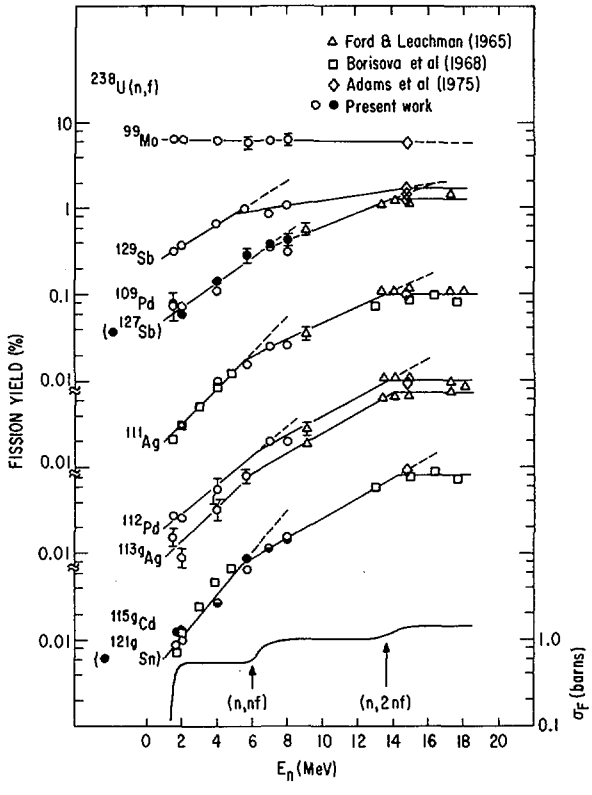

FIG.4. Fission yields and cross-section σ_F for fission of ^{238}U by monoenergetic neutrons as a function of neutron energy. From Ref.[7].

The results of these measurements for near-symmetric fission masses are shown in Fig. 4 for ^{239}U and in Fig. 5 for ^{233}Th. The results of Ford and Leachman [4], Borisova, et al., [5] and Adams, et al., [18] are also shown in Fig. 4. The results of Turkevich, Niday and Tompkins [19], Ford and Leachman [4] and Dubrovina, et al., [6] are also shown in Fig. 5. An average value of the 14-MeV neutron yields given by Crouch [20] and Meek and Rider [21] is plotted in Fig. 5.

The yields (Y) of the near-symmetric fission masses increase rapidly with E_n for both ^{239}U and ^{233}Th with those for ^{233}Th increasing more rapidly initially. The onset of second-chance fission in ^{239}U is marked by a pronounced change in slope of the Y vs. E_n curves and perhaps by a slight dip. In ^{233}Th a definite dip occurs at those energies where second-chance fission becomes possible. The onset of third-chance fission in both fissioning systems is marked by another change in slope of the Y vs. E_n curves. In Fig. 6 the Y vs. E_n curves of the valley fission product ^{115}Cd are compared for both ^{233}Th and ^{239}U.

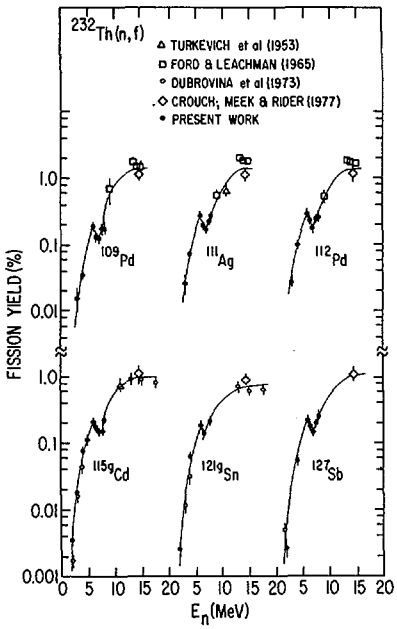

FIG.5. Fission yields of near-symmetric masses for fission of ^{232}Th by monoenergetic neutrons as a function of neutron energy.

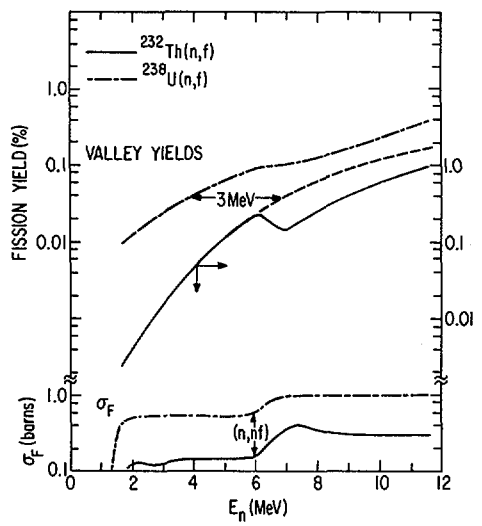

FIG.6. Fission yield of the valley fission product ^{115}Cd and the fission cross-section σ_F as a function of neutron energy for $^{232}Th(n,f)$ and $^{238}U(n,f)$. The dashed curve (- - - -) represents the first-chance fission yield of ^{115}Cd for $^{232}Th(n,f)$ calculated for $E_n > 6$ MeV.

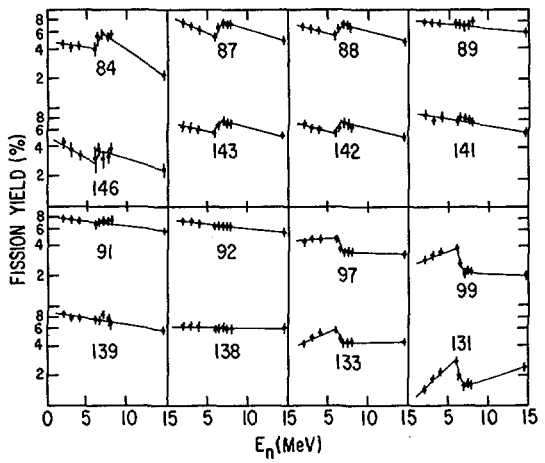

FIG. 7. Fission yields of asymmetric masses for fission of ^{232}Th by monoenergetic neutrons as a function of neutron energy. The yields of complementary masses are shown assuming three neutrons are emitted per fission event.

In contrast to the near-symmetric fission mass yields, those of asymmetric masses near the peaks in the mass distribution decrease slightly with increasing E_n for ^{239}U. This is shown for ^{99}Mo in Fig. 4. The yield behavior with E_n of the corresponding masses for ^{233}Th is more complex as seen in Fig. 7. This shows that the yields of masses more asymmetric than the peak-yield masses increase sharply at the onset of second-chance fission; whereas the yields of more symmetric masses decrease sharply.

3. ANALYSIS

In analyzing the data, first-chance fission yields were calculated for neutron energies at which both first- and second-chance fission could occur. This was done by use of the measured fission cross sections (σ_F) for ^{233}Th [22] and ^{239}U [23] as shown in Fig. 6. The measured yields at these energies may be written as

$$Y(E_n) = \frac{\sigma_{F-I}}{\sigma_F} Y_I(E_n) + \frac{\sigma_{F-II}}{\sigma_F} Y_{II}(E_n-\varepsilon_n) \quad (4)$$

where the subscripts I and II refer respectively to first- and second-chance fission. The second-chance fission yield Y_{II} is evaluated in the first-chance fission energy region $(E_n-\varepsilon_n)$, where ε_n ($\sim$6 MeV) is the sum of the binding energy and kinetic energy of a neutron emitted from the compound ^{233}Th or ^{239}U nucleus prior to fission. This analysis assumes that the fission yield from an excited ^{232}Th or ^{238}U nucleus is the same as that from an excited ^{233}Th or ^{239}U nucleus at the same incident neutron energy, $(E_n-\varepsilon_n)$. Values of σ_{F-I} were obtained by extrapolating horizontally the fission cross section σ_F vs. E_n curve just prior to the onset of

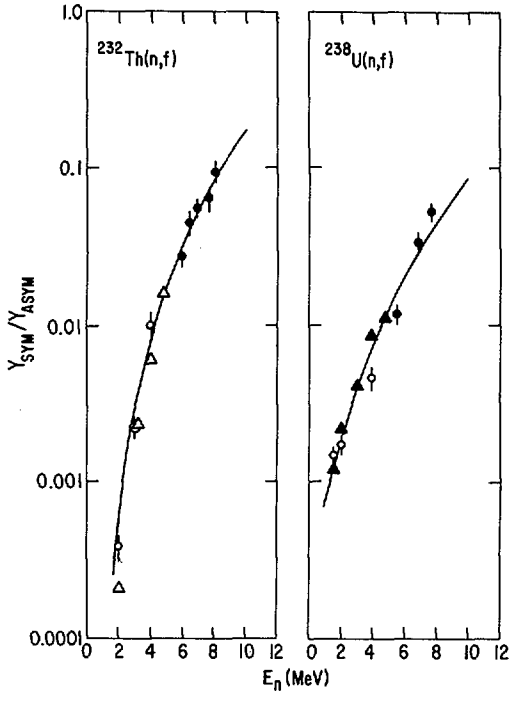

FIG.8. Ratio of symmetric-to-asymmetric yields for first-chance fission of ^{233}Th and ^{239}U as a function of neutron energy. Circles are present data and represent the ratio of ^{115}Cd-to-^{140}Ba yields. Open circles are for yields measured in the energy region for which only first-chance fission occurs. Solid circles are for yields deduced by the method described in the text. Open triangles are the data of Ref.[6] and represent the ratio of ^{115}Cd-to-^{89}Sr yields. Solid triangles are the data of Ref.[5] and represent the ratio of ^{115}Cd-to-$\frac{1}{2}(^{99}Mo + ^{140}Ba)$ yields. The solid curves are fits to the present data by means of Eq.(5).

second-chance fission. This gives values of 0.14 barn for ^{233}Th and 0.56 barn for ^{239}U. Such a procedure is fairly straightforward for ^{239}U since the fission cross section curve is a fairly flat plateau in the energy region where only first-chance fission occurs. However, the fission cross section curve for ^{233}Th exhibits some structure in the energy region for which only first-chance fission occurs. There is, therefore, some ambiguity associated with the value of 0.14 barn used for σ_{F-I}. Values of σ_{F-II} were deduced by subtracting σ_{F-I} from σ_F. Values of Y_I were then calculated by substituting the above quantities into Eq. (4). The dashed curve in Fig. 6 indicates the calculated first-chance ^{115}Cd yield for ^{233}Th.

The ratio of ^{115}Cd-to-^{140}Ba yields for first-chance fission of the thorium and uranium systems are shown as circles in Fig. 8. Open circles are the result of measured first-chance fission yields. Solid circles are the result of first-chance fission yields deduced by means of Eq. (4).

TABLE I. PARAMETERS OBTAINED FOR Eq.(5) IN ITS FIT TO FIRST-CHANCE FISSION DATA

Parameter	^{232}Th(n,f)	^{238}U(n,f)
c_1	9.59 amu/MeV	9.59 amu/MeV
c_2	11.35 amu/MeV	11.35 amu/MeV
$a_1=A_f/c_1$	24.3 MeV^{-1}	24.9 MeV^{-1}
$a_2=A_f/c_2$	20.5 MeV^{-1}	21.0 MeV^{-1}
E_1	-0.5 MeV	2.4 MeV
E_2	2.6 MeV	6.8 MeV

For comparison the results of Dubrovina, et al., [6] for ^{115}Cd-to-^{89}Sr yields are given as open triangles for ^{233}Th. The results of Borisova, et al., [5] for ^{115}Cd-to-½(^{99}Mo + ^{140}Ba) yields are given as solid triangles for ^{239}U. Since the ratio of ^{140}Ba-to-^{89}Sr yields averages 1.15 in the region where only first-chance fission occurs for ^{232}Th [6] and the ratio of ^{99}Mo-to-^{140}Ba yields averages 1.13 in the corresponding region for ^{238}U [5], the present data are seen to agree very well with the data of Refs. 5 and 6.

Although Eq. (2) applies to yields of pre-neutron-emission fission fragments, it is assumed that the yields of the post-neutron-emission fission products ^{115}Cd and ^{140}Ba represent well the yields of pre-neutron-emission progenitors which are assumed for simplicity to be respectively ^{117}Rh and ^{141}Xe. The respective complements of these fragments are ^{116}Rh and ^{92}Kr for ^{232}Th(n,f) and ^{122}Ag and ^{98}Sr for ^{238}U(n,f).

In applying Eq. (2) to the data shown in Fig. 8 it was assumed that the pre-exponential factor $k_1(E_1^*)/k_2(E_2^*)$ was equal to one. The level density parameter was defined as $a_i=A_f/c_i$, where A_f is the mass of the fissioning nucleus, and c_i is a constant $\approx$10. The values of c_i were constrained to be the same for both ^{233}Th and ^{239}U. This is reasonable since, for ^{141}Xe (the ^{140}Ba progenitor), the shell effects are the same for both fissioning systems (point H in Fig. 1) and the complementary fragments are found at a β-deformation of 0.4 (near point B in Fig. 1) [10]. Similarly, for ^{117}Rh (the ^{115}Cd progenitor), the shell effects are the same for both fissioning systems at a β-deformation of 0.7, and the complementary fragments are found at the same deformation (to the right of point D in Fig. 1). The larger deformations for the near-symmetric fission fragments is indicated by the dip in the total kinetic energy near symmetry observed in the fission of both ^{232}Th [24] and ^{238}U [25,26] by energetic neutrons, assuming a small pre-scission kinetic energy. Re-writing E_i^* as $E_n + E_i$, Eq. (2) then becomes

$$Y_1/Y_2 = \exp\left[2\left((A_f/c_1)\cdot(E_n+E_1)\right)^{1/2} - 2\left((A_f/c_2)\cdot(E_n+E_2)\right)^{1/2}\right] \qquad (5)$$

TABLE II. ENERGIES USED IN Eq.(6)

Energy	^{232}Th(n,f) (MeV)	^{238}U(n,f) (MeV)
B_n	4.955[a]	4.783[a]
B_f	6.44[b]	6.15[b]
E_{LD1}	0.01[c]	0.06[e]
E_{LD2}	2.72[d]	1.91[f]
E_1[g]	-0.5	2.4
E_2[g]	2.6	6.8
$E_{DIS}-\Delta E_{SP1}(T)$[h]	0.995	3.83
$E_{DIS}-\Delta E_{SP2}(T)$[h]	6.805	10.08
$\Delta E_{SP1}(T)-\Delta E_{SP2}(T)$[i]	5.81	6.25
$\Delta E_{SP1}(T)$[j]	.69	1.19
$\Delta E_{SP2}(T)$[j]	-5.62	-7.78
$\Delta E_{SP1}(T)-\Delta E_{SP2}(T)$[k]	6.31	8.97

[a] Values determined from experimental masses given in Ref. [13].

[b] Experimental values given in Table II of Ref. [13].

[c] Calculated for a 117/116 mass split in ^{233}Th.

[d] Calculated for a 141/92 mass split in ^{233}Th.

[e] Calculated for a 122/117 mass split in ^{239}U.

[f] Calculated for a 141/98 mass split in ^{239}U.

[g] Values from the present work assumed valid for $E_n \approx$ 4.5 MeV.

[h] Calculated by means of Eq. (6).

[i] Calculated by subtracting values of $E_{DIS}-\Delta E_{SPi}(T)$ for a given fissioning system.

[j] Values based on the scission-point model of fission described in Ref. [10].

[k] Calculated by subtracting values of $\Delta E_{SPi}(T)$ for a given fissioning system.

TABLE III. TEMPERATURE-CORRECTED AND NORMALIZED VALUES OF THE SINGLE-PARTICLE CORRECTION ENERGIES

Energy	^{232}Th(n,f) (MeV)	^{238}U(n,f) (MeV)
Temperature-corrected values		
$\Delta E_{SP1}(T)$	0.64	1.04
$\Delta E_{SP2}(T)$	-4.79	-6.06
$\Delta E_{SP1}(T)-\Delta E_{SP2}(T)$ (calculated)	5.43	7.10
$\Delta E_{SP1}(T)-\Delta E_{SP2}(T)$ (experimental)	5.81	6.25
Values normalized to the experimentally derived value of $\Delta E_{SP1}(T)-\Delta E_{SP2}(T)$		
$\Delta E_{SP1}(T)$	0.68	0.92
$\Delta E_{SP2}(T)$	-5.13	-5.33

Application of Eq. (5) simultaneously to the uranium and thorium data gave the preliminary least-squares best fits shown by the solid curves in Fig. 8. Values of the parameters c_i, a_i, and E_i obtained for ^{233}Th and ^{239}U are given in Table I. The values of a_1, a_2, E_1, and E_2 determined for ^{239}U are significantly smaller than the respective values of 31.1, 27.4, 3.6, and 7.1 obtained by Borisova, et al., [5]. Their energies, E_1 and E_2, are reported as "corresponding to the fission threshold of ^{238}U, that is, for E_n=1.5 MeV." Substituting their values into Eq. (5) does not give a good fit to the data. The least squares fit to the level density parameter, a_i, gives quite reasonable values of $A_f/9.59$ and $A_f/11.35$ for the symmetric and asymmetric mass splits, respectively.

Since $E_i = E_i^* - E_n$, Eq. (3) can be rewritten to give

$$E_i - B_n + B_f + E_{LDi} = E_{DIS} - \Delta E_{SPi}(T) \qquad (6)$$

The measured or calculated quantities on the left-hand side of Eq. (6) are listed in Table II. The values of $E_{DIS}-\Delta E_{SPi}(T)$ at $E_n \sim 4.5$ to 5 MeV are also given in Table II. The values of $\Delta E_{SP1}(T)-\Delta E_{SP2}(T)$ listed in the table are obtained by subtracting the two values of $E_{DIS}-\Delta E_{SPi}(T)$ for

a given fissioning system. To determine E_{DIS} an estimate of $\Delta E_{SPi}(T)$ is needed. Values were taken from data described by the scission-point model of fission [10] and are listed below the dashed line in Table II. However, these calculated values are appropriate for $E_i^*=0$. (The experimental values are for $E_i^* \simeq 4.5 + E_i$ MeV.) Therefore, the calculated values were corrected to correspond to the experimental excitation energies. The temperature-corrected values, $\Delta E_{SPi}(T)$ and $\Delta E_{SP_1}(T)-\Delta E_{SP_2}(T)$ are given in Table III. The calculated and experimentally derived values of $\Delta E_{SP_1}(T)-\Delta E_{SP_2}(T)$ agree to within 7% for ^{233}Th and 12% for ^{239}U. This agreement is rather gratifying in view of the uncertainties in the Strutinski method for calculating shell effects for deformed nuclear shapes [27] and the use of an independent fragment model [10] for their derivation. To bring the calculated values of $\Delta E_{SPi}(T)$ into agreement with the experimental values, the former were normalized to give the experimentally derived values of $\Delta E_{SP_1}(T)-\Delta E_{SP_2}(T)$. These values are listed in Table III. Adding the normalized values of $\Delta E_{SPi}(T)$ to the values of $E_{DIS}-\Delta E_{SPi}(T)$ given in Table II yields E_{DIS} values of 1.7 MeV for ^{233}Th and 4.8 MeV for ^{239}U, a difference of 3.1 MeV.

4. DISCUSSION

A number of assumptions have been made in the above analyses that affect the accuracy of the deduced E_{DIS} values for the ^{233}Th and ^{239}U compound nuclei. Certainly one may question the applicability of the Fermi gas level density at such low values of E_i^*. Nevertheless, the data cannot be fit with large values of E_{DIS}. Therefore, the picture of complete damping between the saddle point and the point where masses are fixed appears to be eliminated. The values obtained for E_{DIS} are also consistent with the discussion on pairing in the scission-point model [10] which attributes the strong odd-even effect observed in the TKE distribution for the fission of ^{229}Th with thermal neutrons, shown in Fig. 9 [28], to the very low scission-point temperature expected in thorium systems.

The difference of 3.1 MeV between values of E_{DIS} for ^{239}U and ^{233}Th is much less sensitive to the assumptions made and can, in fact, be seen directly in the data before analysis (see Fig. 6). The 3.1 MeV E_{DIS} difference between ^{239}U and ^{233}Th is also consistent with the difference between $\bar{\nu}_p$ for the two nuclides, which is $\sim$0.6 neutron for a given incident neutron energy [29]. Since the number of neutrons emitted per fission is a measure of E_{DIS} plus the average fragment deformation energy and the difference in $\bar{\nu}_p$ between ^{239}U and ^{233}Th is accounted for by the difference in E_{DIS}, one may conclude that the deformation energies at the scission point for these two fissioning systems are approximately equal. Guet, et al., [30] in a study of long-range alpha particles in ^{235}U(n,f), decide that only a compact scission shape with relatively low pre-scission kinetic energy (<10 MeV) is consistent with their data. If pre-scission kinetic energy is small, then the total kinetic energy is dominated by the post-scission kinetic energy. The latter can be approximated by

$$(TKE)_{post} = Z_1 Z_2 e^2/D \qquad (7)$$

where D is the distance between the charge centers at scission. Since the total deformation energy is shown to be equal for ^{233}Th and ^{239}U, then D should also be nearly equal for systems which are so similar. One may therefore calculate the expected TKE differences for the most probable charge divisions (Z = 54 and 38 for ^{239}U and Z = 54 and 36 for ^{233}Th).

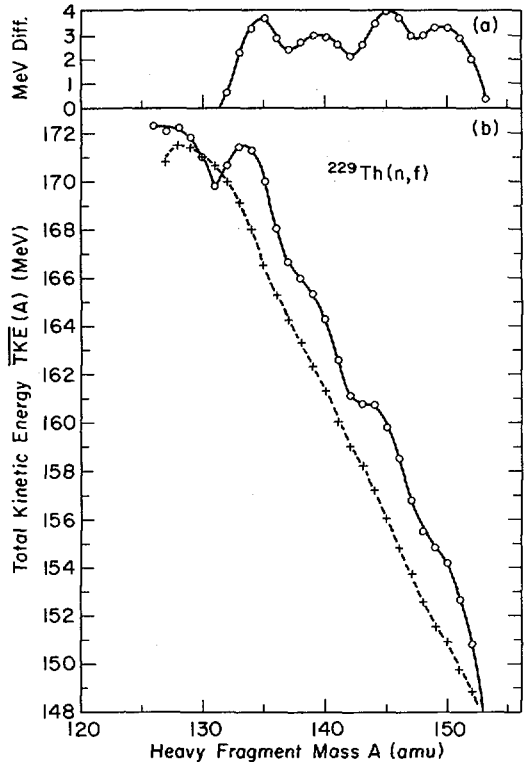

FIG.9. Average total kinetic energy for thermal-neutron-induced fission of ^{229}Th as a function of primary heavy-fragment mass. The dashed curve in (b) shows TKE (A) values for the thermal-neutron-induced fission of ^{233}U multiplied by 0.944. The curve shown in (a) represents the differences between the two curves shown in (b). From Ref.[28].

This amounts to a 5.6% difference or ∿9 MeV for compact scission shapes deduced by Guet, et al., [30]. Experimental values of $\overline{TKE}$ are ∿172.5 MeV for ^{239}U [26] and ∿163 MeV for ^{233}Th [24], a 5.8% difference or 9.5 MeV. The 0.5-MeV difference between the calculated and experimental energies indicates very little difference in the pre-scission kinetic energy for the two fissioning systems. Since all dynamic calculations that predict appreciable amounts of pre-scission kinetic energy indicate a strong dependence on the parameter $Z^2/A^{1/3}$ in the actinide region of the elements [31], one concludes that the pre-scission kinetic energy is small, i.e., less than 10 MeV, consistent with Guet, et al. [30].

In view of the experimental evidence we conclude that fission occurs with small amounts of dissipation energy, small amounts of pre-scission kinetic energy, and compact shapes at the scission point. Such a situation is incompatible with current dynamic calculations. Original one-body viscosity calculations yield compact shapes but large amounts of E_{DIS} and

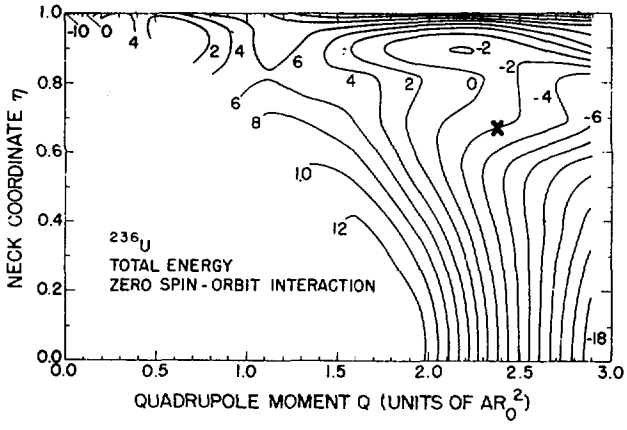

FIG.10. Contours in the Q-η plane of the microscopic-macroscopic potential energy of ^{236}U with zero spin-orbit interaction, in units of MeV. The scission point suggested in the present paper is denoted by an X. From Ref.[3].

essentially no pre-scission kinetic energy [3]. Two-body viscosity calculations give very extended shapes with varying but always large amounts of pre-scission kinetic energy [2,3]. In Fig. 10 is shown the potential energy surface for ^{236}U as a function of neck constriction and total elongation of the system. This figure was taken from the recent paper by Negele, et al., [3] on fission dynamics. Two valleys in the potential energy surface are apparent in the figure. The upper valley is quite flat descending from the second saddle point and exhibits stability against constriction of the neck. This valley leads to the extended shapes at scission predicted by the two-body viscosity calculations. The lower valley is associated with approaching fragments in heavy ion reactions. It exhibits little stability against neck constriction and can lead to more compact shapes at scission. A small ridge separates the two valleys. At elongations greater than 17 fm ($\sim 2.25/AR_0^2$ units), the potential energy of the lower valley becomes less than that of the upper valley. Also, the upper valley is very flat in the region of 17-18 fm, exhibiting a slight saddle point. This is similar to the scission saddle described by Nörenberg [12] where the attractive forces of the neck balance or even over-balance the repulsive Coulomb force. Davies, et al., [31] show that rupture occurs for neck thicknesses of ~ 2 fm. Previous calculations assumed that scission occurs for zero neck thicknesses. The experimental evidence of small dissipation energy, small pre-scission kinetic energy, and compact shapes together with the 2-fm neck thickness indicate that scission occurs at $\eta \gtrsim .68$ and $Q \gtrsim 2.4$, indicated by an x in Fig. 10. This corresponds to a separation between charge centers of 17-18 fm. The approximate energy release from the second saddle to this scission position for ^{236}U is ~ 9 MeV, in good agreement with the presently proposed sum of dissipation energy and pre-scission kinetic energy for ^{239}U. It is suggested that dynamical calculations be undertaken to determine whether the fissioning system can be diverted from the upper valley in the region of the third saddle point, i.e., 17-18 fm, to the lower valley where scission can occur with parameters more consistent with those derived from experiment.

REFERENCES

[1] KOONIN, S.E., NIX, J.R., Phys. Rev. C 13 (1976) 209.
[2] DAVIES, K.T.R., SIERK, A.J., NIX, J.R., Phys. Rev. C 13 (1976) 2385.
[3] NEGELE, J.W., KOONIN, S.E., MÖLLER, P., NIX, J.R., SIERK, A.J., Phys. Rev. C 17 (1978) 1098.
[4] FORD, G.P., LEACHMAN, R.B., Phys. Rev. 137 (1965) 826.
[5] BORISOVA, I., DUBROVINA, S.M., NOVGRODTSEVA, V.I., PECHLIN, V.A., SHIGIN, V.A., SHUBKO, V.M., Yad, Fiz. 6 (1967) 454 [Sov. J. Nucl. Phys. 6 (1968) 331].
[6] DUBROVINA, S.M., NOVGRODTSEVA, V.I., MOROZOV, L.N., PECHLIN, V.A., CHISTYAKOV, L.V., SHIGIN, V.A., SHUBKO, V.M., Yad. Fiz. 17 (1973) 470 [Sov. J. Nucl. Phys. 17 (1973) 240].
[7] NAGY, S., FLYNN, K.F., GINDLER, J.E., MEADOWS, J.W., GLENDENIN, L.E., Phys. Rev. C 17 (1978) 163.
[8] GINDLER, J.E., GLENDENIN, L.E., MEADOWS, J.W., Nucl. Sci. Eng. 70 (1979) 101.
[9] GLENDENIN, L.E., GINDLER, J.E., AHMAD, I., MEADOWS, J.W., Abstracts of Papers, American Chemical Society, 177th National Meeting, Honolulu, Hawaii, April 2-6, 1979, NUCL-4.
[10] WILKINS, B.D., STEINBERG, E.P., CHASMAN, R.R., Phys. Rev. C 14 (1976) 1832.
[11] FONG, P., Statistical Theory of Nuclear Fission, Gordon and Breach, New York (1969).
[12] NÖRENBERG, W., Physics and Chemistry of Fission (Proc. 2nd IAEA Symp., Vienna, 1969) IAEA, Vienna (1969) 51.
[13] MYERS, W.D., SWIATECKI, W.J., Nuclear Masses and Deformations, Lawrence Radiation Laboratory Rep. UCRL-11980 (1965).
[14] MOSEL, U., SCHMITT, H.W., Phys. Rev. C 4 (1971) 2185.
[15] JENSEN, A.S., DAMGAARD, J., Nucl. Phys. A203 (1973) 578.
[16] ZIEGENHAIN, K.H., LUSTIG, H.J., HAHN, J., MARUHN, J.A., GREINER, W., SCHEID, W., Fizika 9 suppl. 4 (1977) 559.
[17] MORETTO, L.G., Phys. Lett. 40B (1972) 1.
[18] ADAMS, D.E., JAMES, W.D., BECK, J.N., KURODA, P.K., J. Inorg. Nucl. Chem. 37 (1975) 419.
[19] TURKEVICH, A., NIDAY, J.B., TOMPKINS, A., Phys. Rev. 89 (1953) 552.
[20] CROUCH, E.A.C., At. Data Nucl. Data Tables 19 (1977) 419.
[21] MEEK, M.E., RIDER, B.F., Compilation of Fission Product Yields, NEDO-12154-2, Vallecitos Nuclear Center (1977).
[22] MEADOWS, J., POENITZ, W., SMITH, A., SMITH, D., WHALEN, J., HOWERTON, R., Evaluated Nuclear Data File of Th-232, Argonne National Laboratory Rep. ANL-NDM-35 (1978).
[23] POENITZ, W., PENNINGTON, E., SMITH, A.B., HOWERTON, R., Evaluated Fast Neutron Cross Sections of Uranium-238, Argonne National Laboratory Rep. ANL-NDM-32 (1977).
[24] SERGACHEV, A.I., VOROB'EVA, V.G., KUZ'MINOV, B.D., MIKHAILOV, V.B., TARASKO, M.Z., Yad. Fiz. 7 (1968) 778 [Sov. J. Nucl. Phys. 7 (1968) 475].
[25] SINCHENKO, V.I., SERGACHEV, A.S., MIKHAILOV, V.B., VOROB'EVA, V.G., TARASKO, M.Z., KUZ'MINOV, B.D., Yad. Fiz. 6 (1968) 708 [Sov. J. Nucl. Phys. 6 (1968) 516].
[26] VOROB'EVA, V.G., KUZ'MINOV, B.D., SERGACHEV, A.I., TARASKO, M.Z., Yad. Fiz. 9 (1969) 296 [Sov. J. Nucl. Phys. 9 (1969) 175].
[27] STRUTINSKI, V.M., Nucl. Phys. A95 (1967) 420.
[28] UNIK, J.P., GINDLER, J.E., GLENDENIN, L.E., FLYNN, K.F., GORSKI, A., SJOBLOM, R.K., Physics and Chemistry of Fission (Proc. 3rd IAEA Symp., Rochester, N.Y., 1973) 2, IAEA, Vienna (1974) 19.

[29] MANERO, F., KONSHIN, V.A., At. Energy Rev. 10 (1972) 637.
[30] GUET, C., SIGNARBIEUX, C., PERRIN, P., NIFENECKER, H., ASHGAR, M., CAITUCOLLI, F., LEROUX, B., Nucl. Phys. A314 (1979) 1.
[31] DAVIES, K.T.R., MANAGAN, R.A., NIX, J.R., SIERK, A.J., Phys. Rev. C 16 (1977) 1890.

DISCUSSION

H.J. SPECHT: This may be an appropriate point to take up again the discussion we had following Dr. David's paper (see SM-241/C6 in these Proceedings). Dr. David found, in full conformity with your conclusion regarding only weak dissipation in ^{232}Th + n, that there was a surprising increase in the total kinetic energy with excitation in ^{232}Th(α, α'). I have just been told by Dr. Bauer of Livermore that there are now data by Caldwell and co-workers on $\bar{\nu}$ in ^{232}Th (γ, f) clearly showing that $\bar{\nu}$ decreases, or at least remains constant, up to about 8 MeV, thereby supporting Dr. David's results.

R.W. BAUER: Yes, the new photofission data referred to have been obtained by Caldwell, Berman and co-workers as a result of collaboration between Los Alamos and Livermore. Figure A is taken from a paper recently submitted for publication in Nuclear Science and Engineering.

P. DAVID: The data show that there are steps at the same excitation energies at which we observed steps in the TKE for the ^{232}Th (^{4}He, ^{4}He'f) reaction. We will use these new data to calculate further $\overline{\text{TKE}}$. I have no doubt that the positive slope $\partial \text{TKE}/\partial E_x \approx 1$, indicating the pairing gap, as I showed in my paper, will still hold good.

A.F. MICHAUDON: It is most interesting to see these new data from Livermore on $\bar{\nu}$ for photofission of ^{232}Th. The decrease, followed suddenly by an increase in $\bar{\nu}$ versus photon energy, is unexpected. But, of course, when comparing such data with those for the ^{232}Th(n, f) reaction discussed earlier, one has to bear in mind that the two fissioning nuclei are different in each reaction, as already pointed out, and that the incident photon, or neutron, energies should shift by an amount equal to the neutron separation energy. I should like to ask Dr. David whether his kinetic energy data for the ^{232}Th $(\alpha, \alpha' f)$ reaction show a change in slope at the energy where the $\bar{\nu}$ variation with incident photoenergy for ^{232}Th (γ, f) presents a change in sign.

P. DAVID: Yes, the decrease in $\bar{\nu}$ with E_x changes to a positive slope at the same excitation energy at which the TKE shows the opposite behaviour: the slope $\partial \overline{\text{TKE}}/\partial E_x$ changes from about + 1.5 to about 0. If we include the new data from Caldwell et al. in our analysis, we can bring down the slope $\partial \overline{\text{TKE}}/\partial E_x$ over the excitation energy level (B_f, B_f + 1.5 MeV) to about unity, which is then a strong indication of the pairing gap at the saddle.

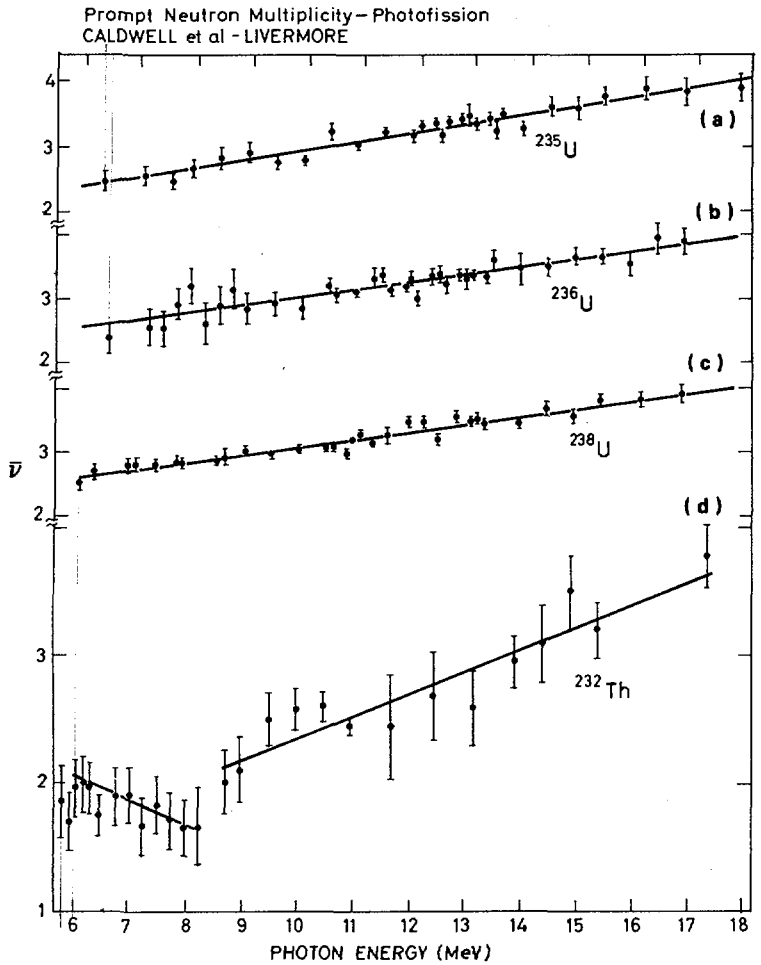

FIG.A. Photofission data by Caldwell et al., Livermore.

H.A. NIFENECKER: I think a word of caution is needed with regard to any interpretation of localized variation in kinetic energy with excitation energy as the result of purely dynamic effects. In his paper, Dr. Asghar (see SM-241/F3 of these Proceedings) showed how much kinetic energy may depend, in the long run, on the nature of the fissioning nucleus. Change in potential energy with quasi-particle excitations may be responsible for kinetic energy variation. Further, in the case of thorium very compact shapes may be suppressed at low energy and become available at higher energies when the phase space increases.

M. ASGHAR: Dr. Gindler, don't you think that the different behaviour of ^{232}Th and ^{238}U might be due to the sudden change in phase beyond ^{236}U that I discussed this morning (SM-241/F3)?

J.E. GINDLER: It is difficult to say how the dissipation energy behaves, since we have only two cases to deal with. We need at least a third case in order to determine any trends. We are currently working with ^{233}U and may be in a position to establish some sort of pattern after completion of the work.

VISCOSITY EFFECTS AT LOW EXCITATION IN THE NEUTRON FISSION OF ^{239}Pu

R.L. WALSH*, J.W. BOLDEMAN, M.E. ELCOMBE
Australian Atomic Energy Commission,
Research Establishment,
Lucas Heights, Sutherland, New South Wales,
Australia

Abstract

VISCOSITY EFFECTS AT LOW EXCITATION IN THE NEUTRON FISSION OF ^{239}Pu.

The dissipation of the collective energy at the saddle point for ^{239}Pu(n,f) has been investigated by a measurement of fragment kinetic energies and mass yields. Significant disagreement exists in previous studies. Measurements were made at E_n = 0.296, 0.081 and 0.033 eV, a region where the relative fission contribution from individual (J,K,π) collective channels can be calculated. A triple-axis spectrometer was used to provide a monoenergetic neutron beam. The data were analysed by direct comparison of the raw pulse height distributions at the three neutron energies and also by the usual surface barrier calibration procedure. The measured average total kinetic energy difference between E_n = 0.296 and 0.033 eV was $|\Delta\bar{E}_K| = 185 \pm 75$ keV. From the mass yield measurements it was shown that mass yield changes contributed only 15 keV of this difference. The measured $\bar{E}_K$ variation confirms the known $\bar{\nu}$ variation in the same energy region. The present data imply an $\bar{E}_K$ difference between pure $J = 0^+$ and 1^+ levels of 430 ± 180 keV. One interpretation of this result is that viscosity effects in the ^{240}Pu system are significant.

1. INTRODUCTION

Significant progress has been made in calculating the potential energy surfaces of fissioning nuclei [1]. However, to fully describe the fission process, the dynamical effects of collective inertia and viscosity in the descent from the saddle point to scission must also be known. Experimental data on fragment properties can provide such dynamical information. For example, there is the question of how the collective energy of the compound nucleus is dissipated between the saddle point and scission. For ^{233}U(n,f), discrete changes in the collective energy have been observed directly as discrete changes of the same size and direction in the average total fragment kinetic energy $\bar{E}_K$ [2]. Further, the average number of prompt neutrons emitted per fission, $\bar{\nu}_p$, was observed to show the same variation as $\bar{E}_K$ but of opposite sign [2], as expected from energy balance considerations.

---

* Also University of Wollongong, Wollongong, NSW, Australia.

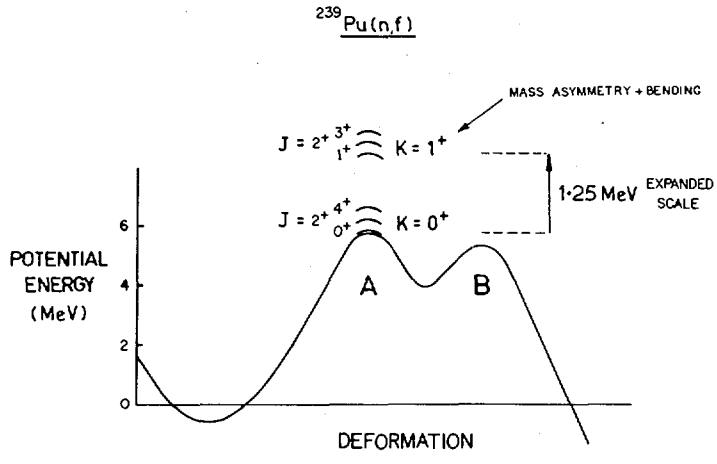

FIG.1. Collective levels at the saddle point for ^{240}Pu, for resonance energy fission.

These data provide strong evidence that, for ^{233}U(n,f) at low excitation energy, the collective energy at the saddle point is only weakly coupled to the single-particle degrees of freedom during the barrier descent. A similar conclusion for the system ^{235}U(n,f) was reported in Ref. [3]. That is, these systems are essentially adiabatic (low viscosity).

For the case of ^{239}Pu(n,f), however, the question of collective energy dissipation has remained unanswered, mainly because of conflicting experimental results. The situation can be illustrated by reference to Fig.1. This shows the collective levels at the saddle point for ^{240}Pu. For resonance energy neutrons, fission occurs via $J = 0^+$ and 1^+ levels only. The nice feature of the ^{239}Pu(n,f) system at resonance energies, a feature which makes the system close to unique, is that all the $J = 1^+$ strength occurs through the $K = 1^+$ band shown, and 90% of the $J = 0^+$ strength through the $K = 0^+$ ground-state band. Thus it is possible to isolate effects related to unique (J,K,π) channels. This is not possible with most other (n,f) systems, unless beam polarization or target alignment methods are used. The remaining 10% of the $J = 0^+$ strength occurs through a 'double-gamma' vibrational band 1.0 MeV above the ground-state band (not shown in Fig.1). Data used to estimate the energies of the collective bands are presented below Table II.

If the coupling between collective and single-particle degrees of freedom is weak for ^{239}Pu(n,f), as it is for ^{233}U(n,f), then $\bar{E}_K$ for fission through $J = 1^+$ levels (i.e. the $K = 1^+$ band) should exceed $\bar{E}_K$ for $J = 0^+$ levels (the $K = 0^+$ ground-state band) by 1.25 MeV. Experimental results for this $\bar{E}_K$ difference are summarized in Table I. The data of Ref. [4] were obtained from a direct fragment kinetic energy comparison, using filtered neutron beams. $\bar{E}_K$ for the large $J = 1^+$ resonance

TABLE I. SUMMARY OF PREVIOUS RESULTS FOR $\bar{E}_K$ ($J = 1^+$) – $\bar{E}_K$ ($J = 0^+$) FOR ^{239}Pu(n,f) AT RESONANCE NEUTRON ENERGIES

Method	$\bar{E}_K$ ($J = 1^+$) – $\bar{E}_K$ ($J = 0^+$) (MeV)
Kinetic-energy measurements [4]	1.5 ± 0.1 [a] → system non-viscous
$\bar{\nu}$ measurements [6]	0.40 ± 0.10 → system viscous?
$\bar{\nu}$ measurements [7]	0.11 ± 0.05 → system viscous?

[a] The value reported in Ref. [4] of 0.75 ± 0.05 MeV must be increased to take account of the $J = 1^+$ contribution in the Be-filtered events.

at $E_n = 0.296$ eV was compared with $\bar{E}_K$ for $E_n \sim 0.005$ eV, where the bound $J = 0^+$ resonance [5] below the neutron binding energy gives a significant contribution. The 1.5 ± 0.1 MeV value found for $\bar{E}_K$ ($J = 1^+$) – $\bar{E}_K$ ($J = 0^+$) implies that the system is non-viscous. However, two measurements of $\bar{\nu}$ in the resonance region [6, 7] obtained for the difference $\bar{\nu}$ ($J = 0^+$) – $\bar{\nu}$ ($J = 1^+$) values of 1.8 and 0.5% of $\bar{\nu}$, respectively, after correction for the small (n,γ f) effect [8]. Converted to $\bar{E}_K$ differences (via 0.13 n MeV^{-1}), these are equivalent to 0.40 ± 0.10 and 0.11 ± 0.05 MeV. Although in mild disagreement with each other, both these values suggested that the discrete nature of the collective levels at the saddle point (Fig.1) is not preserved after scission, e.g. that the system is viscous.

To examine this problem we have measured fragment kinetic energies and mass yields for ^{239}Pu(n,f) in the resonance region.

2. EXPERIMENTAL METHOD

The measurements were made at neutron energies $E_n = 0.296$, 0.081 and 0.033 eV, an energy region similar to the kinetic energy study of Ref. [4]. The $J = 1^+$ resonance for ^{239}Pu(n,f) at $E_n = 0.296$ eV is shown in Fig.2. For decreasing energies below 0.296 eV, the proportion of $J = 0^+$ fissions (associated with the bound level) increases. Table II shows the proportions of fissions occurring

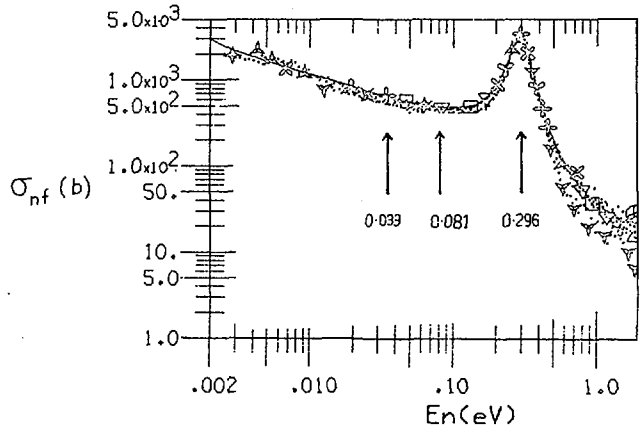

FIG.2. Neutron fission cross-section σ_{nf} for ^{239}Pu. The arrows show the energies used for the present measurements.

through the (J,K,π) channels open at each neutron energy studied, calculated from the Breit-Wigner single-level formula and from the data of Ref. [9]. In this calculation, no assumptions are made concerning the resonance parameters of the bound $J = 0^+$ level. The accurately known resonance parameters of the $J = 1^+$ level at 0.296 eV give absolute values for $\bar{\sigma}_{nf}$ ($J = 1^+$). The total fission cross-section is also known accurately [11]. Therefore, their difference gives σ_{nf} ($J = 0^+$). The experimental procedure was to measure fragment kinetic energies at $E_n = 0.296$ and 0.033 eV, to see how much the kinetic energy changes owing to changes in the relative $J = 0^+$ and 1^+ contributions. A measurement at $E_n = 0.081$ eV provided an intermediate value.

A standard double-energy configuration was used, with two surface barrier detectors operated in coincidence viewing a thin ^{239}Pu target, of isotopic purity 99.97%. The detectors were positioned at 2 and 4 cm from the target. The ^{239}Pu thickness was 12 $\mu g \cdot cm^{-2}$, over an area of 1.3 cm^2. The target backing was 15 $\mu g \cdot cm^{-2}$ VYNS and 12 $\mu g \cdot cm^{-2}$ gold. Figure 3 shows the fragment pulse height distribution measured in a single detector. The good peak-to-valley ratio (7:1) and the absence of a tail in the low-energy peak confirm the quality of the ^{239}Pu target.

A monoenergetic neutron beam was provided by a triple-axis spectrometer, in association with the 10 MW reactor HIFAR. A single scatter of the beam from a germanium monochromator was used. The energy resolution and energy accuracy of the beam are given in Table III. The odd index planes of the germanium were used, as these produce no $\lambda/2$ or $\lambda/6$ background components of the main reflected beam (λ). For the runs at $E_n = 0.033$ eV, a ^{239}Pu filter in the beam was used to eliminate the $\lambda/3$ component. (0.033 eV X 9 = 0.297 eV, almost exactly the

TABLE II. PROPORTIONS OF FISSION THROUGH EACH (J, K, π) CHANNEL

E_n (eV)	Relative (J, K, π) strength, %		
	(1, 1, +) E_c = 1.25 MeV[a]	(0, 0, +) E_c = 1.0 MeV	(0, 0, +) E_c = 0.0 MeV
0.296	92	0.9	7.1
0.081	59	4.7	36.3
0.033	46	6.2	47.8

[a] E_c = collective energy of specific K-band.
E_c for $K = 1^+$ band from data of Ref. [10].
E_c for upper $K = 0^+$ band from data of Ref. [9] ($N_{eff} = 0.13$), in reasonable agreement with data of Ref. [10].

energy of the large σ_{nf} resonance. Thus, the $\lambda/3$ is absorbed.) The total contribution from all background components was measured independently at each neutron energy by a second scatter from pyrolitic graphite. The total background contribution was $< 2\%$ of the main λ-beam. Relative flux measurements using thin gold foils showed the beam intensity distribution across the target to be uniform, at each neutron energy.

Since the measured changes in $\bar{E}_K$ were expected to be small, < 0.5 MeV, considerable care was taken to ensure the electronic stability of the measuring system. This stability was 1 part in 2000 over two to three days. Movement of the spectrometer to change the neutron energy produced no observable effect on the stability.

Data were monitored on-line with a PDP11/10 computer and recorded event-by-event on magnetic tape for off-line analysis with an IBM 3031 computer. The measurement procedure was to do repeated runs at $E_n = 0.296$ and 0.033 eV in sequential fashion. Data were recorded at $E_n = 0.296$ eV ($\sim$ 16 h), then at 0.033 eV (6–8 h), then at 0.296 eV again ($\sim$ 16 h) to check the system stability. Data at $E_n = 0.081$ eV were compared with data at $E_n = 0.296$ eV in similar fashion. About 77 000 coincidence events were obtained at $E_n = 0.296$ eV and about 35 000 at each of $E_n = 0.033$ and 0.081 eV.

TABLE III. ENERGY RESOLUTION AND ENERGY ACCURACY OF NEUTRON BEAM

E_n (eV)	λ (Å)	Energy resolution (%, FWHM)	Accuracy of E_n (%)
0.033	1.58	4.2	± 0.6
0.081	1.01	6.8	± 0.9
0.296	0.528	6.8	± 0.9

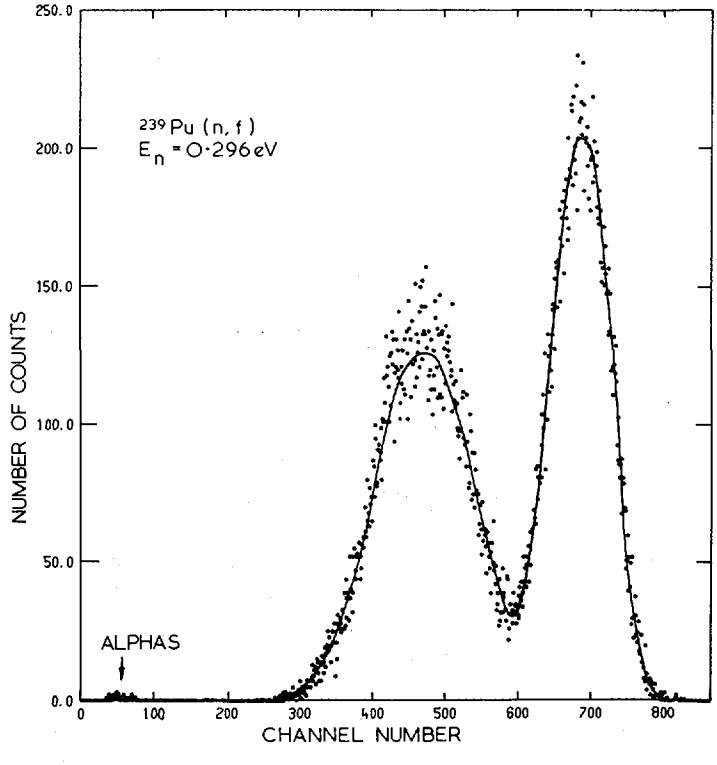

FIG.3. Fragment pulse height distribution for one detector.

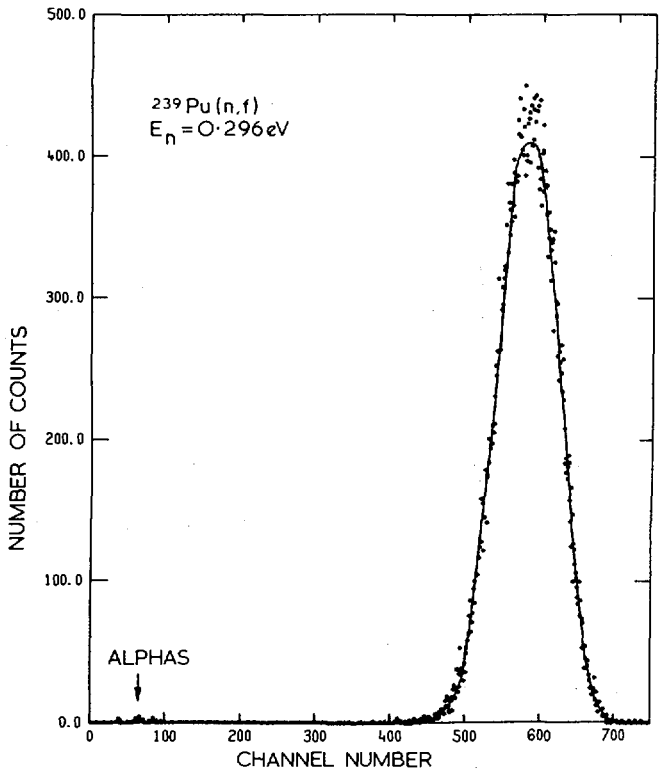

FIG.4. Total pulse height distribution from two complementary fragments.

The data were treated by two methods: (i) The raw data (in channel numbers) were used to calculate the mean position of the fragment total pulse height distribution (Fig.4). This distribution is formed by summing the pulse heights from complementary fragments, event-by-event. The change in position of this mean between runs at different neutron energies was then determined. The energy scale was calibrated from the positions of the light and heavy fragment pulse height peaks and the data of Ref. [12].

(ii) The usual surface barrier detector calibration equation [13, 14] was used to calculate fragment kinetic energies and masses. For each event, an iterative procedure is used, as described in Ref. [15]. Correction for the energy loss of fragments in the target and backing and in the dead-layer of the detectors is inherent in the calibration procedure [13]. The correction for neutron emission uses the ν (m) data for ^{239}Pu(n,f) of Ref. [16]. For each fragment mass m, the kinetic energy dependence of ν (m) is then incorporated by using the $\partial\nu(m)/\partial E_K$ data for ^{235}U(n,f) of [17]. The pre-neutron emission masses were calculated for mass groups 2 amu wide.

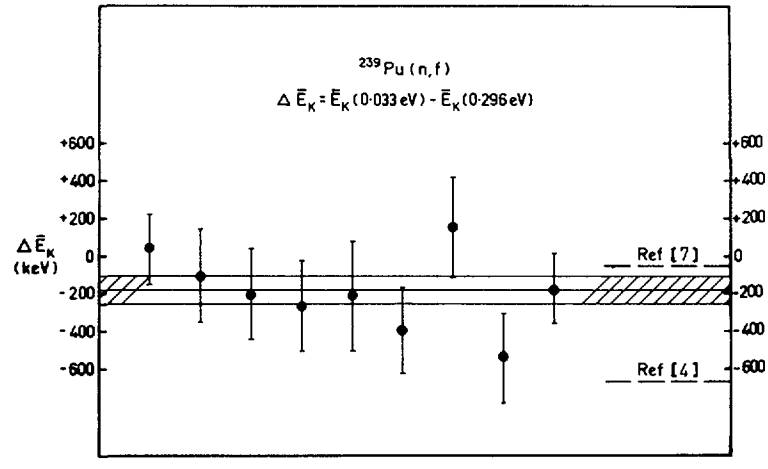

FIG.5. Measured differences in $\bar{E}_K$ between the two neutron energies 0.296 and 0.033 eV.

3. RESULTS AND DISCUSSION

Figure 5 shows the results for the fragment kinetic energy comparison between E_n = 0.296 and 0.033 eV. Each data point shows the change in position of the peak of Fig.4 between the run at E_n = 0.033 eV and the average of the 'before' and 'after' runs at E_n = 0.296 eV (method (i) above). Thus each data point represents one complete cycle. The points are plotted at equal distances along the abscissa in Fig.5; however, they are not necessarily equally spaced in real time. The average shift of the peak was

$$\Delta\bar{E}_K = \bar{E}_K\ (0.033\ \text{eV}) - \bar{E}_K\ (0.296\ \text{eV}) = -185 \pm 75\ \text{keV}$$

The shaded region shows this average value and the error. The analysis by method (ii) gave a value of $\Delta\bar{E}_K$ which agreed with the above value to within 7 keV. From method (ii), $\bar{E}_K$ for E_n = 0.033 eV was found to be $\bar{E}_K$ = 177.2 ± 2 MeV, in good agreement with the value of 177.7 ± 1.8 MeV reported by Ref. [13] in a similar measurement for ^{239}Pu(n_{th},f). The variances of the total pulse height distributions were very similar, for each neutron energy.

The lower dashed line to the right of Fig.5 shows the $\Delta\bar{E}_K$ result that would have been expected from the present measurement according to the data of Ref. [4]. Clearly, there is significant disagreement. The upper dashed line shows the $\Delta\bar{E}_K$ result expected according to the $\bar{\nu}$ data of Ref. [7]. This $\bar{\nu}$ data were

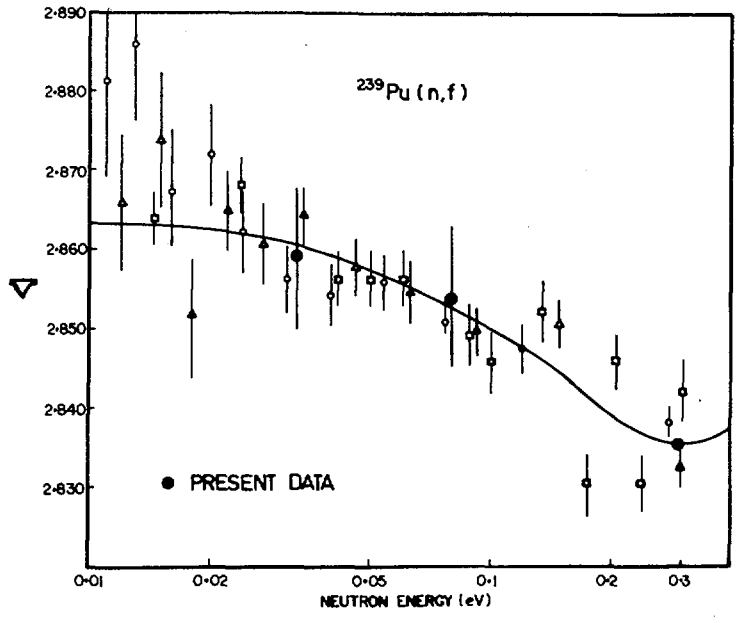

FIG.6. Present $\bar{E}_K$ data converted to $\bar{\nu}$ data and compared with direct $\bar{\nu}$ measurements [6].

obtained for $7 < E_n < 400$ eV. There is smaller disagreement here. The result expected according to the $\bar{\nu}$ variation of Ref. [6],

$$\Delta\bar{E}_K \sim 0.026n/0.13\ \text{nMeV}^{-1} \sim 200\ \text{keV}$$

is in good agreement with the 185-keV value above. For the $\bar{E}_K$ comparison between $E_n = 0.296$ and 0.081 eV, the measured value was $\Delta\bar{E}_K = -145 \pm 75$ keV.

In Fig. 6 the present $\bar{E}_K$ differences measured are shown converted to $\bar{\nu}$ differences and are compared with the direct $\bar{\nu}$ data in the same energy region [6]. The normalization is at the 0.296 eV point. The continuous line is that suggested in Ref. [6] to describe the $\bar{\nu}$ trend. The present $\bar{E}_K$ work confirms the $\bar{\nu}$ variation.

Of course, part of the $\Delta\bar{E}_K$ measured is due to the change in the mass yield distribution. It is known from radiochemical measurements [18, 19] that fission through $J = 0^+$ levels gives a larger amount of symmetric fission than fission through $J = 1^+$ levels. This correction can be calculated as follows: The measured pre-neutron emission mass yield distributions for $E_n = 0.296$ and 0.033 eV are shown in Fig.7 (uncorrected for mass resolution). The two curves are almost identical, except near the symmetric region and near the peaks. The symmetric region is shown in detail in Fig.8. The peak-to-valley ratio for $E_n = 0.296$ eV is

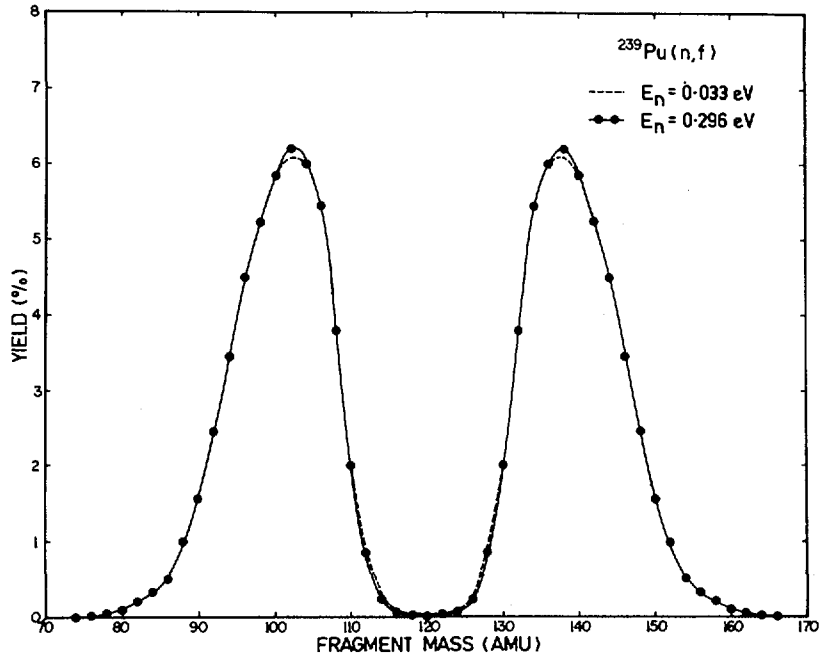

FIG. 7. Mass yields for neutron energies 0.033 and 0.296 eV.

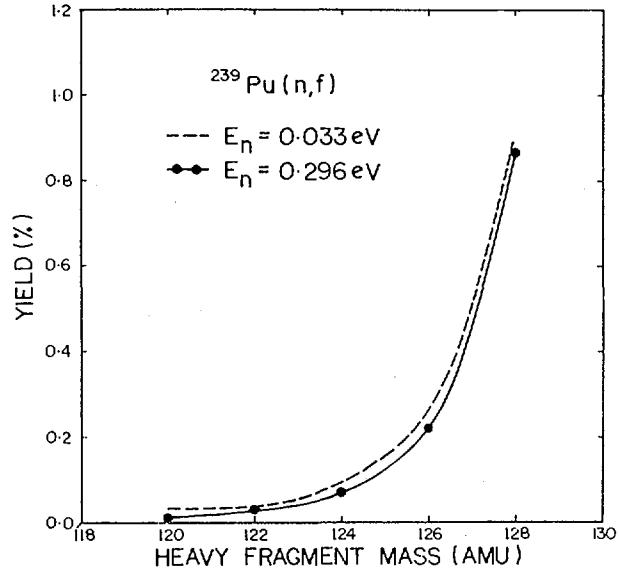

FIG. 8. Comparison of mass yields in symmetric region.

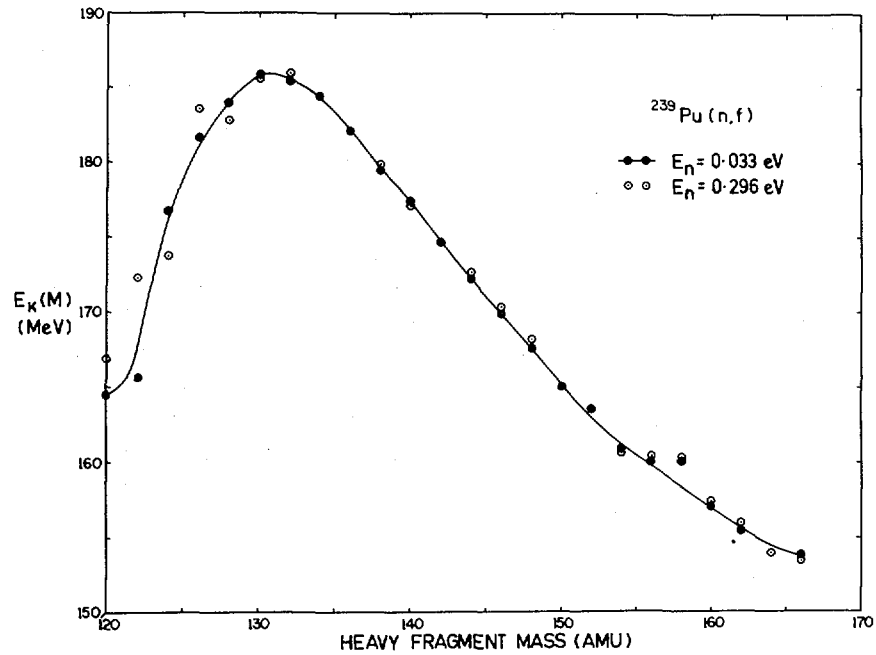

FIG.9. Total fragment kinetic energy versus mass for neutron energies 0.033 and 0.296 eV.

477:1 and for $E_n = 0.033$ eV is 164:1. The factor of ~ 3 difference agrees with the radiochemical data [18, 19]. Figure 9 shows the measured fragment-total-kinetic-energy-versus-mass curve, E_K (m). Again the data for $E_n = 0.296$ and 0.033 eV are very similar, with the 0.296 eV data (open circles) tending to lie slightly higher in energy. The data of Figs 7 and 9 agree closely with the ^{239}Pu(n_{th},f) data of [14]. Using the mass yield data Y (m) and the E_K (m) data, we have

$$\text{Mass yield correction to } \Delta\bar{E}_K = \sum_m E_K(m)\Big|_{0.296\text{ eV}} \times Y(m)\Big|_{0.033\text{ eV}} - \sum_m E_K(m)\Big|_{0.296\text{ eV}} \times Y(m)\Big|_{0.296\text{ eV}}$$

$$= -15 \text{ keV}$$

compare -185 keV measured for $\Delta\bar{E}_K$

Thus, only 15 keV of the kinetic-energy change measured can be attributed to the change in the mass yield distribution. Incorporating this correction, and also a correction of −18 keV due to the reduced mass of the fragments from neutron emission, gives a corrected value of −152 ± 75 keV for the $\bar{E}_K$ change between E_n = 0.296 and 0.033 eV. Consideration of the relative change in the $J = 0^+$ and 1^+ contributions at these two energies (Table II), gives a value of 365 ± 180 keV for the $\bar{E}_K$ difference between *pure* $J = 0^+$ and $J = 1^+$ levels. A further correction to account for the (n,γf) reaction [8] (0.011 n in 0.062 n ~ 18%) gives a final $\bar{E}_K$ difference of 430 ± 180 keV between pure $J = 0^+$ and $J = 1^+$ levels. That is, only ~ 35% of the discrete 1.25 MeV energy difference between the $K = 0^+$ and $K = 1^+$ bands at the saddle point appears after scission in the fragment kinetic-energy mode.

One interpretation of this result is that the coupling between collective and single-particle degrees of freedom is strong, i.e. the ^{240}Pu system is significantly viscous. An alternative interpretation is that mixing of K-values occurs between barrier A and barrier B [20]. This interpretation is perhaps less likely, however, as the difference in heights of barriers A and B for ^{240}Pu is only 0.3–0.5 MeV [21, 22]. If the viscosity interpretation is correct, then a viscous ^{240}Pu system may be contrasted with the lighter uranium systems, which are essentially adiabatic.

ACKNOWLEDGEMENTS

The authors gratefully acknowledge the following people: I.F. Senior and J.J. Fardy for assistance with the target preparation; J. Pauwels (CBNM) for advice on target preparation; I.F. Senior and H.G. Broe for assistance with the experimental apparatus; V. Page for preparation of the VYNS films and for β-γ counting of the gold foils; R.L. Davis for advice on spectrometer problems. The ready cooperation of all HIFAR Operating Staff was greatly appreciated. One of us (RLW) acknowledges the hospitality of Institut für Kernphysik, Kernforschungsanlage Jülich GmbH, during the writing of this paper.

REFERENCES

[1] MÖLLER, P., NIX, J.R., in Physics and Chemistry of Fission (Proc. 3rd Symp. Rochester, 1973) Vol.1, IAEA, Vienna (1974) 103.
[2] BOLDEMAN, J.W., BERTRAM, W.K., WALSH, R.L., Nucl. Phys. A265 (1976) 337.
[3] CLERC, H.G., LANG, W., WOHLFARTH, H., SCHRADER, H., SCHMIDT, K.H., these Proceedings, paper SM/241-F2.
[4] TORASKAR, J., MELKONIAN, E., Phys. Rev. C4 (1971) 267.
[5] VOGT, E., Phys. Rev. 118 (1960) 724.

[6] LEONARD, B.R., Jr., private communication (1976), reported in BOLDEMAN, J.W., Proc. Int. Specialists' Symp. Neutron Standards and Applications, Gaithersburgh (1977) 182. An evaluation of $\bar{\nu}$ data from several US laboratories.
[7] FREHAUT, J., SHACKLETON, D., in Physics and Chemistry of Fission (Proc. 3rd Symp. Rochester, 1973) Vol. 2, IAEA, Vienna (1974) 201.
[8] RYABOV, Yu., TROCHON, J., SHACKLETON, D., FREHAUT, J., Nucl. Phys. **A216** (1973) 395.
[9] DERRIEN, H., BLONS, J., MICHAUDON, A., in Nuclear Data for Reactors (Proc. Conf. Helsinki, 1970) Vol. 1, IAEA, Vienna (1971) 481.
[10] BACK, B.B., BONDORF, J.P., OTROSCHENKO, G.A., PEDERSEN, J., RASMUSSEN, B., Nucl. Phys. **A165** (1971) 449.
[11] GWIN, R., WESTON, L.W., DE SAUSSURE, G., INGLE, R.W., TODD, J.H., GILLESPIE, F.E., HOCKENBURY, R.W., BLOCK, R.C., ORNL Rep. ORNL-4707* Special (1971).
[12] MILTON, J.C.D., FRASER, J.S., Can. J. Phys. **40** (1962) 1626 and ibid. **41** (1963) 817.
[13] SCHMITT, H.W., KIKER, W.E., WILLIAMS, C.W., Phys. Rev. **137** (1965) B837.
[14] NEILER, J.N., WALTER, F.J., SCHMITT, H.W., Phys. Rev. **149** (1966) 894.
[15] BOLDEMAN, J.W., MUSGROVE, A.R. de L., WALSH, R.L., Aust. J. Phys. **24** (1971) 821.
[16] APALIN, V.F., GRITSYUK, Yu., KUTIKOV, I.E., LEBEDEV, V.I., MIKAELIAN, L.A., Nucl. Phys. **71** (1965) 553.
[17] MASLIN, E.E., RODGERS, A.L., CORE, W.G.F., AWRE Rep. AWRE 0–43/67 (1967).
[18] REGIER, R.B., BURGUS, W.H., TROMP, R.L., SORENSEN, B.H., Phys. Rev. **119** (1960) 2017.
[19] COWAN, G.A., BAYHURST, B.P., PRESTWOOD, R.J., GILMORE, J.S., KNOBELOCH, G.W., Phys. Rev. **144** (1966) 979.
[20] STRUTINSY, V.M., PAULI, H.C., Physics and Chemistry of Fission (Proc. 2nd Symp. Vienna, 1969) IAEA, Vienna (1970) 155.
[21] BACK, B.B., HANSEN, O., BRITT, H.C., GARRETT, J.D., Physics and Chemistry of Fission (Proc. 3rd Symp. Rochester, 1973) Vol. 1, IAEA, Vienna (1974) 25.
[22] BRITT, H.C., these Proceedings, paper SM/241-A1.

DISCUSSION

H.C. BRITT: On the basis of theoretical calculations and analysis of fission probability data we believe that the first peak of the fission barrier is most likely to be triaxial. This will cause mixing of K at the first barrier and may possibly lead to a more complex prediction for the expected difference in TKE for 0^+ and 1^+ states.

R.L. WALSH: If K mixing does occur, then it is not clear whether it occurs more at the first barrier, in passing across to the second barrier, or even later. In each case, however, the effect of the mixing is to reduce the amount of the 1.25 MeV energy difference between the saddle point $K = 0^+$ and $K = 1^+$ bands, which may appear after scission as a fragment kinetic energy difference.

A.F. MICHAUDON: I would like to stress the advantage of measuring $\bar{E}_K$ for several ^{239}Pu resonances with pure J quantum numbers, as compared to measurements in the thermal neutron region where there is a mixture of $J = 0^+$ and $J = 1^+$ contributions. In the case of the $^{239}Pu(n, f)$ reaction, the fission cross-section for thermal neutron energy also includes a contribution by a negative energy resonance with poorly known parameters. Even if a good fit to the cross-section is obtained, it is not unique. An equally good fit could also be obtained with other parameters and, consequently, different 0^+ and 1^+ contributions. This illustrates the ambiguities associated with the thermal neutron energy region, where several quantum numbers are involved.

R.L. WALSH: You make the point that a possible error in the resonance analysis of the neutron fission-cross-section for ^{239}Pu might produce an error in our value for the kinetic energy difference between pure $J = 0^+$ and $J = 1^+$ resonances. In particular, such an error might account for the large discrepancy between the $\bar{\nu}_p$ results from ORNL, RPI and Battelle Northwest and our own $\bar{E}_K$ result, and the data from Saclay and Mol (see SM-241/F7 of these Proceedings). But I do not think, in fact, it could. The shape at the fission cross-section in the vicinity of the 1^+ resonance at 0.296 eV is very well known, as shown in the paper. Therefore the contribution of this resonance to the total fission cross-section between 0.01 and 1.0 eV can be accurately obtained. The total fission cross-section is also accurately known (WIN, R., et al., ORNL 4707 (1971)). Hence the $J = 0^+$ contribution, which is just the difference between the two, can be accurately found. The calculation is made independently of the resonance parameters of the bound state $J = 0^+$ resonance. The contribution of higher energy $J = 0^+$ and $J = 1^+$ resonances is negligible in the energy region of our experiment. We stress once again that the data for the very low energy resonance region in the case of $^{239}Pu(n, f)$ differ from the data in the resonance at higher energy.

C.M.C. WAGEMANS: I agree with Dr. Michaudon's comment. I should point out, in addition, that in my opinion the most important result of your measurements is the measured kinetic energy difference of $\approx 170 \pm 75$ keV. Your *calculated* difference of ≈ 0.5 MeV between the 0^+ and 1^+ channels is subject to several assumptions, which make it an indirect result that should be considered with caution.

H.A. NIFENECKER: It is important to note that while the channel analysis of the ^{239}Pu fission cross-section refers to states at the first saddle point, the dynamic properties observable are affected by states at the second saddle point, which is lower in the case of ^{239}Pu. We cannot take it for granted that the 0^+ states fission through the ground state band at the saddle point. The washing out of even-odd effects in plutonium may even be an indication that the nucleus fissions through two quasi-particle states at the saddle point.

FISSION FRAGMENT MASS AND ENERGY DISTRIBUTIONS FOR THE NEUTRON-INDUCED FISSION OF ^{239}Pu AS FUNCTIONS OF THE RESONANCE SPINS*

C.M.C. WAGEMANS
Nuclear Energy Center,
S.C.K./C.E.N. Mol, and
Nuclear Physics Laboratory, Gent

G. WEGENER-PENNING
Nuclear Energy Center,
S.C.K./C.E.N. Mol

H. WEIGMANN, R. BARTHELEMY
CBNM (Euratom), Geel
Belgium

Abstract

FISSION FRAGMENT MASS AND ENERGY DISTRIBUTIONS FOR THE NEUTRON-INDUCED FISSION OF ^{239}Pu AS FUNCTIONS OF THE RESONANCE SPINS.

Measurements were performed at 8-m flight-path of GELINA to study the fission fragment mass and energy distributions for ^{239}Pu (n,f) as functions of the neutron energy. A ^{239}Pu-layer on a transparent backing was mounted in a vacuum chamber and bombarded with neutrons of energies from 2×10^{-2} eV up to about 10^{6} eV. The pulse height spectra of coincident fission fragments were measured with cooled-surface barrier detectors. With the mass and momentum conservation relations, and using the Schmitt-Neiler calibration method to convert the measured pulse heights into energy, fission fragment mass and energy distributions were obtained as functions of the neutron energy. With the same apparatus, also the spontaneous fission of ^{240}Pu was measured during a one-month stop of GELINA. The average pre-neutron emission total kinetic energy is found to be (0.8 ± 0.3) MeV higher for thermal-neutron-induced fission of ^{239}Pu than for spontaneous fission of ^{240}Pu. The mass distributions for both fissioning systems are similar. However, the fine structure is more pronounced, the peak-to-valley ratio is larger, and the peaks are narrower for spontaneous fission. In the neutron resonance region, finally, only small fluctuations in the average total kinetic energy $\overline{E}_K$ from resonance to resonance are observed. However, no difference is observed between the mean $\overline{E}_K$-value for the 0^+ and the 1^+ resonances. This is discussed in terms of the channel theory of fission.

* Research sponsored by NFWO, Belgium.

1. INTRODUCTION

The fissioning system ^{240}Pu is a very suitable case to study the influence of the fission channels on the fragment mass- and energy distributions. Indeed, the spontaneous fission of ^{240}Pu (zero excitation energy) passes completely through the $J^{\pi} = 0^+$ ground-state channel, whilst in the resonance neutron induced fission of ^{239}Pu ($\approx$6.5 MeV excitation energy) well separated $J^{\pi} = 0^+$ and 1^+ states are available. In addition, the study of the fissioning systems mentioned above can give some information on the dynamics of the fission process since very different excitation energies are involved.

To investigate these phenomena, we carried out two series of double energy measurements at the Central Bureau for Nuclear Measurements (Geel). In a first series of measurements resonance neutrons produced by the Geel Linear Accelerator (Gelina) induced fission reactions in a ^{239}Pu target. Secondly the spontaneous fission of ^{240}Pu was compared with the thermal neutron induced fission of ^{239}Pu under almost identical experimental conditions.

2. EXPERIMENTAL PROCEDURE

A ^{239}Pu-layer on a transparent backing was mounted in the center of a vacuum chamber, which was installed at an 8-m flight-path of GELINA. Fission reactions were induced in this target by bombardment with neutrons with energies from 2.10^{-2}eV up to about 10^6eV. The pulse-height spectra of coincident fission fragments were measured with two large surface barrier detectors, which were cooled at a constant temperature in order to realize a good long-term stability of the measuring chains. The mass- and momentum conservation relations and the Schmitt-and Neiler [1] calibration method were used to convert the measured pulse-heights into energy. Using the fission neutron emission data as a function of the fragment mass as obtained by Milton and Fraser [2], pre-neutron emission fission fragment mass- and energy distributions and mass-energy correlations were obtained as a function of the energy of the bombarding neutrons. The advantages of this measuring procedure are that it contains an intrinsic calibration at thermal neutron energy, and that the data are obtained for all neutron energies simultaneously, which allows an accurate intercomparison. In addition, the spontaneous fission of ^{240}Pu was measured during a one month stop of GELINA with the same apparatus. For comparison purposes a ^{239}Pu (n_{th},f) measurement was performed with the same detectors and strictly maintaining the geometrical configuration. The spontaneous fission data were analysed in the same way as described above.

However, no fission neutron emission distributions as a function of the fragment mass are available for the spontaneous fission of ^{240}Pu. We therefore used the ^{239}Pu (n_{th},f) fission neutron data of Milton and Fraser [2] multiplied by the ratio $\bar{\nu}$ ^{240}Pu (s.f) $/\bar{\nu}$ ^{239}Pu (n_{th},f) as given by Mughabghab and Garber [3]. This can be done since it is well known that for all fissioning isotopes the general features of these $\nu(m^*)$-distributions are very similar.

TABLE I. CHARACTERISTICS OF THE PLUTONIUM SAMPLES USED

ISOTOPE	^{239}Pu I	^{239}Pu II	^{240}Pu
CHEMICAL FORM	PuO_2	PuF_3	PuF_3
ENRICHMENT	96.023 %	99.956 %	98.35 %
PREPARATION METHOD	spraying	evaporation	evaporation
LAYER THICKNESS	40 $\mu g/cm^2$	65 $\mu g/cm^2$	93 $\mu g/cm^2$
LAYER DIAMETER	60 mm	20 mm	20 mm
BACKING	vyns	poly-imide	poly-imide
B. THICKNESS	50 $\mu g/cm^2$	20 $\mu g/cm^2$	20 $\mu g/cm^2$
TOTAL MASS Pu	1.13 mg	204 μg	292 μg

The targets used were prepared by the CBNM Sample Preparation Group. Relevant details of these targets are summarized in Table I.

3. RESULTS AND DISCUSSION

3.1. Spontaneous fission measurements

For the study of the spontaneous fission of ^{240}Pu and for the thermal neutron induced fission of ^{239}Pu, very similar targets were used, both prepared by evaporating plutonium-fluoride on two identical poly-imide backings (see Table I). The pre-neutron emission mass-distributions obtained using these targets are shown in Figure 1. In both distributions a definite fine-structure is present, which is more prominent in the spontaneous fission case. More fine-structure appears when windows are put on the energy of the light fragment (E_L) or on the total kinetic energy (E_K), as already discussed elsewhere [4,5]. Moreover, for spontaneous fission the peaks are slightly narrower and, although the measured yield for symmetric mass divisions is strongly affected by the experimental resolution, we also observe a considerably larger peak-to-valley ratio. This higher peak-to-valley ratio in the case of spontaneous fission fits with the picture of two different barriers for symmetric and asymmetric fission [6,7].

The main characteristics of the ^{240}Pu (s.f) and ^{239}Pu (n_{th},f) pre-neutron emission mass- and energy distributions obtained in these measurements are summarized in Table II. From this table it is clear that the average total pre-neutron kinetic energy is (0.8 ± 0.3) MeV larger

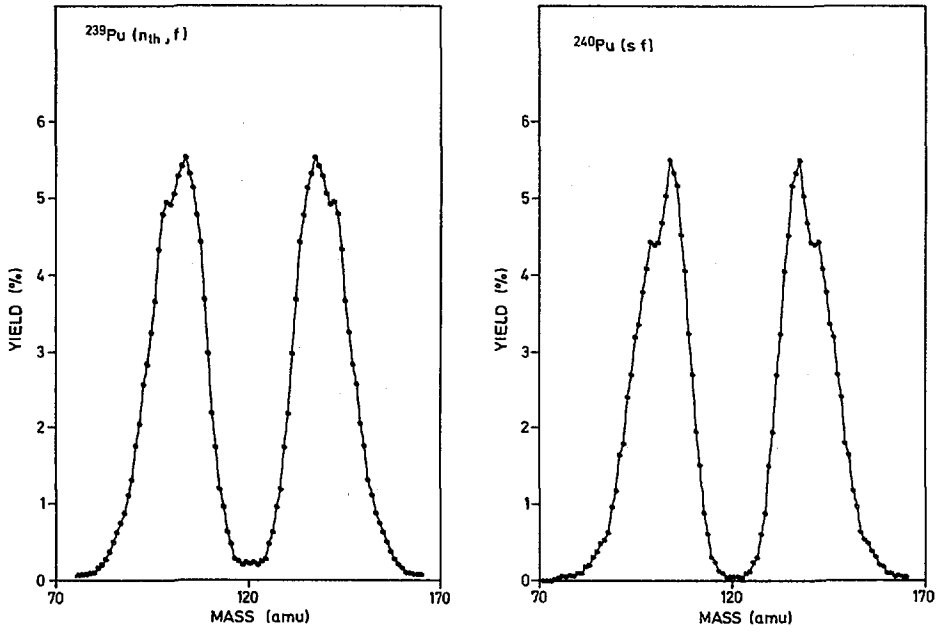

FIG.1. Fission fragment mass distributions for the thermal-neutron-induced fission of ^{239}Pu and for the spontaneous fission of ^{240}Pu.

TABLE II. MAIN CHARACTERISTICS OF THE ^{240}Pu (s f) AND $^{239}Pu(n_{th}, f)$ PRE-NEUTRON EMISSION MASS AND ENERGY DISTRIBUTIONS

	$^{240}Pu(s.f)$		$^{230}Pu(n_{th},f)$	
$\bar{E}_K^*$	177.30 ± 0.20 [a]	MeV	178.10 ± 0.10 [a]	MeV
$\bar{E}_L^*$	103.59 ± 0.13 [b]	MeV	104.33 ± 0.08 [b]	MeV
$\bar{E}_H^*$	73.66 ± 0.13 [b]	MeV	73.73 ± 0.08 [b]	MeV
$\bar{m}_L^*$	100.32 ± 0.13 [b]	amu	100.44 ± 0.08 [b]	amu
$\bar{m}_H^*$	139.68 ± 0.13 [b]	amu	139.56 ± 0.08 [b]	amu
peak/valley	100 ± 35		27 ± 4	

a) statistical error plus error on the gaussian fit.

b) statistical error.

for the thermal neutron induced fission of ^{239}Pu than for the spontaneous fission of ^{240}Pu. This difference is almost completely due to different $\bar{E}^*_I$-values. Furthermore, the present $\bar{E}^*_K$-results are consistent with the difference in fission fragment excitation energies, which may be inferred from the respective $\bar{\nu}$-values. Indeed, the difference in initial excitation energy between both fissioning systems is given in good approximation by

$$\Delta E_{exc} = (\Delta\bar{\nu}_t)\ \bar{B}_n + (\Delta\bar{\nu}_t)\ \bar{E}_\nu + \Delta\bar{E}^*_K$$

$\Delta\bar{\nu}_t$ being the difference in the prompt fission yields of both systems, $\bar{B}_n$ being the mean neutron binding energy and $\bar{E}_\nu$ being the mean kinetic energy of the fission neutrons. With the present $\Delta\bar{E}^*_K$-value this energy balance is in equilibrium, which was not the case with the data of Toraskar and Melkonian [11].

The present results are in good agreement with those of Deruytter and Wegener-Penning [4], but due to improved experimental conditions we obtain a significantly better mass-resolution. Our results generally agree with those of Laidler and Brown [8] and Mostovaya [9,10], but they contradict the data of Toraskar and Melkonian [11]. A critical evaluation of all these results indicates that the additional 6.5 MeV excitation energy available in the thermal neutron induced fission of ^{239}Pu only leads to an additional fission fragment kinetic energy of about 1 MeV compared to the spontaneous fission of ^{240}Pu. This is an important result since this value was one of the basic data used by Lachkar in his dynamic approach to the fission proces [12].

3.2. Neutron induced fission measurements

In order to obtain a significant statistical accuracy in the neutron resonance region, the sample denoted by ^{239}Pu I (see Table I) was used, since it contained the largest amount of fissile material. However, this resulted in a poorer mass-resolution and peak-to-valley ratios of about 15. With this sample about twenty resonances were studied in the energy region 1-100 eV (Fig. 2). GELINA was operated at a repetition frequency of 400 Hz with a burst width of 11 ns. These data were calibrated to the thermal fission of ^{239}Pu during short runs at 100 Hz repetition frequency. The results are summarized in Table III. Since all these data were taken simultaneously, only the statistical errors have to be considered for an intercomparison. From this table it is clear that the mean mass of the light and the heavy fission fragments do not vary from resonance to resonance. Also for the mean total kinetic energy only small fluctuations are present. If we calculate the weighted mean of $\bar{E}^*_K$ for each group of spins, taking into account the spin-values recommended by Derrien [13] which seem to be the best ones at present [14], following results are obtained :

$$\bar{E}^*_K\ (J = 0) = 177.99\ \text{MeV} \pm 0.09\ \text{MeV}$$

$$\bar{E}^*_K\ (J = 1) = 178.04\ \text{MeV} \pm 0.03\ \text{MeV}$$

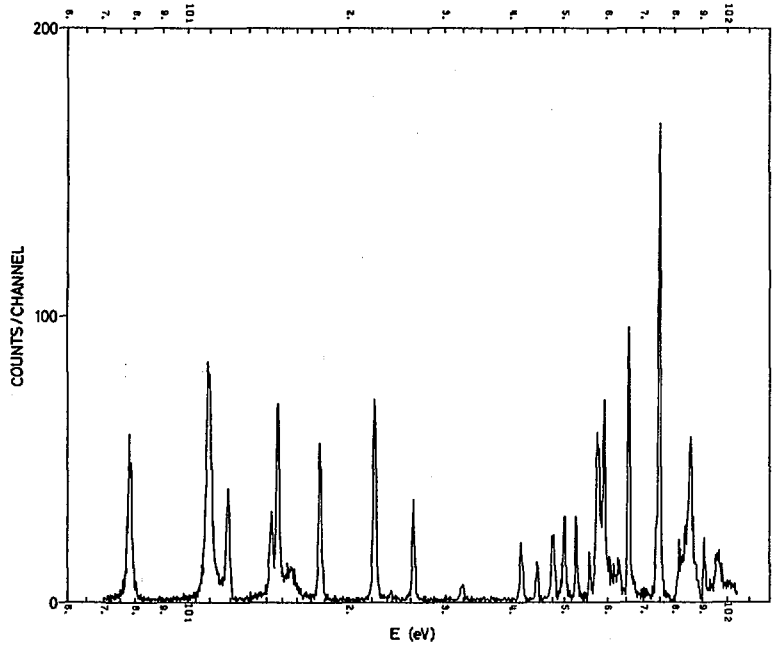

FIG.2. ^{239}Pu (n,f) resonances between 7 and 100 eV neutron energy.

Obviously, no difference is present, which seems to be in contradiction with the results of Melkonian and Mehta [15] who observed a difference of about 1 MeV between the $\bar{E}_K^*$-values for J = 0 and J = 1 resonances. Their conclusions were based on the ^{239}Pu spin values available in 1964. However, if we recalculate the weighted mean of their data, also using the spin values of Derrien [13], following values are obtained after normalization :

$$\bar{E}_K^* \text{ (J = 0)} = 178.00 \text{ MeV and } \bar{E}_K^* \text{ (J = 1)} = 178.01 \text{ MeV}$$

in perfect agreement with our results. Anyhow, in this respect the recent warning by Keyworth and Moore [14] that several ^{239}Pu spin-assignments remain questionable is very important and a reason for precaution.

An additional measurement was performed in the energy region below 1 eV, using the ^{239}Pu II sample which yielded a better resolution but a lower counting rate. Preliminary results indicate a thirty percent higher peak-to-valley ratio for the 0.296 eV resonance compared to the thermal value. This result is in qualitative agreement with the radiochemical data [16-18].
We will not enlarge upon this low-energy region since it is treated in detail by Walsh at al. [19].

TABLE III. MEAN TOTAL KINETIC ENERGY AND MASS VALUES FOR THE ^{239}Pu(n,f) RESONANCES

E_n (eV)	J	$\bar{E}_K^*$(MeV)	$\bar{m}_L^*$	$\bar{m}_H^*$
7.82	1	178.13 ± 0.07 [b]	100.74	139.26
10.93	1	178.00 ± 0.07	100.85	139.15
11.89	1	178.06 ± 0.13	100.94	139.06
14.31 / 14.68	1	178.06 ± 0.09	100.79	139.21
15.46	0	178.01 ± 0.18	100.73	139.27
17.66	1	178.10 ± 0.13	100.84	139.16
26.24	1	177.93 ± 0.15	100.78	139.22
32.31	0	178.21 ± 0.26	100.88	139.12
41.5 [a]	1	177.97 ± 0.10	100.77	139.23
47.6	0	177.79 ± 0.21	100.97	139.03
50 [a]	1	178.06 ± 0.13	100.91	139.09
57.44	0	178.02 ± 0.14	100.83	139.17
59.22	1	178.00 ± 0.19	100.99	139.01
66 [a]	1	178.04 ± 0.10	100.87	139.13
75 [a]	1	177.99 ± 0.12	100.64	139.36
85 [a] [c]	0	178.26 ± 0.12	100.76	139.24

a) poorly separated resonances; the spin of the dominating resonance is taken into account.

b) statistical error.

Finally, we will discuss how the present results fit in the frame of the channel theory of fission. For ^{239}Pu (n,f) several fission characteristics have been studied in the resonance region. A large channel effect has been observed for the Γ_f-values, which yield $\bar{\Gamma}_f(o^+)$ = 2.27 eV and $\bar{\Gamma}_f(1^+)$ = 0.035 eV [20] resulting in very different values for the effective number of open fission channels : N (o^+) = 1.48 resp. N (1^+) = 0.07. Also for the peak-to-valley ratio in the mass-distribution [21] and for the ternary fission yield [22] channel effects have been reported. Very interesting results on the mean number of fission neutrons and on the mean energy of the fission gammas $\bar{E}_\gamma$ were obtained by Shackleton [23], who observed a small but

significant channel dependence of $\bar{\nu}$. His $\bar{\nu}$ and $\bar{E}_\gamma$ data resulted in a small difference in the excitation energy of the fission fragments for both fission channels :

$$E_{f.exc.}\ (0^+) - E_{f.exc.}\ (1^+) = (109 \pm 43)\ \text{keV}$$

Our results on the fission fragment kinetic energy are in agreement with these data : for both spins the subdivision of the total available energy into fragment kinetic and excitation energies is the same within about 100 keV, which seemed not to be the case for the former data of Melkonian and Mehta [15].

4. CONCLUSIONS

The present work confirmed that the additional 6.5 MeV excitation energy available in the thermal neutron induced fission of ^{239}Pu only leads to an additional fission fragment kinetic energy of about 1 MeV compared to the spontaneous fission of ^{240}Pu.

For the ^{239}Pu (n,f) resonances no significant channel effect on the mean total fission fragment kinetic energy was observed, although some precaution is required here due to the uncertainty on the ^{239}Pu resonance spin assignments. Nevertheless, taking into account all the fission characteristics reported up to now, the channel theory seems to be verified for the ^{239}Pu (n,f)-resonances, although the amplitudes of some effects are smaller than expected. This attenuation might be due to the interactions and the energy transfers taking place between saddle and scission points.

ACKNOWLEDGEMENTS

The authors thank Prof. Dr. A. Deruytter, Dr. M. Nève de Mévergnies, Dr. B. Rose and Mr. K. Böckhoff for their interest in this work and for a critical reading of the manuscript. They are also indebted to the CBNM Sample Preparation Group for the preparation of the plutonium samples.

REFERENCES

[1] SCHMITT H., GIBSON W., NEILER J., WALTER F., THOMSON T., Physics and Chemistry of Fission 1, IAEA, Vienna (1965) 531.

[2] MILTON J., FRASER J., Ann. Rev. Nucl. Sci. 16 (1966) 894.

[3] MUGHABGHAB S., GARBER D., Brookhaven National Laboratory Report BNL 325 (1973).

[4] DERUYTTER A., WEGENER-PENNING G., Physics and Chemistry of Fission 2, IAEA, Vienna (1974) 51.

[5] ASGHAR M., CAITUCOLI F., PERRIN P., WAGEMANS C., Nucl. Phys. A 311 (1978) 205.

[6] KONECNY E., SPECHT H., WEBER J., Physics and Chemistry of Fission, 2, IAEA, Vienna (1974) 3.

[7] BRITT H., these proceedings

[8] LAIDLER J., BROWN F., Journ. Inorg. Nucl. Chem. 24 (1962) 1485.

[9] MOSTOVAYA T., Peaceful Uses of Atomic Energy (Proc. Second Int. Conf. Geneva, 1958) 15, UN, New York (1958) 433.

[10] OKOLOVICH V., SMIRENKIN G., Sov. Phys. JETP 16 (1963) 1313.

[11] TORASKAR J., MELKONIAN E., Phys. Rev. C4 (1971) 267 and 1391.

[12] LACHKAR J., PATIN Y., SIGAUD J., J. de Phys. L. 36, (1975) 79.

[13] DERRIEN H., Report NEANDC(E) 163 U (1974) 243.

[14] KEYWORTH G., MOORE M., Neutron Physics and Nuclear Data (Proc. Int. Conf. Harwell, 1978), OECD, Paris (1978) 241.

[15] MELKONIAN E., MEHTA G., Physics and Chemistry of Fission, 2, IAEA, Vienna (1965) 355.

[16] REGIER R., BURGUS W., TROMP R., SORENSEN B., Phys. Rev. 119 (1960) 2017.

[17] VAN ASSCHE P., VANDENPUT G., JACOBS L., VAN DEN CRUYCE J., SILVERANS B., Nuclear Physics with Thermal and Resonance Energy Neutrons (Proc. Symp. Petten, 1973), Report RCN-203 (1973) 95.

[18] KAISER T., VON GUNTEN H., Phys. Rev. C 17 (1978) 1510.

[19] WALSH R., BOLDEMAN J., ELCOMBE M., these proceedings.

[20] BLONS J., DERRIEN H., MICHAUDON A., Nuclear Data for Reactors (Proc. Int. Conf. Helsinki, 1970) 2, IAEA, Vienna (1970) 161.

[21] COWAN G., BAYHURST B., PRESTWOOD R., GILMORE J., KNOBELOCH G., Phys. Rev. 144 (1966) 979.

[22] WAGEMANS C., DERUYTTER A., Nucl. Phys. A 212 (1973) 556.

[23] SHACKLETON D., Dr. Sc. Thesis, University of Paris-Sud, 1974.

DISCUSSION

Yu.M. TSIPENYUK: Can you say anything about the J dependence of the mass distribution?

C.M.C. WAGEMANS: In the neutron energy region studied (5–100 eV) we observed no significant difference in the mass distributions for both spin groups. However, such differences are mainly to be expected in the symmetric fission region. On account of the relatively large ^{239}Pu target used in our measurements the experimental resolution was rather poor in this region and did not permit observation of differences in the peak/valley ratio.

R.L. WALSH: I would like to make two comments. First, whereas your value of $\Delta\bar{E}_K \approx 50$ keV between the $J = 0^+$ and $J = 1^+$ levels agrees with the $\bar{\nu}_p$ data obtained by Fréhaut and Shackleton, it does not tally with the value of $\Delta\bar{E}_K \approx 500$ keV implied by the $\bar{\nu}_p$ data from RPI, ORNL and Battelle Northwest. The higher value of $\Delta\bar{E}_K$ is in agreement with our own result.

Second, it would be worthwhile including the kinetic energy dependence of $\bar{\nu}_p(m)$ in your calculation of the neutron emission correction. In other words, you should use a matrix of values of ν (M, E_K), where E_K is the total kinetic energy for a given mass split. Values for the $\partial\bar{\nu}_p/\partial E_K|_{m=const}$ dependence can be derived for ^{239}Pu(n, f) from data on other nuclei, for example, ^{235}U(n, f).

C.M.C. WAGEMANS: I did not consider the kinetic energy difference implied by the American data on $\bar{\nu}$ that you quote, since they relate to the lower energy region (< 0.5 eV). Since our own $\bar{E}_K$ measurements cover the resonance region from 5 to 100 eV, the obvious $\bar{\nu}$ data to use are Shackleton's which were also calculated in this region.

With regard to your second point, I do not think that the use of $\bar{\nu}_p(m)$ instead of $\nu(m, E_K)$ would significantly alter our results. Indeed, since the same correction for neutron emission has been made for *all* resonances, the relative behaviour of $\bar{E}_K$ for these resonances should not be affected.

DISTRIBUTION OF NUCLEAR CHARGE AND ANGULAR MOMENTUM IN CHAINS 132–137, 99, AND 102 OF $^{235}U(n_{th}, f)$ AT VARIOUS KINETIC ENERGIES AND IONIC CHARGE STATES OF THE FRAGMENTS

H.O. DENSCHLAG, H. BRAUN, W. FAUBEL,
G. FISCHBACH, H. MEIXLER, G. PAFFRATH,
W. PÖRSCH, M. WEIS
Institut für Kernchemie,
Universität Mainz, Mainz, Federal Republic of Germany

H. SCHRADER, G. SIEGERT
Institut Laue-Langevin, Grenoble, France

J. BLACHOT
Centre d'études nucléaires, Grenoble, France

Z.B. ALFASSI*
Ben Gurion University, Beer Sheva, Israel

H.N. ERTEN*
Middle East Technical University, Ankara, Turkey

T. IZAK-BIRAN*
Soreq Nuclear Research Centre, Yavne, Israel

T. TAMAI*
Kyoto University Research Reactor Institute, Japan

A.C. WAHL*
Washington University, St. Louis, Missouri, USA

K. WOLFSBERG*
Los Alamos Scientific Laboratory, Los Alamos,
New Mexico, USA

* Guest scientist at Universität Mainz.

Abstract

DISTRIBUTION OF NUCLEAR CHARGE AND ANGULAR MOMENTUM IN CHAINS 132–137, 99, AND 102 IN $^{235}U(n_{th}, f)$ AT VARIOUS KINETIC ENERGIES AND IONIC CHARGE STATES OF THE FRAGMENTS.

The fission product yields of the members of the decay chains 132–137, 99, and 102 in $^{235}U(n_{th}, f)$ are measured at various kinetic energies and ionic charge states of the fragments using the mass separator for unslowed fission products 'LOHENGRIN'. The results are discussed with respect to four aspects:

(1) A preferential formation of neutron-rich chain members found at high kinetic energy of the fragments is predominantly due to decreasing prompt-neutron evaporation. A particularly large effect in chain 132 is attributed to the double shell closure in ^{132}Sn.

(2) The persistence of an even-odd pairing effect in the yields throughout the range of kinetic energies studied leads to the conclusion that the high internal excitation energy of the fragments is tied up mainly in the form of collective energy (e.g. deformation energy) rather than single-particle excitation.

(3) In chains 132, 134, 135, and 137, the yield distribution at constant kinetic energy was found to be invariant with the ionic charge state of the isotopes separated. Deviations from this behaviour found in chains 99, 102, 133, and 136 are interpreted as being due to Auger events following a converted transition in the decay of ns isomers taking place in the vacuum of the separator.

(4) A pronounced variation of the independent formation ratio of individual isomeric states with the kinetic energy of the fragments provides direct information on the controversial topic of the change of angular momentum of fission fragments as a function of deformation (scission distance).

1. Introduction

Radiochemical yield measurements have been a useful tool in the study of nuclear fission, providing some information on nuclear temperatures and angular momentum at the scission point through determination of even-odd factors and of isomeric yield ratios.

Radiochemical measurements generally supply information on quantities averaged e.g. over the kinetic energy. Correction for the emission of prompt neutrons (or γ-rays) is possible only in terms of their average values thus producing a somewhat blurred picture of the initial conditions.

The mass separator LOHENGRIN [1,2,3] may be used to improve this situation as it allows the separation of fission products according to their initial kinetic energy. The total

energy of a fission into two given products is constant. In consequence, the kinetic energy of fission fragments is inversely correlated to their internal excitation energy, and a fission fragment pair of particular kinetic energy will possess a well defined total excitation energy and will therefore emit a particular number of neutrons and/or γ-rays. A particular kinetic energy is also presumably connected to a well defined distance of the charge centers at the scission point, i.e. a particular scission configuration.
Measurements of the yield distribution of the light-wing fission products have been carried out at LOHENGRIN using various kinds of dE/dx-detectors [4-11] for the elemental assignment of the isobars. These measurements concentrated on the mean kinetic energy of the fission fragments, but some measurements at other kinetic energies were included [7,8,10]. The most recent survey will be given in these proceedings[11]. Unfortunately, this method is limited to the light-wing fission products because of resolution problems. Therefore, the study of the heavy-region fission products presented in the following is based on a radiochemical method. This method has the disadvantage of depending on the decay characteristics of each individual nuclide measured. In consequence, it is much more laborious than the physical methods. It has the other drawback that nuclides near stability cannot be measured with high accuracy. It has, however, the advantage that the yields of individual isomers can be differentiated. The possibility of measuring the independent yields of individual isomers has induced us to include light-wing chains 99 and 102 in our programme.

2. Experimental

Due to space limitations only the principal approach will be described here, and further details will be given in separate papers [12].
The fission products were produced inside the mass separator LOHENGRIN of the Institut Laue-Langevin in Grenoble. UO_2-targets with a thickness of 40 or 100 $\mu g/cm^2$ were used. In some

of the experiments they were covered with a nickel foil of 0.5 μm thickness. In all cases the energy loss of the fragments was determined experimentally by measuring the fragment beam intensity at various kinetic energies and comparing the maximum of the distribution with the most probable kinetic energy of the same mass as obtained by Schmitt et al. [13]. The values of kinetic energies given in this paper have all been corrected for energy loss in the target and due to prompt neutron emission.

The beam of fission products separated according to mass, ionic charge state, and kinetic energy was stopped in a fast transport tape outside the separator. The collection of activity was restricted to a length of 200 mm of tape (as compared to the total length of 720 mm of the exit slit) in order to maintain an energy resolution of $\pm$ 1.5% (ca.1 MeV) and to have a uniform deposition profile along the collection length. The collected fission products were transported to a shielded and absolutely calibrated counting position (Ge(Li) detector and zig-zag mechanism) either continuously or in a start-stop mode, and the γ-rays associated with their β-decay were counted. The velocity of transportation was chosen according to the half-lives of the nuclides studied. Appropriate corrections for growth and decay during collection, transport, and counting, and for detection efficiency allow the calculation of the number of atoms of the individual chain members produced. The fractional yields were obtained by two methods:

a) They were determined from the absolute activity of a descendant with a fractional cumulative yield nearly equal to unity (e.g. ^{134}I, ^{137}Xe, $^{99m+g}Nb$, and ^{135}Xe). Descendants too long-lived for on-line counting (e.g. 78 h - ^{132}Te, 20.8 h-^{133}I, and 9.35 h-^{135}Xe) were (partly) collected on a strip of aluminium foil (generally 25-50 mm wide) maintained fixed in front of the moving tape system during the whole experiment. The activity on this collector strip was measured after the on-line experiment using a well shielded Ge(Li) detector.

b) In chain 136 this method could not be used due to the stability of Xe. Therefore, the total number of fragments was counted directly by inserting a surface barrier detector into the beam of fragments inside LOHENGRIN.

Method a) is preferred over method b) as it is less sensitive to impurities in the separated masses.

Generally, the limited count rates required a fair detection efficiency (source-to-detector distance ca. 2 cm). This in turn made necessary a careful correction of summing loss [14,15] both in the calibration of the detectors and in the actual measurements.

The evaluation of the data relies on the decay properties (half-lives, absolute γ-line intensities, conversion coefficients, branching ratios, etc.) of the nuclides measured. In many cases these values were not known and had to be determined in separate radiochemical experiments. Space does not allow the description of these measurements here. The values used are, however, given in Table I.

3. Results and Discussion

The fractional independent yields obtained will be presented and discussed in two sections. The first section will deal with the influence of the ionic charge state of the fragments on the yields observed. In the second section the variation of the yields with the kinetic energy of the fragments will be treated.

3.1. Fractional independent yields at various ionic charge states of the fragments

In chains 132, 134, 135, and 137, the yield distribution at constant kinetic energy was found to be invariant with the ionic charge state of the isotopes separated. An example of this type of behaviour is shown in Fig. 1 for chain 134. In chains 136, 99, 102, and 133, however, a marked dependence of the yields on the charge state of the ions is observed.

TABLE I. DECAY PROPERTIES USED IN THE EVALUATION OF THE MEASUREMENTS[a]

Mass number	Nuclide	$T_{1/2}$[s]	E_γ[keV]	I_γ	P_1	P_2
99	Y	2.3(1.6)	122	0.41		
	Zr	2.0	468 546	0.58 0.46		
	Nb[1/2$^-$]	168	253 351	0.079 0.059	0.29	
	Nb[9/2$^+$]	15	137	0.90(0.0214)	0.71	
	Mo	66.0[h]				1
102 [b]	Zr	2.2	600	0.075		
	Nb[high]	4.3	446	0.10	0.33	
	Nb[low]	1.3	400	0.12	0.67	
	Mo	690				1
132	Sn	40	247	0.417		
	Sb[8$^-$]	252	150	0.658	0	
	Sb[4$^+$]	168	974 696	1 (1) 0.69(1)	1	
	Te	77.8[h]	228	0.88		1
133	Sb	2.34[m]	1096	0.32		
	Te[11/2$^-$]	55.4 [m]	912	0.62	0.29	
	Te[3/2$^+$]	12.45[m]	312	0.70	0.71	0.16
	I	1248 [m]	530	0.89		0.84
134	Sb	11	297 1279	0.97 1		
	Te	2508	211 767	0.248 0.297		
	I[8$^-$]	228	272	0.79		
	I[4$^+$]	3156	847 884	0.956 0.654	1	1
135	Te	18	603	0.254		
	I	6.59[h]	1260	0.286		
	Xe[11/2$^-$]	15.3 [m]	526	0.799	0.147	
	Xe[1/2$^+$]	9.17[h]	250	0.902	0.853	1

TABLE I (cont.)

136	Te	17.5	332	0.36		
	I[5⁻]	46.0	381	1.0		
	I[2⁻]	83.0	1313 1321	0.67(1) 0.25	1	
	Xe	stable				1
137	Te	3.5	243	0.15		
	I	24.7	1219	0.134		
	Xe	229.8	455	0.31		

[a] $T_{1/2}$ Half-life of isotope.
E_γ Energy of γ-ray(s) evaluated.
I_γ Absolute line intensity of γ-ray (value in parentheses refers to the feeding of the same γ-ray in the decay of an isomer).
P_1 Fraction of β-decay to isomer indicated.
P_2 Fraction of decay of isomer to nuclide indicated.
Values from [16] or [17] when available, otherwise [12].

[b] Preliminary data, further radiochemical studies in progress.

The results of the first three chains mentioned are shown in Figs. 2 - 4.
Similar effects were observed by Siegert et al. [18] and by Clerc et al. [7,19] for the light-wing fission products. They were explained as being due to the emission of Auger electrons following converted γ-ray transitions of nanosecond (ns) isomers taking place while these isomers are flying through the vacuum of the separator before entering the magnetic and electric fields (time period from 10^{-14} s until $2 \cdot 10^{-6}$ s after fission). The increase in the mean ionic charge due to the Auger effect will lead to an increased yield of a nuclide with such an isomeric state at high ionic charge states as is observed for $^{136}I[5^-]$ and $^{136}I[2^-]$ (Fig.2), ^{99}Zr (Fig.3), $^{102}Nb[1^+]$ (Fig.4), and for $^{133m+g}Te$

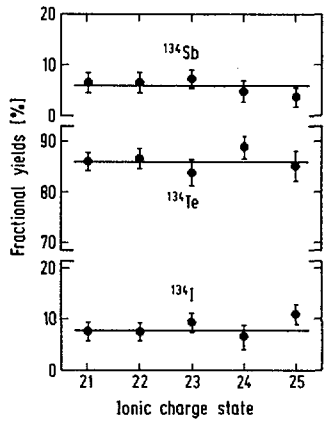

FIG.1. Fractional cumulative (Sb) and independent (Te, I) yields in chain 134 at various ionic charge states of the fragments. Kinetic energy E_k = 77.2 [MeV].

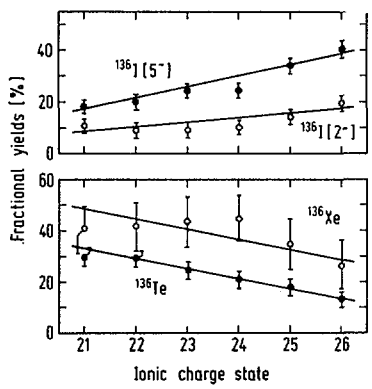

FIG.2. Fractional cumulative (Te) and independent (I, Xe) yields in chain 136 at various ionic charge states of the fragments. Spin and parity of iodine isomers indicated in brackets. E_k = 75.2 [MeV].

(not shown). The fact that fractional yields have been plotted leads to seemingly decreasing yields for the other unaffected isotopes (^{136}Xe, ^{136}Te in Fig.2, ^{99}Y in Fig.3, ^{102}Zr, ^{102}Nb[h] in Fig.4). The yields of the isomers of ^{99}Nb (Fig.3) appear to be practically constant. This could be interpreted as indicating the presence of another - less effective - isomeric transition in that chain feeding the two isomers and

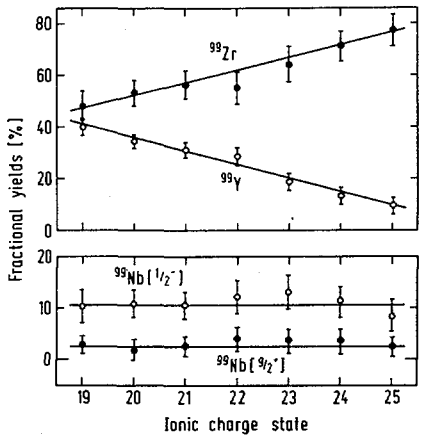

FIG.3. Fractional cumulative (Y) and independent (Zr, Nb) yields in chain 99 at various ionic charge states of the fragments. Spin and parity of Nb-isomers indicated in brackets. $E_k = 102.7$ *[MeV].*

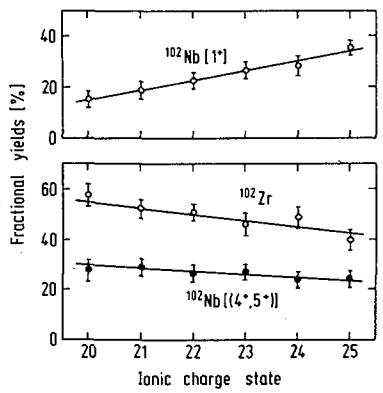

FIG.4. Fractional cumulative (Zr) and independent (Nb) yields in chain 102 at various ionic charge states of the fragments. Assumed spins and parities of Nb-isomers indicated in brackets. $E_k = 102.5$ *[MeV].*

compensating for the expected decrease in yield. In this context it is interesting to note that in chain 102 the ns isomer seems to be feeding only the low-spin isomer of Nb whereas in chains 99 and 136 both isomers are apparently fed to nearly the same extent. It should be stated here that the results concerning chain 102 require further confirmation as

TABLE II. NANOSECOND ISOMERS POSSIBLY RESPONSIBLE FOR HIGHER-THAN-AVERAGE IONIC CHARGES OF FISSION PRODUCTS IN LOHENGRIN

Fission Product of High Ionic Charge	Nanosecond Isomer [20]
^{99}Zr	∿ 15 ns - ^{99m}Zr
	∿300 ns - ^{99m}Zr
^{99}Nb	7 ns isomer of mass 99 and unidentified Z
	100 ns isomer of mass 99 and unidentified Z
^{102}Nb	271 ns isomer of mass 102 and unidentified Z
	<4 ns - ^{102}Zr ?
^{133}Te	∿85 ns isomer of mass 133 and unidentified Z
	750 ns isomer of mass 133 and unidentified Z
^{136}I	3 ns - ^{136m}I

they are based on preliminary information concerning the decay characteristics (see Table I). In the present examples, as in the cases identified in Refs. [18] and [19], ns isomers that could be responsible for the effect have been detected independently by Clark et al. [20] (Table II).
However, the identification of these isomers is not fully conclusive as numerous additional ns isomers have been detected [20], in particular in chains 132, 134, 135, and 137. These chains, however, have shown no dependence on the ionic charge state.
It seems desirable to give additional support to the interpretation given above, e.g. by measuring the half-live of the parent assumed responsible for the increased ionic charge. This can be done by introducing into LOHENGRIN a thin foil which will re-equilibrate the ionic charge of the ions in flight. A 're-equilibration' prior to the decay of the isomer will not affect the increased average charge while a re-equilibration after decay will remove the effect. Therefore, the measurement of the average ionic charge as a function of

the target-to-foil distance will allow the calculation of the desired lifetime as the velocity of the ions can be calculated from their energy.

3.2. Fractional independent yields at various kinetic energies of the fragments

The yields measured for the various fission product chain members and kinetic energies are given in Table III.
The yields indicated refer to the cumulative yield of the last chain member shown. This yield can generally be assumed to be identical with the chain yield. In some cases, however (e.g. in chain 133 at low kinetic energy), the independent yield of the subsequent chain member (^{133}I) is not negligible even though it could not be measured. In these cases,possible effects on Z_p values and even-odd factors discussed subsequently have been taken into account.
The yields of individual isomeric states are indicated in Table III. In two cases (chains 134 and 135), however, the yields of the individual isomers had to be determined in separate experiments, and therefore the fragment kinetic energies were not identical. In these cases the yields(^{135}Xe) or the fraction of high-spin isomer relative to the total,

$$F_h = \frac{Y_{FI}(\text{high-spin isomer})}{Y_{FI}(\text{both isomers})}$$

(^{134}I), are given separately in Table III.
In general, good agreement is observed between radiochemical yield values [21] and the yields obtained in the present experiments at the mean kinetic energy of the fragments. There is also general agreement concerning chains 99 and 102 with the data obtained at LOHENGRIN (at mean kinetic energy) using physical methods [6,8].
A typical example of the change in yields with varying kinetic energy of the fragments is shown in Fig.5. This example has been chosen as it allows a comparison with results of Clerc et al.[7,7a] at two kinetic energies of the fragments. The agreement seems reasonable. Other measurements at other kinetic energies [8] agree in their trends. Some deviations

TABLE III. EXPERIMENTAL FRACTIONAL YIELDS OF FISSION PRODUCTS INDICATED, AND CORRESPONDING Z_p AND EOF VALUES OBTAINED BY FITTING A GAUSSIAN CURVE MODULATED BY EVEN-ODD FACTORS

A = 99 q = 21^+ $\bar{E}_k$ = 102.2[MeV] $\bar{\nu}$ = 1.54

E_k	Y	Zr	Nb[$1/2^-$]	Nb[$9/2^+$]	$Z_p(\sigma=0.60)$	EOF
96.7	13.8±2.0	58.9±7.3	15.8±3.9	11.5±4	40.15±0.08	1.00±0.17
100.0	22.7±2.5	59.2±8.0	11.5±3.5	6.6±4.4	39.95±0.09	0.98±0.17
102.7	31.3±3.7	55.5±6.0	10.7±3.0	2.5±2.0	39.81±0.10	0.95±0.16
105.7	39.5±4.0	49.4±6.1	8.7±4.0	2.4±2.0	39.72±0.11	0.88±0.17
107.8	49.1±3.9	39.8±5.0	10.9±4.5	<0.5	39.66±0.12	0.75±0.17

A = 102 q = 22^+ $\bar{E}_k$ = 102.5[MeV] $\bar{\nu}$ = 1.40

E_k	Zr	Nb[high]	Nb[low]	$Z_p(\sigma=0.56)$	EOF=1.25
95.6	27.2±2.8	46.6±5.0	26.2±3.5	41.03±0.12	
96.5	26.5±2.8	40.7±4.3	32.8±3.5	41.05±0.14	
99.0	42.0±4.0	36.0±4.0	22.0±3.5	40.79±0.09	
102.5	51.1±5.5	26.2±4.6	22.7±3.5	40.63±0.10	
105.1	55.2±5.6	24.0±4.0	20.8±3.5	40.56±0.10	
106.8	55.1±5.6	17.9±4.0	27.0±3.5	40.56±0.12	
107.8	64.3±6.5	15.1±4.0	20.6±3.5	40.37±0.14	

A = 132 q = 23^+ $\bar{E}_k$ = 79.8 [MeV] $\bar{\nu}$ = 0.49

E_k	Sn	Sb[8^-]	Sb[4^+]	Te	$Z_p(\sigma=0.56)$	EOF
75.3	5.3±2.0	11.5±2.0	15.8±3.0	67.4±5	51.58±0.18	1.57±0.28
78.9	13.9±2.0	13.1±0.8	31.8±4.2	41.2±4	51.22±0.06	1.36±0.12
79.8	14.4±2.0	14.0±1.0	31.1±3.0	40.5±3.0	51.21±0.05	1.36±0.11
82.6	19.5±4.0	16.1±3.0	39.0±3.7	25.4±3.8	51.05±0.07	1.18±0.15
86.6	34.9±4.0	10.6±2.6	33.1±4.5	21.4±4.6	50.90±0.07	1.47±0.20

A = 133 q = 23^+ $\bar{E}_k$ = 78.5 [MeV] $\bar{\nu}$ = 0.65

E_k	Sb	Te[$11/2^-$]	Te[$3/2^+$]	$Z_p(\sigma=0.56)$	EOF=1.25
68.7	17.1±6.2	66.7±8.4	16.2±1.6	52.03±0.20	
73.3	28.9±3.2	49.8±4.2	21.3±1.2	51.75±0.12	
79.7	50.6±3.0	28.9±3.0	20.5±2.0	51.37±0.12	
83.4	66.9±1.5	15.4±2.0	17.7±1.0	51.17±0.16	

TABLE III (cont.)

A = 134 q = 23^+ $\bar{E}_k$ = 77.2 [MeV] $\bar{\nu}$ = 0.85

E_k	Sb	Te	I	$Z_p(\sigma=0.47)$	EOF
71.7	4.3±0.2	71.8±0.2	23.9±0.2	52.26±0.02	1.18±0.02
75.4	4.4±0.2	80.9±1.4	14.7±1.4	52.18±0.03	1.41±0.06
79.0	7.3±1.2	83.8±2.0	9.0±0.8	52.03±0.04	1.44±0.11
81.8	7.0±0.4	87.3±3.4	5.8±2.2	51.97±0.07	1.65±0.30
84.7	10.4±0.6	82.5±3.6	7.1±3.2	51.94±0.09	1.39±0.26

A = 135 q = 24^+ $\bar{E}_k$ = 75.0 [MeV] $\bar{\nu}$ = 0.99

E_k	Te	I	Xe	$Z_p(\sigma=0.56)$	EOF
70.2	29.2±1.3	66.8±1.3	4.0±2.0	52.61±0.09	0.75±0.10
71.5	43.1±1.4	53.4±1.4	3.5±2.0	52.50±0.10	0.90±0.12
73.0	44.3±1.7	52.4±1.7	3.3±2.0	52.49±0.08	0.91±0.13
75.0	60.2±2.3	37.3±2.3	2.5±2.0	52.35±0.05	1.00±0.04
75.7	64.1±2.4	33.4±2.4	2.5±2.0	52.28±0.05	0.99±0.04
78.5	78.4±2.7	19.8±2.7	1.8±2.0	52.07±0.07	1.05±0.04
78.8	75.5±1.8	23 ±1.8	1.5±2.0	52.13±0.06	1.04±0.04
81.2	84.0±4.0	15.5±4.0	0.5±2.0	51.95±0.07	1.04±0.10

A = 136 q = 24^+ $\bar{E}_k$ = 74.0 [MeV] $\bar{\nu}$ = 1.07

E_k	Te	$I[2^-]$	$I[5^-]$	Xe	$Z_p(\sigma=0.56)$	EOF
68.6	5.1±1.5	9.2±2.1	23.0±5.5	62.7±6.1	53.59±0.18	1.40±0.26
72.3	11.9±3.0	13.6±2.9	28.8±5.9	45.9±11.5	53.27±0.10	1.38±0.18
75.5	17.3±4.5	12.2±3.0	25.3±5.2	45.3±13.1	53.19±0.11	1.61±0.12
79.5	19.6±4.9	17.6±5.0	20.2±4.3	42.6±14.3	53.15±0.12	1.63±0.13

A = 137 q = 21^+ $\bar{E}_k$ = 73.0 [MeV] $\bar{\nu}$ = 1.11

E_k	Te	I	Xe	$Z_p(\sigma=0.56)$	EOF
66.8	9.0±0.2	31.6±8.0	59.4±7.8	53.38±0.05	1.60±0.23
68.1	2.8±0.3	30.4±6.9	66.8±6.9	53.67±0.06	1.27±0.20
69.6	6.8±0.2	40.7±8.6	52.5±8.4	53.41±0.07	1.28±0.20
71.8	5.8±0.2	40.5±9.0	53.7±8.4	53.44±0.06	1.24±0.19
72.2	8.1±0.3	45.1±9.2	46.8±8.8	53.35±0.05	1.23±0.18
72.7	7.0±0.2	40.4±8.7	52.6±8.5	53.40±0.05	1.29±0.19
73.3	9.2±0.4	44.3±9.2	46.5±8.8	53.32±0.06	1.28±0.19
75.5	10.9±0.5	45.5±9.5	43.6±9.0	53.28±0.06	1.29±0.19
77.0	14.9±0.8	47.5±10.0	37.6±9.2	53.18±0.07	1.31±0.20
79.2	18.6±1.0	44.3±10.3	37.1±9.2	53.14±0.08	1.43±0.20
81.7	14.8±1.0	53.9±10.3	31.3±9.3	53.15±0.09	1.17±0.20

TABLE III (cont.)

A=134: E_k	$F_h(^{134}I)$
72.8	0.347±0.029
75.4	0.352±0.019
77.5	0.283±0.066
79.1	0.195±0.017
81.5	0.096±0.007

A=135: E_k	Xe[11/2$^-$]	Xe[1/2$^+$]
72.0	2.34±0.15	<3
75.0	0.94±0.12	<3
75.7	0.67±0.08	<3
79.8	0.29±0.14	<3

Explanation of symbols:

A mass number of chain,

q ionic charge state of fragments separated,

$\overline{E}_k$ mean kinetic energy of fragments from [13],

$\overline{\nu}$ number of prompt neutrons emitted from fragments of mass A from [22],

E_k primary kinetic energy of fragment observed (corrected for energy loss in the target and by prompt neutron emission) [MeV],

F_h Fraction of independent yield of high-spin isomer in relation to total independent yield of nuclide,

Z_p, EOF, σ : see equations (1,2).

at low kinetic energies are presumably due to their use of a thick UO_2-target (400 $\mu g/cm^2$) and the consequent loss in energy resolution.

The trend observed in Fig.5 and common to all chains studied (Table III) is an increase with increasing kinetic energy of the yield of the chain member with the lowest nuclear charge at the expense of the chain members with higher nuclear charges. The slight maximum found for the intermediate chain member ^{99}Zr resulting from some gain in yield from ^{99}Nb and from some subsequent loss to ^{99}Y at higher energies is found even more pronounced in other chains (e.g. in chain 132). The observed effects are among other reasons due to the decrease in prompt neutron emission with decreasing excitation energy (increasing kinetic energy) of the fragments.

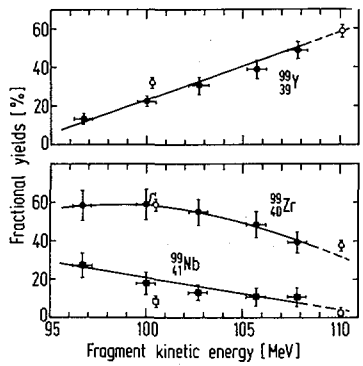

FIG.5. Fractional cumulative (Y) and independent (Zr, Nb) yields in chain 99 at various kinetic energies of the fragments ($q = 21^+$). Blank points from [7,7a], full points this work.

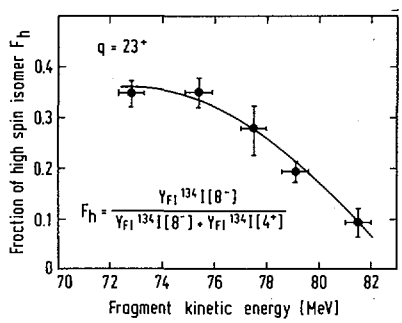

FIG.6. Fraction of independent yield of $^{134}I\,[8^-]$ relative to total independent yield of $^{134}I\,[8^-]$ and $[4^+]$ at various kinetic energies of the fragments.

Besides the change in element yields mentioned, a strong variation in the independent yields of isomeric states is observed in this work for the first time. This effect, consisting of a decrease of F_h, and observed in chains 99, 102, 132, 133, 134, 135, and 136 (Table III) is illustrated in Fig.6 for chain 134.

In the following, the changes in yields will first be discussed in terms generally used for a discussion of charge distribution in nuclear fission, i.e. Z_p, σ, and even-odd factors (EOF) [22,23,24]. Finally, the changes in the independent yields of isomers will be discussed with respect to the angular momentum of the fission fragments and scission point configurations.

In order to study the effects of kinetic energy on the charge distribution, Gaussian type curves modulated by even-odd factors, as given below, were fitted to the observed yields.

$$(1) \qquad FI(Z) = N^{-1} \int_{Z-1/2}^{Z+1/2} EOF(Z)\cdot P(Z)\cdot dZ \quad , \quad \text{and}$$

$$(2) \qquad FC(Z) = N^{-1} \int_{Z=-\infty}^{Z+1/2} EOF(Z)\cdot P(Z)\cdot dZ$$

$$\text{with:} \quad P(Z) = (2\pi\sigma^2)^{-1/2}\cdot\exp[-0.5\cdot((Z-Z_p)/\sigma)^2].$$

FI (FC): fractional independent (cumulative) yields.

N is a normalization factor assuring that the sum of all fractional independent yields within one chain remains equal to unity after the modulation by even-odd factors.

$$N = \int_{Z=-\infty}^{Z=+\infty} EOF(Z)\cdot P(Z)\cdot dZ$$

This curve is described completely by a set of three variables:

Z_p: the most probable charge,
σ : the width parameter of the curve, and
EOF: the even-odd pairing factor.

Calculation of the three parameters requires the knowledge of at least four yields. However, the present experiments provide only two or three element yields per chain (Table III). Therefore, only some of the values could be calculated explicitly[1]. Whenever three yields were measured, both Z_p and EOF were calculated. In the other cases only Z_p was calculated.

[1] The calculation was carried out using the fit-program ORGLSW.

In these cases the assumed values of σ and/or EOF were based on independent information, e.g. the radiochemical yield distribution. Fortunately, the results obtained for Z_p are quite insensitive to the assumed values of σ and/or EOF since the yields used were those of the most prominent chain members. Even the simple calculation of the average nuclear charge $\overline{Z}$ according to [5,9] leads to almost identical results. Although the absolute size of EOF is sometimes affected by the choice of σ, fortunately the change in EOF with the kinetic energy of the fragments is practically not affected as long as σ itself does not vary with energy.

The present method of evaluation is preferred over the method used in Refs. [5] and [9], because it allows the handling of incomplete sets of data more easily in a self-consistent way. The main advantage of the present method is, however, that it provides a well-defined EOF value, whereas the other method uses the oscillation of σ', the square root of the second moment of the charge distribution, to obtain an even-odd factor in a less direct way.

The resulting Z_p and EOF values are given in Table III. The Z_p values are plotted in Fig.7 versus the deviation from average fragment kinetic energy $(E_k-\overline{E}_k)$. The data points in the figure may be compared with a drawn-out line representing Z_{UCD}, the nuclear charge calculated assuming unchanged charge density according to the equation:

$$(3)\quad Z_{UCD}(E_k) = (A + \nu_A(E_k)) \cdot \frac{Z_F}{A_F}$$

$$\text{with}\quad \nu_A(E_k) = \overline{\nu}_A - \frac{E_k-\overline{E}_k}{7}\ , \quad \text{when } \overline{\nu}_A - \frac{E_k-\overline{E}_k}{7} \text{ positive,}$$

$$\text{else } \nu_A(E_k) = 0,$$

where

- A mass number of fission product,
- $\nu_A(E_k)$ number of prompt neutrons emitted by chain of mass A at kinetic energy E_k,
- $\overline{\nu}_A$ mean number of prompt neutrons emitted by chain A (from [22]),
- Z_F, A_F charge and mass of compund nucleus.

The relation assumes that about 7 MeV have to be spent in order to evaporate a neutron [25]. It could be shown that the

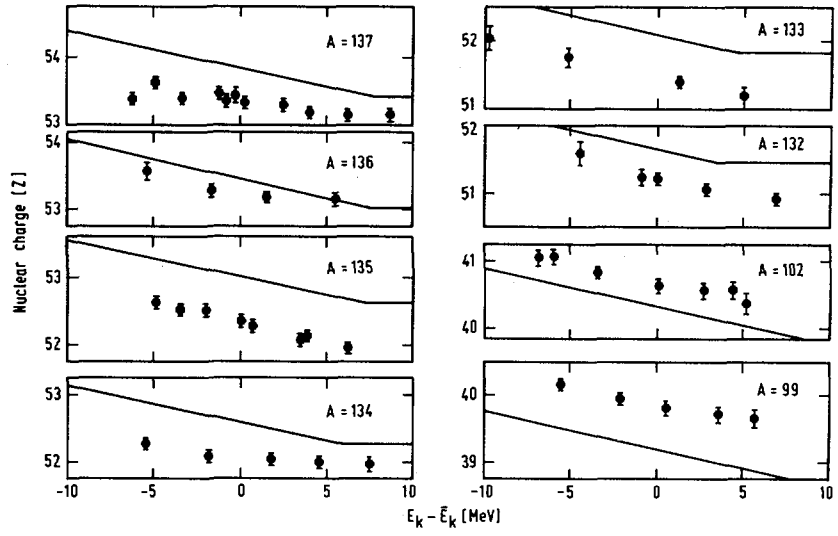

FIG.7. Z_p-values (data points) from Table III and Z_{UCD} (drawn-out line) as calculated from Eq.(2) at various kinetic energies of the fragments (E_k). For better comparability the kinetic energies have been normalized to the mean kinetic energy ($\bar{E}_k$) of the fragments of the same mass (from Ref.[13]).

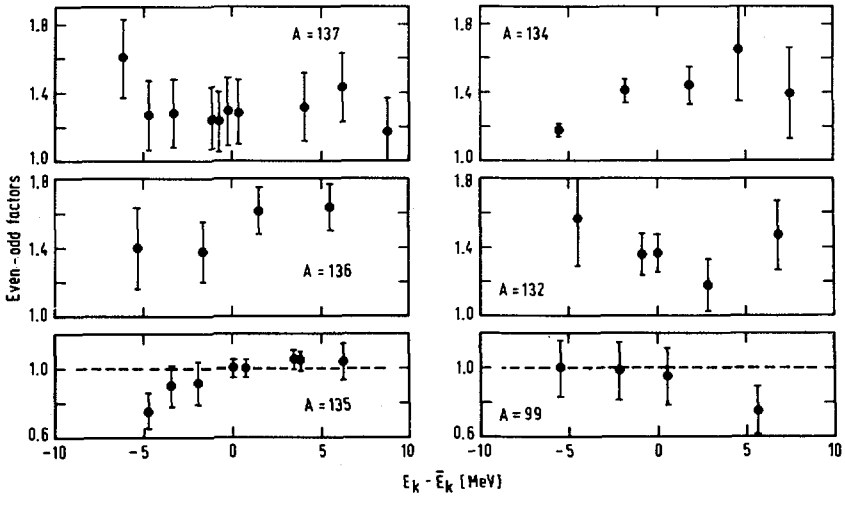

FIG.8. Even-odd factors (EOF values) from Table III at various kinetic energies of the fragments (E_k). For better comparability the kinetic energies have been normalized to the mean kinetic energy ($\bar{E}_k$) of the fragments of the same mass (from Ref. [13]).

number of neutrons emitted at the mean kinetic energy $\bar{E}_k$ corresponds to the mean number of neutrons emitted at all kinetic energies.

The distance between the experimental points (Z_p) in Fig.7 and the line (Z_{UCD}) represents the parameter ΔZ ($=Z_p - Z_{UCD}$) used to describe the charge polarization in the fissioning nucleus [22].

At a first glance, the change in Z_p (data points) is essentially parallel to the change in Z_{UCD}, indicating that the decrease in prompt neutron emission with decreasing excitation energy of the fragments has the dominating influence on the variation of the experimental yields, and that the distribution of protons and neutrons at scission is roughly independent of the scission distance. Looking more closely, however, one finds deviations from this simple behaviour:

(1) The Z_p values in chains 137,136,and 134 seem to approach the Z_{UCD}-line at high kinetic energies. This trend was actually predicted for all chains by Wilkins et al.[26]. The differences in the behaviour of neighbouring chains can possibly be attributed to an uneven distribution of excitation energy among complementary fragments [27].

(2) In chain 132 the opposite effect is found; the gap between Z_p and Z_{UCD} somewhat widens at high kinetic energies, when prompt neutron emission has ceased. Possibly, this is due to the influence of the double shell closure in $^{132}_{50}Sn^{82}$.

The even-odd factors given in Table III are plotted in Fig.8 versus $E_k - \bar{E}_k$.

The behaviour is somewhat complicated as was also found for the light-wing fission products [5,9]. There are chains showing practically no even-odd effect (99,135), and others with strong effects (A = 132, 134, 136, and 137). The most interesting result is certainly the observation that the effect is apparently preserved over the whole span of kinetic energies, which indicates that the internal excitation energy of more than 15 MeV (corresponding to low kinetic energy) is tied up almost exclusively in collective degrees of freedom, e.g. deformation energy. The results in chains 132 and 137,

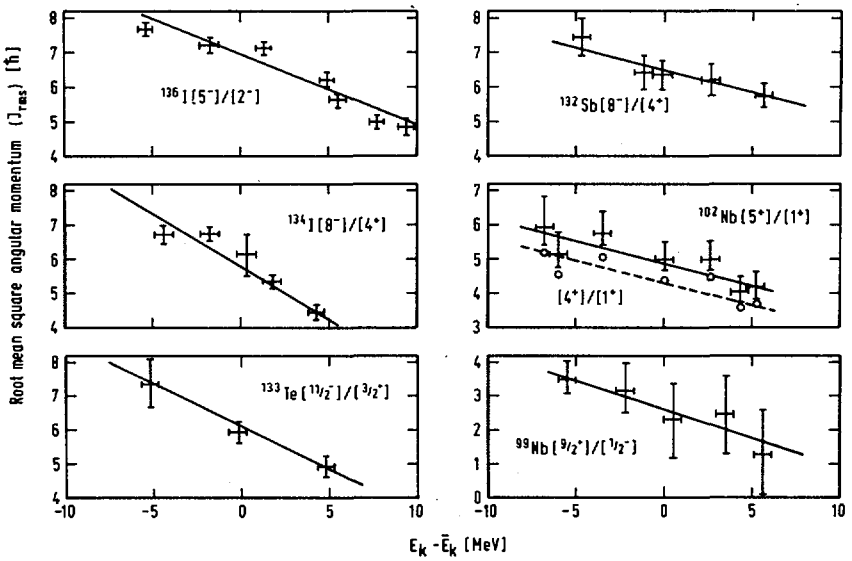

FIG.9. Root-mean-square angular momentum of fission fragments calculated from the independent formation ratios of single isomeric states characterized by their spins and parties at various kinetic energies of the fragments (E_k). For better comparability the kinetic energies have been normalized to the mean kinetic energy ($\bar{E}_k$) of the fragments of the same mass (from [13]). The results obtained for Nb-102 are based on preliminary decay characteristics and have been calculated for two values of high spin.

TABLE IV. COEFFICIENTS DESCRIBING THE CHANGE IN ROOT-MEAN-SQUARE ANGULAR MOMENTUM (J_{rms}) WITH FRAGMENT KINETIC ENERGY

Fragment mass number (A)	$\Delta J_{rms}/\Delta E_k$ [ħ/MeV]
99	- 0.17 ± 0.10
102 [5⁺/1⁺] [a]	- 0.13 ± 0.05
102 [4⁺/1⁺] [a]	- 0.11 ± 0.04
132	- 0.13 ± 0.05
133	- 0.27 ± 0.07
134	- 0.31 ± 0.03
136	- 0.20 ± 0.02

[a] Obtained for the two assumed spin combinations; results of chain 102 are based on preliminary information on decay characteristics (see footnote to Table I).

showing a possible minimum in the even-odd factors around $\bar{E}_k$, could be interpreted as supporting results of Nifenecker et al. [27], indicating that the 'intrinsic excitation energy' (total energy minus kinetic (coulombic) and deformation energies) shows a maximum for those fragments carrying the mean kinetic energy. However, the results of chain 134 contradict this interpretation, and the results of chain 136 do not support it. Measurements of more chains are needed to answer this question.

One of the most interesting results of the present work certainly concerns the independent yields of the individual isomers and their variation with kinetic energy.

Using the formalism developed by Huizenga and Vandenbosch [28,29] and the equations as explicitly written down in [30], the ratios of independent yields of the isomers as given in Table III were converted into the root mean square angular momentum (J_{rms}) of the fission fragments. The resulting values are plotted in Fig.9 as a function of $E_k-\bar{E}_k$.

The values obtained for the mean kinetic energy of the fragments ($E_k-\bar{E}_k = 0$ in Fig.9) cluster around 6-7 $\hbar$ for the heavy fission products and somewhat less for the light fission products in agreement with results obtained by other groups, e.g. Wilhelmy et al. [31]. The unusually low value of J_{rms} for ^{99}Nb may be due to nonstatistical effects in the de-exitation of ^{99}Nb fission fragments [32,28].

The most striking effect observed in Fig.9 is the pronounced decrease in J_{rms} by about 3 $\hbar$ per 10-15 MeV. This effect, expected on theoretical grounds[31,33,34], has long been debated since the limited experimental information available was contradictory. Wilhelmy et al. [31] concluded from the relative intensities of ($6^+ \rightarrow 4^+ \rightarrow 2^+ \rightarrow 0^+$) cascade transitions at three kinetic energy intervals (total span 20-30 MeV for heavy or light fragment) that the value of J_{rms} is on the average (within $\pm$ 1 $\hbar$) independent of the fragment total kinetic energy. Nifenecker et al.[27], however, estimated from the correlation of the total γ-ray energy and the neutron multiplicity in the fission of ^{252}Cf and ^{235}U that the average spin of the fission fragments should increase by one unit for an increase of excitation energy of approximately 7 MeV

(corresponding to a $\Delta J_{rms}/\Delta E = -0.14\ \hbar/MeV$). The results of the present work, based on a fit of data points in Fig.9, are compiled in Table IV. There is general agreement with the value of Nifenecker. A comparison of the values obtained for individual chains could possibly be used to provide information on fragment stiffness at the scission point.

Acknowledgements

The authors wish to express their gratitude to Professor Dr. G. Herrmann for his continuous interest, valuable discussions, and support throughout this project.
They are also indebted to Professor Dr. G. Friedlander for valuable discussions and for reading the manuscript.
Financial support by the Bundesministerium für Forschung und Technologie, by the Alexander von Humboldt-Stiftung (H.N.E., T.T., and A.C.W.) , by GSI Darmstadt (K.W.), and by the Minerva-Stiftung (Z.B.A. and T.I.-B.) is also gratefully acknowledged.

References

1. E.Moll, H.Schrader, G.Siegert, M.Asghar, J.P.Bocquet, G.Bailleul, J.P.Gautheron, J.Greif, G.I.Crawford, C.Chauvin, H.Ewald, H.Wollnik, P.Armbruster, G.Fiebig, H.Lawin, K.Sistemich, Nucl.Instr. and Methods 123, 615 (1975).
2. E.Moll, P.Armbruster, H.Ewald, G.Fiebig, H.Lawin, H.Wollnik, in Proc. Int. Conf. on electromagnetic isotope separators and the techniques of their applications, Marburg 1970, Report BMBW-FBK 70-28,241(1970).
3. E.Moll, G.Siegert, M.Asghar, G.Bailleul, J.P.Bocquet, J.P.Gautheron, J.Greif, H.Hammers, H.Schrader, P.Armbruster, G.Fiebig, H.Lawin, K.Sistemich, H.Ewald, H.Wollnik, in Proc. 8th Int. EMIS Conf., Skövde,Sweden 1973, G.Anderson, G.Holmén Eds.(Gothenburg 1973) p.249.
4. G.Siegert, H.Wollnik, J.Greif, G.Fiedler, M.Asghar, G.Bailleul, J.P.Bocquet, J.P.Gautheron, H.Schrader, H.Ewald, P.Armbruster, Phys. Letters 53 B, 45 (1974).
5. G.Siegert, H.Wollnik, J.Greif, R.Decker, G.Fiedler, B.Pfeiffer, Phys. Rev. C 14, 1864 (1976).

6. H.Wollnik, G.Siegert, J.Greif, G.Fiedler, in Proceedings of the 3rd International Conference on Nuclei far from Stability, Cargèse (1976), Report CERN 76-13 (1976).

7. H.-G.Clerc, W.Lang, H.Wohlfarth, K.H.Schmidt, H.Schrader, in Proceedings of the 3rd International Conference on Nuclei far from Stability, Cargèse (1976), Report CERN 76-13 (1976) and (a) Report IKDA 76/5.

8. H.-G.Clerc, K.H.Schmidt, H.Wohlfarth, W.Lang, H.Schrader, K.E.Pferdekämper, R.Jungmann, M.Asghar, J.P.Bocquet, G.Siegert, Nucl. Phys. A 247, 74 (1975).

9. H.-G.Clerc, W.Lang, H.Wohlfarth, K.H.Schmidt, H.Schrader, K.E.Pferdekämper, R.Jungmann, Z.Physik A 274, 203 (1975).

10. H.Wohlfarth, W.Lang, H.-G.Clerc, H.Schrader, K.H.Schmidt, H.Dann, Phys. Letters 63 B, 275 (1976).

11. H.-G.Clerc, W.Lang, H.Wohlfarth, H.Schrader, K.H.Schmidt, these proceedings, contribution F 2.

12. H.O.Denschlag et al., to be published.

13. H.W.Schmitt, J.H.Neiler, F.J.Walter, Phys. Rev. 141, 1146 (1966).

14. K.Debertin, U.Schötzig, submitted to Nucl. Instr. and Methods (1978).

15. R.J.Gehrke, R.G.Helmer, R.C.Greenwood, Nucl. Instr. and Methods 147, 405 (1977).

16. Nuclear Data Sheets.

17. Table of Isotopes, C.M.Lederer, V.S.Shirley (Eds.), Wiley (New York) (1978).

18. G.Siegert, J.Greif, H.Wollnik, R.Decker, G.Fiedler, W.Kaiser, B.Pfeiffer, Report AED-Conf-76-072-007.

19. H.Wohlfarth, W.Lang, H.Dann, H.-G.Clerc, K.H.Schmidt, H.Schrader, Report IKDA 78/6.

20. R.G.Clark, L.E.Glendenin, W.L.Talbert Jr., in Physics and Chemistry of Fission (Proc. Symposium Rochester, 1973), IAEA, Vienna (1974), Vol.II, p.221.

21. B.F.Rider, M.E.Meek, Compilation of Fission Product Yields, Report NEDO-12154-2(D)(1977).

22. A.C.Wahl, A.E.Norris, R.A.Rouse, J.C.Williams, in Physics and Chemistry of Fission (Proc. Symposium Vienna, 1969), IAEA, Vienna (1969), p.813.

23. S.Amiel, H.Feldstein, in Physics and Chemistry of Fission (Proc. Symposium Rochester, 1974), IAEA, Vienna (1974), Vol.II, p.65.

24. A.C.Wahl, Contribution to Second Advisory Group Meeting on Fission Product Nuclear Data, IAEA Petten (1977), to appear as Report INDC-(NDS)-87, p.215-244.

25. R.Vandenbosch, J.R.Huizenga, Nuclear Fission, Academic Press, New York (1973).

26. B.D.Wilkins, E.P.Steinberg, R.R.Chasman, Phys. Rev. C 14, 1832 (1976).

27. H.Nifenecker, G.Signarbieux, R.Babinet, J.Poitou, in Physics and Chemistry of Fission (Proc. Symposium Rochester, 1973), IAEA, Vienna (1974), Vol.II, p.117.
28. J.R.Huizenga, R.Vandenbosch, Phys. Rev. 120, 1305 (1960).
29. R.Vandenbosch, J.R.Huizenga, Phys. Rev. 120, 1313 (1960).
30. D.G.Madland, T.R.England, Nucl.Sci.Eng. 64, 859 (1977), and Report LA-6595-Ms(1976).
31. J.B.Wilhelmy, E.Cheifetz, R.C.Jared, S.G.Thompson, H.R.Bowman, J.O.Rasmussen, Phys. Rev. C 5, 2041 (1972).
32. M.Weis, Doctoral thesis, Mainz 1979.
33. J.R.Nix, W.J.Swiatecki, Nucl. Phys. 71,1 (1965).
34. J.O.Rasmussen, W.Nörenberg, H.J.Mang, Nucl. Phys., A 136, 456 (1969).

DISCUSSION

O. W. B. SCHULT: How much detail do we know of the shape of the wings of the nuclear charge distribution for a given mass? In other words, what is the fractional yield for values of $Z-Z_p$ larger than 2 or 3?

H. O. DENSCHLAG: Low counting statistics and uncertainty in the correction factors for secondary formation of the elements close to stability prevented us from obtaining very low yields with the LOHENGRIN mass separator. Consequently we have no information on the bahaviour of these yields as a function of the kinetic energy of the fragments.

M. SCHMID: Perhaps I can throw some light on this question. In our work we have been able to measure fission yields of nuclides that lie some way from the centre of the distributions. It has been found that yields in the wings of the distributions are significantly enhanced over the range expected from Wahl's systematics. The deviation may be as high as a factor of 100 for $|Z-Z_p| \approx 3$.

M. ASGHAR: The electron inelastic scattering from deformed rare-earth nuclei shows that at $\beta \approx 0.3$ the nuclear charge is already more or less preformed into two charge centres. Are these data consistent with fragment charge 'clustering' at a later stage, following the fragment mass freezing that you have discussed?

H. O. DENSCHLAG: It is difficult, I think, to ascertain whether the results you mention are consistent with our data since the position of a medium-A deformed nucleus in its ground state is quite different from a scissioning system. It seems to me that the nuclear charge clustering you refer to is too weak to survive the drastic changes occurring during scission.

P. FONG: We are concerned with two important quantities at the scission point – the initial kinetic energy of fragments, and the excitation energy. In drawing conclusions with regard to these quantities we should not ignore other

important evidence related to them. The fact that fission fragments have high spin indicates that the excitation is reasonably high. The evidence from long-range α-particle angular distributions is that the initial kinetic energy is very low. These two facts are compatible, but other conflicting evidence will have to be reconciled.

H. O. DENSCHLAG: It seems to me that the persistence of the odd-even pairing effect excludes higher values of single-particle excitation at the scission point. Hence we should conclude that the excitation energy occurs in collective degrees of freedom and deformation seems to be the most reasonable assumption. It is further supported by our findings regarding the dependence of the angular momentum of the fragments on their kinetic energy.

EFFECT OF FRAGMENT KINETIC ENERGY ON THE SUPPLY OF ISOMERIC STATES IN ^{236}U FISSION*

J.P. BOCQUET**, F. SCHUSSLER, E. MONNAND
Centre d'études nucléaires, Grenoble Cedex,
France

K. SISTEMICH
Institut für Kernphysik, Kernforschungsanlage Jülich,
Federal Republic of Germany

Abstract

EFFECT OF FRAGMENT KINETIC ENERGY ON THE SUPPLY OF ISOMERIC STATES IN ^{236}U FISSION.

Isomeric ratios (yield of high-spin state over yield of low-spin state) have been measured for the following isotopes: ^{88}Br (6.3 μs), ^{95}Y (57 μs), ^{97}Y (1.2s), ^{98}Y (0.8 and 8 μs), ^{131}Sn (50 s) and ^{132}Te (28 and 3.9 μs), and as a function of the kinetic energy of the fission fragments from ^{236}U. – The angular momentum of the corresponding fission fragments has been calculated by using a statistical de-excitation model for the fission fragments. Thus the dependence of the angular momentum on the excitation energy has been obtained in each case. The results are not in agreement with a saw-tooth behaviour of the angular momentum with mass number and the dependence of angular momentum on the excitation energy is strongly affected by the individual structures of the nuclei.

1. INTRODUCTION

The knowledge of the scission configuration is essential for a better understanding of the dynamics of nuclear fission. One of the parameters characterizing the scission configuration is the angular momentum of the nascent fission fragments. From investigations of the prompt gamma-radiations of the fragments it has been concluded that the initial angular momenta are large on the average and that they are oriented perpendicular to the axis of thetwo fragments [1]. A saw-tooth like dependence of the angular momenta on the fragment mass has been obtained, assuming that the angular momentum is proportional to the average number of gamma-rays emitted by the fragment [2,3]. This behaviour is in agreement with theoretical predictions [4] for several fissile materials, while the determination of the initial angular momentum of individual fragments for the Cf^{252} spontaneous fission indicates a more complex dependence on the nuclear structure of the fragments [5].

---

* Experiment held at the Institut Laue-Langevin.

** And USM/Grenoble (France).

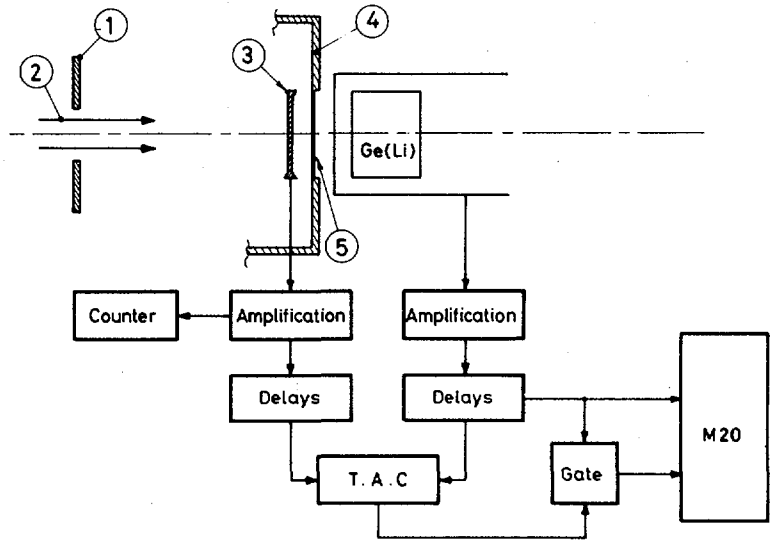

FIG.1. The experimental arrangement of Lohengrin:
1) beam collimator (1 cm diameter) located at about 20 cm from the stopper;
2) ion beam from Lohengrin;
3) surface-barrier detector;
4) vacuum chamber of Lohengrin;
5) thin aluminium window.

In the present investigation the populations of some fragments isomeric states in U^{235} thermal-neutron induced fission have been measured as a function of the fragment kinetic energy, at the separator Lohengrin [6]. The dependence of individual fragments initial momenta on their excitation energy can thus be obtained. This dependence can be correlated to changes in the scission configuration and therefore should provide valuable informations on scission. A slight rise of the angular momentum with decreasing kinetic energy of the fragment (or increasing excitation energy) has been obtained [7] from the neutrons and gamma-rays emitted by the fragments, while for Cf^{252} [5] the value of the angular momentum was independant (within ± 1 unit) of the fragment kinetic energy. The present experiment is taking advantage from the good energy resolution [8] of Lohengrin and from several new isomeric states identified with the same instrument [9, 10]. The isomeric ratio is converted into a root-mean-square angular momentum of the fragment and the result is compared to other experimental results and theoretical predictions.

2. EXPERIMENTAL TECHNIQUE

The Lohengrin facility [6,8] separates the fragments recoiling from a thin source of U^{235}, by means of a magnetic and an electrostatic field. The fragments having a given mass and kinetic energy are selected by a proper

setting of the fields. Two types of experiments were performed since both gamma-decaying states (with half-lives in the μsec region) and beta-decaying isomers have been investigated.

The experimental set-up which has been used for the determination of the feeding of μsec isomers is shown in Fig.1. The fragments were stopped in a proton transmission surface barrier detector (200 μ thickness) which started a time-to-amplitude converter (TAC). The gamma-radiation was observed with a Ge(Li) diode (50cm^3 volume, 2.5 keV resolution for the 1332 keV line) which stopped the TAC. The time range of the TAC was selected to match the half-life of the isomeric state, so that it could be used to select the isomeric gamma-ray from the radiations following the beta-decay of the fragments. The spectra from the Ge(Li) either gated with the TAC signals or ungated were both stored into an Intertechnique M20 multichannel-analyser. For the measurements of the β-decaying isomers only the ungated spectra were stored, and for the case of Sn^{131} a small gas transport device was used in order to reduce the influence of the gamma-rays background emitted by Lohengrin.

The measurements were performed over the whole range of kinetic energies of the individual fragments, within the limits of a reasonable beam intensity (running time for a measurement not exceeding 10 hours). Typically a range of 10 MeV below and above the most probable value of E_K (kinetic energy of the final product) has been covered and for all cases some measurements correspond to an excitation energy where no neutron emission is possible.

The number of fission fragments was monitored with the thin surface barrier detector in the case of μsec-isomers and the beam surface is limited by a diaphragm (see Fig.1) so that the ungated spectrum of the Ge(Li) was corresponding to the same number of fission fragments as the gated one. Additionally the fragment beam was controlled with a surface barrier detector of high energy resolution before and after each measurement. This allowed the identification of fragments with different masses in the beam. Due to the separating properties of Lohengrin any contaminating mass (which occur usually on the wings of the kinetic energy distribution) has a kinetic energy which differs by several MeV (about 5% of the kinetic energy) from that of the investigated fragment [8].

3. DATA ANALYSIS

3.1. Obtention of the experimental isomeric yields

From the measured ungated gamma-ray spectra, the intensities (N_γ) of the gamma-transitions characteristic of each isomer can be obtained (beta decaying isomers). A sufficient knowledge of the beta-decay schemes of the different isomers has been obtained from the spectroscopic work performed at Lohengrin [9-11]. In the case of the μsec isomers, the gated spectra were used and the gamma-lines intensities have been corrected for the losses due to the time-of-flight through the separator ($\simeq$ 1.8 μsec for the light fission fragments and $\simeq$ 2.2 μsec for the heavy ones). For a given value of the kinetic energy, the population of the isomeric state relative to the ground state of the considered nucleus, can be obtained from the relative intensities of a gamma-line characteristic of the isomer in the gated spectrum and of a gamma-line characteristic of the beta-decaying ground state in the ungated spectrum. Unfortunately, this procedure can be used only for the kinetic energies having a good statistical precision, since the gamma-background from Lohengrin (mainly rare gases), is important in the ungated spectrum (see Fig.2 for instance). For the

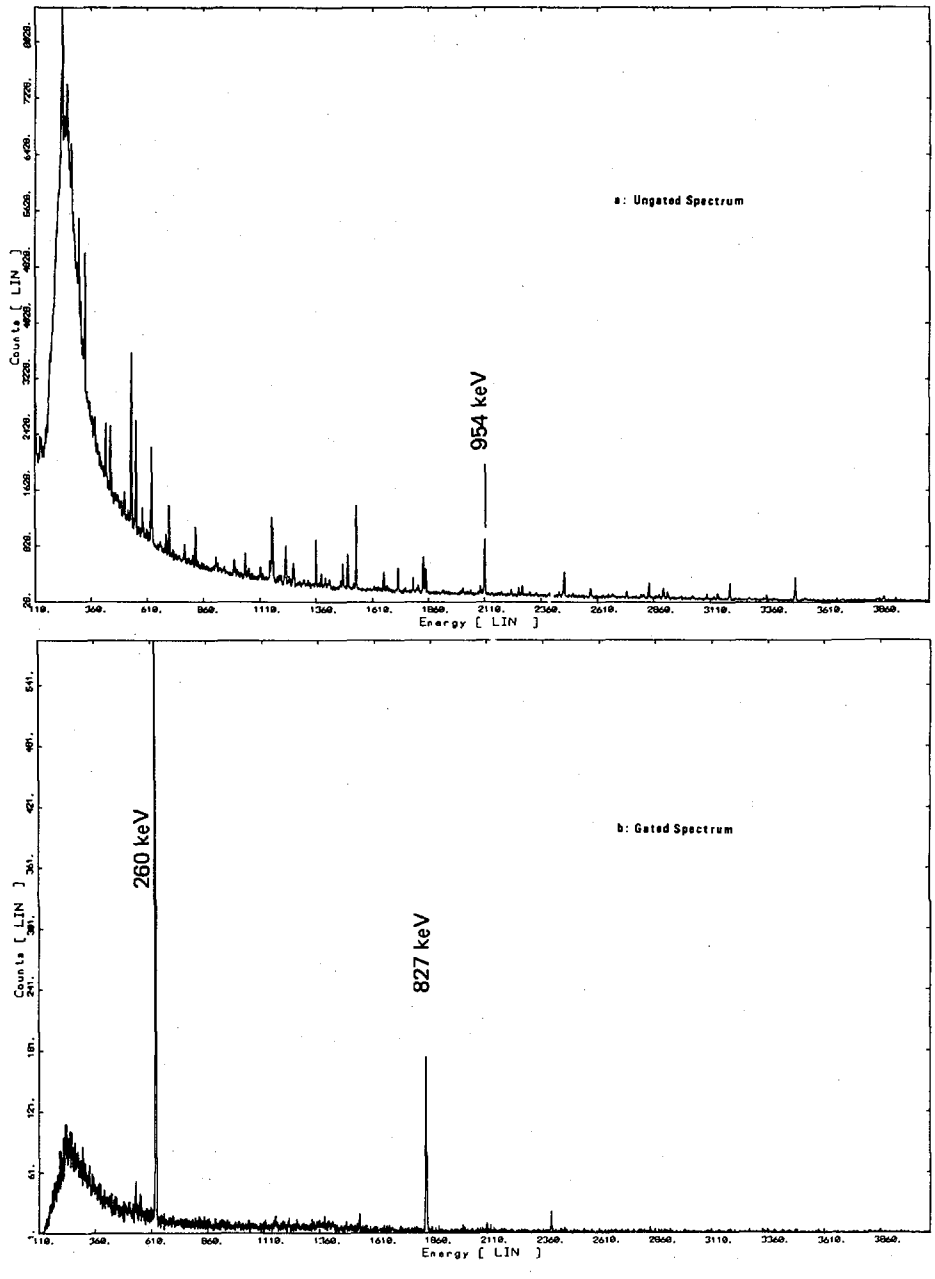

FIG.2a) Ungated gamma spectrum measured on ^{95}Y for the most probable kinetic energy (measuring time ≈ two hours).

b) Corresponding gated spectrum showing the very strong background reduction due to the coincidence (time window ≈ 80 μs).

TABLE I. SPECTROSCOPIC FEATURES OF THE MEASURED ISOMERIC AND GROUND STATES

Nucleus	Low-spin state			High-spin state			Gamma lines used in the measurement	
	$T_{1/2}$	E (MeV)	I	$T_{1/2}$	E (MeV)	I	Ungated spectrum	Gated spectrum
Br^{88}	16.6sec	0.0	(1^-)	6.3μsec	0.270	(4^-)	0.159, 0.775	0.111, 0.159
Y^{95}	10.9mn	0.0	$\frac{1}{2}$	57 μsec	1.088	$\frac{9^+}{2}$	0.954, 0.686	0.260, 0.827
Y^{97}	3.7 sec	0.0	$\frac{1^-}{2}$	1.2 sec	0.667	$\frac{9^+}{2}$	0.970, 1.996	
Y^{98}	8 μsec	0.495	3^+	0.8μsec	1.179	(9^+)		0.185, 0.203
Sn^{131}	33 sec	0.0	$\frac{3^+}{2}$	50 sec	0.434	$\frac{11^-}{2}$	0.305, 0.450 0.798	
Te^{132}	78 h.	0.0	0^+	28 μsec	1.925	7^-		0.697, 0.974
				3.9μsec	2.700	10^+		0.776, 0.926

low counting rates, the variations of the population of the isomeric states with E_k were obtained from a normalization of N_γ to the number of nuclei of the corresponding isotope in the beam. This number is the product of the number of fragments of the considered mass with the relative fission yield of the investigated isotope (taken from ref. 12 and 13). Thus, the determination of the absolute gamma-ray efficiency of the experimental set-up is not necessary to obtain the absolute isomeric yields. The results are given in Table II, while the main properties of the studied isotopes are listed in Table I. In the case of Y^{98} and Te^{132}, the ratio of two different isomeric states could be studied and the experimental values (Table II) are derived from the gated spectra alone, thus minimizing the systematic errors.

3.2. Calculation of the excitation energy (E^*) of the fragments

The experimental isomeric yields as a function of the fragments kinetic energy, must be transformed into the angular momentum of the fragments (root-mean squared values) expressed as a function of the excitation energy of the fragments (E^*).

TABLE II. THE EXPERIMENTAL ISOMERIC RATIOS $[\sigma_{High} + (\sigma_{Low})]$ AS A FUNCTION OF THE EXCITATION ENERGY OF THE INITIAL NUCLEUS (E*) OR OF THE DIFFERENCE WITH THE MOST PROBABLE KINETIC ENERGY, $(E - E_p)$.

$(E-E_p)$ KIN (MeV)	E^* (MeV)	$\frac{\sigma_{High}}{\sigma_{High}+\sigma_{Low}}$		$(E-E_p)$ KIN (MeV)	E^* (MeV)	$\frac{\sigma_{High}}{\sigma_{High}+\sigma_{Low}}$	
- 9.8	17.5 ± 1.0	0.23 ± 0.02		- 8.8	11.5 ± 1.	0.75 ± 0.02	
- 7.6	15.8 ± 1.0	0.24 ± 0.02		- 6.8	10.3 ± 1.	0.70 ± 0.02	
- 5.5	14. ± 1.0	0.26 ± 0.02		- 4.8	9.1 ± 0.8	0.70 ± 0.02	
- 3.4	12.7 ± 1.0	0.26 ± 0.02		- 2.9	7.9 ± 0.8	0.67 ± 0.02	
- 1.3	11.5 ± 1.0	0.26 ± 0.02	Br^{88}	- 1.	6.8 ± 0.7	0.67 ± 0.02	Sn^{131}
+ 0.8	10.5 ± 1.0	0.28 ± 0.02		+ 1	5.6 ± 0.6	0.67 ± 0.02	
+ 2.9	9.1 ± 1.0	0.26 ± 0.02		+ 3	4.4 ± 0.5	0.66 ± 0.02	
+ 5.2	7.2 ± 1.0	0.26 ± 0.02		+ 4.9	3.2 ± 0.5	0.64 ± 0.02	
+ 7.2	5.8 ± 1.0	0.25 ± 0.02		+ 5.9	2.6 ± 0.5	0.64 ± 0.02	
+ 9.2	4.2 ± 1.0	0.23 ± 0.02		+ 6.8	2.2 ± 0.5	0.62 ± 0.02	
				+ 8	1.4 ± 0.5	0.59 ± 0.02	
- 11.0	25.0 ± 1.0	0.46 ± 0.08					
- 7.0	21.0 ± 1.0	0.46 ± 0.08		- 12	26.5 ± 2.0	0.15 ± 0.02	
- 3.0	17.0 ± 1.0	0.43 ± 0.08	Y^{95}	- 8.1	22.0 ± 1.0	0.10 ± 0.01	Y^{98}
+ 1.0	10.5 ± 1.0	0.35 ± 0.07		- 4.3	17.8 ± 1.0	0.11 ± 0.01	
+ 5.0	9.8 ± 1.0	0.37 ± 0.07		- 0.4	13.6 ± 1.0	0.11 ± 0.01	
+ 9.0	5.0 ± 1.0	0.24 ± 0.05		+ 3.5	10.8 ± 1.0	0.096± 0.01	
				+ 7.3	7.2 ± 1.0	0.098± 0.01	
- 6.9	20.0 ± 1.0	0.58 ± 0.05					
- 3.1	17.7 ± 1.0	0.58 ± 0.04	Y^{97}	- 7.6	9.2 ± 1.0	0.35 ± 0.02	
+ 0.8	14.0 ± 1.0	0.53 ± 0.03		- 5.4	8.0 ± 1.0	0.36 ± 0.04	Te^{132}
+ 4.6	9.2 ± 1.0	0.52 ± 0.03		- 3.2	6.6 ± 0.8	0.25 ± 0.03	
+ 8.4	5.4 ± 1.0	0.59 ± 0.08		- 1	5.8 ± 0.8	0.30 ± 0.03	
				+ 1.2	4.8 ± 0.8	0.26 ± 0.04	
				+ 3.4	3.5 ± 0.8	0.25 ± 0.05	
				+ 5.7	2.2 ± 0.8	0.19 ± 0.06	

The conversion of E_K into E^*_{Total} is obtained from the calculation of the energy release in the condidered fission event : $Q(M_1,M_2)$ and the use of the conservation laws :

$$E^*_{Total} = Q(M_1 M_2) - E_K(M_1)\,\frac{236}{M_2}$$

where $E_K(M_1)$ represents the initial kinetic energy of a fragment having an initial mass M_1 and E^*_{Total} is the total excitation energy of both fragments. $Q(M_1,M_2)$ has been calculated with the mass formula of G.T. Garvey and al. [14]. The values of E^* for a given fragment has been deduced from E^*_{Total} under the assumption that the excitation energy is divided in fission proportional to the average number of prompt neutrons emitted by each fragment. The average number of neutrons emitted by each fragment has been

studied as a function of the total kinetic energy by H. Nifenecker and al. [7] and the ratio ν_L/ν_H stays reasonably constant over the energy range, thus supporting our assumption.

The isotopes which have been investigated at Lohengrin are partially produced after the emission of prompt neutrons, hence the calculation of E^* has to be performed for different initial masses corresponding to the emission of 0, 1, 2, 3 or 4 neutrons, the final mass beeing constant. The relation $E^*(E_K)$ is finally obtained after introduction of the number of emitted neutrons as a function of E^*, as calculated by the statistical deexcitation model described in the next section. The availability of the whole procedure can be tested in reproducing the average number of emitted prompt neutrons for the investigated mass chain (the nuclei which have been studied represent always the most (or very close to) probable charge split for a given mass).

The uncertainties of the calculated values of E^*_{Total} are estimated to be $\approx$ 1.0 - 1.5 MeV on the average. They result from the uncertainties on Q($\approx$ 0.5 MeV), from the change of E_K through the emission of neutrons ($\approx$ 0.7 MeV) and from the energy dispersion of the fragments in the Uranium target ($\approx$ 0.7 MeV).

3.3. Calculation of the initial angular momenta of the fragments

The average initial angular momenta are deduced from the absolute feedings of the isomeric states using the statistical model analysis developed by D.P. Min and M. Martinot [15] (program MAMI).

The competition between neutron and gamma emission is calculated for each step of the deexcitation path of a fission fragment created with the excitation energy E^* and the spin J . Thus the populations of the different discrete levels in the final nucleus can be obtained as a function of E^* and J. For each nucleus in the cascade, the known discrete levels can be introduced and for energies above a thereshold E_1, a semi-phenomenological level density formula is used [16]. The value of E_1 corresponds for each nucleus to the limit of the experimentaly observed levels. The gamma-ray emission is restricted to E_1, E_2 and M_1 transitions with energy below 5 MeV, and a corrective factor depending of the multipolarity of the transitions and of the mass region is applied to the transition probabilities. The corrective factors have been determined from a large set of experimental data [17]. The transmission coefficients used to determine the neutron emission rate result from an optical model calculation [18], the optical model parameters being taken from ref.19.

To compare the theoretical calculation with the experimental results of Table II, one has to assume a distribution of initial angular momenta for the fragments. The most commonly used distribution of spins corresponds to :

$$P(J) \propto (2J+1) \exp\left[\frac{-J(J+1)}{B^2}\right]$$

where B represents a parameter similar to a spin cut-off and is approximately equal to the root-mean-square value of J: J_{RMS}.

The theoretical isomeric ratio $R(E^*,J)$, which corresponds to an initial excitation energy E^* and an initial angular momentum J, is obtained from calculated populations of the discrete levels in the final nucleus by :

$$R(E^*, J) = \sigma_H/(\sigma_H + \sigma_L)$$

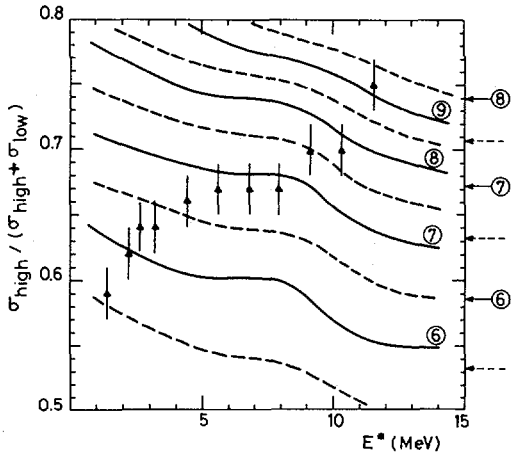

FIG.3. Determination of J_{RMS} by comparing the theoretical values of $\sigma_{High}/(\sigma_{High} + \sigma_{Low})$ obtained for different values of the parameter B (full and dotted lines), with the experimental results (triangles with uncertainties), for ^{131}Sn. On the right-hand side of the figure, the arrows indicate the results of the simplified calculation (isomeric ratios considered independent of excitation energy) from Madland et al. [20].

where σ_H and σ_L represent the total populations of the high and low spin levels, respectively, taking into account, as much as possible, the experimental knowledge of the decay scheme. For each value of E^*, the isomeric ratio corresponding to the spin distribution P(J) can be calculated by

$$R'(E^*) = \frac{\sum_J R(E^*, J)\, P(J)}{\sum_J P(J)}$$

for different values of the parameter B or J_{RMS}. The result of such a calculation is shown in Fig.3. The experimental values of $R(E^*)$ are indicated and the theoretical values of $R'(E^*)$ correspond to the continuous lines and to different values of J_{RMS}. Each experimental value of $R(E^*)$ can thus be transformed into an interpolated value of J_{RMS}, reproducing the measured isomeric ratio.

4. DISCUSSION OF THE EXPERIMENTAL RESULTS

The dependence of isomeric ratios on kinetic energy has been measured for the following isotopes : Br^{88}, Y^{95}, Y^{97}, Y^{98}, Sn^{131} and Te^{132}. Two of them are β-decaying isomers (Y^{97}, Sn^{131}) and the others have half-lives in the μsec range. For Y^{98} and Te^{132} several isomeric states are

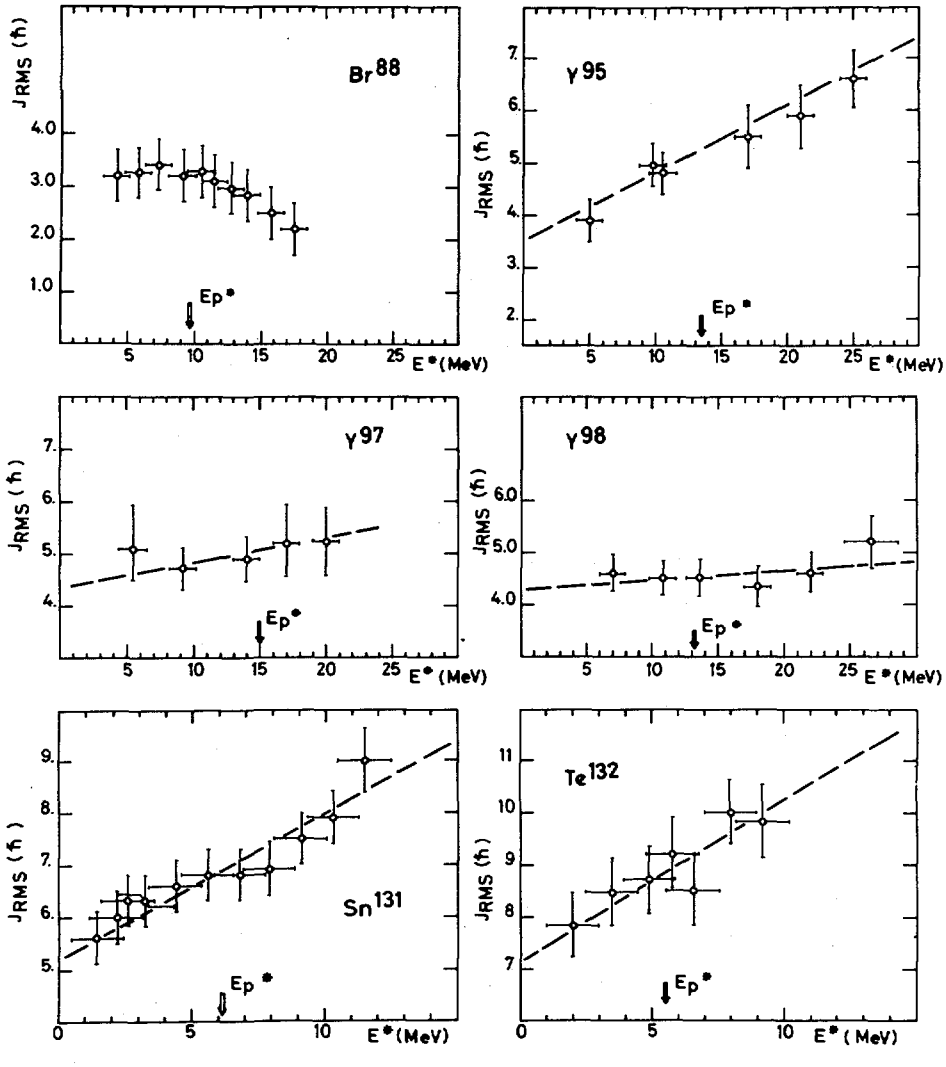

FIG.4. Experimental results of Table II transformed into J_{RMS} (E) dependences, using the statistical model of de-excitation of the initial fragments [15]. The most probable excitation energy E_p^* is indicated on each diagram.*

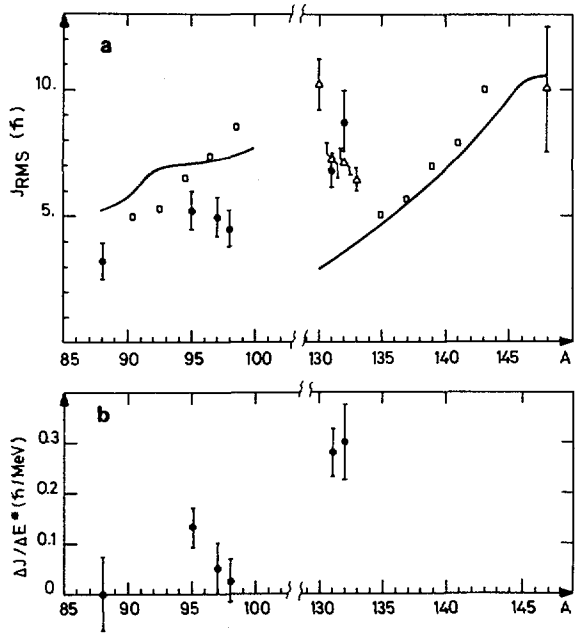

FIG.5a) Comparison of the values of J_{RMS} (E_p^*) obtained in this experiment with other existing results for ^{236}U fission:

- ● *this experiment;*
- Δ *experimental values deduced from isomeric ratios and compiled or measured by Aumann [21];*
- □ *experimental values from prompt gamma;*
- — *theoretical calculations of K. Dietrich (adiabatic case).*

b) Slope of J_{RMS} (E^*) dependences as functions of the mass of the final fragment.

reached by fission and the ratio of two isomeric states yields has been studied, thus avoiding a normalization of the gated gamma-lines to the ungated ones (see Tables I and II).

The calculation procedure developed in the preceding section has been applied to the experimental values, and the deduced dependences $J_{RMS}(E^*)$ are plotted in Fig.4.

The J_{RMS} value obtained for the most probable excitation energy E_p^* can be compared to other measurements performed on U^{235} thermal neutron fission. Two types of experimental information have led to the angular momentum of the fission fragm ents :

- the isomeric ratio measurements (taken from ref.21)
- the prompt-gamma radiations (ref.2).

There is a general agreement between the present results for masses 130 and 132, and the J_{RMS} values calculated from the isomeric yields measurements (Fig.5) in the same mass region. However the values of J deduced from the prompt-gamma radiations are not in agreement neither in the

light nor in the heavy group. The angular momentum in this last case is deduced from the average number of gammas emitted by a given mass, with the assumption that the fragments are mainly deexited by cascades of streched E2-transitions of collective character.

The observed discrepancy could be understood in the light group if the gamma cascades were only partly stretched, thus reducing the angular momenta given by [2] around masses 95-100. Unfortunately the same argument would not hold for masses around 130-133, since the result from the prompt gamma is too low in that case.

The saw-tooth behaviour for the angular momentum has also been deduced from a theoretical calculation by K. Dietrich and al. [4]. They predict a very low angular momentum around masses 130-132 ($J_{RMS} \approx 3$-$4\ \hbar$), no matter what temperature is chosen for scission (their result depends on this parameter). On the other hand the angular-momentum obtained from isomeric ratios in this mass region are not so much dependent of the deexcitation model since the number of emitted neutrons is very low in the average (≈ 0.3 - 0.5). Therefore it might not be correct to associate so closely the angular momentum of the fragments to their deformation or to the number of quanta emitted.

Another information is coming out of the experiment : the dependence of J_{RMS} with the excitation energy of the fragment. If one consider the Fig.4 the most striking feature is the very weak dependence for masses in the light group and the stronger influence of the excitation energy in the heavy group. We have plotted in Fig.5 b) the slopes $\Delta J / \Delta E^{*}$ ($\hbar$/MeV) obtained for the different masses. Several estimates of this quantity have already been made either on experimental or theoretical grounds. For instance an average slope of 0.14 $\hbar$/MeV has been obtained by H. Nifenecker [7] from the observed correlation between the total γ-ray energy and the neutron multiplicity in Cf^{252} and U^{235}, while J.M. Wilhelmy and al. [5] considered in Cf^{252} that the value of J was constant (within $\pm$ 1 h). The present measurement, no longer resulting from an average, is associated to a definite fragment and must be strongly influenced by the individual structure of the nucleus studied Nevertheless there seems to be a general trend to have less than the average in the light group (if we consider that the average value could be ≈ 0.14 $\hbar$/MeV) and more than the average (about twice as much) for masses 131 and 132. These masses which are known to be spherical seem to have more changes in their shape at scission than for the light group but this assumption results again from an association of the angular momentum with the deformation, which might be questionable.

5. CONCLUSION

From the dependence of several isomeric ratios on the kinetic energy of the fragments in U^{236} fission, one has derived, making use of a new statistical model for the deexcitation of the fission fragments, the influence of the excitation energy of some fragments on their angular momentum.

The saw-tooth behaviour of the angular momenta with the fragment mass is not reproduced by the isomer-ratio experimental results, indicating that the angular momentum of the fragments might not be so strongly correlated to their deformation.

The dependence of the angular momentum on the excitation energy is stronger for masses close to spherical shapes than for the others.

We are grateful to R. Sellam, J.W. Grüter and K. Sadler for their participation in the early stage of the experiment.

We wish to acknowledge D.P.Min and M. Martinot for their computer code MAMI, constant advices and fruitfull discussions. We had also valuable opportunities for discussions with P. Armbruster, K. Dietrich and H. Nifenecker.

REFERENCES

[1] VANDENBOSCH, R., HUIZENGA, J.R., Nuclear Fission, Academic Press, New York and London, 1973.
[2] ARMBRUSTER, P., LABUS, H., REICHELT, K., Z. Natur. 26a (1971) p. 512.
[3] PLEASONTON, F., Nucl. Phys. A312 (1973) p. 413.
[4] DIETRICH, K., ZIELINSKA-PFABE, M., Annals of Phys. to be published.
[5] WILHELMY, J.B., CHEIFETZ, E., JARED, R.C., THOMPSON, S.G., BOWMAN, H.R. and RASMUSSEN, J.O., Phys. Rev C5 (1972) 2041.
[6] MOLL, E. SCHRADER, H., SIEGERT, G., ASGHAR, M., BOCQUET, J.P., BAILLEUL, G., GAUTHERON, J.P., GREIF, J., CRAWFORD, G.I., CHAUVIN, C., EWALD, H., WOLLNIK, H., ARMBRUSTER, P., FIEBIG, G., LAWIN, H., SISTEMICH, K., Nucl. Instr . 123, 615 (1975).
[7] NIFENECKER, H., SIGNARBIEUX, C., BABINET, R., POITOU, J., Phys. and Chem. of Fission, Rochester 1973 (USA), IAEA, 1974 Vol.II p. 117.
[8] ARMBRUSTER, P., ASGHAR, M., BOCQUET, J.P., DECKER, R., EWALD, H., GREIF, J., MOLL, E., PFEIFFER, B., SCHRADER, H., SCHUSSLER, F., SIEGERT, G., WOLLNIK, H., Nucl. Instr . Meth. 139 (1976) p. 213.
[9] MONNAND, E., BLACHOT, J., SCHUSSLER, F., BOCQUET, J.P., PFEIFFER, B., SADLER, G., SELIC, H.A., KHAN, T.A., LAUPPE, W.D., LAWIN, H., SISTEMICH, K., Proceedings of the 3rd Int. Conf. on Nuclei far from Stability (Cargese) 1976, P. 477, p.495.
[10] SCHUSSLER, F., BLACHOT, J., BOCQUET, J.P., MONNAND, E., Z. Physik A281 (1977) p. 229.
[11] SISTEMICH, K., SADLER, G., KHAN, T.A., LAWIN, H., LAUPPE, W.D., SELIC, H.A., SCHUSSLER, F., BLACHOT, J., MONNAND, E., BOCQUET, J.P., PFEIFFER, B., Z. Physik A 281 (1977) p. 169.
[12] CLERC, H.-G., LANG, W., WOHLFARTH, H., SCHRADER, H., SCHMIDT, K.-H., these Proceedings.
[13] DENCHLAG, O., private communication/
[14] GARVEY, G.T., GERACE, W.J., JAFFE, R.L., TALMI, I., KELSON, I., Rev. Mod. Phys 41 (1969) n°4.
[15] MIN, D.P., MARTINOT, M., to be published.
[16] GILBERT, A. and CAMERON, A.G.W., Can. J. Phys., 43 , 1446 (1965).
[17] BERTRAND, F., MARTINOT, M. and VERGES, N., "Nuclear Data in Science and echnology", Vol.2, p.353 ; IAEA, Vienna 1973 and further unpublised results.
[18] KIKUCHI, Y., CEA-N-1532, INDC (FR) 3/L, Saclay (1972).
[19] PEREY, C.M. and PEREY, F.G., Nucl. Data Tables, 17, 1 (1976).
[20] MADLAND, D.G., ENGLAND, T.R., LA-6595-MS (ENDF 241), Los Alamos (Nov.1976).
[21] AUMAN, D.C., GÜCKEL, W., NIRSCHI, E. and ZEISING, H., Phys. Rev. C16, (1977) p. 254.

DISCUSSION

K. M. DIETRICH: In the model calculation that I carried out together with Dr. Pfabé, the angular momenta of the fragments result from bending modes

at scission, i.e. they stem from a collective mode in the system. If a nascent fragment is spherical in the scission region – as in the case of the 132 mass range in our model – it cannot acquire angular momentum through the bending mechanism. This is why we obtain a dip in the dependence of the average angular momentum on the fragment mass A_{fr} around $A_{fr} \approx 132$.

J. P. BOCQUET: Thank you for the comment.

E. CHEIFETZ: I can also add a few words on the problem of angular momentum. While looking at the prompt de-excitation of gamma rays in the ground state band of fragments we have found angular distributions consistent with complete alignment of the fragments at the scission point in barium isotopes. This suggests that the angular momentum is due to the deformation of the fragments at scission and not to their internal excitation. However, in the decay of ^{134}Te via the transition $6^+ \rightarrow 4^+$ we also found strong alignment, though it was not necessarily complete. It is believed that this nucleus does not deform at scission. The measurement shows that the supposedly spherical nuclei have collective motion coherent with the opposite fragment and not only internal excitation.

J. B. WILHELMY: Dr. Bocquet, do you expect any difficulty in determining the absolute value of the angular momentum on the basis of a statistical analysis in the ^{132}Sn closed-shell region?

J. P. BOCQUET: The statistical analysis we made introduces experimentally established discrete levels for each nucleus of the cascade, and one is free to select the energy from which the statistical level of density will be used. In the case of ^{131}Sn, we tested the sensitivity of the isomer ratio to the position of the matching point and found it negligible. In the region around mass 132 the experimentally established discrete levels have been used up to 1.5–3MeV.

POLAR EMISSION IN FISSION

E. PIASECKI, L. NOWICKI
Institute of Nuclear Research,
Świerk, Poland

Abstract

POLAR EMISSION IN FISSION.

Experimental information concerning polar emission is surveyed. The available data relate to the intensity, the angular distribution of polar particles, the energy spectra of polar particles and fission fragments, and to the mass distributions of fission fragments recorded in coincidence with polar particles. – The following hypotheses regarding the nature of this phenomenon are discussed: pre-scission emission from the fragment polar tips, snapping of the nuclear surface, bending of the trajectory by the nuclear force, diffraction and transmission through fission fragments, reactions induced by scission neutrons, the rotating remnants of the necks, delayed tripartition and evaporation from fission fragments. So far, no one of these hypotheses was able to describe all the existing data, although some of them seen to be promising.

1. INTRODUCTION

The details of the ternary-fission mechanism are still unclear. It is, however, generally believed that light, charged particles, which once in a few hundreds of cases accompany fission, are born somewhere in the vicinity of scission and subsequently accelerated and focused almost perpendicularly to the fission axis by the Coulomb field of the fission fragments [1]. In classical terms, the strong deflection off the fission axis should give rise to shadow cones centred along the fission axis (Fig. 1). It can be calculated [2] that from particles starting from any place between the fission fragments such a cone should be very wide: the angle θ_{min} in Fig. 1 should be, at least, 45°.

In spite of this naive picture, it was found some ten years ago that a surprisingly high portion of alphas (the dominating tripartition particles) can be recorded in the vicinity of the fission axis [3]. So far, this was observed in ^{235}U (n_{th},f) [3–12], ^{233}U(n_{th},f) [11], in spontaneous fission of ^{252}Cf [13–15] and, possibly, in the fission of ^{238}U by 42–MeV protons [16].

It is the aim of this paper to review the experimental information accumulated up to now on this phenomenon which we call 'polar emission' (PE) as well as to discuss some ideas concerning its nature.

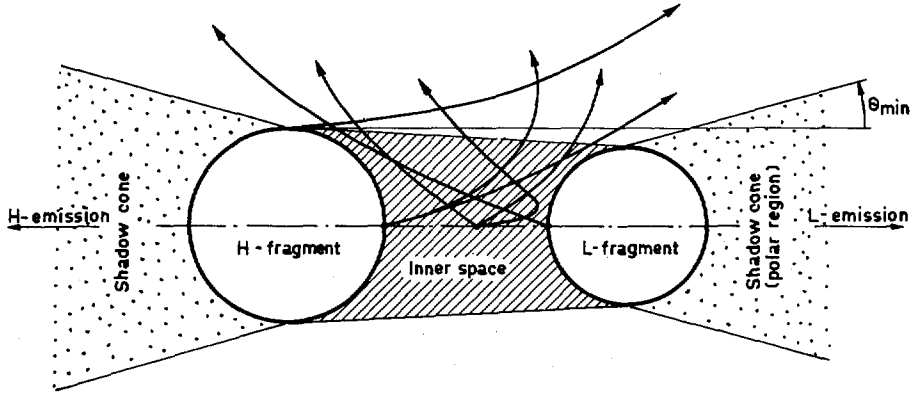

FIG.1. Idea of shadow cones. According to the classical model, the charged particles emitted from the 'inner space' should be deflected off the fission axis giving rise to the shadow cones of the opening angle θ_{min}.

2. EXPERIMENTAL CHARACTERISTICS OF POLAR EMISSION

It seems that the main experimental features (intensity, energy spectra) are only weakly dependent on the fissioning nuclei [11], although some differences were noticed and will be discussed in the following.

2.1. Angular distribution

The angular distribution of light, charged particles with respect to the fission axis is, unfortunately, known only very approximately, for extreme angles. The poor angular resolution ($7°-15°$) obtained so far did not allow us to see any fine structure of this distribution, even if such a structure did exist. Various authors seem, however, to agree that, after passing some critical angle, the intensity of emission (per solid angle) does not decrease but, on the contrary, has a tendency to increase when one approaches the fission axis [3, 7, 12, 14, 16] (Fig.2). This tendency is particularly striking in the case of proton emission, which can be seen in Fig.3, taken from Ref.[14]. Unfortunately, this is the only published angular distribution of protons measured in the full range of angles, and it should be taken with some caution, not only because it was obtained without distinguishing between the light and heavy fragments (thus the results are symmetrized about 90°), but also because the measurements were taken at extremely few experimental points. The main source of our reservations is, however, the fact that the energy of protons recorded in the polar region by the

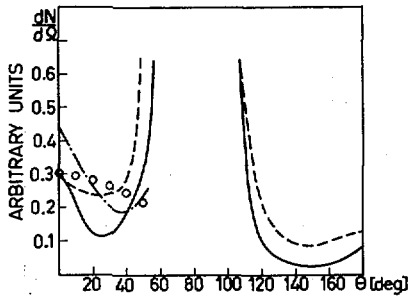

FIG.2. Angular distribution of α-particles from the ^{236}U fission determined by E. Piasecki et al. [7] (solid line), Adamov et al. [14] (dot-dash line) and Caïtucoli et al. [12] (dashed line). The circles show what the shape of the polar component distribution should look like if the particles were emitted isotropically from the fully accelerated fragments.

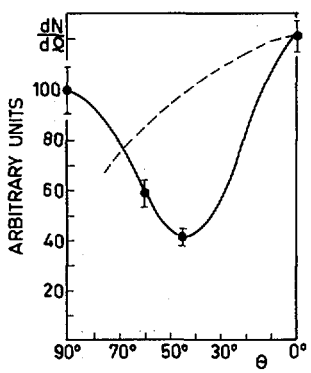

FIG.3. Angular distribution of protons from the ^{252}Cf fission measured by Adamov et al.[14]. The dashed line shows the anticipated shape of the polar component if the protons were isotropically emitted from the fully accelerated fragments.

authors of Ref.[14] is half that determined in other works. On the other hand, the general shape of the angular distribution was confirmed by the measurements of a Polish group (unpublished data), who observed even stronger enhancing of proton emission intensity at the polar angles than that seen in Ref.[14]. This is, moreover, confirmed by the data on the relative intensities of polar protons and alphas (see below). As we shall see, the angular distribution of protons is very important in testing various hypotheses on the nature of polar emission; thus, a more precise determination of this distribution would be of great value.

TABLE I. EXPERIMENTAL INTENSITY RATIOS

L and H relate to emission along the light- and heavy-fragment trajectories, respectively. The errors given in the table are statistical ones and the estimated maximum systematic errors involved in particle identification are given in parentheses.

Particle	^{236}U					^{252}Cf			
	Ternary fission Dakowski et al. [20]	Polar emission Piasecki et al. [9]			P/E ratio[b]	Ternary fission Whetstone et al. [21]	Polar emission Nowicki et al. [22]		
		L-emission[a]	H-emission[a]	L/H ratio			L-emission[a]	H-emission[a]	L/H ratio
P	1.15 ± 0.15	30.5 ± 2 (± 0.6)	44.5 ± 4 (± 1)	2.0 ± 0.2	0.17 ± 0.03	1.6 ± 0.2	35.0 ± 2 (± 1)	33.0 ± 3 (± 1)	3.9 ± 0.3
d	0.5 ± 0.1	2.8 ± 0.5 (± 0.6)	3.4 ± 0.9 (± 0.7)	2.4 ± 0.9	$(3 \pm 1) \times 10^{-2}$	0.63 ± 0.03	7.2 ± 0.6 (± 1.5)	5.7 ± 1.1 (± 1.2)	4.8 ± 1
t	6.2 ± 0.5	9.2 ± 1.2 (± 0.9)	8.0 ± 1.5 (± 0.8)	3.3 ± 0.6	$(7.2 \pm 1.3) \times 10^{-3}$	5.9 ± 0.2	13 ± 1 (± 2)	18 ± 2 (± 3)	2.7 ± 0.3
^4He	100	100	100	2.9 ± 4	5×10^{-3}	100	100	100	3.8 ± 0.2
^6He	1.1 ± 0.2	< 0.06	< 0.2	–		2.4 ± 0.5	< 0.05	< 0.2	–

[a] The α-particle intensity is assumed to be 100.

[b] The P/E values were obtained based on the 5×10^{-3} value for alphas.

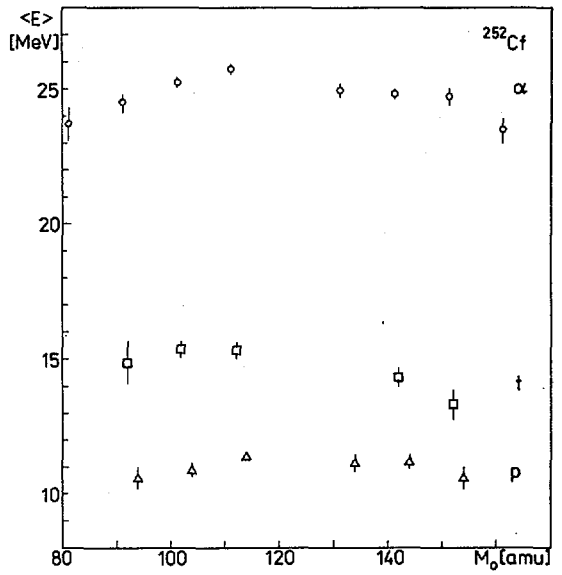

FIG.4. Dependence of the mean energy of polar particles in the laboratory system on the mass of the fragment moving in the same direction. The data relate to fission of ^{252}Cf.

2.2. Intensity

To determine the intensity of PE, one has, in some way, to decompose the angular distribution into two components: PE and conventional tripartition ('equatorial emission', as it is sometimes called [18]). If we use some arbitrary convention setting the borderlines, e.g. at 25° and 155° (the angles being measured with respect to the light-fragment trajectory), the intensity ratio P/E of the polar to equatorial α-particles in the case of ^{235}U(n_{th},f) is about 5×10^{-3}, based on the angular distribution obtained in Ref.[7]. Other works suggest a value higher, by a factor of 1.5–2 (Fig.2). Another, model-dependent approach to decomposition of the angular distribution gives a ten times larger P/E ratio; then, however, the P value concerns not only the particles moving along the fission axis, but all the particles hypothetically emitted from the accelerated fragments (see Appendix).

The polar emission intensity of other particles (protons, deuterons, tritons and ^{6}He) was predicted by calculations based on the hypothesis that polar particles are evaporated in-flight from the fission fragments [19]. Soon afterwards, these predictions were confirmed experimentally [8, 14]. Although the angular distributions for these particles are even less certain, the relative intensities can be determined quite accurately, if we consistently use the abovementioned convention (Table I).

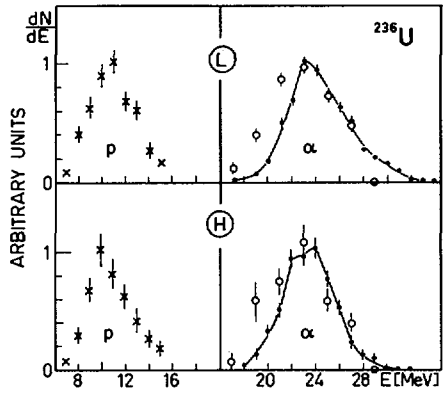

FIG.5. Energy spectra (in the laboratory system) of the polar protons and α-particles emitted along the light (L) and heavy (H) fragment trajectory in ^{236}U fission. Open circles relate to data taken from Ref.[11], other data are from Ref. [9]. The curve is only a guide to the eye.

TABLE II. ENERGY (in MeV) OF POLAR PARTICLES IN THE LABORATORY SYSTEM

The errors are only statistical.

Particle	Fissioning nucleus	Mean value		Dispersion		Reference
		L-emission	H-emission	L-emission	H-emission	
α	^{234}U	22.8 ± 0.1	22.2 ± 0.3	3.0 ± 0.2	2.8 ± 0.4	Andreev et al. [11]
	^{236}U	22.8 ± 0.2	22.5 ± 0.4	3.0 ± 0.2	2.8 ± 0.5	Andreev et al. [11]
	^{236}U	24.5 ± 0.1	23.5 ± 0.1	2.9 ± 0.1	2.5 ± 0.1	Piasecki et al. [9]
	^{252}Cf	25.5 ± 0.1	24.8 ± 0.1	3.4 ± 0.1	2.7 ± 0.1	Nowicki et al. [22]
t	^{236}U	15.3 ± 0.2	13.6 ± 0.3	2.7 ± 0.2	2.0 ± 0.2	Piasecki et al. [9]
	^{252}Cf	15.3 ± 0.2	14.0 ± 0.3	2.6 ± 0.2	2.6 ± 0.3	Nowicki et al. [22]
d	^{236}U	13.1 ± 0.3	11.6 ± 0.3			Piasecki et al. [9]
	^{252}Cf	13.6 ± 0.2	12.8 ± 0.5			Nowicki et al. [22]
p	^{236}U	11.2 ± 0.1	11.2 ± 0.2	2.5 ± 0.2	2.8 ± 0.3	Piasecki et al. [9]
	^{252}Cf	11.4 ± 0.2	11.3 ± 0.1	2.2 ± 0.1	2.0 ± 0.1	Nowicki et al. [22]

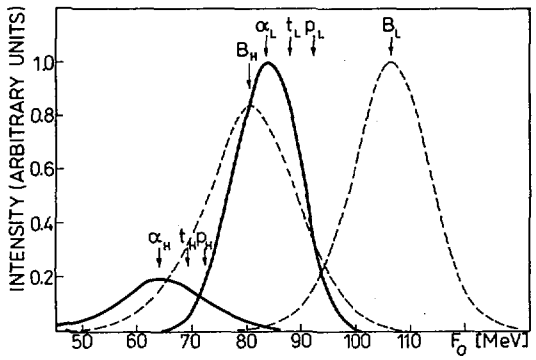

FIG.6. Comparison of fission energy spectra in bipartition of ^{252}Cf (dashed line) with the spectra of fragments measured in coincidence with polar α-particles moving in the same direction [22]. For the polar protons and tritons, only the peak positions are indicated.

The difference between the intensities of emission of various particles in PE and in conventional tripartition is remarkable, e.g. ^{6}He nuclei were never observed at the extreme angles, although over 5000 polar events were recorded by the Polish group alone (in tripartition, the intensity ratio ^{6}He/^{4}He is about 0.02). On the other hand, the protons, which are observed in conventional tripartition with intensities about hundred times lower than that of the alphas, constitute about one third of all polar particles. In fact, from the relative intensities of protons and alphas in PE and tripartition and from the P/E ratio for α-particles, we can easily calculate that P/E for protons is equal to about 0.2 if the convention 0°– 25° for the polar angles is used. Such a large P/E value means that the intensity ratio N(0°)/N(90°) is probably even twice as large as that shown in Fig.3.

2.3. Energy spectra of polar particles

The energy of polar particles is definitely higher than that emitted in conventional tripartition [3, 5–11, 13, 14] although it seems that this energy changes smoothly on passing from the 'equatorial' to the 'polar' range of angles [7, 15]. As in the case of equatorial emission [23], this energy is only weakly dependent on the fragment mass ratio [9, 22] (Fig.4), but it seems that the character of this dependence is different. Somewhat controversial is the question of asymmetry of the energy peaks, observed in Refs [7, 9, 10, 22], but not in other papers (see, e.g. Fig. 5); all the authors agree, however, that the polar spectra are almost twice as narrow as the equatorial ones. The first two moments of the spectra are given in Table II.

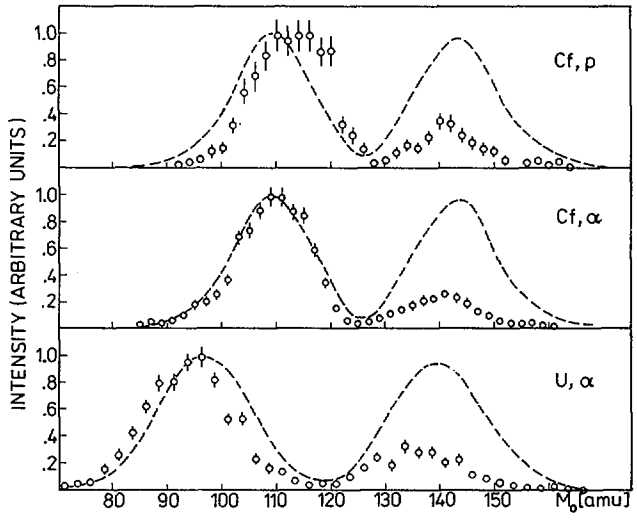

FIG. 7. Comparison of fission fragment mass distributions in bipartition (dashed line) with that measured in coincidence with polar particles moving in the same direction [9, 22].

2.4. Fission fragment energy spectra

It is characteristic of PE (Fig.6) that the kinetic energy of fission fragments moving in the same direction as the charged particles is markedly lower than in bipartition [3, 4, 6, 7, 9, 11, 22], the shift being the largest for α-particles. Part of this effect is simply due to linear momentum conservation and thus it is independent of the mechanism of the process (e.g. whether it is a one-step or a sequential one). However, the well-established (although smaller) decrease of kinetic energy of the fragments moving in the opposite direction obviously cannot be explained by recoil. Since the energy shift is independent of the fragment mass ratio [11], this observation points to some differences in the scission configuration of the average case of bipartition and that accompanied by polar emission. To obtain the magnitude of this difference, one has to make some assumptions as to the time delay of emission with respect to scission. If we assume, e.g. that the emission takes place in the vicinity of scission, we can calculate for ^{236}U fission that the polar α-particle accompanies those fission modes in which the final total kinetic energy of the fragments would normally be by about 15 MeV smaller (and the excitation energy higher) than the average. If this difference is only due to the larger fragment deformation at the moment of scission, it would mean that PE occurs most frequently when the scissioning nucleus is stretched about 10 per cent more than usually in scission. If, eventually, the emission takes place from the fully accelerated fragments, then this additional stretching is only half as large.

TABLE III. DECREASE (in amu) OF THE LIGHT-FRAGMENT MEAN MASS IN POLAR EMISSION AND TRIPARTITION WITH RESPECT TO BIPARTITION. The figures indicate by how much, on the average, the light fragment is lighter in PE (and tripartition) than in binary fission.

Particle	Fissioning nucleus	Polar emission			Tripartition	
		L-emission	H-emission			
α	^{234}U	2.0 ± 0.3	0.3 ∓ 0.7	Andreev et al. [11]		
	^{236}U	2.5 ± 0.4	0.7 ± 0.8	Andreev et al. [11]	2	Schmitt et al. [24] Asghar et al. [25]
		2.9 ± 0.2	0.4 ± 0.4	Piasecki et al. [9]		
	^{252}Cf	0.4 ± 0.2	0.6 ± 0.4	Nowicki et al. [22]	3.0 ± 0.15	Nardi et al. [26]
t	^{236}U	0.6 ± 0.7	1.9 ± 1.4	Piasecki et al. [9]		
	^{252}Cf	−1.0 ± 0.4	0.2 ± 0.8	Nowicki et al. [22]		
p	^{236}U	−1.2 ± 0.4	−0.4 ± 0.6	Piasecki et al. [9]		
	^{252}Cf	−3.4 ± 0.3	−1.9 ± 0.6	Nowicki et al. [22]	−3.2 ± 0.5	Nardi et al. [26]

2.5. Fragment mass distribution

Some mass distributions of fission fragments moving in the same direction as the polar particles, taken from Refs [9, 22], are presented in Fig.7. Comparison with the mass distribution of binary-fission fragments measured under the same experimental conditions shows (Table III) that, in the case of α-polar emission from ^{236}U, the final mass of the light fragment moving along the particle trajectory is, on the average, about 2.5 amu smaller than in bipartition, which is similar to the result for equatorial emission [24, 25]. Similar results were obtained in Ref. [11] for α-polar emission also for the thermal-neutron fission of ^{233}U. Such a shift with respect to the binary-fission results is not observed, however, for the light-fragment peak in the case of α-PE in ^{252}Cf, although it is seen in tripartition. In the proton PE in ^{252}Cf fission, the final mass of the light fragment is even heavier than in bipartition, which agrees with the result obtained by Nardi et al. [26] for the proton tripartition of this element. A similar, although weaker shift is also observed in the case of proton PE in $^{235}U(n_{th}, f)$.

Thus, we see that the fragment mass shifts differ in U and Cf and the shifts are also quite different in the cases of α and proton polar emission. Moreover, we see from Table III, where the values of the peak shifts are given, that they

also depend on the direction of emission. We shall see later how some degree of order can be brought into this confusing situation.

Other experimental characteristics of PE will be discussed together with the theoretical predictions.

3. HYPOTHESES ON THE NATURE OF POLAR EMISSION

Since the discovery of PE various hypotheses were advanced, trying to explain why the shadow cones actually do not exist. Most of these hypotheses look so natural that, if they proved to be true, they would make PE a trivial phenomenon. It seems, however, that this is not the case. We shall briefly discuss the proposed explanations of PE, approximately in the order of increasing delay between scission and the moment of appearence of the charged particle in the polar region.

3.1. Pre-scission emission?

A very original hypothesis concerning the mechanism of tripartition was advanced by Cârjan et al. in a series of papers [17, 18, 27]. According to them, the charged particles are emitted not during or after scission, but shortly before scission. We shall not quote the arguments, which, in the opinion of the authors of Refs [17, 18, 27], exclude the generally accepted point of view, and shall refer the reader to the original papers. More relevant here is the result of calculations of the α-particle clustering probability as a function of the site on the nucleus surface. According to the authors of Refs [17, 18, 27], shortly before scission the α-particle pre-formation probability is highest in the neck, but a small portion of the alphas is formed on (and can be released from) the fragment polar tips.

Another possibility, suggested in Ref. [27], is that an α-particle clustered in the neck remains for some time in the nucleus while it is deforming towards scission and gains its kinetic energy through the one-body mechanism (i.e. by collisions with the moving walls of the neck) until the emission is energetically possible. During this process, after several reflections from the potential wall, some clusters (or protons) could move to the polar tips, being subsequently emitted from this region of lowered Coulomb barrier. Of course, such a mechanism needs a very long mean free path in the nuclear interior, which cannot, however, be excluded.

Usually, it is taken for granted that α-particles interact so strongly with nuclear matter that they barely penetrate the nuclear skin. One should, however, remember the very low initial energy of the tripartition alphas. There are some indications, both theoretical and experimental [28, 29], that at low projectile

energy the imaginary part of the optical potential changes from the volume to the surface type. At low energy, experimentalists usually cannot distinguish between them, since both types yield (within experimental accuracy) the same angular distributions. This is connected with the fact that, even if we assume a surface imaginary potential, the α-particle penetrability through the nucleus is of the order of $10^{-4} - 10^{-2}$, which, under usual circumstances, is difficult to notice at small angles on the background of Rutherford scattering. It could, however, be seen in the shadow produced by the fission fragments.

It is difficult to assess the validity of this interesting hypothesis, until detailed predictions concerning, e.g. angular distributions, emission intensity of various particles or energy spectra based on this hypothesis are available. We should, however, like to point out two difficulties of the model. First, if the polar particles are really clustered at and emitted from the poles, what mechanism transfers the energy from the rapidly necking-in areas to the polar tips, making the cluster emission possible just before the instant of scission? The second difficulty is connected with the mass distribution. The author of Ref.[27] writes: "If the existing deficit of four mass units is corrected, the mass distribution in α-accompanied fission, aside from being a little narrower, coincides in all respects with that in binary fission. [...]. Only those emissions made before the moment of scission could preserve the mass distribution". However, as we see in Table III, this argument does not hold in the case of proton tripartition or PE. In particular, in the case of ^{252}Cf, after the proton is emitted, the light fragment occurs to be heavier, on the average by a few mass units, than in bipartition, independently of the direction of emission (tripartition or PE); thus, it is clear that (bipartition) mass distribution is not preserved.

Of course, it can finally occur that our reservations are only of marginal importance; the model certainly deserves further elaboration since at the present stage it cannot be subjected to any detailed testing.

3.2. Snapping of the nuclear surface?

According to another hypothesis, advanced by Halpern [1], PE arises from the same cause as equatorial emission, i.e. "from the snapping back of nuclear surface just after scission. The snapping at the outer ends of the system is expected to be less pronounced than at the centre because the outer ends are presumably more rounded. One would therefore expect fewer polar α-particles than perpendicular (i.e. normal) ternary particles".

In another version of this concept, the remnant of the neck (a 'navel') could be transferred to the outer pole because of, e.g. fragment vibration.

Although potentially both suggestions can explain the effect of focusing along the fission axis, neither was elaborated in detail. One can expect, however, that at least according to the 'vibrational' model the probability of PE is larger

TABLE IV. DIFFERENCE (in amu) OF THE FRAGMENT MASS IN POLAR EMISSION (BEFORE PARTICLE EMISSION) AND IN BIPARTITION

The figures in the table indicate how much, on the average, the polarly emitting fragment is heavier than in bipartition, assuming that in L-emission the particle is emitted from the light fragment and in H-emission from the heavy one. The values with asterisk are these before particle emission.

Particle	Fissioning nucleus	L-emission $\langle M_L^* \rangle - \langle M_L^B \rangle$	H-emission $\langle M_H^* \rangle - \langle M_H^B \rangle$	Reference
α	^{234}U	1.5 ± 0.4	0.7 ± 0.8	Andreev et al. [11]
	^{236}U	1.5 ± 0.4	0.7 ± 0.8	Andreev et al. [11]
		1.1 ± 0.2	0.4 ± 0.4	Piasecki et al. [9]
	^{252}Cf	3.6 ± 0.2	0.6 ± 0.4	Nowicki et al. [22]
t	^{236}U	2.4 ± 0.7	1.9 ± 1.4	Piasecki et al. [9]
	^{252}Cf	4.0 ± 0.4	0.2 ± 0.8	Nowicki et al. [22]
p	^{236}U	2.2 ± 0.4	−0.4 ± 0.6	Piasecki et al. [9]
	^{252}Cf	4.4 ± 0.3	−1.9 ± 0.6	Nowicki et al. [22]

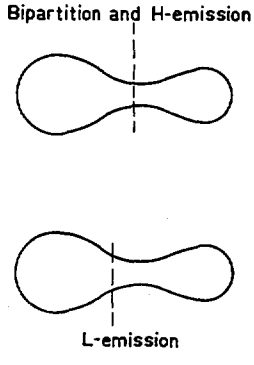

FIG.8. A scheme of possible differences between the scission points for the cases of bipartition and polar emission.

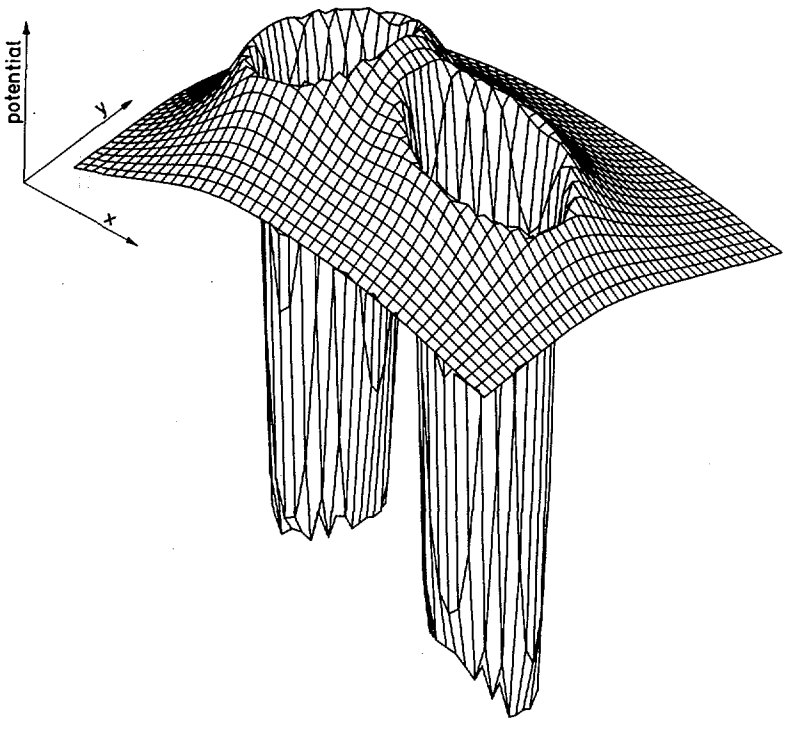

FIG.9. The Coulomb plus nuclear potential of the α-particle interaction with the ^{252}Cf fission fragments. The centres of the fragments are here at a distance of 26 fm, the deformation of the light fragment is $\beta = 0.3$, the heavy one is undeformed.

for the fragments with longer navel. Let us consider the experimental situation. If we assume, according to the above concepts, that the emission along the light-fragment trajectory (L-emission) takes place really from the light fragment and similarly in the case of H-emission, we can answer the question of how much heavier, on the average, than in bipartition was the emitting fragment. From Table IV, it is seen that L-emission occurs when the light fragment is (on the average) heavier than, usually, by two (in U) or four (in Cf) mass units, while for the H-emission the emitting fragment should be of almost usual mass. The situation can be sketched in the following way (Fig.8): for L-emission, the light-fragment navel should be longer than usually, while for H-emission the neck can snap in the usual place. It is not clear whether such a picture is only of mnemo-technical value. Certainly, the situation in the case of L-emission looks 'natural' in the framework of the 'vibration' model; in H-emission the situation is, however, less clear, and the case of proton emission in ^{252}Cf fission even seems to be in conflict with what could be expected.

3.3. Bending of the trajectory by nuclear force?

The shadow cones were calculated [2] in the spirit of usual tripartition model calculations, in which the three relevant bodies are approximated by the charged points. This approximation is, however, a very rough one [30]. When calculating a potential felt by an α-particle in the vicinity of fission fragments, we see the areas (the ridges in Fig. 9) where the repulsive Coulomb forces are balanced by the attractive nuclear ones. Thus although the majority of particles emitted from the neck are deflected off the fission axis, giving rise to the equatorial emission, or are absorbed by the fragments, one can imagine that there is a particular range of impact parameters and velocities for which the particle trajectory is bent into the polar region.

We performed the classical calculations [31] in which the motion of the three bodies was simulated by numerical integration of Newton equations, and the initial spatial and momentum configurations were varied in an attempt to reproduce the experimental data. The sizes and deformations of the relevant bodies were taken into account and, in addition to the nuclear and Coulomb forces, the phenomenological friction term was accounted for. It appeared that it is possible to find the initial conditions for which α-particles are scattered into the polar angles. We were, however, unable to reproduce the experimental intensities and kinetic energy distributions simultaneously, especially for the polar protons. Also, the calculated angular distribution could not explain the probably occurring focusing of particles along the fission axis.

3.4. A wave phenomenon?

Lack of success in using the classical model can hardly be surprising, especially if we take into account the very low starting energy of the light particles (of the order of 1 MeV). The ratio of the fragment radius to the wavelength λ at the point of closest approach, being only of the order of 2–5 for α-particles and even less for protons, certainly leaves much place for the wave effects.

The problem of scattering of a spherical wave emerging between two nuclei is non-standard in nuclear physics and, although interesting, is not easy to solve; we are aware of only two such attempts. Andreev et al. [11] reported that by numerical integration of the time-independent Schrödinger equation they obtained for α-particles the P/E ratio of the order observed in experiment. Similar calculations by Kordyasz [32] indicate also that one can fit the experimental value of P/E not only for the alphas and tritons, but also for protons, where the $N(0°)/N(90°)$ ratio is very high (Fig. 3), provided the fragments are sufficiently close to one another at the moment of emission. The 'mechanism' of obtaining high P/E values is especially well seen in the case of protons (Fig. 10): the flux

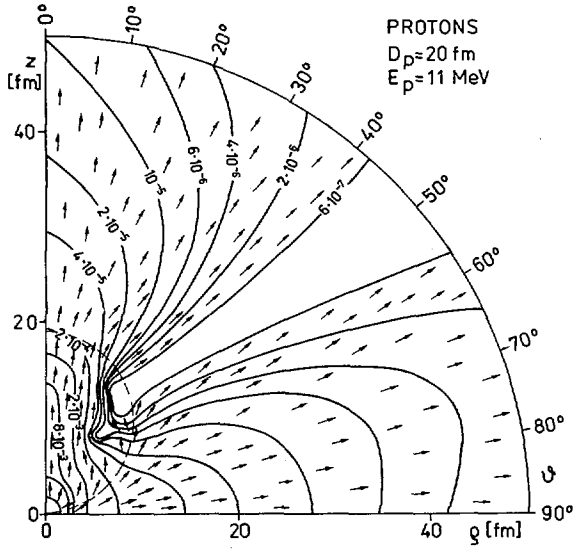

FIG.10. Current density $\vec{J}$ of protons emitted from the centre of the reference system and scattered on spherical fragments. In view of symmetry only one quarter is shown. The arrows indicate unit vectors $\vec{J}/|\vec{J}|$. Points with the same $|\vec{J}|$ value are connected by contour lines labelled by arbitrary units. The fission axis lies along the Z-co-ordinate. The proton energy (at infinity) is equal to 11 MeV, the fragment centres are 20 fm apart. The dashed line indicates the potential ridge.

from the spherical wave is 'drained' by the close fragments, which diminishes the intensity of equatorial emission and simultaneously enhances the particle flux through and around the fragments into the polar region.

An interesting result is the prediction of a diffraction pattern which should be observed in angular distribution of tritons of some particular energy. It is, however, not yet clear to what extent this prediction follows from the drastic approximations made (it is assumed that the fragments are not deformed and are of equal size and that the interfragment distance is fixed all the time; it is also assumed that the source of particles lies strictly in the centre system).

On the whole, although the first results are encouraging, one should be very cautious in drawing final conclusions since at the present stage the predictive power of the model is too weak to permit a detailed verification. It should be remembered here that the classical 'prototype' of this model, discussed in the previous section, was able to 'explain' the P/E intensity ratio, and only the requirement of simultaneous description of other experimental data unveiled its inapplicability.

3.5. Effect of the scission neutrons?

The question of scission neutrons is very controversial (see, e.g. Refs [33, 34]), if we, however, assume their existence, we can expect that they will induce, with some probability, the (n, charged particle) reaction on fission fragments. The yield of charged particles would depend on the neutron spectrum, reaction thresholds and cross-sections, fission fragment composition and, of course, on the probability of the scission neutron emission.

Making use of the existing systematics of cross-sections for the (n,p) reaction [35, 36] and assuming that the scission neutron spectrum is not much harder than that given in Ref. [34], we calculated that, under the most favourable conditions, such a mechanism can be responsible for only three per cent of the observed proton polar emission intensity.

3.6. A rotating navel?

It is well known that the bending vibrations of the fissioning nucleus result in the rotation of fragments. We can imagine that the remnant of the neck (the 'navel') will exist some time after the scission, before it finally dissolves in the nucleus. There is some probability that such a structure on the nuclear surface (a kind of 'hot spot') will emit particles (or clusters) because of the energy stored in the form of deformation. Owing to the fragment rotation, in some cases the emission may take place when the navel is in favourable position for PE (emission of the clusters, when the fragment is rotated through a smaller – or larger – angle, would give rise to equatorial emission).

This model can be eliminated without detailed calculations since the emission intensity should decrease monotonically with the rotation angle, which makes an explanation of the shape of angular distribution impossible.

3.7. Delayed tripartition?

The wide shadow cones for particles emitted from the 'inner space' of Fig. 1 can obviously be expected only if the emission takes place when the interfragment distance is small, of the order of 21–26 fm. Can we explain the PE phenomenon by assuming that the particle is emitted (as in the usual tripartition) from the fission fragment side facing the second fragment, but with a considerable delay with respect to the scission moment? The answer is: no [2]. The reason is that for significant reduction of the shadow-cone opening angle, say to 20°, the emission has to be delayed by at least 8×10^{-21} s, when the fragments are already 160–200 fm apart (were we to explain the recent measurements by Caïtucoli et al. [12], this delay would have to be equal even to 2.5×10^{-20} s). After such a long time, the emission 'upstream' (i.e. towards the second fragment) should be equally

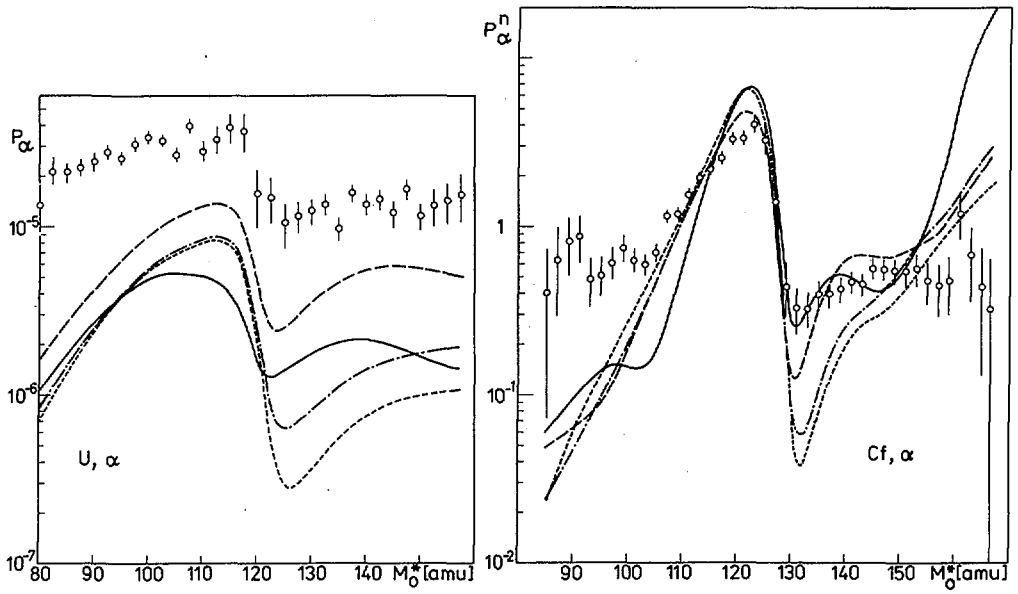

FIG.11. Probability of α-particle emission as function of mass of the emitting fragment. For the ^{236}U case, absolute experimental and calculated distributions are shown, for the Cf fission normalized distributions,

$$p_\alpha^N(M_0^*) \equiv \frac{N(M_0^*)/\int N(M_0^*)\,dM_0^*}{N_B(M_0^*)/\int N_B(M_0^*)\,dM_0^*}$$

are given, where N_B denotes the binary fission mass yield. The curves were calculated by using various level density formulas: Kataria et al. [41] (short-dash), Il'inov et al. [39] (dot-dashed), Tyuran et al. [37](solid lines) and Ignatyuk [40] (long-lines). In this and all the following figures, geometry and resolution effects (see Appendix) were taken into account.

probable as the emission 'downstream'. Since in the latter case the fragment and light-particle velocities should add, we should observe, in addition to the usual PE, the 'high-energy PE'. For instance, in the case of emission from the lighter fragment the α-particle should have a kinetic energy of about 67 MeV. However, it was experimentally checked that the 'high-energy PE' does not exist, which disproves the 'delayed-tripartition' hypothesis.

3.8. Evaporation from fission fragments?

It is well-known that fission fragments de-excite mainly through neutron and γ-ray emission. It is, however, obvious that the charged-particle evaporation channel should compete, but there is still the question of intensity: is this enough to explain polar emission?

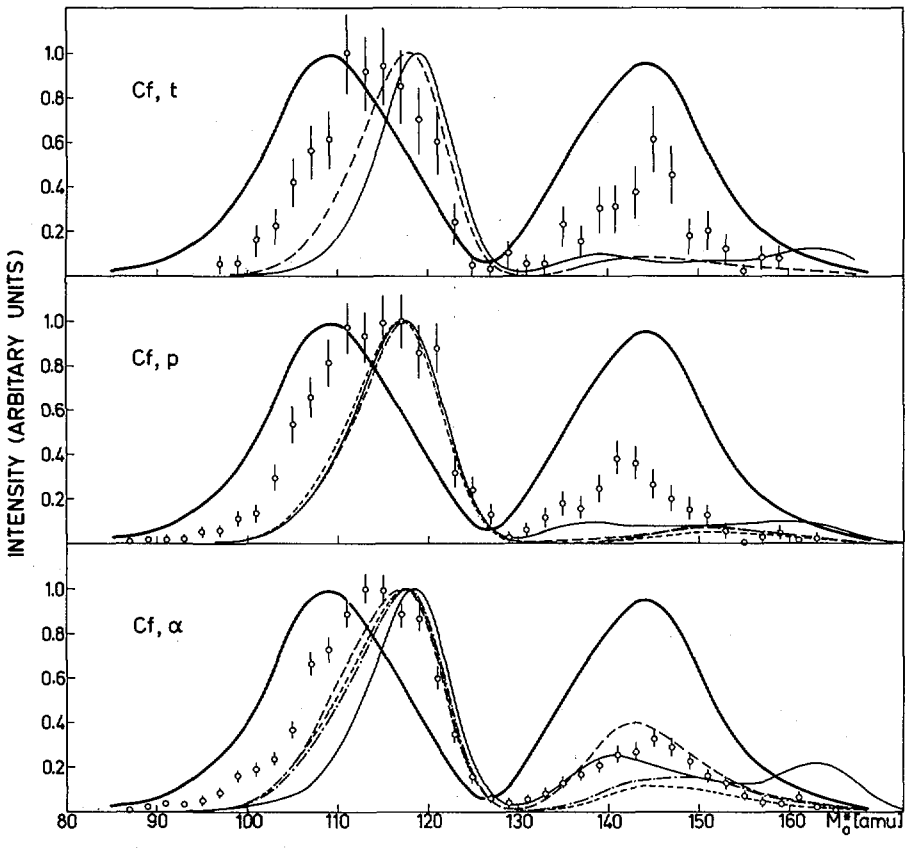

FIG. 12. Comparison of the measured and calculated mass distributions of the polarly emitting fragments. The bipartition data (measured in the same experiment) are represented by bold lines, for the other lines see caption to Fig. 11. All the distributions are normalized to unity in the peak.

The evaporation calculations are the most detailed ones of all those discussed here: they refer virtually to all available experimental data, although for the price of using a pretty large number of parameters. The main principle underlying such calculations was [7, 19], however, that all the relevant distributions (masses, charges, excitation energies, spins) were taken from binary-fission data and that the distributions undergo modification during the de-excitation process only under the influence of penetrability and statistical factors. The parameters were varied only to learn about the sensitivity of the results to input data uncertainties.

Recently performed calculations [22] are an updated version of those described in Refs [7, 19]. The results were modified mainly because of the change of the Fermi-gas level density formula (with the parameter $a = A/\text{const}$)

for more sophisticated formulas providing for shell and deformation effects [37–41]. When comparing experiment and calculations, important geometry and experimental resolution effects were accounted for (see Appendix).

The results are as follows: For fission of ^{236}U, where absolute-intensity data exist, the calculated intensity is too low by a factor of 2–5, which could be explained by parameter uncertainties (especially of the optical-model interaction radius, the separation energies far from the β-stability line, and of the excitation energy distribution far from the mean value). An exception is H-emission of protons, where the intensity is too low by a factor of 10.

The relative intensity of emission of various particles is sometimes reproduced surprisingly well, e.g. the calculated intensity ratio of protons to alphas for L-emission in U is about 0.45 (experimental value: 0.42 ± 0.03), for H-emission in Cf about 0.45 (experiment: 0.40 ± 0.05), of deuterons to alphas in the Cf H-emission is $(6-7) \times 10^{-2}$, while the experiment yields $(6.7 \pm 1.3) \times 10^{-2}$, etc. In some cases, however, the calculated results differ by a factor of three from the experimental ones.

The intensity ratio L/H of emission along the light- and heavy-fragment trajectories is best reproduced in the case of alphas, where (in contrast to the previous calculations) the agreement is almost within the experimental error. Even more, the calculated dependence of the emission probability on the fragment mass $p_\alpha(M_0^*)$, where M_0^* is the mass of the fragment before emission, is also similar to the experimental result (Fig.11). For other particles, the calculated L/H ratio is usually larger by a factor of two to three than the experimental one although the general character of $p(M_0^*)$ reminds of the experimental dependence.

The measured and calculated fission fragment mass distributions are compared in Fig.12. The information it provides is essentially the same as in Fig.11 since, in terms of the evaporation model, the mass distribution of polarly emitting fragments is determined by the product of $p(M_0^*)$ and binary-fission mass yield. This way of presentation shows, however, that the agreement is not so good as might have been supposed from the data given in the previous figure.

The characteristic feature of the evaporation model is the strong dependence of the emission probability of charged particles on the excitation energy U of the emitting nucleus. Unfortunately, the measurement of U for single fragments is very difficult. Nevertheless, it was possible to determine the total excitation energy of both fission fragments U_t by using the Q-values for the particular fragment mass ratios and the kinetic-energy data [22]. It deserves stressing that the 'experimental' value of U_t was obtained under the assumption that emission takes place from accelerated fragments. Thus, the value of U_t is meaningless when the emission takes place with a delay smaller than, say, 5×10^{-21} s with respect to the scission moment. Comparison of the calculated and measured dependences of the emission probability on U_t shows (Fig.13) that for some fragment mass intervals the calculated dependence is in quantitative agreement with the experimental one, although there are also some masses for which a clear disagreement is observed.

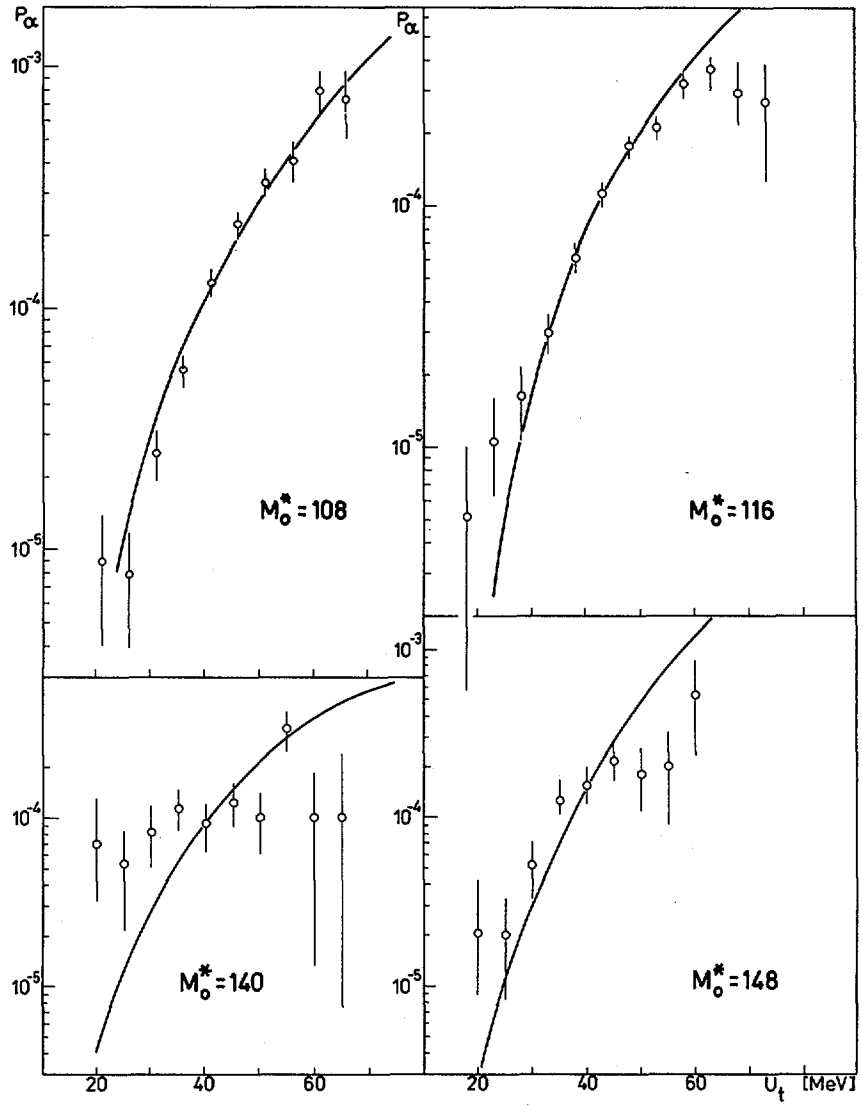

FIG. 13. Probability of emission of α-particles in ^{252}Cf fission as a function of excitation energy of both fission fragments U_t. The results are shown for the emitting fragment mass intervals of 8 amu and centred on the given values of the pre-emission mass M_0^*. Since only the shapes are of interest here, the experimental distributions are normalized at 40 MeV to the theoretical ones. The calculated shapes are practically independent of the level density formula used. The experimental data in this and all the next figures were obtained under the assumption of emission from the accelerated fragments.

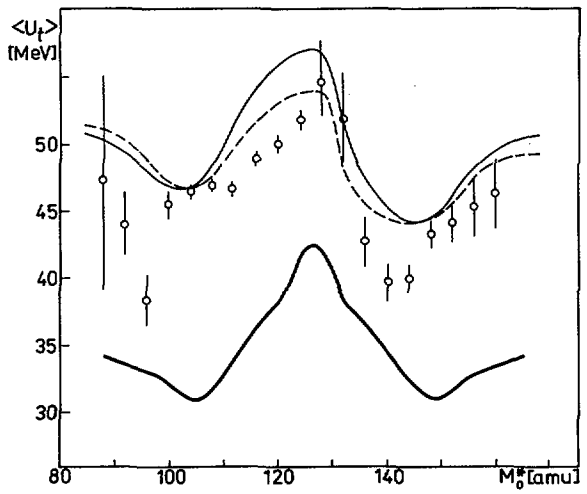

FIG.14. Calculated and experimental dependences of mean total excitation energy of both fission fragments U_t on the emitting fragment mass. The bold line represents the experimental result for bipartition. The other curves represent the calculated results obtained with the use of the level density formula given by Truran et al. [37] (solid line) and Ignatyuk [40] (dashed line). For other level densities [38, 39, 41], the results lie between these two lines.

The total excitation energy of fragments is, in the case of PE, as was stated in Section 2.4., higher than usually in bipartition. In terms of the evaporation hypothesis, this is, of course, due to the fact that the probability of charged-particle emission increases with U_t. The calculated dependence of the mean value of U_t in PE on the emitting fragment mass is compared with experimental results in Fig.14, where we see that the agreement is quite good.

For the sake of balance, we shall give some arguments against the evaporation hypothesis. The first one is due to Andreev et al. [11], who measured the PE intensity in ^{234}U and ^{236}U and found that these intensities differ by about 30 per cent. Since, as the authors argue, the evaporation from the fragments should (judging from the $\tilde{\nu}$-values) be similar in these cases, PE cannot be caused by evaporation. This reasoning is not fully convincing since the probability of charged-particle evaporation depends on the excitation energy almost exponentially whereas $\tilde{\nu}$ depends only linearly. The quantitative comparison of PE intensity in ^{236}U and ^{252}Cf fission made recently [22], gave, however, a result which also disagrees with the evaporation calculations. Other observations concerning the kinetic-energy and angular distribution of polar particles are also in significant disagreement with the hypothesis considered.

In Fig.15, we see some channel energy spectra of polar particles. While for protons the agreement between theory and experiment is quite good, the

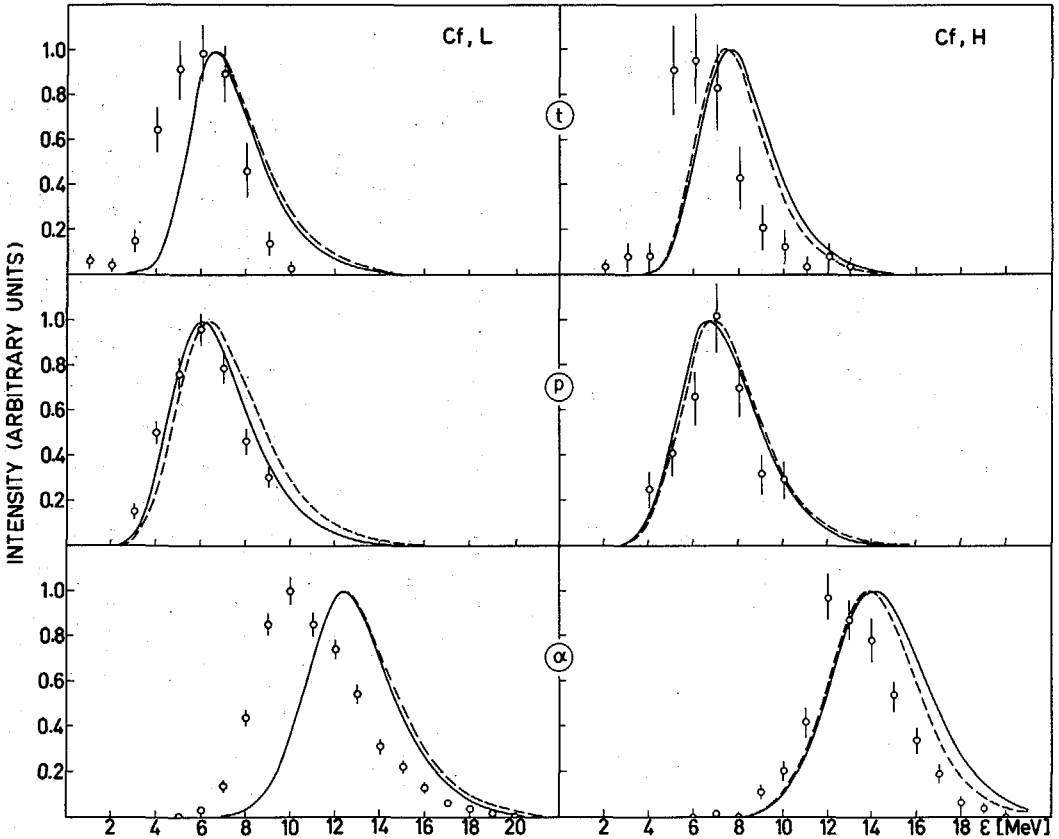

FIG.15. The channel energy spectra of polar particles emitted in ^{252}Cf fission along the light (L) and heavy (H) fragment trajectories. For the labelling of the curves, see caption to Fig.14. For level densities from Refs [38, 39, 41], the results lie between the lines. All spectra are normalized to unity in the peak.

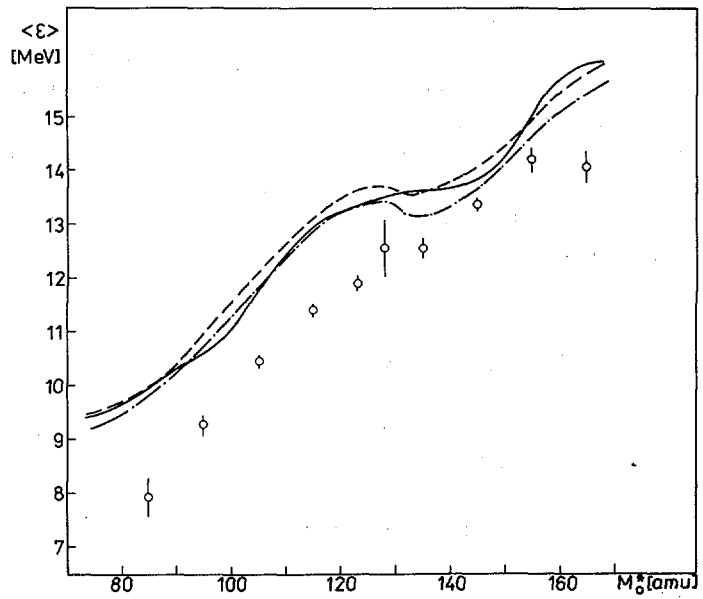

FIG.16. Dependence of the mean channel energy of polar α-particles from ^{252}Cf fission on the emitting fragment mass. For the labelling of the calculated curves, see caption to Fig.11. For level densities from Refs [38, 41], the results lie between the lines shown in the figure.

calculated spectra of tritons and alphas lie clearly too high (although the shapes are reproduced very well). Particularly large disagreement is observed for L-emission, which is clearly visible in Fig.16, where the mean channel energy of α-particles is given as a function of fragment mass for the case of ^{252}Cf fission. We consider the 0.5 – 1.5-MeV difference between experiment and theory to be significant since, in contrast to the emission probability, the calculated energy spectra are only weakly dependent on the parameter uncertainties. Moreover, it is apparently impossible to explain the energy discrepancies by the parameter uncertainties since the decrease in the too large particle energy by changing any parameter used in the calculations (apart from the fragment radii) entails a decrease in the already too small absolute intensity. Another difficulty is connected with the dependence of the channel energy on the total excitation energy U_t, which appears to be much weaker than predicted by the calculations [22].

The next strong argument against the evaporation hypothesis of PE are angular distributions, although (as we stressed in Section 2.1.) they are not known very accurately. The observed focusing along the fission axis is too large to be explained by in-flight emission enlarged by (a small) anisotropy of emission in the centre-of-mass (of fragment + particle) system. This is particularly clear in the

case of protons, where, in terms of the statistical mode, the emission (in the centre-of-mass system) should be almost isotropic. Transformation to the lab system should result in a much flatter distribution than was observed experimentally, which is shown in Fig.3.

Concluding, we face an intriguing alternative: either the evaporation hypothesis is true, then the disagreements with experiment are caused by the inapplicability of the standard statistical approach, or it is false, then the observed extent of agreement is even more surprising.

4. SUMMARY AND CONCLUSIONS

We have reviewed experimental data pertaining to polar emission and learned that, although rich information has already been gathered, there is a need for more precise measurements of, e.g. angular distributions, or for experiments on the dependence of the phenomenon of the fissioning nucleus on the excitation energy.

We have also discussed eight hypotheses concerning the nature of PE and come to the conclusion that four of them are false, one (evaporation) is able to describe some experimental data quite well, which is quite surprising since the hypothesis is apparently also wrong, another one (the nuclear-surface snapping) is too vague for quantitative verification. What is left, is the hypothesis of prescission emission and another one trying to explain the phenomenon by the wave features of matter. Unfortunately, both are in a preliminary stage and their predictive power is, as yet, too weak for a comparison with the experiment. However, at least one of them (the latter) can easily be generalized, and, in fact, quite realistic calculations are in progress.

We can ask what we can, in fact, learn from studying such a rare process, occurring once per 10^5 fissions. Obviously, the answer cannot be very precise until we explain what polar emission, in fact, is, so we have to resort to speculations. If, e.g. it will finally be explained as a diffraction of the wave going out from the scission point, we shall perhaps gain a new tool for determining the scission configuration since, according to the calculations performed, it strongly influences the competition between equatorial and polar emissions. If, as a second example, we shall somehow manage to explain PE as an evaporation process, then it will be possible to use it as a kind of thermometer for determining the fission fragment excitation energy, much more precise than the old 'neutron' one.

As long as the PE is not understood, its main value lies probably in that it signalizes some gaps in our knowledge. It remains to be seen whether these gaps concern some peculiarities of fission fragment de-excitation, of the 'proximity' scattering of the spherical wave, the very long mean free path of α-particles in the nuclear interior, or something else. Let us hope that it will be something interesting.

Appendix

COMMENTS ON THE COMPARISON BETWEEN EXPERIMENTAL DATA ON POLAR EMISSION AND EVAPORATION CALCULATIONS

If polar emission takes place from the accelerated fission fragments, as it is assumed, e.g. in the evaporation calculations, only a part of the emitted particles can be observed in the polar region (0°–25°). To compare the results of evaporation calculations with experimental data recorded only in the polar region, we may extrapolate these data to the full range of angles proceeding, e.g. as in Ref. [7], i.e. assuming that in the centre-of-mass system the particles are emitted with an angular distribution of the type that is given by statistical theory [42], and fit this distribution to the data. Next, integrating this distribution over all angles (not only the polar ones!) we obtain the extrapolated intensity. Such a procedure, applied in Ref. [7] to the case of α-emission in ^{236}U fission, resulted in a P/E value of about 0.02. (Of course, using of the word 'polar' after extrapolation is somewhat misleading since it now concerns all the particles emitted from the accelerated fragments, not only those recorded at the polar angles.) The P/E value can be even larger since we cannot exclude the possibility that high anisotropy in the centre-of-mass system (in Ref. [7], $N(0°)/N(90°) \approx 8$) was caused by some systematic error. If we assume isotropy of emission in the centre-of-mass system, which is close to the predictions based on the statistical model, we reach a value of 0.05. Thus, in the case of α-emission in ^{236}U fission, only about 10 per cent of all the alphas emitted from the fragments would be seen in the polar region.

Moreover, we should keep in mind that the degree of the forward focusing of light particles depends on the particle and fragment velocities; thus, e.g. the slower particles are more effectively focused and recorded with higher geometrical efficiency, which results in a distortion of the measured spectra. The experimental results presented in Section 3.8 are already corrected for this effect.

As regards the question of experimental resolution, we chose to smear the calculated distributions (simulating experimental effects) instead of making a deconvolution of the experimental data since the results of deconvolution are inherently much more ambiguous.

ACKNOWLEDGEMENTS

The authors wish to thank Drs M. Dakowski, J. Błocki, Z. Sujkowski, N. Cârjan, H.-G. Clerc, M. Kisieliński, A. Kordyasz, J. Sobolewski and P. Koczoń for interesting and fruitful discussions.

REFERENCES

[1] HALPERN, I., Annu. Rev. Nucl. Sci. **21** (1971) 245.
[2] PIASECKI, E., DAKOWSKI, M., BŁOCKI, J., NOWICKI, L., INR Report 1720/IA/PL/A (1977).
[3] PIASECKI, E., DAKOWSKI, M., KROGULSKI, T., TYS, J., CHWASZCZEWSKA, J., Phys. Lett. **33B** 8 (1970) 568.
[4] SCHRÖDER, I.G., Bull. Am. Phys. Soc. II **17** 4 (1972) 441.
[5] NADKARNI, D.M., KATARIA, S.K., KAPOOR, S.S., RAMA RAO, P.N., Nucl. Phys. **A196** (1972) 209.
[6] ANDREEV, V.N., NEDOPEKIN, V.G., ROGOV, V.I., Yad. Fiz. **18** 5 (1973) 976.
[7] PIASECKI, E., BŁOCKI, J., Nucl. Phys. **A208** (1973) 381; Nucl. Phys. **A212** (1973) 628.
[8] PIASECKI, E., DAKOWSKI, M., KORDYASZ, A., in Physics and Chemistry of Fission (Proc. Symp. Rochester, 1973) Vol.2, IAEA, Vienna (1974) 383.
[9] PIASECKI, E., SOWIŃSKI, M., NOWICKI, L., KORDYASZ, A., CIEŚLAK, E., CZARNACKI, W., Nucl. Phys. **A255** (1975) 387.
[10] WILHELM, I., BAYER, R., ČVANDA, J., DLOUHY, Z., Nucl. Phys. **A262** (1976) 301.
[11] ANDREEV, V.N., NEDOPEKIN, V.G., ROGOV, V.I., Yad. Fiz. **25** 4 (1977) 732.
[12] CAÏTUCOLI, F., LEROUX, B., PERRIN, P., BARREAU, G., ASGHAR, M., CÂRJAN, N., these Proceedings.
[13] ADAMS, J.A., ROY, R.R., Nucl. Sci. Eng. **63** (1977) 41.
[14] ADAMOV, V.M., DRAPCHINSKY, L.V., KOVALENKO, S.S., PETRZHAK, K.A., PLESKACHEVSKY, L.A., TYUTYUGIN, I.I., Phys. Lett. **48B** 4 (1973) 311.
[15] CUMPSTEY, D.E., VASS, D.G., these Proceedings.
[16] RAJAGOPALAN, M., THOMAS, T.D., Phys. Rev. **C5** 4 (1972) 1402.
[17] CÂRJAN, N., SÂNDULESCU, A., PASHKEVICH, V.V., Phys. Rev. **C11** 3 (1975) 782.
[18] CÂRJAN, N., J. Phys. 37 (1976) 1279.
[19] PIASECKI, E., BŁOCKI, J., Acta Phys. Pol. **B5** 2 (1974) 247.
[20] DAKOWSKI, M., CHWASZCZEWSKA, J., KROGULSKI, T., PIASECKI, E., SOWIŃSKI, M., Phys. Lett. **25B** (1967) 213.
[21] WHETSTONE, S.L., Jr., THOMAS, T.D., Phys. Rev. **154** (1967) 1174.
[22] NOWICKI, L., PIASECKI, E., KORDYASZ, A., KISIELIŃSKI, M., SOBOLEWSKI, J., CZARNACKI, W., KARWOWSKI, H., KOCZOŃ, P., SIGNARBIEUX, C., to be published.
[23] MEHTA, S.K., POITOU, J., RIBRAG, M., SIGNARBIEUX, C., Phys. Rev. **C7** 1 (1973) 373.
[24] SCHMITT, H.W., NEILER, J.H., WALTER, F.J., CHETHAM-STRODE, A., Phys. Rev. Lett. **9** 10 (1962) 427.
[25] ASGHAR, M., CARLES, C., CHASTEL, R., DOAN, T.P., RIBRAG, M., SIGNARBIEUX, C., Nucl. Phys. **A145** (1970) 657.
[26] NARDI, E., GAZIT, Y., KATCOFF, S., Phys. Rev. **C1** 6 (1970) 2101.
[27] CÂRJAN, N., PhD Thesis, Institut für Kernphysik, Technische Hochschule Darmstadt (1977).
[28] SINHA, B., Phys. Rev. **C11** 5 (1975) 1546.
[29] BUDZANOWSKI, A., DABROWSKI, M., FREINDL, L., GROTOWSKI, K., MICEK, S., PŁANETA, R., STRZAŁKOWSKI, A., BOSMAN, M., LELEUX, P., MACQ, P., MEULDERS, J.P., PIRART, C., Phys. Rev. **C17** 3 (1978) 951.
[30] DAKOWSKI, M., PIASECKI, E., NOWICKI, L., Nucl. Phys. **A315** (1979) 370.
[31] DAKOWSKI, M., PIASECKI, E., NOWICKI, L., Acta Phys. Pol. **B9** 10 (1978) 933.
[32] KORDYASZ, A., to be published.

[33] SKARSVÅG, K., Phys. Scr. 7 (1973) 160.
[34] PIKSAYKIN, V.M., DYACHENKO, P.P., KUTSAEVA, L.S., Yad. Fiz. 25 4 (1977) 723.
[35] LEVKOVSKY, V.N., Yad. Fiz. 18 4 (1973) 705.
[36] TROFIMOV, Yu. N., Proc. 4th All-Union Neutron Physics Conference (Kiev, 1977) Moscow (1978) 140.
[37] TRUKAN, J.W., CAMERON, A.G.W., HILF, E., in Properties of Nuclei Far from the Region of β-stability (Proc. Int. Conf. Leysin, 1970) Vol. 2, CERN, Geneva (1970) 275.
[38] IGNATYUK, A.V., SMIRENKIN, G.N., TISHIN, A.S., Yad. Fiz. 21 3 (1975) 485.
[39] IL'INOV, A.S., CHEREPANOV, E.A., Report P-0064, Inst. Nucl. Res., Tomsk (Moscow, 1977).
[40] IGNATYUK, A.V., Proc. of the Summer School, Alushta (1978) 505.
[41] KATARIA, S.K., RAMAMURTHY, V.S., KAPOOR, S.S., Phys. Rev. C18 1 (1978) 549.
[42] ERICSON, T., Adv. Phys. 9 (1960) 425.

DISCUSSION

D. HOFFMAN: Have I understood correctly that the mass distributions were quite different for particle emission? More particularly, was the yield for the heavy-mass peak rather low?

E. PIASECKI: Yes, that is right. We were dealing with the mass distribution of fragments moving in the same direction as the light particle. The lower heavy-fragment yield simply means that more polar particles are emitted along the light fragment trajectory than in the opposite direction.

N. CÂRJAN: Although it is not my purpose to defend the evaporation hypothesis, I still think that, on the basis of your analyses, it cannot be rejected in general terms, since you were actually testing a particular evaporation model. For instance, a feature of your model is the fact that the evaporation of the polar particles occurs neither before nor immediately after scission, but rather when there is full acceleration of the fission fragments – which means about 10^{-18} s after the scission moment (VANDENBOSCH, R., HUIZENGA, J. R., Nuclear Fusion, Academic Press, New York and London (1973) 336). I wonder whether the life-time for particle emission is not shorter, especially if the fragments are already highly excited at their separation (in some cases the excitation energy considerably exceeds the barrier for particle emission). In such a case the problem is no longer a two-body one, and evaporation should be combined with three-body trajectory calculations.

E. PIASECKI: Let me first say in reply that the time for acceleration up to 90% of the final energy is of the order of 10^{-20} s, which is mentioned in Ref. [19] of my paper. It is highly improbable that as short a time as this would be sufficient for evaporation of the charged particle.

The second point is that charged particle evaporation competes effectively with neutron evaporation when the excitation energy is higher than it normally is in bipartition. From Fig. 14 you can see that an excitation energy as high as 50 MeV is necessary. It is hard to believe that the fragments possess as high an excitation energy as this immediately after scission.

Thirdly, evaporation during fragment acceleration should give rise to considerable smearing of the polar particle energy spectra, but this is in fact not observed experimentally. It is only the shapes (widths) of the spectra that are well produced by the evaporation theory. May I refer you to my Fig. 15.

Moreover, anisotropy of the emission (in the laboratory system) from the non-accelerated fragments should differ from the experimental results to an even higher degree.

D. G. VASS: I should like to draw attention to evidence supporting the view that the emission of the 'polar' α-particles occurs after the fragments have reached, or at least nearly reached, their final velocities. Andreev and co-workers (ANDREEV, V. M., et al., Sov. J. Nucl. Phys. **25** (1977) 390 (original Yad. Fiz. **25** (1977) 732)) have measured the energies of the fragments associated with polar emission and those of binary fission fragments as a function of fragment mass. They have found that the energies of the fragments emitted in the opposite direction to the polar α-particles are almost the same as those of the binary fragments, whereas the energies of the fragments emitted in the same direction as the polar α-particles are 15–20 MeV lower than for the corresponding binary fragments. To my mind, this indicated that the 'complementary' fragment is not directly involved in the emission process.

I accept that the experimental yields cannot be explained satisfactorily on the basis of the model in which the polar particles are evaporated from fully accelerated fragments, as you point out. But this does not mean that we should reject the 'post-scission' hypothesis. It does mean, however, that we have to re-examine possible mechanisms governing the emission of alpha particles from fragments that are fully or almost fully accelerated.

E. PIASECKI: I am not aware of any post-scission hypothesis able to explain the experimental data, but I suppose that a model of that kind could be devised. I would not agree, however, with the first of your comments, since the reduction in the kinetic energy of fragments moving in the opposite direction to the polar particle is well established and – the most important thing – it is rather well reproduced by the evaporation model, as I show in Fig. 14. I would not say, though, that this is a strong argument against the 'near-scission' hypothesis, as it simply means that the scission configuration in polar emission differs slightly from that of binary fission.

J. P. THEOBALD: In view of the fact that the polar protons behave quite differently, compared with the orthogonal particles, why do you treat them in terms of the same mechanism as the composite particles?

E. PIASECKI: Well, it would clearly be preferable to avoid devising models for each kind of particles. Besides that, we do not know for sure that it would help very much to do so. For example, the energy spectrum calculated in terms of a statistical model agrees best with precisely those proton states that, as I show, differ extensively at the same time from the angular distribution anticipated on the basis of this model.

J. B. WILHELMY: Since many of the light fission fragments are strongly deformed, do you think the use of a deformed optical model analysis would enable the evaporation process to explain the polar emission?

E. PIASECKI: Interestingly enough, we made an attempt of this kind a few years ago – see Ref. [19] of the paper – to explain the discrepancy between the theoretical and experimental alpha energy spectra, which is much greater for the light (deformed) fragments. The trouble is that the optical model would affect only the emission from the light fragments and as a result the good agreement that we have for the light/heavy intensity ratio would be destroyed.

M. DAKOWSKI: The angular distributions for long-range particles are very different for the models discussed. Experiments with an angular resolution of 0.5–1° would be especially interesting, among other things, for testing the diffraction hypothesis. They are also possible nowadays by means of the larger modern detector arrays.

E. PIASECKI: Yes, I agree.

A MULTIPARAMETER INVESTIGATION OF THE ^{3}H AND ^{4}He EMISSION IN THE FISSION OF ^{252}Cf

D.E. CUMPSTEY*, D.G. VASS
Department of Physics,
University of Edinburgh,
Edinburgh,
Scotland, United Kingdom

Abstract

A MULTIPARAMETER INVESTIGATION OF THE ^{3}H AND ^{4}He EMISSION IN THE FISSION OF ^{252}Cf.

A specially designed xenon scintillation detector, with enhancement of the scintillation intensities by an applied electric field, was used to detect fission fragments from a ^{252}Cf source mounted on the cathode of a parallel-plate electrode assembly inside the scintillation cell. The energies of the fission fragments were determined from the amplitudes of the scintillation pulses, while analyses of the pulse profiles provided information about their orientations. A $\Delta E \times E$ telescope, consisting of two surface barrier detectors mounted on the axis of the detector behind the source, was used to detect the ternary particles. For each ternary event, the light particle involved was identified, its total energy calculated correcting for energy losses, the energy of the associated fragment measured and the angle of emission of the particle relative to the direction of the light fragment determined allowing for the effect of the recoil momenta imparted to the fragments by the ternary particle. – The gross energy distributions of the ^{3}H and ^{4}He particles, their relative total yields and the angular distributions of their yields were measured. The energy distributions at 19 angles between 0° and 180° were observed, and the variations with angle of the most probable energies and the widths of the ^{3}H and ^{4}He distributions were determined. The variations with angle of the relative yields and the ratio of the most probable energies of ^{3}H to ^{4}He suggest that the nuclear configurations at the instant of release of the ^{3}H and ^{4}He particles are almost identical for 'broadside' emissions, but may be slightly different for 'polar' emissions.

1. INTRODUCTION

There have been several studies of the ternary fission of ^{252}Cf, in which correlations between various parameters have been investigated, and those relevant to the present investigation are compared in Table I. The early work has been reviewed by Feather [1] and Halpern [2] . In order to place the present study in context the parameters measured by us are also listed in the table.

---

* Now at the Department of Medical Physics and Bio-engineering, University of Aberdeen, Aberdeen, Scotland, UK.

TABLE I. SUMMARY OF STUDIES OF THE TERNARY FISSION OF ^{252}Cf

	Ref	Yields of Light Particles Y_{TOT}	Gross Energy Distributions $N(E)$	Gross Angular Distributions $Y(\theta)$	Energy Distributions as f(θ) $N_\theta(E)$	Angular Distributions as f(E) $Y_E(\theta)$	Polar Emission	Mean & Standard Deviation of $N_\theta(E)$ $\bar{E}(\theta)$ & $\sigma(\theta)$	Fragment Energy Spectra as f(θ) $N_\theta(E_F)$	Total Kinetic Energy T	Mass Ratio R	Angular Distributions as f(R) $Y_R(\theta)$
Whetstone and Thomas (1967)	[3]	✓	✓									
Cosper, Cerni & Gatti (1967)	[4]	✓	✓									
Fraenkel (1967)	[5]		✓	✓		✓		✓		✓	✓	
Raisbeck & Thomas (1968)	[6]	✓	✓	✓	✓							
Nardi et al (1969)	[7]		✓							✓	✓	
Adamov et al (1971)	[8]				✓	✓						
Rajagopalan & Thomas (1972)	[9]			✓								
Fluss et al (1973)	[10]		✓	✓		✓		✓			✓	✓
Tsuji et al (1974)	[11]			✓	✓			✓				
Adamov et al (1974)	[12]			✓	✓		✓		✓			
Present investigation		✓	✓	✓	✓	✓	✓	✓	✓			

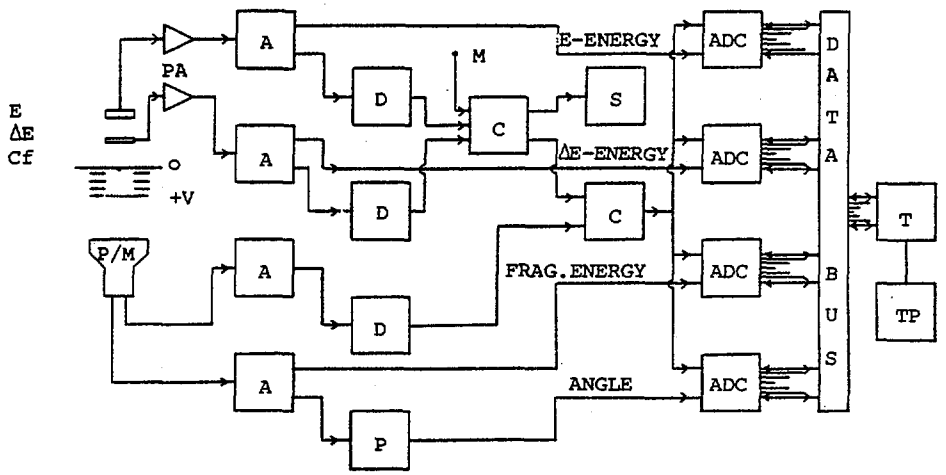

FIG.1. A block diagram of the electronics showing also the arrangement of the fission fragment scintillation detector and the ΔE × E telescope.
A – amplifier, ADC – analogue-to-digital converter, C – coincidence unit, D – discriminator, PA – pre-amplifier, P/M – photomultiplier, P – pulse-shape analyser, S – scaler, T – temporary data store, TP – teletype punch; the signal M monitors the status of the gas purification system of the xenon scintillator.

2. EXPERIMENTAL ARRANGEMENT

The arrangement of the fragment and light charged particle detectors used in the experiment is shown in Fig.1.

2.1 The fragment detector

Fission fragments emitted from a ^{252}Cf source, 1mm dia and having a fission rate of ~850 s^{-1}, were detected in a xenon proportional-scintillation detector in which the intensities of the scintillations were enhanced by the application of an electric field. With the pressure of the xenon gas set at 760 torr, the range R(A,Z,E) in xenon of any fragment (mass number A, charge number Z and energy E) was about half the separation (15mm) between the cathode plane and the anode mesh in the scintillation cell. The amplitude of the pulse from the photomultiplier, which viewed the active region between the cathode and anode, was proportional to the energy of the fragment. For a fragment emitted at an angle ω to the axis of the detector the fall time T depended on the projection R(A,Z,E) cos ω of the track along the axis. The range of a fragment does not, however, depend significantly on its atomic mass and charge numbers [13], and so for a selected fragment energy the fall time T of the pulse from the photomultiplier was determined solely by the value of cos ω. The fall time of the photomultiplier pulse was measured using a pulse shape analyser, Ortec model 458. This analyser generated, for subsequent pulse height analysis, a pulse whose amplitude was proportional to the fall time between 90% and 10% of the photomultiplier pulse height.

2.2 The light charged particle detector.

The light charged particles, after passing through the 11.1 mg cm^{-2} thick nickel backing of the source, were detected in a ΔExE telescope mounted on the axis of the system. The telescope consisted of a totally depleted surface barrier detector 50μ thick and a partially depleted surface barrier detector 1000μ thick, Ortec types TD - 15 - 50 - 50 and BA - 24 - 50 - 100 respectively. A circular aperture 5 mm dia in a thin steel plate inserted between the ΔE and E detectors defined the acceptance angle of the telescope as ± 8.4°.

2.3 The electronics.

A standard coincidence arrangement was used in which two coincidence requirements were imposed, Fig.1. The first requirement of a coincidence between the signals from the ΔE and E detectors rejected "noise" from the telescope. The second requirement of a coincidence between the output signal from the ΔExE coincidence unit, indicating the detection of a light charged particle, and a signal from the linear channel of the xenon proportional-scintillation detector, acknowledging the detection of one or in a few cases both of the associated heavy fragments, was used to select the ternary fission events for analysis. The resolving time, 2τ, of the coincidence circuits was 1.4 μs.

For each ternary event selected, the four signals corresponding to the amplitude of the scintillation pulse, its fall time and the amplitudes of the pulses from the ΔE and E detectors were digitised by the analogue-to-digital converters (ADCs). The digital data were stored event by event in a data buffer [14] and transferred to punched tape about every 8 hrs. The ternary fission rate was ~30 hr^{-1}, and data were collected continuously for 3? days with frequent calibration checks. The random event rate was negligible.

3. DATA ANALYSIS

3.1 The identity of the light charged particle.

The pulse height responses of the two surface barrier detectors were calibrated in terms of energy using a 0.2μCi source consisting of the α-emitters ^{239}Pu, ^{241}Am and ^{244}Cm. The 22,000 ternary fission events recorded were mapped on to the $\Delta E \times (E+\Delta E)$ plane to determine the regions corresponding to the various types of particles of mass and charge numbers, m and z. Groups of ^{1}H, ^{3}H, ^{4}He and ^{6}He particles together with a few of the more exotic light nuclei were observed, consistent with the relationship $\Delta E \times (E+\Delta E) \propto mz^2$ (approx). The regions corresponding to the ^{3}H and ^{4}He particles, which are the subject of this study, were easily identified and clearly defined.

3.2 The total energy of the light charged particle.

Having identified the light particle in an event, its total energy was calculated correcting for the energy losses in the xenon gas between the ΔE and E detectors and also between the Ni foil of the source and the ΔE detector. The appropriate range-energy relationships required to do this were obtained from the data tabulated by Northcliffe and Schilling [15]. The energy distributions for the ^{3}H and ^{4}He particles determined in this way agreed well with distributions obtained in a control measurement using

the ΔExE telescope in exactly the same arrangement but in vacuum, indicating that the corrections were reliable. The distribution in xenon was ~5% wider than that in vacuum due to energy straggling in the gas. The calculations were extended to correct for the energy losses in the Ni backing of the source.

3.3 The energy of the fission fragment.

Daily, the responses of the linear and fall time channels of the xenon proportional-scintillation detector were recorded with the coincidence requirements cancelled. The pulse height distributions obtained from the linear channel before and after the collection of each day's ternary fission data were summed to provide a calibration distribution. The pulse height distribution, due to the binary fission fragments from ^{252}Cf, was similar in quality to that obtained using a surface barrier detector, Ortec heavy ion detector type F - 60 - 300 - 60, [16]. The procedure established by Schmitt et al [17] was used to provide the "pulse height-energy " calibration for the individual ternary fission fragments detected that day, and also for each of the binary fission fragments recorded as required for the angle calibration described below.

3.4 The angle of emission of the fragment relative to the detector axis.

The ^{252}Cf source used in this investigation was a thin, uniform deposit mounted flush with the surface of the cathode in the scintillation cell, and so the binary fission fragments were emitted isotropically into the detector. As shown already the fall time T of the pulse from the proportional-scintillation detector depended solely on cos ω for a given fragment energy, the mimimum and maximum fall times, T_{MIN} and T_{MAX}, occurring for cos ω = 0 and 1 respectively. It may be shown [16] for isotropic emission that

$$\cos\omega = 1 - \left[y(E,T,T_{MAX}) \,/\, y(E,T_{MIN},T_{MAX}) \right] \quad \text{for } 0 \leq \omega \leq \frac{\pi}{2}$$

where $y(E,T,T_{MAX})$ is the yield of fragments of energy E with pulse fall times in the range T to T_{MAX} (corresponding to emission at angles between ω and 0). This relationship was exploited to determine the "cos ω - T" calibration curve at each energy. Strictly the expression is valid only if the energy response of the detector is the same for all angles. For fragments emitted at grazing angles ($\omega \gtrsim 84^{o}$), the absorption of energy in the source was significant and due allowance was made for this in the calibration procedure. The angular resolution of the detector was estimated to be about 2 degrees.

3.5 The angle of emission of the light charged particle relative to the light fragment direction.

Since only one fragment was detected for each ternary fission event, light and heavy fragments were identified on the basis of their kinetic energies. Fragments with energies greater than 85 MeV were classed as light, and fragments with lower energies as heavy [5]. The angle of emission Θ of the light charged particle relative to the direction of the light fragment was calculated in each case. For light fragments recoiling into the gas detector, Θ was simply (π - ω). Where the heavy fragment recoiled into the gas, Fig.2, the effect of the recoil momenta, imparted to the fragments by the light charged particle, had to be taken into account.

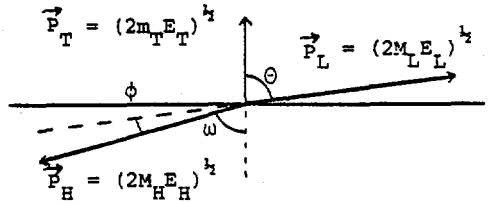

FIG.2. Diagram showing the vector relationship between the momenta $\vec{P}_L$, $\vec{P}_H$, $\vec{P}_T$ of the light and heavy fragments and the ternary particle respectively, when the heavy fragment recoils into the gas detector at an angle ω to the detector axis. The masses and energies of the particles are denoted by (M_L, E_L), (M_H, E_H) and (m_T, E_T).

In such cases, $\Theta = \pi - (\omega+\phi)$ with ϕ given according to the conservation of momentum by the expression

$$\tan \phi = (2m_T E_T)^{\frac{1}{2}} \sin \omega \left\{ (2M_H E_H)^{\frac{1}{2}} - (2m_T E_T)^{\frac{1}{2}} \cos \omega \right\}^{-1}$$

Apart from ϕ, the only unknown is M_H which was estimated with sufficient accuracy by assuming that the total energy of the ternary fission fragments is 168 MeV for all mass divisions; this is correct within about ± 10 MeV. Thus we obtained

$$M_H = (252 - m_T) \left[\frac{(168-E_H)}{168} \right]$$

The effect of the recoil momenta on M_H, itself, was neglected.

3.6 The angular resolution of the spectrometer.

For investigating the angular dependence of the properties of the light charged particles, the range of values of cos Θ from -1 to +1 was split into 20 equal intervals with Δcos Θ = 0.1, each being equal in solid angle. The absorption of energy from fragments leaving the source at grazing angles led to ambiguities between values of cos Θ in the adjacent intervals (-0.1→ 0.0) and (0.0→+0.1). All such events were therefore simply assigned to the interval ($-0.1 \lesssim \cos\Theta \lesssim +0.1$) and allowance made for the larger solid angle subtended in that case.

A Monte Carlo type computation was performed to find the mean angle of emission and the angular resolution of the distribution of the particles selected in each 'Δcos Θ' group, taking account of the acceptance angle of ± 8.4° for the ΔExE telescope. It was found that the mean angle of emission corresponded, as expected, to the mid-point value of cos Θ for the 'Δcos Θ' group , and the full widths at half the maximum height were 13° for groups with $-0.3 \lesssim \cos\Theta \lesssim 0.3$, 14° for $-0.9 \lesssim \cos\Theta < -0.3$, $0.3 < \cos\Theta \lesssim 0.9$ and 17° for $-1.0 \lesssim \cos < -0.9$, $+0.9 < \cos\Theta \lesssim 1.0$.

3.7 The calibrated and corrected data.

At this stage, for each ternary fission event the energy of the fission fragment, the identity and energy of the associated light charged particle, and the angle of emission of that particle relative to the direction of the light fragment were listed.

4. RESULTS

4.1 The gross energy distributions of the ^{4}He and ^{3}H particles.

The energy distributions of the ^{4}He and ^{3}H particles emitted over all angles were plotted and Gaussian curves fitted to them. The fits are very good over the energies ranges of the measurements, 13.3 to 37.0 MeV for ^{4}He and 5.5 to 21.0 MeV for ^{3}H particles. In Table II we compare the mean energies and widths (FWHM) of the distributions, obtained from the parameters of the Gaussian curves, with previous measurements. Our values for the widths were reduced by 7% in both cases to allow for the widening due to straggling in the xenon gas and Ni foil of the source. Weighting all measurements equally, the average values of the various parameters have been calculated, see Table II. The agreement amongst the various measurements is good.

4.2 The relative total yields of ^{3}H to ^{4}He particles.

The ratio of the total yields of ^{3}H to ^{4}He particles was estimated by using the Gaussian curves to extrapolate the energy distributions to zero energy and taking the ratio of the total counts in the distributions. The value obtained is compared with previous measurements in Table II. In all cases the relative yields were estimated on the basis of extrapolations of measured distributions, as here, except for the value of Raisbeck and Thomas [6]. They calculated the relative yield over the energy range of the particles as measured in their experiment. They have estimated that the yield of ^{4}He particles over all energies is about 5% greater than their observed yield. We estimate that about 12% of the ^{3}H yield lies below their energy threshold of 5 MeV. This leads to a relative total yield of about 7%, when the missing low energy contributions are included, which is in good agreement with our value.

4.3 Angular distributions of the yields of ^{4}He and ^{3}H particles.

The yields of ^{4}He particles detected above the 13.3 MeV threshold and of ^{3}H particles above 5.5 MeV were determined at each angle, and the variations of the yields with angle are shown in Figs. 3 and 4.

We obtained a most probable angle of emission for the ^{4}He particles of $85^\circ \pm 1^\circ$ and a width (FWHM) of $21^\circ \pm 1^\circ$ which after correction for the instrumental resolution of $\sim 13^\circ$ over the peak, becomes $17^\circ \pm 1^\circ$. These values are compared with previous measurements in Table III. Clearly the more recent experiments indicate that the width is narrower than suggested by the earlier measurements.

Fluss et al [10] used an experimental arrangement having a mean angular dispersion of about 5° which is significantly better than that of 12° in the arrangement used by Tsuji et al [11] and of 13° used here.

TABLE II. ^4He AND ^3H PARAMETERS

^4He Mean Energy (MeV)	^4He FWHM (MeV)	^3H Mean Energy (MeV)	^3H FWHM (MeV)	$(\frac{\text{Yield of } ^3H}{\text{Yield of } ^4He}) \times 100$ %	Ref.
16.0 ± 0.5	11.5 ± 0.5	8 ± 1	6 ± 1	5.9 ± 0.2	[3]
16.0 ± 0.2	10.2 ± 0.4	8.0 ± 0.3	6.2 ± 0.6	8.46 ± 0.28	[4]
15	13 (a)	-	-	-	[5]
15 (a)	10 (a)	8 (a)	8 (a)	7.0 (b)	[6]
15.5	10 (a)	-	-	-	[10]
16.1 ± 0.8	13.0 ± 0.7	9.0 ± 0.5	8.2 ± 0.5	7.4 ± 0.3	[(c)]
15.6 ± 0.5	11.3 ± 1.4	8.3 ± 0.5	7.1 ± 1.2	7.2 ± 1.0	Average

(a) Estimated from their figures.

(b) Measured value of 6.5 ± 0.5 adjusted to include low energy events; see text section 4.2.

(c) Present measurement

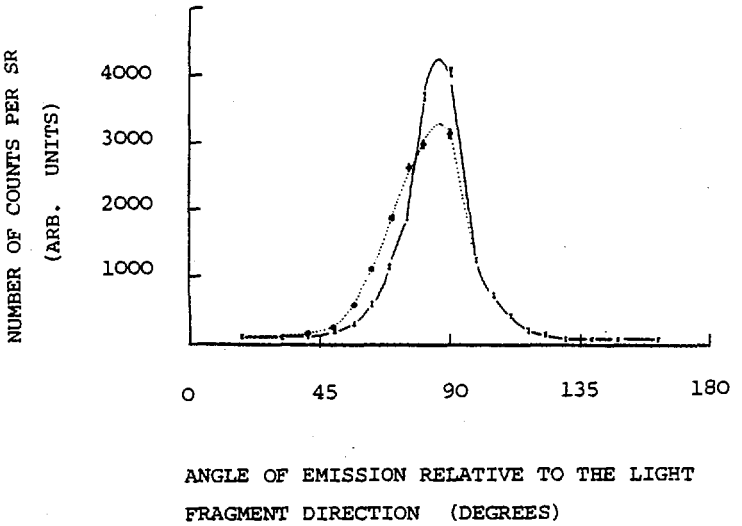

FIG.3. The angular dependence of the yield of ^{4}He particles from ^{252}Cf (solid curve). The variation without correction for the effects of the recoil momenta imparted to the fission fragments by the ^{4}He particles is indicated by the curve .. Φ ...

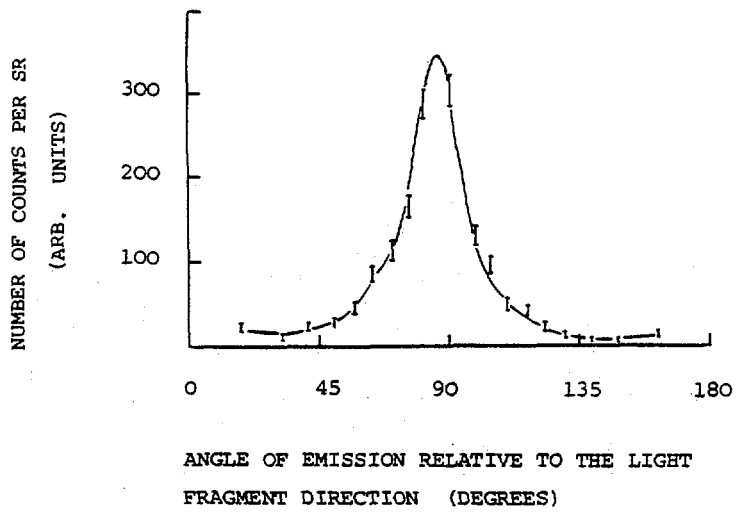

FIG.4. The angular dependence of the yield of ^{3}H particles, corrected for the effects of the recoil momenta.

TABLE III. VALUES FOR ^{4}He FROM VARIOUS SOURCES

^{4}He				
Most probable angle (relative to light fragment direction) (Degrees)	FWHM (Degrees)	Energy threshold (MeV)	^{4}He particle selection	Ref.
84 (a)	32	11.0	No	[5]
92 (b)	34 (b)	13.0	No	[8]
82	23.5	7.0	Yes	[9]
84.3 ± 0.7	18.5 ± 1.0	11.0	No	[10]
84.3	18.3	12.5	No	[11]
85.0 ± 1.0	17.0 ± 1.0	13.3	Yes	[c]
84.5 ± 0.5	17.0 ± 1.0	(~12)	Suggested Values	

(a) Corrected for recoil momenta effects in [10]

(b) Angle relative to fission axis, no distinction between light and heavy fragment directions.

(c) Present measurements.

However, in all of these measurements the light charged particle was detected in coincidence with only one of the heavy fragments, and therefore allowance had to be made for the effect of the recoil momenta imparted to the heavy fragments by the light charged particle when determining its angle of emission relative to the direction of the light fragment. Fluss et al and Tsuji et al applied fixed corrections of 4.3° and 4.5° respectively, wherever corrections were required. We calculated the correction angle required in every case to within 0.4° as described above. Reanalysis of our data applying instead a fixed correction of 4.5° led to an angular width of 22° ± 1° and hence a corrected width of 18° ± 1°, which is in good agreement with the other measurements. An indication of the importance of the correction for the recoil momenta may be obtained from Fig. 3, where the uncorrected angular distribution(i.e. ϕ = 0 in all cases, section 3.5) is plotted. We conclude therefore that the lower value of 17° ± 1° is reliable, and indeed is consistent with the previous observations. Guet et al [18] have recently obtained a comparable value (18.7° ± 0.8°) for the ^{4}He distribution in the thermal neutron induced fission of ^{236}U *.

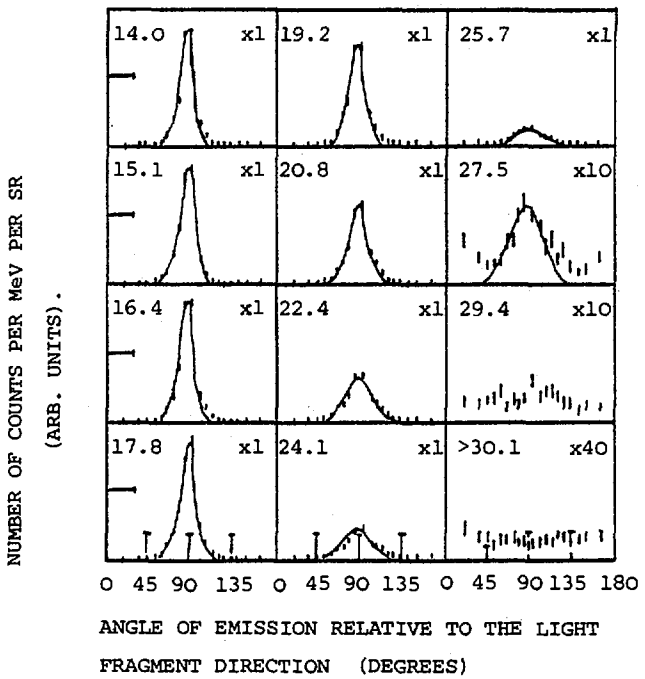

FIG.5. The angular distributions of the ^{4}He particles within selected ^{4}He energy ranges identified by the mean energy in MeV. These correspond to the following ranges (in MeV): 14.0 (13.3–14.3), 15.1 (14.3–15.5), 16.4 (15.5–16.8), 17.8 (16.8–18.3), 19.2 (18.3–19.9), 20.8 (19.9–21.5), 22.4 (21.5–23.2), 24.1 (23.2–25.0), 25.7 (25.0–26.6), 27.5 (26.6–28.4), 29.4 (28.4–30.1) and lastly energies > 30.1. For clarity, the individual distributions have been scaled by the factors indicated.

The recoil momenta also influence the determination of the most probable angle of emission. On the basis of the measurements since 1973, the most probable angle of emission relative to the direction of the light fragment for ^{4}He emission above ~12 MeV is $84.5^\circ \pm 0.5^\circ$. This compares with $82.0^\circ \pm 0.4^\circ$ for energies above 12.5 MeV in the $^{235}U(n_{th},f)$ reactions [18].

For ^{3}H particles, the most probable angle of emission is $86.5^\circ \pm 1.0^\circ$ and the width $17^\circ \pm 1^\circ$ after correction for the instrumental resolution. Raisbeck and Thomas [6] have suggested that the angular distribution of the yield of ^{3}H particles is about 4° or 5° wider than for ^{4}He particles. Their suggestion was based on measurements of angular distributions of the light charged particles relative to the fission axis. Similarly in the measurements made by Adamov et al [12] at a few angles, no distinction was made between the light and heavy fragment directions. When the distinction is made and corrections for the recoil momenta are applied, we find that the angular variations for ^{3}H and ^{4}He particles are very similar.

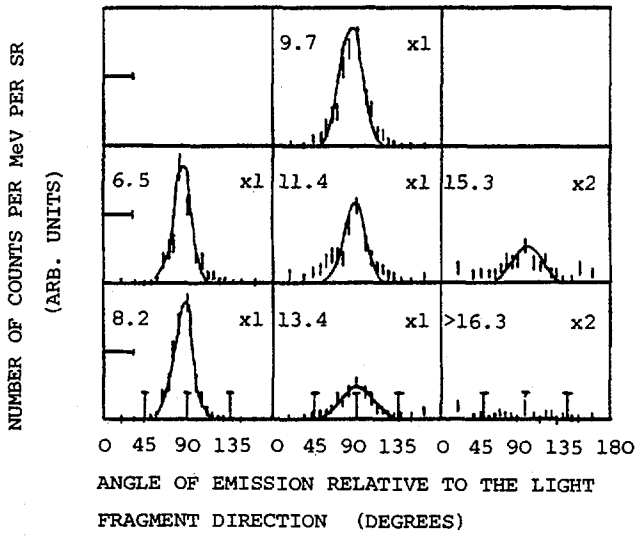

FIG. 6. The angular distributions of the ^3H particles within selected ^3H energy ranges identified by the mean energy in MeV. These correspond to the following ranges (in MeV): 6.5 (5.5–7.1), 8.2 (7.1–8.8), 9.7 (8.8–10.5), 11.4 (10.5–12.4), 13.4 (12.4–14.3), 15.3 (14.3–16.3) and lastly energies > 16.3. For clarity, the individual distributions have been scaled by the factors indicated.

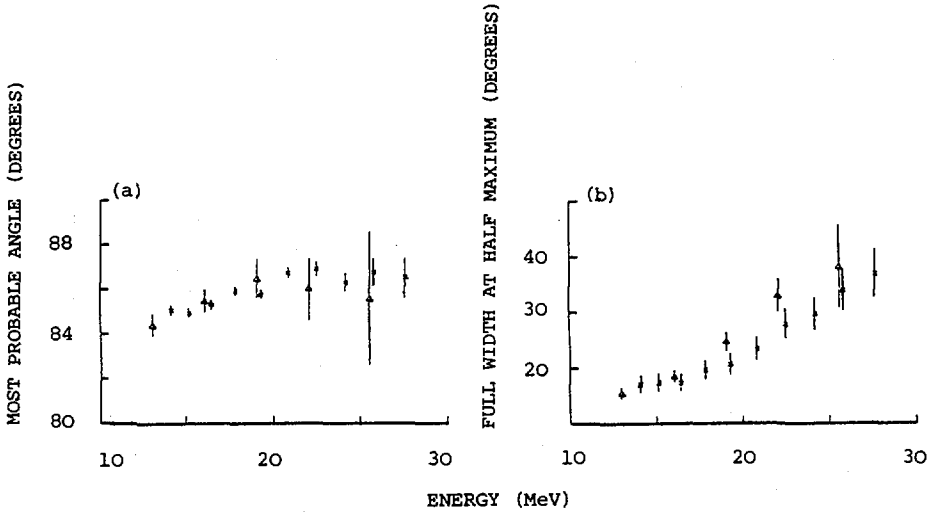

FIG. 7. The variation with energy for ^4He particles of (a) the most probable angle of emission and (b) the full width at half-maximum of the angular distributions. Measurements: Δ Fluss et al. [10], X present experiment.

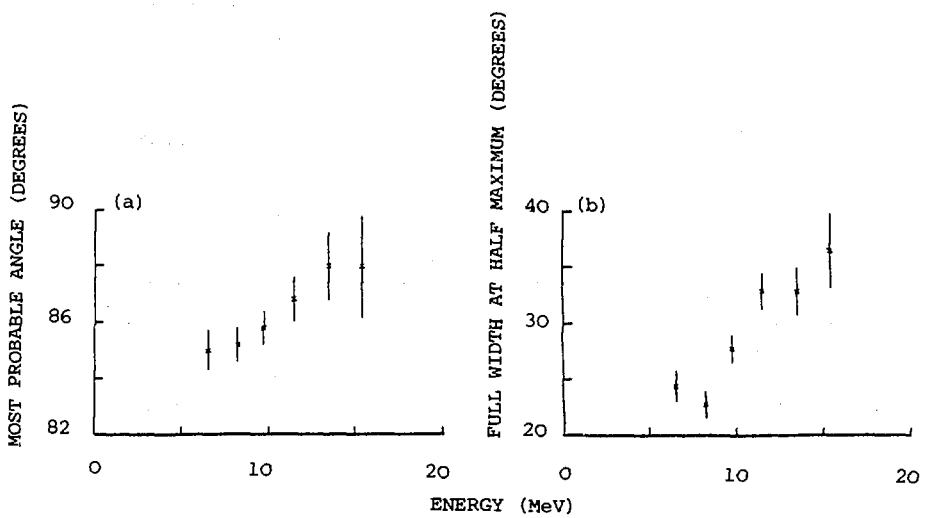

FIG.8. The variation with energy for ^{3}H particles of (a) the most probable angle of emission and (b) the full width at half-maximum of the angular distribution.

4.4 The variation of the angular distributions with energy.

The angular distributions of the yields for selected energy intervals of the ^{4}He and ^{3}H particles are shown in Figs. 5 and 6. Although the variation of the total yield with angle is not symmetrical, it was nevertheless possible to fit Gaussian curves between 53° and 120° to the individual distributions for ^{4}He energies below 23.2 MeV in Fig.5 and for ^{3}H energies below 14.3 MeV in Fig.6. As the ^{4}He energy is increased above $\sim$ 23 MeV the emission becomes isotropic and then peaked towards the polar angles; the highest energy ^{4}He particles are emitted along the fission axis. A similar trend occurs for the ^{3}H emission.

The variations of the most probable angles of emission and the widths of the distributions with energy are shown in Fig.7 for the ^{4}He emission, where the results of Fluss et al [10] are also plotted, and in Fig.8 for the ^{3}H emission. Adamov et al [8], who made no distinction between the light and heavy fragment directions, also found that the width increased rapidly with energy consistent with the trend in Fig.7(b). When a fixed correction angle for the effect of the recoil momenta is applied in every case, as by Fluss et al [10], it leads to widened distributions except where the correction happens to be reasonably accurate for the events selected. As the emission in the peak occurs near 90°, a correction of 4.3° is only reasonably accurate for a large number of events near 16 MeV, see section 3.5. Also with such a fixed correction the most probable angle will appear too low at ^{4}He energies above ~16 MeV and too high at lower energies. These tendencies show up in Figs.7 (a) and (b) when comparing the data of Fluss et al with that obtained in the present experiment in which accurate event by event corrections were made.

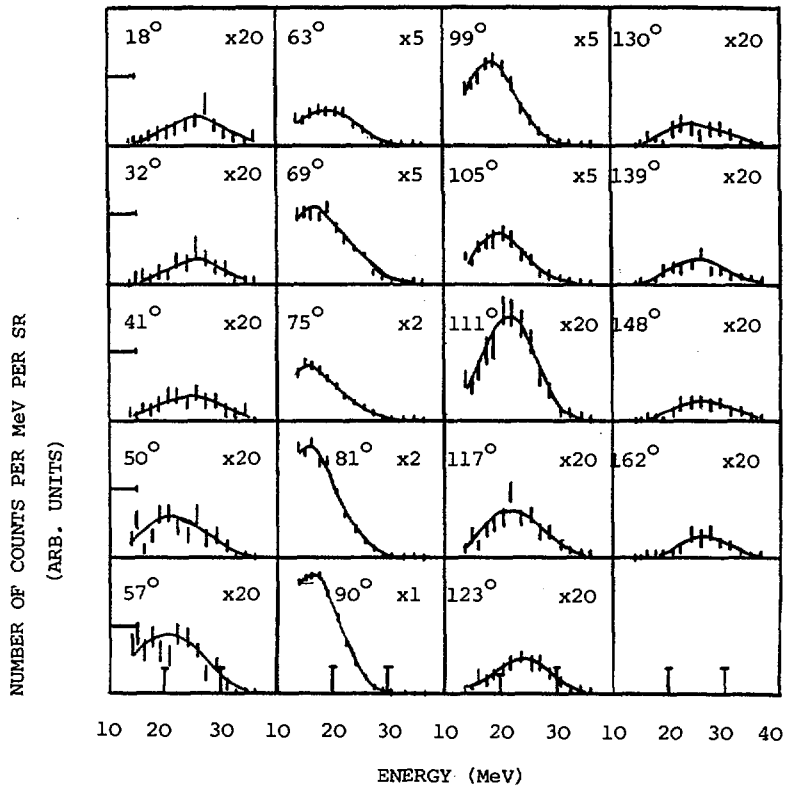

FIG.9. The energy distributions of the ^{4}He particles emitted with the mean angles specified. These correspond to the following angular ranges: 18 (0–26), 32 (26–37), 41 (37–46), 50 (46–53), 57 (53–60), 63 (60–66), 69 (66–72), 75 (72–78), 81 (78–84), 90 (84–96), 99 (96–102), 105 (102–108), 111 (108–114), 117 (114–120), 123 (120–127), 130 (127–134), 139 (134–143), 148 (143–154) and 162 (154–180). For clarity, the individual distributions have been scaled by the factors indicated.

4.5 The variations of the energy distributions with angle.

The energy distributions of the ^{4}He and ^{3}H particles emitted at each of the 19 angles were determined, and Gaussian curves fitted to most of them, Figs. 9 and 10.

The variation of the most probably energy with angle of emission relative to the light fragment direction for the ^{4}He particles is shown in Fig.11(a), where the results of previous measurements are also plotted. The pioneering measurements of Fraenkel [5] have not been included since the angular resolution of his spectrometer was not fine enough to follow rapid variations with angle. We note the striking similarities in the ternary fission of ^{236}U* and ^{252}Cf despite the differences in binary fission,

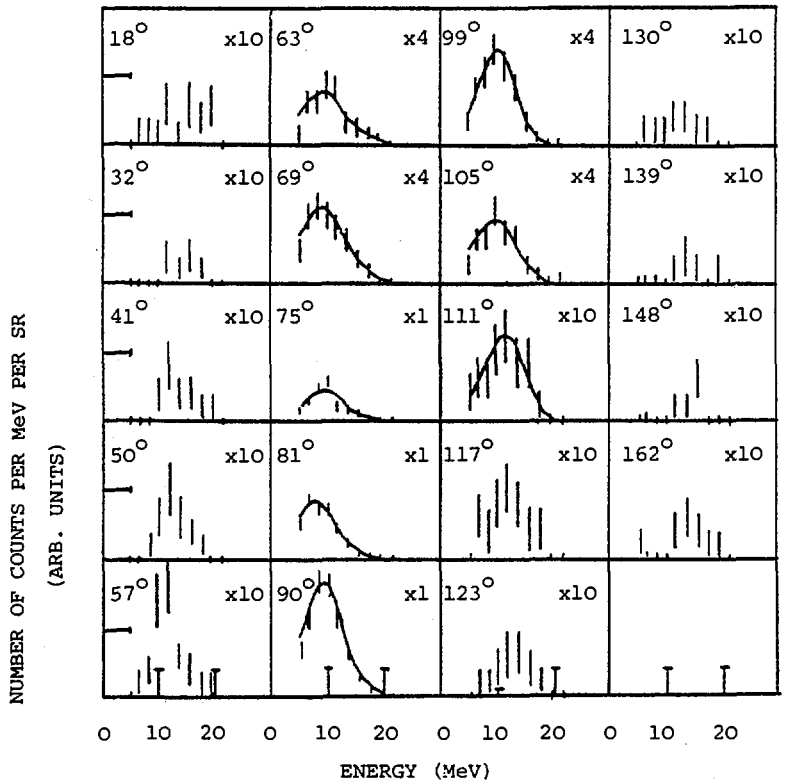

FIG.10. The energy distributions of the ^{3}H particles (presented as in Fig.9 for the ^{4}He data).

especially the different mass-yield distributions. Our results show that the most probable energy has a mimimum value of 15.5 ± 0.8 MeV at 84° ± 1° (the same angle at which the yield is a maximum) and maximum values of 26.0 ± 0.5 MeV along the fission axis.
Piasecki et al [19] found that the most probable energy has a miminum value ~15.5 MeV near 83° rising on either side to values of 24 MeV and 23 MeV at 0° and 180° respectively for the fission of $^{236}U^{*}$.

The variation with angle of the standard deviation of the Gaussian curves fitted to the observed ^{4}He energy distributions is shown in Fig.11(b) The average value of the standard deviation as measured is about 5 MeV, and this becomes 4.6 ± 0.3 MeV when the correction is made for straggling. By comparison Tsuji et al [11] found an average value of 3.8 MeV over the angular range 65° to 115°.

The variation of the most probable energy of the low yield ^{3}H particles is shown in Fig. 12 (a). Although the statistical accuracy of the energy distributions at polar angles is poor the mean (most probable) energies may be determined fairly accurately provided we assume that the

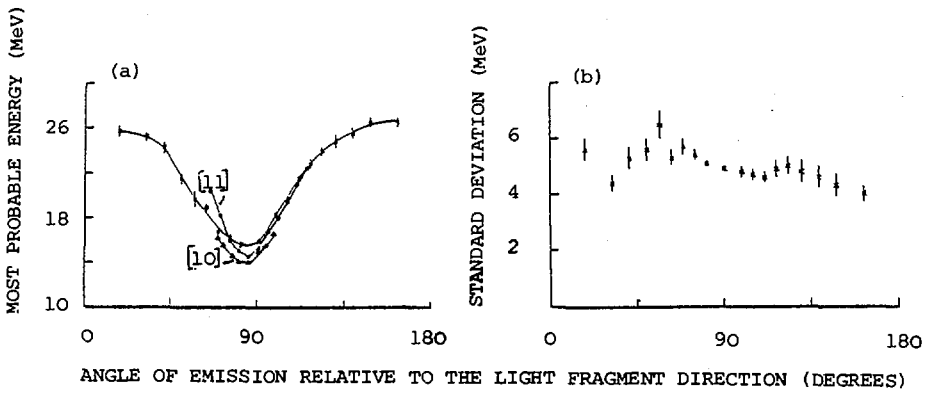

FIG.11. The variation with angle for ^{4}He particles of (a) the most probable energy of emission and (b) the standard deviation of the Gaussian curve fitted to the energy distribution within each angle group. Measurements: Δ Fluss et al. [10], ○ Tsuji et al. [11], X present experiment.

form of the distribution at each angle is indeed Gaussian. The standard deviations of the ^{3}H energy distributions do not vary significantly over the range of angles 60° to 120°, Fig.12 (b). The mean value of the standard deviation, after correcting for straggling, is about 3.3 MeV.

4.6 Polar emissions.

The only measurements, at least known to the authors, of the polar emissions from ^{252}Cf are due to Adamov et al [12]; Atneosen and Thomas [20] found no significant yield from ^{252}Cf although they did observe "polar" emission in the proton induced fission of ^{235}U. The percentage relative yields of ^{3}H to ^{4}He particles along the fission axis, irrespective of light and heavy fragment directions, is 19 ± 5% compared to 5% found by Adamov et al [12]. Their low value may possibly be due to misidentification of ^{3}H as ^{4}He events. There is a peak in their ^{4}He energy distribution at the most probable energy of the ^{3}H particles, and they themselves suggest that the peak is anomalous and possibly due to scattering. The corresponding value for the fission of ^{236}U* is 9 ± 2% from the data published by Piasecki et al [19, 21].

5. DISCUSSION

We have concentrated on the experimental aspects of the emission of the ternary particles in fission. These may according to the various models be emitted prior to scission [22], at scission [1, 2] or after scission [23]. Unfortunately comparisons of the results of model dependent calculations with experimental measurements do not provide as yet unambiguous support for one particular model. However the observation of narrower angular distributions has important implications for the various models [24,25,26,18], since this enables valid scission configurations to be found with lower initial kinetic energies than previously thought possible.

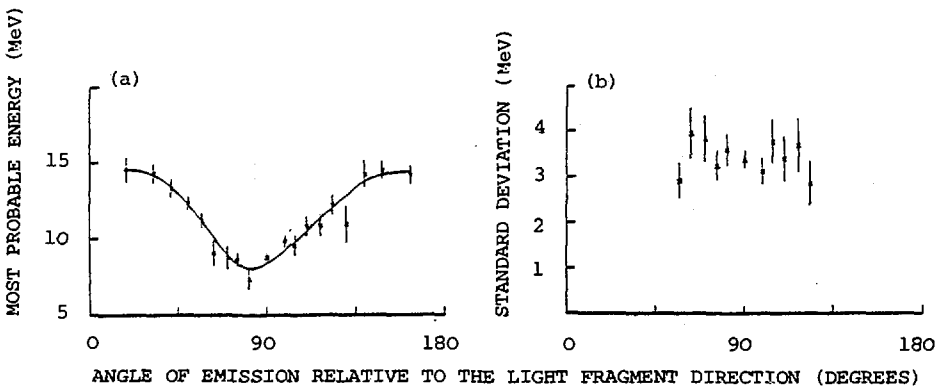

FIG.12. The variation with angle for ^{3}H particles of (a) the most probable energy of emission and (b) the standard deviation of the Gaussian curve fitted to the energy distribution within each angle group.

That the distributions for ^{252}Cf are narrower apparently than those in the fission of $^{236}U^{*}$ is of special significance [18].

From our data we conclude that the ratio of the total (extrapolated) yields of ^{3}H and ^{4}He particles increases significantly towards the polar angles, Fig. 13. However, it should be noted that the relative yields measured by Adamov et al [12] for ^{252}Cf and those for the fission of $^{236}U^{*}$ by Piasecki et al [19,21] do not necessarily support this conclusion. A much more marked increase towards polar angles has been observed for the relative yields of ^{1}H to ^{4}He particles [12], but the energy variations are different in the two cases.

The ratio of the most probable energies of the ^{4}He to ^{3}H particles as a function of angle is shown in Fig. 14. There is a tendency for values close to 2 to occur over the central region 60° to 135°, and for values near 1.8 - values which are only slightly different from 2.0 but the difference appears to be statistically significant- to occur towards the polar angles 60° to 0° and 135° to 180°. This ratio does not depend critically on the absolute energy calibration of the detectors or on the absolute angular calibration; it does however depend on the linearity of the pulse hight response with energy of the ΔExE telescope. We note that ^{3}H and ^{4}He particles emitted near 90° and near the polar angles have been treated in exactly the same way. If the configurations at the instant of release of a ^{4}He and a ^{3}H particle were identical except for the different charges carried by the light particles, then the ratio would be exactly 2; the fragments however share one unit of charge extra in the case of the ^{3}H emission. Tentatively we conclude therefore that the configurations at the instant of release of ^{3}H and ^{4}He particles are more or less identical for those events leading to 'broadside' emissions, but may be slightly different for 'polar' emissions.

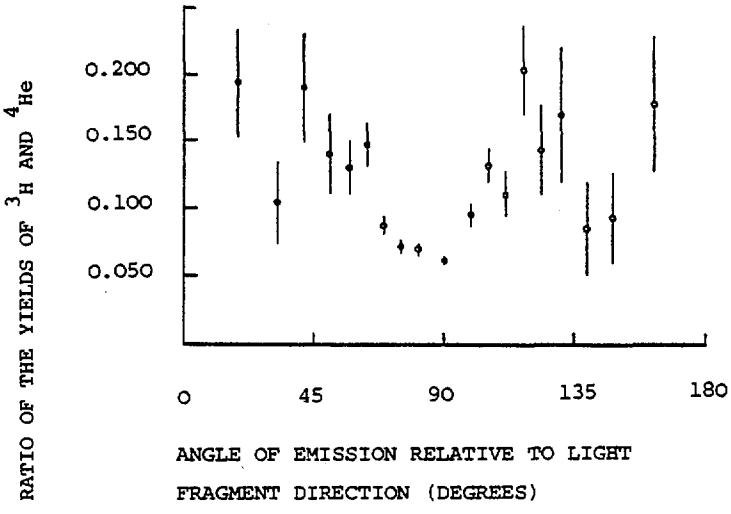

FIG.13. The ratio of the total (extrapolated) yields of the ^{3}H and ^{4}He particles as a function of the angle of emission.

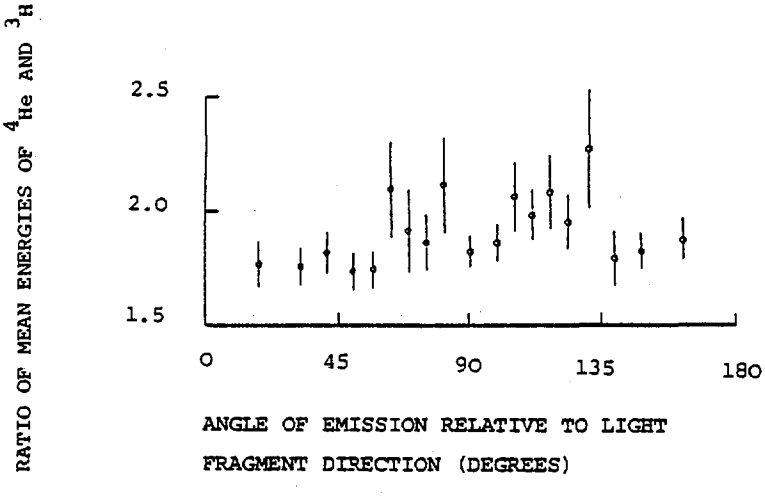

FIG.14. The ratio of the mean energies of the ^{4}He and ^{3}H particles as a function of the angle of emission.

Finally we note that the evidence in Figs.13 and 14 suggests that both the relative energies and the relative yields of ^{3}H to ^{4}He increase towards polar angles. It is conceivable that one physical parameter is responsible for both variations. Also these observations do not necessarily imply a different basic mechanism for 'broadside' and 'polar' emissions. Finally, it is desirable that further experimental work should be undertaken to investigate these trends in more detail.

REFERENCES

[1] FEATHER, N., in Physics and Chemistry of Fission (Proc. Symp. Vienna, 1969), IAEA, Vienna (1969) 83.

[2] HALPERN, I., Ann. Rev. Nucl. Sci. 21 (1971) 245.

[3] WHETSTONE, S.L. and THOMAS, T.D., Phys. Rev. 154 (1967) 1174.

[4] COSPER, S.W., CERNI, J., and GATTI, R.C., Phys. Rev. 154 (1967) 1193.

[5] FRAENKEL, Z., Phys. Rev. 156 (1967) 1283.

[6] RAISBECK, G.M. and THOMAS, T.D., Phys. Rev. 172 (1968) 1272.

[7] NARDI, E., GAZIT, Y. and KALCOFF, S., Phys. Rev. 182 (1969) 1244.

[8] ADAMOV, V.M., DRAPCHINSKII, L.V., KOVALENCKO, S.S., PETRAZHAK, K.A. and TYUTYUGIN, I.I., Sov.J. Nucl. Phys. 13 (1971) 540.

[9] RAJAGOPALAN, M. and THOMAS, T.D., Phys. Rev. C5 (1972) 2064 .

[10] FLUSS, M.J., KAUFMANN, S.B., STEINBERG, E.P. and WILKINS, B.D., Phys. Rev. C7 (1973) 353.

[11] TSUJI, K., KATASE, A., YASHIDA, Y., KATAYAMA, T., TOYOFUKU, F. and YAMAMOTO, H., in Physics and Chemistry of Fission 2 (Proc. Symp. Rochester, U.S.A., 1973), IAEA, Vienna (1974) 405.

[12] ADAMOV, V.M., DRAPCHINSKII, L.V., KOVALENCKO, S.S., PETRAZHAK, K.A., PLESKACHEVSKY, L.A. and TYUTYUGIN, I.I., Phys. Lett. 48B (1974) 311.

[13] HARVEY, B.G., Ann. Rev. Nucl. Sci., 10 (1960) 235.

[14] CUMPSTEY, D.E. and VASS, D.G. Nucl. Instr. and Meth. 134 (1976) 601.

[15] NORTHCLIFFE, L.C. and SCHILLING, R.F., Nucl. Data Tables A7 (1970) 233.

[16] CUMPSTEY, D.E. and VASS, D.G., (To be published).

[17] SCHMITT, H.W. and PLEASONTON, F., Nucl. Instr. and Meth 40 (1966) 204.

[18] GUET, C., SIGNARBIEUX, C., PERRIN, P., NIFENECKER, H., LEROUX, B. and ASGHAR, M., J.Phys. - Lett. 39 (1978) L-213.

[19] PIASECKI, E. and BLOCKI, J., Nucl. Phys. A208 (1973) 381.

[20] ATNEOSEN, R.A. and THOMAS, T.D., Phys. Rev. B139 (1965) 307.

[21] PIASECKI, E., SOWINSKI, M., NOWICKI, L., KORDVASZ, A., CIESLAK, E. and CZARNACKI, W., Nucl. Phys. A255 (1975) 387.

[22] CARJAN, N., J.Phys. 37 (1976) 1279.

[23] VASS, D.G., Proc. Roy. Soc. Edin. A70 (1971-72) 295.

[24] FOSSATI, F. and PINELLI, T., Nucl. Phys. A249 (1975) 185.

[25] KRISHNARAJULU, B. and MEHTA, G.K., Pramana 4 (1975) 74.

[26] FONG, P., Phys. Rev. C16 (1977) 251.

DISCUSSION

C. M. C. WAGEMANS: What a pity that your measurements, which certainly represent a lot of hard work, have been made at such a high discrimination level – 13.5 MeV in the case of alpha particles. Results obtained recently by Guet and co-workers at Grenoble, and also by ourselves, on the thermal-neutron-induced ternary fission of ^{235}U clearly indicate a marked deviation from a Gaussian shape in the low-energy part of the ternary alpha spectrum. I should therefore like to ask you whether there was any special reason for using that discrimination level?

D. G. VASS: In our experiments the energy threshold was set mainly by the energy lost by the light charged particles in the nickel backing of the source and in the xenon gas. We were developing a new type of detector and decided, as a precaution, to use a more robust source. Obviously, a thinner backing could have been used with advantage.

As you can see from Fig. A, the energy spectrum of the ^{4}He particles, recorded in coincidence with fragments, is fitted reasonably well over the high-energy region by a Gaussian curve. However, when we extrapolate this curve to zero energy, we see that it does not pass through the origin and indeed extends to negative energy values. This is physically unreasonable, and in my view supports your observation that the distribution deviates from a Gaussian shape at low energies. From Fig. B we see that the triton distribution behaves in similar fashion.

N. CÂRJAN: Your ^{252}Cf measurements show that the polar alpha particles emitted in the direction of the light fragment have ~ 1 MeV less energy than those emitted in the direction of the heavy fragment, whereas Dr. Piasecki has reported the opposite for ^{236}U*. We know from trajectory calculations that we can go from one situation to another by varying the initial alpha particle kinetic energy. The ^{236}U case would correspond to low kinetic energy and ^{252}Cf to high initial kinetic energy.

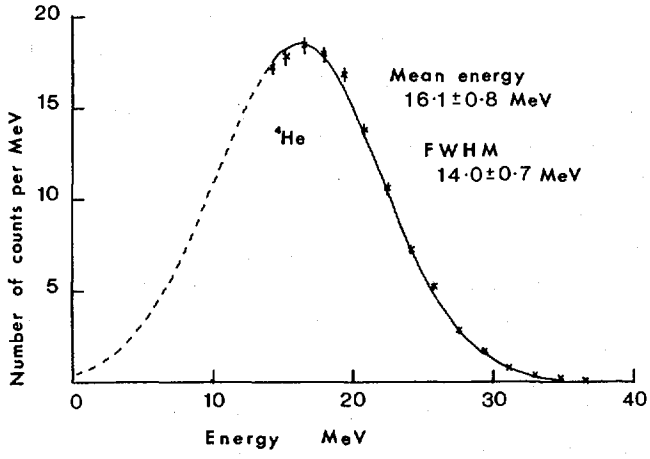

FIG.A. Fission spectrum of ⁴He particles.

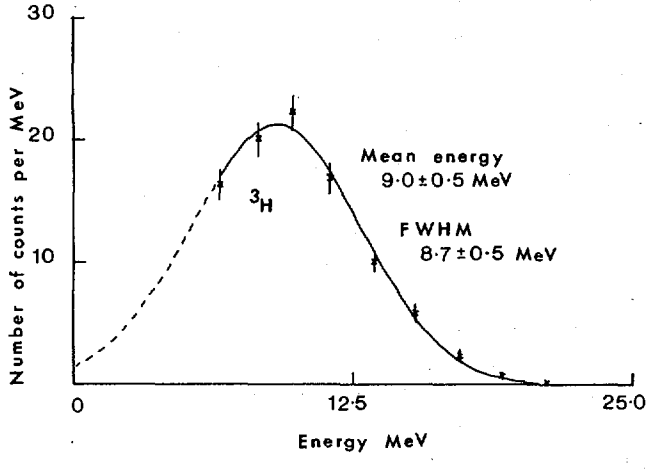

FIG.B. Fission spectrum of ³H particles.

According to the quoted errors, this difference is significant and in such a case could provide a supplementary test for the various emission hypotheses that have been proposed so far (see SM-241/F11 in these Proceedings).

D. G. VASS: When comparing the values for the energy of the polar alpha particles I would advise caution in reading too much significance into differences of ~ 1 MeV in absolute energies between the measurements. For example, there are considerable variations in the mean energy values for the normal ternary alpha

particles obtained by various groups, as shown in Table II of our paper, which possibly arise from difficulties in calibrating the alpha particle spectrometers accurately over the complete energy range.

I agree that the different relative trends within each set of measurements for the ternary fission of $^{236}U^{*}$ and ^{252}Cf may indeed be significant. It is an interesting point worth investigating in more detail.

S. S. KAPOOR: How did you estimate the angular resolution attained by your electronic method of measuring angles, and what is its value? It is very important, I think, for the angular resolution function to be determined experimentally and it should not have any tail so that one can really be sure one is looking at polar alpha particles.

We have also employed an electronic method based on a back-to-back-gridded ion chamber for multiparametric study of alpha emission involving measurement of a variety of correlations. But we have determined the angular resolution of the system experimentally. Some of the details of this method can be found in Extended Synopsis SM-241/F19.

D. G. VASS: We estimate the intrinsic angular resolution of the fragment detector to be about 2°, taking into account the straggling of the fragments in the gas and the precision with which the decay times of the scintillation pulses can be measured. The precise value is relatively unimportant, since the acceptance angle of the coincidence spectrometer was set very much higher than this value at all angles, as I mention in Section 3.6 of the paper. Unfortunately, we have not been able to measure the angular resolution function experimentally, and I agree that it would be highly desirable to do so.

With regard to possible contamination of the polar spectra by "normal" ternary events, this would require either a light charged particle or a fission fragment to be deflected through ~ 90°. There are too few light charged particles of sufficiently high energy between 60° and 120° to provide, after scattering, a significant contribution to events in the polar regions. If a heavy fragment were scattered through 90° (or even 60°), it would lose a considerable fraction of its kinetic energy. There is no evidence from the energy spectrum of the fragments associated with the polar particles that such a large angle scattering actually occurs.

H. A. NIFENECKER: In your experimental set-up the target is positioned at an angle of 90° to the direction of the alpha particles. Don't you think that this system creates problems for light fragment detection near the most probable angle of 83°?

D. G. VASS: Yes it does. The problems occur near 90° rather than at the polar angles, but fortunately they are not too great. We detected the fragments associated with the light charged particles entering the $\Delta E \times E$ telescope in more than 99% of the cases. Therefore we do not lose many events by complete absorption of the fragments in the source. However, we do observe that

fragments emitted at grazing angles, i.e. $\omega \gtrsim 86°$, lose a significant portion of their kinetic energies in the source, even though the ^{252}Cf deposit is extremely thin. We have made allowance for such effects in our analysis (see, e.g. Section 3.6 of our paper.).

M. DAKOWSKI: I am surprised to see that you have not presented your experimental results for protons. The existing data on protons, especially angular distributions in the vicinity of polar angles, appear to be very different from those for alpha particles. More precise data would be very useful for understanding polar emission.

D. G. VASS: We did detect the protons, but since the E detector for our $\Delta E \times E$ telescope was not quite thick enough for complete stoppage of the most energetic protons, we could not determine their energy spectrum unambiguously. We therefore decided not to present the proton data.

ON THE COMPATIBILITY OF LRA FISSION DISTRIBUTIONS WITH COMPACT SCISSION

C.R. GUET*, H.A. NIFENECKER**, C. SIGNARBIEUX†, M. ASGHAR††

* Institut Laue-Langevin, Grenoble Cedex, France

** Centre d'études nucléaires, Grenoble Cedex, France

† Centre d'études nucléaires, Gif-sur-Yvette, France

†† Centre Euratom, Ispra Varese, Italy

Abstract

ON THE COMPATIBILITY OF LRA FISSION DISTRIBUTIONS WITH COMPACT SCISSION.

It is shown that most of the experimental data available on α-accompanied fission are consistent with the assumption that scission configurations are rather compact and that the kinetic energy acquired by the fission fragments before scission is low. A set of 'scission parameters' for α-accompanied fission of ^{236}U (n_{th}) is derived and is found, within trivial corrections, to be valid for ^{252}Cf spontaneous fission and for emission of unstable ^{5}He.

1. INTRODUCTION

The angular distribution of α-particles emitted in fission (with a probability of the order of 10^{-3}) is known to be rather strongly peaked perpendicular to the fission fragment direction. This relatively sharp peaking is qualitatively understood by assuming the two following points : i) the α-particle emerges from the "neck" region ie between the fragments and follows then a trajectory governed by the coulomb field of the fission fragments, ii) the emission occurs when the fragments are still close together and thus able to focus the particle in the orthogonal direction. Since the trajectories are determined by the initial conditions the α-particle should be an unique probe of the dynamical and static state of the scissionning system. Moreover the most typical features (mass distribution, mass-energy correlations, neutron emission, etc ..) observed in binary and ternary fission have been shown to be rather similar [1-4] within trivial discrepancies due to the presence of the third particle. Thus one is naturally led to extend the information obtained from α-accompanied fission to the more general case of binary fission. As underlined by H. Nifenecker [5] at this conference, the present state in the dynamics of fission is still the object of strong contradictions. Many aspects of fission are well understood if one assumes some kind of semi-statistical equilibrium at scission [6] ie a strong damping of the fission mode from saddle to scission. But, on the other side the observation of odd-even effects in charge division and in kinetic energy seems to prove that superfluidity is conserved in a large extent during the descent towards scission. Thus, in this last case on should expect a rather high pre-scission kinetic energy (unless damping can occur without breaking pairs).

Thus, it would be very important to provide some reliable value, ε, for this pre-scission kinetic energy as well as information on the deformations involved at scission. The first value for ε which was proposed was that of Fraenkel [2,8]. Their analysis of the first detailed experiment of α-accompanied fission of Cf^{252} led to the conclusion that the fission fragments were already moving apart with some 20% of their final kinetic energy (i.e. ε = 40 MeV) when the α-particle was released. This value was close to that predicted by Nix et al. [9] when considering the dynamics of the fissioning nucleus as described by a non-viscous liquid drop. On the other extreme, Fong [10] found that the experimental results could be reproduced with a value for ε less than 1 MeV. Then further works based in new experiments with improved accuracy proposed a rather wide spectrum of ε values. The general trend was for high values lying between 25 and 60 MeV (see, for example, Musgrove [11], Kataze [12], Krogulski et al[13]), although lower values around 8-10 MeV have been found to fit the results (see Rajagopalan et al. [14] and Raisbeck et al. [15]).

The basic ambiguity of any three-body trajectories model lies in the impossibility to compute the trajectories backwards. Therefore, one has to try a set of initial dynamical variables, perform the calculations and compare the results at infinity with the experimental ones. A priori, there is no unique solution. Nevertheless, the more measured correlations are reproduced the less freedom is kept for fixing the initial configuration.

The present contribution deals with an analysis of our own data on ternary fission of U^{236} [16]. In this detailed investigation, the energy and angular distributions of the α-particles were measured as a function of mass and kinetic energy of the fission fragments. Among other results, three of them seem to be rather critical for the knowledge of the degree of damping of the fission mode along the descent from saddle to scission and the subsequent scission configurations since they will appear to be strongly selective for the initial parameterization. They are :

1. The width of the angular distribution is 18.5° which is very close to that measured for ^{252}Cf [17].
2. This width appears to decrease sensitively for increasing values of the total fission fragment kinetic energy, Ek.
3. The negative anticorrelation between the kinetic energy of the light particle and that of the fragments.

In section II we shall discuss the model, its approximation and its physical relevance.

In section III, results of the calculations, corresponding to the best choice of initial parameters are compared to experimental results on LRA fission of U^{236}. The calculations are also extended to spontaneous fission of Cf^{252} and to other light particles, especially the unstable He^5.

We shall conclude by trying to interprete the best set of initial "scission-parameters" in the framework of the current theoretical approaches of scission.

2. THE MODEL

The model used for obtaining the initial condition (which by excess of language we can call "scission-parameters") is basically similar to that of Boneh et al. and its modified version by Gavron [18]. There are, however significant differences in the definition of the initial set of parameters which is going to be selected by trial and error method in order

to fit the experimental results. In a recent publication Dakowski et al.[19] claimed that these models were just "erroneous". For avoiding severe a priori suspicions, we will present our model in detail and try to justify it. The first basic approximation is to use classical mechanics for computing the trajectories. This is clearly reasonable and has just the consequence that interference effects, if any, will be washed out. The second and third approximation which might be more doubtful (see Dakowski et al.) consist to assume that the interaction between the three particles is a pure monopole-monopole Coulomb interaction without any higher order term and without any nuclear component. It is clear that the fission fragments born at scission experience a strong deformation, the conventional deformation parameter β being around 0.5-0.8. Moreover the fragments start to oscillate rather rapidly about their mass centers as they separate. The lowest multipole ($l = 2$) surface oscillation of a fission fragment considered as an idealized non-viscous liquid drop has a period in time around $(1\text{-}1.5)10^{-21}$ sec. During a quarter of that period the nucleons placed at the inside tips of the fragments will move towards the centers of their respective fragments by about 1.5-2 fm.

We computed the trajectories of the three fragments during that time the initial conditions being that selected below for fitting the experimental results : the fission fragments would have moved by roughly 1-1.5 fm whereas an α-particle initially placed on the symetry axis with an initial kinetic of 1 MeV will at most be displaced by 2 fm. Thus the speed of retraction of the nuclear surface (which should be added to the motion of the fragments) is higher than the velocity of the particle in the beginning of the separation. This should prevent particles from being absorbed by the heavy fragments. It shows, too, that fixing some static deformation at scission may be irrelevant with respect to the α-trajectories. Although one could easily include these oscillations in the model, it seems reasonable to just consider the mean shape i.e a sphere for each fragment. Regarding the effects of the nuclear force, the α-particle was assumed to have a spherical gaussian density distribution with a r.m.s radius of 1.28 fm whereas each fragments nuclear density distribution was represented by a spherical Fermi function :

$$f(r) = 1/[1 + \exp((r-C)/a)]$$

with $C = 1.16\ A^{1/3}$ and $a = 0.5$ fm. An overlap of the densities of the α-particle and one fragment at a maximum one third of their respective most probable value can be represented by the following distance between the charge centers :

$$R_m = 1.16\ A^{1/3} + 2.2$$

This value determines for the α-particle the closest approach to the fragment center. For $R < R_m$ the particle is trapped, and for $R > R_m$ the pure Coulomb interaction is supposed to be valid. This was checked by adding to the Coulomb force a nuclear attractive force, which, as in ref[19] is defined as the gradient of the real part of a spherical Woods-Saxon potential which parameters are $V_0 = 50$ MeV, $a = 0.55$ fm and $R_V = 1.2.A^{1/3}$. In agreement with Dakowski et al halfof the events accepted in the pure Coulomb case were here rejected (absorbed by the fragments), but this did not affect significantly, the typical final distributions as shown in Fig. 7. The reason for that should be searched in the definition of the various initial distributions and thus will be discussed later.

Fig. 1 shows a schematic initial configuration for α-accompanied fission. The fission fragments with mass A_L and A_H and charges Z_L and Z_H are

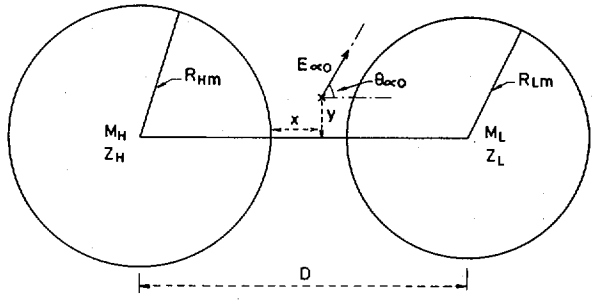

FIG.1. Schematic scission configuration.

spheres of radii R_{Lm} and R_{Hm} as defined above and whose respective centers are at a distance $\bar{D}$ apart from each other. Their initial velocities along the fission axis are determined from the initial total kinetic energy of the fragments denoted as ε. The position of the light particle with mass M_α, charge Z_α has for coordinates x and y. Its initial direction is fixed by the angle θ_0 from the direction of the light fragment and its initial kinetic energy is $E_{\alpha 0}$.

All these parameters obey some statistical distributions and will therefore be selected by a Monte-Carlo procedure. Thus, the light fragment mass distribution (which is known experimentally) is assumed to be gaussian shaped with a mean value $\langle A_L \rangle$ = 92 amu and a standard deviation σ_{A_L} = 6 amu. Charges are then deduced from M_L by assuming conservation of the ratio A/Z. The three initial linear momentum components of the light particle were assumed to be normally distributed with equal standard deviations around the mean-value zero :

$$Pi = 0 \; ; \; \sigma_{p_i} = \sigma_p \; ; \; i = x, y, z$$

Consequently the initial light-particle kinetic energy, $E_{\alpha 0}$, equal to the sum P_i^2, has a Maxwellian distribution with an average value

$$\bar{E}_{\alpha_0} = 3 \sigma_p^2$$

and with a characteristic temperature

$$T = 2 \sigma_p^2$$

Each selected $E_{\alpha 0}$ was then corrected by a deformation parameter equal to $(D/\bar{D})^2$ where D is the center distance selected in the considered event and $\bar{D}$ the most probable value for D. This correction which is weak (±10°) will be very helpful for the correlations between the kinetic energies of particles and fragments. It is not unphysical, if one thinks that the release of the particle might be done at the expense of the energy stored in deformation.

The initial angle θ_0 is naturally defined as :

$$\cos\theta_0 = P_x . (P_x^2 + P_y^2 + P_z^2)^{-1/2}$$

It is seen to be centered around 90°.

Generally, in most of the previous works, the authors assume that the emission point is preferentially located near the Coulomb potential energy minimum. This assumption first proposed by Halpern does not seem to be

very justified (see ref [20]) and is not in fact crucial. We prefer to assume that the emission point are equally distributed in the neck region ie along the fission axis on the distance D-(R_{Lm} + R_{Hm}). This choice which indeed is arbitrary plays a very important role since the final direction of the light particle is strongly determined by the initial position.

The y-coordinate was initially chosen to be normally distributed around the axis (y = 0) with a spread related to that of its conjuguate momentum, Py, via the uncertainty principle. Let us note that taking an emission point out of the axis (at a physically reasonable distance) does not bring any significant modification on the final results. Especially we shall see that the reproduction of the lower part of the final kinetic energy spectrum of the particle needs not any critical requirement of a spread in y. Moreover, if the out-of-axis emission is to be seriously taken into account, one should then perform the calculations in three dimensions which increases sensitively the computing time. A relevant observable that we should reproduce in our calculations is the final kinetic energy of the fragments, E_K. In binary fission E_K is the sum of the energy ε acquired prior to scission and the energy acquired after scission. This last energy is well approximated by the Coulomb interaction between the two spheres separated by D. This is related to what was discussed when considering the effects of deformation. Thus :

$$E_K = \varepsilon + \frac{Z_L Z_H}{D}$$

In ternary fission the previous equation is a bit complicated by the presence of the light particle which acts as a perturbation. The energy conservation principle will allow us to write :

$$E_K + E_\alpha = C + \varepsilon + E_{\alpha_0} \qquad (1)$$

C is the total Coulomb energy of the scission configuration, and E_α the final kinetic energy of the particle.

It was already shown by Boneh et al [8] that the spread in the variables associated to the particle could not account for the final spread in E_K. We calculated that the largest variations of initial conditions on the particle which were compatible with the final kinetic energy distribution of the α-particle led to a width (FWHM) in E_K which was definitely less than 10 MeV. This spread in E_K should be compared to around 20 MeV measured by differents authors [16, 4]. Thus the measured spread in E_K is essentially due to the fluctuations in ε and ρ . Note that this means that even in ternary fission E_K is still a physically significant parameter for selecting a scission configuration.

Whether the fluctuations in E_K proceed preferentially from that of ε or that of ρ stays an open question. Following the argumentation of Björnholm two extremes situations can be considered :

i) all the nuclei follow the same sequence of shapes leading to scission. This can be the path in the deformations space which minimizes the total potential energy. Thus, there is a one-to-one correspondence between E_K and ε and the spread in ρ is negligible, $\sigma_D \ll \sigma_\varepsilon$;

ii) the nuclei proceed to scission by other paths leading to more or less elongated shapes at scission. In this case compact configurations will be associated with the higher values of E_K and the stretched ones to its lower values. Thus we have the strong inequality, $\sigma_\varepsilon \ll \sigma_D$.

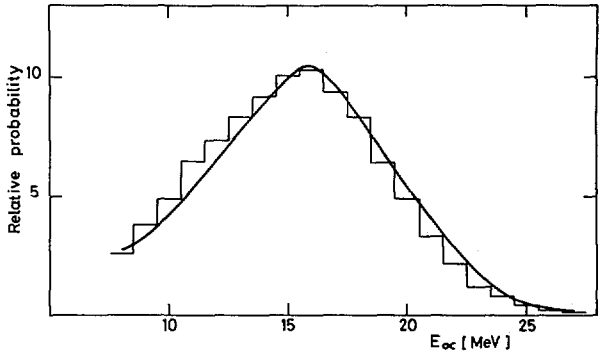

FIG.2. Comparison of measured (histogram) and calculated (full line) kinetic energy distributions of the α-particle.

Both cases were considered in the present calculations. We shall see that some measured correlations are unambigously advocating for the second alternative. The mean values $\bar{D}$ and $\bar{\varepsilon}$ cannot obviously be selected indepently as the final kinetic energies of both the light particle and the fission fragments have to be restored. The spread σ_D and σ_ε were forced to reproduce the final spread $\sigma(E_K)$. The dependence of E_K with the mass division was insured by introducing an adequate dependence of D upon the light fragment mass.

3. RESULTS

The main experimental observables to be reproduced are :
1) The total kinetic energy distribution of the fission fragments.
2) The kinetic energy of the α-particle.
3) The correlation between these kinetic energies.
4) The angular distribution of the α-particle with respect to the light fragment direction.
5) The correlation between the final direction and the final kinetic energy of the α-particle.
6) The dependence of the final direction of the particle upon the mass-ratio of the fission fragments.
7) The dependence of the angular distribution upon the total fragment kinetic energy.

In order to reach the best set of initial parameters able to fit reasonably well all these data, numerous calculations were performed. In each calculation, one the five parameters was changed, the others being kept constant. These five parameters are D, σ_D, ε, σ_ε, and σ_p and we assume that the emission point is uniformly distributed along the fission axis between the two fragments considered as black spheres. Note that the requirements 1) and 2) are already strongly selective with respect to the mean values $\bar{D}$, $\bar{\varepsilon}$ and $E\alpha_0(\sim 3\sigma_D^2)$ since the final kinetic energies Eα and E_K are determined to a large extent by their own initial values and by the initial Coulomb potential.

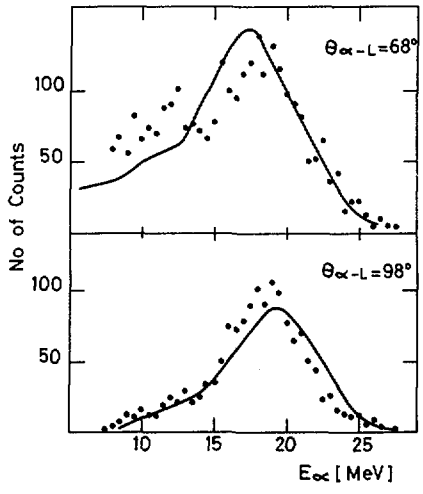

FIG.3. Comparison of measured (points) and calculated (full line) kinetic energy distributions of the α-particle detected at different angles.

The best set of "scission parameters" is presented in Table I. The pre-scission kinetic energy is 8 MeV corresponding to an interfragment distance of 20.7 fm. It should be noted that severe difficulties were met when starting far from these values on both sides.

In the following we shall review all the comparisons.

3.1. The kinetic energy of the α-particle

The calculated kinetic energy spectrum averaged over all mass ratios is compared to the measured one in Fig.2. Both spectra are associated to α-particles detected between 65° and 100° from the light fragment direction. A good agreement is seen, which is not surprising since this observable was naturally given a special weight in the selection of the initial set. As a matter of fact the kinetic energy of the light particle in ternary fission, varies significantly with the nature of the particle.

The experimental spectrum is clearly asymetric, the low-energy part (Eα < 12 MeV) being sensitively enhanced with regards to a normal distribution. This is well reproduced in the calculations. In our experiment [16] we observed that this low-energy enhancement is much more pronounced for the lower angles $\theta_{\alpha-L}$ between the α-particle and light fragment directions. Fig.3 shows the kinetic energy spectra measured at $\theta_{\alpha-L}$ = 68° and $\theta_{\alpha-L}$ = 98°. The calculations let also appearalow-energy tail at the lower angle whereas there is almost no deviation from the normal distribution at $\theta_{\alpha-L}$ = 98° just as measured. The reason for the distortion of the calculated distribution lies in the possibility for a few particles to experience some kind of backscattering in the Coulomb field of the heavy fragments. As it will be seem later, the final direction is very much dependent of the initial position of the particle.Thus in order to come at infinity at an angle $\theta_{\alpha-L}$ around 65-70°, the particle should originate from a rather well defined region close to the heavy fragment (a region of high Coulomb potential). It will be strongly repelled and follow a trajectory which is

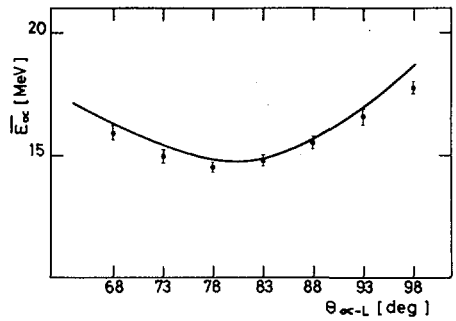

FIG.4. Comparison of measured (points) and calculated (full line) variations of the average particle energy $\bar{E}_\alpha$ with the angle $\theta_{\alpha\text{-}L}$.

approximatively linear. Its kinetic energy at the end will be relatively high. However, this region near the heavy fragment can be reached by particles originally emitted in the proximity of the light one with an initial momentum directed towards the heavy fragment. After a first acceleration the particle is slowed down when approaching the heavy charge and then strongly deflected leading to a low final angle with a relatively low kinetic energy since a part was taken by the recoiling heavy fragment. These drastic modifications of the trajectories occur in the very beginning of the process, in a time interval less than 10^{-21} sec when the fission fragments are still close to each other. It comes out of the calculations that the deflection effect is not so much pronounced for the extreme high angles ($\theta_{\alpha\text{-}L} \sim 100°$) which correspond to direct trajectories from the proximity of the light fragment. This is just due to the asymetry of the problem with respect to the shapes and forces and this is in nice agreement with the experiment.

The calculated variations of the mean kinetic energy $\bar{E}\alpha$ (calculated for events with $E\alpha > 8$ MeV) as a function of final angle $\theta_{\alpha\text{-}L}$ is compared to the experimental data in Fig.4. The mean value $\bar{E}\alpha$ is minimum for the most probable angle. The observed dissymetry around this point is just related to what is discussed above. One major difficulty in most of the previous calculations based on a three-point-charge model (see for example ref [8] and ref [18]) has been to obtain the correct correlation between the kinetic energies $E\alpha$ and E_K. In Fig.5 the mean value $\bar{E}_K$ is plotted against $E\alpha$ and compared to experiment. The measured slope $\langle dE_K/dE\alpha \rangle$ is in the linear approximation roughly equal to -0.45 whereas the calculated one lies rather around -0.7. This correlation as obtained in the model and which in fact is not strictly linear, is the result of two conflictual tendencies. First for a given distance D between the charge-centers the final energies E_K and $E\alpha$ are fully anti-correlated since their sum has to be equal to the initial energy (see eq.1) which is dominated by the potential energy depending on D. The perturbations given by the distributions of ε and $E\alpha_0$ are not sufficient to reduce positively this anticorrelation. This is illustrated by the dashed line of Fig.5, which corresponds to a solution in which the whole dispersion of E_K was attributed to that of ε ($\sigma_\varepsilon = 5$ MeV, $\sigma_D = 0.$). On the opposite, varying the distance D will tend

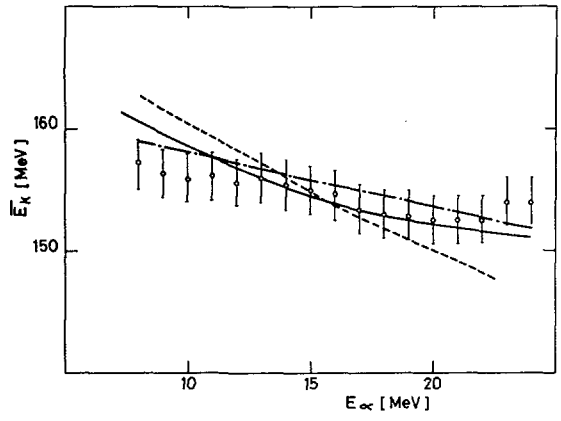

FIG.5. Variation of the average total fission fragment kinetic energy $\bar{E}_K$ with the α-particle kinetic energy. Experimental results are those of Ref. [16] (Φ) *and Ref.* [4] (– · – ·). *The different assumptions for the calculations are:* $\sigma_D \gg \sigma_\epsilon$ *(full line);* $\sigma_\epsilon \gg \sigma_D$ *(dashed line).*

to create a positive correlation between E_K and Eα since both of them increase when decreasing D. We observe that for high values of Eα, above 20 MeV, the effect of D becomes predominant unless we impose a dependence of $E\alpha_0$ upon D as discussed in section 2.

The alternative way to look at the correlation (Eα, E_K) is to plot the main value $\bar{E}\alpha$ against E_K as in fig.6 where the experimental points are ours and in fair agreement with previous ones. However we note that the variation of $\bar{E}\alpha$ versus E_K is not purely linear as it has also been observed in the case of spontaneous fission of Cf^{252} [3] . The theoretical curve measured in the experiment-like conditions (M = 90-95 amu) is fitting rather well the measured in the high yield region. The m ean slope $\langle dE\alpha/dE_K \rangle$ is there equal to -0.13. On the same figure the results of two other trials are shown : first we kept the same mean values for the initial parameters but took the alternative $\sigma_\epsilon >> \sigma_D$; the anti-correlation becomes definitely too strong. The second trial consisted of taking a high value for ε, 25 MeV, the other quantities $\bar{D}$ and σ_p being adjusted for fitting the distributions of Eα and E_K. The dispersion of E_K is again assumed to be essentially that of ε. The resulting slope is again too large, although it is more reasonable than for ε = 8 MeV. Boneh et al. [8] claimed that the observed anti-correlation required a high pre-scission kinetic energy (around 40 MeV). We claim that the correlation can also be understood under the assumption that ε is small provided the interfragment distance D is allowed to vary according to a normal distribution.

3.2. The angular distribution of the α-particles

When the point of emission moves along the axis from the edge of the heavy fragment to the edge of the light one, all other parameters between distributed as usual, the average final angle goes linearly from 75° to 87°. Its dispersion is, for reasons of deflection effects as seen in the previous paragraph, larger near the edges. The angular distribution of α-particles with kinetic energies over

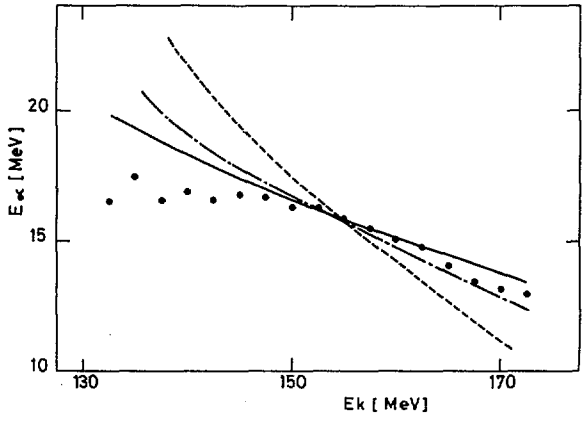

FIG.6. Variation of the average α-kinetic energy with the total fission fragment kinetic energy for a given mass division (M_L = 90–95 amu). Experimental points: (●). Calculations are for: (–) $\sigma_D \gg \sigma_\epsilon$ and ϵ = 8 MeV; (·····) $\sigma_\epsilon \gg \sigma_D$ and ϵ = 8 MeV; (– · – · –) $\sigma_\epsilon \gg \sigma_D$ and ϵ = 25 MeV.

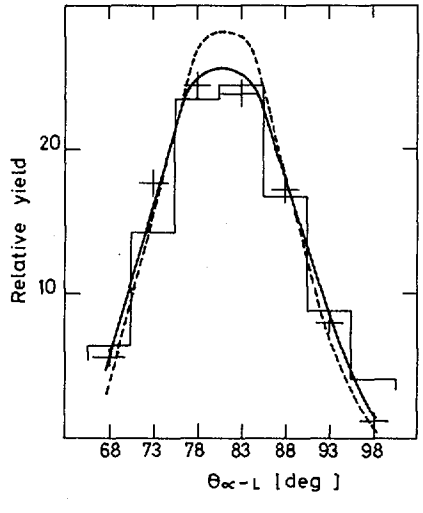

FIG.7. Angular distribution of the α-particle with respect to the light fragment. The measured histogram is from Ref. [16]. Calculations including nuclear forces are shown by (+). The full and dashed lines differ by the size of the neck (see text).

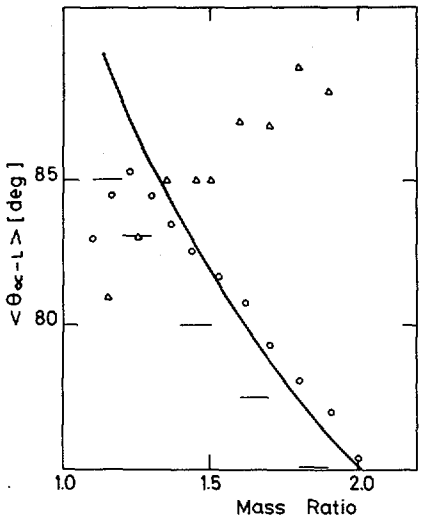

FIG.8. Most probable angle of light particle as a function of mass ratio. Experimental results are from Ref. [16] (○); *Ref.* [23] (–); *Ref.* [31] (Δ). *The calculated curve is shown by the full line.*

8 MeV is reported in Fig.7 together with the calculated distribution = The most probable value of 81° is in excellent agreement with our own . measurement, 81.3° ± 0.4° and other recent works, [21], [22]. It is important to note that no preferential emission point is needed in order to obtain this final angle. The calculated and measured angular widths are also in very nice agreement. Of course, this width is very sensitive to the extension of the region of emission points thus to the parametre D and to the radii R_{Lm} and R_{Hm} (see section 2) which are assigned to the fragments. For illustration, we have run a case in which these radii were both increased by 0.5 fm ; in such a case the sum of the radii is about 16.5 fm and the neck region is thus reduced in length by 20%. As visible in Fig.7, no drastic change of the angular distribution is felt. There is, of course a slight diminution of the angular width from 18.7° down to 17.3° a value which is still reasonable with regards to the experimental one, 18.3° ± 0.4°. The width goes up to 24° when the interfragment distance is distributed around 23.1 fm (i.e ε = 25 MeV).

The α-particle angular distribution is known to become significantly broader and broader as the kinetic energy of the particle increases. This comes naturally out of the calculations and is explained [8] by the fact that the particles with high initial kinetic energy escape faster from the "storm-region" and are thus less focused by the fission fragments. The slight variation of the average angle with Eα is due to the same reason.

The dependence of the angular correlation upon the mass ratio, R, of the main fragments has been, up to recently, known very poorly and is very controversial. We hope that our own results have helped to shed some light on this point by showing that the most probable angle $\langle\theta_{\alpha-L}\rangle$ increases with light fragment mass (see Fig.8) thus confirming the results of Gazit

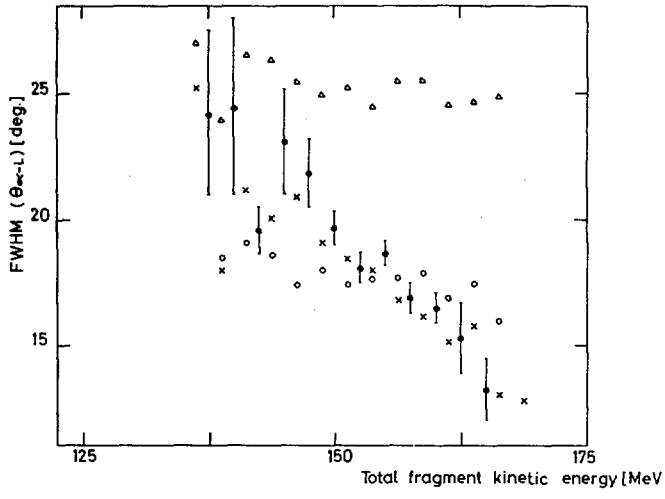

FIG.9. Angular width (FWHM) as a function of total fragment kinetic energy of the mass interval $M_L = 91-93$ and with the condition that $E\alpha > 9.5$ MeV. Experimental results: Ref. [16] (Φ). Calculations are for (X): $\sigma_D \gg \sigma_\epsilon$ and $\epsilon = 8$ MeV; (○) $\sigma_\epsilon \gg \sigma_D$ and $\epsilon = 8$ MeV; (Δ) $\sigma_\epsilon \gg \epsilon_D$ and $\epsilon = 25$ MeV.

et al. [23] and partly those of Choudhuri et al. [20]. The calculated variation is again in excellent agreement with the experimental one. However, the dip between calculated and measured points is seen to become rather important as symetric mass division is approached. Anyhow the variation with mass seems to be due to a large extent to the asymetric Coulomb repulsion of each fragment rather than to a mass-dependent position of the particle between the fragments as speculated in previous works. For instance, the calculations of α-trajectoires starting from initial conditions derived from the statistical theory [24], [25] let appear no significant dependence of the angular correlation upon mass ratio. In this approach, the initial position of the particle is determined from the most probable deformation shapes provided by the statistical theory. The measured data tend to show that describing the deformations involved at scission as pure static deformations and keeping them unchanged as the fragments separate is certainly an overstatement (see Section 2).

The last correlation that we want to discuss expresses the diminution of the angular spread of the α-particle at the total fission fragment kinetic energy increases. In Fig. 9 we show the dependence of the width (FWHM) on E_K only for a given mass interval but same trends are present for other mass bins [16]. It has been shown in the previous paper [16] that this strong correlation was not a trivial consequence of other correlations. The selected set of initial parameters (Table I) permits us to obtain a very similar calculated behaviour. Other possibilities were tried as for the correlation ($E\alpha$, E_K). Evidently, the alternative with $\sigma_D \gg \sigma_\epsilon$ is the unique one able to provide such a dependence. Assuming the opposite, i.e $\sigma_\epsilon \gg \sigma_D$, ε being high or not, leads to a constancy of

TABLE I. FIT TO α-ACCOMPANIED FISSION OF ^{236}U. SEE THE TEXT FOR THE DEFINITION OF PARAMETERS

Parameter	D	ϵ	X	E_{α_o}
Type of distribution	Gaussian	Gaussian	Uniform	Maxwellian
Mean value	20.7 fm	8 MeV	Centre of the neck	1.5 MeV
Standard deviation	0.9 fm	0.5 MeV	∞	1.2 MeV

the angular spread for all possible values of E_K. The reason for these behaviours is clear : high values of E_K correspond to short interfragment distances and thus to a strong localisation of the particle between the fragments and finally to a small angular dispersion. On the contrary a low value of E_K means undirectly that a large initial space was available for the α-particle which leads to a large final angular width. Note that an increase of D of 1 fm implies a broadening of the width of 3°

3.3. Other fissioning system and other light particles

The late experimental investigations have let appear a very strong similarity between the α-accompanied fission of $U^{235}(n_{th})$ and Cf^{252} (spont.). Both angular distributions show nearly identical widths : 18.5° ± 0.5°. The mean angles are slightly different : 81° ± 0.5 for U^{236} and 84.3 ± 0.7 for Cf^{252} [17], [26]. We showed in the previous paper that the variations of the α-kinetic energy spectra with the final angle were also very similar in these two fissioning systems as well as the correlation $(E\alpha, E_K)$ characterized by linear regression coefficients $\langle dE\alpha/dE_K \rangle$ and $\langle dE_K/dE\alpha \rangle$ being respectively ∿ -0.1 and ∿ -0.45 in both cases. All these similarities lead us to assume that the average initial configuration at scission does not differ so much from U^{236} to Cf^{252}.

Since the change of 16 units in the atomic mass induces an increase of about 0.3 fm of the sum of the fragments radii the interfragment distance was adjusted to 21 fm in order to keep the neck extension as the same as in U^{236} fission. All other parameters of Table I were kept (ϵ stays equal to 8 MeV) except the mean light fragment mass which was put equal to 105. The results of the calculations were surprisingly close to experimental data as shown in Table II.

The angular width is found to be a little bit smaller in the Cf^{252} fission than in U^{236}. This point is evidently very crucial since it could help for providing information on the dependence of ϵ on the fissility parameter.

TABLE II. COMPARISON OF CALCULATED OBSERVABLES TO THE MEASURED ONES IN THE CASE OF ^{252}Cf FISSION.

Observable	Mean total fission fragment kinetic energy: $\bar{E}_K$	Mean α-particle kinetic energy E_α	Mean angle $\theta_{\alpha\text{-}L}$	Angular width FWHM ($\theta_{\alpha\text{-}L}$)
measured	174.5 MeV[a]	16.0 MeV[b]	84.3°[c]	18.5°[c]
calculated	175.4 MeV	15.7 MeV	83.6°	18°

[a]Ref. [32]; [b]Ref. [7]; [c]Ref. [17].

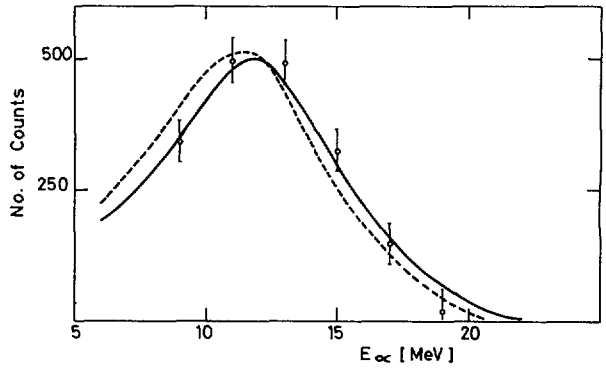

FIG.10. Kinetic-energy spectrum of α-particles emitted in the decay of ^{5}He accompanying the fission of ^{252}Cf. Experimental results are from Ref. [27]. *Calculations are for: ^{252}Cf* (——); ^{236}U (- - - -).

Among light charged particles emitted in fission, the unstable He^5 particle has a privilegied role. It decays into an α-particle and a neutron with a period T1/2 = 8.10^{-22} sec, thus at a time when it is still in the vicinity of the fission fragments and not yet fully accelerated. Therefore, the He^5 data provide information from a fairly well determined time after scission and thus they exclude the freedom of extrapolating the solution backwards or towards in time as it is in principle possible when the emitted particle is stable. To our knowledge there has been only one experimental investigation of He^5 emission in fission : Cheifetz et al. [27] could select He^5 events in spontaneous fission of Cf^{252} by looking for the coincident neutron-He^4 events with both particles having the same direction. They measured the kinetic energy spectrum

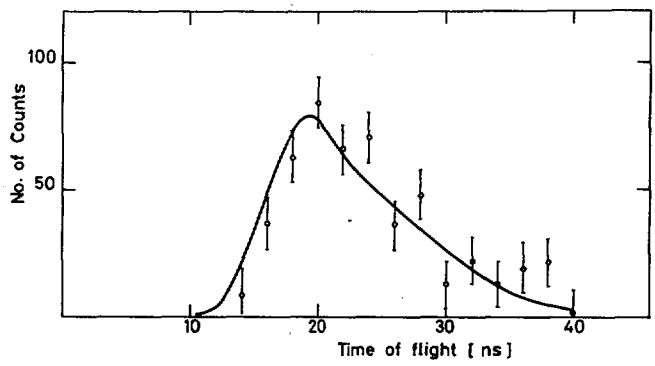

FIG.11. Fit to the time-of-flight of the neutron associated with ^{5}He decay in ^{252}Cf fission.

of the α-particle in coincidence with the neutron time-of-flight. Following the prescription of Gavron et al. [18] we calculated these observables under the same conditions as in the experiment. The initial set of scission-parameters was exactly the same as for He^4 i.e, D = 21 fm. An excellent agreement with experiment is found as shown by Fig.10 and Fig.11 . Although his description of the initial configuration is different from ours, Gavron [18] found a range from 7 to 14 MeV for the pre-scission kinetic energy in which our value of 8 MeV fits well. Our calculations showed that the corresponding averaged energy of the He^5 particle at the time of its decay is about 5.5 MeV.

Although few experimental data on other light charged particles are available, we have tried our initial set of "scission parameters" for deuteron, triton, ^{6}He and ^{6}Li. The final angles are found not to depend upon the nature of the particle whereas the kinetic energies are in good agreement with the experimental values of ref [7].

4. CONCLUSION

We have shown that it is possible to fit most of the typical features of α-accompanied fission of $U^{235}(n_{th})$, by assuming that the fission fragments are already moving apart when the α-particle is released but with a relatively low kinetic energy of 8 MeV (which corresponds to around 5% of their final total kinetic E_K energy).

The second important assumption was to describe the fluctuations of E_K as due to fluctuations of the fission fragment deformations at scission which in their turn we expressed as fluctuations of the interfragment distance D. This assumption is unambiguously necessary for interpreting the decrease of the width of the angular distribution of the α-particle as E_K increases and is also a serious help for finding back the negative correlation between $E\alpha$ and E_K. The close similarity between the angular widths measured in the thermal U^{236} fission and in spontaneous Cf^{252} fission have been understood by assuming the same pre-scission kinetic energy in both systems. This might be very useful with regards to any dynamical theory of

fission, since such a theory should predict the dependence of the pre-scission kinetic energy, if any, on the fissility parameter Z^2/A. As an example, the dynamical theory of the non-viscous liquid drop predicts for U^{236} that about 25 MeV is already acquired as translational energy before scission and that it reaches 40 MeV for Cf^{252} [1], [28]. When adding a dissipating term to the equation of motion of the liquid drop between saddle and scission these pre-scission energies are both reduced by about 30% in case of two-body viscosity[29]. In the formalism of one-body dissipation as treated by Blocki et al. [30] they are almost vanishing and should not anyhow depend on Z^2/A.

It is, of course, very desirable to have more experimental information (specially angular distributions) from other fissioning systems in order to be able to give a definite answer to this very important question. It will be also extremely useful to get more accurate and complete results about the emission of the unstable He^5 particle, which as we have seen, seems to confirm our assumption of rather compact scission configurations.

REFERENCES

[1] SCHMITT, H.W., NEILER, J.H., WALTER, F.J. and CHETHAM-STRODE, A., Phys. Rev. Lett. 9 (1962) 427.
[2] FRAENKEL, Z., Phys. Rev. 156 (1967) 1283.
[3] MEHTA, G.K., POITOU, J., RIBRAG, M. and SIGNARBIEUX, C., Phys. Rev. C7 (1973) 373.
[4] ASGHAR, M., CARLES, C., CHASTEL, R., DOAN, T.P., RIGRAG, M. and SIGNARBIEUX, C., Nucl. Phys. A145 (1970) 657.
[5] NIFENECKER, H.A., BLACHOT, J., BOCQUET, J.P., BRISSOT, R., CRANÇON, J., MARIOLOPOULOS, G., RISTORI, Ch., This Conference, paper SM/241-F1.
[6] WILKINS, B.D., STEINBERG, E.P. and KAUFMAN, S.B., Phys. Rev. C14 (1976) 1832.
[7] COSPER, S.W., CERNY J. and GATTI, R.C., Phys. Rev. 154 (1967) 1193.
[8] BONEH, Y., FRAENKEL, Z. and NEBENZAHL, I., Phys. Rev. 156 (1967) 1305.
[9] NIX, J.R., Nucl. Phys. A130 (1969) 241.
[10] FONG, P., Phys. Rev. C2 (1970) 735.
[11] MUSGROVE, A.R.L., Aust. J. Phys. 24 (1971) 129.
[12] KATAZE, A., J. Phys. Soc. Jap. 25 (1968) 933.
[13] KROGULSKI, T. and BLOCKI, J., Nucl. Phys. A144 (1970) 617.
[14] RAJAGOPALAN, M. and THOMAS, T.D., Phys. Rev. C5 (1972) 2064.
[15] RAISBECK, G.M. and THOMAS, T.D., Phys. Rev. 172 (1968) 1272.
[16] GUET, C., SIGNARBIEUX, C., PERRIN, P., NIFENECKER, H., ASGHAR, M., CAITUCOLI, F., and LEROUX, B., Nucl. Phys. A314 (1979 1.
[17] TSUJI, K., KATAZE, A., YOSHIDA, Y., KATAYAMA, T., TOYOFUKU, F. and YAMAMOTO, H., Proc. Third Symp. on physics and chemistry of fission, Rochester, 1973 (IAEA, Vienna, 1974) p.405.
[18] GAVRON, A., PHys. Rev. C11 (1975) 580.
[19] DAKOWSKI, M., PIASECKI, E., and NOWICKI, L., Nucl. Phys. A315 (1979) 370.
[20] CHOUDHURY, R.K., and RAMAMURTHY, U.S., Phys. Rev. C18 (1978) 2213.
[21] GRACHOV, V.T., SELIVERSTOV, D.M. and SMIRNOV, N.N., unpublished.
[22] PIASECKI, E. and BLOCKI, J., Nucl. Phys. A208 (1973) 381.
[23] GAZIT, Y., KATAZE, A., BEN-DAVID, G. and MOREH, R., Phys. Rev. C4 (1971) 223.

[24] BROWN, C., and FONG, P., Phys. Rev. C16(1977) 243.
[25] FONG, P., Phys. Rev. C16 (1977) 251.
[26] FLUSS, M.J., KAUFMAN, S.B., STEINBERG, E.P. and WILKINS, B.D., Phys. Rev. C7 (1973) 353.
[27] CHEIFETZ, E., EYLON, B., FRAENKEL, Z., and GAVRON, A., Phys. Rev. Lett. 29 085 (1972).
[28] HASSE, R.W., Habilitationsschrift, München University (1977).
[29] NEGELE, J.W. et al., Phys. Rev. C 17 (1978) 1098.
[30] BLOCKI, J., BONEH, Y., NIX, J.R., RANDRUP, J., ROBEL, M., SIERK, A. J. and SWIATECKI, W.J., Preprint LBL, 6536 (1977).
[31] CARLES, C., ASGHAR, M., DOAN, T.P. and CHASTEL, R. , Proc. Second Symp. on physics and chemistry of fission, Vienna, 1969 (IAEA, Vienna, 1969) p.119.
[32] NARDI, E. and FRAENKEL, Z., Phys. Rev. C2 (1970) 1156.

DISCUSSION

P. FONG: I am rather disturbed by the spherical-nucleus approximation that you have used. We know that fission fragments are deformed and that the deformation differs as a function of the stiff constant. These deformation shapes determine the initial position of the alpha particle, which in turn determines the final angular and energy distributions. This important piece of information is lost in the spherical approximation. I feel that this is a crucial point, since it rules out the high initial kinetic energy of the fragments. For light fragments in the 50-neutron shell region, the alpha particle would be pushed towards the heavy particle. Only when the initial kinetic energy of the alpha particles is very low, let us say about 1 MeV, will the particle reverse and move towards the light fragment, as has been actually observed. So I repeat that this important result is lost if you use the spherical approximation.

C. R. GUET: I believe that there is direct experimental evidence to show that the emission point position is closely related to the fragment deformations. You should note, however, that the variation in mean angle with mass ratio is easily interpreted in terms of the asymmetric Coulomb repulsion of the fragments, without any specification of the position of the initial point. All the deformation effects are averaged to the extent that allowance for a distribution of the charge distance D is sufficient to take them into account.

In answer to your second point, I should say that the deflections that you mention are possible in the case of our selection of an initial alpha particle kinetic energy at ~1.5 MeV. Furthermore, these deflection effects are very useful for understanding the enhancement of low-energy particles at small final angles.

Finally, the value of 8 MeV for the pre-scission kinetic energy of fission fragments is, within the framework of this model, an upper limit.

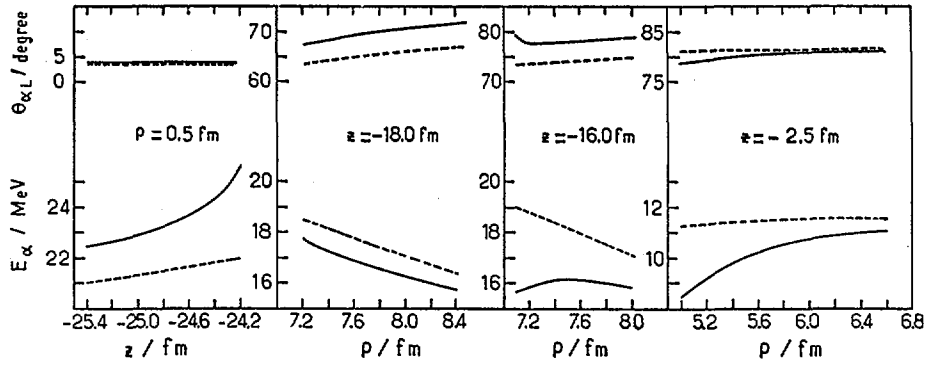

FIG. A. Final α-particle energies and directions obtained with point-charge approximation (dashed lines) and exact calculation (solid lines).

N. CÂRJAN: I would like to add the following remarks to what Dr. Fong has said. Determination of the configuration of the fissioning system at the moment of alpha particle emission, using the three point charge model, is very probably unreliable.

The problem of the validity of the point charge approximation would take too long to discuss, but I will try to give you an idea of its validity by means of Fig. A, which illustrates the differences between the final alpha particle energies and directions obtained with the point-charge approximation (dashed lines) and with an exact calculation (solid lines) for some selected initial conditions and non-viscous liquid drop nuclear dynamics. $D/R_0 = 2.9$ and $E_\alpha = 0$. These differences are expected to be inversely proportional to the velocity of fission fragment motion, and, therefore, for more realistic nuclear dynamics they are even greater than those shown here.

In connection with what you have said for the benefit of the fission theorists, I would like to recall that the configuration at the moment of alpha particle emission is probably related to, though not identical with, the scission configuration in binary fission. To obtain this relationship we have to understand the mechanism governing the emission of these particles.

According to the only mechanism quantitatively developed (CÂRJAN, N., J. Phys. 37 (1976) 1279), there is no incompatibility between the fact that the binary fission energies are different in the case of ^{236}U and ^{235}Cf, and the fact that the fragments have the same kinetic energies at the moment of alpha particle emission in these two nuclei. This is because in the above-mentioned model the moment of alpha emission is related to the saddle moment and not to scission. The alpha emission occurs between saddle and scission at the same distance from the saddle for all nuclei, i.e. at the same pre-scission kinetic energy.

C. R. GUET: Unfortunately, I am not familiar with the work you have done, but it would of course be very interesting to check to what extent our approximations are correct. It may seem rather surprising that a model as crude as the one we have used here can reproduce the experimental data quite well, but it definitely does, and the approximations have been shown to be physically reasonable.

With regard to your second comment, I agree completely that our conclusions are meaningful only on the assumption that the emission occurs at scission. It is to be noted that this assumption is strongly supported by experimental data. I shall be most interested to see how the predictions of a model postulating emission at saddle will compare with experimental correlations that are now well established.

УГЛОВОЕ РАСПРЕДЕЛЕНИЕ И ДИФФЕРЕНЦИАЛЬНЫЕ ЭНЕРГЕТИЧЕСКИЕ СПЕКТРЫ НЕЙТРОНОВ СПОНТАННОГО ДЕЛЕНИЯ ^{252}Cf

О.И.БАТЕНКОВ, М.В.БЛИНОВ, В.А.ВИТЕНКО
Радиевый институт им.В.Г.Хлопина,
Ленинград,
Союз Советских Социалистических Республик

Abstract–Аннотация

ANGULAR DISTRIBUTION AND DIFFERENTIAL ENERGY SPECTRA OF SPONTANEOUS ^{252}Cf FISSION NEUTRONS.

The energy spectra and numbers of neutrons emitted at various angles in relation to the axis of ^{252}Cf fission fragment separation were measured by the time-of-flight method. Within the region of the angles 45–90° the neutron yield was greater than that for a simple evaporation model. Preferential emission was not observed at small angles. In an analysis of the results the influence of various effects on emission characteristics was considered. The agreement of experimental and theoretical data improves considerably when the possibility of neutron emission from incompletely accelerated fragments and from the fissionable nucleus is taken into account.

УГЛОВОЕ РАСПРЕДЕЛЕНИЕ И ДИФФЕРЕНЦИАЛЬНЫЕ ЭНЕРГЕТИЧЕСКИЕ СПЕКТРЫ НЕЙТРОНОВ СПОНТАННОГО ДЕЛЕНИЯ ^{252}Cf.

Методом времени пролета проведены измерения энергетических спектров и числа нейтронов, испускаемых под различными углами относительно оси разлета осколков деления ^{252}Cf. В области углов 45-90° зарегистрирован повышенный выход нейтронов по сравнению с простой испарительной моделью. Под малыми углами преимущественной эмиссии не обнаружено. При анализе результатов рассмотрено влияние различных эффектов на характеристики эмиссии. Согласие экспериментальных и расчетных данных существенно улучшается при учете возможной эмиссии нейтронов из неполностью ускоренных осколков и из делящегося ядра.

1. ВВЕДЕНИЕ

Измерение энергетических спектров и числа нейтронов, испускаемых под различными углами к направлению движения осколков при спонтанном делении ^{252}Cf, впервые проведены Бауманом и др. [1]. В этой работе было найдено, что подавляющая часть (80-90%) нейтронов деления ^{252}Cf испаряется на поздней стадии процесса деления – из возбужденных осколков, ускорившихся до конечных скоростей. Наиболее существенные отклонения от этой модели авторы работы [1] объяснили изотропной эмиссией в лабораторной системе 10-20% полного числа нейтронов на каком-то дру-

гом более раннем этапе деления ядра. В этой же работе наблюдался преимущественный вылет нейтронов под малыми углами к оси деления и в связи с этим отмечалась необходимость тщательных измерений в этой области.

В нескольких последующих экспериментальных работах [2-4] были сделаны попытки выяснить природу "изотропной" (в лабораторной системе) компоненты нейтронов. Эти исследования были направлены на выяснение связи величины отклонения от испарительной модели с характеристиками процесса деления. Однако, однозначного объяснения в этих работах получено не было.

В теоретических работах [5-7] была показана возможность и оценена вероятность испускания изотропной компоненты нейтронов деления на различных этапах процесса спонтанного деления ^{252}Cf – при движении ядра к точке разрыва, в момент разрыва и в процессе установления равновесной формы осколков. В работах [8, 9] найдено, что, не вводя предположений о дополнительной "изотропной" компоненте, можно объяснить результаты работы [1], если не целиком, то во всяком случае в значительной степени, испарением нейтронов в процессе ускорения осколков. Таким образом, высказывались различные предположения о природе части нейтронной эмиссии, которую называют "изотропной" или "разделительной", хотя ее происхождение до сих пор остается неясным. Характеристики этой компоненты представляют особый интерес, так как они могут дать полезную информацию о динамике процесса деления. Для выяснения этого трудного вопроса экспериментальным путем необходимы детальные исследования угловых и энергетических распределений нейтронов деления. С этой целью нами начато последовательное изучение этих распределений и их корреляций с характеристиками осколков при спонтанном делении ^{252}Cf.

В докладе сообщаются результаты первого этапа работы – измерения числа нейтронов и их энергетических спектров для разных углов вылета нейтронов относительно оси разлета осколков. Эти данные пока не связываются с массами и кинетическими энергиями осколков.

2. МЕТОДИКА ИЗМЕРЕНИЙ И РЕЗУЛЬТАТЫ

Для определения энергии нейтронов использовался метод времени пролета, а регистрация нейтронов осуществлялась кристаллом стильбена (диаметр 50 мм, толщина 25 мм) с фотоумножителем ФЭУ-30. Осколки деления ^{252}Cf регистрировались полупроводниковым кремниевым счетчиком, помещенным в вакуумную камеру. Слой калифорния в виде пятна диаметром 2 мм (10^5 спонтанных делений в секунду) располагался на расстояниях 25 или 50 мм от счетчика. Перед счетчиком осколков помещались диафрагмы, диаметр которых в различных опытах составлял от 2 до 4 мм. Это обеспечивало угловое разрешение до 3^0. Использовались две пролетные базы – 50 и 100 см. Временнбе разрешение системы, определенное по пику гамма-квантов деления, было равно 1,5 нс. Иэмерения под всеми углами для контроля производились с помощью двух нейтронных детекторов, находящихся под углом 90^0 один к другому.

Электронная система спектрометра включала схему нейтрон-гамма разделения, основанную на различии времен высвечивания в стильбене. Необходимость введения этой схемы была вызвана тем, что при делении испускается значительное количество запаздывающих гамма-квантов с временами эмиссии более 1 нс, которые могут искажать временной спектр нейтронов. Для компенсации влияния большого амплитудного диапазона регистрируемых импульсов на временнбе разрешение использовался блок формирования со "следящим"порогом. Спектрометр имел систему амплитудной стабилизации по обоим каналам. В нейтронном канале использовался светодиод, установленный около катода фотоумножителя. Стабилизация в осколочном тракте обеспечивалась поддержанием постоянной скорости счета импульсов в заданном узком интервале амплитуд. Регистрация и обработка данных производились с помощью ЭВМ М-6000.

При конструировании вакуумной камеры, нейтронных детекторов и других составных частей спектрометра обращалось особое внимание на уменьшение их масс, так как наши предварительные эксперименты показали большое влияние эффектов рассеяния на форму спектров нейтронов деления.

Для определения эффективности нейтронного детектора использовался газовый сцинтилляционный счетчик с регистрацией осколков в угле 2π. Зависимость эффективности от энергии нейтронов находилась путем сравнения измеренного распределения с интегральным спектром нейтронов деления ^{252}Cf, полученным на основе оценки результатов целого ряда работ [10].

Угловое распределение нейтронов измерялось через $2{,}5^0$ в области малых углов и далее через 10^0. Порог регистрации нейтронов составлял около 0,2 МэВ. Энергетические спектры анализировались в области энергий 0,5-10 МэВ.

В экспериментальные данные вводились поправки на угловое и энергетическое разрешения. Сравнение данных, полученных с помощью двух нейтронных детекторов с несколько отличающимися порогами регистрации, а также сравнение результатов для двух различных пролетных расстояний показали их согласие в пределах ошибок опыта.

На рис. 1 и 2 приведены измеренные в настоящей работе угловое распределение нейтронов и зависимость средних энергий спектров от угла вылета. Здесь же представлены для сравнения данные Баумана и др. [1], поскольку только в этой работе проведены измерения во всем интервале углов ($0\text{-}90^0$). Как следует из рисунка, угловые распределения довольно близки. Что касается средних энергий, то полученные нами данные для этой области в целом заметно ниже. Можно попытаться провести сравнение результатов обеих работ через суммарный спектр, который получается интегрированием дифференциальных спектров. В работе [1] средняя энергия такого спектра $\bar{E}$ равна 2,34 МэВ, а в нашем случае – 2,15 МэВ. Средняя энергия оцененного интегрального спектра нейтронов спонтанного деления ^{252}Cf, согласно последним литературным данным [10], равна 2,13 МэВ, что почти на 10% ниже, чем получено Бауманом и др. С этим, по-видимому, и связаны завышенные значения $\bar{E}$ дифференциальных спектров в работе [1].

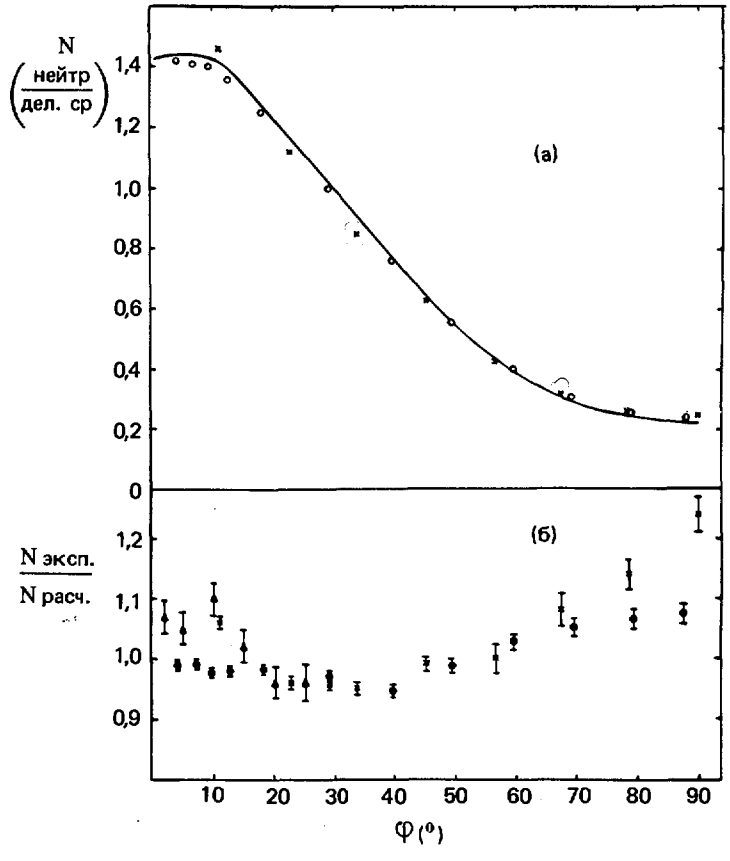

Рис.1. Угловое распределение нейтронов спонтанного деления ^{252}Cf: а) экспериментальная зависимость числа нейтронов от угла эмиссии в лабораторной системе; б) зависимость отношения экспериментальных данных к расчетным от угла эмиссии.

○ – данные, полученные авторами, × – данные работы [1], *Δ – экспериментальные данные работы* [11], *расчет из работы* [1]. *Сплошная кривая построена по расчетам авторов работы.*

2. АНАЛИЗ РЕЗУЛЬТАТОВ И ОБСУЖДЕНИЕ

При анализе результатов с помощью программы, основанной на методе наименьших квадратов, был проведен поиск спектра в системе центра масс, который бы наилучшим образом удовлетворял экспериментальным данным, полученным под всеми углами. Расчет проводился для суперпозиции вкладов тяжелого и легкого осколков, характеризуемых средними скоростями групп. Предполагалось, что эмиссионные спектры нейтронов для этих групп одинаковы в соответствии с выводами работы [1] и не зависят от угла эмиссии, которая происходит из полностью ускоренных осколков.

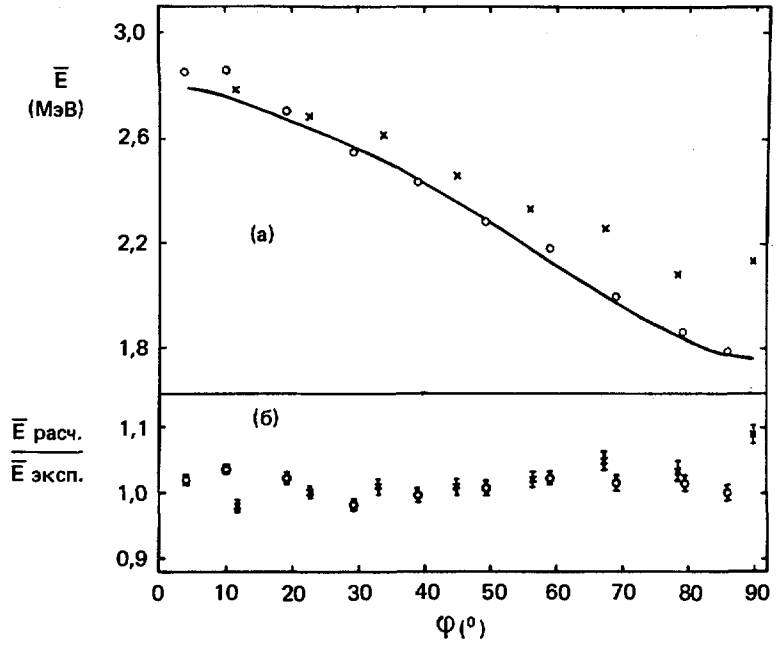

Рис.2. Зависимость средних энергий дифференциальных спектров от угла эмиссии в лабораторной системе: а) экспериментальные данные; б) отношение экспериментальных данных к расчетным.
○ – данные, полученные авторами, × – данные работы [1]. *Сплошная кривая построена по расчетам авторов работы.*

Форма эмиссионного спектра принималась в виде $N(\eta) \sim \sum_i \frac{\alpha_i}{T_i^2} \eta \sigma_c e^{-\eta/T_i}$

где η – энергия нейтрона в системе центра масс, T_i – температура с относительным вкладом α_i и σ_c – сечение захвата нейтрона с энергией η. Применялось трехтемпературное приближение. Для лучшего согласия данных оказалось необходимым ввести зависимость σ_c от энергии нейтрона, которая использовалась в виде $\sigma_c = \sigma_o (1 + \frac{c}{\sqrt{\eta}})$. Подбор величин α и T показал, что ни при каких значениях параметров не удается согласовать экспериментальные и расчетные данные для всех углов и всех энергетических интервалов. Наилучшее согласие ($\chi^2 = 1022$, 228 точек) было достигнуто при $\alpha_1 = 0{,}647$, $T_1 = 0{,}957$ МэВ, $\alpha_2 = 0{,}339$, $T_2 = 0{,}472$ МэВ, $\alpha_3 = 0{,}014$, $T_3 = 0{,}142$ МэВ и $C = 0{,}50$.

На рис.1 и 2 изображены отношения экспериментальных данных к расчетным. Общий ход зависимости для числа нейтронов коррелирует с результатами работы [1].

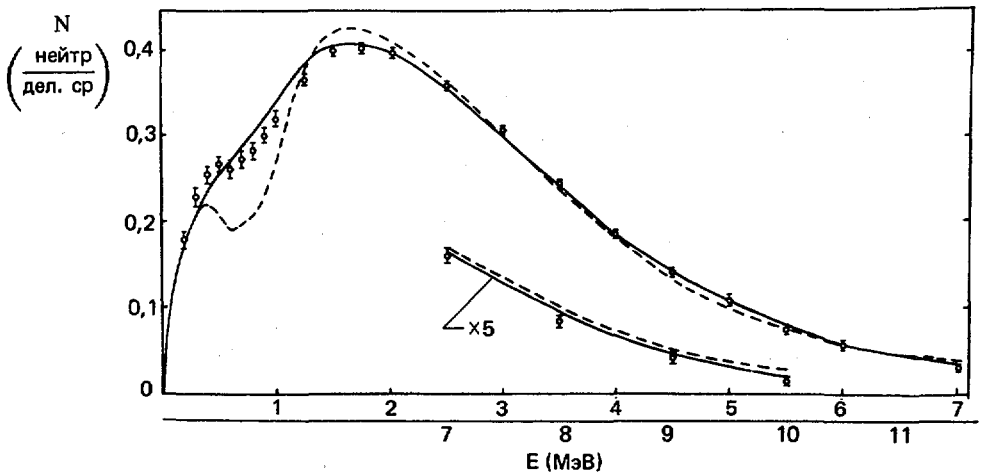

Рис. 3. Энергетический спектр нейтронов спонтанного деления ^{252}Cf для угла $\varphi = 4^0$.
○ – экспериментальные данные. Сплошная кривая построена по расчетам авторов работы, пунктирная – по данным работы [1].

Начиная примерно с угла 45^0, отклонение от расчетных величин постепенно увеличивается. Что касается малых углов, то наши данные не показывают какой-либо преимущественной эмиссии нейтронов в этой области в отличие от результатов работы [1]. В значительной мере это связано с тем, что наш спектр в системе центра масс мягче, чем полученный в работе [1], а низкотемпературная компонента играет существенную роль в распределении интенсивности под малыми углами. Предположение о такой возможности объяснения этого эффекта высказывалось недавно в работе [11]. На рис. 3 показаны полученные нами экспериментальный и расчетный спектры для угла 4^0 и расчетный спектр по данным работы [1] для того же угла. Отличие наблюдается для области 0,5-1,0 МэВ, где проявляются нейтроны низких энергий в системе центра масс. Отметим, что минимальный угол, при котором в работе [1] производились измерения, был равен 11^0. Описание спектра под этим углом еще не очень критично к низкоэнергетической компоненте спектра в системе центра масс в отличие от углов менее 5^0, что и сказалось на выборе ее в работе [1].

Мы попытались согласовать расчетные и экспериментальные данные для всех углов путем введения угловой анизотропии эмиссии в системе центра масс, однако это не привело к улучшению согласования. Представлялось важным также учесть возможность испускания нейтронов в процессе ускорения осколков. Если бы удалось найти убедительное доказательство подобного явления, то появилась бы возможность измерения очень малых времен испускания нейтронов (менее 10^{-20}с). Мы провели подгонку с учетом такого эффекта в основном аналогично расчету Пик-Ильичака [8] и нашли, что χ^2 существенно уменьшается. χ^2 уменьшалось значительно

(примерно в два раза) и при введении изотропной компоненты эмиссии в лабораторной системе. Таким образом заметное уменьшение χ^2 происходило при учете каждого из последних двух эффектов. Однако при улучшении общего согласования отдельные участки спектров подгонялись не очень хорошо, и поэтому нет возможности говорить об удовлетворительном согласии данных в целом. Сравнительно лучшее согласие данных получается или при одновременном учете изотропной компоненты в лабораторной системе и эмиссии нейтронов в процессе ускорения осколков, или введением анизотропной компоненты в системе, связанной с делящимся ядром.

Проводимые в настоящее время измерения угловых и энергетических распределений нейтронов для фиксированных масс и кинетических энергий осколков позволят более определенно ответить на изучаемый вопрос о механизме эмиссии нейтронов спонтанного деления ^{252}Cf.

ЛИТЕРАТУРА

[1] BOWMAN, H.R., THOMPSON, S.L., MILTON, J.C., SWIATECKI, W.J., Phys. Rev. 126 (1962) 2120.

[2] БЛИНОВ, М.В., КАЗАРИНОВ, Н.М., КРИСЮК, И.Т., Ядерная физика 16 (1972) 1155.

[3] ВАСИЛЬЕВ, Ю.А., СИДОРОВ, Л.В., ЧУЛКОВ, Н.М., Нейтронная физика (Материалы 3-й Всесоюзной конференции по нейтронной физике, Киев, 1975 г.) 5, М., ЦНИИатоминформ, (1976) 86.

[4] ПИКСАЙКИН, В.М., ДЬЯЧЕНКО, П.П., КУЦАЕВА, Л.С., Ядерная физика 25 4 (1977) 723.

[5] FULLER, R.W., Phys. Rev. 126 (1962) 684.

[6] BONEH, J., FRANKEL, Z., Phys. Rev. C10 (1974) 893.

[7] РУБЧЕНЯ, В.А., Препринт РИ-28 (1974).

[8] ПИК-ПИЧАК, Г.А., Ядерная физика 10 2 (1969) 321.

[9] SKARSVAG, K., Phys. Scripta 7(1973) 160.

[10] STEWART, L., EISENHAUER, C., Neutron Standards and Applications (Proc. Symp.) 493 NBS Special Publication (1977) 198.

[11] ПИКСАЙКИН, В.М., ДЬЯЧЕНКО, П.П., АНИКИН, Г.В., СЕРЕГИНА, Е.А., АХМЕДОВ, Г.М., СТАВИНСКИЙ, В.С., Ядерная физика 28 2 (8) (1978) 314.

FISSION PROPERTIES OF VERY HEAVY ACTINIDES

D. HOFFMAN*
Lawrence Berkeley Laboratory,
University of California,
Berkeley, California

Los Alamos Scientific Laboratory,
Los Alamos, New Mexico

United States of America

Abstract

FISSION PROPERTIES OF VERY HEAVY ACTINIDES.

The existing data on neutron-emission, kinetic-energy and mass distributions, and half-lives for spontaneous fission of the heavy actinides are reviewed. A comparison of the data for the Fm isotopes with heavier and lighter nuclides suggests that the properties of the heavy Fm isotopes may be unique and can qualitatively be explained on the basis of fragment shell effects, i.e. symmetric fission results in two fragments with configurations close to the doubly magic ^{132}Sn nucleus. The effect of excitation energy and the use of systematics and theoretical predictions of fission properties and half-lives in the identification of new heavy-element isotopes are discussed.

I. INTRODUCTION

Much progress has been made in studying the properties of the low-energy fission of the heavy actinides since the last Symposium on the Physics and Chemistry of Fission [1] in 1973. At that time, a trend toward increased yields of symmetric mass division for both spontaneous fission (SF) and thermal-neutron induced fission (n,f) had been observed [2-5] as the mass of the fissioning nucleus was increased. For ^{257}Fm(n,f), the heaviest nuclide studied at that time, symmetric mass division was found [4] to be most probable, although the distribution was very broad. The average total kinetic energy ($\overline{TKE}$) for SF and (n,f) of nuclides from ^{230}Th to ^{256}Fm was fit rather well by Unik et al. [2] with a linear function of the symmetric-fission coulomb repulsion parameter, $Z^2/A^{1/3}$. The effect of excitation energy, E_x, on $\overline{TKE}$ had also been investigated and in several cases the extra excitation energy of around 6 MeV for (n,f) over SF had been found to increase the yields of symmetric mass division and the $\overline{TKE}$ for the same fissioning nuclide. However, in some cases the

---

* John Simon Guggenheim Fellow on sabbatical leave from the Chemistry and Nuclear Chemistry Division, Los Alamos Scientific Laboratory, Los Alamos, New Mexico.

This work was supported in part by the US Department of Energy.

increased E_x resulted in increased neutron emission and a correspondingly smaller increase in $\overline{TKE}$ [2]. A review [6] of the data to early 1974 indicated that whether or not the $\overline{TKE}$ increases with E_x for a specific fissioning system depends on the result of averaging a large number of different energy dependences for individual fragment pairs, taking into account that as the fragment yields change with E_x, the statistical weights of the individual fragments change. Different fragment pairs were found to react differently to changes in E_x although the maximum TKE at low E_x was found for fragment masses around 132. At higher excitation energies, a decrease in $\overline{TKE}$ was noted for fragments around mass 132 which suggests a decreasing influence of fragment shells at higher E_x. Neutron emission from the fragments is also affected by the same considerations and varies with the excitation energy and deformation of the fragments. For symmetric mass division of ^{257}Fm (SF), TKE's which approached the Q value for fission had been reported [3], indicating that the fragments must have lower excitation energies which might be expected to result in the emission of fewer neutrons from the fragments. Indeed, it was reported [7] at the 1973 conference that the average neutron emission per fission, $\bar{\nu}$, for these symmetric mass splits with high TKE is only about 1 for ^{257}Fm while it is 3 for ^{252}Cf. It was postulated that the high TKE and low $\bar{\nu}$ observed for ^{257}Fm (SF) were because the fragments were becoming more spherical as they more closely approached the doubly magic ^{132}Sn configuration. This suggested that the effects should be still more pronounced for the heavier Fm isotopes. Whether or not these effects continue for elements of atomic number greater than 100 and for neutron numbers of 157 or more for other elements is important in assessing the relative importance of fragment shell effects near scission, the height of the second barrier relative to the ground state, and the question of adiabaticity [8] in nuclear fission.

Although measurements of SF properties for these heavy actinide isotopes are extremely difficult because of the short half-lives and small production cross sections, much new information has been reported since 1973. I will discuss some of the new data for low-energy fission of the heavy actinides, defined here as those with $Z \geq 98$, in terms of the half-lives, fragment mass and kinetic energy distributions, neutron emission, and the use of SF properties and systematics in the identification of new heavy element isotopes.

II. HALF-LIVES

Systematic trends in the SF half-lives of actinide and transactinide isotopes have been observed for the even-even actinide isotopes [9]. In general, the half-lives are shorter for the higher Z nuclides. However, beginning with curium, a pronounced stabilizing effect for 152 neutrons has been observed experimentally, and consequently, the half-life values overlap from one element to the next and even for a given Z. The calculations of Randrup et al. [10] and Baran et al. [11, 12] reproduce the general trends very well, but for a given nuclide can show deviations of several orders of magnitude. This is particularly apparent at ^{258}Fm where a "SF disaster" appears to have occurred--the SF half-life [13] being only 380 μs, a factor of some 10^6 lower than the calculated value.

This might be explained on the basis of the disappearance of the second fission barrier for ^{258}Fm. Recently a half-life of 12.3 minutes has been measured [14] for ^{256}Cf which has the same number of neutrons as ^{258}Fm. This indicates a reduction in half-life for the addition of 2 neutrons to ^{254}Cf (60 days) of 1.4×10^{-4} compared to 1.9×10^{-3} from ^{252}Cf to ^{254}Cf. Although the half-life reduction for 2 neutrons between ^{254}Cf and ^{256}Cf is a factor of 10 larger than between ^{252}Cf and ^{254}Cf, no real "disaster" at 158 neutrons is indicated.

The theoretical calculations do not treat the odd nucleon cases in general, but the extra hindrance associated with the SF of nuclides having an odd number of protons or neutrons has been recognized for some time [15, 16]. The hindrance is typically of the order of 10^5, but has been found to be as small as 10 and as large as 10^{10}. The hindrance associated with N = 157 nuclei due to the hindrance of the 9/2+[615] neutron orbital has been calculated [16] and appears to be consistent with the data for ^{257}Fm, ^{259}No, and ^{261}104. The measurement of a 10% SF branch [17] for 1.5-s ^{260}105 indicates a hindrance of about 10^3 for the odd proton over predictions [16] for even 104 isotopes. The SF half-life of 1.5 seconds [18] measured for ^{259}Fm also indicates a hindrance factor of about 4×10^3 for the odd neutron orbital, assuming that ^{258}Fm and ^{259}Fm would otherwise have about the same SF half-lives. The half-life of 95 min for ^{259}Md [19] indicates a hindrance for the odd proton of more than 10^7 relative to ^{258}Fm. If the second fission barriers no longer exist for isotopes of the even-even trans-nobelium elements, then the SF half-lives may be expected to be very short, i.e., milliseconds or less, and relatively constant with N. However, if the stabilizing effect of the N = 152 shell experimentally observed in Cf through No persists, half-lives in the region of N = 152 might be longer than calculated [10]. The recent dynamical calculations of Baran et al. [12] which additionally include the effect of ε_6 deformations, show that the effect on the potential barrier is considerable and increases the half-lives calculated for the Fm isotopes as much as two orders of magnitude for ^{252}Fm. The calculated change in half-life systematics for trans-nobelium isotopes is less abrupt than proposed by Oganessian et al. [20], and gives much longer half-lives than those calculated by Randrup et al. [10]. It is clearly very important to obtain measurements of the SF half-lives of these isotopes in order to check the validity of various theoretical approaches and for extrapolation to still heavier regions. Because of the very short half-lives of these nuclides, their production via complex heavy ion reactions with only nanobarn cross sections, and decay by SF which effectively destroys information concerning the Z of the fissioning parent nucleus, unequivocal assignment to a given Z and A is extremely difficult. However, much progress is being made in "on-line" observations of SF properties, including measurement of fragment kinetic energies and mass distributions, and coincidence measurements between characteristic x-rays, following electron-capture or alpha decay, and short-lived SF activities in order to determine the Z of the fissioning nuclide.

III. FRAGMENT MASS AND KINETIC-ENERGY DISTRIBUTION

Kinetic-energy distributions have recently been obtained for SF of ^{256}Cf, ^{254}Fm, ^{258}Fm, ^{259}Fm, ^{259}Md, and ^{252}No [14, 18, 19, 21, 22] from

TABLE I. LOW-ENERGY FISSION PROPERTIES OF SOME HEAVY-ELEMENT ISOTOPES

Fissioning Nuclide[a]	SF $T_{1/2}$ (seconds)	Peak-to Valley Ratio[b]	$\overline{TKE}$[c] (MeV)	$\sigma_{\overline{TKE}}$	$\bar{\nu}_T$[d]
^{250}Cf	5.4×10^{11}	>300(RC)	187.0	11.3	3.49
$^{250}Cf^*$	-	$\geq$ 50(RC)	189.1	13.0	-
^{252}Cf	2.7×10^{9}	$\geq$750(RC)	185.7	11.6	3.735
$^{252}Cf^*$	-	$\approx$20(RC)	185	15.5	-
^{254}Cf	5.2×10^{6}	$\geq$145(RC)	186.9	11.8	3.89
^{256}Cf	7.4×10^{2}	Asymm.(SS)	189.8	14.6	-
^{253}Es	2.0×10^{13}	326(RC)	191	13.4	-
$^{255}Es^*$	-	$\approx$8(SS)	194.3	15.9	-
^{254}Fm	2.0×10^{7}	$\approx$42(RC)	195.1	11.7	3.96
^{256}Fm	1.0×10^{4}	12(SS)	197.9	14.4	3.70
$^{256}Fm^*$	-	2.5(RC)	195.5‡	18	-
^{257}Fm	4.1×10^{9}	$\approx$1.5(SS)	197.6	15.3	3.77
^{258}Fm	3.8×10^{-4}	Symm., σ = 8(SS)	238‡	14	-
$^{258}Fm^*$	-	Symm.,broad(SS)	197	-	-
^{259}Fm	1.5×10^{0}	Symm., σ = 11(SS)	242‡	21	-
^{259}Md	5.7×10^{3}	Symm., σ = 13(SS)	189‡	44	-
^{252}No	8.6×10^{0}	Asymm.(SS)	202.4	15.4	4.15

[a] This is either the spontaneously fissioning nuclide or the excited compound nucleus formed by (n,f) and designated by *.

[b] Peak-to-valley ratios from radiochemical (RC) or solid-state (SS) measurements from compilation in Ref. 6, p. 159 and Refs. 2, 14, 18, 19, 21-26, 31, 32.

[c] These average values of the pre-neutron emission TKE's except for those designated by ‡ which are most probable pre-neutron emission values from a provisional mass analysis without corrections for neutron emission. Data from compilation in Ref. 6, p. 159 and Refs. 2, 14, 18, 19, 21-26.

[d] Data from Refs. 6, 7, 38, 40, 41.

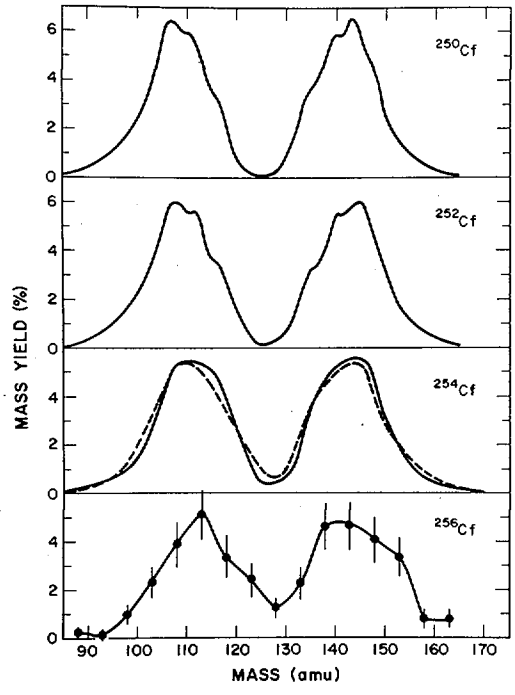

FIG.1. Pre-neutron emission mass-yield distributions for ^{250}Cf [2], ^{252}Cf [2], ^{254}Cf (solid curve from Ref. [2]; dashed curve from Ref. [14]), and ^{256}Cf [14]. The data for ^{254}Cf and ^{256}Cf from Ref. [14] were analysed in 5-amu mass bins using an empirical neutron correction similar to that for ^{252}Cf.

measurements of the kinetic energies of coincident fragments. Total kinetic energies and fragment mass distributions were also derived from these data. Mass distributions for ^{250}Cf, ^{253}Es, ^{254}Fm, and ^{254}Cf have been obtained from radiochemical measurements [21, 23-26]. The results of these measurements are summarized in Table I together with properties reported earlier for SF and (n,f) of some other trans-berkelium actinide isotopes. The peak-to-valley (P/V) ratios for the mass distributions can be seen to decrease rapidly with the addition of 2 protons between Cf and Fm isotopes having the same number of neutrons: e.g., ≥750 for ^{252}Cf to ≈42 for ^{254}Fm; ≥145 for ^{254}Cf to 2.5 for ^{256}Fm; asymmetric for ^{256}Cf to narrowly symmetric for ^{258}Fm. The P/V ratios also decrease with the addition of neutrons for both Cf and Fm as illustrated in Figs. 1 and 2. Only a small change is shown in going from ^{250}Cf to ^{256}Cf while an abrupt change to symmetric fission occurs for the Fm isotopes at N = 158. The valley disappears completely between ^{257}Fm and ^{258}Fm, and narrow, symmetric mass distributions [14, 18] have been measured for ^{258}Fm and ^{259}Fm. The mass distribution for ^{259}Md has also been found [17] to be symmetric and narrow.

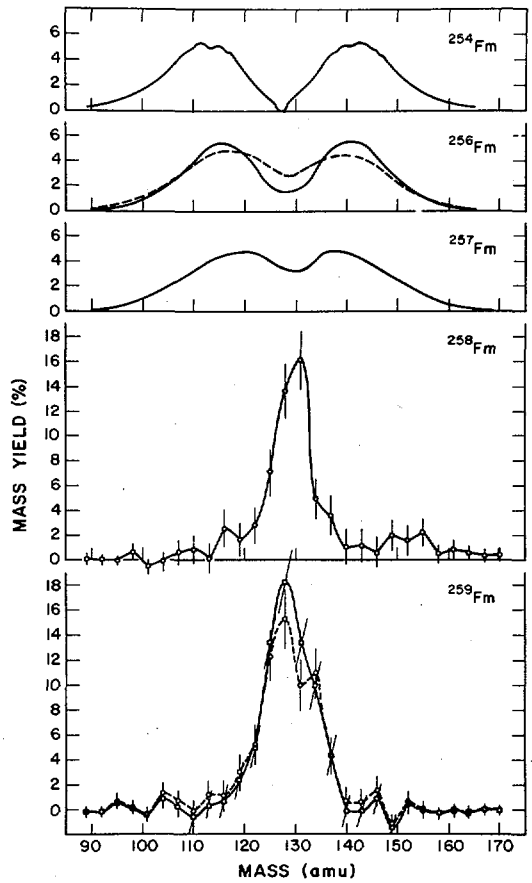

FIG.2. Pre-neutron emission mass yield curves for ^{254}Fm [21], ^{256}Fm [2], ^{257}Fm [3], ^{258}Fm [14], and ^{259}Fm [18]. The solid curve for ^{256}Fm is a pre-neutron emission curve from Ref. [2], while the dashed curve is a provisional mass analysis for ^{256}Fm measured in the same experimental set-up as used for ^{259}Fm [14].

A plot of $\overline{TKE}$ vs $Z^2/A^{1/3}$ is shown in Fig. 3 with some data for the heavy actinides. The dashed line represents the fit of Viola [27] to the function $\overline{TKE} = B(Z^2/A^{1/3}) + C$ with B = 0.1071 and C = 22.2. The solid line is that of Unik et al. [2] with B = 0.13323 and C = -11.64. In general, most of the data fall between these two lines except for ^{258}Fm and ^{259}Fm which are 40 MeV or so higher. Schmitt and Mosel [28] have predicted that the $\overline{TKE}$ for nuclides having masses of 260 to 275 would also be substantially higher than these linear extrapolations, but the measurement [29] of ^{262}105(104) does not show this. However, the $\overline{TKE}$ for ^{259}Md, which also exhibits symmetric mass division, is below

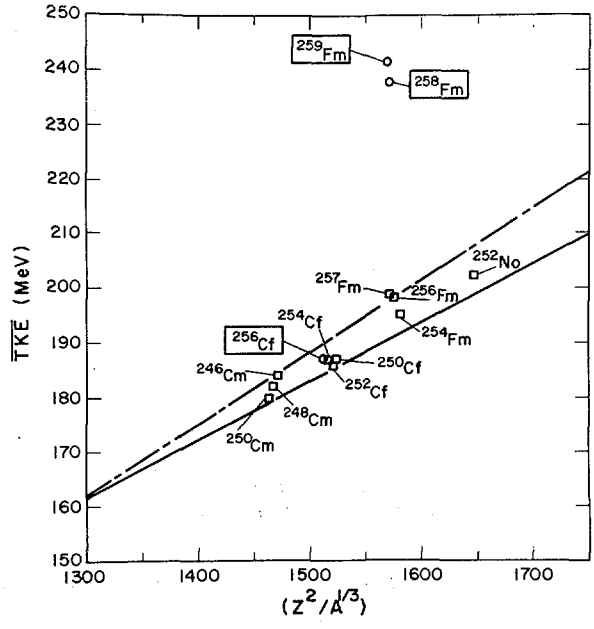

FIG.3. $\overline{TKE}$ versus $Z^2/A^{1/3}$ for heavy actinide isotopes. Solid line represents linear fit of Viola [27]*; dashed line is from Unik et al.* [2]*. The data for ^{258}Fm and ^{259}Fm are most probable TKE's* [14, 18].

the lines although the TKE distribution for ^{259}Md was found [19] to be extremely broad (σ = 44 MeV or FWHM = 103 MeV). The value for ^{252}No appears to be perfectly "normal." The $\overline{TKE}$'s of 238 to 242 MeV for ^{258}Fm and ^{259}Fm approach the total energy of about 250 MeV estimated to be available from fission. This is also the case for symmetric mass division of ^{257}Fm where some events with TKE as high as 240 to 260 MeV, as well as some very low TKE events, were observed. Similarly, the very large σ for the TKE distribution from ^{259}Md indicates some events with very high TKE.

The dip in $\overline{TKE}$ near symmetry which is $\approx$20 MeV for $^{236}U^*$ decreases for the heavier fissioning systems and for $^{255}Es^*$ has essentially disappeared. Similarly, for SF the dip at symmetry, which is around 15 MeV for ^{246}Cm, decreases to only a few MeV for ^{250}Cf. The $\overline{TKE}$ as a function of mass fraction, M_H/A, for the Cf and Fm isotopes is shown in Figs. 4 and 5 respectively. A gradual increase in the $\overline{TKE}$ at symmetry with mass of the fissioning nuclide is observed for the Cf isotopes until for ^{256}Cf the $\overline{TKE}$ at symmetry is highest by a few MeV. For the Fm isotopes, the $\overline{TKE}$ at symmetry increases by 15 MeV between ^{256}Fm and ^{257}Fm and by 20 MeV between ^{257}Fm and ^{259}Fm. A comparison of these trends in the form of contour plots of TKE as a function of mass fraction is shown in Fig. 6 for ^{254}Cf, ^{256}Fm, and ^{257}Fm. The greatly increased yield of symmetric mass division of ^{257}Fm compared to lighter actinides

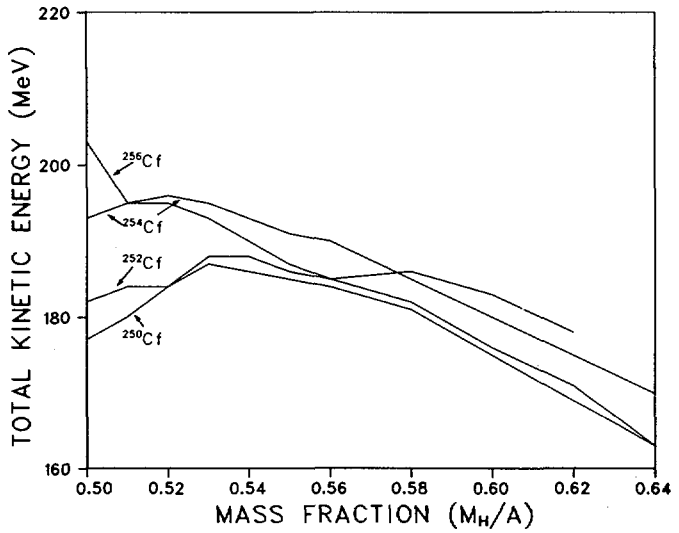

FIG.4. $\overline{TKE}$ *versus mass fraction for Cf isotopes. (Data from Refs* [2, 14].*)*

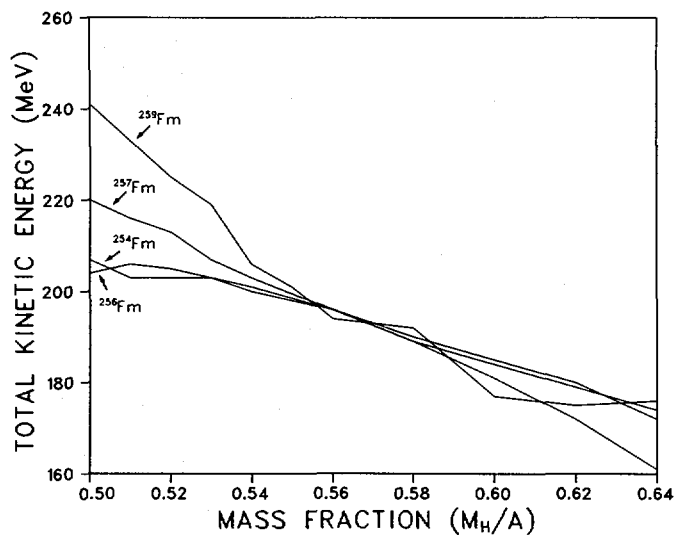

FIG.5. $\overline{TKE}$ *versus mass fraction for Fm isotopes. (Data from Refs* [2, 3, 14].*)*

has been explained on the basis of the approach of the fragments from symmetric mass division to the doubly magic ^{132}Sn configuration. The high TKE at symmetry then results because of coulomb repulsion which is a maximum for spherical shapes. The large spread in TKE at symmetry indicates a large difference in fragment shapes and that some of the fragments must still be highly deformed. Thus ^{257}Fm would appear to be in a "transition" region. The very high TKE's and narrow, symmetric mass distributions for ^{258}Fm and ^{259}Fm can also be explained on the basis of near spherical fragments which give the maximum TKE's. Since these approach the Q values for fission, the excitation energy of the fragments and subsequent neutron or gamma emission should be small. Although the measured [19] mass distribution for SF of ^{259}Md is symmetric and rather narrow, the very broad TKE distribution indicates a range of fragment shapes as for ^{257}Fm, again with some of the events having TKE's which approach the Q-value. However, it should be noted that for ^{259}Md, the most probable mass split is symmetric even for events with TKE <200 MeV while for ^{257}Fm the mass distribution becomes asymmetric for the lower TKE's. The effect of the odd proton is apparently very strong, and it has been suggested [30] that three-body fragmentation may be occurring, and accounts for the observed low TKE. Measurements of charge distribution for these highly symmetric systems would be extremely interesting, but are probably not feasible because of the short half-lives and low production cross sections.

IV. EFFECTS OF EXCITATION ENERGY

In general, increased excitation energy is expected to "wash out" shell effects. If the mass asymmetry and decrease in $\overline{TKE}$ at symmetry for the SF of ^{250}Cf, ^{252}Cf, and ^{256}Fm are attributed to shell effects, then an increase in yields and $\overline{TKE}$ at symmetry for (n,f) relative to SF would be expected. Some of the pertinent data are summarized in Table I. Indeed, a decrease in the P/V ratios, indicating an increase in the yield of symmetric mass division, has been observed [2, 31] for ^{250}Cf*, ^{252}Cf*, and ^{256}Fm* (Fig. 7) relative to SF of the same nuclides. A small increase [2] in $\overline{TKE}$ for ^{250}Cf* and small decreases [5] in $\overline{TKE}$ for ^{252}Cf* and ^{256}Fm* have been found relative to SF of ^{250}Cf, ^{252}Cf, and ^{256}Fm. The changes do not appear to be large, and for symmetric mass division, the $\overline{TKE}$'s for both ^{250}Cf* and ^{256}Fm* are higher than for SF of these nuclides. Although these results may appear contradictory, whether or not the overall $\overline{TKE}$ increases or decreases with increasing E_x depends on the details of each fissioning system, and is the result of averaging many different energy dependences for individual fragment pairs as their yields change with E_x.

In the case of ^{258}Fm*, the effect of extra E_x was quite clearly to decrease [4] the $\overline{TKE}$ and to broaden the mass distribution [4, 32] significantly relative to ^{258}Fm (SF) as shown in Fig. 8. Perhaps the apparently conflicting results for ^{258}Fm* and ^{256}Fm* shown in Figs. 7 and 8 can be explained by postulating that for ^{256}Fm and lighter actinides, fragment shells may tend to stabilize asymmetric mass division while in ^{258}Fm the fragment shell effects stabilize symmetric division into two near doubly magic fragments. Thus the effect of the extra excitation energy in outweighing the shell effects increases the yield

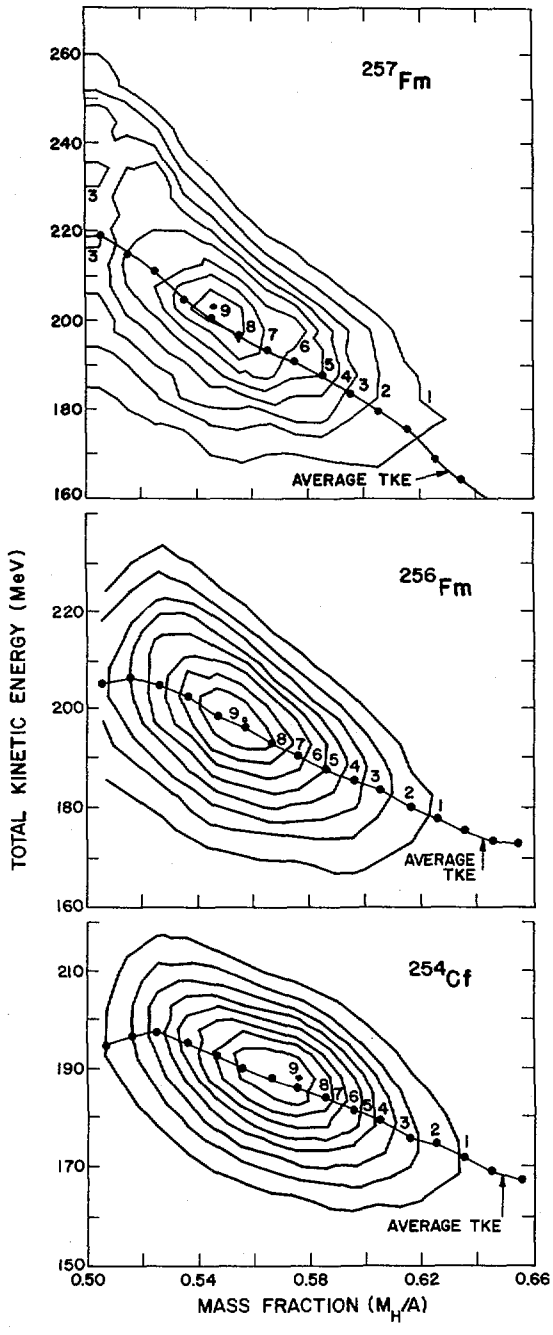

FIG. 6. Contour plots of TKE versus mass fraction for ^{254}Cf, ^{256}Fm, and ^{257}Fm [41]. The contours are lines of relative numbers of events based on data groupings 5 MeV X 0.01 units of mass fraction.

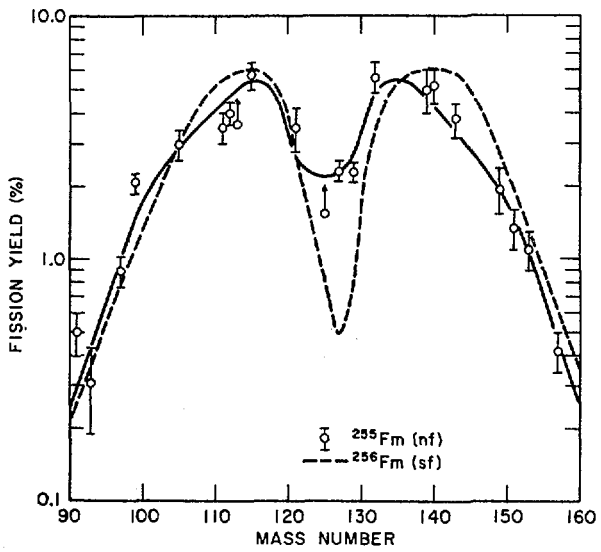

FIG. 7. Mass-yield curves for $^{256}Fm^*$ and ^{256}Fm [31].

of symmetric mass splits for $^{256}Fm^*$, while for $^{258}Fm^*$ the mass distribution is broadened and the yields at symmetry are decreased relative to ^{258}Fm (SF). The large reduction in the yield of symmetric, near spherical mass splits for $^{258}Fm^*$ also significantly reduces the $\overline{TKE}$.

Recently, direct reaction studies [33] of the prompt fission of $^{255}Es^*$, $^{256}Es^*$, and $^{255}Fm^*$ at E_x from threshold to ≈15 MeV and $^{256}Fm^*$ from 10 to 24 MeV via the (d,pf), (t,pf), (^{3}He,df), and (^{3}He,pf) reactions on ^{254}Es have given information about the effect of E_x on fragment energies and mass yields. The mass distribution for $^{255}Es^*$ at E_x = 4 to 6 MeV was nearly the same as for ^{254}Es (n,f) but showed significant increases in the yields near symmetry. In general, the yield of symmetric mass division increased monotonically with increasing TKE. The yield of symmetric fission for events with TKE > 210 MeV decreased for all these nuclides with increasing E_x. For a given E_x, the yield of symmetric, high TKE fission was highest for $^{256}Fm^*$ and decreased in the order $^{255}Fm^*$, $^{256}Es^*$, $^{255}Es^*$. The TKE generally decreased and these asymmetric mass distributions broadened with increasing E_x over the range studied. These results seem to be consistent with the weakening of shell effects with increasing E_x.

The mass distribution of $^{256}No^*$ at a E_x of ≈25 MeV has been measured radiochemically [34] to be asymmetric, but at ≈53 MeV, it becomes nearly symmetric. Apparently, shell effects are still stabilizing asymmetric fission to some extent up to ≈25 MeV, while for the heavy Fm isotopes rather dramatic changes are seen in the mass distributions for thermal neutron fission compared to spontaneous fission

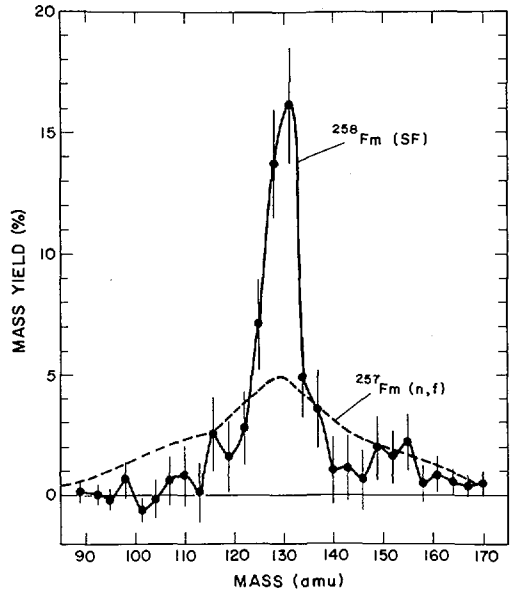

FIG. 8. Mass-yield curves for ^{258}Fm [4] and ^{258}Fm [14].*

even though the excitation energy is only about 6 MeV. This may indicate a rather small difference in potential energy for the asymmetric and symmetric paths to fission with a resulting high degree of sensitivity to E_x.

V. NEUTRON EMISSION

The average number of neutrons emitted per fission event, $\bar{\nu}_T$, for low energy fission generally increases with Z as shown in Fig. 9. (Values for $\bar{\nu}_T$ for thermal neutron fission have been corrected to zero E_x.) For the heavier actinides, $\bar{\nu}_T$ also tends to increase with mass for a given Z. However, this trend is not shown by the Fm isotopes where $\bar{\nu}_T$ is lower for masses 256 and 257 than for 254, although within the quoted errors it might be regarded as nearly constant.

The average values for the number of prompt neutrons emitted per fission event are, of course, not integral, but the probability for emitting a given number of neutrons has been measured for the low-energy fission of a large number of nuclides. It was early shown [35] that these "multiplicity" distributions could be approximated by a Gaussian distribution. Originally, most of the data could be fit with $\sigma_\nu = 1.08$ ($\sigma_\nu^2 = 1.17$), except for ^{252}Cf which required the use of $\sigma = 1.21$.

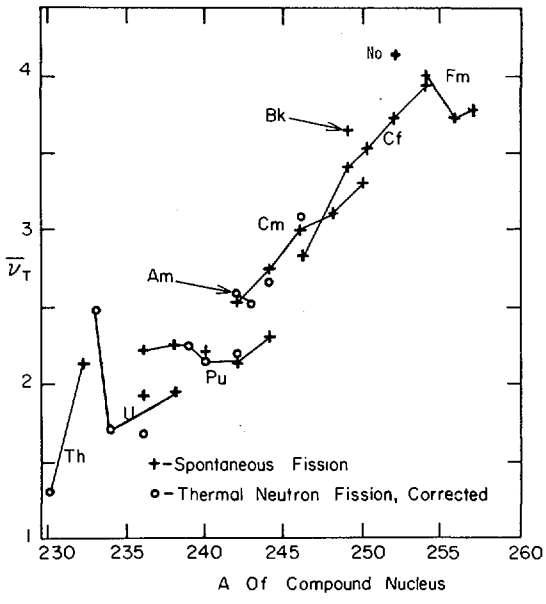

FIG.9. Experimental values of $\bar{\nu}_T$ as a function of A of the compound nucleus. Data for SF are shown by +. Measurements for $\bar{\nu}_T$ for (n,f) fission have been corrected to zero excitation energy using $d\bar{\nu}_T/dE_x = 0.11\ MeV^{-1}$ and are shown by ○. (Data from Refs [6, 31, 38].)

The variances for many heavier nuclides have now been measured and are plotted in Fig. 10. The variance for ^{252}Cf no longer appears to be anomalous. The variances are relatively constant for the isotopes of a given element, except for Fm, where much larger values are observed for masses 256 and 257. The variance of 4.0 ± 1.3 reported [36] for ^{252}102 is still larger, even considering the quoted error. It was proposed by Dakowski et al. [37] that there was a correlation between σ^2_ν and the fragment mass distribution, the highest σ^2_ν being observed for the most symmetric distribution, i.e., the lowest P/V ratio. Some variances for neutron emission and TKE and P/V ratios are given in Table II and do, indeed, show such a trend. However, this may be attributed to the fact that ^{256}Fm, ^{257}Fm, and ^{252}102 are in transition regions, i.e., symmetric mass division results in fragments which although close to the spherical, doubly magic ^{132}Sn configuration, are still rather soft to deformation and thus exhibit a large difference in fragment shapes ranging from rather deformed to nearly spherical. This could account for the large variances, for both ν and TKE. However, the trend is reversed for the highest TKE events (TKE > 240 MeV) from SF of ^{257}Fm. These have been found [7] to exhibit a very narrow, symmetric mass distribution (P/V ≈ 0), but σ^2_ν is only 0.9. (The $\bar{\nu}$ for these events is also low, 0.9 ± 0.1, as might be expected because the TKE is approaching the estimated Q value for fission.)

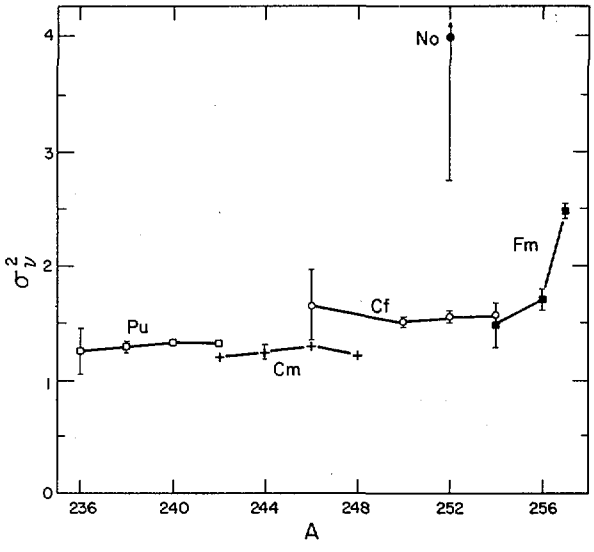

FIG.10. Variances of the neutron multiplicity distributions, σ^2_ν, plotted as a function of Z and A of the fissioning nucleus. (Data from Refs [36, 38, 40, 41].)

Lazarev [38] has recently reviewed the data for σ^2_ν and σ^2_{TKE} for low energy fission and summarized their dependences on A, Z, E_x, and the fissility parameter. He found that the ratio $\sigma^2_\nu/\sigma^2_{TKE}$ is nearly constant for all the heavy nuclides studied to date. If this relationship continues for ^{259}Fm and ^{259}Md, which have very high σ^2_{TKE} values, then σ^2_ν should also be very high and would continue the trend with increasing σ^2_ν values toward low P/V ratios, i.e., more symmetric fission. However, it might be argued that for higher mass Fm isotopes, σ^2_ν and σ^2_{TKE} should both become very small as the fragments all become nearly spherical which results in maximum TKE's which approach Q, and results in low E_x, and hence less neutron and gamma emission. It might be postulated that fissioning systems with Z > 100 would again be in a transition region, e.g., ^{259}Md, and the variances and $\bar{\nu}$ would increase as the fragments move away from the ^{132}Sn configuration. Relatively little detailed information for neutron emission as a function of fragment mass and kinetic energy has been obtained for heavy actinide nuclei except for ^{252}Cf where a minimum in $\bar{\nu}$ of $\approx$0.5 was found [39] in the region of A = 130. Such information is necessary for each fissioning system in order to obtain accurate pre-neutron emission kinetic-energy and mass distributions from kinetic energy measurements or to obtain pre-neutron masses from radiochemical measurements. Direct measurements of both the kinetic energies and velocities of the fragments require very intense sources which are not available for the heavier actinides, but $\bar{\nu}$(M) functions for ^{255}Es*, ^{254}Fm, and ^{256}Fm have been deduced [2, 23] by an iterative method involving comparison of radiochemical and kinetic-energy measurements of the fragment yields.

TABLE II. PEAK-TO-VALLEY RATIOS, P/V, AND VARIANCES, σ_ν^2, OF THE UNFOLDED NEUTRON MULTIPLICITY DISTRIBUTIONS FOR SPONTANEOUS AND THERMAL-NEUTRON FISSION (*) OF SOME ACTINIDE ISOTOPES (Refs [2, 6, 7, 12, 17, 18, 21, 22, 23, 36–41])

Nuclide	σ_ν^2	P/V	σ_{TKE}^2
$^{234}U^*$	1.208 ± 0.008	440	98.0
$^{236}U^*$	1.236 ± 0.008	620	106.1
$^{240}Pu^*$	1.40 ± 0.01	150	132.3
^{242}Cm	1.21 ± 0.03	>700	-
^{244}Cm	1.23 ± 0.05	>5700	122.6
^{250}Cf	1.49 ± 0.03	>300	127.7
^{252}Cf	1.57 ± 0.01	≥750	134.6
^{254}Cf	1.56 ± 0.01	≥145	139.2
^{253}Es	-	326	179.6
$^{255}Es^*$	-	≈8	252.8
^{254}Fm	1.50 ± 0.20	≈42	162.6
^{256}Fm	1.82 ± 0.08	12	207.4
^{257}Fm	2.51 ± 0.02	≈1.5	197.5
^{257}Fm(TKE>235 MeV)	0.09 ± 0.02	Sym.(0)	-
^{258}Fm	?	Sym.(0)	≈200
^{259}Fm	?	Sym.(0)	≈400
^{259}Md	?	Sym.(0)	≈1900
$^{252}102$	4.0 ± 1.3	Asym.	222

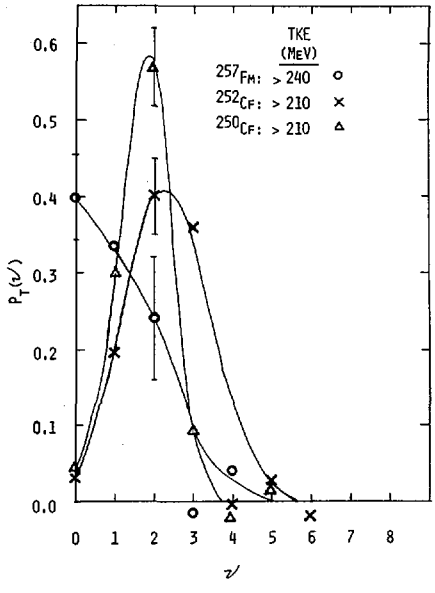

FIG.11. $P_t(\nu)$ for ^{250}Cf, ^{252}Cf, and ^{257}Fm for the fission events having the highest TKE's [40].

As in the case of ^{252}Cf, minimum neutron emission is found around mass 130 and can be correlated with the low deformation, closed-shell structure of these fragments.

Measurements of $\overline{\nu}$ and σ_ν^2 as a function of fragment TKE and mass ratio have been made [40, 41] for the SF of ^{250}Cf, ^{252}Cf, ^{254}Cf, ^{256}Fm, ^{257}Fm, and the "unfolded" multiplicity distributions were obtained for all except ^{256}Fm. The $\overline{\nu}$'s for $^{250,252,254}Cf$ and $^{256,257}Fm$ were found to decrease monotonically with increasing TKE for a given mass split. This might be expected since the total energy is constant and is manifested primarily either in E_x or TKE of the fragments. Thus as the TKE increases, E_x and hence the energy available for the emission of neutrons (and photons), must necessarily decrease. This effect is most pronounced for ^{257}Fm.

A comparison of the $P_t(\nu)$ distributions for the highest TKE events from ^{250}Cf, ^{252}Cf, and ^{257}Fm is shown in Fig. 11 and illustrates the large probability for the emission of 0 neutrons for ^{257}Fm for events with TKE > 240 MeV. This is consistent with a large fraction of these fragments being nearly spherical with resultant high TKE's which are nearly equal to the Q value. The measured $\overline{TKE}$'s for ^{258}Fm and ^{259}Fm of $\approx$240 MeV are also close to the estimated Q value of around 250 MeV and indicate that the fragments must emit very few neutrons and are probably nearly spherical.

VI. DISCUSSION

The existing data on mass, kinetic-energy, and neutron-emission distributions for low-energy fission of the heaviest actinides and the effect of modest excitation energy on these properties have been reviewed. Most of the data are consistent with the systematics established for the lighter actinides, but the properties of the heavy fermium isotopes appear to be unique. The rather abrupt change in properties observed for SF of ^{258}Fm and ^{259}Fm which fission symmetrically with a very high TKE seems to be associated with the approach of the fragments from symmetric mass division to the spherical, doubly magic ^{132}Sn configuration. The maximum yield of symmetric fragments with associated very high TKE and low neutron emission, and the resulting decrease in these effects with increasing excitation energy seem to be best described by the asymmetric two-center shell model (ATCSM) calculations of Mustafa et al. [8, 42, 43] and the scission-point model of Wilkins et al. [44]. The cluster model of Gönnenwein et al. [45] also appears to qualitatively describe these results and the differences in mass distributions for Cf and Fm isotopes. Due to the formation of Z = 50 clusters in Fm (which cannot occur in lighter elements), symmetric mass division is energetically favored, the fragment deformation is small, and the TKE high compared to lighter actinides. However, the competition of both symmetric and asymmetric substructure effects should result in large variances, particularly for lower mass Fm isotopes. Almost equal barriers for symmetric and asymmetric fission should result and account for the observed sensitivity of fission properties to small increases in E_x. Maruhn and Greiner [46] have used the concept of mass symmetry, treated as a dynamical collective coordinate based on the ATCSM, to calculate mass distributions for ^{226}Ra, ^{236}U, and ^{258}Fm which are in qualitative agreement with the data. Ultimately, dynamical calculations which relate the potential energy surface of the fissioning nucleus with those of the fragments will probably be required for a complete understanding of the fission process.

The calculations of Mustafa and Ferguson [8] for $98 \geq Z \leq 106$ show that the transition from asymmetric to symmetric mass division occurs at N = 158 for Fm, a lower value than for the other elements. The calculated potential energy surfaces are rather shallow for both ^{256}Fm and ^{258}Fm, consistent with their sensitivity to the addition of small E_x. They predict that the transition to mass symmetry should occur at N = 160 for No, and at N = 162 for Cf and elements 104 and 106. This is in agreement with the observed asymmetric mass distribution for ^{256}Cf. Their calculation for ^{252}No also indicates a preference for asymmetric mass division, in agreement with experiment.

They performed calculations for two odd nuclides, ^{257}Fm and ^{262}105, and found a preference for symmetric fission for ^{257}Fm (similar to ^{258}Fm) and asymmetric fission for ^{262}105. However, for ^{262}105, they found symmetric shapes to be preferred before the second saddle with asymmetric shapes becoming increasingly favored as the neck radius decreases en route to scission. They find similar results for ^{256}Cf and ^{256}Fm for which a preference for asymmetric mass division is shown even though there is no second barrier.

Mustafa and Ferguson find that the second barrier to fission has disappeared in Fm for N > 154, while for elements 102 and 104 the barriers persist for N > 154 but are below the ground state, and disappear entirely for large N. Element 106 isotopes show essentially no barrier. They argue that the observation of asymmetric fission for ^{262}105, even though it does not show a second barrier, may indicate that the process is adiabatic. Recent calculations of Mustafa [47] indicate that a rapid descent from saddle to scission does not lead to symmetric fission for the heavy Fm isotopes and is thus inconsistent with the measured mass distribution data. He therefore suggests that the potential energy surfaces are moving slowly near scission where fragment shell effects are strong. It is important to measure the properties of more trans-fermium isotopes to check this hypothesis and determine whether or not they all fission asymetrically and whether the TKE's are high as for ^{258}Fm and ^{259}Fm or whether they can again be represented by a linear extrapolation from the lower Z actinides.

Wilkins, Steinberg, and Chasman [44] have used a static model based on the assumption of statistical equilibrium at the scission point to calculate the relative probabilities of formation of complementary fission fragment pairs as determined from the relative potential energies of two nearly touching, coaxial spheroids. They are able to reproduce the general trends in kinetic-energy, charge, and mass distributions for Po to Fm isotopes. They are also able to interpret variations in neutron emission and $\overline{\text{TKE}}$ based on the fragment configurations at scission. The observed dip in $\overline{\text{TKE}}$ for symmetric mass division for the lighter actinides is explained on the basis that the deformation for symmetric mass splits of fissioning nuclides such as ^{235}U is considerably larger than for asymmetric splits, and hence the coulomb repulsion and $\overline{\text{TKE}}$ will be less at symmetry. They predict the transition to mass symmetry at A = 258 for Fm, but with one spherical and one highly deformed fragment due to stabilization of a deformed neutron shell at $\beta = 0.85$. This results in a maximum $\overline{\text{TKE}}$ of 220 MeV, somewhat lower than the observed $\overline{\text{TKE}}$ of about 240 MeV for ^{258}Fm and ^{259}Fm. They expect the maximum $\overline{\text{TKE}}$ for Fm isotopes to be $\approx$225 MeV for ^{262}Fm rather than for ^{264}Fm because of this deformed shell at 80 neutrons. However, the total deformation at symmetry for heavy Fm isotopes is small with resulting higher $\overline{\text{TKE}}$ for symmetric relative to asymmetric mass division thus explaining the experimentally observed disappearance of the "dip" in $\overline{\text{TKE}}$ at symmetry for the Fm isotopes. They predict large variances for TKE and neutron emission in the ^{258}Fm to ^{264}Fm region because of the large differences in the deformation of the fragments. This is experimentally observed for the TKE and neutron emission of the "transition" nuclide ^{257}Fm, but the $\overline{\text{TKE}}$ data for ^{258}Fm and ^{259}Fm seem to be better explained by two near spherical fragments [48].

Perhaps the low $\overline{\text{TKE}}$ and extremely large variance in TKE and the narrow, symmetric mass distribution observed for ^{259}Md can be explained on the basis of the stabilization of more deformed fragments for symmetric mass division. At A = 284, Wilkins et al. [44] predict a configuration which is symmetric in deformation as well as mass with a total deformation, $\beta_1 + \beta_2 = 1.30$, similar to that for lighter actinides. This suggests a return to the $\overline{\text{TKE}}$ systematics as a linear

function of $Z^2/A^{1/3}$ which have been found for lighter actinides [2, 27] rather than the high $\overline{TKE}$ predicted by Schmitt and Mosel [48] using a static scission model.

The mass distribution for ^{258}Fm calculated by Wilkins et al. [44] is triple-peaked while the data for ^{258}Fm (SF) show a very narrow symmetric mass distribution with essentially no asymmetric mass division. Their calculated mass distribution is more consistent with the data for $^{258}Fm^*$ where the effect of the extra E_x is to broaden the mass distribution and increase the yield of the asymmetric component. Apparently, the details of the mass distribution are very sensitive to small changes in the potential energy surfaces and the overall agreement of their calculations with experimental data is relatively good over a broad range of fissioning systems using only a single set of parameters for the collective temperature, intrinsic temperature, and the spheroid separation distance.

Mosel [49] and Nix [50] have recently reviewed the various theoretical approaches to nuclear fission including the use of the Strutinsky "shell-correction" method [51], recent self-consistent calculations, and attempts to understand the descent from the second saddle to scission, nuclear viscosity, and the time scales involved.

Further measurements of the fission properties of the trans-fermium isotopes are needed in order to check the various theoretical approaches by determining whether there is a return to asymmetric mass distributions and lower TKE's. The measurements for ^{252}No and $^{262}105(104)$ indicate that this is the case but more data are needed. As the SF half-lives become still shorter, these measurements become increasingly difficult. Methods for measuring the SF properties for millisecond activities [52] will have to be developed. Another problem involves the unequivocal assignment of the Z and A of these nuclides. Assignment on the basis of half-life or fission properties alone is difficult because of the large overlap in properties, although the TKE and mass distributions of the heavy Fm isotopes appear to be unique. The TKE of the higher Z elements may well revert to a linear extrapolation based on asymmetric fission of lower Z actinides. The assumption of compound nucleus formation with the subsequent emission of neutrons becomes increasingly risky for heavy ions on heavy element targets. It is known [53] that SF activity from ^{256}Md-^{256}Fm is formed with a relatively large cross section from bombardments of ^{248}Cm and ^{249}Bk with ^{18}O and recently evidence [54] for the production of ^{259}Fm in bombardments of ^{248}Cm with ^{18}O has been obtained. Thus a variety of nuclides can be formed in these reactions making identification and measurement of properties exceedingly difficult. Methods such as those of Bemis et al. [17] for measuring coincidences between characteristic x-rays following electron-capture or alpha decay, and short-lived SF activities can perhaps be used if sufficient activity can be produced. Hopefully, with the development of these and other ingenious techniques, it will be possible to elucidate the fission properties and unequivocally identify the many short SF activities of the actinide and trans-actinide elements which are produced in heavy ion bombardments. Knowledge of their properties and production modes should be invaluable in our understanding of nuclear fission and in extending the periodic table still further.

ACKNOWLEDGEMENTS

It is a pleasure to acknowledge the receipt of a Fellowship Award from the John Simon Guggenheim Foundation, the support of the Los Alamos Scientific Laboratory, and the hospitality of the Nuclear Science Division of the Lawrence Berkeley Laboratory. I also wish to thank Dr. G.T. Seaborg for his continued interest and support and Kathleen Van Der Haeghen for her help in the preparation of this manuscript.

REFERENCES

[1] Proc. IAEA Symp. Phys. Chem. of Fission, 3rd, Rochester, New York, 1973 (IAEA, Vienna) Vol. II (1974) 191.

[2] UNIK, J.P., GINDLER, J.E., GLENDENIN, L.E. FLYNN, K.F., GORSKI, A., and SJOBLOM, R.K., in Proc. IAEA Symp. Phys. Chem. of Fission, 3rd, Rochester, New York, 1973 (IAEA, Vienna) Vol. II (1974) 19.

[3] BALAGNA, J.P., FORD, G.P., HOFFMAN, D.C., and KNIGHT, J.D., Phys. Rev. Lett. 26 (1971) 145.

[4] JOHN, W., HULET, E.K., LOUGHEED, R.W., and WESOLOWSKI, J.J., Phys. Rev. Lett. 27 (1971) 45.

[5] RAGAINI, R.C., HULET, E.K., LOUGHEED, R.W., and WILD, J.F., Phys. Rev. C 9 (1974) 399.

[6] HOFFMAN, D.C., and HOFFMAN, M.M., Ann. Rev. Nucl. Sci. 24 (1974) 24.

[7] BALAGNA, J.P., FARRELL, J.A., FORD, G.P., HEMMENDINGER, A., HOFFMAN, D.C., VEESER, L.R., and WILHELMY, J.B., Proc. IAEA Symp. Phys. Chem. of Fission, 3rd, Rochester, New York, 1973 (IAEA, Vienna) Vol. II (1974) 191.

[8] MUSTAFA, M.G. and FERGUSON, R.L., Phys. Rev. C 18 (1978) 301.

[9] NURMIA, M., SIKKELAND, T., SILVA, R., GHIORSO, A., Phys. Lett. 26B (1967) 78.

[10] RANDRUP, J., LARSON, S.E., MÖLLER, P., NILSON, S.G., POMORSKI, K., and SOBICZEWSKI, A., Phys. Rev. C 13 (1976) 229.

[11] BARAN, A. et al., Proc. 3rd Intl. Conf. on Nuclei Far from Stability, Cargèse, Corsica, CERN, Geneva (1976) 558; Phys. Lett 76B (1978) 8.

[12] BARAN, A., POMORSKI, K., LARSON, S.E., MÖLLER, P., NILSSON, S.G., RANDRUP, J., LUKASIAK, A., SOBICZEWSKI, A., Fourth IAEA Symposium on Physics and Chemistry of Fission, Jülich, Germany, 14-18 May, 1979, Paper D4.

[13] HULET, E.K., WILD, J.F., LOUGHEED, R.W., EVANS, J.E., QUALHEIM, B.J., NURMIA, M., and GHIORSO, A., Phys. Rev. Lett. 26 (1971) 523.

[14] HOFFMAN, D.C., WILHELMY, J.B., WEBER, J., DANIELS, W.R., LASL; HULET, E.K., LANDRUM, J.H., LOUGHEED, R.W., WILD, J.F., LLL, Detection of the new isotopes, 12.3 minute ^{256}Cf and 43-minute ^{258}Md, Los Alamos Scientific Laboratory Report LA-UR-77-2901 (1977); International Meeting on Reactions of Heavy Ions with Nuclei and Synthesis of New Elements, 13-16 December (1977) Dubna.

[15] JOHANSSON, S.A.E., Nucl. Phys. 12 (1959) 449.

[16] RANDRUP, J., TSANG, C.F., MÖLLER, P., NILSSON, S.G., and LARSON, S.E, Nucl. Phys. A 217 (1973) 221.

[17] BEMIS, JR., E.E., DITTNER, P.F., SILVA, R., HAHN, R.L., TARRANT, J.R., HUNT, L.D., HENSLEY, D.C., Phys. Rev C 16 (1977) 1146.

[18] HOFFMAN, D.C., WEBER, J., WILHELMY, J.B., HULET, E.K., LOUGHEED, R.W., LANDRUM, J.H., and WILD, J.F., Transplutonium 1975, Proc. 4th Int. Transplutonium Element Symposium, North Holland, Amsterdam, (1976) 363; Proc. 3rd Int. Conf. on Nuclei Far From Stability, Cargèse, Corsica, CERN, Geneva (1976) 558.
[19] WILD, J.F., HULET, E.K., LOUGHEED, R.W., LANDRUM, J.H., NITSCHKE, J.M., and GHIORSO, A., ACS/CSJ Chemical Congress, April 2-6, 1979, Honolulu, Hawaii, Abstracts, NUCL-64.
[20] OGANESSIAN, Yu. Ts., DEMIN, A.G., ILJINOV, A.S., TRETYAKOVA, S.P., PLEVE, A.A., PENIONZHKEVICH, Yu. E., IVANOV, M.P., TRETYAKOV, Yu. P., Nucl. Phys. A239 (1975) 157.
[21] GINDLER, J.E., FLYNN, K.F., GLENDENIN, L.E., SJOBLOM, R.K., Phys. Rev. C 16 (1977) 1483.
[22] BEMIS, JR., C.E., FERGUSON, R.L., PLASIL, F., SILVA, R.J., PLEASANTON, F., and HAHN, R.L., Phys. Rev. C 15 (1977) 705.
[23] FLYNN, K.F., GINDLER, J.E., GLENDENIN, L.E., J. Inorg. Nucl. Chem. 39 (1977) 759).
[24] FLYNN, K.F., GINDLER, J.E., GLENDENIN, L.E., SJOBLOM, R.K., J. Inorg. Nucl. Chem. 38 (1976) 661.
[25] WOLFSBERG, K. and FORD, G.P., American Chemical Society 167th National Meeting, Los Angeles, March 31-April 5, 1974, NUCL-21.
[26] FLYNN, K., GINDLER, J., GLENDENIN, L., GORSKI, A., SJOBLOM, F., and UNIK, J., American Chemical Society, 167th National Meeting, Los Angeles, March 31-April 5, 1974, NUCL-22.
[27] VIOLA, V., Nucl. Data 1 (1966) 391.
[28] SCHMITT, H.W., and MOSEL, U., Nucl. Phys. A 186 (1972) 1.
[29] BEMIS, JR., C.E., FERGUSON, R.L., PLASIL, F., SILVA, R.J., O'KELLEY, G.D., KIEFER, M.L., HAHN, R.L., HENSLEY, D.C., HULET, E.K., and LOUGHEED, R.W., Phys. Rev. Lett. 39 (1977) 1246.
[30] HULET, E.K., WILD, J.F., LOUGHEED, R.W., BAISDEN, P.A., LANDRUM, J.H., DOUGAN, R.J., MUSTAFA, M., GHIORSO, A. and NITSCHKE, J.M., IAEA Symp. Phys. Chem. of Fission, 4th, Jülich, Germany, 14-18 May, 1979, Paper F15.
[31] FLYNN, K.F., GINDLER, J.E., SJOBLOM, R.K., J. Inorg. Nucl. Chem. 37 (1975) 881.
[32] FLYNN, K.R., GINDLER, J.E., GLENDENIN, L.E., Phys. Rev. C 12 (1975) 1478.
[33] WILHELMY, J.B., BRITT, H.C., CHEIFITZ, E., HOFFMAN, D.C., DUPZYK, R.J., LOUGHEED, R.W., to be published.
[34] KALPAKCHIEVA, R., et al., Phys. Lett. 69B (1977) 287.
[35] TERRELL, J., Phys. Rev. 127 (1957) 880.
[36] LAZAREV, Yu.A., NEFEDIEV, O.K., OGANESSIAN, Yu.Ts., DAKOWSKI, M., Phys. Lett 52B (1974) 321.
[37] DAKOWSKI, M., LAZAREV, Yu.A., OGANESSIAN, Yu.Ts., Yad. Fiz. 17 (1973) 692.
[38] LAZAREV, Yu.A., Atomic Energy Rev. 15 (1977) 75.
[39] BOWMAN, H.R., MILTON, J.C.D., THOMPSON, S.G., and SWIATECKI, W., Phys. Rev. 129 (1963) 2133.
[40] HOFFMAN, D.C., American Chemical Society, 167th National Meeting, Los Angeles, March 31-April 5, 1974, NUCL-15; LAUR-73-1683.
[41] HOFFMAN, D.C., FORD, G.P., BALAGNA, J.P., and VEESER, L.R., Phys. Rev. C, to be published.
[42] MUSTAFA, M.G., Phys. Rev. C 11 (1975) 1059.
[43] MUSTAFA, M.G., MOSEL, U., SCHMITT, H.W., Phys. Rev. C 7 (1973) 1519.

[44] WILKINS, B.D., STEINBERG, E.P., and CHASMAN, R.R., Phys. Rev. C 14 (1976) 1832.
[45] GÖNNENWEIN, F., SCHULTHEIS, H., SCHULTHEIS, R., and WILDERMUTH, K., Phys. Lett. 57B (1975) 313.
[46] MARUHN, J. and GREINER, W., Phys. Rev. Lett. 32 (1974) 548.
[47] MUSTAFA, M.G., Proc. IAEA Symp. Phys. Chem. Fission, 4th, Jülich, Germany, 14-18 May, 1979.
[48] SCHMITT, H.W., MOSEL, U., Nucl. Phys. A186 (1972) 1.
[49] MOSEL, U., "Theory of Nuclear Fission: A Review," Specialists Meeting on Fast Neutron Fission Cross Sections, NEANDC/NEARCP, Argonne National Laboratory, June 28-30, 1976.
[50] NIX, J.R., ACS/CSJ Chemical Congress, Honolulu, Hawaii, April 2-6, 1979, Abstracts, NUCL-59.
[51] STRUTINSKY, V.M., Nucl. Phys. A95 (1967) 420; A122 (1968) 1.
[52] GAEGGLER, H., SEIDEL, W., POPEKO, G.S., SMIRNOV, V.I., SUBBOTIN, V.G., TER-AKOPIAN, G.M., CHELNOKOV, L.P., Nucl. Inst. Meth. 150 (1978) 173.
[53] NITSCHKE, J.M., GHIORSO, A., NURMIA, M.J., SOMERVILLE, L.P., HULET, E.K., ILLIGE, J.D., LOUGHEED, R.W., ACS/CSJ Chemical Congress, Honolulu, Hawaii, April 2-6, 1979, Abstracts, NUCL-66.
[54] HOFFMAN, D.C., LEE, D., GHIORSO, A., NURMIA, M.J., NITSCHKE, J.M., ALEKLETT, K. (1979) private communication.

DISCUSSION

P. ARMBRUSTER: We have heard an excellent account of the cold fragmentation of nuclear matter in the symmetric fission of ^{258}Fm. I would like to mention another case of cold fragmentation found recently in thermal-neutron-induced fission of ^{233}U during an experiment carried out jointly by research workers from Darmstadt, Munich and Grenoble at ILL. For very high TKE approximating the reaction Q value, it was found that ^{234}U splits into several mass pairs with N = 60 and N = 82, predominantly into ^{100}Zr/^{134}Te. The TKE approaches the Q value to within (2 ± 2) MeV, i.e. the excitation energy of the fragmented system is not higher than the energy gained in the capture of the fission-inducing neutron. A deformation of about 2:1 is derived for the ^{100}Zr fragment, in qualitative agreement with the postulated deformed shell at N = 62. The yield of the cold fragmentation is less than 10^{-2}%, comparable with the symmetric mass splits. This finding demonstrates clearly that nuclear-structure effects dominate fragmentation at very low excitation energies. Fission shows us that only when nuclear matter is prevented from being intrinsically heated (E_x<10 MeV) is a preferential production of close shell nuclei to be observed. This is a lesson we should keep in mind when discussing the production of SHE's.

M. ASGHAR: Dr. Hoffman, I am delighted to see the microcosm of fission in the fermium isotopes, where the N = 82 and Z = 50 spherical shells seem to determine the transition from asymmetric to symmetric fission. In the light

actinides fission changes from symmetric to asymmetric with the mass of the fissioning system. However, this is not due to the N = 82 and Z = 50 spherical shells, as was thought for many years, but to the N ~ 88 deformed shell in the heavy fragment and the N = 50 spherical shell in the light fragment.

Furthermore, in connection with Dr. Armbruster's comments on what he calls cold fragmentation in fission for the mass ratio 134/100 - here ^{134}Tb has an N = 82 spherical shell and ^{100}Zr has an N = 60 deformed shell - from ^{233}U (n_{th}, f), I think one could cite many such examples, such as the mass ratio 146/90, where the N ≈ 88 deformed shell and N = 50 spherical shell fix the configuration. I refer you to my paper at this meeting (see SM-241/F3 of these Proceedings).

D. HOFFMAN: It seems that in the case of the heavy fermium isotopes we are dealing with two spherical fragments, since the $\overline{\text{TKE}}$ of about 240 MeV is approaching the Q value, whereas if only one fragment were deformed, the $\overline{\text{TKE}}$ would be lower. Wilkins, Steinberg and Chasman predict ≈ 220 MeV for the $\overline{\text{TKE}}$ based on one spherical and one deformed fragment.

K. SISTEMICH: You might be interested to know of a cold system of fission products that we have observed during the fission ^{235}U induced by thermal neutrons. There exists a μs isomer with high spin in ^{132}Sn. Using the Lohengrin mass separator at ILL Grenoble, we have studied the feeding of this state at ~5 MeV as a function of the kinetic energies of the products. We have observed the production of ^{132}Sn in this excited state even when the total available excitation energy is only just sufficient to reach the 5 MeV level. This means that the complementary nucleus 104 Mo is cold and that fission preferentially yields products with high spin over a statistical excitation energy distribution.

R.H. IYER: Dr. Hoffman, what sort of experimental techniques did you use to obtain the mass yield distribution? I should also like to urge you to extend your measurements to cover the far asymmetric region, since I believe some very interesting phenomena, such as shell effects, seem to take place in this region during the fission of very heavy elements.

D. HOFFMAN: My review included data from both radiochemical and double-kinetic-energy measurements. In the case of ^{258}Fm and ^{259}Fm, double-kinetic-energy measurements with solid-state detectors were used and ≈ 500 SF events were detected. For example, ^{259}Fm was produced via the (t,p) reaction on ^{257}Fm targets of ≈ 10^9 atoms. In the case of the ^{248}Cm + ^{18}O reaction producing nuclei (which may be ^{259}Fm), with a 1.5 half-life, some 700 SF events were detected. With so few events, we would not be able to see low-probability events.

THE SPONTANEOUS FISSION OF ^{259}Md*

E.K. HULET, J.F. WILD, R.W. LOUGHEED,
P.A. BAISDEN, J.H. LANDRUM, R.J. DOUGAN,
M. MUSTAFA, A. GHIORSO, J.M. NITSCHKE
University of California,
Lawrence Livermore Laboratory,
Livermore, California,
United States of America

Abstract

THE SPONTANEOUS FISSION OF ^{259}Md.

The mass and kinetic energy distributions of fission fragments from the spontaneous fission of the newly discovered nuclide ^{259}Md have been obtained. Mendelevium-259 was identified as the E.C. daughter of ^{259}No and was found to decay entirely ($> 95\%$) by spontaneous fission with a 95-min half-life. From the kinetic energies measured for 397 pairs of coincident fragments, a mass distribution has been derived that is symmetric with $\sigma = 13$ amu. Mendelevium-259, together with ^{258}Fm and ^{259}Fm, forms a select group of three nuclides whose mass division in spontaneous fission is highly symmetric. Unlike the total-kinetic-energy (TKE) distributions of ^{258}Fm and ^{259}Fm, which peak at $\approx$ 240 MeV, this distribution for ^{259}Md is broad and is 50 MeV lower in energy. The authors' analysis of the mass and energy distribution shows that events near mass symmetry also exhibit a broad TKE distribution, with one third of the symmetric events having TKE's less than 200 MeV. The association of low TKE's with symmetric mass division in the fission of very heavy actinides is anomalous and inconsistent with theories based upon the emergence of fragment shells near the scission point. The authors assume either three-body fragmentation or peculiar fragment shapes as the cause for the large consumption of Coulomb energy observed for a significant fraction of symmetric fissions in ^{259}Md.

INTRODUCTION

During the past decade, the mass and kinetic energy distributions have been measured for numerous spontaneously-fissioning (SF) nuclides in the region $92 \leq Z \leq 100$. With the exception of ^{258}Fm and ^{259}Fm, the mass divisions were found to be decidedly asymmetric with the most probable total kinetic energy (TKE) increasing slowly from $\approx$ 180 to $\approx$ 200 MeV with increasing Z of the fissioning nucleus. The mass distributions for the SF of ^{258}Fm and ^{259}Fm, on the other hand, are strongly symmetric and exhibit TKE's that are 40 to 50 MeV higher than predicted by systematics [1,2]. This rather abrupt change in fission properties, beginning with the heavy Fm isotopes, has brought about significant new

* Work performed under the auspices of the US Department of Energy by the Lawrence Livermore Laboratory under contract number W-7405-ENG-48.

insights concerning the fission process and has provided a new testing ground for fission theory. A major result has been to stress the importance of the part fragment shells play in the mass and energy division during fission.

The progress of nuclear fission theory in recent years has centered around the double-humped fission barrier caused by the stability of several nuclear shapes in the actinide region. The double-humped feature arises from shell corrections superimposed upon a smoothly varying, liquid-drop potential [3]. Some believe that the inner barrier is responsible for symmetric fission and the outer barrier for asymmetric fission [4]. Calculations by Randrup et al. [5] suggest that the outer barrier disappears in the heavy actinide region, which could account for the observed transition from an asymmetric to symmetric mass division in the heaviest Fm isotopes. On the other hand, if the mass division is governed by the potential energy surface in the vicinity of scission, that is, the descent to the scission point is adiabatic, then the shell structure of the nascent fragments would determine the mass division [6]. According to this argument, the anomalous fission behavior of ^{258}Fm and ^{259}Fm would be due to their ability to fission into two ultra-stable, Sn-like fragments, $Z = 50$, $N \approx 82$.

Currently, fragment shell structure is viewed as the dominant factor in determining the fission mass split and the TKE. The TKE is traced to fragment shells because the TKE appears to be related to the ability of the fragments to remove deformation energy. However, the fission properties of ^{258}Fm and ^{259}Fm represent too limited a test of the validity of this or other possible hypotheses. The fission properties of the lighter Fm isotopes and a wide mass range of Cf isotopes have been examined to supply a baseline of systematic behavior. But to provide more extensive tests of the influence of fragment-shell structure or the effects from the disappearance of the second barrier on fission, we need SF data from selected nuclides in the transfermium region. In this region, it is particularly important that the neutron-rich nuclides be investigated because only here are the effects of the outer barrier fully suppressed. Also, if the fragments are to approach the $N = 82$ shell, then the fissioning species must be very neutron-rich.

We have started a systematic study of fission in this region with an investigation of ^{259}Md, and we plan to continue with studies of the millisecond isotopes, ^{258}No and ^{260}[104]. The nuclide ^{262}[105] provides the only other case directly relevant to fission theory in the $Z>100$ region [7]. The mass distribution from the fission of ^{262}[105] was interpreted to be probably asymmetric, although less than 200 events were observed, together with a high background from the fission of ^{256}Fm coproduced in the bombardments. By studying the fission of ^{259}Md, which has the same number of neutrons as ^{258}Fm, we have begun to follow the trend in fission properties from symmetric fission in ^{258}Fm to possibly asymmetric fission in ^{262}[105].

Our first experiments were aimed at identifying the source of spontaneous fission activity which was earlier thought to belong to the decay of ^{259}No [8]. We chemically identified this activity as arising from Md following the E.C. decay of 62-min ^{259}No. After establishing a half-life for this new nuclide, we characterized the decay modes and partial half-lives for both ^{259}Md and ^{259}No. The SF properties of ^{259}Md were next investigated and these results are the main subject we treat in this paper.

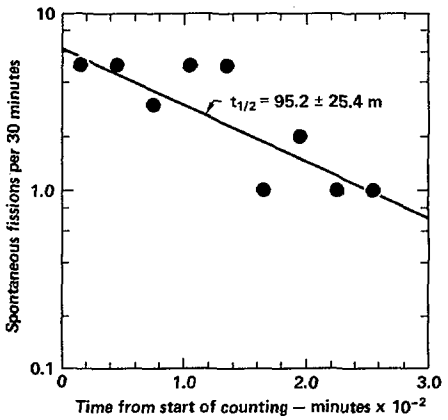

FIG.1. The decay of spontaneous fission activity in samples of Md chemically separated from ^{259}No.

It should be noted that fission studies of these very heavy nuclei are exceedingly difficult and the results are by no means predictable.

EXPERIMENTAL

In all experiments, we initially prepared a pure sample of the parent, 62-min ^{259}No, from which the ^{259}Md would grow following E.C. decay. The ^{259}No was produced by the bombardment of a target of ^{248}Cm with 96-MeV ^{18}O ions from the 88-in cyclotron at the Lawrence Berkeley Laboratory. Products of the (^{18}O, α3n) reaction recoiling from the target were collected on a thin foil of either Pd or Au positioned directly behind the target. At the end of a bombardment typically 2-h long, the recoil foil was dissolved. The Pd or Au from the dissolved recoil collection foil was removed by adsorption on an anion-exchange column. The eluate, containing mainly No^{2+} and other trivalent actinides, was evaporated to dryness, redissolved in 0.1 M HCl, and eluted from a chromatographic-extraction column consisting of HDEHP dissolved in n-heptane, adsorbed on a fluoroplastic powder. This column adsorbed all of the trivalent actinides, including ^{256}Fm, ^{254}Fm, ^{248}Cm transferred from the target, and any other potential SF contaminant. We thus were assured of producing an isotopically pure source of ^{259}Md SF activity. Finally, we eliminated most of the inactive mass contamination, such as Ca or Mg, by means of a small cation-exchange column.

In the identification experiments, we evaporated samples of the purified ^{259}No parent onto Pt disks which were then pulse-height analyzed using surface-barrier detectors. The output from the counting system was routed through an ADC to a PDP-15 computer which recorded the energy and time of occurrence of each alpha and fission event on magnetic tape for subsequent off-line data analysis. A decay curve of the SF activity coming from samples of isolated Md is shown in Fig. 1 and indicates a single component decaying with a half-life of 95 min.

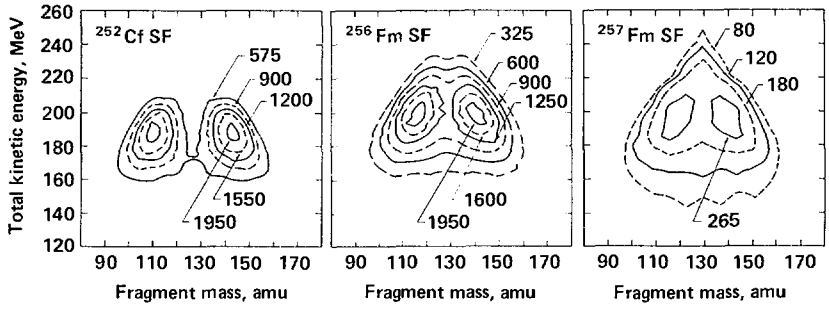

FIG.2. Contour diagrams of counts versus fragment mass and total kinetic energy for three nuclides used in calibrating the surface-barrier detectors. Numbers on the contours refer to the number of events.

To characterize the SF decay properties of ^{259}Md, we arranged two coincidence counting systems, each consisting of two 450-mm^2 surface-barrier detectors mounted facing one another inside a vacuum chamber. Samples of ^{259}No-^{259}Md evaporated on thin VYNS films (typically 25-35 μg/cm^2) were placed between the detectors. Fission fragments from an event were detected in coincidence and the kinetic energy of each fragment was measured. As before, the output from the counting system was processed by the PDP-15 computer, which recorded the fragment energies and event times on magnetic tape. The mass of each fragment was derived from kinematic considerations.

We used a ^{252}Cf SF source to calibrate the fragment-energy response of the detectors, and employed the mass-independent calibration procedure of Schmitt, Kiker, and Williams [9]. The ^{252}Cf source on VYNS film was similar in thickness to the ^{259}Md sources, which reduced our calibration errors due to differing source thickness. Shortly after collecting the SF data for ^{259}Md, we prepared sources of ^{256}Fm (2.6 h, 92% SF) and ^{257}Fm (101 d, 0.2% SF) on VYNS film and analyzed these in our coincidence counting system. The kinetic energy and mass distributions of these two nuclides are already known [10,11] and they, therefore, served to verify our calibrations. The mass vs TKE distributions for ^{256}Fm and ^{257}Fm, as well as that obtained for ^{252}Cf, are shown in the contour plots of Fig. 2.

RESULTS AND DISCUSSION

We became aware that ^{259}No did not possess a spontaneous fission mode of decay when no SF activity was found in samples of ^{259}No immediately after chemical separation. But as the ^{259}No decayed with a 1-h half-life, SF activity grew in and eventually decayed with a new half-life of 95 min. The 95-min SF activity was proven to be associated with ^{259}Md by chemical separation of Md from purified No and observation of the 95-min decay of spontaneous fissions in the Md fraction. Mendelevium was repeatedly separated from a sample of pure ^{259}No and from this we were able to show that the growth period for ^{259}Md corresponded to the 1-h half-life of ^{259}No. An α-decay branch in ^{259}Md was not observed in

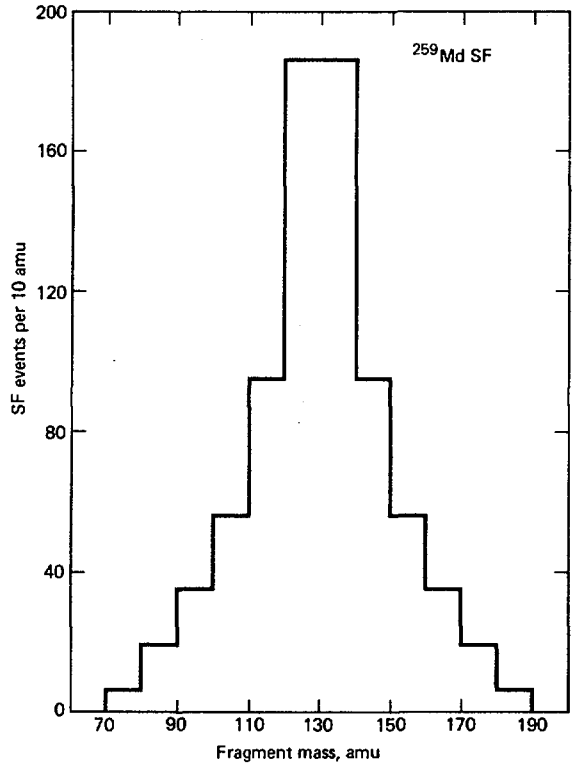

FIG.3. Provisional mass distribution for the spontaneous fission of ^{259}Md.

the α spectra obtained with pure Md samples. These data would allow an upper limit of 5% for α-decay by ^{259}Md; thus, the predominant decay mode is spontaneous fission. The decay sequence is summarized as follows:

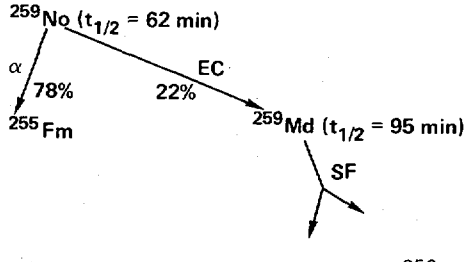

Our experiments do not rule out the possibility of ^{259}Md decaying by E.C. to 1.5-s ^{259}Fm, which would then be the source of the observed SF activity. However, this seems unlikely because most (but not all) mass equations [12, 13] and closed decay-cycle calculations [14] indicate that ^{259}Md is stable with respect to decay toward ^{259}Fm and, indeed, that ^{259}Fm is β^- unstable.

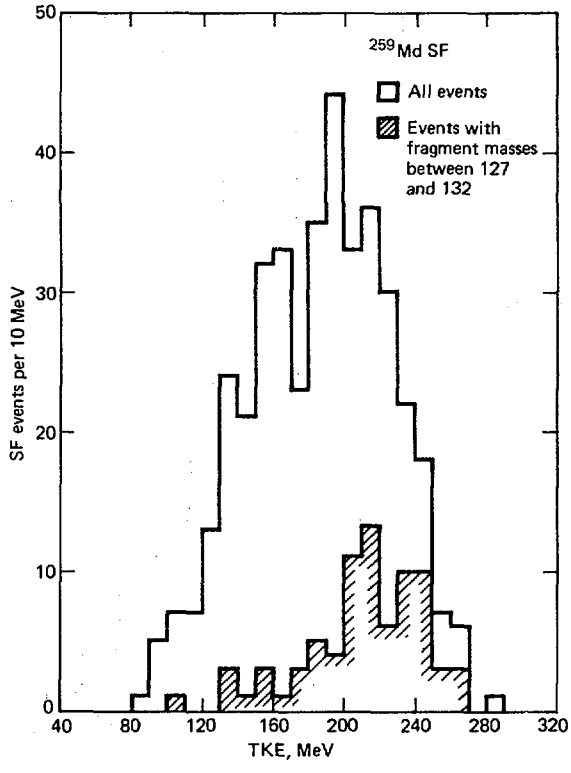

FIG.4. Post-neutron total-kinetic-energy (TKE) distributions for the spontaneous fission of ^{259}Md. The most probable TKE is 187.5 MeV. The shaded region is the TKE distribution for a 5-amu wide band of fission events at mass symmetry.

Following the identification of the new isotope ^{259}Md, we performed eighteen separate bombardments in which ^{259}No was chemically separated, deposited on thin films, and the energies of coincident fission fragments measured. A total of 397 fragment pairs was obtained from which we calculated mass and kinetic energy distributions. The mass distribution, illustrated in Fig. 3, is seen to be highly symmetric; however, there are indications of a small asymmetric component. This symmetric mass division is most comparable with the symmetric fission of ^{258}Fm and ^{259}Fm, the only other nuclides found so far that yield highly symmetric mass distributions. In the way of further comparisons to ^{259}Md, both the SF and neutron-induced fission of ^{257}Fm [11,15] contain a much larger component of asymmetric mass division.

The distribution of total kinetic energy (TKE) is shown in Fig. 4. The most probable TKE is 188 MeV while the average TKE is 185 MeV. The most probable TKE's measured for the nuclides ^{256}Fm and ^{257}Fm were found to be 195.0 MeV and 187.5 MeV, respectively, which can be compared

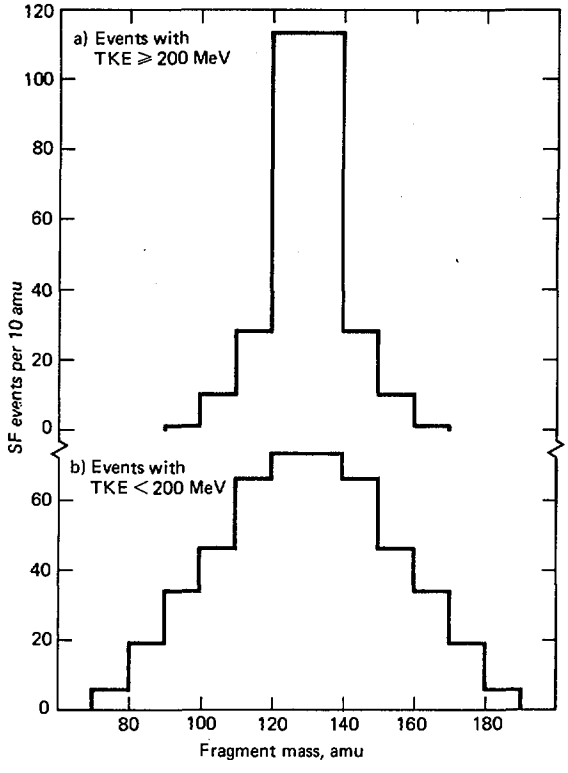

FIG.5. Provisional mass distributions for the spontaneous fission of ^{259}Md separated into two groups according to the total kinetic energy. The lower curve clearly shows a symmetric mass distribution for fission events with low kinetic energies.

with the post-neutron TKE's of 194.8 MeV and 195.1 MeV measured for these Fm isotopes by Unik et al. [10] and Balagna and co-workers [11]. Although our TKE for ^{257}Fm is low, the ^{256}Fm value is easily within the error limits of the measurements and we are satisfied with the accuracy of our calibrations.

As a result of comparing the SF properties of ^{259}Md with those of ^{256}Fm through ^{259}Fm, we find that ^{259}Md is unique. Although the mass distribution is closely comparable to the symmetric division in ^{258}Fm and ^{259}Fm, the most probable TKE is ≈50 MeV lower than found for these heavy Fm isotopes. The ^{259}Md TKE is most comparable to those of ^{256}Fm and ^{257}Fm. Such a low TKE associated with symmetric mass division is unusual and is inconsistent with current fission theory in which fragment shells appear to govern the fission process. Symmetric division of the heavy Fm isotopes leads to fragments approaching the magic nucleon numbers Z = 50, N = 82 which, due to their spherical rigidity, possess low deformation and internal excitation energy. Therefore, fissions with near-symmetric mass division exhibit correspondingly higher TKE's than those with asymmetric division, which yields fragments that are soft toward deformation.

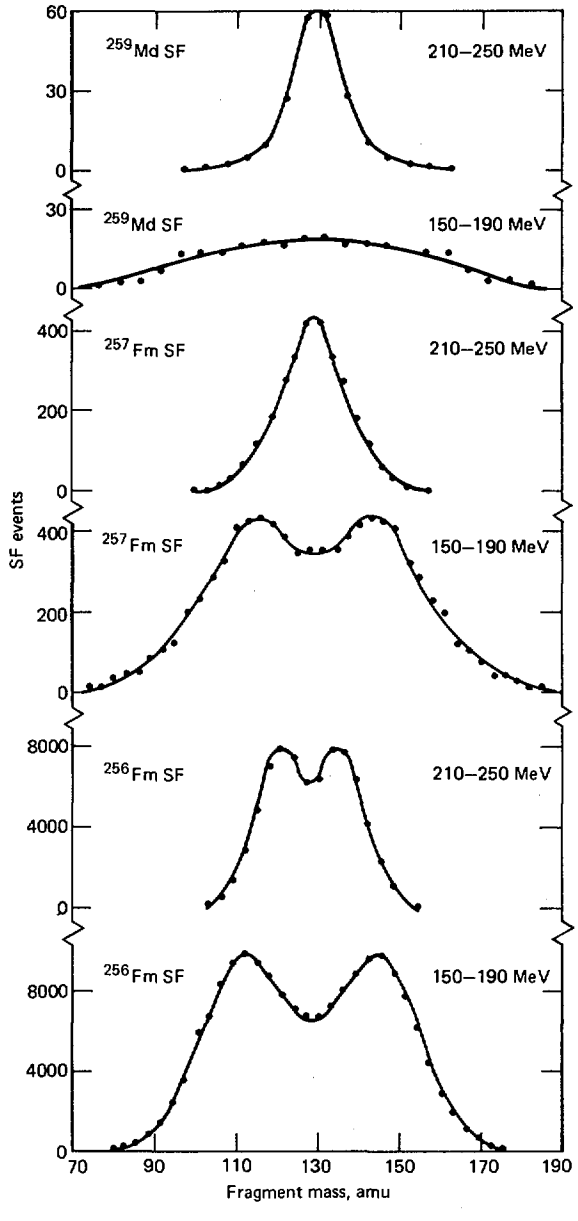

FIG.6. Provisional mass distributions for ^{259}Md, ^{257}Fm, and ^{256}Fm sorted into groups as a function of their total kinetic energies. Each curve shows the mass distribution for fission events with total kinetic energies within a 40-MeV band. Only ^{259}Md retains a semblance of a symmetric distribution in low-kinetic-energy fission.

To determine the extent of this deficit in TKE for ^{259}Md, we sorted our coincident events with respect to selected bands of TKE or mass. We then estimated the extent of correlation between symmetric mass division and high TKE. In the shaded section of Fig. 4, we see that events very close to mass symmetry have an average TKE about 20 MeV greater than the most probable TKE observed for all events. These high kinetic energy events seem to support the two-spheroid model of Schmitt and Mosel [16], based on fragment shell effects. However, about 35% of these highly symmetric fissions still exhibit TKE's less than 200 MeV. If broad energy cuts are taken for those events above and below 200 MeV, the mass distributions shown in Fig. 5 are obtained. The greater portion of symmetric mass divisions result in higher than average TKE's, but a significant percentage are associated with low kinetic energies. Finally, in Fig. 6, where the ^{259}Md mass distributions are compared with those of ^{256}Fm and ^{257}Fm, we find that only ^{259}Md yields a symmetric mass distribution in fission with TKE's under 200 MeV.

In sum, our analysis indicates we are observing a unique fission mode in the SF of ^{259}Md. To account for the 40-50 MeV loss in TKE for about a third of the symmetric events, it would be necessary to admit about 60 MeV of internal excitation and deformation energy in the fragments or to hypothesize three-body fragmentation whereby a light particle and two heavy fragments are emitted at the scission point. The storage of 60 MeV internal energy in the fragments is much more than can be accounted for by collective motions, angular rotation, or internal heating. Highly deformed symmetric fragments, in principle, can incorporate such a large potential energy. However, there is no evidence of such events (i.e., sizeable symmetric fission with TKE's <200 MeV) in the nearby Fm isotopes. Most fission studies have indicated a maximum excitation energy of ≈10 MeV in each fragment [17]. On the other hand, we estimate that light-particle emission would remove at least 25 to 30 MeV from the fissioning system and would be energetically favored if the particle is hydrogen-like (p,d,t). The emission of a Z = 1 particle obviously provides the opportunity for the remaining mass to divide into two Z = 50 fragments, which would be stabilized by filled proton shells. A test of this hypothesis is underway, but we expect it will require another long series of experiments to detect and identify light particles coming from the SF of ^{259}Md.

A trend toward mass asymmetry in the SF of nuclides with atomic numbers greater than that of Fm is barely discernible. The fission of ^{262}[105] is very probably asymmetric but ^{259}Md is only slightly less symmetric than ^{258}Fm and ^{259}Fm. Therefore, it might be expected that neutron rich nuclides between Md and element 105 would show a sharp reduction in symmetric fission properties, but the present evidence is still too slight to offer this as any more than a prediction. Only after the fission properties of other neutron-rich nuclides such as ^{258}No and ^{260}[104] have been measured can a trend be established.

REFERENCES

[1] HOFFMANN, D. C., WILHELMY, J. B., WEBER, J., DANIELS, W.R., LASL; HULET, E.K., LANDRUM, J. H., LOUGHEED, R. W., WILD, J. F., LLL, Detection of the new isotopes, 12.3-minute ^{256}Cf and 43-minute ^{258}Md, Los Alamos Scientific Laboratory Report LA-UR-77-2901 (1977); International Meeting on Reactions of Heavy Ions with Nuclei and Synthesis of New Elements, 13-16 December, 1977, Dubna.

[2] HOFFMANN, D. C., WEBER, J., WILHELMY, J. B., HULET, E. K., LOUGHEED, R. W., LANDRUM, J. H., and WILD, J. F., "Transplutonium 1975" (Proc. 4th Int. Transplutonium Element Symposium, North Holland, Amsterdam, 1976) 363; Proc. 3rd Int. Conf. on Nuclei Far From Stability, Cargèse, Corsica (CERN, Geneva, 1976) 558.

[3] STRUTINSKY, V. M., Nucl. Phys. A95 (1967) 420; A122 (1968) 1. MEYERS, W. D. and SWIATECKI, W. J., Nucl. Phys. 81 (1966) 1.

[4] MÖLLER, P. and NILSSON, S. G., Phys. Lett. 31B (1970) 283. PAULI, H. C., LEDERGERBER, T. and BRACK, M., Phys. Lett. 34B (1971) 264.

[5] RANDRUP, J., TSANG, C. F., MÖLLER, P., and NILSSON, S.G., Nucl. Phys. A217 (1973) 221.

[6] MOSEL, U. and SCHMITT, H. W., Phys. Rev. C4 (1971) 2185.

[7] BEMIS, JR., C.E., FERGUSON, R. L., PLASIL, F., SILVA, R. J., O'KELLEY, G. D., KIEFER, M. L., HAHN, R. L., HENSLEY, D. C., HULET, E. K., and LOUGHEED, R. W., Phys. Rev. Lett 39 (1977) 1246.

[8] SILVA, R. J., DITTNER, P. F., MALLORY, M. L., KELLER, O. L., ESKOLA, P., ESKOLA, K., NURMIA, M., and GHIORSO, A., Nucl. Phys. A216 (1973) 97.

[9] SCHMITT, H.W., KIKER, W. E., and WILLIAMS, C. W., Phys. Rev. B137 (1965) 837.

[10] UNIK, J. P., GINDLER, J. E., GLENDENIN, L. E., FLYNN, K. F., GORSKI, A., and SJOBLOM, R. K., (Proc. 3rd IAEA Symp. Phys. Chem. of Fission, Rochester, New York, 1973), IAEA, Vienna, Vol. II (1974) 19.

[11] BALAGNA, J. P., FORD, G. P., HOFFMANN, D. C., and KNIGHT, J. D., Phys. Rev. Lett. 26 (1971) 145.

[12] WAPSTRA, A. H. and BOS, K., Atomic Data Nucl. Data Tables 17 (1976) 593.

[13] KOLESNIKOV, N. N. and DEMIN, A. G., Joint Institute for Nuclear Research, Dubna, USSR, reprint P6-9421 (1975); Lawrence Livermore Laboratory Translation UCRL-11098.

[14] VIOLA, JR., V. E., SWANT, J. A., and GRABER, J., Atomic Data Nucl. Data Tables 13 (1974) 60.

[15] JOHN, W., HULET, E. K., LOUGHEED, R. W., and WESOLOWSKI, J. J., Phys. Rev. Lett. 27 (1971) 45.

[16] SCHMITT, H. W. and MOSEL, U., Nucl. Phys. A186 (1972) 1.

[17] SCHULTHEIS, H. and SCHULTHEIS, R., Phys. Rev. C18 (1978) 317.

DISCUSSION

H.A. NIFENECKER: According to Dr. Hoffman, the assumptions made with regard to variation in $\bar{\nu}$ (M) may change a symmetric distribution into an asymmetric one or vice versa. The shape of these variations may depend on the kinetic energy, and therefore the low-kinetic-energy symmetric events may be in fact asymmetric. Z identification using a DE-E fragment telescope might help to remove the ambiguity.

E.K. HULET: The mass distribution of ^{259}Md, unlike that of ^{257}Fm noted by Dr. Hoffman, is highly symmetric, and therefore, much less likely to be converted into a pre-neutron asymmetric distribution by the $\bar{\nu}$ (M) correction. The evaporation of large numbers of neutrons by the fragments implies high excitation energies that could, in principle, reduce the total energy available. However, the question remains why it is possible for the fragments from the fission of ^{259}Md to be highly excited, while those from ^{258}Fm and ^{259}Fm are not. The average total kinetic energies for ^{258}Fm and ^{259}Fm were ~240 MeV, which leaves only about 10 MeV available for fragment excitation.

J.B. WILHELMY: Did you find that the ^{259}No decays by EC into ^{259}Md?

E.K. HULET: Yes, Md was chemically separated from ^{259}No isolated after the bombardments. The 95-minute spontaneous fission decay of ^{259}Md was observed in this Md sample.

J.B. WILHELMY: I should also like to ask whether you made certain that the chemically prepared sources were 'thin'. Is there any danger that the observed broad KE distribution could be caused by a 'thick' source? And a further question is, have there been any potential energy surface calculations in support of the idea of light-particle emission in this region?

E.K. HULET: The sources were not especially thin, but only a small fraction of the energy broadening could have been due to source thickness. This was established by noting the half-widths of the total kinetic energy distributions for the calibration standards - ^{252}Cf and ^{256}Fm - which were narrow. These standards were prepared identically with the ^{259}Md samples.

The answer to your second question is yes. Some calculations have been made by M.G. Mustafa, using the two-centre shell mode. They showed that light particle emission was favourable. Nevertheless, these calculations are not decisive, since some rather crude approximations were made to account for the potential of the light particle.

EVIDENCE FOR THE OCCURRENCE OF NEW SHOULDERS IN LOW-ENERGY-FISSION MASS DISTRIBUTION

R.H. IYER, V.K. BHARGAVA, V.K. RAO,
S.G. MARATHE, S.M. SAHAKUNDU
Radiochemistry Division,
Bhabha Atomic Research Centre,
Trombay, Bombay, India

Abstract

EVIDENCE FOR THE OCCURRENCE OF NEW SHOULDERS IN LOW-ENERGY-FISSION MASS DISTRIBUTION.

The results of investigations aimed at defining the nature of the low-yield wing portions of the mass yield curve in the reactor-neutron-induced highly asymmetric binary fission of ^{238}U are reported. Fission yields for mass chains 66, 67, 72, 73, 77, 161, 167, 171, 172, 173, 175, and 177, together with the upper limits for the yields of mass chains 179, 183 and 199, were determined relative to ^{99}Mo by using stringent radiochemical techniques and have been used to obtain the complete mass yield curve. The yields of these mass numbers are in the range of $10^{-3} - 10^{-6}$%. The yields of mass chains 66 – 67 on the lighter mass side and 171 – 177 on the heavier mass side were found to be about three orders of magnitude higher than the normally expected trend. This observation, coupled with the upper limits for mass chains 179, 183 and 199, unambiguously shows the presence of 'shoulders' in the very asymmetric mass region which the authors attribute to the possible influence of the 28-proton shell in low-energy fission. Some interesting new features concerning low-energy highly asymmetric fission seem to emerge from these studies. Various plausible explanations for the occurrence of the new shoulders in low-energy-fission mass distribution are discussed in the light of recently available experimental and theoretical data from other laboratories.

1. INTRODUCTION

Very few experimental measurements are reported in the literature on the yields of low-yield products formed in the highly asymmetric fission ($70 \geqslant A \geqslant 160$) of heavy elements. The main reason for the lack of experimental data on fission yields in this region is that measurements of such low-cross-section events involve considerable effort at developing radiochemical separation procedures capable of separating activities of the order of a few counts per minute in a radiochemically pure form from highly irradiated targets. Fortunately, the capabilities of radiochemical techniques have undergone significant revision in recent years, and this fact, coupled with the availability of low-background

counting systems, makes radiochemical techniques important in the study of rare and low-cross-section processes such as ternary fission [1], very asymmetric binary fission, etc.

This communication is concerned with some of the results of a long-range programme of work on the determination of fission yields in the neutron-induced highly asymmetric fission of actinide elements. It was recognized that the expected yields of products are in the range of $10^{-6} - 10^{-7}$%, which are too low to be of any consequence to the reactor designers. The main motivation for initiating this programme arose from the lack of experimental data. Such measurements would help both in checking the correctness of extrapolations/predictions of yields in the low-yield wing portions of the mass yield curve and in more precisely defining the nature and trends of yields in extremely asymmetric mass splits in low-energy fission. It would also give some insight into the effect of nucleon shells, if any, in the far-asymmetric mass splits since such shell effects are best preserved at low excitation energies.

In this paper, we report the results of a set of measurements on the low-yield products in the reactor neutron-induced fission of ^{238}U and ^{235}U. Some of the results have appeared elsewhere [2, 3]. The results are considered in the light of recently available experimental and theoretical data from other laboratories [4 – 6]. Some interesting new facts concerning low-energy highly asymmetric fission seem to emerge from these studies. Suggestions for future experiments to further pin down this rare fission mode are also discussed in this paper.

2. EXPERIMENTAL SET-UP

Enriched ^{235}U (93.4%) and depleted ^{238}U (0.21% ^{235}U) were used in the experiments. Before irradiation, the targets were extensively purified by extracting uranium from 2M nitric acid into 30% tributyl phosphate (TBP) in xylene, followed by anion exchange purification from 8M hydrochloric acid using a Dowex-2X8 (50 – 100 mesh) column. The solvent extraction-cum-ion exchange cycle was repeated four times. All reagents used were of high purity.

About 0.5 – 1.0 g of depleted ^{238}U and 2 – 3 mg of enriched ^{235}U in the form of uranyl nitrate hexahydrate were triply sealed in PVC (polyvinyl chloride) bags. The depleted uranium sample was wrapped in 0.3-mm-thick cadmium metal foils. The targets were irradiated in the maximum flux position (10^{12} n · cm^{-2} · s^{-1}) of the swimming-pool reactor APSARA for periods ranging from 8 – 48 hours depending upon the half-lives of the products to be isolated. After irradiation, the targets, in general, were dissolved in dilute hydrochloric acid in the presence of 10 – 20 mg of added carriers of the fission products. The existing radiochemical procedures were either suitably modified [7], or new procedures were developed [8, 9] to meet the stringent requirements of radio-

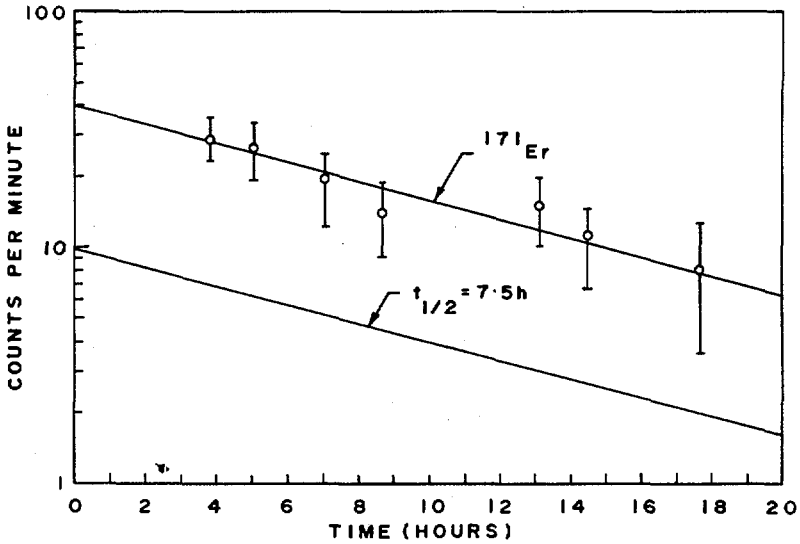

FIG. 1. Beta decay curve of ^{171}Er.

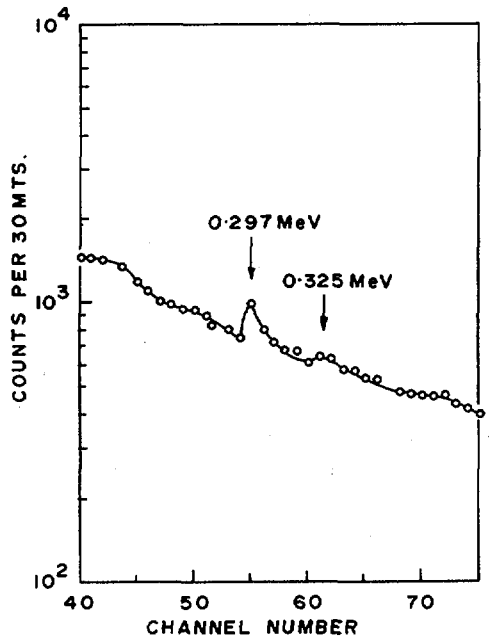

FIG. 2. Gamma spectrum of ^{73}Ga.

TABLE I. FISSION YIELDS OF SOME HIGHLY ASYMMETRIC PRODUCTS IN THE REACTOR-NEUTRON-INDUCED FISSION OF ^{238}U AND ^{235}U

S. No.	Nuclide	Fission yields (%)	
		^{238}U	^{235}U
1	^{66}Ni	$(4.01 \pm 1.6) \times 10^{-6}$	$\leqslant 4.60 \times 10^{-9}$
2	^{67}Cu	$(2.32 \pm 0.93) \times 10^{-5}$	$\leqslant 1.60 \times 10^{-8}$
3	^{72}Zn	$(6.54 \pm 2.50) \times 10^{-5}$	$(5.85 \pm 2.34) \times 10^{-6}$
4	^{73}Ga	$(2.19 \pm 0.44) \times 10^{-4}$	–
5	^{77}As	$(1.51 \pm 0.64) \times 10^{-3}$	–
6	^{161}Tb	$(6.45 \pm 2.58) \times 10^{-4}$	$(1.32 \pm 0.52) \times 10^{-4}$
7	^{167}Ho	$(4.08 \pm 0.80) \times 10^{-5}$	–
8	^{171}Er	$(5.04 \pm 2.0) \times 10^{-6}$	–
9	^{172}Er	$(9.40 \pm 3.76) \times 10^{-6}$	–
10	^{173}Tm	$(6.17 \pm 2.50) \times 10^{-6}$	–
11	^{175}Yb	$(8.0 \pm 3.20) \times 10^{-6}$	$\leqslant 2.4 \times 10^{-8}$
12	^{177}Lu	$(6.60 \pm 2.64) \times 10^{-6}$	$\leqslant 1.8 \times 10^{-8}$
13	^{179}Lu	$\leqslant 2.41 \times 10^{-7}$	–
14	^{183}Ta	$\leqslant 1.13 \pm 10^{-8}$	–
15	^{199}Au	$\leqslant 4.66 \pm 10^{-9}$	–

chemical purity of the products isolated. A brief summary of the procedures used is given in the Appendix. The activities were mounted in the form of suitable precipitates of known stoichiometry and counted in low-background beta proportional counters with anti-coincidence shielding (background 0.5 – 1.0 cpm). The samples were counted long enough to accumulate sufficient counts to reduce the statistical uncertainty in counting. The radiochemical purity was checked from the half-lives in all cases and from the gamma spectrum wherever possible using a NaI(Tl) detector, coupled to a multichannel analyser. A typical beta decay curve and a gamma spectrum are shown in Figs 1 and 2, respectively.

The observed activities were corrected for chemical yield, decay and counting efficiency. Fission yields were calculated relative to ^{99}Mo yield using the equation

$$Y_i\,(\%) = \frac{Y_{^{99}Mo}\,(\%)\,N_i}{N_{^{99}Mo}} \qquad (1)$$

where Y_i is the yield of the particular nuclide, i, produced in the irradiation, and N_i is its number of atoms formed. $Y_{^{99}Mo}$ and $N_{^{99}Mo}$ are the corresponding yield and number of atoms of ^{99}Mo formed. The number of atoms N_i were calculated by using the relation

$$N_i = \frac{A_i t}{(1 - e^{-\lambda t})} \qquad (2)$$

Here A_i is the activity (in dpm) associated with the nuclide, i, at the end of the bombardment, and t is the time of irradiation (in minutes). The yield of ^{99}Mo was assumed to be 6.2%. The corrections for independent yields [10] to obtain the total isobaric chain yield as well as the contribution from epi-Cd fission of ^{235}U were estimated and found to be negligible in comparison with the uncertainties associated with the reported yields.

3. RESULTS AND DISCUSSION

Table I gives the cumulative fission yields of 15 mass chains (A = 66, 67, 72, 73, 77 in the lighter region and A = 161, 167, 171, 172, 173, 175, 177, 179, 183 and 199 on the heavier side) in the reactor neutron fission of ^{238}U. Also included in Table I are the yields of some of these highly asymmetric products in the thermal-neutron fission of ^{235}U for comparison. The yields are of the order of $10^{-3} - 10^{-6}$ % for the mass chains in the highly asymmetric region. The values reported for mass chains 179, 183, and 199 are only upper limits since the activities isolated could not be identified unambiguously as due to ^{179}Lu, ^{183}Ta and ^{199}Au, respectively. Similarly, the yields reported for ^{235}U fission (Table I) are also upper limits only. The estimated uncertainties in yield values range from ± 20% to ± 40% for the highly asymmetric products. The uncertainties include errors from chemical yield determinations, counter efficiencies, decay systematics of the nuclides involved, counting statistics, etc.

3.1. Effect of target impurities

Since the highly asymmetric products are very low-cross-section events, the effect of target impurities which might give rise to the products of our interest by neutron activation was considered seriously. The relevant nuclear reactions leading to the formation of the products of interest by non-fission events have been listed in Table II. The target material was exhaustively purified before irradiation by a repeated ion-exchange-cum-solvent extraction method and the impurity fraction was analysed by spectrographic and activation analyses to

TABLE II. POSSIBLE MODES OF FORMATION OF FISSION PRODUCTS BY NON-FISSION REACTIONS IN A REACTOR

Nuclide		Nuclear reaction
^{66}Ni	a)	$^{64}Ni \xrightarrow{(n,\gamma)} {}^{65}Ni \xrightarrow{(n,\gamma)} {}^{66}Ni$
^{67}Cu	a)	$^{65}Cu \xrightarrow{(n,\gamma)} {}^{66}Cu \xrightarrow{(n,\gamma)} {}^{67}Cu$
	b)	$^{67}Zn \xrightarrow{(n,p)} {}^{67}Cu$
^{72}Zn	a)	$^{70}Zn \xrightarrow{(n,\gamma)} {}^{71}Zn \xrightarrow{(n,\gamma)} {}^{72}Zn$
^{73}Ga	a)	$^{71}Ga \xrightarrow{(n,\gamma)} {}^{72}Ga \xrightarrow{(n,\gamma)} {}^{73}Ga$
	b)	$^{73}Ge \xrightarrow{(n,p)} {}^{73}Ga$
^{77}As	a)	$^{75}As \xrightarrow{(n,\gamma)} {}^{76}As \xrightarrow{(n,\gamma)} {}^{77}As$
	b)	$^{76}Ge \xrightarrow{(n,\gamma)} {}^{77}Ge \xrightarrow{\beta^-} {}^{77}As$
	c)	$^{77}Se \xrightarrow{(n,p)} {}^{77}As$
^{161}Tb	a)	$^{159}Tb \xrightarrow{(n,\gamma)} {}^{160}Tb \xrightarrow{(n,\gamma)} {}^{161}Tb$
	b)	$^{160}Gd \xrightarrow{(n,\gamma)} {}^{161}Gd \xrightarrow{\beta^-} {}^{161}Tb$
	c)	$^{161}Dy \xrightarrow{(n,p)} {}^{161}Tb$
^{167}Ho	a)	$^{165}Ho \xrightarrow{(n,\gamma)} {}^{166}Ho \xrightarrow{(n,\gamma)} {}^{167}Ho$
	b)	$^{167}Er \xrightarrow{(n,\gamma)} {}^{167}Ho$
$^{171,172}Er$	a)	$^{170}Er \xrightarrow{(n,\gamma)} {}^{171}Er \xrightarrow{(n,\gamma)} {}^{172}Er$

TABLE II (cont.)

Nuclide		Nuclear reaction
^{173}Tm	a)	$^{173}Yb \xrightarrow{(n,p)} {}^{173}Tm$
^{175}Yb	a)	$^{174}Yb \xrightarrow{(n,\gamma)} {}^{175}Yb$
	b)	$^{175}Lu \xrightarrow{(n,p)} {}^{175}Yb$
^{177}Lu	a)	$^{176}Lu \xrightarrow{(n,\gamma)} {}^{177}Lu$
	b)	$^{176}Yb \xrightarrow{(n,\gamma)} {}^{177}Yb \xrightarrow{\beta^-} {}^{177}Lu$
	c)	$^{177}Hf \xrightarrow{(n,p)} {}^{177}Lu$
^{179}Lu	a)	$^{179}Hf \xrightarrow{(n,p)} {}^{179}Lu$
^{183}Ta	a)	$^{181}Ta \xrightarrow{(n,\gamma)} {}^{182}Ta \xrightarrow{(n,\gamma)} {}^{183}Ta$
	b)	$^{183}W \xrightarrow{(n,p)} {}^{183}Ta$
^{199}Au	a)	$^{197}Au \xrightarrow{(n,\gamma)} {}^{198}Au \xrightarrow{(n,\gamma)} {}^{199}Au$
	b)	$^{199}Hg \xrightarrow{(n,p)} {}^{199}Au$

ensure that the products of our interest could not arise by activation. Impurity fractions equivalent to 5-g amounts of the target material were used for these analyses while the targets used for irradiations were 5 – 10 times less in all the cases. Spectrographic analysis did not show the presence of any of the three rare earths Lu, Yb and Er. Activation analysis revealed the presence of some un-identified long-lived activity in the impurity fraction as well as reagent blank in the case of lutetium (probably due to natural lutetium activity). Similar long-lived tails were observed in the decay curve of ^{177}Lu and ^{179}Lu separated from irradiated uranium targets. Natural lutetium shows about 0.7 cpm · mg^{-1} due

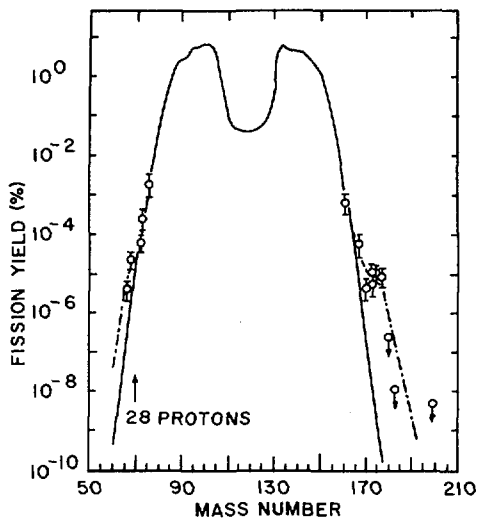

FIG. 3. Mass distribution in the fission of ^{238}U by reactor neutrons.

to ^{176}Lu in the counter used. It may be noted in this context that the presence of about 0.02 ppm of Lu in the target may give rise to 10^4 dpm of ^{177}Lu activity by $^{176}Lu(n,\gamma)^{177}Lu$ reaction under the conditions of irradiation. The absence of such abnormal ^{177}Lu activity in the irradiated uranium targets coupled with the result of the impurity analyses by spectrographic and activation methods is taken as evidence for the purity of the targets employed. The presence of Zn impurity (0.7 ppm) was detected in depleted uranium sample. The formation of ^{66}Ni by the $^{70}Zn(n,n\alpha)$ reaction may be regarded as negligible in view of the low cross-section for the reaction. The correction for the fission yield of ^{67}Cu due to $^{67}Zn(n,p)^{67}Cu$ was found to be less than 1% on the basis of available data [11] on reaction cross-section and threshold energy. All other possibilities of nuclear reactions leading to the formation of ^{66}Ni, ^{67}Cu, ^{172}Er, ^{175}Yb and ^{177}Lu were considered while calculating the yields, and their effect was found to be negligible. It may be noted that the formation of ^{172}Er by non-fission nuclear reactions under reactor neutron irradiation is extremely improbable. The formation of ^{171}Er and ^{179}Lu by the reactions $^{170}Er(n,\gamma)^{171}Er$ and $^{179}Hf(n,p)^{179}Lu$ are ruled out as could be expected from the target impurity analyses in which Hf and heavier rare earths have been found to be absent. The nuclides ^{167}Ho, ^{173}Tm and ^{73}Ga which could result from the nuclear reactions $^{167}Er(n,p)^{167}Ho$, $^{173}Yb(n,p)^{173}Tm$ and successive neutron capture by ^{71}Ga and $^{73}Ge(n,p)^{73}Ga$, respectively, have also been estimated to be negligible under the experimental conditions. In general, the depleted uranyl nitrate targets appeared to have been extremely pure for the purpose of these studies.

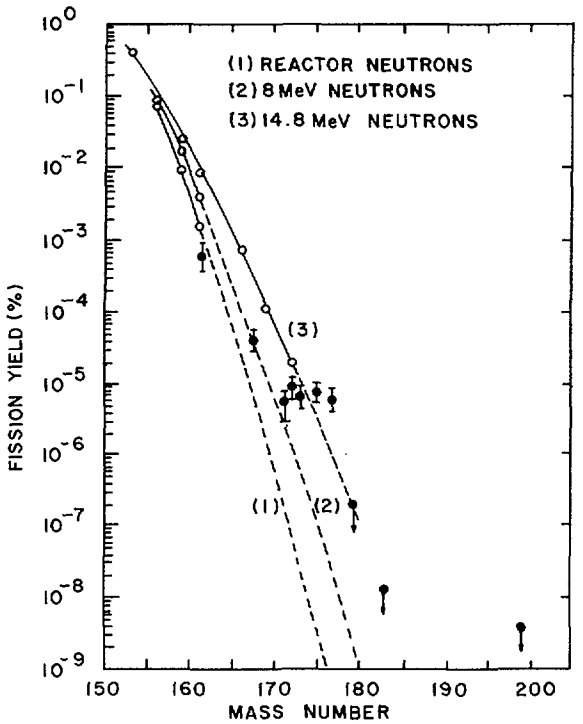

FIG. 4. Low-yield products in the heavier mass region from fission of ^{238}U with neutrons of different energies.

3.2. Features of the mass distribution curve – new shoulders in the low-yield wings

Figure 3 shows the complete experimental mass yield curve for the reactor neutron fission of ^{238}U in the mass range 66–199 using the data from Table I (for the highly asymmetric region) and from the literature [12] (for the mass range 72–161). The dotted portions of the mass yield curve represent computer extrapolations up to A = 60 on the lighter wing and up to A = 180 on the heavier wing portions by assuming a Gaussian distribution of the yields

$$Y = \frac{F}{\sqrt{2\pi}\sigma} \exp\left[-\frac{1}{2}\left(\frac{A-\bar{A}}{\sigma}\right)^2\right] \qquad (3)$$

where σ is the width of the gaussian, F is the normalizing factor and $\bar{A} = 118.18$, on the assumption of a prompt neutron emission of 2.64. The Gaussian width σ

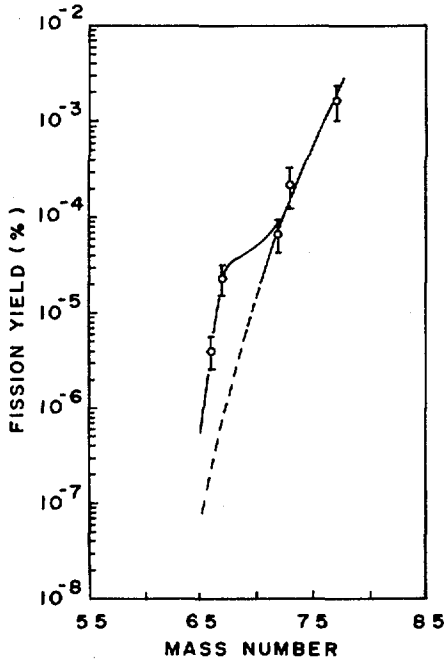

FIG.5a. Mass distribution in lighter wing in the fission of ^{238}U by reactor neutrons.

was found to depend critically on the range of mass numbers used in the calculation. The extrapolations in Fig.3 were made by using mass yield data [12] for A = 155 − 161 on the heavier side and for A = 83 − 72 on the lighter side. These mass numbers lie in the vicinity of the highly asymmetric mass regions we are concerned with in the present studies.

For an understanding of the energy dependence of the yields of very asymmetric products in the fission of ^{238}U induced by neutrons of different energies, the present data have been compared with the data of Nethaway [13] on A ⩾ 160 in the 14-MeV-neutron-induced fission of ^{238}U as well as with other data up to A = 161 available in the literature [12]. This is illustrated in Fig.4, where the dotted portions are computer extrapolations. It is evident from this figure that the yields of very asymmetric products are sensitive to the excitation energy of the compound nucleus, a trend well established in the case of symmetric fission. The yields measured by us for mass chains A = 161, 167, 171, 172, 173, 175 and 177 follow the general trend although they are a few orders of magnitude higher than the corresponding computed values as seen from the figure. The same

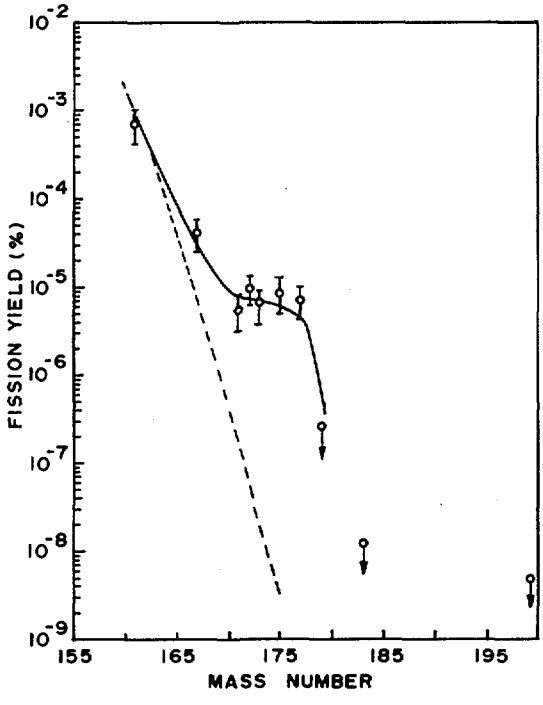

FIG.5b. Mass distribution in heavier wing in the fission of ^{238}U by reactor neutrons.

trend holds good in the lighter wing, too. This tendency for the yields to increase with increasing asymmetry of the mass division at a given excitation energy of the compound nucleus (e.g. reactor neutron fission of ^{238}U), however, does not continue infinitely as can be seen from the upper limits reported by us for mass chains 179, 183 and 199. This is more evident from Figs 5a and 5b in which the yields of highly asymmetric products obtained in the present studies are plotted separately for the lighter and heavier wing portions, respectively.

A perusal of the results shown in Figs 3 – 5 reveals the following trends in the highly asymmetric mass distribution:

(i) The yields for mass chains 66 – 67 on the lighter side and 171 – 177 on the heavier side are nearly three orders of magnitude higher than the computed values and this large increase is beyond experimental uncertainties. (ii) The tendency for the yields to increase does not continue beyond A = 177. Thus, in the wing portions of the mass yield curve the yields first decrease smoothly, then show a slight increase around A = 66 – 67 and A = 171 – 177 and again show a

fall. These observations lead us to believe that there are 'shoulders' or 'bumps' in the low-yield wings of the mass yield curve. This is the first experimental observation of new shoulders in the low-energy fission of ^{238}U. Very recently observation of similar shoulders have been reported from Duke University in the fission of $^{235,236}Np$ [14].

3.3. Plausible explanations for the occurrence of shoulders

Various plausible explanations for the occurrence of these new shoulders in low-energy fission may be considered such as a) effect of the 28-proton shell [3, 5]; b) influence of deformed heavy fragment shells [6] and c) emission of heavy-ion clusters [4].

The familiar asymmetric mass devision, fixation of the position of the heavier peak and the observation of 'spikes' in the mass distribution curve, etc. are best understood in terms of the influence of the 82-neutron shell in fission. There is a 28-proton shell in the region $A \sim 66-67$, where the yields of ^{66}Ni and ^{67}Cu (the only nuclides with convenient chemical and nuclear properties which were amenable to experimental measurements) are found to be higher than expected giving rise to a 'shoulder' in this region. We attribute this 'shoulder' to the influence of the 28-proton shell which forces the yields in this region to be higher than normal in much the same way as the 82-neutron shell forces the yields to be higher around $A = 132$. The shoulder on the heavier wing around $A = 171 - 177$ is considered to be complementary to the one on the lighter wing. This seems justified since we estimated neutron emission in far asymmetric splits ($A_L \sim 66 - 67$ and $A_H \sim 171 - 177$) to be negligible [3, 15]. Further, it appears that the influence of the 28-proton shell is much weaker than that of the 82-neutron shell.

If we assume that shell effects (28-proton) are responsible for the observed shoulders in the fast fission of ^{238}U, then this fact, coupled with the strong energy dependence of very asymmetric fission, enables us to make some interesting speculations concerning fission mass distributions. For example, whereas shell effects are best preserved at lower excitation energy (e.g. thermal neutron fission of heavy elements) the sharp decrease in yields of highly asymmetric products (Fig.4) with decrease in excitation energy of the compound nucleus would make experimental measurement of yields and observation of 'shoulders' difficult. In fact, none of the very asymmetric products isolated in the fast fission of ^{238}U could be detected in the thermal-neutron fission of ^{235}U (Table I). On the other hand, at higher excitation energies, say in the 14-MeV neutron fission of ^{238}U [13] even though the yields of very asymmetric products are higher and easily measurable, it is possible that the weak 28-proton-shell effect gets washed off resulting in the disappearance of 'shoulders'. This is illustrated in Fig.6, where the yield values shown are only order-of-magnitude estimates derived from the

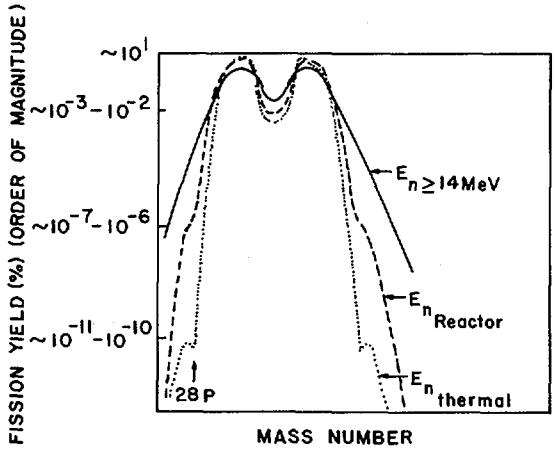

FIG. 6. Effect of neutron energy in fission mass distribution.

known trends in fission yields. Thus, for reactor-neutron-induced fission of ^{238}U which lies between thermal-neutron fission of ^{235}U and 14-MeV neutron fission of ^{238}U with respect to the excitation energy of the compound nucleus, we clearly observe the influence of both the 82-neutron and the 28-proton shells. Figure 7 shows an extension of this idea where we indicate the possibility of the influence of the 82-proton core on fission mass distribution giving rise to additional shoulders at A ~ 208 and the complementary product at A ~ 30. The values of yields shown are only order-of-magnitude estimates, based on the variation of yields with asymmetry of mass division. Experimental measurements and observation of these new shoulders in actinide isotopes would be extremely difficult. It may, perhaps, be possible to observe such shoulders in the fission of very heavy and super-heavy nuclei where, because of the general broadening of the mass yield curve with increasing mass number of the fissioning nucleus [16], the yields of extremely asymmetric products are expected to be significant and measurable.

Theoretical support for these observations has recently become available from the fragmentation potential calculations of Greiner et al. [17 – 20]. These calculations are available for ^{226}Ra, ^{235}U and ^{258}Fm and, very recently, for ^{238}U and ^{252}No [5]. New mass asymmetry valleys are shown to appear in the fragmentation potential $V(\ell,\eta)$ as a function of length, ℓ (elongation of the compound nucleus) and the mass asymmetry co-ordinate $\eta = (A_1 - A_2)/(A_1 + A_2)$, where A_1 and A_2 represent the mass numbers of the two fragments. The new valleys arise owing to the correct treatment of shell corrections such that for separated fragments the shell corrections equal the sum of the shell corrections of the

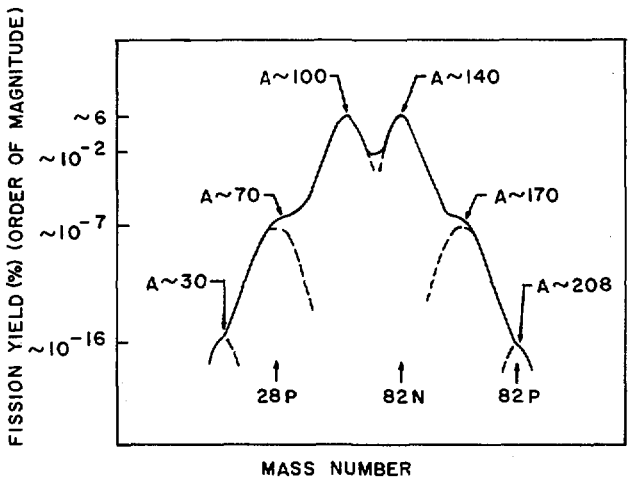

FIG. 7. Possible influence of the nucleon shells (28 P, 82 N, 82 P) in fission mass distribution.

individual fragments. New minima in the fragmentation potential are shown to appear in the case of ^{238}U [5] because of the shell corrections for the smaller fragment with Z = 28, and N = 50 or Z = N = 28. These minima in the fragmentation potential appear as shoulders in the mass distribution curve and in the case of ^{238}U the predicted positions of the shoulders agree well with the experiment although the calculated and measured yield values are significantly different.

In another calculation [21] for the fission of ^{236}U, additional peaks in the mass distribution were predicted arising from the dynamical effects of collective friction while running down the potential barrier.

Wilkins et al. [6] have, from considerations of deformation stiffness, suggested that the heavy fragment resulting from a highly asymmetric split will be highly deformed whereas the lighter fragment will tend to be close to spherical. Based on a static scission point model Wilkins et al. predict new deformed shells corresponding to N = 66, 88, 106, etc. and Z = 38, 44, 66, etc. The deformed shells at N = 106 (deformation parameter = 0.8) and at Z = 66 (deformation parameter = 1.0) which are of interest in our present studies are shown to add coherently to lower the potential energy of the total system, thereby enhancing the yields in the mass region around A ~ 172. The increase in the yield on the lighter side A ~ 66 – 67 is considered to be a reflection of the one on the heavier side.

In a recent communication [4], de Carvalho et al. reported experimental evidence for the emission of heavy ions in the mass range 20 – 70 in the spontaneous and low-energy-photon-induced fussion of ^{238}U. These are based

on the observation of short-range tracks (different from spontaneous binary fission and alpha tracks) in nuclear emulsion loaded with uranium. Such spontaneous emission of heavy ions which are less massive than ordinary fission fragments, if they occur independently of the usual binary fission, should give rise to complementary, very heavy fragments resulting in additional 'shoulders' similar to what we have observed in the fast-neutron fission of ^{238}U.

4. CONCLUSIONS

To sum up, the first experimental evidence for the occurrence of new shoulders in the highly asymmetric binary fission of ^{238}U can be attributed to various possibilities such as the possible influence of the 28-proton shell in fission, the influence of nucleonic shells in the deformed heavier fragments or an altogether new possibility of emission of heavy ions from an excited nucleus. It is speculated that for very heavy and super-heavy nuclei, very asymmetric binary fission may be a new decaying mode [5]. More experimental work is needed to understand and further pin down this interesting mode of fission.

5. SUGGESTIONS FOR FUTURE EXPERIMENTS

Several factors such as availability of extremely high-purity actinide isotopes in sufficient quantities (tens of milligrams) as target materials, availability of low-energy, high-flux ($\sim 10^{12}$ n $\cdot$ cm^{-2} $\cdot$ s^{-1}) and monoenergetic neutrons, etc. need to be considered in designing future experiments. From a consideration of the strong dependence of very asymmetric fission on the excitation energy of the compound nucleus vis-à-vis the nucleonic shell effects in fission, it appears that a neutron energy in the range $1 - 4$ MeV is most ideal. Similarly, studies on the spontaneous fission of ^{252}Cf appear particularly attractive since the system has sufficiently high Z ($Z = 98$) and lowest excitation energy. It also satisfies the important criterion of eliminating the problem of activation of impurities since the recoiling fission fragments can be conveniently collected in a catcher foil and separated radiochemically. Some indications of increased yields in the high-mass region ($A \geqslant 161$) already exist in the published work of Nervik [22] on spontaneous fission of ^{252}Cf. A careful radiochemical re-investigation using a strong ^{252}Cf source of about 100 μg is desirable to obtain further evidence for the existence of the highly asymmetric fission mode in this system. Studies on ^{232}Th(n,f) or ^{244}Pu(n,f) in which the N/Z ratio is similar to the ratio of fragment shells $N = 106$ and $Z = 66$ can resolve the problem of the role of deformed shells on highly asymmetric fission. Thermal neutron fission of ^{239}Pu also appears to be an interesting case from the following considerations: a) Pronounced shell

effects leading to the occurrence of shoulders are expected in thermal fission; b) because of the higher mass number compared to ^{235}U, the mass distribution is expected to be broader and the yields in the high-mass region ($A > 160$) are expected to be higher, making measurements feasible; c) higher fission cross-section of ^{239}Pu compared to ^{235}U and the absence of ^{239}Np as an activation impurity (as in the case of ^{238}U) make separation and purification of heavier rare earths easier. At present, experiments are underway in our laboratory on the determination of the yields of very asymmetric products in the thermal-neutron fission of ^{239}Pu.

ACKNOWLEDGEMENT

The authors are thankful to Dr. M.V. Ramaniah, Director, Radiological Group, BARC, for his interest and encouragement during the course of this work.

Appendix

RADIOCHEMICAL SEPARATION PROCEDURES

A brief summary of the radiochemical procedures employed in these studies is given below:

(A) Separation of heavier rare earths: A new radiochemical separation scheme for the separation of rare earths from fission products was developed [8]. Additional anion exchange separation steps were incorporated for the separation of ^{239}Np. Individual rare earths could be separated by using two cation exchange operations using NTA (nitrilo triacetic acid) and α-HIBA (alpha hydroxy isobutyric acid) as eluants.

(B) Nickel: ^{66}Ni was separated by using the standard radiochemical procedure involving extraction of the Ni-dimethyl-glyoxime complex into chloroform.

(C) Copper: ^{67}Cu was separated by extracting Cu-diethyl dithio carbamate (Cu-DDC) complex into n-butyl acetate at pH 8.5. Copper was finally precipitated as Cu-alpha benzoin oxime complex for mounting.

(D) Zinc: ^{72}Zn was separated along with copper as Zn – DDC complex. Selective stripping of Zn was accomplished with 0.16M HCl. Zn was finally precipitated as $Zn(NH)_4PO_4$, in which form it was mounted and counted.

(E) Gallium: ^{73}Ga was separated by extracting with diisopropyl ketone in 6M HCl. Gallium was stripped back at pH 5–6. Finally, Ga was precipitated and mounted as the oxinate.

(F) Arsenic: ^{77}As was separated by standard radiochemical procedure in which As_2S_3 was extracted with 50% HIO_3 in $CHCl_3$. The sample was mounted as As_2S_3 for counting.

(G) Tantalum: Ta was precipitated as hydroxide and dissolved in $HF\text{-}HNO_3$ mixture. It was extracted in methyl iso-butyl ketone and back-extracted by fresh dilute H_2O_2 solution. This procedure was repeated 3 – 4 times. Finally, the hydroxide was converted to oxide (Ta_2O_5) by heating in a platinum crucible, in which form it was mounted and counted.

(H) Gold: A radiochemical procedure for the separation of gold from irradiated uranium targets as reported by Iyer et al. [1] was used for the separation of ^{199}Au. $AuCl_4$ was extracted repeatedly with ethyl acetate. Gold was finally reduced to metallic form and mounted for counting.

REFERENCES

[1] IYER, R.H., COBBLE, J.W., Phys. Rev. **172** (1968) 1186.
[2] RAO, V.K., BHARGAVA, V.K., MARATHE, S.G., SAHAKUNDU, S.M., IYER, R.H., Phys. Rev. C **9** (1974) 1506.
[3] RAO, V.K., BHARGAVA, V.K., MARATHE, S.G., SAHAKUNDU, S.M., IYER, R.H., Phys. Rev. C (1979) to be published.
[4] de CARVALHO, H.G., MARTINS, J.B., TAVARES, O.A.P., Centro Brasileiro de Pesquisas Fisicas, Rio de Janeiro, Brazil, Rep. A 0025/77 (1977).
[5] SANDULESCU, A., LUSTIG, H.J., HAHN, J., GREINER, W., J. Phys. G. Nucl. Phys. **4** 11 (1978) 279.
[6] WILKINS, B.D., STEINBERG, E.P., CHASMAN, R.R., Phys. Rev. C **14** (1976) 1832.
[7] FLYNN, K., Argonne National Laboratory Report No. ANL-75-24 (1975).
[8] BHARGAVA, V.K., RAO, V.K., MARATHE, S.G., SAHAKUNDU, S.M., IYER, R.H., J. Radioanal. Chem. **47** (1978) 5.
[9] SAHAKUNDU, S.M., MARATHE, S.G., BHARGAVA, V.K., RAO, V.K., IYER, R.H., J. Radioanal. Chem. **13** (1973) 37.
[10] WAHL, A.C., NORRIS, A.E., ROUSE, R.A., WILLIAMS, J.C., in Physics and Chemistry of Fission (Proc. 2nd Int. Symp. Vienna, 1969), IAEA, Vienna (1969) 813.
[11] ALLEV, A.I., et al., Handbook of Nuclear Data for Neutron Activation Analysis, Israel Program for Scientific Translation, Jerusalem (1970).
[12] FLYNN, K.F., GLENDENIN, L.E., Argonne National Laboratory Report No. ANAL-7749 (1970).
[13] NETHAWAY, D.R., MENDOZA, B., VOSS, T.E., Phys. Rev. **182** (1969) 1251.
[14] EPHERSON, D.H., Ph. D. Thesis, Duke University (1978).

[15] MACMURDO, K.W., COBBLE, J.W., Phys. Rev. **182** (1969) 1303.
[16] HYDE, E.K., Nuclear Properties of Heavy Elements, Fission Phenomena, Vol.3, Prentice Hall, Englewood Cliffs, New Jersey (1964).
[17] MARUHN, J., GREINER, W., Phys. Rev. Lett. **32** (1974) 548.
[18] GUPTA, R.K., SCHEID, W., GREINER, W., Phys. Rev. Lett. **35** (1975) 353.
[19] GUPTA, R.K., Particles and Nucleus **8** (1977) 4.
[20] GUPTA, R.K., Z. Phys. A **281** (1977) 159.
[21] MARUHN, J., GREINER, W., Phys. Rev. C **13** (1976) 2404.
[22] NERVIK, N.E., Phys. Rev. **119** (1960) 1685.

DISCUSSION

M. ASGHAR: What is the reason for the absence of shoulders in the yield curve for ^{235}U? I feel it cannot be the excitation energy that is at fault.

R.H. IYER: I think it is mainly due to the excitation energy dependence of the highly asymmetric products that I discussed in detail.

FISSION OF LIGHT AND MEDIUM-HEAVY NUCLEI INDUCED BY 600-MeV PROTONS

G. ANDERSSON, M. ARESKOUG, H.-Å. GUSTAFSSON,
G. HYLTEN, B. SCHRØDER
Department of Physics, University of Lund,
and
Department of Nuclear Physics, Lund Institute of Technology,
Lund, Sweden

E. HAGEBØ
Department of Chemistry, University of Oslo,
Oslo, Norway

Abstract

FISSION OF LIGHT AND MEDIUM-HEAVY NUCLEI INDUCED BY 600-MeV PROTONS.

The fission of ^{89}Y, $^{121,123}Sb$ and ^{139}La induced by 600-MeV protons is studied with the double-kinetic-energy method. The binary character of the process is demonstrated for Y with an in-plane angular-correlation curve. The total kinetic energies at symmetric mass division are corrected for the effects of neutron evaporation after fission and found to be in good agreement with Viola's empirical relationship. For La, strong indications of a stable asymmetric mass distribution are observed, which can be explained from similar arguments as those used for the actinides. In the investigated mass range, i.e. masses at and above Y, no indication is found of the Businaro-Gallone limit expected to occur somewhere in the mass range A = 100 to A = 140.

1 INTRODUCTION

Various macroscopic models are used in connection with the interpretation of fission phenomena. Some of the energy terms in these models are shape-dependent and the associated constants are partly determined from fits to experimentally obtained fission barrier heights for nuclei in a mass range around A=200. Macroscopic fission barrier heights calculated with the models [1-4] agree in that mass range for obvious reasons; however, for medium-heavy and light nuclei the predictions disagree. For a given nucleus the calculated barrier heights may differ as much as 10-15 MeV. The models agree, however, perfectly on the value of x_{BG}, the critical Businaro-Gallone limit [5], defined as

the value of the fissility parameter x below which the symmetric saddle point goes unstable against the mass-asymmetry coordinate. Due to differences in the evaluation of x the Businaro-Gallone point is predicted to appear somewhere in the mass range A=100 [1-3] to A=140 [4]. A dramatic change in the fragment mass distribution, from symmetric to highly asymmetric, is expected when approaching and passing the critical mass value as shown by the calculations of ref. [6].

In a series of experiments we have studied the fission process in medium-heavy and light nuclei using 600 MeV protons as bombarding particles. The goal of these investigations was to collect experimental data relevant to the answering of the questions: 1) How does the fission barrier height vary for medium-heavy and light elements and 2) does the critical Businaro-Gallone limit exist, if so where is it located. In the present paper we will mainly concentrate on the second of these questions and discuss the properties of fission products from fission induced in La, Sb and Y. We have earlier found that La has fission characteristics differing from those shown by other medium-heavy nuclei [7-9]. Both the width and shape of the mass distribution indicated the possibility of a stable asymmetric mass division for La [8], whereas the mass distributions of the other investigated nuclei were symmetric and gaussian shaped as expected from liquid drop model calculations [6]. Below we will present new data for La obtained in order to investigate these questions further.

The lightest element studied earlier was Ag [7,8] close to or below the calculated location of the Businaro-Gallone point [1-4]. Due to the wide mass distribution obtained for La it was difficult to outrule the location of x_{BG} corresponding to A=100 although we for Ag observed a value of the $FWHM_A$ (full width at half maximum height of the mass distribution) a factor of about 3 lower than calculated in ref. [6]. The elements Sb and Y were included in the new measurements in order to obtain further experimental data points below La.

2 EXPERIMENTAL PROCEDURE

The experiment was performed at the CERN synchro-cyclotron. Thin samples of La, Sb and Y, all of natural composition, were irradia-

TABLE I. SAMPLE CHARACTERISTICS

Element	$^{89}_{39}Y$	$^{121,123}_{51}Sb$	$^{139}_{57}La$
Thickness ($\mu g/cm^2$)[a]	124	233	155
Major impurities (ng/cm^2)[b]	Fe 8.1 Ca 34 Cl 36 S 213	Fe <2.0 Cu <2.0	Ta 302

[a] The error in the thickness determination is 8%.

[b] The detection limit is typically 2 ng/cm^2.

ted with 600 MeV protons with beam intensities of 20-50 nA and a duty factor of about 0.5.

Samples were fabricated by vacuumevaporation of LaF_3, metallic Sb and metallic Y on 40$\mu g/cm^2$ thick carbon foils. The thicknesses and major impurities were determined using the PIXE-method [10], see Table I. The 0.2 % impurity of Ta in the La sample originates from the Ta-boat used in the evaporation. From the fission cross sections of La and Ta [7,9] it is estimated that about 4 % of the events collected in the case of the La sample will be caused by fission induced in Ta. The majority of these events was excluded on the basis of the larger total kinetic energy release for Ta compared to La.

Samples and detectors were placed in a vacuum scattering chamber during irradiations. Coincidences were measured with two detector arms. One arm was kept fixed at 90° with respect to the incoming proton beam, the other moved in-plane to the desired position.

The arm fixed at 90° contained a transmission start detector and a Si surface barrier stop detector. The time-of-flight distance was 12.9 cm. The transmission detector consisted of a 20 $\mu g/cm^2$ carbon foil, placed at 45° with respect to the time-of-flight path, viewed by two channel electron multiplier plates (CEMP) [11]. On the passage of a heavy ion electrons are emitted from the carbon foil, and these are partly collected on the CEMP-detector resulting in an amplification of about 10^8.

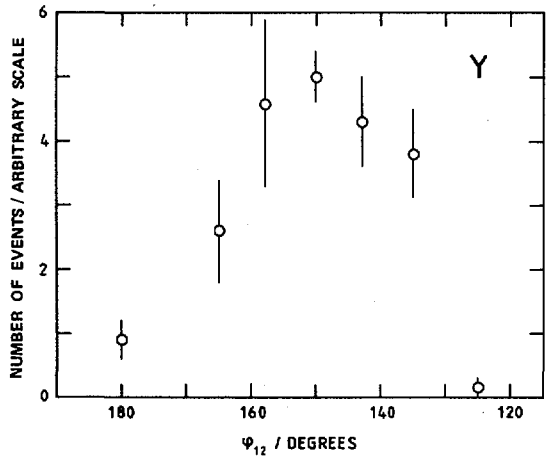

FIG.1. Fission product angular correlation with detector 1 fixed at 90° with respect to the incoming proton beam. The in-plane angular-correlation curve shown was obtained for Y.

With a source of ^{252}Cf the efficiency was found better than 95 % for fission fragments and the time resolution around 0.8 ns.

On the moveable arm a gasionization chamber [12] was placed. It consisted of 9.4 cm of 90% Ar- 10% CH_4 gas at a pressure of 20 torr for energy loss measurements. Inside the chamber a Si surface barrier detector was used for residual energy measurements. The entrance window, dia. 20 mm, was a 20 $\mu g/cm^2$ thick plastic foil supported by a Ni mesh with 97% open area. The purpose of the gasionization chamber was to eliminate a large proportion of the background events from the analysis. The Si detectors and the gasionization chamber were energy-calibrated with alpha-particles and fission fragments from a thin ^{252}Cf source.

For each coincident event, i.e. with signals above 5 MeV in both Si-detectors within 100 ns, we registered on tape event by event two energy signals (Si-detectors), one energy loss signal from the gasionization chamber and three time-of-flight signals. These latter were measures of the time differences between the start detector and each Si-detector and between the two Si-detectors. Under beam-conditions the time resolution was deteriorated from 0.8 ns to about 2 ns which prevented any accurate velocity measurements. The time information obtained

TABLE II. SUMMARY OF EXPERIMENTAL RESULTS

Element	Y	Sb	La
Number of events analysed	128	81	267
$\langle T_{tot} \rangle_{sym}$ (MeV)[a]	46.5	69.6	77.7
$\sigma\langle T_{tot} \rangle_{sym}$ (MeV)	8.3	9.3	11.0
$FWHM_{T_{tot}}$ (MeV)	30±3	20±3	30±3

[a] Uncorrected for the effects of neutron evaporation.

TABLE III. CALCULATED FISSION CHARACTERISTICS

Element	Y	Sb	La
A_F	82	114	130
Z_F	38	49	55
$\langle E_{tot} \rangle_{sym}$ (MeV)[a]	56.8	82.5	88.6

[a] Corrected for the effects of neutron evaporation.

was merely used in the off-line analysis to reduce the coincidence window to around 2 ns. The experiment is thus to be characterized as a double-kinetic-energy measurement.

3 RESULTS

The kinetic energies of coincident fission products were determined from the surface barrier and gasionization detector amplitudes

using the calibration procedure suggested by Kaufman et al. [13]. Energy losses in sample, backing and transmission detector, typically 2-5 MeV for each product, were corrected for using electronic and nuclear stopping power data according to the formalism of Münzel [14]. The in-plane angular correlation curve for Y is shown in Fig. 1 which gives the relative coincidence rate as a function of the angle between the two detector arms. The occurence of a coincident event was determined from the measured times-of-flight and the energy loss in the gasionization chamber. Similar angular correlation curves have been obtained for Ag, La and Tb [15].

From the single product kinetic energies of complementary products, E_1 and E_2, the masses were obtained from the approximate relation

$$M_1 = A_F \, E_2 \, / \, T_{tot} \qquad (1)$$

where A_F is the estimated mass of the fissioning nucleus (see Table III) and $T_{tot}=E_1+E_2$ the total kinetic energy in the center of mass system. The distributions of the relative masses $U=M_1/A_F$ are shown for La in Fig. 2 and for Y and Sb in Fig. 3. According to ref. [16] the mass resolution in double-kinetic-energy measurements may be obtained from the variances observed for E_1 and E_2. The mass resolution for U (one standard deviation) is estimated to be 0.11 for Y, 0.08 for Sb and 0.07 for La.

A summary of kinetic energy results is presented in Table II. The values of $\langle T_{tot} \rangle_{sym}$ and $\sigma\langle T_{tot} \rangle_{sym}$ apply to symmetric mass divisions. We estimate the energy resolution in the experiment to be 2.5 MeV taking into account uncertainties connected with energy loss corrections and the calibration procedure.

4 DISCUSSION

In the case of fission induced by 600 MeV protons the reaction is considered to be devided into two steps. First the fast intranuclear cascade resulting in cascade residuals with broad distributions in excitation energy, imparted linear and angular momenta, mass and charge [17], followed by the slow evaporation step in which fission may compete. Fission-spallation competition calculations were performed for Ag, La and

Tb [15] the results of which were used in the present work to estimate the properties of the fissioning nuclei (see Table III). The average value of the imparted angular momentum turns out to be about 10 ħ with a standard deviation around 10 ħ.

4.1. Angular correlations

The in-plane angular correlation curve for Y shown in Fig. 1 reflects the influence of experimental conditions, reaction steps prior to fission and the fission process itself. The shift in the position of the center of gravity from 180^{o} is caused by the in the cascade imparted linear momentum. An analysis of the contributions to the width of the angular correlation curve [18] indicates that the width is mainly determined by experimental conditions and the distribution of momenta imparted in the cascade. Evaporation before and after fission has only a minor influence on the width.

4.2. Kinetic energy release

The total kinetic energy values at symmetric mass divisions $<T_{tot}>_{sym}$ (see Table II) were corrected for the effects of neutron evaporation after fission following the procedure of ref. [19]. The corrected value is obtained from the relation

$$E_{tot} = T_{tot} \, (1 + E_F \, / \, \{ \, 12.5 \, A_F \, \} \,) \qquad (2)$$

where E_F is the estimated excitation energy of the fissioning nucleus. The relation is an approximation of the expression given in ref. [19], however, sufficiently accurate for our purposes. In the fission-spallation competition calculations on Ag, La and Tb [15] we found values of E_F around 200 MeV and this value was also used in the present work.

The values of $<E_{tot}>_{sym}$ at symmetric mass divisions for Y, Ag, Sb, La and Tb are compared to calculated values in Fig. 4. The experimental points are in good agreement with the empirical relation of Viola [20]. The two macroscopic model calculations [4,6] are approximately 10 MeV below the experimental data points. Other experimental investigations of the total kinetic energy release in the fission of medium-heavy and light nuclei also favour the Viola's empirical relation [21-23].

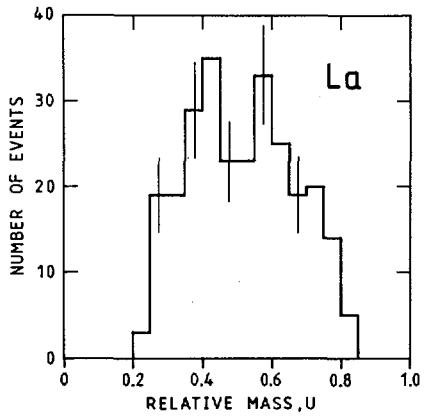

FIG.2. The distribution of relative mass U obtained in the fission induced by 600-MeV protons in La.

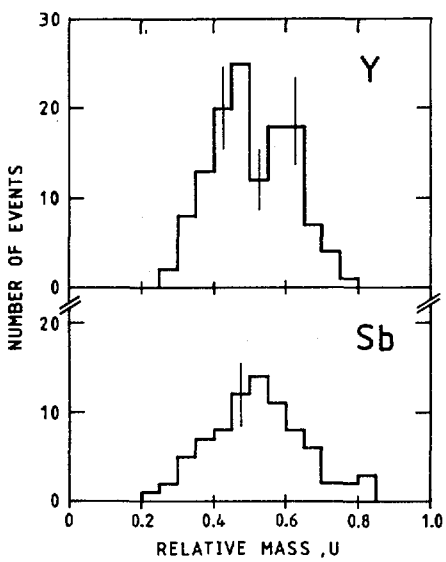

FIG.3. The distributions of relative mass U obtained for Y and Sb.

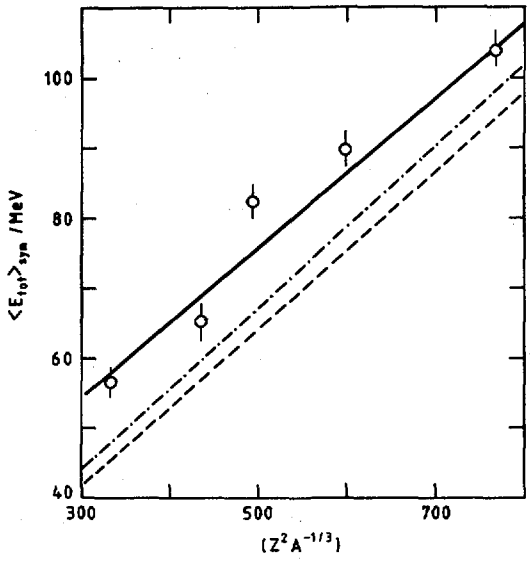

FIG.4. The experimental values of the total kinetic energy release $\langle E_{tot}\rangle_{sym}$ at symmetric mass division corrected for the effects of neutron evaporation after fission compared to calculated values. The curves are:
1) The empirical relationship of Viola [20] *given by $E_{tot} = 0.1071Z^2/A^{1/3} + 22.2$ (solid line),*
2) the liquid-drop-model calculation of Nix [6] *(dashed line), and*
3) the prediction of Krappe and Nix [4] *with a friction coefficient $\mu = 0.02$ TP (dash-dot line).*

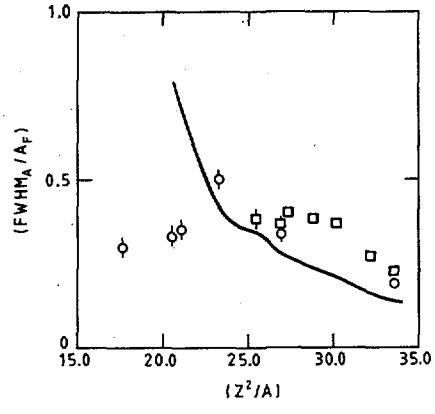

FIG.5. Experimental values of the relative width of the mass distribution in fission of medium-heavy and light nuclei induced by 600-MeV protons (present work, circles) and 1-GeV protons ([9], *squares). The solid curve is calculated with the formalism of Ref.* [6] *with the critical Businaro-Gallone limit located at Z^2/A around 20.*

4.3. Mass distributions

The mass distributions obtained are shown in Figs. 2 and 3 for La and for Y and Sb, respectively. In the case of La there is a clear indication of a stable asymmetric mass division. For Sb and Y symmetric shapes seem appropriate, the low value observed for Y in the interval 0.5 to 0.55 is caused by the bin division used. In fig. 5 the values of $FWHM_A/A_F$ are shown versus the parameter Z^2/A. This figure thus displayes the observed width of the mass distributions relative to the maximum possible widths. We have included data obtained at Gatchina [9] with 1 GeV protons. Apart from La the values of $FWHM_A/A_F$ are rather constant in sharp contrast to the liquid drop model prediction (solid curve). This curve was calculated as described in ref. [8] using the formalism of Nix [6]. The steep rise observed is connected with the location of the critical Businaro-Gallone point close to Ag (Z^2/A approximately 20). From the behaviour of the experimental data we may thus conclude that we have seen no sign of the Businaro-Gallone limit, although the lightest element investigated (Y) is well below the limit predicted by macroscopic theories.

The width and shape of the mass distribution for La suggest that for this nucleus the mass distribution is influenced by shell effects. Such effects, either at the saddle point [24] or at the scission point [25], are found to cause the stable asymmetric mass distributions observed in the actinide region. The shell effects are known to disappear when the excitation energy of the fissioning nucleus is increased, and at bombarding energies around 100 MeV the shell effects are normally completely washed out. For medium-heavy and light nuclei excitation energies around 200 MeV seems appropriate and one would expect shell effects to be uneffective in the fission process of these nuclei. The stiffness against mass-asymmetric deformations [6] is much lower for La than for the actinides and one would expect medium-heavy nuclei to be softer to this type of deformations. This could extend the excitation energy range in which shell effects can survive. For medium-heavy nuclei the saddle- and scission point configurations are expected to be close [6] and shell effects in the fragments could be the reason for the observed mass distribution. The excitation energy of the fragments is estimated to 100 MeV.

Recently Johansson [26] suggested an interesting explanation to the possible mass asymmetry for La. In ref. [27] he calculated the stability of heavy nuclei against an octupole deformation and found certain regions very soft to this deformation. For elongated shapes stable octupole deformations was found. For the actinides a linear relationship was established between the mass ratio of the fission fragments and the degree of octupole deformation at the saddle point. The asymmetric mass distribution in the actinide region was found to be correlated with the occurence of special levels in the employed Nilsson level diagram [28]. Johansson observed that these levels, of opposite parity obeying certain selection rules, show a periodic shell effect and suggested that the mass asymmetry might also show this shell effect. Thus mass asymmetry was expected to appear around proton number 72 [27] and a very preliminary study shows that the neutron number 78 seems to favour asymmetric fission [26]. A close examination of the results from Gatchina [9,29] shows that the mass distribution obtained for W (proton number 74) is indeed similar to those observed for moderatly excited nuclei in the actinide region.

Turning to La the explanation suggested by Johansson [26,27] could imply that for neutron numbers close to 78 there will be two asymmetric valleys with deformation energies below that of the symmetric path. The exact location in deformation space is not known at present. The crucial influence of neutron number 78 could explain why Plasil et al. [21] did not observe any mass asymmetry in the fission induced by ^{20}Ne in ^{107}Ag. In this case the value of $FWHM_A/A_F$ is close to 0.3 in agreement with the values shown in Fig. 5. The maximum neutron number is in this case 70, however, well below the important value 78.

We may thus conclude that the explanation briefly described above is quite promising and quantitative calculations will be performed following these ideas. The mechanism behind the survival of shell effects to the high excitation energies expected in the fission of medium-heavy and light nuclei is, however, not understood at present.

ACKNOWLEDGEMENTS

The authors are indebted to S.A.E. Johansson, P. Möller and S.G. Nilsson for helpful discussions. We thank B. Sundqvist for pro-

viding the thin plastic windows used in the gasionization chamber. We are indebted to the CERN synchro-cyclotron staff for the excellent beam quality achieved. The work has been supported by the Swedish Natural Science Research Council and in part by the Norwegian Research Council for Science and the Humanities.

REFERENCES

[1] MYERS,W.D.,SWIATECKI,W.J., Ark. Fys. 36(1967)343.
[2] MYERS,W.D.,SWIATECKI,W.J., Ann. Phys. (New York) 84(1974)186.
[3] MYERS,W.D., Nucl. Data Tables 17(1976)411.
[4] KRAPPE,H.J.,NIX,J.R., Physics and Chemistry of Fission (Proc. Symp. Rochester, 1973) 1, IAEA,Vienna(1974)159.
[5] BUSINARO,U.L.,GALLONE,S., Nuovo Cim. 1(1955)629.
[6] NIX,J.R., Nucl. Phys. A130(1969)241.
[7] ANDERSSON,G.,et al., Phys. Letters 64B(1976)421.
[8] ANDERSSON,G.,et al., Phys. Letters 71B(1977)279.
[9] SEMENCHUK,G.G.,et al., Phys. Letters 69B(1977)49.
[10] JOHANSSON,T.B.,AKSELSSON,R.,JOHANSSON,S.A.E., Nucl. Instr. and Meth. 84(1970)141.
[11] GABOR,G.,et al., Nucl. Instr. and Meth. 130(1975)65.
[12] FOWLER,M.M.,JARED,R.C., Nucl. Instr. and Meth. 124(1975)341.
[13] KAUFMAN,S.B.,et al., Nucl. Instr. and Meth. 115(1974)47.
[14] MÜNZEL,H., Methodik und Ergebnisse radiochemischer Reichweite-Untersuchungen, Kernforschungszentrum Karlsruhe Rep. KFK 693 (1967).
[15] ANDERSSON,G.,et al., submitted to Nucl. Phys.
[16] BOHN,E.M.,et al., Nucl. Instr. and Meth. 109(1973)605.
[17] BERTINI,H.W., Phys. Rev. 188(1969)1711.
[18] ANDERSSON,G.,et al., Nucl. Instr. and Meth., in press.
[19] BORDERIE,B.,et al., Nucl. Phys. A220(1974)93.
[20] VIOLA Jr.,V.E., Nucl. Data 1(1966)391.
[21] PLASIL,F.,FERGUSON,R.L.,PLEASONTON,F., Physics and Chemistry of Fission (Proc. Symp. Rochester, 1973) 2, IAEA,Vienna(1974)319.
[22] GELBKE,C.K.,et al., Nucl. Phys. A269(1976)460.
[23] CABOT,C.,et al., Nucl. Phys. A244(1975)134.
[24] MÖLLER,P., Nucl. Phys. A192(1972)529.

[25] WILKINS,B.D.,et al., Phys. Rev. C14(1976)1832.
[26] JOHANSSON,S.A.E., private communication.
[27] JOHANSSON,S.A.E., Nucl. Phys. 22(1961)529.
[28] NILSSON,S.G., Mat. Fys. Medd. Dan. Vid. Selsk. 2916(1955).
[29] KOTOV,A.A.,et al., Sov. J. Nucl. Phys. 20(1975)251.

DISCUSSION

E. CHEIFETZ: You excite your nuclei up to about 600 MeV, though the excitation of the fissioning species itself is not known. Is it possible, do you think, that some 10-15 neutrons are emitted prior to the fissioning, thereby bringing the fissility parameter up by 10-20%, and thus above the Businaro-Gallone point?

B. SCHRØDER: Fission-spallation competition calculations that have been performed for La indicate that some 5-10 nucleons are emitted. I don't think that this will change the Z^2/A value to any extent, since both neutrons and protons are emitted.

H.H. DUHM: In ^{3}He-induced fission on ^{169}Tm at $E_{^3He}$ = 40 MeV we have observed, within the low statistical figure of ~ 600-800 collected fission events, a dip in the mass distribution for symmetric fission, the two peaks being separated by ~ 8-10 mass units.

R.L. FERGUSON: Dr. Schrøder, the Businaro-Gallone point is transformed into a curve with angular momentum and would decrease the fissility parameter value at which the Businaro-Gallone transition occurs. Does your system have enough angular momentum to affect your conclusion?

B. SCHRØDER: Fission-spallation calculations indicate 10 ħ as a mean with a width of 10 ħ.

I.S. GRANT: Were you able to deduce the barriers in these reactions, or were the uncertainties introduced by the evaporation calculation too great?

B. SCHRØDER: Barriers were deduced for La, Ag and Tb. They show that for Tb the liquid-drop barrier has to be reduced to 80% of the theoretical value. For La and Ag the reduction was found to be ~ 65%.

FRAGMENT PROPERTIES AND PARTICLE EMISSION (THEORY)
(Session G)

Chairman

B.G. YANKOV
USSR

ESTIMATE OF ODD-EVEN EFFECTS IN NUCLEAR FISSION

G. SCHÜTTE
University of Heidelberg,
Federal Republic of Germany

Abstract

ESTIMATE OF ODD-EVEN EFFECTS IN NUCLEAR FISSION.

The excitation of a fissioning nucleus during the passage from the saddle to the scission point starting cold at the saddle is described in the framework of the cranking model. Although the single-particle potential is of Nilsson type the model can be expected to give estimates for realistic nuclei because of the structure of the single-particle spectrum. The pairing force is treated in the BCS-formalism. In the first step the Hilbert space is limited to the BCS-ground state and to single and multiple pair excitations. In this space, the time-dependent Schrödinger equation is solved correctly. The non-analytic excitation as a function of the collective deformation velocity is thereby taken care of. The coupling to broken pair states is then taken into account by calculating a decay width for the pair excitations in second-order perturbation theory. Statistical arguments on the coupling-matrix elements are used in this development. From the amount of pair breaking the ratio of even-even and odd-odd fragmentation is estimated. An even fragmentation of the neutrons occurs with a probability of about 0.6.

1. Introduction

During the last conference on nuclear fission in Rochester first numerical calculations in the frame of the cranking model were presented to study the dynamical excitation of a fissioning nucleus on its way from the saddle to the scission point [1] . The basic assumption of the model was a self-consistent time-dependent single-particle potential in which the nucleons are excited by the moving walls and by residual interactions. The self-consistent time dependence was replaced by the dependence on time-dependent deformation parameters. The deformation path $q_i(\alpha)$ in a multidimensional parameter space q_i had to be and will be guessed. The deformation velocity $\dot{\alpha}$ along such a path was determined by conservation of the energy in the mean.

The Hilbert space was limited in these calculations to 2-quasi-particle excitations for the sake of numerical feasibility [2] . Two results must be quoted here: (1) The quasi-adiabatic approximation leading to the Inglis mass parameter fails; (2) pair breaking is weak, even if a residual interaction of about 2 MeV couples the quasi-particle excitations. One reason for the latter result is due to the large derivatives of the single-particle energies with respect to the deformation . Furthermore pair breaking due to the ∂_t -matrix elements is inhibited by both small matrix elements and large energy separation of coupled states (6 MeV) compared to the excitations of pairs (2Δ = 1.5 MeV).

The first result has meanwhile been studied analytically [3, 4]. The complete expansion in powers of the collective velocity has been constructed in ref.[4]. For systems which change their intrinsic structure and which hence exhibit pseudo-crossings the systematic expansion diverges. Pseudo-crossings occur for any known single-particle potential relevant to fission; also, pairing does not result in a convergent series, although the smallest distance ΔE at the pseudo-crossings is increased from a few hundred keV to 1.5 MeV.

Result (2) is used to establish the simple model described in the following subsection in which the residual interaction is neglected. Result (1) shows up again in this model where occupation probabilities are non-analytic functions of the deformation velocity. In section 3 the residual interaction is taken into account by calculating a width of the states of the simple model.

2. Simple Model

For the deformation process the nuclear Hamiltonian is approximated by a time-dependent shell model Hamiltonian plus a pairing force. Hence, the time-dependent Schrödinger equation must be solved:

$$i\dot{\Psi} = \mathcal{H}\Psi = \left(T + \mathcal{U}(\alpha(t)) + V_p\right)\Psi \tag{1}$$

with kinetic energy T, single-particle potential U and pairing force V_p. The pairing force can be treated by the usual Bogoliubov transformation to quasi-particles. In this first step all residual interactions among the quasi-particles are neglected [5]. They are switched on in the next section. Therefore, the Hamiltonian $\mathcal{H}$ is written in terms of quasi-particle creation and annihilation operators α_ν^+ and α_ν:

$$\mathcal{H} = \sum \varepsilon_\nu \left(\alpha_\nu^+ \alpha_\nu + \alpha_{\bar{\nu}}^+ \alpha_{\bar{\nu}}\right) \tag{2}$$

The BCS-energies are given by

$$\varepsilon_\nu = \sqrt{(e_\nu - \lambda)^2 + \Delta^2} \tag{3}$$

with the gap parameter Δ, the chemical potential λ and the single-particle energy e_ν. First, a deforming Nilsson potential is assumed. The changes when going to a realistic potential are discussed in section 5. Of course, for the Hamiltonian (2) equation (1) results still in breaking of pairs due to the ∂_t-matrix elements. However, this effect is suppressed by almost two orders of magnitude as discussed above. Therefore, the Hilbert space is confined in this step to the BCS-ground state and single and multiple pair excitations:

$$|0\rangle \;,\; \alpha_{\bar{\nu}}^+ \alpha_\nu^+ |0\rangle \;, \ldots \tag{4}$$

The index $\bar{\nu}$ denotes the time-reversed state to ν . All these states result in an even-even fragmentation, because the single-particle states φ_ν and $\varphi_{\bar{\nu}}$ have the same spatial density distribution. If the blocking effect is neglected the solution of (1) can be written in the form (for details s. [5]):

$$\Psi_\nu = \prod \left(d_\nu + c_\nu \exp\left(2i \int_0^t \varepsilon_\nu \, d\tau\right) \alpha_{\bar{\nu}}^\dagger \, \alpha_\nu^\dagger \right) |0\rangle \tag{5}$$

if the coefficients d_ν and c_ν fulfil the equation:

$$\dot{c}_\nu = \langle 0 | \partial_t | \bar{\nu}\, \nu \rangle \exp\left(2i \int \varepsilon_\nu \, d\tau\right) d_\nu$$

$$\dot{d}_\nu = -\langle 0 | \partial_t | \bar{\nu}\, \nu \rangle \exp\left(-2i \int \varepsilon_\nu \, d\tau\right) c_\nu \tag{6}$$

There is no coupling between different single-particle indices ν due to the neglect of the blocking effect. If the gap parameter Δ , the chemical potential λ and the derivative e'_ν of the single-particle energy are essentially constant over an interval where the matrix element $\langle 0 | \partial_t | \bar{\nu}\, \nu \rangle$ is large - i.e. the region where the single-particle energy e_ν crosses the Fermi energy - then eqs. (6) are of the Landau--Zener type. The solution for the probability $|c_\nu|^2$ of a pair $\bar{\nu}\,\nu$ being occupied in combination with any other pair is asymptotically

$$|c_\nu|^2 = \exp\left(-\frac{\pi \, \Delta^2}{|\dot{\alpha}\, e'_\nu|}\right) \tag{7}$$

This asymptotic value is essentially attained in an interval $2\Delta/e'_\nu$ beyond the crossing of e_ν with λ . The non-analytic form as function of $\dot{\alpha}$ shows that an expansion in powers of $\dot{\alpha}$ is bound to fail.

3. Residual Coupling to Broken Pairs

In the preceding section the Schrödinger equation has been solved in the restricted Hilbert space of pair excitations. These are denoted by Greek letters in this section. There is, however, residual coupling to the orthogonal space of broken pairs denoted by Latin letters. It is due to residual interactions and the ∂_t -matrix elements. Correspondingly the Schrödinger equation is split into two coupled parts [6]

$$i\,\dot{a}_\nu = \sum \langle \nu | H' | \mu \rangle \exp\left(i \int (E_\nu - E_\mu) d\tau\right) a_\mu + \sum \langle \nu | H' | n \rangle \exp\left(i \int (E_\nu - E_n) d\tau\right) a_n \tag{8a}$$

$$i\,\dot{a}_n = \sum \langle n | H' | \mu \rangle \exp\left(i \int (E_n - E_\mu) d\tau\right) a_\mu + \sum \langle n | H' | m \rangle \exp\left(i \int (E_n - E_m) d\tau\right) a_m \tag{8b}$$

The first line is just the equation in the restricted space. The form of the coupling matrix H' depends on whether a moving or a static adiabatic basis has been used and if there is additional residual interaction not taken into account in the basis. The statistical assumptions of this section may depend on the choice of the basis, but no attempt is made to look into this point. It is plausible that one should put as much coherent and collective motion into the basis as possible. The last term in the set of equations (8b) is neglected, because (1) the amplitudes a_m are small compared to a_μ , and (2) the coupling matrix elements $\langle n|H'|m\rangle$ can be assumed to have random sign. This is due to the complicated nature of the static adiabatic states $|m\rangle$. Also the residual interaction V_r may be assumed to be diagonalized within the subspace $|m\rangle$.

The assumption of a random sign of $\langle n|H'|\nu\rangle$ as a function of n gives

$$\sum_n \langle \nu|H'|n\rangle_t \langle n|H'|\mu\rangle_{t'} \varphi_n^{\nu,\mu} \approx \sum \langle \nu|H'|n\rangle_t \langle n|H'|\nu\rangle \varphi_n^{\nu,\nu} \delta_{\nu,\mu} \tag{9}$$

for any function $\varphi_n^{\nu,\mu}$ which is smooth in n compared to the matrix elements. The indices t and t' denote time arguments of the matrix elements. If the integrated first part of eq. (8b) is inserted into (8a), the function $\varphi_n^{\nu,\nu}$ is just the propagator

$$\varphi_n^{\nu,\nu} = \exp\left(i \int_{t'}^{t} (E_\nu - E_n)\, d\tau\right) \tag{10}$$

By this step a system of integro-differential equations for the a_ν is obtained. Since the matrix elements decrease with increasing energy difference $E_\nu - E_n$ the sum over n in (9) results in a short correlation time t-t' as will be seen below. Therefore, the amplitude $a_\nu(t')$ can be taken out of the integral at time t and a system of differential equations for a_ν is achieved:

$$i\dot{a}_\nu = \sum \langle \nu|H'|\mu\rangle \exp\left(i \int (E_\nu - E_\mu)\, d\tau\right) a_\mu - i\Gamma_\nu a_\nu(t) \tag{11}$$

The decay rate Γ_ν is given by

$$\Gamma_\nu = \int_0^t dt' \sum_n \langle \nu|H'|n\rangle_t \langle n|H'|\nu\rangle_{t'} \exp\left(i \int_{t'}^{t} (E_\nu - E_n)\, d\tau\right) \tag{12}$$

It can be estimated in the following way.

After the state $|\nu\rangle$ is occupied the energy E_ν is a sum of rising BCS-energies of the form (3), because all the corresponding single-particle energies e_ν have crossed the Fermi surface. Consequently, for these times E_ν is a steeply rising function of t with slope β_ν . In contrast, the energies E_n are a sum of rising and falling BCS-energies - or, if the residual interaction has been diagonalized

among the states $|n\rangle$ they are wiggly lines. Therefore, on the average, they may be replaced by constants. Next, the sum over n is converted into an integral over E' with a density of states $\varrho(E')$. The ansatz

$$\varrho(E')\,\langle\nu|H'|E'\rangle_t\,\langle E'|H'|\nu\rangle_{t'} = (V^2\varrho)\exp\left[-\frac{(E'-E_\nu(t))^2}{2D^2}-\frac{(E'-E_\nu(t'))^2}{2D^2}\right] \tag{13}$$

gives then the result

$$\Gamma_\nu = \pi(V^2\varrho)\left[1+\frac{\beta_\nu^2}{D^4}\right]^{-1/2} \tag{14}$$

The expression $V^2\varrho$ reminding of the "spreading width" should be rather independent of the energy and is consequently estimated from low energy data of ref. [2] : V = 0.1 MeV, ϱ = 10 MeV^{-1}. Each BCS-energy entering E_ν has a slope of about 20 MeV as function of α . In the deformed harmonic oscillator potential α is defined in terms of the oscillator constants $\alpha = \omega_\perp/\omega_z$. The velocity $\dot\alpha$ is of the order of 1 MeV. Hence, the slope of an s-pair excitation is β_s = 2s MeV^2. The reach D of the residual coupling is a few MeV (~ 6 MeV). This gives

$$\Gamma_\nu \sim 0.3 \text{ MeV} \tag{15}$$

The result is rather independent of the state ν .

4. Pair Breaking

The probability W of finding the nucleus in a paired state after time t can now be calculated. The pairs $\bar\nu\nu$ are ordered according to the time t_ν when the corresponding single-particle energy e_ν crosses the Fermi energy. The sum of the occupation probability of all single and multiple pair excitations containing pair "1" decays with a rate 2Γ starting at t_1. Analogously the sum of all pair excitations containing pair "2" but not "1" start decaying at time t_2. Hence using average values for $|c_\nu|^2$ and $|d_\nu|^2$ in eq.(5) gives[1]:

$$W = |c|^2\sum_{i=0}^{N-1}|d|^{2i}\,e^{-2\Gamma(t-t_{i+1})} + |d|^{2N} = |c|^2 e^{-2\Gamma(t-t_1)}\,\frac{|d|^{2N}e^{2\Gamma(t-t_1)}-1}{|d|^2 e^{2\Gamma\tau}-1} + |d|^{2N} \tag{16}$$

The interval τ is an average value of $t_{i+1}-t_i$.

---

[1] Formula (3.14) of Ref.[1] and Eq.(5) in the Extended Synopses distributed at the Symposium are erroneous.

During the passage from the saddle to the scission point the pair excitations which correspond always to an even-even fragmentation decay into states containing broken pairs. As long as there is no neck broken pairs corresponding to even and to odd mass splits are created with equal probability. In the later stages, however, a pair excitation located in one fragment decays preferentially into states located in that fragment. For short range correlations the volume overlap of the two emerging fragments gives this unequal coupling to even and odd fragmentation. In the simple model considered here there is no neck at all and, hence, there is no localization of states in one or the other half of the elongated cigar. For an estimate it is argued that odd fragmentation is created only in the early stages when there is no neck and that it is no longer possible after the nucleus necks in. From the hydrodynamical calculations of Nix et al. [7] the time for the first stage would be 2.5×10^{-21}s.

With an average value for $|c|^2$ of 0.3 the occupation probability W of paired states is about 20% at that time. There are many more states containing broken pairs than pair excitations (2^{2N} compared to 2^N, if N single-particle energies crossed the Fermi energy). Hence 40% of the fragments have odd neutron number and 60% even neutron number.

5. Conclusion

This result will certainly undergo some changes if more realistic single-particle energies and deformations are used. These changes are, however, not expected to be drastic, because (1) in the Woods-Saxon potentials the Nilsson spectrum is still clearly visible as diabatic spectrum the pseudo-crossings being very close [8], and (2) the bulk part of the odd fragmentation is created in the early stages of the descent from saddle to scission where the quadrupole deformation is indeed dominant.

REFERENCES

[1] SCHÜTTE, G., WILETS, L., in Physics and Chemistry of Fission (Proc. 3rd Int. Symp. Vienna, 1972) Vol.1, IAEA, Vienna (1973) 503.
[2] SCHÜTTE, G., WILETS, L., Nucl. Phys. A252 (1975) 21; LEDERGERBER, T., PALTIEL, Z., PAULI, H.C., SCHÜTTE, G., YARIV, Y., FRAENKEL, Z., Phys. Lett. **56B** (1975) 417.
[3] STRUTINSKY, V.M., Z. Phys. A280 (1977) 99.
[4] SCHÜTTE, G., Z. Phys. A283 (1977) 183.
[5] SCHÜTTE, G., WILETS, L., Z. Phys. A286 (1978) 313.
[6] SCHÜTTE, G., Z. Phys. A288 (1978) 161.
[7] DAVIES, K.T.R., SIERK, A.J., NIX, J.R., Phys. Rev. **C13** (1976) 2385.
[8] PAULI, H.C., Phys. Rep. 7C (1973) 36.

DISCUSSION

H.A. NIFENECKER: Would you not agree that since, according to your theory, odd fragments stem from early pair breaking, the excitation energy of even Z splits should be higher than that of odd Z splits? In such a case there should be a correlation between the probability of odd splits and the magnitude of even-odd effects on excitation energy.

G. SCHÜTTE: I did not perform a calculation of the excitation energy and energy difference between odd and even fragments, which is in any case complicated. But I would say that the odd fragments have higher excitation energies since the density of broken pair states increases with increasing energy. The breaking of a pair therefore uses up energy in most cases.

STUDIES IN THE STATISTICAL THEORY OF NUCLEAR FISSION AND EXPLANATION OF FRAGMENT MASS ASYMMETRY IN TERMS OF NUCLEON-EXCHANGE MECHANISM

M. PRAKASH, V.S. RAMAMURTHY, S.S. KAPOOR
Bhabha Atomic Research Centre, Trombay,
Bombay, India

Abstract

STUDIES IN THE STATISTICAL THEORY OF NUCLEAR FISSION AND EXPLANATION OF FRAGMENT MASS ASYMMETRY IN TERMS OF NUCLEON-EXCHANGE MECHANISM.

The statistical theory of fission based on full equilibrium at scission is explored in detail, with several improvements. These include a diffuse surface description of deformed fragments near scission, and better mass and level density formulas as inputs. The use of adjustable parameters is avoided so that the capabilities and limitations of statistical theory may be learnt more thoroughly. – In view of the failure of the statistical theory of full equilibrium to provide a satisfactory quantitative explanation of the mass distributions, a model of mass distributions based on a nucleon-exchange mechanism has been developed which does not involve the use of any free parameters. In this approach, the crucial factor which decides the shape of the fragment mass distributions is the systematics of the differences in the chemical potentials of the pair fragment nuclei near scission. Results for the fission of ^{236}U are presented. It is shown that a satisfactory explanation of the fragment mass distributions and their excitation energy dependence is obtained on the basis of the proposed model.

1. INTRODUCTION

Several attempts have been made in the past to explain the observed fragment mass and charge distributions in the fission process. These attempts are based on such widely different assumptions as the complete statistical equilibrium at scission [1, 2], partial equilibrium between collective and single-particle degrees of freedom at scission [3, 4], the statistical equilibrium at the mass-asymmetric outer barrier with and without consideration of the dynamics of descent to scission [5, 6], and others [7, 8]. It is well known that these efforts have not yet resulted in a fully satisfactory explanation of the observed features of fission, nor has it been possible to put these various approaches to rigorous tests against the experimental data in view of the presence of adjustable parameters.

In the first part of the present work, we have carried out calculations of the fragment mass and energy distributions in low-energy fission in the framework of the statistical model of Fong [1]. This was prompted by the availability of better inputs to the statistical model, i.e. reliable mass formulas and level density

estimates, and more accurate calculations of interaction energies between two nuclei in proximity so that we learn about the capabilities as well as the limitations of this model. A conscious effort was made to avoid the use of adjustable parameters, and emphasis was placed on examining results ensuing from a consistent set of rules. Results of calculations for ^{236}U revealed features such as the observed dip at symmetry in the total fragment kinetic energies, the saw-tooth nature of the fragment deformation energy curve, etc. However, although the calculated mass yield curve was asymmetric, it was found to peak at mass 132 instead of at mass 140, as observed experimentally. This appears to be a failure common to most of the calculations reported on the basis of statistical theory [2, 4].

In the second part of this work, investigations were performed on the basis of the fact that nucleon-exchange processes occur during the fission process, similar to those observed in heavy-ion reactions [9, 10]. Following an earlier suggestion [11], a stochastic model description of this nucleon-exchange mechanism has been developed and is applied to the case of fission of ^{236}U. It is found that this approach provides a satisfactory explanation of the observed mass distributions.

2. STATISTICAL THEORY OF COMPLETE EQUILIBRIUM AT SCISSION

When full equilibrium is assumed to prevail among all degrees of freedom during the descent from saddle to scission, the final distributions become independent of the dynamics during the descent and are mainly governed by the phase space available near scission. The calculation of the yield for specified charge and mass identity of the fragments is performed by following three distinct steps. These are

i) the specification of the scission configuration;
ii) the calculation of the scission energy in order to obtain the energy available for internal excitation; and
iii) the calculation of the phase space available.

2.1. Specification of the scission configuration

The nucleus near the scission point is described by two co-axial fragments with diffuse matter distributions [12], whose equivalent sharp surfaces are separated by a distance d, along the line joining their centres. The diffuse density distribution is given by

$$\rho(\vec{r}_1) = \frac{\rho_0}{4\pi a^3} \int_V d^3 r_1' \frac{e^{-|\vec{r}_1 - \vec{r}_1'|/a}}{|\vec{r}_1 - \vec{r}_1'|/a} \tag{1}$$

where the integration is over a given sharp surface shape whose volume is V, and where $\rho_0 V = A$, A being the mass number of the fragment. a is the range of the Yukawa folding function. Following Myers [13], a value of $a = 1.0\ \text{fm}/\sqrt{2}$, is used in the present work. In the present calculations, the sharp-surface deformations of the individual fragments are described by spheroidal deformations ϵ_2 in the Nilsson model notation [14].

2.2. Calculation of the scission energy

The potential energy of the system near scission is assumed to be given by

$$E_{sc} = E_1(N_1, Z_1, \epsilon_2^1) + E_2(N_2, Z_2, \epsilon_2^2) + E_{int}(N_1, Z_1, \epsilon_2^1;\ N_2, Z_2, \epsilon_2^2;\ d) \qquad (2)$$

where E_1, E_2 are the self-energies of the individual nascent fragments with deformations ϵ_2^1 and ϵ_2^2, respectively, and E_{int} is the interaction energy between the two fragments. N_1, Z_1 and N_2, Z_2 specify the neutron and proton numbers of the two fragments. For the calculation of the individual fragment energies E_1, E_2, we follow the standard macroscopic-microscopic approach [15, 16], and write

$$E_{1,2} = E_{1,2}^{smooth} + \Delta E_{1,2} \qquad (3)$$

where $E_{1,2}^{smooth}$ forms the major part of the total potential energy and varies smoothly with respect to nucleon numbers and fragment deformations, and ΔE is the correction term due to shell and pairing effects. For the calculation of the smooth part, the liquid-drop mass formula of Howard and Seeger [17] was used. The microscopic part consisting of the shell and pairing corrections was obtained by using the Strutinsky smearing procedure [18] over the single-particle levels of the deformed-Nilsson-model harmonic-oscillator potential of Seeger and Perisho [19].

The interaction energy E_{int} is taken as the sum of Coulomb and nuclear parts. The Coulomb energy is given by

$$E_c = \frac{1}{2} \iint d^3r_1\, d^3r_2\, \rho_e(\vec{r}_1)\ \rho_e(\vec{r}_2)/|\vec{r}_1 - \vec{r}_2| \qquad (4)$$

where $\rho_e(\vec{r}_1)$ and $\rho_e(\vec{r}_2)$ are the charge density distributions of the two fragments. The nuclear interaction energy arising out of the finite range of the nuclear forces is given by [12, 20]

$$E_n = \frac{1}{2} \iint d^3r_1\, d^3r_2\, V(\vec{r}_{12})\ \rho(\vec{r}_1)\ \rho(\vec{r}_2)/\rho_0^2 \qquad (5)$$

where $V(\vec{r}_{12})$ is an effective Yukawa two-nucleon interaction. For the calculation of the interaction energies in the diffuse-surface model, the set of values of constants provided by Arnould and Howard [21] has been used. For axially symmetric deformations of the fragments, the six-dimensional integrals in Eqs (4) and (5) can be reduced to three-dimensional integrals in cylindrical co-ordinates and have been evaluated by the use of Gauss-Legendre quadrature formulas.

The energy released E_R at the scission point is then obtained from

$$E_R = E^* - E_{sc} \tag{6}$$

where E^* is the total energy of the initial compound nucleus and E_{sc} is the potential energy of the nucleus at the scission point. Under the assumption of complete statistical equilibrium, the excitation energy at scission is almost equal to E_R.

2.3. Calculation of the phase space

Nuclear level densities play a central role in the calculation of the available phase space. Direct numerical calculations of level densities from the single-particle levels of the fragments have been used earlier [2] and include the well-known excitation energy dependence of shell effects on level densities. However, these calculations depend sensitively on the details of the single-particle level scheme used, and there is need for a suitable normalization of the values to an appropriate average liquid-drop-model behaviour as is done in the case of nuclear-potential-energy calculations. A recently proposed level density formula [22], which takes into account the influence of nuclear-shell structure on level densities, their excitation energy dependence and the liquid-drop normalization has been used in this work. The level density in this approach is given by

$$\rho(E_x) = C \exp [S(E_x)] \tag{7}$$

$$\text{where } C = \pi^{1/2}/(12\, a^{1/4}\, E_x^{5/4}). \tag{8}$$

The entropy S and the excitation energy E_x of the system are given by

$$S = 2aT + \frac{\Delta_s}{T}\left[\frac{\pi^2 W^2 T^2 \cosh(\pi WT)}{\sinh^2(\pi WT)} - \frac{\pi WT}{\sinh(\pi WT)}\right] \tag{9}$$

$$E_x = aT^2 + \Delta_s\left[\frac{\pi^2 W^2 T^2 \cosh(\pi WT)}{\sinh^2(\pi WT)} - 1\right] \tag{10}$$

where T is the temperature, Δ_S is the ground-state shell correction of the corresponding shape and W is a constant given by $W = W_0 A^{1/3}$, $W_0 = 0.185\ MeV^{-1}$. For deformed nuclei, the nuclear level density parameter a can be expressed as

$$a = \gamma A (1 - \beta A^{-1/3} B_S) \tag{11}$$

where B_S is the nuclear surface area relative to spherical shape, $\gamma = 0.176$ and $\beta = 1.0$ [22]. Using the above expressions for entropy and excitation energy, the total entropy of the fragment system is obtained under the assumption of temperature equilibration between the two fragments.

2.4. Calculation of the observable quantities in fission

To predict physical observables as energy distributions, yield distributions, etc. the following equation is used:

$$Y(Z_1, A_1, \epsilon_2^1;\ Z_2, A_2, \epsilon_2^2) = \text{const} \times \rho(Z_1, A_1, \epsilon_2^1;\ Z_2, A_2, \epsilon_2^2, E_X) \tag{12}$$

The yield distributions for specified charge and mass identities of the fragments are obtained by integrating over all possible deformations, i.e.

$$Y(Z_1, A_1;\ Z_2, A_2) = \text{const} \int\int d\epsilon_2^1\ d\epsilon_2^2\ (Z_1, A_1, \epsilon_2^1;\ Z_2, A_2, \epsilon_2^2;\ d, E_X) \tag{13}$$

where E_X is the excitation energy corresponding to the deformations $(\epsilon_2^1, \epsilon_2^2)$ of the two fragments, and d is the distance between fragment tips starting from which pure Coulombic separation of fragments starts [23]. The yield distributions of specified masses alone are obtained by integrating the charge variables also in the above equation.

For a given mass and charge configuration of the fragments, the asymptotic fragment kinetic energies and excitation energies can be obtained from the interaction and deformation energies at the point where pure Coulombic separation starts. The most probable values of these quantities are obtained by the phase space maximization condition given by

$$\left.\frac{\partial \rho}{\partial \epsilon_2^1}\right|_{\epsilon_2^1 = \tilde{\epsilon}_2^1} = \left.\frac{\partial \rho}{\partial \epsilon_2^2}\right|_{\epsilon_2^2 = \tilde{\epsilon}_2^2} = 0 \tag{14}$$

In practice, these values are obtained numerically by studying the contour map of the level density as a function of the deformations of the fragments and by

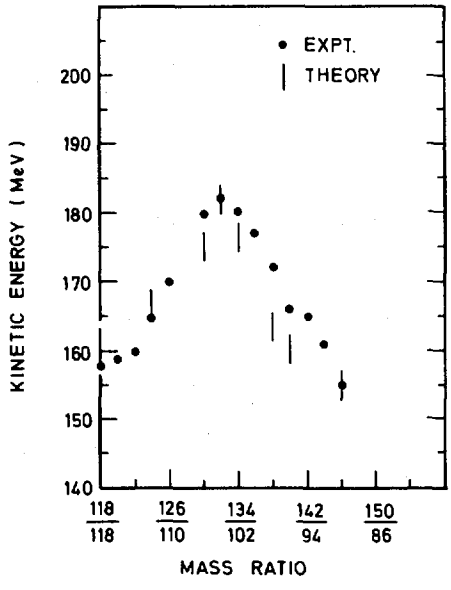

FIG.1. Comparison of the calculated interaction energies at scission with experimental mean kinetic energies of fragments as a function of mass ratio, for thermal-neutron-induced fission of ^{235}U. The closed circles represent the experimental data of Schmitt [24] *and the crosses represent the calculated values.*

searching for level density maxima in such a plot. The most probable deformation energy of a fragment is obtained as the difference between the energy of the deformed fragment at scission and the energy of the ground-state equilibrium shape of that fragment. In the above calculations, the distance between fragment tips d at which pure Coulomb separation starts is obtained by a study of the post-scission dynamics of fission fragments with the inclusion of dissipative forces [23]. In such a study, one determines the distance at which the energy released starts being converted into kinetic energy, instead of being pumped into the excitation energy of the fragments.

2.5. Results

2.5.1. Calculated fragment interaction and deformation energies

In Fig. 1 we show the most probable values of the calculated interaction energies as a function of fragment mass ratio. The distance d for each mass ratio was obtained on the basis of dynamical calculations with the inclusion of dissipative forces [23] and was found to be 2 ± 0.2 fm for the range of masses

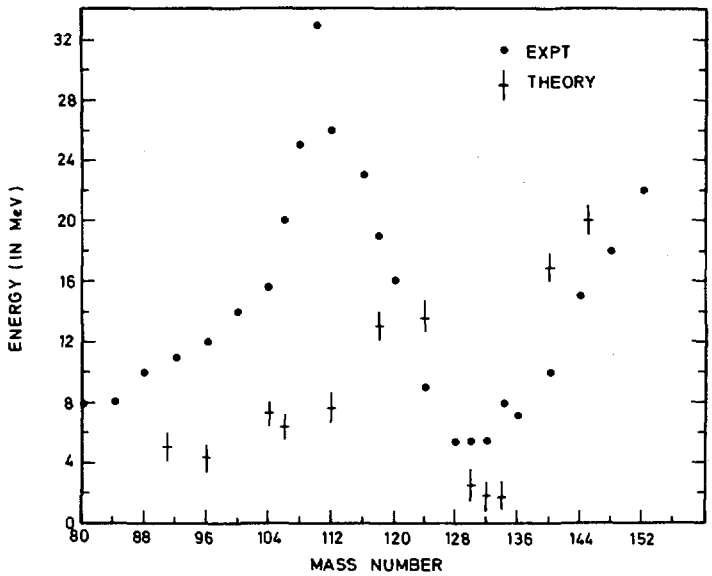

FIG.2. Calculated deformation energies at scission and experimental fragment excitation energies for the thermal neutron fission of ^{235}U. The experimental excitation energies are those deduced by Schmitt [24].

studied. For the sake of comparison, the experimental kinetic energies [24] are also shown in this figure. It is seen that the dip at symmetry and the peak at $A \cong 132$ are well reproduced. A finer comparison between the calculated interaction energies and the experimental kinetic energies is not justified in view of the neglect of higher-order deformations, post-scission dynamics of the fragments, etc. Figure 2 shows a plot of the calculated deformation energies versus the mass ratio. For comparison, we also show the experimental fragment excitation energies as obtained from prompt neutron and γ emission data [24]. It is seen that the deformation energy forms a sizable portion of the final observed excitation energy and exhibits the well-known saw-tooth shape with a minimum around $A \cong 132$. Further quantitative comparisons are not warranted as pointed out earlier.

2.5.2. Fragment mass distributions

In Fig. 3, we show the calculated results on mass yields for the thermal-neutron-induced fission of ^{235}U and make a comparison with the experimental data [25]. It is seen that, although the calculated mass distribution is asymmetric, the peak occurs at mass number $A \cong 132$ and not at $A \cong 140$, as observed experimentally. This shows that the earlier conclusions of Ignatyuk [2] that the

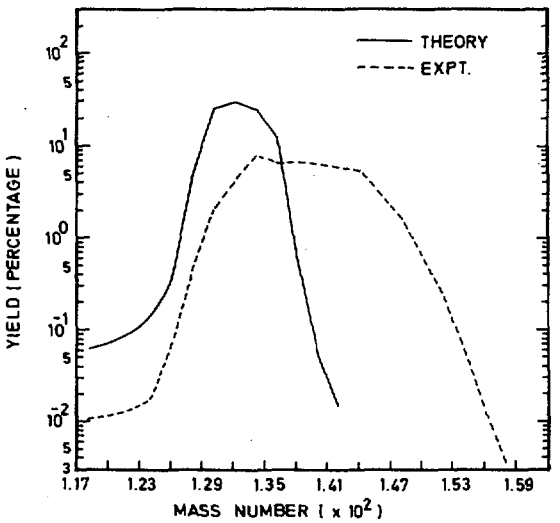

FIG.3. Calculated heavy fragment mass yields for thermal-neutron fission of ^{235}U in the full equilibrium model. The dashed line represents the experimental data of Flynn and Glendenin [25].

position of the most probable mass split is not reproduced by the statistical theory of complete equilibrium is not altered despite the present improvements. We are, therefore, led to the conclusion that although qualitative agreement as regards the shape of the asymmetric mass distributions is found in the framework of the statistical theory of complete equilibrium, quantitative agreement concerning the position of the asymmetric peak and the width of the mass distributions is not obtained.

3. EXPLANATION OF MASS ASYMMETRY IN FISSION IN TERMS OF NUCLEON-EXCHANGE MECHANISM

A stochastic approach of the nucleon-exchange processes in fission was suggested earlier [11] to account for the mass asymmetry. However, these calculations involved the use of some adjustable parameters. In addition, doubt also existed at that time as to whether there is enough time for such nucleon exchanges to take place during the last stages of the fission process. It is now well-known that in heavy-ion deep inelastic collisions, a considerable number

of nucleon-exchanges take place between the colliding partners in a reaction time as small as 1 to 10 X 10^{-22} s [9, 10]. Encouraged by the overwhelming experimental evidence for the occurrence of nucleon-exchange phenomena between two nuclei in close proximity, we have now developed a parameter-free approach applicable to fission to calculate the fragment mass distributions on the basis of the nucleon-exchange mechanism.

3.1. Physical basis of the nucleon-exchange model

The fissioning nucleus near scission consists of two diffuse surface nuclei with overlapping matter distributions, in the process of receding from each other. If we assume that during the initial stages of nascent fragment separation, there exists a time interval in which the relative motion of the two fragments is slower than the nucleon traversal time, then nucleon-exchange processes should occur until a significant overlap of nuclear matter exists. That enough time may be available for such nucleon-exchange processes to occur has been indicated in a recent study on the effect of dissipative forces on nascent fragment separation [23] and also in the dynamical study of Błocki et al. [26]. The probability for the transfer of a nucleon from one of the nascent fragments to the other would, at any instant, depend on the configuration of the nucleus at that instant and is expected to be independent of the previous history of the fissioning nucleus. The process can, therefore, be treated as a stochastic one, and the final mass distributions can be determined solely on the basis of the nucleon-exchange mechanism operating near scission. From the study of deep-inelastic collisions in heavy-ion reactions, it is known that the energy equilibration time is much shorter than that of mass equilibration [9]. It is, therefore, reasonable to assume that near scission nucleon transfers take place between two nascent fragment nuclei in close proximity in thermal equilibrium. In the case of heavy-ion deep-inelastic collisions, the contact time is generally not sufficient to achieve full mass equilibration. The charge-to-mass ratio is, however, found to equilibrate more rapidly, and the distributions in deep-inelastic collisions show that equilibrated N/Z ratio is achieved. case of fission, it is expected that equilibration in both N/Z ratio and the mass-asymmetric degree of freedom will be realized owing to the existence of larger nuclear overlaps and contact times in this case as compared to deep-inelastic heavy-ion collisions.

In the following, we describe the theoretical formulation of nucleon-exchange process between two nuclei in close proximity, for the calculation of equilibrium mass distributions. We first start with a one-component system. Referring to the configuration of the two interacting nuclei at scission by the suffixes L and H, we shall determine the equilibrium mass distribution of the system H only, that of L being determined from mass conservation. If $p_{m,n}$ denotes the probability that the system H having m nucleons goes over to a configuration with n nucleons

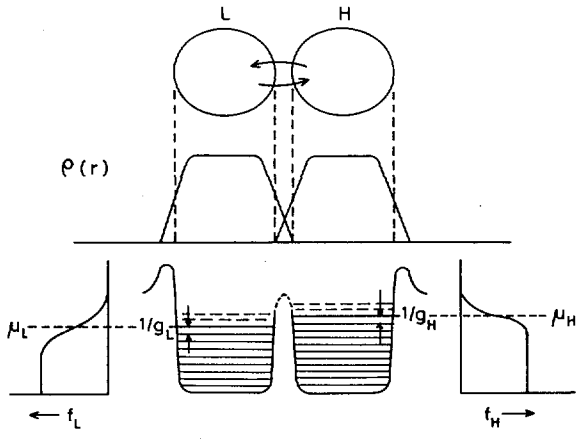

FIG.4. Schematic diagram illustrating the nucleon-exchange mechanism between the fragments L and H. $\rho_{L,H}(r)$ represents the diffuse densities, $g_{L,H}$ are the single-particle level densities, $f_{L,H}$ are the Fermi-Dirac occupation probabilities and $\mu_{L,H}$ are the chemical potentials of the fragments L and H, respectively.

because of nucleon transfers in a time t, the following relations connect the yields W_n and W_m of the respective systems:

$$W_n(t + \Delta t) = \sum_m W_m(t)\, p_{m,n} \tag{15}$$

$$\sum_n p_{m,n} = 1 \tag{16}$$

Under the mass equilibrium conditions ($W_n(t + \Delta t) = W_n(t)$) and considering single-nucleon transfers to be the predominant mode of exchange of nucleons, the ratio of the yields of the fragment masses m + 1 and m is given by [11]

$$\frac{W_{m+1}}{W_m} = \frac{p_{m,m+1}}{p_{m+1,m}} \tag{17}$$

The central quantities deciding the mass distributions are, therefore, the transition probabilities $p_{m,m+1}$ and $p_{m+1,m}$, which can be designated by the single-nucleon

transfer probabilities T_{LH} and T_{HL}, from the fragment L to H, and from the fragment H to L, respectively. Figure 4 illustrates the mechanism of nucleon transfers between the two fragment nuclei in close proximity. On the basis of Fermi's golden rule, the nucleon transfer probability from the light to the heavy fragment, T_{LH}, can be written as

$$T_{LH} = \int_0^\infty g_L(E_1)\, f_L(E_1)\, dE_1\, \frac{2\pi}{\hbar} \left| M_{LH} \right|^2 g_H(E_2)\, [1 - f_H(E_2)]\, \delta(E_1 - E_2) \quad (18)$$

Number of nucleons in the light fragment in an energy bin

Matrix element of transfer

Density of available states (holes) in the heavy fragment

where $g_{L,H}$ are the single-particle level densities, $f_{L,H}$ are the Fermi-Dirac occupation probabilities, and M_{LH} is the matrix element of transfer. Since the main contribution to the integral in Eq. (18) comes from a small energy interval around the chemical potentials of L and H, the quantities $g_{L,H}$ and the matrix element of transfer can be calculated at the corresponding chemical potentials and taken out of the integral. With these approximations, we have

$$T_{LH} = 2\pi\hbar^{-1} |M_{LH}|^2\, g_L(\mu_L)\, g_H(\mu_H)\, I_{LH} \quad (19)$$

$$I_{LH} = \int_0^\infty f_L(E)\, [1 - f_H(E)]\, dE \quad (20)$$

where μ_L and μ_H are the chemical potentials of L and H, respectively. We have evaluated the integral I_{LH} exactly; for the nuclear case, where the chemical potentials are considerably larger than the temperatures involved, it is given by [27]

$$I_{LH} = (\mu_H - \mu_L)\, [\exp[(\mu_H - \mu_L)/T] - 1]^{-1} \quad (21)$$

Similar expressions can be written for nucleon transfer from the heavy fragment to the light one. It may be noted from Eqs (19) and (21) that the main driving force for the transfer of nucleons from one nucleus to another is the difference in their chemical potentials.

It is also interesting to note that, with the above nucleon transfer probabilities, the nucleon drift coefficient D_v and the diffusion coefficient D_A defined at any instant as

$$D_v = \int h\, p_{m,\, m+h}\, dh$$

$$D_A = \int h^2\, p_{m,\, m+h}\, dh$$

are given by

$$D_V = -R_{LH}\,(\mu_H - \mu_L) \tag{22}$$

$$D_A = R_{LH}\,(\mu_H - \mu_L)\coth\,[(\mu_H - \mu_L)/2T] \tag{23}$$

where

$$R_{LH} = 2\pi\hbar^{-1}\,|M|^2\, g_L\,(\mu_L)\, g_H\,(\mu_H)$$

$h = 0, \pm 1$ (single-nucleon transfers only)

and $M_{LH} = M_{HL} = M$ (microscopic reversibility).
It can be seen that the above equations for D_v and D_A follow the well-known Einstein relation in the asymptotic limit of high temperatures.

Making use of Eqs (17–21) the following result can be obtained for the yield W of the heavy fragment, which is x nucleons removed from the symmetric mass s;

$$\frac{W_{s+x}}{W_s} = \left[\frac{|M_{ss}|^2}{|M_{s+x,\,s-x}|^2}\right]\left[\frac{g_s^2}{g_{s+x}\, g_{s-x}}\right] \tag{24}$$

$$\times\left[e^{\sum_{i=1}^{} -(\mu_{s+i} - \mu_{s-i})/T_i}\;\frac{e^{(\mu_{s+x} - \mu_{s-x})/T_x} - 1}{(\mu_{s+x} - \mu_{s-x})/T_0}\right]$$

where W_s is the yield of the symmetric fragment.

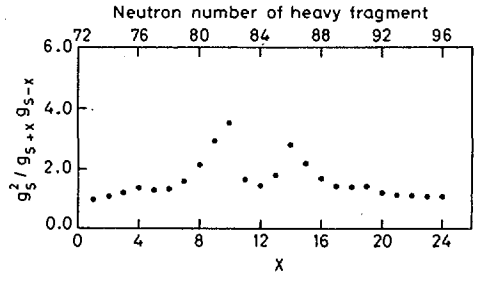

FIG.5. The single-particle level density factor of Eq. (24) as a function of the neutron number of the heavy fragment.

3.2. Results and discussion

Of the three terms on the right-hand side of Eq. (24), the first term containing the matrix element of nucleon transfer is the least known. It is, however, reasonable to assume that the matrix element will not vary significantly with the mass ratio. The first term is, therefore, taken to be nearly unity in the present calculations.

The value of the term in the second bracket will be unity for all values of x if an equidistant model is assumed for g.

It is, however, possible to calculate this quantity by taking into consideration the shell structure as follows. In the spirit of the macroscopic-microscopic approach for nuclear masses, the single-particle level density can be written as

$$g(\epsilon) = g_0(\epsilon) + \delta g(\epsilon)$$

$$= g_0(\epsilon) + \frac{W^2 \Delta}{\cos(W\mu - \phi)} \cos(W\epsilon - \phi) \qquad (25)$$

where g_0 represents the overall smooth component, Δ is the ground-state shell correction energy for the relevant shape, μ is the chemical potential, ϕ is a suitable phase factor and W is the fundamental frequency of oscillation of δg. If $g(\epsilon)$ is calculated at the chemical potential μ, we have

$$g(\mu) = g_0(\mu) + W^2 \Delta \qquad (26)$$

We show in Fig. 5 the value of the term $(g_s^2/g_{s+x}\, g_{s-x})$ calculated by using Eq. (26) for various values of x. The value of g_0 for neutrons was taken as [22]

$$g_0 = 6\gamma(1 - \beta B_s A^{-1/3})N/\pi^2 \qquad (27)$$

with $\gamma = 0.176$, $\beta = 1.0$ and $W_0 = 0.185\ \text{MeV}^{-1}$. Here, B_s is the nuclear surface area relative to spherical shape, N is the neutron number and A is the mass of the nucleus. It is seen that, with the incorporation of shell effects, the quantity $(g_s^2/g_{s+x}\, g_{s-x})$ exhibits some structure, but its magnitude is confined to within 1 and 4. It is, therefore, clear that this term does not play a very significant role in determining the mass distributions.

We now turn our attention to the term in the last bracket of Eq. (24), which depends on the differences in the chemical potentials $(\mu_H - \mu_L)$ and the temperatures of not only the final configuration for which the mass yield is to be determined but also of all the intermediate configurations which are realized. Since in the actual case of a fissioning nucleus there are two components, protons and neutrons, the above exchange mechanism can be treated in two dimensions [11]. For the purpose of calculating the mass distributions the problem can, however, be simplified to calculations in one dimension considering only neutron exchanges keeping the N/Z ratio close to the observed values, since the N/Z ratio equilibrates faster than the mass.

The difference in the chemical potentials, $\mu_H - \mu_L$, is equal to the negative of the difference in the nucleon separation energies of the two fragments in the limit of zero temperature, neglecting the small re-arrangement energies. At finite temperatures, it is possible to include a temperature dependence of the chemical potential explicitly on the basis of a model single-particle level scheme. For the level scheme given in Eq. (25), the following relations hold:

$$\mu(T) = \mu(0) + [\mu(0) - \mu^{LDM}]\left[\frac{\pi WT}{\sinh \pi WT} - 1\right] \tag{28}$$

$$\mu_H(0) - \mu_L(0) = S_L - S_H$$

$$\mu_H^{LDM} - \mu_L^{LDM} = S_L^{LDM} - S_H^{LDM}$$

where the quantities S, S^{LDM} are the separation energies calculated with and without the shell correction term in the masses.

Figure 6 shows the calculated values of the chemical potential differences $\mu_H - \mu_L$ versus N_H for three cases of mean fragment temperatures T = 0.5, 1.0 and 2.0 MeV. Taking guidance from the known systematics of fragment charge distribution for a given mass [28], we have assumed that the light fragments are richer in charge by about half a unit than that given by unchanged charge division in all regions except for the symmetric-mass region $M_H/M_L < 1.2$, where an unchanged charge division was assumed. The separation energies were calculated for the fragment deformations obtained in Section 2. Figure 7 shows the corresponding equilibrium mass distributions of the heavy fragments without the

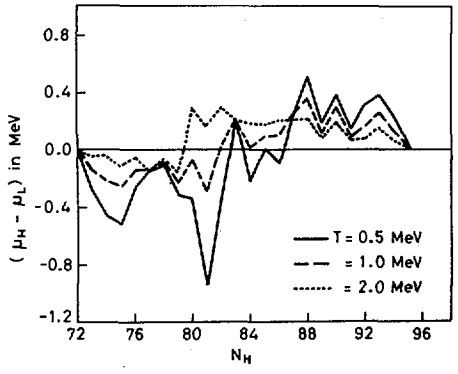

FIG.6. Difference in the chemical potentials of the light and heavy fragments as a function of the neutron member of the heavy fragment. The individual separation energies are calculated for the most probable deformations of the light and heavy fragments. Results are shown for mean fragment temperatures T = 0.5, 1.0 and 2.0 MeV.

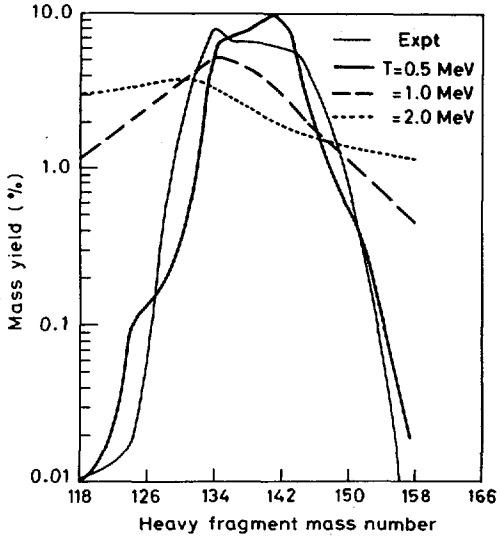

FIG.7. Comparison of the calculated yields in the nucleon-exchange model with the experimental yields for the use of thermal-neutron fission of ^{235}U. Calculated results are shown for mean fragment temperatures T = 0.5, 1.0 and 2.0 MeV. The experimental data (dark full curve) are those given by Flynn and Glendenin [25].

inclusion of the first two terms on the right-hand side of Eq. (24), which have been shown to be not very significant in deciding the mass distributions. For the sake of comparison, the experimental mass distribution in the case of $^{235}U(n_{th}, f)$ is also shown [25]. It can be seen that the experimental mass distribution is close to the calculated equilibrium mass distribution with a mean fragment temperature of T = 0.5 MeV. Considering that this value of T is nearly equal to the scission temperatures obtained in Section 2, and that no free parameters are involved in the calculation, this agreement can be taken as an evidence for the relevance of the proposed nuclear exchange mechanism in deciding the fragment mass distributions. It is also gratifying to note that the well-known filling up of the symmetric valley with increasing excitation energy is brought out by the present calculations.

From the above discussion, it is interesting to note that the most crucial factor determining the shape of the fragment mass distributions in Fig. 7 and responsible for the observed asymmetry in fission is the systematics of the difference in the chemical potentials of the various complementary mass configurations of the fragment nuclei shown in Fig. 6. The fact that the difference in the chemical potentials $\mu_H - \mu_L$ is negative for all the configurations up to neutron number $N \cong 86$ and is positive for all the configurations above 86 is responsible for the increasing yields of the heavy fragments up to $N \cong 86$ and the decrease thereafter. Qualitatively, we may say that there exists a driving force for a net nucleonic current from the light fragment to the heavy fragment up to $N \cong 86$ and from heavy to light beyond this number. In conclusion, this model of nucleon exchanges without any free parameter predicts an equilibrium mass distribution of two fragment nuclei in close proximity, which is very close to the observed fragment mass distributions in low-energy fission. Further calculations with this model to the case of other fissioning nuclei which include two-dimensional calculations with respect to individual neutron and proton transfers to calculate also the charge distributions are in progress.

4. SUMMARY

In the first part of this paper, detailed investigations have been carried out on the theoretical predictions of the fragment mass and energy distributions in the framework of the statistical theory of complete equilibrium at scission, without use of any adjustable parameters. With the best available inputs to the calculations, while qualitative agreement with the known features in fission was obtained, the calculated fragment mass distributions were not found to be in quantitative agreement with experimental results. The calculated peak of the mass distribution in $^{235}U(n_{th}, f)$ was found to be at mass 132 as against the experimental peak around mass 140.

In the second part of this work, it is shown that a satisfactory explanation of the mass distributions can be obtained on the basis of a nucleon-exchange mechanism operating near the scission point similar to that observed in heavy-ion deep-inelastic collisions. A stochastic description of the nucleon-exchange process is formulated, and the transition probabilities are related to the differences in the chemical potentials of the pair fragment configurations. It is found that in the case of low-energy fission of ^{236}U, there exists a driving force for a net nucleonic current to flow from the light fragment to the heavy one up to a neutron number of 86 (mass number 140) in the heavy fragment and from heavy to light beyond this number. This fact results in a peak in the mass distributions at mass number 140 of the heavy fragment.

REFERENCES

[1] FONG, P., Phys. Rev. **102** (1956) 434; Statistical Theory of Nuclear Fission, Gordon and Breach, New York (1969).
[2] IGNATYUK, A.V., Sov. J. Nucl. Phys. **9** (1969) 208.
[3] NÖRENBERG, W., in Physics and Chemistry of Fission (Proc. 2nd Int. Symp. Vienna, 1969) IAEA, Vienna (1969) 41.
[4] WILKINS, B.D., STEINBERG, E.P., CHASMAN, R.R., Phys. Rev. **C14** (1976) 1832.
[5] HASSE, R.W., Nucl. Phys. **A128** (1969) 609.
[6] KAPOOR, S.S., RAMAMURTHY, V.S., in Physics and Chemistry of Fission (Proc. 3rd Int. Symp. Rochester, 1974) IAEA, New York (1975) 375.
[7] SCHMITT, H.W., MUSTAFA, M.G., ibid., 421.
[8] MARUHN, J., GREINER, W., LICHTNER, P., DRECHSEL, D., ibid., 569.
[9] SCHRODER, W.U., HUIZENGA, J.R., Ann. Rev. Nucl. Sci. **27** (1977) 465.
[10] LEFORT, M., NGO. Ch., Ann. Phys. **3** (1978) 5.
[11] RAMANNA, R., SUBRAMANIAN, R., AIYER, R.N., Nucl. Phys. **67** (1965) 529; RAMAMURTHY, V.S., RAMANNA, R., in Physics and Chemistry of Fission (Proc. 2nd Int. Symp. Vienna, 1969) IAEA, Vienna (1969) 51; RAMAMURTHY, V.S., PhD thesis, University of Bombay (1971).
[12] DAVIES, K.T.R., NIX, J.R., Phys. Rev. **C14** (1976) 1977.
[13] MYERS, W.D., Nucl. Phys. **A204** (1973) 465; Lawrence Radiation Laboratory Rep. LBL-4342 (1975).
[14] NILSSON, B., Nucl. Phys. **A129** (1969) 445.
[15] BRACK, M., DAMGAARD, J., PAULI, H.C., JENSEN, A.S., STRUTINSKY, V.M., WONG, C.Y., Rev. Mod. Phys. **44** (1972) 320.
[16] NIX, J.R., Ann. Rev. Nucl. Sci. **22** (1972) 65.
[17] HOWARD, W.M., SEEGER, P.A., Nucl. Phys. **A238** (1975) 491.
[18] STRUTINSKY, V.M., Sov. J. Nucl. Phys. **3** (1966) 449; Nucl. Phys. **A95** (1967) 420.
[19] SEEGER, P.A., PERISHO, R.C., Los Alamos Scientific Laboratory Rep. LA-3751 (1967).
[20] KRAPPE, H.J., NIX, J.R., in Physics and Chemistry of Fission (Proc. 3rd Int. Symp. Rochester, 1974) IAEA, New York (1973) 159.
[21] ARNOULD, M., HOWARD, W.M., Nucl. Phys. **A274** (1974) 295.
[22] KATARIA, S.K., RAMAMURTHY, V.S., KAPOOR, S.S., Phys. Rev. **C18** (1978) 549.

[23] PRAKASH, M., RAMAMURTHY, V.S., KATARIA, S.K., KAPOOR, S.S., Phys. Lett. **81B** (1979) 136; PRAKASH, M., Phys. Rev. **C18** (1979).
[24] SCHMITT, H.W., NEILER, J.N., WALLER, P.S., Phys. Rev. **141** (1966) 146; SCHMITT, H.W., in Why and How Should we Investigate Nuclides far off the Stability Line (Proc. Int. Conf. Lysekil, 1966) Stockholm (1967) 633.
[25] FLYNN, K.F., GLENDENIN, L.E., Argonne National Laboratory Rep. ANL-7749 (1970).
[26] BŁOCKI, J., BONEH, Y., NIX, J.R., RANDRUP, J., ROBEL, M., SIERK, A.J., SWIATECKI, W.J., Ann. Phys. **113** (1978) 330.
[27] PRAKASH, M., PhD thesis, University of Bombay (1979).
[28] WAHL, A.C., FERGUSON, R.L., NETHAWAY, D.R., TROUTNER, D.E., WOLFSBERG, K., Phys. Rev. **126** (1962) 1112.

DISCUSSION

P. FONG: If you assume statistical equilibrium, why not just apply the general principles of statistical equilibrium for calculation, instead of using a particular transport mechanism? The same may be said of two gases in equilibrium through a particular connecting mechanism. The general principle always leads to the correct result. A particular transport mechanism may sometimes result in a perpetual motion machine, a concept which, of course, is invalid.

S.S. KAPOOR: As I stated, our calculations are based on your statistical theory and show the heavy fragment peak at 132, and not around 140 as observed experimentally. The calculations based on the 'nuclear-exchange' model, however, give the right peak position and width. So the nuclear-exchange model is different from the statistical theory. In the nuclear-exchange model the separation energy and, therefore, shell effects of all intermediate configurations are involved, while in the statistical theory only the phase space of the masses under consideration is important.

G. SCHÜTTE: You calculate the transition probability from one fragment to the other in a first-order perturbation. How can you maintain the thermodynamic equilibrium between the two fragments in this case?

S.S. KAPOOR: We have learnt from heavy-ion deep-inelastic collisions that the equilibration time in the energy degree of freedom can be much shorter than in the mass asymmetry degree of freedom. Hence it can be assumed that there is temperature equilibrium between the fragments, while the mass exchange is being considered.

R. SCHULTHEIS: I am surprised that you obtain quite different mass distributions in your radium and fermium calculation, although you have used the same deformation energy. Does this mean that your results are somewhat insensitive to deformation energy?

S.S. KAPOOR: No, I don't think so. In this model the results strongly depend on the difference SL-SH of the separation energies for the complementary fragments. In the case of a given heavy mass, the complementary fragments are quite different for radium and fermium, so there is a difference in the two sets of results. For the sake of simplicity of calculation, we assumed a universal deformation energy versus mass curve, in the same way as we speak of a universal $\bar{\nu}(M)$ curve. I suppose that with a little more computational effort, it might not have been necessary to do so.

P. SCHUK: You calculate the mass spread in a phenomenologically independent particle model. The time-dependent Hartree–Fock method, which uses a more sophisticated independent-particle model, gives a mass spread that is too low. How do you reconcile this fact with your model?

S.S. KAPOOR: The independent-particle-model picture was intended to illustrate and explain our nuclear-exchange model. The mass yields were shown to depend primarily on the differences in the separation energies, which are taken from 'experimental' nuclear-mass data.

NEW PERSPECTIVES OF THE STATISTICAL THEORY OF FISSION

P. FONG
Physics Department, Emory University,
Atlanta, Georgia,
United States of America

Abstract

NEW PERSPECTIVES OF THE STATISTICAL THEORY OF FISSION.

Recent studies on spin distribution, excitation energy and its variance shed new light on the statistical theory of fission. They establish the conceptual validity of the statistical approach and correctly predict new experimental results. Together with earlier studies it can now be concluded that the statistical theory has generally explained all the phenomena it is designed to explain, i.e. those pertaining to the late stage of fission, and any theory capable of explaining these facts must be statistical in nature. Recent dynamical study based on the one-body dissipation mechanism leads to results in excellent agreement with those of the statistical theory and therefore may be regarded as the dynamical interpretation of the statistical theory. The long controversy between these two approaches concerning the perennial question of asymmetric fission is now resolved.

1. INTRODUCTION

The asymmetric-fission and related late-stage fission problems have puzzled nuclear scientists for four decades. It seems that, by generally reasonable arguments, a fissioning nucleus should split into two comparable fragments. Indeed this is the case for light nuclides and very heavy nuclides, and for all nuclides at high energy fission. But there is one glaring exception. For the nuclides we are most interested in, i.e. ^{233}U, ^{235}U, ^{239}Pu and many neighbouring ones, fission at low energy is strikingly asymmetric. The two fragments are mostly of the mass ratio of 3:2 and the probability of symmetric fission is only 10^{-3} of that of asymmetric fission. Why is the more likely process of symmetric fission so severely inhibited?

The problem has engaged many theorists and experimentalists. Experiments were designed to test theories but, to the surprise of all, later results on kinetic energy and prompt-neutron distributions were so startling that the mystery was greatly compounded.

It soon became apparent that these and many other related problems form a group related to the fission process in the late stage – that from the saddle point to the scission point. It requires an understanding of the dynamical process in this stage to work out theories of distributions of mass, charge, kinetic energy,

prompt neutrons and so on, of the fission products. Asymmetric fission is just the most outstanding feature and provides a severe test to any theory dealing with the fission process in the late stage. The problem thus goes to the heart of the mechanism of fission.

To be sure, there were important discoveries and problems in other fields of fission (angular distribution of fission products, fission isomers, etc.) but most have been solved satisfactorily (collective states at the saddle point, double-humped potential barrier, etc.) within a reasonable time.

In 1974 Specht [1] published a review on nuclear fission. One of the two conclusions summarizing the paper reads thus: "As far as the understanding of fragment mass distribution is concerned, however, there are still major open problems."

In the same year I published a paper [2] reporting a statistical-theory calculation of the asymmetric mass distribution which incorporates the Strutinsky correction. For the first time a theoretical mass distribution curve agreeing with the essential features of the experimental results is obtained and the phenomenon of asymmetric fission is quantitatively explained. Previously, over the years, the statistical theory has successfully explained charge distributions [3], kinetic-energy distribution [4], energy dependence of the distributions [5], prompt-neutron distribution [4], ternary fission [6] and spontaneous fission [5]. Also it has already partially explained asymmetric fission – it predicts asymmetric fission with symmetric fission suppressed by a factor of 10^{-3}, the only flaw being that the mass ratio predicted is 1.3 instead of 1.45 experimentally observed. This small discrepancy, disregarding the other overwhelming agreements, seemed sufficient to convince many workers to take a position against the statistical theory. Herculean efforts were invested in various dynamical approaches, not realizing that the chance of a basically different theory's explaining the same large body of experimental information concerning the late stage of fission is statistically very small. Even after the 1974 calculation of mass distribution removing the last discrepancy, the trend continued.

This is a rare instance in the history of science that massive experimental evidence was ignored to pursue alternative theories. The result can be expected: either the alternative theory, such as the Maruhn-Greiner theory [7] turns out to be equivalent to the statistical theory [8], or to be contradicted by experimental results as described in the following.

A year ago Negele et al. [9] published extensive results of dynamical calculations. Seven different dynamical prescriptions were pursued. These have nearly exhausted our intellectual resources on this problem at the present time. In a recent paper [10] I pointed out that six of the seven lead to results contradicted by experimental results of prompt neutron and spin distributions. The remaining one, based on Swiatecki's one-body dissipation according to the Fermi gas model in a liquid-drop-model approach and not contradicted by experimental results,

leads to results of scission time and kinetic energy at the scission point in excellent agreement with those of the statistical theory. It dissipates enough energy and implies statistical equilibriums. The long controversy between the statistical and dynamical approaches can now be resolved. The statistical theory is, in principle, a special case of the dynamical theory and, if correct, should be derivable from the right dynamics of the system. While originally proposed on an ad-hoc basis, the statistical theory may now be regarded as originating from a dynamics based on the one-body dissipation mechanism. The two approaches thus converge and the one-body dissipation mechanism may be regarded as the dynamical interpretation of the statistical theory – even though this interpretation leads to an even more bewildering problem that the nuclear matter behaves both as a gas and as a liquid.

In a typical dynamical theory we would expect the co-ordinates and the corresponding velocities to be functions of time $q_i(t)$, $\dot{q}_i(t)$. Once we have a non-vanishing $\dot{q}_i(t)$ we would expect a non-vanishing change of the co-ordinate Δq_i including the elongation co-ordinate q_e. The experimental results of kinetic energy, prompt-neutron and long-range α-particle distributions determine conclusively that the change of the elongation co-ordinate is very small, and that the velocity $\dot{q}_e(t)$ is nearly zero [11, 12]. It is unfortunate that this point is overlooked by many theorists. This means that there is no authentic dynamics. A nearly zero velocity implies a quasi-static process which is the basis of the statistical theory.

Thus the fact that nature chooses the statistical option is ascertained by experiments. This simplifies the work of the theorists. They need to do only two things: develop a statistical theory to explain the experimental results and develop a theory of nuclear matter to explain nature's choice of the statistical option. The first is not contingent on the second because we know from experimental facts that the statistical approach is correct.

The situation is similar to that of the nuclear-shell theory. The overwhelming experimental evidence supporting the shell structure is sufficient to pursue the shell theory without having to work out a theory of nuclear matter that proves the existence of shell structure. That issue is left to the nuclear many-body theory, which is a separate problem. The validity of shell theory is not contingent on the successful development of the many-body theory. As far as nuclear structure is concerned the problem is solved by the shell theory. Likewise the perennial problem of fission is solved by the statistical theory. What remains is a separate problem of nuclear matter. Historically, the statistical theory was developed at a time when the experimental proof was far from conclusive. It was a venture and was, therefore, subject to various kinds of criticisms.

A number of criticisms have been directed at the detailed working-out of the statistical principle including the choice of the 'scission point' for statistical calculation and the use of the level density formula. These questions have been answered adequately in the paper published a year ago [11].

Whereas the verification of the statistical theory predictions on mass, charge, energy and neutron distributions is important and crucial, it is also desirable to confirm the direct physical manifestations of the quasi-static process. In the very early stage of development, predictions on such manifestations have been made including the distribution of the initial kinetic energy of the fission fragments at the scission point (average 0.5 MeV) and the distribution of the spin of the fission products. It took more than a dozen years to find experimental results to verify these predictions. The initial kinetic energy can be checked by the long-range α-particle angular distributions [13] which have been studied by many groups with a substantial amount of controversy that was resolved only recently in favor of the statistical theory [12]. Evidence from the spin distribution supporting the theory has been discussed in a recent paper [14]. More detailed calculation is presented in the following.

2. SPIN DISTRIBUTION OF FISSION PRODUCTS

The statistical theory of the spin distribution of fission products was developed in the first paper [15] more than twenty years ago. For a compound nucleus with a spin much less than 10 (applicable to thermal-neutron fission of ^{235}U) the spins of the two fragments are nearly equal (designated by J). The J distribution for a given fragment of mass A_1 (and also for its complement of mass A_2) is given by

$$N(J) = (2J+1)^2 e^{-\left(J+\frac{1}{2}\right)^2 \frac{1}{gT}} \tag{1}$$

where g is the harmonic average of $g_1(A_1)$ and $g_2(A_2)$ with the function g(A) given in terms of the mass M and radius R of the nucleus of mass number A by

$$g(A) = \frac{2}{5}\frac{MR^2}{\hbar^2} \sim A^{5/3} \tag{2}$$

and T is the nuclear temperature, which is the same for the two fragments (thermal equilibrium), and thus equal to

$$T = \sqrt{\frac{E_1 + E_2}{a_1 + a_2}} \tag{3}$$

where E_1, E_2 and a_1, a_2 are the excitation energies and the level density constants of the two fragments 1 and 2 respectively. A typical value of gT for thermal neutron fission of ^{235}U is 63.2.

The J distribution is thus fairly broad, centred on a most probable J value given by

$$J_m = \sqrt{gT} - \frac{1}{2} \tag{4}$$

A typical value of the most probable J for thermal neutron fission of ^{235}U is 7.2. This agrees quite well with the experimental value of 7 obtained by Armbruster, Labus and Reichelt [16]. However, the recent value of Aumann et al. [17] for this quantity is 10. The origin of the discrepancy is not known. Perhaps in the latter work the determination of spin by isomeric ratio of ^{148}Pm favours fission products of high spin and thus accentuates the high spin end of the distribution curve [Eq.(1)].

Equation (4) shows that the most probable spin changes with the mass ratio not only through the dependence on excitation energy $E_1 + E_2$, which varies with the mass ratio, but also through the dependence of g on the mass numbers A_1 and A_2. The latter effect is much weaker and, therefore, we may conclude that the fission modes with larger excitation energies (the more abundant modes in mass distribution according to the statistical theory) will have higher spin. In other words, there is a positive correlation between spin and mass yield. The most probable spin as a function of fragment mass in thermal neutron fission of ^{235}U determined by Eq.(4) based on excitation energy values given in the first paper [15] is shown in Fig.1.

No experimental information is available for comparison. Preliminary results of Loveland do show that in both ^{235}U and ^{252}Cf the most probable fission modes (mass ratio 1.45 for ^{235}U and 1.27 for ^{252}Cf).correspond to the highest spin. Thus the positive correlation is corroborated.

This agreement represents not just another successful application of the statistical theory but a direct proof of the basic assumption of the statistical theory which calls for the dissipation of most of the kinetic energy appearing in the fission process into heat energy (excitation energy). The explanation of asymmetric fission is based on the idea that asymmetric fission products have higher excitation energy at the scission point E_s and thus greater level density leading to larger probability. Higher excitation leads to higher spin. Spin is unchanged from the scission point to the point when the fragments are infinitely apart – the point at which experimental observation is made. Therefore, the observed spin values give us direct information on the crucial quantity E_s. The results of Loveland that the most probable asymmetric fission modes in both ^{235}U and ^{252}Cf do correspond to maximum spin are a direct confirmation of the basic idea of the statistical theory.

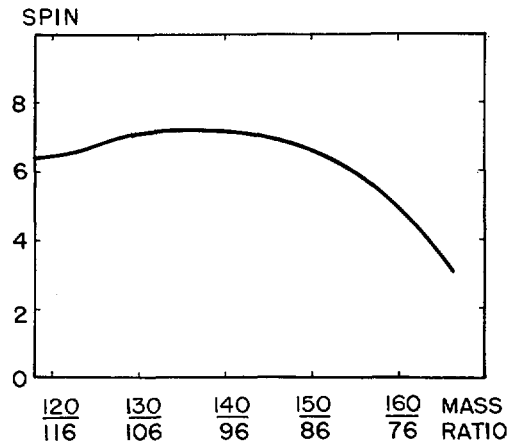

FIG. 1. Spin of fission products of thermal neutron fission of ^{235}U as a function of the mass ratio of fission calculated according to the statistical theory.

For spontaneous fission of ^{252}Cf a similar calculation cannot yet be made but it can be estimated that the spin value is about one unit higher than that of ^{235}U because of the change of both g and T.

Aumann et al.'s results of high-energy α-fission of Th [17] may be predicted according to the statistical theory of high-energy fission because the compound nucleus is ^{236}U, the same as that in thermal neutron fission of ^{235}U. While the trend of higher spin for higher energy is borne out by the calculation, the experimental values are consistently higher than the theoretical value as we have already observed in Aumann et al.'s results for thermal neutron fission. The statistical theory predicts an energy dependence of the spin according to $\sqrt{T}$. Aumann et al.'s values seem to indicate a linear dependence on T.

3. EXCITATION ENERGY OF FISSION PRODUCTS

In all the previous years attempts have been made to find experimental information on the crucial quantity E_s. However, the excitation energy we can observe experimentally is that when the fragments are infinitely far apart, E_f. E_f differs from E_s by the addition of the deformation energy of the fragments. E_f can be ascertained by the number of prompt neutrons. Because of the uncertainty of the deformation energy no clear-cut conclusion can be drawn concerning the validity of the basic statistical assumption. Recently Asghar et al.

[18] have studied the mass distributions of fission products of thermal neutron fission of ^{235}U for various ranges of E_f. The systematic trend of variation can be accounted for by the statistical theory as follows. The experimental information thus corroborates the theory.

Asghar et al. began the investigation after Newson had re-analysed the ORNL fission data along this line. The emphasis of both investigations has been on the fine structure of the distribution curve which may be correlated to even-odd variation or shell structure. We shift the interest to the gross structure of the distribution. Since the statistical theory relates the fission yields to the excitation energies, these experimental studies may shed light on the theory. As already mentioned, the excitation energy crucial to the statistical theory is that at the scission point, E_s, whereas the excitation energy involved in these studies is that at the point of infinite separation, E_f. No direct comparison with the theory can be made. In spite of this some significant conclusions can still be drawn based on the experimental results.

For very small excitation energies E_f the corresponding fission events are characterized by large Coulomb energy at the scission point and very small deformation of the fragments. The scission point is closely represented by two undeformed fragments in point contact. The uncertainty of deformation energy disappears in this case; the two excitation energies E_s and E_f are not much different. It is evident that the dominant factor determining the excitation energy E_f is the close shell structure of the undeformed fragments which favours the doubly magic region around mass number 132. According to the statistical theory these fission modes will appear with large probability. The experimental results of Asghar et al. indeed show that for excitation energies of the order of a few MeV the mass distribution curves are all very narrowly peaked around mass 134.

At the other extreme, for large excitation energies E_f, the corresponding scission point is characterized with small Coulomb energy and large deformation energy (the system is highly stretched out). The two excitation energies E_s and E_f become quite different. The amount of deformation energy not only depends on the degree of deformation (which is related and can be determined by the Coulomb energy) but also on the stiff constant of the fragments. For nearly symmetric fission fragments, which are between shells and are soft against deformation, the deformation energy is smaller (for the same amount of deformation). Therefore, the excitation energy at the scission point is higher and, according to the statistical theory, should appear with greater yields. This explains the observed shift [18] of the peak of the mass distribution curve of a fixed excitation energy toward symmetric fission with respect to the increase of excitation energy E_f at the high end.

The experimental results of Asghar et al. at the low- and high-energy ends of the excitation can thus be explained by the statistical theory. In the middle the mass distribution curves are not much different from the total, undifferentiated

mass distribution curve and therefore do not present new information calling for explanation.

The excitation energy E_f distribution curve (Fig.2 of Ref.[18]) reflects the well-known kinetic energy distribution for a fixed fragments pair. The most probable value of this distribution, 24 MeV, agrees well with the empirical estimate of the average excitation energy E_f based on the energy of prompt neutrons and prompt γ-rays [15].

4. THE VARIANCE OF KINETIC-ENERGY DISTRIBUTION

The problem of kinetic energy distribution of fission products has been extensively studied. One aspect that has not received much attention is the variation of the variance of the total fission fragment kinetic energy $\sigma^2_{E_k}$ and the closely related variance of the total number of prompt neutrons σ^2_ν. The statistical theory derivation of $\sigma^2_{E_k}$ was worked out twenty-five years ago [15]. Recently Lazarev [19] has reviewed the available experimental information and compared the results with various theoretical calculations including that of the statistical theory. He found unusual features that none of the theories can explain. Both $\sigma^2_{E_k}$ and σ^2_ν increase slowly with the charge number Z of the fissioning nucleus for $Z < 96$ which is expected from the statistical theory. But for $Z > 96$ they increase rapidly which is totally unexpected.

The theoretical formula of $\sigma^2_{E_k}$ derived by the statistical theory used by Lazarev for numerical calculation and comparison comes from the first paper [15] in which the shell effect on nuclear masses is taken into account but that on the nuclear stiff constant is not. The latter is necessary to explain the dip of the kinetic energy curve in the symmetric fission region and the saw-tooth shape of the prompt neutron distribution curve $\nu(A)$ [4]. It should be included in the calculation of $\sigma^2_{E_k}$ as well. Without it there is no surprise that Lazarev found disagreement with experimental results. In fact, as explained below, this effect seems to be just what is needed to explain the rapid increase of the variance curves after $Z = 96$ experimentally observed.

The stiff constant is large for closed shell nuclei and small between the shells. Asymmetric fission modes generally involve one fragment near a closed shell whereas symmetric fission modes involve none. Thus symmetric fission products are softer and can be easily stretched. Their $\sigma^2_{E_k}$ and σ^2_ν are expected to be larger than those of asymmetric fission. For the low actinides asymmetric fission dominates; the average $\sigma^2_{E_k}$ and σ^2_ν are those of asymmetric fission modes which are small. As Z increases, probability of symmetric fission increases

rapidly and the average variance is increased to reflect the contribution of the symmetric fission modes that have larger variances. (Eventually in the very high actinide region the closed shell fission products move to the symmetric fission region but the distribution is sufficiently broad to include many soft fragments now in the asymmetric fission region. Thus the variances remain high.) The experimental results are thus explained. That $\sigma^2_{E_k}$ of symmetric fission is much greater than that of asymmetric fission has been reported experimentally by Gavron and Fraenkel [20].

The fact that the variances for thermal neutron fission are greater than those of spontaneous fission is likely to be due to the dependence of the variances on the excitation energy as prescribed by the statistical theory [15]. The increase of symmetric fission yields in thermal neutron fission over spontaneous fission may also have a part to play.

The statistical theory has the merit, among all theories, to give rise to the largest possible variances because all degrees of freedom are fully realized. A strict dynamical theory always leads to zero variances.

Another piece of work on the variance and covariance of neutron numbers and kinetic energies of the fragments may be mentioned. Signarbieux et al. [21] found the correlation of the excitation energies of the two fragments is practically zero for all mass ratios. They claimed that this result proves that at the moment of scission, an important part of the energy gained by the system at the expense of the potential energy is dissipated in other degrees of freedom than the pure elongation and suggests that the speed of evolution of the system could be sufficiently slow to justify the hypothesis of the quasi-equilibrium state at the moment of scission.

5. CONCLUSION

Recent studies on spin distribution, excitation energy and its variance shed new light on the statistical theory of fission. They establish the conceptual validity of the statistical approach and correctly predict new experimental results. Together with earlier studies it can now be concluded that the statistical theory has generally explained all the phenomena it is designed to explain, i.e. those pertaining to the late stage of fission, and any theory capable of explaining these facts must be statistical in nature. Recent dynamical study based on the one-body dissipation mechanism leads to results in excellent agreement with those of the statistical theory and therefore may be regarded as the dynamical interpretation of the statistical theory. The long controversy between these two approaches concerning the perennial question of asymmetric fission is now resolved.

REFERENCES

[1] SPECHT, H.J., Rev. Mod. Phys. **46** (1974) 773.
[2] FONG, P., Phys. Rev. C **10** (1974) 1122.
[3] WING, J., FONG, P., Phys. Rev. **157** (1967) 1038.
[4] FONG, P., Phys. Rev. Lett. **11** (1963) 375.
[5] FONG, P., Dissertation, University of Chicago (1953).
[6] FONG, P., Phys. Rev. C3 (1971) 2025.
[7] MARUHN, J., GREINER, W., Phys. Rev. Lett. 32 (1974) 548.
[8] FONG, P., Phys. Rev. Lett. 34 (1975) 699.
[9] NEGELE, J.W., KOONIN, S.E., MÖLLER, P., NIX, J.R., SIERK, A.J., Phys. Rev. C **17** (1978) 1098.
[10] FONG, P., Phys. Rev. C **19** (1979) 868.
[11] FONG, P., Phys. Rev. C **17** (1978) 1731.
[12] FONG, P., Phys. Rev. C **16** (1977) 251.
[13] FONG, P., Phys. Rev. C **2** (1970) 735.
[14] FONG, P., Phys. Rev. C **17** (1978) 1879.
[15] FONG, P., Phys. Rev. **102** (1956) 434.
[16] ARMBRUSTER, P., LABUS, H., REICHELT, K., Z. Naturforsch. **26a** (1971) 512.
[17] AUMANN, D.C., GÜCKEL, W., NIRSCHL, E., ZEISING, H., Phys. Rev. C **16** (1977) 254.
[18] ASGHAR, M., GUET, C., PERRIN, P., Nucl. Phys. A**298** (1978) 13.
[19] LAZAREV, Yu.A., At. Energy Rev. **15** (1977) 75.
[20] GAVRON, A., FRAENKEL, Z., Phys. Rev. C 9 (1974) 637.
[21] SIGNARBIEUX. C., BABINET, R., NIFENECKER, H., POITOU, J., Physics and Chemistry of Fission (Proc. Symp. Rochester, NY, 1973) Vol.2, IAEA, Vienna (1974) 179.

DISCUSSION

D. HOFFMAN: Can your statistical theory explain the transition from asymmetric to symmetric mass distribution and very high TKE observed for spontaneous fission of the fermium isotopes at mass 258 and 259?

P. FONG: Yes, this point is discussed in a paper I published entitled "Symmetric fission of ^{258}Fm" (Phys. Rev. C**9** (1974) 2448).

E. PIASECKI: You mention that your theory can explain the ternary-fission data. I think you may be overoptimistic in that respect. I know you can explain the mean value of the emission angle, but the width of the angular distribution is, at least, of the same importance. I am aware of only one study in which the author claimed that his calculations could reproduce the experimental value of the width using the results of your theory as input data, and that was one by VITTA, P.B. (Nucl. Phys. A **170** (1971) 417),but it was subsequently shown that his calculations were wrong. Can you comment on this?

P. FONG: I know that Vitta's calculation missed a Jacobian of transformation, which may affect the results somewhat but will not radically alter the situation.

In any case the existence of the width indicates some statistics. The fully statistical theory offers a better chance of explaining the large widths that are often observed in fission.

K.M. DIETRICH: Let me try to make it clear why there may be some hesitation on the part of various authors to consider your theory as the final form of a statistical theory, and let me also emphasize that I do so with all due respect for the fruitfulness of your original idea and the impetus it has given to fission research. A final statistical theory should provide the distribution of the system over the potential landscape as a function of time, i.e. it should describe the full evolution of the shape degrees beyond the saddle point. Your statistical theory relates the observed cross-sections with the level density at the 'scission point'. This level density depends essentially on the potential energy at the scission point and, therefore, also on your actual choice of scission point. It would, of course, be preferable for the theory to *determine* the distribution of the system in the scission region. It is then conceivable that the result of such a theory would justify the choice of the scission point that you have to make, and possibly also the assumption of complete statistical equilibrium, as implied by your ansatz.

P. FONG: Thank you for your comment. A detailed calculation of the mass distribution depends on calculations of two quantities - the excitation energy and the level density formula. The calculation of excitation energy, according to the Strutinsky prescription, can be relied upon since the method has been used extensively with remarkable success. The level density formula for a deformed nucleus affected by nuclear cells is less certain. Ignatyuk has calculated the level density constant a for a deformed nucleus as a function of the mass number, including the magic numbers, and has found a smaller a for closed-shell nuclei. Another way to express the shell effect is to take a smooth constant a but to reduce the excitation energy by a fixed amount. This point has been investigated (Phys. Rev. **C 17** (1978) 1731) and the conclusion has been drawn that no matter how the shell effect is treated, the prediction of asymmetric fission remains unaltered. Although there are uncertainties that will have to be ironed out in the future, the origin of asymmetric fission seems to be clearly established.

DYNAMICAL THEORIES OF FISSION
(Session H)

Chairman

P. FONG
USA

TDHF, A SELF-CONSISTENT DESCRIPTION OF FISSION – PRESENT AND PROSPECTIVE

H. FLOCARD
Division de physique théorique,
Institut de physique nucléaire,
Orsay, France

Abstract

TDHF, A SELF-CONSISTENT DESCRIPTION OF FISSION – PRESENT AND PROSPECTIVE.
The present status in self-consistent calculations of fission is reviewed and some perspectives are indicated.

Tracing back the development of a large-amplitude collective phenomenon like fission to the motion of the individual nucleons is now made possible by the progress of the self-consistent theories derived from time-dependent Hartree-Fock (TDHF). Despite the unavoidable simplifications of these theories and the associated restrictions in our understanding, for the first time we have at our disposal a dynamical model in which the fission collective path and the dynamics originate from the interplay of the microscopic variables. That these theories enjoy now a rapid expansion is probably not coincidental. In spite of the length of the calculations that they imply their growth cannot be attributed to the sole improvement of computer technology. They fulfil a need of present nuclear physics. In most of the theoretical descriptions of fission the physicist acts between the microscopic and macroscopic stages of the model. As a filter he comprehends, or at least tries to, the mostly incoherent motion of the nucleons and selects few dominant collective modes which he parameterizes so as to achieve, with minimum analytical or numerical difficulty, a maximum adequacy to what the thinks is the correct physical picture. The microscopic aspects may be re-introduced afterwards in a more or less simplified way. At least for the static case, the method derived by Strutinsky [1] has shown how to correct liquid-drop energy curves for the shell effects. Another example is the one-body viscosity model [2] where the incoherent motion of the nucleons modifies the dynamics of fission by the addition of a damping term. The achievements of this type of methods in the domain of nuclear fission are well known to everybody. The natural and constant need for improvement is, however, hard to satisfy along this line of work. In fission, where only the shapes of the starting point (one nucleus) and the final point of the motion (two fragments) are known, once the simplest analytical parameterizations of the more natural collective variables (say, elongation and necking) have

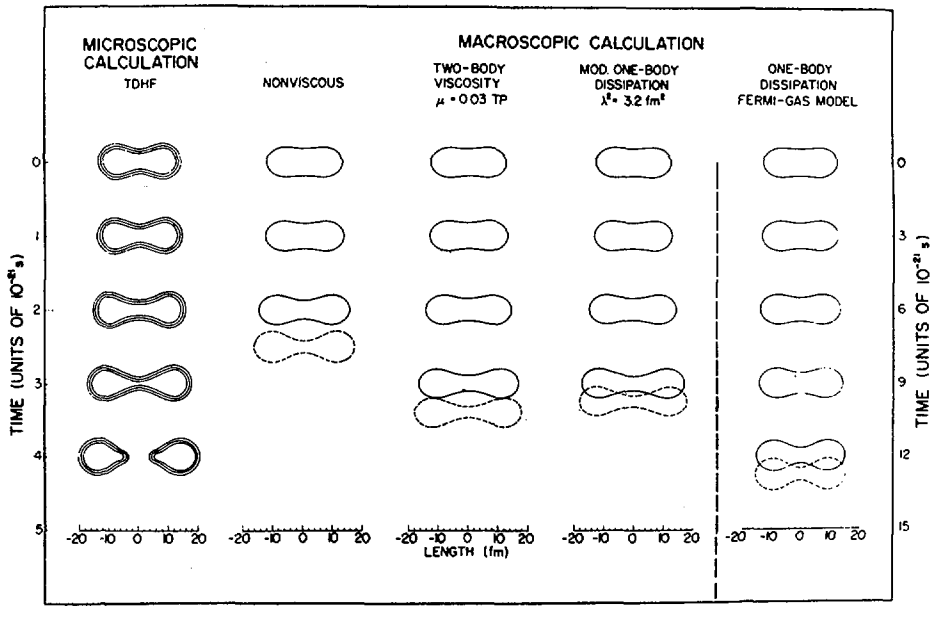

FIG. 1. Comparison of time evolution of densities calculated in a self-consistent model with those of several classical calculations.

been investigated, it becomes difficult to improve. In other words, the collective path is only qualitatively determined and further elaboration and complication of the already used collective variables would probably be dangerous because it would more rely on analytical ingeniousness than on deeper physical insight. One may also argue that the variables are well enough defined and what is needed is a better understanding of their interplay with the incoherent nucleonic bath. To these questions: which collective variables? how many? and how do they interact with incoherent nucleon motion? , TDHF can certainly give some useful answers. These answers will not be found in this paper which is mainly of a prospective character, but undoubtedly in the publications of a near future.

The TDHF physicist abandons the position of an augur who after an inspection of the entrails of the Fermi sea predicts how fission will take place, for the less ambitious position of an observer. Once the starting positions of the nucleons have been chosen, and in the case of fission there is not much choice, their collective behaviour proceeds naturally. The explanation of the fission process is then pushed back to the nucleon two-body interaction and the shell-model picture of the nuclei as described by Hartree-Fock. The real problem in TDHF

beyond the difficulty of solving the equations is the analysis of their results. An analysis of the time evolution of the nuclear density and current can give an idea of the dominant collective variables. But other methods exist like that using the adiabatic approximation to TDHF [3]. The interaction between the fission modes and the incoherent modes and the nature of the transfer of energy between them raises more difficult questions. However, in the present situation we have already hints on how the problem could be tackled.

Let us now turn to an example of such a TDHF calculation. It is proposed in the paper by Negele, Koonin, Möller, Nix and Sierk which up to now is the only reference available [4]. Their main result is shown in the first column of Fig.1. It describes the time evolution of the nuclear density of the ^{236}U nucleus. The picture shows the contour lines of the total density for the values 0.02, 0.08 and 0.14 fm^{-3}. The middle line, therefore, corresponds to the external surface of a sharp-edge nucleus, and the other two lines give us an idea of the surface width. The starting point of the calculation is provided by a constrained Hartree-Fock calculation using the quadrupole operator as constraint. In this way, the static Hartree-Fock fission curve has been computed. The starting point of the dynamical calculation is the top of the fission barrier. An advantage of this choice, in addition of its being natural for the description of neutron-induced fission, is that the extrema of the constrained Hartree-Fock energy curve do not depend on the particular choice of the constraining operator. Such a starting point is, in principle, uniquely defined. A slight modification is, however, necessary so as to push the nucleus out of this unstable – but nevertheless equilibrium – position. The authors have chosen a point on the fission curve 1 MeV below the top of the barrier. There is probably some arbitrariness in this choice, and a study of the influence of the choice of the starting point might prove interesting, but for an exploratory work as Ref.[4] this is certainly reasonably good. In Fig.1 one can make several observations: scission takes place in less than 3.5×10^{-21} s; the scission shape is rather compact; the surface width remains remarkably constant during the evolution, and the fragments display, after scission, a marked octupole deformation. In fact, the multipolarity of the post-scission shapes is probably higher since each fragment exhibits a very definite bulge. This is interesting since this collective co-ordinate is absent from most of the models that describe fission in terms of few collective variables. We shall come later to the results concerning fission-fragment kinetic energies.

Before going over to a comparison of the results with those obtained by means of classical collective models, we must recall some of the limitations of the calculation as they are presented in Ref. [4]. One may, first, mention the numerical problems related to the discretization of the wave-functions on a spatial mesh. The authors estimate that it corresponds to, at least, 130 MeV inaccuracy for the system under consideration. This, at first sight, might seem very large compared to typical energies encountered in the study of fission but the authors express their confidence that this uncertainty in the absolute value of the energy will not affect a

dynamical process where only relative energies matter[1]. The possible effects of this numerical uncertainty might still be worth a further study because the error, more particularly, affects the high-lying levels close to the Fermi surface which are among the most active partakers in fission.

More important are probably the limitations imposed on the individual wave-functions and the consequences of the approximate treatment of pairing. Several symmetries have been imposed on the single-particle wave-functions. First, the spin-orbit terms in the Hartree-Fock energies and potentials have been omitted. Each TDHF orbit is, thus, doubly degenerate. This simplication which has been imposed by computational considerations might have an effect on heavy systems where the spin-orbit term mixes the shells and decreases the amplitude of the shell effects. Second, it has been assumed that the single-particle wave-functions possess axial symmetry and reflection symmetry. From a practical point of view this reduces the otherwise three-dimensional problem to a two-dimensional one. Unfortunately, there are consequences on the dynamics. One is evidently the restriction to symmetric fission. In addition, the H.F. orbitals can now be sorted in blocks corresponding to distinct parities and projection of $\vec{J}$ on the fission axis. These blocks are not connected by the TDHF Hamiltonian so that the number of nucleons in each block is a constant of motion. In such a restricted sub-space of Slater determinants fission cannot occur. For this reason it has been necessary to go beyond the pure TDHF formalism.

A solution compatible with the symmetry requirements consists in enlarging the variational space to include B.C.S. wave-functions so that a path connecting separated fragments exists. To the H.F. energy is now added a pairing energy term. The variation of the total energy provides a set of coupled equations; the first equations, formally identical with the TDHF equations, govern the spatial and time evolution of the single-particle wave-functions, while the second ones specify the time evolution of the occupation probabilities of each orbital. To define the pairing energy one has used an additional parameter[2] homogeneous to a gap Δ which, unfortunately, has an ambiguous meaning. It can partly be considered as providing an improvement of TDHF with approximate treatment of pairing. However, the true motivation for its introduction is the need to cure the lack of residual interaction at the crossings of levels with different quantum numbers. When two such levels cross, the residual interaction breaking the symmetry of the problem which could be neglected for two well separated levels becomes preponderant. Depending on its strength and on the velocity of the crossing, it will cause

---

[1] This claim is supported by a discussion of deformation energy curves for a system which is, however, much lighter (^{58}Ni).

[2] In fact, two because the number and the nature of the single-particle orbits which are considered in the calculation can also affect the results.

a transfer of occupation probability from one level to the other. In the calculations of Ref.[4], the gap Δ acts precisely in this way. It should therefore be considered as a simple way to mock a residual mean field interaction ensuring the coupling of levels with different parities and angular projection. This was noticed in Ref.[5] where the identity of the second set of TDHF-BCS equations with a Landau-Zener equation parameterized by Δ, was shown. Because of this dual nature it is difficult to estimate what should be a reasonable value for Δ. The question as to whether it is possible to reproduce symmetry-breaking terms in the average field by means of Landau-Zener transfers and a unique constant, therefore neglecting all spatial effects, is probably even more important.

The influence of Δ on the results is strong. It causes the time evolution of the fission process to increase from 2.2×10^{-21} s for $\Delta = 6.0$ MeV to 5.0×10^{-21} s for $\Delta = 0.7$ MeV. The calculation shown in Fig.1 has been made with $\Delta = 2$ MeV. In principle, the specific choice of Δ should also modify the starting point because the static deformation energy curve changes with the gap. The influence on the shape at scission is very large. For small values of Δ one obtains elongated scission shapes because the fission occurs predominantly by deformation of the wave-functions rather than a promotion into the orbits that finally will be occupied in the fragments. When Δ is large the wave-functions corresponding to two separated fragments with spherical shapes are more rapidly populated and a compact scission shape is obtained. This influence is also reflected in the fission kinetic energy. While the translational kinetic energy at scission does not much depend on Δ, the large differences in shape configurations induce variations of the Coulomb energy by several tens of MeV. A very good agreement with experiment is obtained for $\Delta = 6$ MeV. When Δ is decreased to 2 MeV the fission kinetic energy is underestimated by 15%. To summarize the conclusions of Ref.[4] concerning the influence of Δ, one may say that the modifications of the TDHF formalism so as to allow for the coupling of all single-particle states has noticeably changed the nature of the physics involved. The gap Δ whose interpretation is up to now not very clear appears as a major factor in deciding the qualitative and quantitative features of the self-consistent results. From this point of view, Ref.[4] can only be considered as the first consequent step toward an evaluation of TDHF predictions about fission.

Having in mind these restrictions about the meaning of the self-consistent calculations, let us now compare the results with those of classical calculations as they are shown in Fig.1. Three calculations using different Rayleigh dissipation functions are proposed. The first correspond to the ordinary fluid viscosity labelled here as two-body. The second and the third ones are labelled one-body according to the underlying physical idea that dissipation occurs from the sole exchange of energy between the nuclear surface and a bath of otherwise non-interacting nucleons. The relationship between TDHF and fluid hydrodynamics is difficult to understand. A connection between the two formalisms is generally achieved at the cost of a

truncation of TDHF equations which very likely mutilates their physical meaning. For this reason, we shall not spend much time on a comparison with two-body viscosity results. One may simply note that, for $\Delta = 2$ MeV, scission is achieved in a time interval similar to that of TDHF but with more elongated shapes. We shall not insist on the modified one-body viscosity results either. The corresponding dissipation function has been introduced in Ref.[6] to correct a deficiency of the ordinary one-body dissipation formula which reads

$$\frac{dE_{coll}}{dt} = \frac{3}{4}\rho_m v_F \int v_n^2 \, ds \qquad (1)$$

In the above formula, ρ_m is the mass density, v_F the Fermi velocity and v_n the normal velocity of the nuclear surface. The formula is evidently not Galilean-invariant although in most cases this can be cured[3] by a proper definition of v_n^2. To restore Galilean invariance, the modified one-body formula proposes the replacement of v_n by the difference between the normal velocity of the surface and that of the Fermi sea, and approximates this difference by a term proportional to $\partial v_n/\partial n$. In principle the spirit of the one-body method has been preserved in this operation. However, the evaluation of the derivatives necessitates the knowledge of the distribution of velocities close to the surface and, therefore, becomes highly model-dependent. This is exemplified by the behaviour of the modified one-body dissipation as a function of the multipolarity of the vibrations when it is calculated on the assumption of an irrotational fluid behaviour for the internal density. Since in such a case there is no global translation one would expect at least approximate agreement between the two one-body formulas. On the contrary, one finds that dissipation decreases with multipolarity for ordinary one-body viscosity and increases when formula (1) is corrected according to Ref.[6]. We, therefore, think that the physical picture behind the modified one-body viscosity is more complex than is suggested by its name and that all of it is not elucidated. On the left-hand side of Fig.1 (with a different time scale) one sees the evolution of shapes when friction is governed by one-body viscosity. The scission time is four times longer than that predicted by TDHF BCS and the scission shape is more compact. We have already seen that the modifications in the formalism introduced with the gap Δ greatly change the significance of the self-consistent results. On the other hand, the simple parameterization of the nuclear shapes used in the classical model may explain a lengthening of the scission time. We have mentioned that complex motions of the surface corresponding to high multipole modes are less damped by one-body friction. These modes which, as has been noted above, participate during

[3] This is more difficult for the fission case because of the continuous transition between the saddle point where there are apparently no reasons for correcting the formula and the scission configuration where formula (1) violates Galilean invariance.

the self-consistent evolution might favour a faster rupture of the neck. To make the comparison totally meaningful it would therefore be worthwhile to enlarge the number of collective variables used in the classical models so as to include the sequence of shapes occurring during the TDHF evolution. With the results of Ref.[4] we cannot decide whether TDHF and one-body viscosity correspond to the same physical picture. This will be left to more elaborate TDHF and classical calculations.

Grossly speaking, the dissipation function defined by formula (1) is derived from two assumptions. First, the collective variables of interest are those which define the surface of the nucleus and the only exchange of energy which matters arises from an interaction of this surface with the perfect Fermi gas of the nucleons. Second, the irreversibility of this exchange of energy is a consequence of the instantaneous equilibration of the internal Fermi gas. Immediately after the collision with the surface, the nucleon loses its memory of the peculiarities of the shock so that the internal distribution of velocities is preserved as a function of time. These two assumptions are of very different nature. One expects the first one to be true in a model like TDHF which emphasizes the notions of independent particle and average potential well.

As a pedagogical example, we propose in Fig.2 a calculation of the collision of a finite slab of nuclear matter on infinite nuclear matter [7]. This system was chosen because it minimizes the importance of both surface and shell effects. In Fig.2, we have plotted several contour lines of the Wigner function. This quantity is defined as the Fourier transform with respect to the relative distance $\vec{r}_1-\vec{r}_2$ of the H.F. one-body density operator $\rho(\vec{r}_1,\vec{r}_2)$. It is the best quantal equivalent of the classical phase space density $f(\vec{r},\vec{p})$. Let us now compare its time evolution to that of the classical density corresponding to the one-body picture. For a one-dimensional problem the two-dimensional phase space of the static semi-infinite matter is bounded by the horizontal lines $\pm k_F$ in the momentum direction and the vertical line of the surface. A typical nucleon trajectory is shown as a dash-dot line on the upper part of Fig.2. The nucleon with momentum k travels freely through the nuclear medium until it reaches the surface where it bounces back with momentum $-k$. In the impinging slab whose phase-space density has also a momentum width of $2k_F$ the same phenomenon occurs but displaced by the momentum k_I of the incident slab. When the slabs come into contact the nuclear surface between them disappears. The nucleons of the slab with positive velocities will then flow across the semi-infinite matter which, conversely, will create a back-flow of nucleons. This is schematized in the upper part of Fig.2. The signatures of the independent-particle picture are the left-right flow of nucleons from the projectile with momentum larger than k_F and that of nucleons from semi-infinite matter with momentum less than k_I-k_F going in the opposite direction. The classical evolution is reproduced accurately by that of the Wigner function as shown by the first three pictures at the bottom of Fig.2. Thus the dynamical picture inherent to the one-body viscosity model is also contained in TDHF.

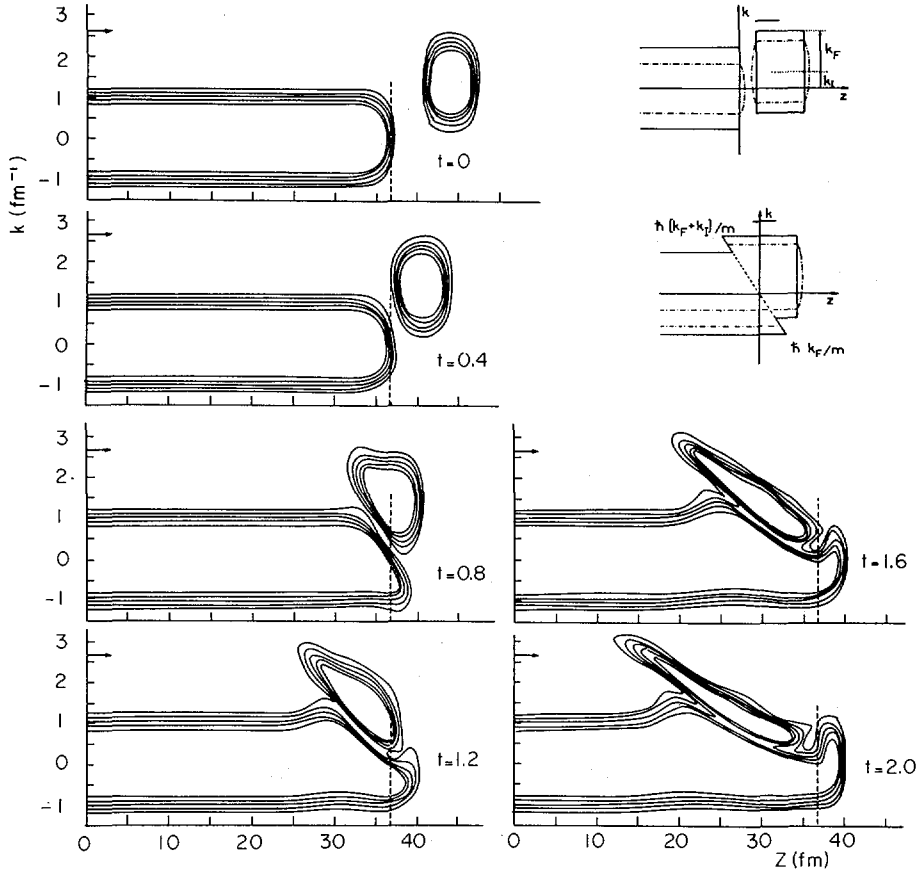

FIG. 2. Density in phase space at several times of the collision of a finite stab with semi-infinite matter. Times are given in units of 10^{-22} s, distances z in fm and momenta k in fm^{-1}.

The assumption of immediate equilibration of the internal momentum density is much more difficult to check. First, the one-dimensional calculation described above cannot be used since it describes only compressional excitations instead of the surface motions for which formula (1) is relevant. Even for an appropriate TDHF calculation one would face the problem of defining what should be considered as the interior of the nucleus and what is the surface. Probably, no unambiguous answer exists to this question since all nucleon wave-functions are partly inside and at the surface of the nucleus.

The preceding considerations underline the difficulties one encounters in trying to interpret TDHF results in the light of the available models. We have

also indicated the limitations of present self-consistent calculations. Let us now imagine what could be done in the near future in view of the present state of the art. Since the solution of three-dimensional TDHF equations is now mastered, the calculation of a fission trajectory without any symmetry limitations on the single-particle wave-functions should very soon provide us with definite TDHF predictions concerning the fission time path and kinetic energies. In the same way as mass transfers have been calculated for heavy-ion collisions, it will be possible to estimate mass widths and kinetic energy distributions. In addition, the adiabatic approximation to TDHF which is well suited for a collective motion like fission provides now a natural way to extract from the TDHF results collective co-ordinates [8], potentials and collective mass parameters. From a knowledge of these results and the time evolution given by TDHF the dissipation function will be calculated. This programme of work for which the tools are ready will certainly help us to comprehend this still puzzling problem: fission.

REFERENCES

[1] BRACK, M., DAMGAARD, J., JENSEN, A.S., PAULI, H.C., STRUTINSKY, V.M., WONG, C.Y., Rev. Mod. Phys. **44** (1972) 320.
[2] BLOCKI, J., BONEH, Y., NIX, J.R., RANDRUP, H., ROBEL, M., SIERK, A.J., SWIATECKI, W.J., Ann. Phys. (NY) **113** (1978) 330.
[3] VILLARS, F.M.H., Nucl. Phys. **A285** (1977) 269; GOEKE, K., REINHARD, P.G., Ann. Phys. (NY) **112** (1978) 328; BARANGER, M., VENERONI, M., Ann. Phys. (NY) **114** (1978) 123.
[4] NEGELE, J.W., KOONIN, S.E., MÖLLER, P., NIX, J.R., SIERK, A.J., Phys. Rev. **C17** (1978) 1098.
[5] BLOCKI, J., FLOCARD, H., Nucl. Phys. **A273** (1976) 45.
[6] SIERK, A.J., KOONIN, S.E., NIX, J.R., Phys. Rev. **C17** (1978) 646.
[7] KÖHLER, S., FLOCARD, H., accepted for publication in J. Nucl. Phys.
[8] BONCHE, P., DOUBRE, H., QUENTIN, P., Phys. Lett. **82B** (1979) 5.

DISCUSSION

G. SCHÜTTE: To ensure fission at all in the TDHF calculation, there is need for an artificial gap. Did you therefore ensure artificially that the adiabatic approximation was valid?

H. FLOCARD: I do not think that the two questions are necessarily connected. As I stated, the gap introduced into the calculation has a marked effect on the velocity of motion, but it is still impossible to say which value of Δ, if any, is the more reasonable. The validity of the adiabatic approximation can be checked

in two ways. First, within the adiabatic limit, there are self-consistent checks that show whether the approximation is valid or not. Second, the adiabatic results can be compared with a pure TDHF calculation of fission, which still remains to be made.

P. SCHUK: Do you think that sub-barrier fission could be treated on the basis of TDHF?

H. FLOCARD: No, sub-barrier fission seems to be beyond the possibilities of pure TDHF calculations.

K.W. GOEKE: The initial condition for the TDHF calculations you have reported is a quadrupole CHF colution ~1 MeV below the second barrier. This is an approximation for a full adiabatic TDHF solution that determines the initial condition to be used in TDHF. Since the ATDHF method might lead to a constraining operator different from the quadrupole moment, I personally expect considerable changes in the TDHF results if they start from such improved initial conditions. A combined ATDHF-TDHF treatment of this kind is particularly necessary when one deals with sub-barrier processes, since in ATDHF all the quantum effects associated with a barrier penetration of this kind can be dealt with. There is no point in worrying about the validity of the adiabatic approximation, as it can be checked exactly by simply expressions describing the coupling of the collective to the non-collective degrees of freedom, which allow us to decide whether further channels have to be incorporated or how important friction effects are likely to be.

H.A. NIFENECKER: Dr. Flocard, it is gratifying to see that TDHF seems to justify at least one aspect of one-body dissipation. Since the TDHF calculations were carried out with a paired systems, is it not implicit that we are justified in generalizing the one-body friction to cover wall reflection of nucleon pairs?

H. FLOCARD: In principle yes, but it might be more interesting to estimate the dissipation induced by the breaking of the pair colliding with the surface.

J.B. WILHELMY: Your model calculations appear to show a descent from saddle to scission of several times 10^{-21} s, irrespective of the assumption with regard to viscosity. Do I take this as an established and realistic estimate of the time, or will improved calculations in the future alter it?

H. FLOCARD: In my paper I have tried to indicate all the calculation restrictions that could have a marked effect on the result. It is encouraging to see, however, that the order of magnitude of the fission time does not alter when the value Δ increases from $\Delta = 0.7$ MeV, which would be reasonable for an ordinary gap, to the extreme value $\Delta = 6$ MeV, which can only be explained if Δ is taken as a parameter giving breaking symmetry terms in the mean field.

H.C. PAULI: I think you are taking a rather optimistic view in believing that you can calculate a neutron-induced fission reaction, for example a cross-section. Frankly, I find it hard to believe. Do really you think, for instance, you could calculate Γ_n/Γ_f by your method?

H. FLOCARD: It is possible I may have given you the wrong impression. I only meant to say that it would be reasonable to expect a real TDHF calculation for the last stage of neutron-induced fission, namely motion from the top of the barrier to the scission point, in the near future. In such a calculation one has to rely on other physical models in order to define the starting point. I should say that some people (who do not do the calculations) are highly optimistic that the whole process of neutron-induced fission, from the moment the neutron hits the nucleus, can be studied within the framework of TDHF.

QUANTUM CORRECTIONS TO POTENTIAL ENERGY SURFACES AND THEIR INFLUENCE ON BARRIERS

P.-G. REINHARD
Institut für Kernphysik,
Universität Mainz,
Mainz

K.W. GOEKE
Institut für Kernphysik,
KFA Jülich, Jülich,
and
Physik-Department,
Universität Bonn,
Bonn,
Federal Republic of Germany

Abstract

QUANTUM CORRECTIONS TO POTENTIAL ENERGY SURFACES AND THEIR INFLUENCE ON BARRIERS.

A microscopic theory suitable for the description of fission processes and other large-amplitude collective phenomena is presented. The approach makes use of an optimal collective path, which is constructed by means of adiabatic time-dependent Hartree-Fock (TDHF) techniques as to show maximal de-coupling of collective and non-collective degrees of freedom. Although this involves a classical concept, the theory fully incorporates quantum effects associated with extracting a collective Schrödinger equation from adiabatic time-dependent Hartree-Fock theories (ATDHF). The quantum corrections are discussed extensively, and calculations in the two-centre shell model show, e.g. that they reduce the second barrier by 2 MeV and the life-time by a factor of 10^{-7}. The relationships of the presented quantized ATDHF approach to the random-phase approximation (RPA) and a generalized dynamic generator co-ordinate method are investigated. For the construction of the optimal fission path, simple step-by-step methods are suggested.

1. Introduction

During the last decade, microscopic theories for the dynamic description of fission and other large amplitude collective phenomena have been extensively studied [1,2]. In contrast to induced fission the spontaneous

decay is independent of initial conditions and can be viewed as a collective motion along a large amplitude eigenmode of the system describable in terms of a few collective coordinates q and a collective Hamiltonian $H_C(q,\partial_q)$. Microscopic theories aim to deduce the H_C from a given many-body Hamiltonian $H(x_i,\partial_{x_i})$. Since a direct coordinate transformation $\{x_i\} \to q$ is unfeasible, most attempts to obtain H_C employ the concept of a collective path. This is a set of Slater determinants $|q\rangle$ in BCS states labelled with a collective parameter q which reflects the various distortions of the wave function during the process. A wide range of choices for the path $|q\rangle$ has been used, the cluster model, the deformed shell model or constrained Hartree-Fock. The dynamic extension of the path $|q,p\rangle$, where p is to describe the average collective momentum, is usually evaluated by means of cranking like approaches [3,4]. Just recently theories like time dependent Hartree-Fock [5-7] (TDHF) and adiabatic TDHF [7-11] have become fashionable, which seem to be promising tools towards an unambiguous choice of the path $|q,p\rangle$.

A consistent microscopic theory of collective motion using collective paths has to consider basically two questions: 1) A unique prescription for evaluating a quantized H_C for a given path $|q,p\rangle$, 2) the determination of an optimal path $|q,p\rangle$. In the present paper we discuss solutions to both problems, with an emphasis on the quantum effects in H_C. (Since friction effects are not discussed, the approach as it stands is limited to subbarrier processes. There, of course, quantum effects are most important.)

2. Derivation of a quantized collective Hamiltonian

For a given path $|q,p\rangle$ one immediately obtains a classical Hamiltonian

$$\mathcal{H}_C(q,p) = \langle qp|H|qp\rangle = \frac{p^2}{2\mathcal{M}(q)} + \mathcal{V}(q) \tag{2.1}$$

where $\mathcal{V}(q) = \langle q|H|q\rangle$ and $\mathcal{M}^{-1}(q) = \langle q|[\hat{Q},[H,\hat{Q}]]|q\rangle$ if we define (in the adiabatic limit) $\hat{Q}$ as $|q,p\rangle = (1+ip\hat{Q})|q\rangle$. The problem is now the extraction of a quantized collective Hamiltonian $\hat{H}_C$, e.g. of the form (with $\hat{p} = -i\partial_q$)

$$\hat{H}_C = :\hat{p}^2 \frac{1}{2M(q)}: + V(q) \tag{2.2}$$

where we choose the $\hat{p}$-ordering to be given as

$$:\hat{p}^2 \frac{1}{2M}: = -\frac{1}{4}\{\partial_q^2 \frac{1}{2M} + \partial_q \frac{1}{M}\partial_q + \frac{1}{2M}\partial_q^2\} \tag{2.3}$$

There one has to consider that M(q) and V(q) are not to be identified directly with the corresponding classical quantities $\mathcal{M}(q)$ and $\mathcal{V}(q)$ since the latter ones contain quantum fluctuations. Those arise due to the fact that the states $|qp\rangle$ are wave packets with respect to the collective operators $\hat{Q}$ and $\hat{P}$, having a certain width $\Delta P^2 = \langle qp|(\hat{P}-p)^2|qp\rangle$ and $\Delta Q^2 = \langle qp|(Q-q)^2|qp\rangle$. In order to obtain the quantized H_C one has to identify the quantum fluctuations in $\mathcal{H}_C$ and to extract them. This yields [9]

$$M(q) = \mathcal{M}(q) \qquad V(q) = \mathcal{V}(q) - \frac{\Delta Q^2}{2}\frac{\partial^2 \mathcal{V}}{\partial q^2} - \frac{\Delta P^2}{2\mathcal{M}} \tag{2.4}$$

Obviously the correction terms in the potential in eq. (2.4) are zero point energies, which can be readily evaluated. Actually the zero point energies depend on the structure of the kinetic energy operator, eq. (2.4). This can be chosen at convenience. However, in order to achieve consistency one has to evaluate the correction terms accordingly. Thus the old question in quantizing $\mathcal{H}_C$, viz. to find out the proper $\hat{p}$-ordering, has been replaced by a precise prescription how to evaluate quantum corrections for a given kinetic energy operator. The result is then unambiguous.

It is necessary to investigate the relationship of the present approach to the generator coordinate method (GCM). There one constructs from the collective path $|q\rangle$ the superposition $|\Psi\rangle = \int dq\, f(q)|q\rangle$ and obtains the collective quantized Hamiltonian by means of a narrow overlap

expansion of the Griffin-Hill-Wheeler equation $\int \langle q'|H-E|q\rangle f(q)dq = 0$. This yields up to $\hbar^2$ an expression, which is identical to eqs. (2.3-2.5) except that the collective mass of GCM differs from the cranking one. Thus one has to generalize [13] the GCM to the two parameter ansatz $|\Psi\rangle = \int dqdp\, f(q,p)|qp\rangle$. The key to derive a Schrödinger equation in terms of q from this ansatz consists in transforming the modified GCM ansatz to an equivalent one in terms of RPA-correlated states $|\Psi\rangle = \int dq\, f(q)|q\rangle_{corr}$. One can now derive [14] a Schrödinger equation from this GCM which turns out to be identical to the one derived above by a consistent quantization of $\mathcal{H}_C(q,p)$.

Altogether we have exposed a simple means to derive from a microscopically calculated classical Hamiltonian $\mathcal{H} = p^2/2\mathcal{M} + \mathcal{V}$ the corresponding quantum-mechanical collective Schrödinger equation (2.4). The evaluation only involves the calculation of the widths ΔQ^2, ΔP^2 which is easy to perform. (For most of the systems and most of the collective modes one can even approximate $\Delta P^2 = (4\,\Delta Q^2)^{-1}$.) The quantum correction corresponds to a local correlation energy which has to be subtracted from the classical $\mathcal{V}(q)$. Hence they lower the potential energy surface and change its shape. Thus the position of minima and maxima, curvatures and barrier heights are affected, see refs. 15,16. They will depend on the collective mode considered.

The above formalism has been applied to giant resonances in refs. [15]. The relevance for fission dynamics has been studied [16] in the conventional Two-Center-Shell-Model (TCSM) including smoothing, ℓ-s- and ℓ^2-force and a schematic BCS treatment with constant pairing matrix elements. The potential energy surface $\mathcal{V}(q)$ has been evaluated using the liquid drop formula with Strutinsky corrections. As the collective parameter the elongation Λ is used. All other model parameters are minimized to a given

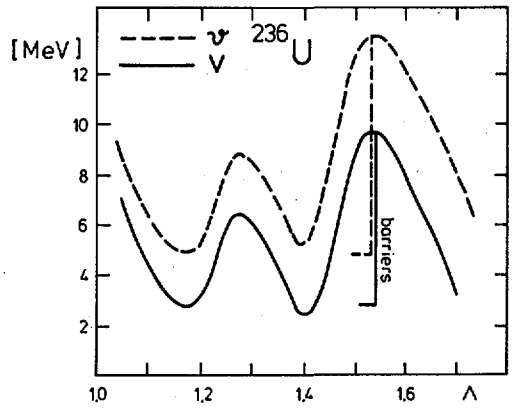

FIG.1. The classical ($\mathcal{V}$) and the quantum-mechanical (V) potential energy surfaces for ^{236}U are plotted versus the elongation Λ. They are evaluated by means of liquid-drop-plus-shell corrections, which are based on a two-centre shell model including ℓ^2-, ℓs-terms and asymmetry. The quantum corrections, V(Λ)-$\mathcal{V}$(Λ), are calculated by using the Inglis cranking model. The elongation Λ measures the extension of the system in units of the equivalent radius (Λ = 1 spherical, Λ → ∞ fission).

value of Λ. The quantum corrections are evaluated for the Λ-mode and the rotational degrees of freedom.

In fig. 1 the classical potential energy surface $\mathcal{V}$(Λ) and the quantum corrected one V(Λ) are given for ^{236}U for symmetric fission. One realizes immediately that the quantum corrections lower the second barrier by about 2 MeV which makes them non-negligible. The lifetime for decay from the second minimum is reduced by $5 \cdot 10^{-4}$ and from the first minimum by about 10^{-7}. (If one assumes that the liquid drop incorporates already all quantum effects, one is left merely with zero point energies of the shell corrections, which change the $\mathcal{V}$ only by 0.5 MeV. For the estimate of the quantum corrections in case of fully microscopic calculations this has no meaning.)

3. Higher order corrections

In the previous section, we have evaluated the quantum corrections to the classical mass $\mathcal{M}(q)$ and potential $\mathcal{V}(q)$ only up to terms of the order of $\hbar^2$. This is the first step to a systematic improvement involving $\hbar^{2n}$ and correspondingly widths like $\langle qp|(Q-q)^{2n}|qp\rangle$ or $\langle qp|(P-q)^{2n}|qp\rangle$. These higher order corrections have been evaluated and studied, again for the TCSM as an example, in ref. [17]. They come out to be negligible for heavy and medium heavy systems. In light nuclei, however, they can become considerable. For nearly spherical systems there might occur problems in applying the above formalism to the rotational degree of freedom since the respective overlaps are not Gaussian. A remedy to this has been given in ref. [18].

Up to now, we have assumed that quantum corrections can be expanded systematically in orders of $\hbar^2$. These are, however, cases where this assumption becomes questionable. An interesting example is the case, where $\xi = (V_1-V_2)/(V_1+V_2)$ is considered as a collective coordinate describing the mass distribution between the fragments. A rising ξ, e.g., lowers the levels in the fragment 1 and rises those in fragment 2. At a level crossing, then, a pair of particles is transferred from fragment 2 to 1. In the overlapping region this transition is weakened by the strong residual interaction (pairing). Near the scission point, however, the redistribution of particles becomes more and more sudden and an $\hbar^n$-expansion is bound to fail. These effects have been studied schematically in ref. [19], with the result that the GOA and the application of the cranking mass formula become questionable if the mass varies along the collective mode by more than a factor 10.

4. The optimal choice of the fission path

In deriving the quantum corrections to the classical potential-energy surface, we assumed the collective path to be given by some educated guess.

A careful choice of the path is very important in order to really find the valley within all the degrees of freedom and to decouple the collective motion from the intrinsic one. (A not well chosen path, e.g., will predict a larger friction than physically justified and will not even be stable along real coordinates q and p; see ref. [20].) Thus a consistent microscopic theory for collective motion should also ask for an optimal collective path. It should be distinguished by the fact that it minimizes the residual coupling to the intrinsic degrees of freedom.

If one assumes $|q,p>$ to be a Slater determinant, this aim can actually be achieved by employing the TDHF theory. TDHF describes the optimal time evolution of a general Slater determinant by

$$\delta<\Phi(t)|H-i\partial_t|\Phi(t)> \qquad (4.1)$$

In a time dependent treatment of collective motion along the path $|q,p>$ we consider $q=q(t)$ and $p=p(t)$, to be determined by

$$\delta<q,p|H-\dot{q}P+\dot{p}Q|q,p> = 0 \qquad (4.2)$$

If collective motion is well established, it is usually also slow. Thus eq. (4.2) will be considered in its adiabatic limit, which is given by the expansion $|q,p> = (1+ip\hat{Q} - \frac{1}{2}p^2\hat{Q}^2 - \frac{i}{2}p^2\frac{\partial\hat{Q}}{\partial p})|q>$. The decoupled collective path is required to be close to a particular solution of eq. (4.1) under the assumption that the system is always nearly in its local equilibrium. This means that the motion is quasistatic and all noncollective degrees of freedom have sufficient time to equilibrate. Furthermore the solution given in terms of a trajectory $|q(t),p(t)>$ should be approximately independent against a variation of the initial $|q(t_0),p(t_0)>$ within a certain range. This means one requires for the multitude of trajectories a behaviour of fig. 2a rather than the case given in fig. 2b. The final

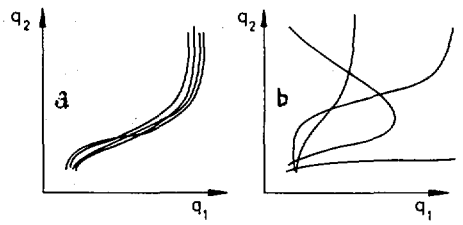

FIG.2. Time-dependent Hartree-Fock trajectories schematically drawn in a two-dimensional space spanned by two relevant degrees of freedom, q_1 and q_2. (b) shows the usual case where the trajectories are strongly dependent on the initial conditions (set in the lower left corner). On the other hand, (a) shows the case of a large-amplitude eigenmode around which the trajectories are bundled and, to some extent, insensitive to the initial velocity and the initial co-ordinate. The collective ATDHF path is constructed to be a representation of the bundle. The spreading of the bundle is given by $\partial_p Q$.

collective path $|q\rangle$ should then be a proper representative of the trajectories of fig. 2a without being necessarily precisely identical with one of them.

Incorporating these requirements in the adiabatic expansion of eq. (4.2) leads to a hierarchy of equations [9] of rising order in p:

$$\delta\langle q|\hat{H} - \frac{\partial \hat{\mathcal{V}}}{\partial q}\hat{Q}|q\rangle = 0 \tag{4.3a}$$

$$\delta\langle q|\left[\hat{H},\hat{Q}\right] + i\, P/\mathcal{M}|q\rangle = 0 \tag{4.3b}$$

and

$$\delta\langle q|\left[\left[\hat{H},\hat{Q}\right],\hat{Q}\right] - 2\mathcal{M}^{-1}\frac{\partial \hat{Q}}{\partial q} - i\left[\hat{H},\frac{\partial \hat{Q}}{\partial p}\right]|q\rangle = 0 \tag{4.4}$$

The eqs. (4.3) are a coupled system to determine the path $|q\rangle$ and the operators Q and P along it. The eq. (4.4) provides an estimate for the degree of decoupling, so to say for the collectivity of the path, found by eq. (4.3).

The path can very simply be determined by transforming eqs. (4.3) to a differential equation for $|\phi(q)>$. From eq. (4.3a) we see that $\hat{Q}$ is proportional to the p-h part of $\hat{H}$ with respect to $|q>$, $H_{ph}(q)$. Inserting this into eq. (4.3b) one obtains [21]

$$\frac{\partial}{\partial q}|q> = c[\hat{H},H_{ph}(q)]\,|q> \qquad (4.5)$$

where c is an unimportant quantity merely fixing the scale q. In the limit of $|q>$ approaching a stationary state like the HF ground state $|q_{HF}>$ the operator P given by $P|q_{HF}> = i\,\frac{\partial}{\partial q}|q_{HF}>$ can be shown to agree with one of the momentum eigenvectors of the RPA. This is satisfying since a large amplitude eigenmode of a system should be extensions of the small amplitude ones. Thus the explicit construction of the path proceeds in four simple steps: First, calculate a stationary point of the system, e.g. the Hartree-Fock point; second, calculate there the RPA and select a proper collective mode (for fission e.g. the low lying collective quadrupole one); third, construct a second point of the path $|q_{HF}+\delta q> = (1-i\delta q P_{RPA})|q_{HF}>$ besides the stationary HF-point $|q_{HF}>$; fourth, use these points as initial conditions to solve the differential equation (4.5) with some standard technique. Preliminary calculations in light nuclei show that these steps are indeed feasible. It seems to be a very promising method for application in nuclear fission [24].

After having evaluated the collective path $|q>$ the degree of decoupling can be checked using eq. (4.4). The strength of the residual coupling is given by the noncollective 1ph matrix elements of $\partial_p Q$, to be determined via eq. (4.4). The criterion of collectivity can thus be written as [21,22]

$$\frac{p^2}{2\mathcal{M}}\frac{||\partial_p Q||}{<Q^2>} \ll \bar{E}_{ph}$$

where $\bar{E}_{ph}$ is the average noncollective ph energy. Furthermore, $\partial_p Q$ allows us to tell which channel is mostly coupled to the collective one. If the coupling is strong to one particular component, this channel might then be considered explicitly by using two collective coordinate parameters rather than one. If a large number of channels couples to the collective one, it might be possible to consider their influence in terms of friction coefficients to be evaluated from $\partial_p Q$. Actually the spreading of the bundle in fig. 2a is given by $\partial_p Q$.

It is remarkable that eqs. (4.3) can also be derived by means of the generator coordinate method. The key for the proof consists in performing a variation of the total energy $E = \langle\Psi|\hat{H}|\Psi\rangle$ with respect to the collective path $|q\rangle$ in $\Psi = \int dq\, f(q)|q\rangle$ in addition to the variation with respect to f. It is interesting to note that the GCM as a thoroughly quantum-mechanical theory incorporates already the quantum corrections and correlation energies and hence it is consistent that for the derivation of eq. (4.3) the $|q\rangle$ in GCM must be replaced by a correlated $|q\rangle_{corr}$. The fact that both approaches, ATDHF and GCM, yield the same equations for the path (4.3) is very satisfying since both theories are of different conceptual origin and use different techniques [23].

5. Summary and conclusion

The present paper exposes a theory suitable for the description of (spontaneous) fission which is based on the concept of a collective path. The approach is fully microscopic and incorporates the relevant quantum effects. The approach has essentially the following three virtues: First, it provides a simple step-by-step method for the explicit construction of the optimal fission path. Second, it provides simple means to check the degree of decoupling of the collective from the noncollective degrees of freedom and allows us to judge whether inclusion of further collective

coordinates is necessary. Third, it provides simple formulae to extract from the collective path the quantized collective Hamiltonian whose eigensolutions determine the tunneling probabilities, lifetimes, etc. The quantum corrections to the classical potential energy surface have been studied in a two-centre-shell-model and for the mass asymmetry. They reduce the second barrier in ^{236}U by 2 MeV and the lifetime by a factor of 10^{-7} and thus seem to be quite important for the realistic description of the process. In preliminary investigations with a three-dimensional ATDHF code the construction of the path and the successive evaluation of quantum effects seems to be a promising tool for a fully microscopic and self-consistent investigation of the dynamics of nuclear fission.

References

[1] "Physics and Chemistry of Fission", Proc. Rochester 1973, IAEA, No. 347.
[2] Brack, M., Damgaard, J., Jensen, A.S., Pauli, H.C., Strutinsky, V.M., Wong, C.Y., Rev.Mod.Phys. 44 (1972) 320.
[3] Goeke, K., Nucl.Phys. A265 (1976) 301.
[4] Goeke, K., Lane, A.M., Martorell, J., Nucl.Phys. A296 (1978) 109.
[5] Bonche, P., Koonin, S., Negele, J., Phys.Rev. C13 (1978) 1226.
[6] Negele, J.W., Koonin, S.E., Möller, P., Nix, J.R., Sierk, A.J., Phys.Rev. C17 (1978) 1098.
[7] Engel, Y.M., Brink, D.M., Goeke, K., Krieger, S.J., Vautherin, D., Nucl.Phys. A249 (1975) 215.
[8] Villars, F., Nucl.Phys. A285 (1977) 269.
[9] Goeke, K., Reinhard, P.-G., Ann.Phys. 112 (1978) 328.
[10] Baranger, M., Veneroni, M., Ann.Phys. 114 (1978) 123.
[11] Rowe, D., Bassermann, R., Can.J.Phys. 54 (1976) 1941.
[12] Reinhard, P.-G., Nucl.Phys. A252 (1975) 120.
[13] Reinhard, P.-G., Goeke, K., J.Phys. G4 (1978) L245.
[14] Goeke, K., Reinhard, P.-G., Ann.Phys., in press.
[15] Goeke, K., Phys.Rev.Lett. 38 (1977) 212;
Goeke, K., Castel, B., Phys.Rev. C19 (1979) 201;
Giannoni, M.J., Moreau, F., Quentin, P., Vautherin, D., Veneroni, M., Phys.Lett. 65B (1976) 305.
[16] Reinhard, P.-G., Nucl.Phys. A252 (1975) 133, Nucl.Phys. A306 (1978) 19.
[17] Reinhard, P.-G., Nucl.Phys. A261 (1976) 291.
[18] Reinhard, P.-G., Z.Physik, 1978
[19] Reinhard, P.-G., Nucl.Phys. A281 (1977) 221.
[20] Reinhard, P.-G., Goeke, K., Phys.Rev. C17 (1978) 1249.
[21] Reinhard, P.-G., Goeke, K., Nucl.Phys. A312 (1978) 121.
[22] Reinhard, P.-G., Goeke, K., Phys.Lett. 69B (1977) 17.
[23] Goeke, K., Reinhard, P.-G., to be published.
[24] Goeke, K., Maruhn, J., Reinhard, P.-G., in preparation.

DISCUSSION

G. SCHÜTTE: You have told us that level crossings cause difficulties and that the adiabatic approximation is valid for nuclei $A > 100$. However, if a nucleus slides down from saddle to scission, there are many level crossings, so I am wondering how you reconcile these two statements.

Since the bulk of the excitation of a fissioning nucleus occurs at the crossings, we do not find an excitation energy proportional to the square of the velocity. This is equally true if there is a pairing gap where there is also a transition probability of the Landau-Zener type. How can one obtain the kinetic energy for a classical Hamiltonian in such a case, and what significance has the requantization?

P:G. REINHARD: The strenght of an adiabatic theory will lie in the pre-scission region. There the residual interaction will remain strong enough to justify the expansion in orders of P^n. Furthermore, the ATDHF model provides a check on the validity of the adiabatic assumption and this is, therefore, not an unverifiable approximation.

H.C. BRITT: You indicate that zero-point and quantum corrections are relatively more important at the second barrier, but for ^{236}U you still seem to obtain a much higher second barrier than is experimentally observed. This appears to be common to many Hartree–Fock approaches and is sometimes interpreted as evidence for a breakdown in the parametrization at large deformations. Could you comment on the comparison of your calculations with the experimental barrier for ^{236}U, where $E_A \sim E_B \sim 6$ MeV?

P:G. REINHARD: The potential-energy state shown is taken from a two-centre shell model and has not been minimized very carefully. It serves only to illustrate the magnitude of the effect.

H.A. NIFENECKER: Zero-point energies of the giant charge oscillation mode and mass asymmetry mode vary considerably along the fission path. How do you include such variations in your calculations?

P:G. REINHARD: We need only subtract the zero-point energies for those channels that are treated explicitly. In modes which are averaged over the ground-state energy the zero-point oscillations are physical and should remain in the potential energy state, analogous to the Born-Oppenheimer approach.

R. SCHULTHEIS: You state that the collective path resulting from your equation is the optimum one. What is the criterion for assessing whether a path is good or not?

P:G. REINHARD: There are two criteria in practice. First, for a given path we can perform a perturbation expansion into the residual Hilbert space. Generally speaking, there will already be a first-order correction. The ATDHF path has the distinguishing feature that the first-order correction vanishes and only a second-order coupling (to the internal motion) remains. The second criterion is to look for the total energy averaged over the path. This energy is minimized by the ATDHF path.

SEMI-CLASSICAL DESCRIPTION OF NUCLEAR DEFORMATIONS FROM SADDLE TO SCISSION

C.R. GUET
Institute Laue-Langevin,
Grenoble Cedex, France

R. BENGTSON
DRF/CPN, CEN-Grenoble, France

M. BRACK
University of Regensburg,
Federal Republic of Germany

Abstract

SEMI-CLASSICAL DESCRIPTION OF NUCLEAR DEFORMATIONS FROM SADDLE TO SCISSION.

The energy density formalism based on the Skyrme force has been used for calculating the deformation energies on the fission of ^{240}Pu. The kinetic energy density is expressed as a functional of the matter density and its derivatives. The fission shapes are described by two ellipsoids connected by a six-order polynomial. The influence of shape parameterization is discussed. Results are compared to both liquid-drop and self-consistent (Hartree-Fock) calculations. In agreement with liquid-drop calculations a well defined 'exit region' is found. Advantages of further developments of semi-classical approximations are discussed.

1. INTRODUCTION

A common feature of the majority of theoretical descriptions of strongly deformed nuclei is that they are based on the Strutinsky prescription. It is then assumed that the binding energy of the nucleus can be divided into two parts, namely one slowly varying part, which describes the average variation of the energy with respect to deformation and particle number and one strongly oscillating part, the so-called shell correction energy. The later part can be calculated, using a single-particle potential of e.g. Woods-Saxon type, the parameters of which are fitted in such a way that the single-particle levels in the ground state are well reproduced. However the total nuclear energy cannot be described by simply adding up the energies of the occupied states. Therefore the slowly varying part of the energy is replaced by a semiempirical energy, calculated for example by means of the liquid drop model. When extending these kinds of calculations to deformations involved in the fission process between the saddle point and the scission point it is obvious that the fall-off of the potential energy, which is of the order tens of MeV, is essentially determined by the liquid drop energy. Since in the later stages of this process a strong necking is developed, terms like curvature energy might be important, and therefore a refined version of the liquid drop model has to be used.

In this paper we shall discuss an alternative approach, which avoids the use of an energy of liquid drop type. In the last ten years considerable progress has been made in the application of Hartree-Fock calculations to heavy nuclei, using an effective interaction of Skyrme type. These kind of calculations reproduce quite well the ground state properties, as reported in ref. [1]. They also allow for a qualitative description of the fission barrier. However, at large deformations the computational difficulties become very serious and thus it is practically impossible to perform the calculations with high accuracy. There exists, however, a way to bypass the time-consuming evaluation of the Hartree-Fock equations, especially, if we are interested only in the averaged, smoothly varying quantities, since the use of semiclassical techniques allows us to find such a solution, without solving the quantum mechanical equations.

2. THE SEMI-CLASSICAL TECHNIQUE

An essential point in the semiclassical calculations is to make an expansion of the density matrix for a given Hamiltonian [2]. In order to obtain such an expansion one may introduce as in ref. [3] the Wigner transform, defined as

$$A_w(\bar{r},\bar{p}) = \int A\left(\bar{r}-\frac{\bar{r}''}{2},\ \bar{r}+\frac{\bar{r}''}{2}\right) e^{i\bar{p}\cdot\bar{r}''/\hbar}\, d^3r'' \tag{1}$$

where $A(\bar{r},\bar{r}') = \langle\bar{r}|\hat{A}|\bar{r}'\rangle$ are the matrix elements of the operator $\hat{A}$ in configuration space, and $(\bar{r},\bar{p})$ denotes a point in the classical phase space.

The Wigner transform can in a natural way be expanded in powers of $\hbar$:

$$A_w(\bar{r},\bar{p}) = \sum_{n=0}^{\infty} A_n(\bar{r},\bar{p})\,\hbar^n \tag{2}$$

which we call the semiclassical expansion of A. The lowest-order term, $A_0(\bar{r},\bar{p})$, corresponds to the classical limit of the operator $\hat{A}$.

The Wigner transform of the Hamiltonian, H_W, is independent of $\hbar$, i.e. H_W coincides with the classical Hamiltonian [3]. Then the Wigner transform of the density matrix can be written

$$\rho_w(\bar{r},\bar{p}) = \sum_{n=0}^{\infty} \rho_{2n}(\bar{r},\bar{p})\,\hbar^{2n} \tag{3}$$

and contains only even powers of $\hbar$ [3]. Once $\rho_W(\bar{r},\bar{p})$ is known it is an easy task to calculate various physical quantities. Thus the normal density is given by

$$\rho(\bar{r}) = \int \frac{d^3p}{(2\pi\hbar)^3}\cdot \rho_w(\bar{r},\bar{p}) \tag{4}$$

and the kinetic energy distribution by

$$\tau(\bar{r}) = \frac{1}{4}\nabla^2\rho(\bar{r}) + \int \frac{d^3p}{(2\pi\hbar)^3}\cdot\frac{p^2}{\hbar^2}\cdot\rho_w(\bar{r},\bar{p}) \tag{5}$$

For nucleons interacting with a Skyrme-force the Hamiltonian in Wigner-space can be written

$$H_w = \frac{1}{2m}f(\bar{r})\,p^2 + V(\bar{r}) \tag{6}$$

where $f(\bar{r})$ is the effective mass and $V(\bar{r})$ is the potential. Since H_W is independent of $\hbar$, the expansion of $\rho_W(\bar{r},\bar{p})$ is given by (3), and one finds, using the eqs. (4) and (5) that

$$\rho = \frac{1}{3\pi^2} k_F^3 + O(\hbar^2) \tag{7}$$

$$\tau = \frac{1}{5\pi^2} k_F^5 + O(\hbar^2) \tag{8}$$

The local Fermi momentum $p_F = k_F \hbar$ is given by

$$\frac{1}{2m} f p_F^2 + V = E_F \tag{9}$$

where E_F is the Fermi energy. The zeroth order terms are immediately recognized as the Thomas-Fermi expressions.

Both $\rho(\bar{r})$ and $\tau(\bar{r})$ are functionals of the potential $V(\bar{r})$ and the Fermi energy E_F. It is however possible to eliminate the dependence on $V(\bar{r})$ and E_F, leading to the following expansion for τ:

$$\tau[\rho] = \tau_0[\rho] + \tau_2[\rho] + \tau_4[\rho] + \ldots \tag{10}$$

Thus τ is a functional of ρ, and a given term τ_n is originating from the terms of order $\hbar^n$ in the Wigner-expansion. The lowest order term is given by

$$\tau_0[\rho] = \frac{3}{5}(3\pi^2)^{2/3} \rho^{5/3} \tag{11}$$

which is the usual Thomas-Fermi term. The expressions for τ_2 and τ_4 can be found in refs [4,3,11].

It should be pointed out that the semiclassical expansions (7) and (8) are only valid up to the classical turning-point, i.e. up to $p_F(\bar{r}) = 0$. Thus the functional $\tau[\rho]$ is in principle not defined outside this point. Although there exist methods for overcoming this limitation [5], we shall not use them here, since it has been shown [6] that assuming the validity of the functional (10) also outside the classical turning point leads to correct results. However, the density given by eq. (7) is in any case unrealistic, since it is undefined outside the turning point. We shall therefore not try to calculate $\rho(\bar{r})$ from the Skyrme-potential by means of eq. (7), but make an ansatz for $\rho(\bar{r})$, which assures a realistic fall off of the density outside the classical turningpoint (see next section). We will then not get a fully selfconsistent density. Instead we optimize the parameterization of the density by minimizing the total energy with respect to the parameters, ρ_0, describing the central density and a_s, describing the diffuseness of the surface. However, for a first application of the semi-classical technique to the fission process we find this simplification justified. The calculation of the total energy E, then becomes simple and can be summarized in the following formulas:

$$E = \int e(\rho)\, d\Omega \tag{12}$$

$$e(\rho) = \frac{\hbar^2}{2m} \cdot \tau(\bar{r}) + v(\bar{r}) + C(\bar{r}) \tag{13}$$

The Skyrme energy density $\mathcal{V}(\vec{r})$ [7] is given by

$$\begin{aligned}\mathcal{V}(\vec{r}) &= \tfrac{1}{2}t_0\left[(1+\tfrac{1}{2}x_0)\rho^2-(x_0+\tfrac{1}{2})(\rho_n^2+\rho_p^2)\right]+\tfrac{1}{4}t_3\rho\rho_n\rho_p \\ &+\tfrac{1}{16}(t_2-3t_1)\rho\Delta\rho+\tfrac{1}{32}(3t_1+t_2)(\rho_n\Delta\rho_n+\rho_p\Delta\rho_p) \\ &-\tfrac{1}{2}W_0(\rho\vec{\nabla}\cdot\vec{J}+\rho_n\vec{\nabla}\cdot\vec{J}_n+\rho_p\vec{\nabla}\cdot\vec{J}_p)+\tfrac{1}{4}(t_1+t_2)\rho\tau+\tfrac{1}{8}(t_2-t_1)(\rho_n\tau_n+\rho_p\tau_p)\end{aligned} \tag{14}$$

where $\rho = \rho_n + \rho_p$, $\tau = \tau_n + \tau_p$ and the spin-density $\vec{J} = \vec{J}_n + \vec{J}_p$, for which the semiclassical expression (given for the neutrons) is [11]

$$\vec{J}_n = -\frac{2m}{\hbar^2}\,\vec{W}_n\,\frac{\rho_n}{f_n} \tag{15}$$

with

$$\vec{W}_n = W_0\left[\vec{\nabla}\rho_n + \tfrac{1}{2}\vec{\nabla}\rho_p\right] \tag{16}$$

The effective mass is

$$f_n = 1 + \frac{2m}{\hbar^2}\left(\alpha\rho_n + \beta\rho_p\right) \tag{17}$$

with

$$\alpha = (t_1 + 3t_2)/8 \tag{18}$$

and

$$\beta = (t_1 + t_2)/4 \tag{19}$$

Integrating all the τ-dependent terms of eq. (13) gives

$$T = T_0 + T_2 + T_4 \tag{20}$$

where

$$T_0 = \frac{\hbar^2}{2m}\cdot\frac{3}{5}\left(3\pi^2\right)^{2/3}\int d\Omega\left[\rho_n^{5/3}+\rho_p^{5/3}+\alpha\left(\rho_n^{8/3}+\rho_p^{8/3}\right)+\beta\left(\rho_p\rho_n^{5/3}+\rho_n\rho_p^{5/3}\right)\right] \tag{21}$$

$$T_2 = \frac{\hbar^2}{2m}\int d\Omega\left\{\frac{1}{36}\left(\frac{|\nabla\rho_n|^2}{\rho_n}+\frac{|\nabla\rho_p|^2}{\rho_p}\right)-\frac{11}{36}\left[\alpha\left(|\nabla\rho_n|^2+|\nabla\rho_p|^2\right)+2\beta\nabla\rho_n\cdot\nabla\rho_p\right]\right\}-\frac{1}{2}E_{so} \tag{22}$$

(E_{so} denotes the spin-orbit term of eq. (14))

$$\begin{aligned}\text{and } T_{4\nu} = \frac{\hbar^2}{2m}\left(3\pi^2\right)^{-2/3}\int d\Omega\Bigg\{&\rho_\nu^{1/3}\left[\frac{1}{810}\left|\frac{\nabla\rho_\nu}{\rho_\nu}\right|^4-\frac{1}{240}\,\frac{|\nabla\rho_\nu|^2\Delta\rho_\nu}{\rho_\nu^3}+\frac{1}{270}\left(\frac{\Delta\rho_\nu}{\rho_\nu}\right)^2\right] \\ &+\rho_\nu^{-2/3}\left[\frac{1}{108}(\Delta\rho_\nu)^2-\frac{1}{1080}\,\frac{|\nabla\rho_\nu|^2\Delta\rho_\nu}{\rho_\nu}-\frac{7}{3240}\,\frac{|\nabla\rho_\nu|^4}{\rho_\nu^2}\right]\Bigg\}\end{aligned} \tag{23}$$

+ terms depending on α, β and $\vec{J}$; $\nu = n, p$

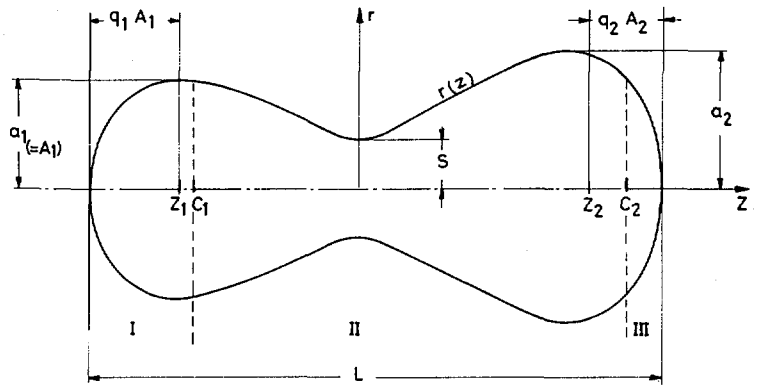

FIG.1. Geometrical meaning of some of the deformation parameters. Left-hand side: matching point (c_1) between ellipsoid centre and neck; right-hand side: matching point (c_2) close to end of nucleus.

We do not calculate the Coulomb energy by integrating the Coulomb energy density $C(\vec{r})$, but instead we follow the prescription of Myers and Swiatecki [8], i.e. we define an equivalent sharp surface, and add a diffuseness correction term, which is independent on the deformation. We also include a Coulomb exchange term of the Slater approximation type [9].

$$E_{ex}(\vec{r}) = -\frac{3e^2}{4}\left(\frac{3}{\pi}\right)^{1/3}\left[\rho_p(\vec{r})\right]^{4/3} \tag{24}$$

3. PARAMETERIZATION OF THE DENSITY

Since we use the density (and not the potential) as the basic input in our calculations, we must find a reliable way of parameterizing the deformed density. We start by defining a sharp surface, as shown in fig. 1. The nucleus is divided into three regions, defined by the matching points c_1 and c_2. The left (I) and the right (III) regions, describing the fragments under formation, are chosen to be parts of ellipsoids, defined by $\pi_i(r,z) = 0$, where

$$\pi_i(r,z) = -r^2 + A_i^2 - \frac{1}{q_i^2}(z - z_i)^2 \qquad (i = 1,2) \tag{25}$$

The index i denotes the two regions and it is possible to choose different deformations for the two fragments. The neck region (II) is described by $\pi_{II}(r,z) = 0$ with

$$\pi_{II}(r,z) = -r^2 + s^2 + tz^2 + uz^3 + vz^4 + wz^5 + yz^6 \tag{26}$$

Since we want the neck to be located at z = 0, $\pi_{II}(r,z)$ does not contain any term proportional to z, and if only cases with reflexional symmetry are considered also the coefficients u and w are zero. Including the matching points, c_i, this parameterization contains 14 parameters. By requiring that r(z) and its three first derivatives are continuous at the matching points the number of parameters is reduced to 6.

Once the sharp surface is determined, the diffuse density is calculated in accordance with ref. [10]. From the functions $\pi_\nu(r,z)$, defined in eqs. (25) and (26), we define a length

$$\ell_\nu(r,z) = \frac{\pi_\nu(r,z)}{|\nabla \pi_\nu(r,z)|} \tag{27}$$

The index ν refers to the three regions in fig. 1. The density is then given by

$$\rho_\nu(r,z) = \frac{\rho_0}{1 + e^{\ell_\nu(r,z)/a_s}} \tag{28}$$

The requirement that r(z) and its three first derivatives are continuous, assures that the density and its two first derivatives become continuous at the limits between the three regions. This is a necessary condition for applying the semiclassical formulas to fourth order. The parameters ρ_0 and a_s are not to be considered as free parameters, since they are determined by minimizing the total energy. In eq. (28) ρ_0 denotes the total density.[1] The individual densities of protons and neutrons are also given by eq. (28) after replacing ρ_0 with ρ_0^p and ρ_0^n respectively, where $\rho_0 = \rho_0^p + \rho_0^n$ and $\rho_0^p/\rho_0^n = Z/N$. The particle number is determined by integrating the density. By requiring a given particle number, one of the remaining deformation parameters can be eliminated. Thus in the most general case we are left with 5 independent parameters. These can of course be chosen in different ways. For practical reasons the following choice seems to be most useful:

1. The total length of the nucleus, $L = z_1 + z_2 + A_1 \cdot q_1 + A_2 \cdot q_2$
2. The radius of the neck, s.
3. The maximal radius of the left fragment, a_1, which is equal to A_1 if $c_1 > z_1$.
4. The maximal radius of the right fragment, a_2, which is equal to A_2 if $c_2 < z_2$.
5. The mass ratio M_L/M_R.

In the present calculations we consider only reflexion symmetric shapes. Consequently we are left with only three independent parameters, namely L, s and the maximal radius of the fragments which we call a.

The above parameterization of the shape is adjusted to describe shapes in the last stage of the fission process, where a neck already has started to be formed. It then allows to describe very compact as well as very elongated shapes, and a considerable variation of the deformation of the fragments can be obtained.

With certain modifications the parameterization can be extended to describe the separated fragments after the scission point. It is, however, not suitable for small deformations, i.e. before the neck is formed. This is directly seen in the calculations, since in this region the matching points are reaching the ends of the fragments and we are left with only the polynomial describing the middle region. The parameterization then

[1] Note that definition (27) leads to a constant surface thickness.

becomes equivalent to the one of ref. [10], except that we have a sixth-order polynomial, allowing for three independent deformation parameters (in the reflexion symmetric case), while ref. [10] uses a fourth-order polynomial, allowing for only two independent deformation parameters.

4. SEMI-CLASSICAL FISSION BARRIERS

It has been shown that when using the Strutinsky smoothed density as input, the functional $\tau[\rho]$ [10] reproduces the Strutinsky averaged energy within a few MeV [11]. We should not expect such an accuracy since we make an independent ansatz for the density. Therefore, before comparing the fission barriers calculated with the semi-classical methods, let us mention a few points. First, the "liquid-drop" barrier height for ^{240}Pu is about 4 MeV, whereas the Strutinsky smoothed barrier obtained from self-consistent H.F. calculations with the Skyrme III potential is about 13 MeV [1]. Furthermore, when defining the density $\rho(\vec{r})$ we assume that the central density ρ_0 and the surface diffuseness, a_s, stay independent of deformation. Moreover, protons and neutrons are assumed to have the same spatial distribution. Self-consistent calculations have shown that these assumptions are not totally satisfactory. Anyhow, we should expect to find a fission barrier which is much higher than the liquid-drop barrier provided our parameterization is reasonable.

The density parameters ρ_0 and a_s have been determined by minimizing the total binding energy at the liquid-drop saddle point. For these calculations we have used the shape parameterization of ref. [10] with c = 1.45 and h = o. The minimization was done in two cases namely with the semi-classical expansion up to the second order (T_2 term only) and then up to the fourth order (T_4 term included). The respective values obtained in each case were $\rho_0 = 0.139$ fm^{-3}, $a_s = 0.330$ fm and $\rho_0 = 0.140$ fm^{-3}, $a_s = 0.409$ fm. In order to check the dependence on deformation, a minimization was performed for the spherical shape in which case we found practically the same value for ρ_0 and a small shift of a few percent for a_s. In the calculations where this variation was neglected the above values were taken. The central density $\rho_0 = 0.140$ fm^{-3} is in excellent agreement to H.F results of ref. [12]. It should be noted that our density has not the same fall-off as a Fermi distribution since the tail of our distribution extends further outside. However, we have calculated an equivalent Fermi diffuseness, d_0, by fitting a Fermi distribution to our density by requiring same central density ρ_0, half radius and particle number. The Fermi diffusenesses are, for both cases considered above, respectively $d_0 = 0.407$ fm and $d_0 = 0.505$ fm. These values should be compared to $d_0 = 0.398$ fm and $d_0 = 0.420$ fm, respectively, as obtained by Grammaticos et al. [3] when optimizing the surface energy by a semi-classical method. In Fig. 2 we show the semi-classical barriers calculated with the T_2-term only (S.C.2 ; ρ_0=0.139fm) and with both T_2 and T_4 terms (S.C.4; ρ_0=0.140 fm). It should be mentioned that the spin-orbit terms in T_4 have been omitted which may move slightly the barrier S.C.4. The maximum of the Strutinsky smoothed H.F. barrier, marked by a cross, is seen to be just in between. The dashed curve shows the barrier calculated without the T_4 term but for density parameters obtained by considering it. It is seen that once these parameters have been properly optimized (inclusion of T_4) the fourth order term does not influence much on the barrier height except for the largest deformations. It should be underlined that the energies calculated with the T_4 term rise steeply, once one goes away from the optimal values ρ_0 and a_s. This explains the relatively large charge in a_s caused by the inclusion

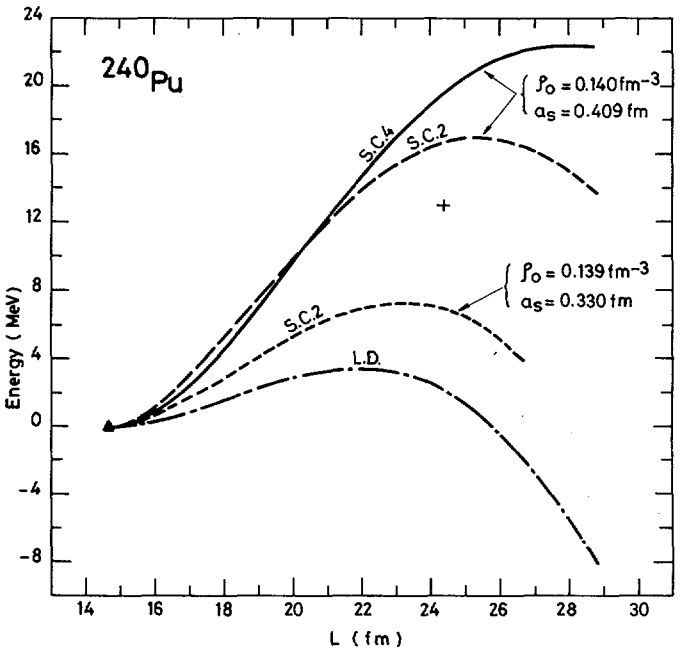

FIG.2. Deformation energy for ^{240}Pu as a function of elongation parameter L. The shape parameterization used for constructing this figure is that of Ref.[10]. *The various curves are discussed in the text.*

of this term. The results shown in fig. 2 are calculated with the {c,h} parameterization of ref. [10] which is very convenient for deformations up to the saddle-point.The parameter h is put equal to zero which corresponds to the liquid-drop valley [10]. The error made by not minimizing with respect to h has been checked for a few cases and found to be negligible.

Note that our calculations in both cases (SC2 and SC4) led to binding energies for the sphere which were less than 5% away from the corresponding Strutinsky smoothed quantity (-1799 MeV as quoted in ref. [1]). Regarding our simplified parameterization of the density distribution and the sensitivity of the binding energy to small changes in the density parameters, this is a fully acceptable result.

5. NUCLEAR DEFORMATIONS INVOLVED IN THE FISSION PROCESS

Although the semi-classical fission barrier heights are too high, they are in relatively good agreement with the smoothed H.F calculations [1] (cf. Fig. 3). It might, therefore,be of interest to investigate the shapes involved in the fission process that the semi-classical calculations predict. For each length, L, of the nucleus the energy has been minimized with respect to the neck radius, s and fragment radius,a. Compared to the

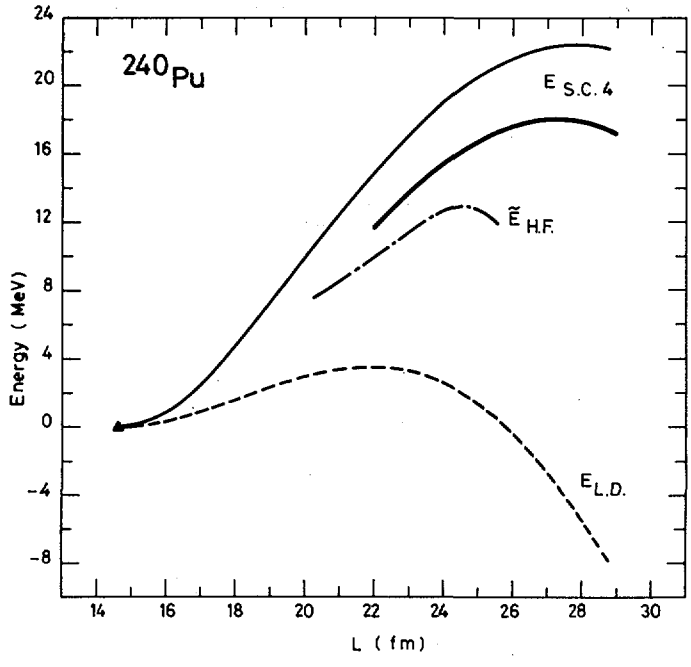

FIG. 3. Solid curves show semi-classical deformation energy, calculated with the T_4-term included. The thin line shows the results obtained with the shape parameterization of Ref.[10], *while the thick line is calculated with the parameterization as defined in Section 3. The curve labelled $E_{H.F.}$ shows the Strutinsky-smoothed H.F. energy (taken from Ref.*[1]*) and the curve labelled $E_{L.D.}$ shows the liquid-drop energy, calculated with the shape parameters of Ref.*[10].

{c,h} parameterization the barrier is lowered at the top by about 4.5 MeV (thick solid line in Fig. 3). In Fig. 4 we show the corresponding values of the parameters s and a (thick lines). The neck starts to develop at $L \approx 23.5$ fm, a length which is almost equal to the sum of the diameters of the resulting fragments shown by the small arrow in Fig. 4. With a further elongation the fragment radius decreases slightly but beyond $L \approx 27$ fm it starts to increase. We interpret this behaviour as if the system starts to feel the individualities of the fragments under formation and thus tries to prevent too elongated fragments since in this semi-classical frame the sphere is energetically favoured. The neck radius is a smoothly decreasing function of L up to $L \approx 29$ fm. However, for $L > 29$ fm the binding energy decreases drastically with decreasing neck radius and there is no longer any static barrier in the s-direction which prevents the fragments to separate, i.e. the "exit-point" is reached. These results are in complete agreement with that of ref. [10] based on the liquid-drop model. The parameter values

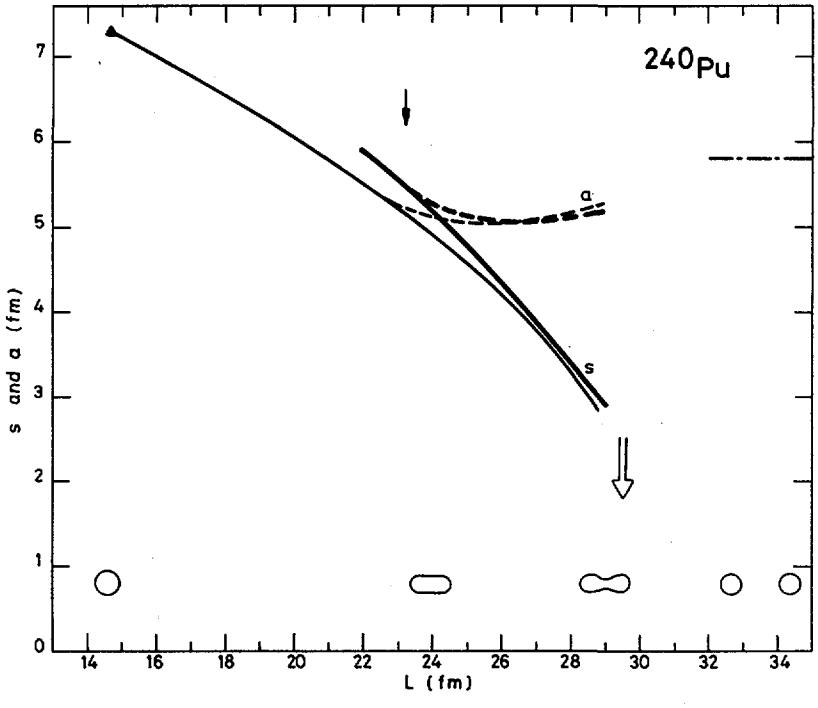

FIG.4. Deformation parameters a and s along the fission path. Thin lines correspond to the shape parameterization of Ref.[10] *and thick lines to that of Section 3. The triangle specifies the spherical shape of* ^{240}Pu *and the open arrow indicates the exit point. The dot-dashed line shows the fragment radius of the two completely separated fragments, which is the limiting value of a for large L. Some typical shapes are shown at the bottom of the figure.*

derived from this reference are also shown in Fig. 4. (Notice that, in this case, a is dependent on s and L and cannot be chosen freely). The results are seen to be rather similar. A somewhat larger difference is obtained on the axis ratio of the fragment as shown in Fig. 5. This axis ratio, q', is defined as $q' = b/a$ where $b = \frac{L}{2} - |z_m|$ with z_m being such that $r(z_m) = a$. (see Fig. 1). In both cases q' decreases strongly with increasing L and goes to 1 near the "exit point". It should be noted that along the fission path the matching points c_i lie outside z_i that is the shapes of the nascent fragments deviate quite much from pure ellipsoidal shapes. Fig. 6 shows some shapes obtained along the fission path.

6. SUMMARY

Our calculations based on the Skyrme-III potential have shown that semi-classical techniques can be applied for describing very deformed nuclei. Regarding the simplifications used in our calculations we find the

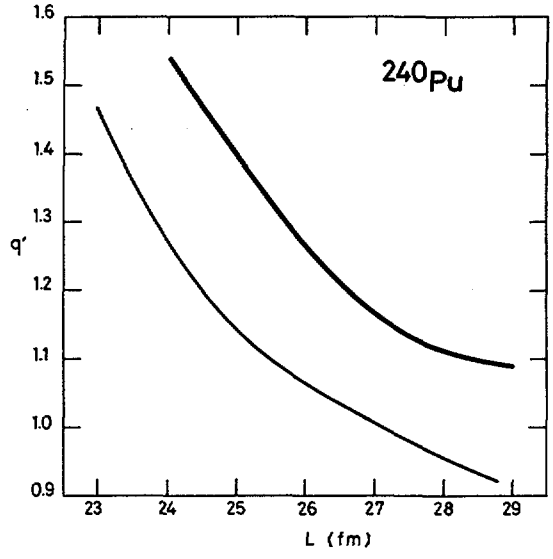

FIG.5. Axis ratio, q', of fragments (for definition, see text). The thin line refers to the parameterization of Ref.[10], *while the thick line refers to that of Section 3.*

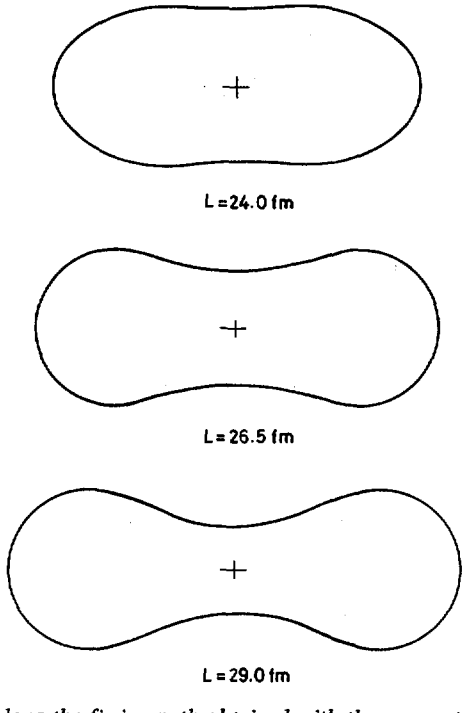

FIG.6. Three shapes along the fission path obtained with the parameterization of Section 3.

agreement with the Strutinsky-smoothed H.F results very encouraging. The too high height for the fission barrier should not be understood as a deficiency of the semi-classical technique but rather as inherent to the Skyrme parameters. As the semi-classical calculations are much less time-consuming than the quantum-mechanical H.F calculations they could easily be used to refit the Skyrme parameters so that they also give reasonable fission barriers. This task would require an improved parameterization of the density or, preferably, a self-consistent calculation of it.

The calculated nuclear shapes along the fission path might be somewhat influenced by the failure of the Skyrme parameters to calculate energies of large deformations. In spite of this uncertainty a strong support is brought to the existence of an "exit point" as obtained in ref. [10]. This "exit-point" is reached for a relatively compact shape of the fissioning system, the neck radius being between 2.5 fm and 3.0 fm.

It should finally be mentioned that it is also possible to treat pair correlations semi-classically. For a preliminary report see ref. [13].

REFERENCES

[1] QUENTIN, P. and FLOCARD, H., Ann. Rev. Nucl. Science (Vol. 28) to appear. See references therein.
[2] WIGNER, E., Phys. Rev. 40 (1932) 749.
[3] GRAMMATICOS, B. and VOROS, A., Annals of Physics, to appear.
[4] BRACK, M., Habilitationschrift, ILL Grenoble, 77BR3465 (1977).
[5] DURAND, M., BRACK, M., SCHUCK, P., Z. Physik A 286 (1978) 381.
[6] CHU, Y.H., JENNINGS, B.K., BRACK, M., Phys. Letter 68B (1977) 407.
[7] VAUTHERIN, D., BRINK, D.M., Phys. Rev. C5 (1972) 626.
[8] MYERS, W.D., SWIATECKI, W.J., Nucl. Phys. 81 (1966) 1.
[9] QUENTIN, P., Thèse d'Etat, Orsay, 1975.
[10] BRACK, M., DAMGAARD, J., PAULI, H.C., HENSEN, A.S., STRUTINSKY, V.M. and WONG, C.Y., Rev. Mod. Phys. 44 (1972) 320.
[11] BRACK, M., JENNINGS, B.K. and CHU, Y.H., Phys. Lett. 65B (1976) 1.
[12] FLOCARD, H., QUENTIN, P., VAUTHERIN, D. and VENERONI, M., Nucl. Phys. A231 (1974) 176.
[13] BENGTSSON, R. and SCHUCK, P., Extended Synopses, this Symposium, p. 245.

DISCUSSION

M. ASGHAR: Your calculation clearly brings out the presence of the 'exit point' predicted by Strutinsky almost 15 years ago solely on the basis of his liquid-drop-model research.

But I want to ask Professor Fong whether the shapes of these fragments at the exit point are similar to those assumed in his work a long time ago.

P. FONG *(Chairman)*: Yes, indeed they are. My earlier calculation was based on rather simple assumptions for the sake of convenience. If it closely corresponds to reality, it is perhaps more by luck than judgement.

A LINEAR-RESPONSE-THEORY TREATMENT OF THE FISSION VISCOSITY TENSOR

A.S. JENSEN, K. REESE
Institute of Physics,
University of Aarhus,
Aarhus,
Denmark

H. HOFMANN
Physik-Department,
Technische Universität München,
Garching,
Federal Republic of Germany

P.J. SIEMENS
Niels Bohr Institute,
University of Copenhagen,
Copenhagen, Denmark
and
The Lawrence Berkeley Laboratory,
University of California,
United States of America

Abstract

A LINEAR-RESPONSE-THEORY TREATMENT OF THE FISSION VISCOSITY TENSOR.

Linear response theory is used to study the dynamics of the fission process. First the equations of motion for a set of collective co-ordinates are given. The crucial quantities are the first and second moments of the response functions. The collective co-ordinates are the deformation parameters and the pairing gap. In the independent-particle model with pairing, expressions for the response functions and their moments are given on the viscosity tensor, i.e. the first moments, which are calculated as functions of deformation, pairing gap and temperature. The corresponding wall-formula results are larger by roughly a factor of two. The damping width in the second well of ^{240}Pu is calculated in the present model and found to be in agreement with the experiment. The treatment of the pairing gap as a dynamic parameter allows a simultaneous determination of the related distributions of fragment mass, excitation energy and pairing gap.

1. INTRODUCTION

The degrees of freedom for a nuclear system are divided into two classes according to their time dependence. The many intrinsic coordinates describe the fast - and the

few collective (external) coordinates describe the slow degrees of freedom. The intrinsic coordinates are treated statistically and time dependent perturbations are applied to the collective coordinates. In this way the average effect of the intrinsic system on the motion of the collective coordinates are included. Using linear response theory these ideas were recently formulated [1,2] and applied [3] to heavy-ion collisions. When the assumptions are valid, classical equations of motion for the collective coordinates are available. We use the same approach to study the dynamics of the fission process.

The set of coupled equations describing the time evolution of the collective coordinates are given in terms of the response functions and static properties of the system. If a moment expansion is appropriate in these equations we obtain

$$\sum_{\mu}(B_{\nu\mu}\ddot{q}_{\mu}+\gamma_{\nu\mu}\dot{q}_{\mu})=-\frac{\partial F}{\partial q_{\nu}};\quad \nu=1,2,\ldots,N \qquad (1)$$

where $\{q_{\nu}\}$ is the set of N collective coordinates, F is the free energy; $B_{\nu\mu}=-\frac{1}{2}{}^{(2)}M_{\nu\mu}$, $\gamma_{\nu\mu}={}^{(1)}M_{\nu\mu}$ where ${}^{(n)}M$ are the moments of the response functions. All the quantities F, B and γ are functions of the coordinates q_{ν} and the temperature T. Here T is related to the excitation energy of the intrinsic system. It was brought into the calculations when the intrinsic degrees of freedom were averaged over a canonical temperature distribution.

For one coordinate eq.(1) has been given previously [2]. The extension in eq.(1) to many collective coordinates seems very reasonable. The general arguments leading to this form will be published elsewhere [4] together with a comprehensive discussion of the approximations and assumptions involved.

This general formulation [4] is aimed at a study of non-harmonic damped large amplitude motion. (Note that the time dependent perturbation used at one point in the derivation does not limit the applications to small amplitudes).

Both for fission and heavy-ion reactions the path obtained by solving the Newton type of equations (eq.(1)) is known to be insufficient. Fluctuations around this average path are essential. An extension to take this into account has been formulated [5] and leads to Fokker-Planck type of equations. The ingredients are the same and the resulting equations also involve the quantities $B_{\nu\mu}$ and $\gamma_{\nu\mu}$. Both average values and distributions around them can then be calculated consistently in the same model.

Convenient collective coordinates appropriate for fission are the deformation parameters. A variety of sets of these are available. We have chosen c, h, and α described in ref. 6. Since pairing is known to be very important we would like to include it. The ordinary static formulation leads to a gap equation determining the gap parameter Δ. In a dynamic treatment there is no reason to believe that Δ should maintain this static value, just as the deformation parameters also assume non-equilibrium values. Consequently we treat Δ as another collective coordinate. The dynamical evolution of the system

will then itself determine the degree of superfluidity, e.g. in the descent from saddle to scission a distribution of Δ-values is obtained completely analogous to the distribution of fragment masses. Thus we study four collective coordinates, c, h, α and Δ.

Clearly the two essential quantities in eq.(1) are the first and second moment of the response functions related to the viscosity - and mass tensors. They are found simultaneously in the model. The expression for the mass tensor is a generalization of the cranking model result. The mass is of course of great interest but it is somewhat better studied than the viscosity. In this paper we shall mainly be concerned with the viscosity and its dependence on the collective coordinates and temperature. The mass will be investigated in more detail in ref. 4. Here we shall only use the results necessary in the study of the first moment and its comparison with experiment.

2. THEORY

2.1. The Hamiltonian

The starting point is the constrained Hartree-Fock method. As a reasonable first approximation we use the effective one-body deformed average potential of the shell model parametrized in terms of the deformation parameters (c, h, α) (see ref. 6). This part of the Hamiltonian is diagonalized giving single particle energies ε_k and creation operators a_k^+. The Hamiltonian with pairing is now taken as

$$H=\sum_k(\varepsilon_k-\lambda)a_k^+a_k - \Delta \sum_{k>0}(a_k^+a_{\bar{k}}^+ + a_{\bar{k}}a_k) \tag{2}$$

which is diagonalized by the usual Boguliubov transformation

$$a_k^+ = u_k\alpha_k^+ - v_k\alpha_{\bar{k}} \tag{3}$$

$$v_k^2 = 1-u_k^2 = \frac{1}{2}\left(1 - \frac{\varepsilon_k-\lambda}{E_k}\right) \tag{4}$$

$$E_k = \sqrt{(\varepsilon_k-\lambda)^2+\Delta^2} \tag{5}$$

where λ is the Fermi energy determined by average particle number conservation. The Hamiltonian is then

$$H= \sum_{k>0}(\varepsilon_k-\lambda-E_k)+\sum_k E_k\alpha_k^+\alpha_k \tag{6}$$

2.2. Response functions

The Hamiltonian at time t is now expanded in terms of the Hamiltonian at t_o where $\delta t=t-t_o$ is small. The perturbing

potential, to be used in the time dependent perturbation treatment, is then found to be

$$\sum_{\nu}(q_{\nu}-q_{\nu}^{(o)})\ \frac{\partial H}{\partial q_{\nu}} \tag{7}$$

Thus the Fourier transform of the imaginary part of the relevant response functions are now [1]

$$\chi''_{\mu\nu}(\omega) = \pi \sum_{m,n} w_m \langle m|\frac{\partial H}{\partial q_{\mu}}|n\rangle\langle n|\frac{\partial H}{\partial q_{\nu}}|m\rangle$$

$$\times[\delta(\omega-\Omega_{nm})-\delta(\omega+\Omega_{nm})] \tag{8}$$

where $|m\rangle$ and $|n\rangle$ are the many body wavefunctions and

$$\Omega_{nm}= \Omega_n-\Omega_m \tag{9}$$

$$w_m=\exp(-\Omega_m/T)/Z(T) \tag{10}$$

where Ω_n are the energy eigenvalues of the many body Hamiltonian which we approximated by H and Z(T) is the grand partition function depending on temperature.

Using the derivative of H found from eq.(6) the response function eq.(8) can be expressed in terms of single particle quantities. The calculation is analogous to that of ref. 3 where pairing was not included. We find

$$\chi''_{\mu\nu}(\omega)=\chi^{(1)}_{\mu\nu}+\chi^{(2)}_{\mu\nu}+\chi^{(3)}_{\mu\nu} \tag{11}$$

$$\chi^{(1)}_{\mu\nu}= \frac{\pi}{2} \sum_{k} A^{\mu}_{k} A^{\nu}_{k}[(1-n(E_k))^2-n^2(E_k)][\delta(\omega+2E_k)-\delta(\omega-2E_k)] \tag{12}$$

$$\chi^{(2)}_{\mu\nu}=\pi \sum_{i\neq k} B^{\mu}_{ik}B^{\nu}_{ki}\, n(E_i)(1-n(E_k))\,[\delta(\omega-E_i+E_k)-\delta(\omega+E_i-E_k)] \tag{13}$$

$$\chi^{(3)}_{\mu\nu}= \frac{\pi}{2} \sum_{i\neq k} C^{\mu}_{ik}C^{\nu}_{ki}[(1-n(E_i))(1-n(E_k))-n(E_i)n(E_k)]$$

$$\times[\delta(\omega+E_i+E_k)-\delta(\omega-E_i-E_k)] \tag{14}$$

where

$$n(E)= \frac{1}{2}(1-\tanh \frac{E}{2T}) \tag{15}$$

$$A_k^\nu = 2E_k \frac{\partial u_k}{\partial q_\nu} / v_k \qquad (16)$$

$$B_{ik}^\nu = (u_i u_k - v_i v_k) \langle i | \frac{\partial V}{\partial q_\nu} | k \rangle \qquad (17)$$

$$C_{ik}^\nu = (u_i v_k + v_i u_k) \langle i | \frac{\partial V}{\partial q_\nu} | k \rangle \qquad (18)$$

Here V is the one-body average potential, which does not depend on Δ. Thus only $\chi^{(1)}_{\Delta\nu}$ contributes to $\chi''_{\Delta\nu}$.

As argued in ref. 3 and 4 this expression for χ'' must be modified by introducing a smearing of the single particle states. The idea is the same as applied in the optical model where the imaginary potential corresponds to a finite width or lifetime of the single particle states. In this case with pairing included the smearing or finite width is of the quasi particle state rather than the single particle state. The response functions are now written

$$\begin{aligned}\chi''_{\mu\nu}(\omega) = \pi \int d\varepsilon \int d\varepsilon' [\delta(\omega - \varepsilon + \varepsilon') - \delta(\omega + \varepsilon - \varepsilon')] \\ \cdot n(\varepsilon)(1 - n(\varepsilon')) \{ \sum_{i \neq k} B^\mu_{ik} B^\nu_{ki} P_i(\varepsilon) P_k(\varepsilon') \\ + \frac{1}{2} \sum_k A^\mu_k A^\nu_k [P_k(\varepsilon) P_k(-\varepsilon') + P_k(-\varepsilon) P_k(\varepsilon')] \\ + \frac{1}{2} \sum_{i \neq k} C^\mu_{ik} C^\nu_{ki} [P_k(\varepsilon) P_i(-\varepsilon') + P_k(-\varepsilon) P_i(\varepsilon')] \qquad (19)\end{aligned}$$

where the integration variables are changed to correspond to zero Fermi energy ($\lambda = 0$) and where

$$P_k(\varepsilon) = \frac{1}{2\pi} \cdot \frac{\Gamma_k}{(\varepsilon - E_k)^2 + \frac{1}{4}\Gamma_k^2} \qquad (20)$$

This Lorentzian function of width Γ_k is chosen because it corresponds to a decaying quasi particle state. For vanishing quasi particle widths Γ_k eq.(19) reduces to eq.(11). The advantages of this particular smearing are discussed in ref. 4. Besides the correct limits for $\Gamma_k = 0$ and for the pairing gap $\Delta = 0$, it has the desirable property that the fluctuation dissipation theorem [1] is fulfilled [4] when the correlation fuction is given by eq.(19) with plus between the two δ-functions.

2.3. The quasi particle width

The quasi particle states should not have infinite lifetimes, due to the residual interactions neglected in the

effective average potential. The corresponding finite width is related to the depth W of the imaginary part of the optical potential by [7]

$$\Gamma = -2W \tag{21}$$

The energy dependence has been studied without pairing in ref. 8. For small energies around the Fermi energy λ the result is

$$\Gamma_k = \Gamma_o(\varepsilon_k - \lambda)^2; \quad \Gamma_o = 0.03 \text{ MeV}^{-1} \tag{22}$$

where the value of Γ_o is for the density corresponding to the interior of the nucleus. For smaller densities, as in the surface region, Γ_o should be somewhat larger. Eq.(22) is valid [8] for negative and perhaps small positive energies ε_k. At higher energies the dependence becomes very complex and eq.(22) may grossly overestimate the width.

The most plausible extension to include pairing effects on the width of the quasi particle state is

$$\Gamma_k = \Gamma_o \cdot E_k^2 \tag{23}$$

The temperature dependence of the width can be obtained using Fermi liquid theory [4]. With the normalization of eq.(23) this leads to

$$\Gamma_k = \Gamma_0(E_k^2 + (\pi T)^2) \tag{24}$$

which is the quasi particle width used in the calculations.

2.3. Moments of the response functions

The time dependent response function is the Fourier transform of eq.(19)

$$\chi''_{\mu\nu}(t) = \frac{1}{2\pi} \int_{-\infty}^{\infty} d\omega \chi''_{\mu\nu}(\omega) e^{-i\omega t} \tag{25}$$

The moments are

$$^{n}M_{\mu\nu} = 2i \int_{-\infty}^{\infty} \chi''_{\mu\nu}(t) \cdot t^n dt \tag{26}$$

which can be evaluated for the three different terms in the response function. We find

$$^{n}M^{(1)}_{\mu\nu} = \sum_k A^{\mu}_k A^{\nu}_k [S^{(n)}_k(\omega=0) \cdot 2^{-n-1} - \int_{-\infty}^{\infty} d\omega n(\omega) P_k(\omega) S^{(n)}_k(-\omega)] \tag{27}$$

$$n_{M_{\mu\nu}}^{(2)} = \sum_{i>k} B_{ik}^{\mu} B_{ki}^{\nu} \int_{-\infty}^{\infty} d\omega n(\omega) [P_i(\omega) S_k^{(n)}(\omega) + P_k(\omega) S_i^{(n)}(\omega)] \quad (28)$$

$$n_{M_{\mu\nu}}^{(3)} = \sum_{i>k} C_{ik}^{\mu} C_{ki}^{\nu} \int_{-\infty}^{\infty} d\omega n(\omega) [P_k(-\omega) S_i^{(n)}(\omega) - P_i(\omega) S_k^{(n)}(-\omega)] \quad (29)$$

where

$$S_k^{(n)}(\omega) = 2\mathrm{Im} \left[\frac{\frac{1}{2}\Gamma_k + i(E_k - \omega)}{\frac{1}{4}\Gamma_k^2 + (E_k - \omega)^2} \right]^{n+1} n! \quad (30)$$

For n=1, the viscosity tensor, the sum of the moments eqs. (27)-(29) may be written

$$^{1}M_{\mu\nu} = \pi \int_{-\infty}^{\infty} (1 - \mathrm{tgh}^2 x) dx \{ \sum_k A_k^{\mu} A_k^{\nu} \cdot P_k(2Tx) P_k(-2Tx) + \sum_{i>k} [B_{ik}^{\mu} B_{ki}^{\nu} P_i(2Tx) P_k(2Tx) + C_{ik}^{\mu} C_{ki}^{\nu} P_i(2Tx) P_k(-2Tx)] \} \quad (31)$$

By changing the integration variable $x = \frac{\omega}{2\pi}$ we obtain a factor $\frac{1}{\pi}(1 - \mathrm{tgh}^2 \frac{\omega}{2T})$ which for small enough T acts as a δ-function. Thus only states around the Fermi energy contribute in the summation. This is of course only true when the quasiparticle widths Γ_k do not increase too strongly with the distance from the Fermi energy.

For temperature T=0 the integration may be performed since all x-dependence disappears except in the first factor. We get

$$^{1}M_{\mu\nu}(T=0) = 2\pi \{ \sum_k A_k^{\mu} A_k^{\nu} P_k(0) P_k(0) + \sum_{i>k} P_k(0) P_i(0) (B_{ik}^{\mu} B_{ki}^{\nu} + C_{ik}^{\mu} C_{ki}^{\nu}) \} \quad (32)$$

which is non-vanishing.

With the width of eq.(24) we get

$$P_k(0) = \frac{\Gamma_o}{2\pi (1 + \frac{1}{4}\Gamma_o^2 E_k^2)} \quad (33)$$

showing that the contribution vanishes only when $E_k \gg 2/\Gamma_o \approx 67$ MeV which certainly not is close to the Fermi energy. A rapid convergence with the distance from λ can therefore not be expected

with the width in eq.(24). This only reflects the fact that eq.(24) is an overestimate of Γ_k and it should not be used too far away from the Fermi energy.

3. NUMERICAL RESULTS

Evaluation of the moments of the response functions is carried out by numerical integration of the expressions eq.(31) and eqs.(27)-(29). The average potential used is a realistic deformed Woods-Saxon potential with spin-orbit and Coulomb terms [6]. For each deformation characterized by (c, h, α) diagonalization give single particle energies and wavefunctions. Then u, v and E in eqs.(16)-(18) are easily obtained for a given pairing gap Δ after the particle number equation is solved to give the Fermi energy.

The necessary matrix elements are given by

$$\langle i|\frac{\partial V}{\partial q_\nu}|k\rangle=(\varepsilon_k-\varepsilon_i)\langle i|\frac{\partial}{\partial q_\nu}|k\rangle+\delta_{ik}\frac{\partial \varepsilon_k}{\partial q_\nu} \qquad (34)$$

which is obtained by numerical differentiations, i.e. by overlap calculation of close lying (in deformation) wavefunctions. This procedure has the advantage that the same computer program as for single particle energies and wavefunctions can be used. Furthermore all terms in the Hamiltonian are included, not only those which a priori are believed to be the most important.

The summations in eq.(31) are extended to an energy interval of 15 MeV around the Fermi energy. With the choice of width in eq.(24) the first moments then have still not converged. For the second asymmetric barrier of ^{238}U an energy interval of 20 MeV leads to an increase of around 5% for Δ=1 MeV and T=1 MeV. As eq.(24) is an overestimate for energies so far above the Fermi energy, the highest states included should contribute less and perhaps the excluded states should give a finite contribution. Thus 15 MeV seems a reasonable choice leading to uncertainties in the first moments of up to 10%.

3.1. Deformation dependence

The deformation dependence is investigated in the symmetric space, i.e. α=0.0. The points chosen lie on a path leading from the ground state over the first barrier, second minimum and second symmetric barrier. The (c,h)-values are given in table 1. In the symmetric space including Δ we have 6 different moments, since the viscosity tensor in general is non-diagonal. In fig. 1 we show the 3 diagonal moments as function of deformation for Δ=T=1 MeV. Aside from point nr. 2 which will be discussed later there is a general increasing tendency with deformation for c and h. From the ground state (0) to the point (7) outside the second symmetric barrier an increase of 6 for c and 14 for h is observed. The Δ-moment only varies with 25%. This picture must be supplemented by the non-diagonal terms, which are often comparable in magnitude to the diagonal terms.

TABLE I. A STUDY OF SYMMETRIC DEFORMATIONS
The first column is the label used on the abscissa of Fig. 1.

Nr.	c	h	
0	1.22	− 0.165	I. min.
1	1.21	0.0	
2	1.20	0.15	I. barr.
3	1.30	0.08	
4	1.415	− 0.012	II. min.
5	1.50	− 0.1	
6	1.625	− 0.061	II. barr.
7	1.70	0.0	

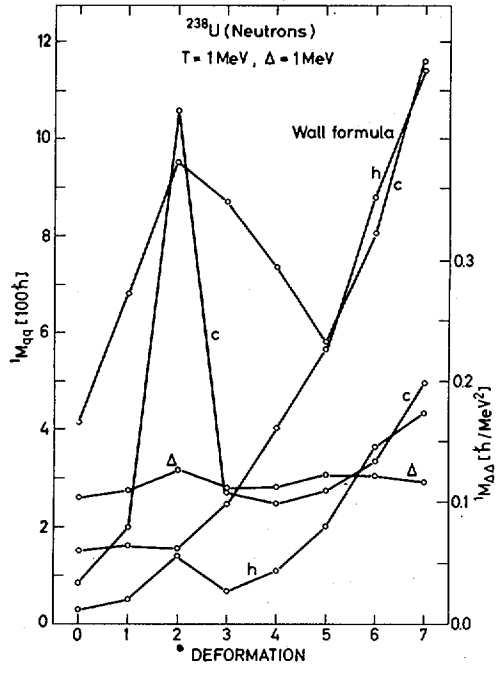

FIG. 1. The diagonal first moments of the response functions for the neutrons of ^{238}U as functions of deformation labelled as shown in Table 1. The scale on the left-hand side corresponds to c and h while that on the right-hand side is for Δ. The different points in deformation are connected by lines to guide the eye. Temperature and gap values are given on the figure. For comparison, we also show the corresponding wall formula results.

The reason for the large value at point 2 is two close lying single particle levels of the same parity and angular momentum projection situated slightly above the Fermi energy. Due to a very large matrix element, this transition is responsible for most of the moment. The very large resulting value in fig. 1 is in other words an extremely pronounced shell effect. Clearly the absolute value of the moment is quite sensitive to small variations of the potential parameters and the particular residual interaction used.

The second moment of point 2 is also almost entirely determined from the above mentioned transition. It seems to present a problem because the mass is large and negative. Of course this is unusual, but perhaps not excluded for small regions in deformation space.

For comparison we show also in fig. 1 the diagonal terms resulting from the wall formula [9]

$$^{1}M_{qq}(\text{wall}) = \rho\bar{v}\int\left(\frac{dn}{dq}\right)^{2} d\sigma \qquad (35)$$

where ρ is the density of neutrons, $\bar{v}$ their average velocity and dn/dq is the change due to q of a surface element perpendicular to the surface. The integral is over the surface. The overall increase with deformation is not very different from the linear response results, but the absolute values are roughly a factor 3 larger for these cases. At this moment such a comparison is not very useful, since the linear response results were for a given Δ and T and the wall formula does not contain pairing and temperature effects. However, for Δ=0 (T=1 MeV) the moments change less than 25% (except point 2). As we shall see later increasing the temperature from T=1 MeV to 3 MeV only increase the moments by around 20%. Furthermore for Γ_ρ=0.04 MeV (see eq.(22)), which is an abnormally high value the moments only increase around 15%. Thus the wall formula estimate for these deformations is about a factor of 2 larger than the linear response results for Δ=0 and T=2 MeV. For the (asymmetric) second barrier (see fig. 2) the overestimate is 1.6 for the h-directions and about 1.0 for the c- and α-direction.

3.2. Temperature and gap dependence

An interesting case is the second asymmetric barrier for ^{238}U. Fig. 2 shows the temperature and gap dependence of the diagonal first moments. The slope at T=0 is zero and the absolute values are all small but finite, i.e. 15 $\hbar$ for h, c, α and 0.015 $\hbar$/MeV^2 for Δ. The fast increase to a flat maximum and the slow decrease afterwards is typical. The maximum is usually between 1 and 2 MeV for the deformations and above 3 MeV for Δ.

The Δ-dependence is also shown on fig. 2. The sharp increase at Δ=0 to a maximum and the following strong decrease is a typical behaviour for the deformations. For the Δ-moment the value at Δ=0 is large (3.2 $\hbar$/MeV) and the following decrease extremely strong.

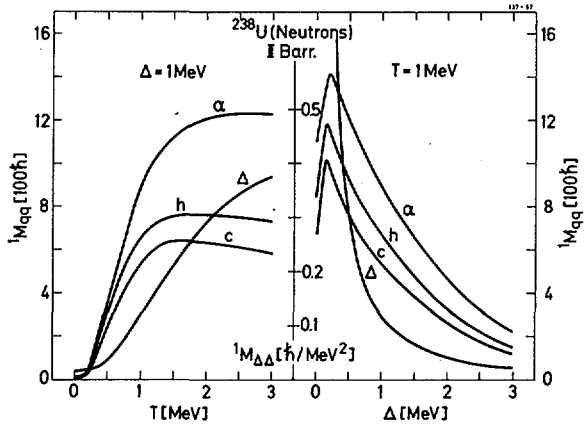

FIG.2. The diagonal first moments of the response functions for the neutrons of ^{238}U at the second (asymmetric) barrier as functions of T for Δ = 1 MeV and as function of Δ for T = 1 MeV. For T = 1 MeV and Δ = 0 the Δ-moment is 3.2 ħ/MeV².

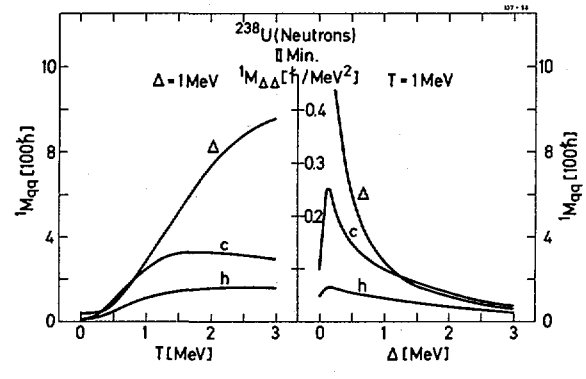

FIG.3. The same as Fig.2 for the second minimum. For T = 1 MeV and Δ = 0 the Δ-moment is 1.7 ħ/MeV².

The typical T and Δ dependence in fig. 2 is also seen in fig. 3 for the second minimum, where the first moments are appreciably smaller than at the second barrier. As an atypical example we show in fig. 4 the results for the first barrier, where the c-moment varies very strongly with Δ and T.

The large value of the viscosity means that the velocity in the c-direction must slow down. The nucleus would therefore try to avoid this point, if possible. Let us assume that only the c- and Δ-degrees of freedom are allowed. Then the

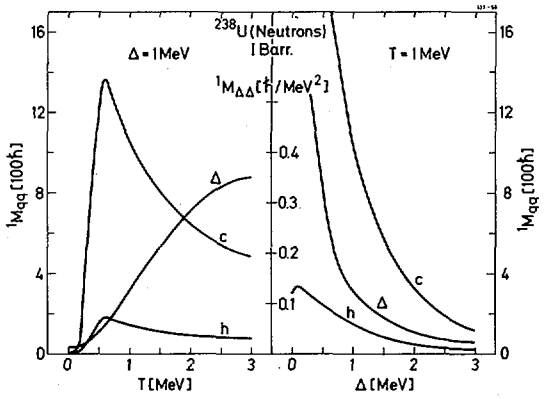

FIG.4. The same as Fig.2 for the first barrier (point 2). For T = 1 MeV and Δ = 0 the Δ-moment is 3.1 ħ²/MeV². For T = 1 MeV, the c-moment is 2300 ħ at Δ = 0 and increases up to a maximum of 3800 ħ at Δ = 0.1 MeV.

nucleus must pass over point 2 in deformation. One possible way to do this would be to move towards the point until the sharp viscosity increase. Then only change Δ to larger values simultaneously with increasing the temperature. This can be done with only a very small increase of intrinsic excitation energy because it is a decreasing function of Δ for fixed T. When T and Δ have assumed large values the viscosity in the c-direction has decreased considerably (see fig. 4) and c can then again change without an enormous loss of collective energy. Of course the actual choice of the nucleus will also depend on the mass and the free energy.

3.3. Comparison to observation

The damping width in the second minimum of ^{240}Pu has been extracted from measurements [10]. The result is Γ_W=0.13 MeV for an excitation energy of 5 MeV above the ground state, i.e. 3 MeV above the bottom of the second well.

This value is to be compared to the calculated value $\gamma/2B$ (see eq.(1)). We obtain 0.096 MeV and 0.2 MeV in the c- and h-direction for Δ=T=0.5 MeV, i.e. for an excitation energy from the neutrons of 1.7 MeV. If the relative proton and neutron contributions to the moments and excitation energy are proportional to their numbers, these "neutron" widths correspond to the "total" widths at 2.8 MeV of excitation. Thus the calculation seems to be in agreement with these experiments. With the mass parameters unchanged the wall formula leads to a Γ_W-value, which is 5-10 times too large.

The same width in the first minimum at 5 MeV of excitation is known to be much larger than the above Γ_W. The calculated value for the c-direction is 0.5 MeV for Δ=0.5 MeV and 1 MeV for Δ=0. In the h-direction the values are about 15% larger. Also this comparison is favorable.

4. SUMMARY

Linear response theory is used to write down the equations of motion for a set of collective coordinates. The crucial parameters are the first and second moments of the response functions. They depend on temperature, collective coordinates and the intrinsic structure of the nucleus in a way which is studied in the independent particle model.

The Hamiltonian correponds to a deformed average potential plus a particle non-conserving pairing term. The collective coordinates are the pairing gap and the deformation parameters of the potential. Expressions for the response functions and their moments are given in terms of temperature, pairing - and single particle states arising from residual interactions.

Numerical results of the first moments are given as function of deformation, pairing gap and temperature. It is small, but finite, for T=0, increases, usually steeply, with T between 0.5 and 1 MeV and is rather flat above T=1.5 MeV. With Δ it increases sharply above Δ=0 to a narrow maximum about Δ=0.2 MeV with a subsequent steep decrease. With increasing elongation of the nucleus the first moment increase on the average for fixed Δ and T. Still fluctuations around this smooth trend are present reflecting the changing shell structure. The results are compared with those obtained from the wall formula which roughly leads to 2 times larger values when we use appropriate Δ and T, i.e. large T ($\gtrsim$ 1 MeV) and small Δ ($\lesssim$ 1 MeV). Calculation of the damping width in the second minimum of ^{240}Pu at a few MeV of excitation is in agreement with experiment.

The mass parameters are not discussed in this paper, but they are calculated simultaneously and from exactly the same ingredients as the viscosity tensor.

The treatment of the pairing gap as a dynamical parameter allow the following very interesting application. Tracing the descent from saddle to scission point gives beside fragment size and excitation energy, the degree of superfluidity, i.e. the Δ-value. Presumable a larger Δ will favour even-even fragments. When the appropriate Fokker-Planck equation is solved, also distributions around the average values will become available. The ingredients for this are still the same quantities, i.e. the moments of the response functions.

In conclusion the approach described in this paper is very promising for applications of detailed dynamical studies of the fission process which is an example of large amplitude, anharmonic, damped collective motion.

REFERENCES

1 Hofmann, H. Siemens, P.J., Nucl.Phys. A257 (1976) 165

2 Hofmann, H., Phys.Lett. 61B (1976) 423

3 Johansen, P.J., Siemens, P.J., Jensen, A.S., and Hofmann, H., Nucl.Phys. A288 (1977) 152

4 Hofmann, H., Siemens, P.J., Ngô, C., Jensen, A.S., and Reese, K., Review to be published

5 Hofmann, H., Siemens, P.J., Nucl.Phys. A275 (1977) 464

6 Brack, M., Damgaard, J., Jensen, A.S., Pauli, H.C., Strutinsky, V.M., and Wong, C.Y., Rev.Mod.Phys. 44 (1972) 320

7 Brown, G.E., Unified Theory of Nuclear Models and Forces (North-Holland, Amsterdam, 1967)

8 Jeukenne, J.P., Lejeune, A., and Mahaux, C., Phys. Rep. 25C (1976) 83

9 Blocki, J., Boneh, Y., Nix, J.R., Randrup, J., Robel, M., Sierk, A.J., and Swiatecki, W.J., Ann.Phys. 113 (1978) 330

10 Glässel, P., Rösler, H., and Specht, H.J., Nucl.Phys. A256 (1976) 220

DISCUSSION

K.M. DIETRICH: I am glad to see that you apply the Hofmann-Siemens linear-response theory to the fission process. I might mention, by the way, that Dr. Pomorski has started work along the same lines. Statistical theories of this kind are, in my opinion, of great interest for an understanding of the fission process. This is the first time that heavy-ion physics has provided a new tool for study of the theory of fission.

Your theory implies that the distribution of the intrinsic degrees of the system is at all times close to statistical equilibrium. But if you describe the evolution of the system, starting from the saddle point, this condition may be better satisfied than in the case of heavy-ion reactions where there is certainly no statistical equilibrium present in the initial phase of the collision. On the other hand, it may be important in fission that only a selected class of intrinsic states is populated, as we have seen from Dr. Schütte's work. I think it would therefore be desirable to incorporate the possibility of partial equilibria into your description.

A.S. JENSEN: We have here assumed full statistical equilibrium leading to the canonical thermal population of excited states. I agree, however, that it is possible to introduce other types of distribution.

A. IWAMOTO: I have two questions. First, which of the two terms contributing to the friction tensor, i.e. the diagonal or the non-diagonal term, makes the more important contribution? Second, is there any consistent method for taking into account the temperature changes during the fission process, especially when treating the gap parameter as a dynamic variable?

A.S. JENSEN: Generally speaking, it can be said that the diagonal term contributes relatively less to the first moment than to the second. Which of the

terms is more important depends on the case considered, especially on the value of the pairing gap parameters.

The answer to your second question is yes. As the collective coordinates evolve in time, the temperature of the nucleus increases in accordance with the total energy conservation condition. No special problem is created in this connection by the present pairing treatment.

H.C. PAULI: I am somewhat puzzled by your statement that the wall formula gives a single-particle state 5 - 10 times larger than the experimental value. As far as I remember, the wall formula reproduces the experimental width of the giant resonance.

A.S. JENSEN: The factor of 5 - 10 mentioned here applies to the special case of the damping of the beta vibrational level at ~3 MeV of excitation in the second well for the ^{240}Pu. The giant resonance you refer to is the different case of dipole vibration that we have not yet considered. I should like to add that in these comparisons with experimental values the viscosity and mass parameter ratio are the relevant quantities. A favourable comparison with this type of experiment is therefore in itself not a test of the viscosity.

DYNAMICS OF THE LATE STAGES IN FISSION

F. DICKMANN
Kernforschungszentrum Karlsruhe GmbH,
Institut für Angewandte Kernphysik,
Karlsruhe, Federal Republic of Germany

Abstract

DYNAMICS OF THE LATE STAGES IN FISSION.

The deformed single-particle plus pairing model employed to evaluate shell and pairing effects on the deformation energy of a fissioning nucleus is extended to include features of the fission dynamics. A momentum operator $\hat{P}$ associated with the fission mode is derived, and the nuclear wave function is determined variationally so as to minimize the expectation value of the Hamiltonian, subject to the constraint that the espectation value of the momentum has a prescribed value: $\delta \langle \hat{H}_{sp}(\alpha) + \hat{H}_{pair} - \lambda\hat{N} - \dot{\alpha}\hat{P} \rangle = 0$. The model Hamiltonian depends on the parameter(s) α characterizing the shape of an equal-potential line close to the Fermi energy λ. The collective velocity $\dot{\alpha}$ and λ are Lagrange multipliers.

INTRODUCTION

A fissioning nucleus on its way from saddle to scission undergoes an accelerated deformation many details of which are not known. The measured kinetic energy of the fission fragments could either result from a strong Coulomb repulsion and a slow relative motion of the fragments in the scission configuration or from a small Coulomb repulsion and a fast relative motion. The additional experimental information that even fragments prevail indicates that pair correlations are effective during the process of fission until the point of scission. A rapid deformation would weaken the pairing correlation analogous to the Coriolis antipairing effect in collective rotations. We perform a theoretical estimate of how fast the deformation leading to fission may be if pairing is to survive.

THE MODEL

A phenomenological model Hamiltonian of a deformed nucleus is – at least conceptually – constructed by a variational determination of the stationary states of a more realistic nuclear Hamiltonian, subject to the constraints that the expectation values of operators characterizing the deformation of the nuclear-mass distribution have prescribed values. The simplified phenomenological model is made to reproduce the stationary states of the original constrained Hamiltonian. It depends on the deformation parameters α. Residual interactions are neglected.

We employ a deformed single-particle plus pairing Hamiltonian:

$$\hat{H}(\alpha) = \hat{H}_{sp}(\alpha) + H_{pair} = E_0(\alpha) + \Sigma_m \; E_m(\alpha)\, \beta^+{}_m(\alpha)\, \beta_m(\alpha)$$

The quasi-particle operators β_m annihilate one-quasi-particle excitations m. The ground state at the deformation α is the quasi-particle vacuum

$|\alpha\rangle : \beta_m(\alpha)|\alpha\rangle = 0$. The parameter(s) α characterize(s) the shape of a fictitious liquid-drop density associated with the nuclear-matter distribution.

From the relation

$$\hat{H}(\alpha + \delta\alpha) \approx H(\alpha) + (\delta\alpha) \cdot \partial\hat{H}_{sp}(\alpha)/\partial\alpha$$

we infer that the single-particle matrix elements of the operator

$$\hat{Q} = \partial\hat{H}_{sp}/\partial\alpha$$

are proportional to those of the constraining operator used to construct the phenomenological model when written in normal order with respect to the static ground state $|\alpha\rangle$. In analogy to the treatment of static deformations, dynamical aspects of the collective motion are introduced by adding a constraining operator $-\dot{\alpha}\hat{P}$ to the static Hamiltonian. The stationary states subject to the new constraint are again obtained variationally:

$$\delta \langle \alpha, \dot{\alpha}|\hat{H}(\alpha) - \lambda\hat{N} - \dot{\alpha}\hat{P}|\alpha, \dot{\alpha}\rangle = 0$$

The conventional ansatz for the momentum operator is

$$\hat{P} = cP_\alpha = c\tfrac{1}{i}\partial/\partial\alpha$$

$\hat{P}_\alpha$ is the generator of an infinitesimal change in the value of α in the static-state vectors:

$$(1 + (\delta\alpha)i\hat{P}_\alpha)|\alpha\rangle = |\alpha + \delta\alpha\rangle$$

The constant of proportionality is

$$c = \frac{\int Q\,(\partial_\alpha \rho_{LDM})\,d^3r}{\langle \alpha|[i\,\hat{P}_\alpha, \hat{Q}]|\alpha\rangle}$$

In this expression, the denominator normalizes the commutator of the operators $\hat{P}$ and $\hat{Q}$. The numerator is necessary because we describe the nuclear deformation in terms of the shape parameter α of the liquid-drop surface rather than by the expectation value $\langle Qr \rangle$. With this definition, the Lagrange parameter $\dot{\alpha}$ is the collective velocity $d\alpha/dt$.

If the dynamic ground state $|\alpha, \dot{\alpha}\rangle$ is determined by treating the constraining operator $\dot{\alpha}\hat{P}$ as a first-order perturbation of the static Hamiltonian, we obtain a

linear relation between $\dot{\alpha}$ and the expectation value of P:

$$\langle \alpha, \dot{\alpha} | \hat{P} | \alpha, \dot{\alpha} r \rangle = m(\alpha)\dot{\alpha}$$

$m(\alpha)$ being the cranking mass. The only matrix elements of the momentum operator entering the cranking model link the static ground state to two quasi-particle states:

$$P_{\mu\bar{\nu}}^{(20)} = \langle \mu\bar{\nu}, \alpha | \hat{P} | \alpha \rangle$$

They can be obtained from the behaviour of the ground state itself under a change of deformation.

In the general non-quasi-static case, matrix elements of the momentum operator between excited static states must be known to determine the dynamic ground state. In our simple model, the excited quasi-particle states are obtained simultaneously with the ground state for any deformation because residual interactions are neglected. We can, therefore, calculate all matrix elements of $\hat{P}$ by using the commutator relations:

$$\partial\beta_m/\partial\alpha = [\beta_m, i\hat{P}_\alpha], \; \partial\beta_m^+/\partial\alpha = [\beta_m^+, i\hat{P}_\alpha]$$

for various quasi-particle states m.

DETERMINATION OF THE DYNAMIC GROUND STATE

In a first step, the expectation value of the constrained Hamiltonian is minimized with respect to Hartree-Fock transformations. For our simple model, this amounts to a numerical diagonalization of the single-particle operator:

$$\hat{H}_{sp}(\alpha) - \dot{\alpha}\hat{P}^{(0)}$$

since the contribution of the pairing force to the H-F-potential is negligible. $\hat{P}^{(0)}$ is that part of the momentum operator P which commutes with the particle-number operator $\hat{N}$. The H-F-eigenvalues $\epsilon_\nu(\alpha,\dot{\alpha})$ are pairwise degenerate as are the eigenvalues of $H_{sp}(\alpha)$; the corresponding eigenvectors are, however, no longer connected by the time-reversal operator. The time-reversal symmetry is lost because the static Hamiltonian is time-even, whereas the momentum operator is time-odd. Since the matrix elements of the momentum operator are complex in the standard representation, the single-particle eigenvectors are also complex.

In the second step, a BCS-ansatz is made for the dyanamic ground state, such that the occupation probability of a level depends on the energy difference $\epsilon_\nu(\alpha,\dot{\alpha}) - \lambda$ and on a single gap parameter Δ. The dynamic ground state minimizes the expectation value of the constrained Hamiltonian with respect to the values of Δ.

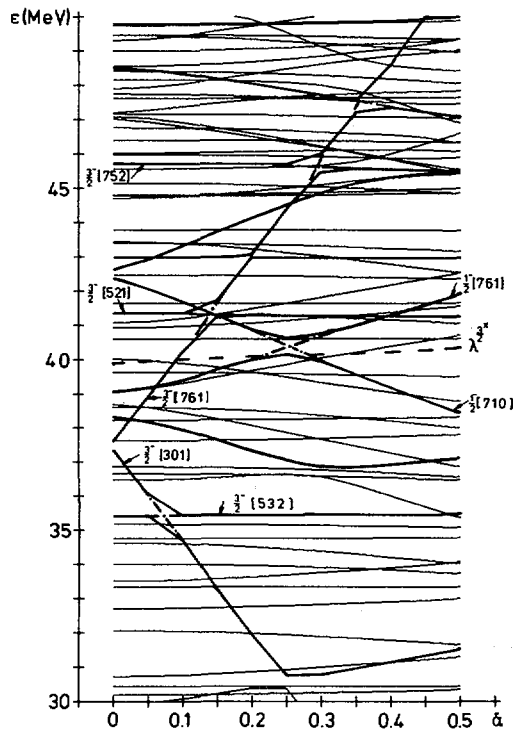

FIG. 1. Proton levels of ^{236}U as functions of the collective velocity for a motion along the static fission line at the second saddle point. Labels indicate asymptotic Nilsson quantum numbers of states strongly coupled by the momentum operator.

NUMERICAL RESULTS

Figure 1 shows that single-particle energies $\epsilon_\nu(\alpha,\dot{\alpha})$ may cross the Fermi energy as the collective velocity $\dot{\alpha}$ increases. In the late stage of fission at and beyond the saddle points, this happens already at low velocity when two static levels from different major shells with the same symmetry properties come energetically close to the Fermi surface and repel each other because of their coupling by the momentum operator. This phenomenon is the analogue of band crossing as observed in nuclear rotations at high spin. It excludes a perturbative treatment of fission dynamics [1]. The dynamical ground state changes its

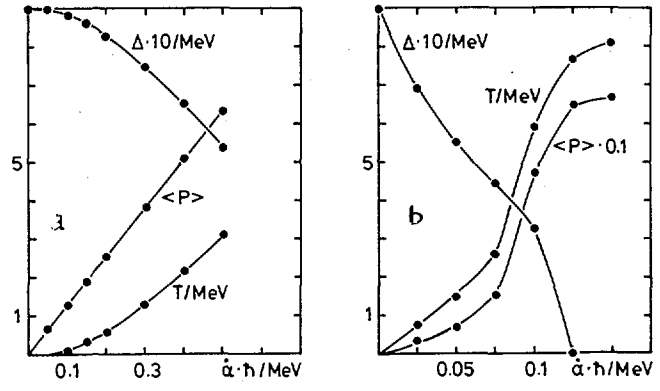

FIG.2. Energy increase T, momentum $\langle \hat{P}_r \rangle$ and pairing gap Δ for the protons of ^{238}U as functions of the velocity $\dot{\alpha}$. (a) The deformation α is the ratio c/a of the spheroid axes which approximate the shape of the ground state. The axis a is twofold. (b) α is the ratio of the largest to the smallest diameter of the nucleus at the second saddle point. The motion proceeds along the quasi-static scission line.

structure in a small velocity interval. The probability of the nucleus being excited instead of staying in the dynamic ground state increases with the slope of the level crossing the Fermi energy [2].

Figure 2 demonstrates the effect of the imposed collective velocity on the expectation values of momentum, energy and pairing gap. In Fig. 2a the ground state of the nucleus is shown to react gently on the imposed velocity of deformation. This is because single-particle states which are coupled by the momentum operator are well separated energetically. For a small velocity, the cranking model is valid. The decrease of the pairing correlations sets in slowly as the velocity is increased. In contrast to Fig. 2a, Fig. 2b shows the situation at the second saddle point. The odd behaviour of the plotted quantities reflects the band crossing depicted in Fig. 1.

CONCLUSIONS AND DISCUSSION

A common feature of the two situations shown in Fig.2 is that the anti-pairing effect of the velocity of deformation is appreciable at a kinetic energy of only a few MeV. Taking proper account of the contribution of the neutrons to the total collective energy of the nucleus we infer that pairing effects will vanish for pre-scission kinetic energies exceeding 10 MeV.

Discussing the reliability of the model Hamiltonian for the present application, we would like to mention that our results do not suffer from the inability

of the model to reproduce nuclear binding energies. We only use properties of the low-lying quasi-particle states for which the model is optimized.

The predicted band-crossing phenomenon is expected to be a real physical effect, even though it may not occur for the specific deformation and velocity for which it was calculated.

More than just one degree of freedom has to be included in order to describe the dynamic coupling of collective modes.

REFERENCES

[1] CHAFFIN, E.F., DICKMANN, F., Phys. Rev. Lett. 37 (1976) 1738.
[2] WILETS, L., Theories of Nuclear Fission, Clarendon Press, Oxford (1964) Chapter 5.

DISCUSSION

G. SCHÜTTE: There are two prescriptions for obtaining the nuclear wave function at the scission point - the dynamic descent from saddle to scission, and your additional constraint on the momentum for a fixed deformation. Do your conclusions regarding the gap parameter depend strongly on the difference between the two wave functions?

F. DICKMANN: Choosing the values of the Lagrange constraints independently, as I have done, does not mean that one has calculated the dynamic descent you refer to. One should rather map the expectation value of the Hamiltonian as a function of the deformation and momentum co-ordinates. Which points are affected by the dynamic path in this multi-dimensional space depends on the initial conditions in which the nucleus is prepared.

K.W. GOEKE: Your doubly-constrained Hartree-Fock method could be considered a unidimensional approximation to the TDHF. This could be shown by writing down the TDHF in terms of classical coordinates. However, in TDHF the occupation of the single-particle levels is determined by the initial condition and the dynamics of the process, whereas in your case the occupation is made on the basis of the single-particle energies. I feel that unless you consider adiabatic motion this can cause tremendous differences.

F. DICKMANN: The purpose of my study was to investigate the way in which the model nucleus reacts to external constraints in terms of deformation and deformation velocity. No attempt was made to attain dynamic equilibrium by specifying the constraining forces as functions of time, which is the aim of TDHF. I consider this a difficult task on account of the instabilities shown by the model nucleus. It would not remain in the simplest time-dependent Hartree-Fock-Bogolyubov state, but would very likely be excited when moving from saddle to scission at finite velocity.

TD-$\mathscr{S}$-HF SINGLE-DETERMINANTAL REACTION THEORY AND THE DESCRIPTION OF MANY-BODY PROCESSES, INCLUDING FISSION

J.J. GRIFFIN, P.C. LICHTNER, M. DWORZECKA,
KIT-KEUNG KAN
The Department of Physics and Astronomy,
The University of Maryland,
College Park, Maryland,
United States of America

Abstract

TD-$\mathscr{S}$-HF SINGLE-DETERMINANTAL REACTION THEORY AND THE DESCRIPTION OF MANY-BODY PROCESSES, INCLUDING FISSION.

The restrictions implied for the time-dependent many-body reaction theory by the (TDHF) single-determinantal assumption are explored by constructive analysis. A restructured TD-$\mathscr{S}$-HF reaction theory is modelled, not after the initial-value form of the Schroedinger reaction theory, but after the (fully equivalent) S-matrix form, under the conditions that (a) only self-consistent TDHF solutions occur in the theory, (b) every wave function obeys the fundamental statistical interpretation of quantum mechanics, and (c) the theory reduces to the exact Schroedinger theory for exact solutions which are single-determinantal. – All these conditions can be accommodated provided that the theory is interpreted on a time-averaged basis, i.e. physical constants of the Schroedinger theory which are time-dependent in the TDHF theory, are interpreted in TD-$\mathscr{S}$-HF in terms of their time averaged values. – The resulting reaction theory, although formulated heuristically, prescribes a well-defined and unambiguous calculational program which, although somewhat more demanding technically than the conventional initial-value TDHF method, is nevertheless more consonant with first principles, structurally and mechanistically. For its physical predictions do not depend upon the precise location of the distant measuring apparatus and are in no way influenced by the spurious cross-channel correlations which arise whenever the description of many reaction channels is imposed upon one single-determinantal solution. – For nuclear structure physics, the 'TDHF-eigenfunctions' provide the first plausible description of exact eigenstates in the time-dependent framework; moreover, they are unencumbered by any restriction to small amplitudes.

1. INTRODUCTION

Since the TDHF method [1] was first computerized as a nuclear model [2], studies based upon its numerical calculation have burgeoned [3]. Recently this method has been applied also to fission studies of the dissipation of collective energy in the descent from saddle to scission [6]. The present report is concerned with the TDHF method in general, and views it as a model of the Schroedinger system, based as it is upon the same variational principle, with only the single additional restriction that the solution be a single determinant.

From this viewpoint the conventional initial-value TDHF method calculated so far offers but a pale replica of the exact Schroedinger reaction theory. Instead of the exhaustive set of (S-matrix) reaction amplitudes between complete sets of asymptotic channel eigenstates of the Schroedinger theory, initial-value TDHF provides a single time-dependent wave function entirely fixed for all time by its initial value. Lacking linearity, TDHF loses also the superposability of its solutions into new solutions by linear combination. In replacing the exact time-independent Hamiltonian, H, by the solution-dependent (i.e. self-consistent) Hartree Fock "Hamiltonian", $\mathcal{H}$, TDHF lose also the orthogonality of its solutions, and the constancy in time of the scalar product analogous the the Schroedinger S-matrix.

These consequences of the self-consistency condition lead to certain fundamental difficulties in the interpretation of the initial-value TDHF solutions [7]. For example, the method predicts time-dependent probabilities for the internal characteristics of the ejectiles, so that the measured quantities are theoretically predicted to depend upon the precise location of the measuring apparatus (non-asymptoticity). In addition, the mean field so essential to the whole method is structurally incapable of describing adequately the full kinematic range of final reaction channels (spurious cross-channel correlation).

That the single determinantal restriction must impose certain limitations upon the theory is obvious, and is recognized frequently and recognized obliquely by statements that the TDHF is a "classical" or a "one-body" theory. But the precise effect of the assumption upon the physical content and the mathematical structure of the theory has seldom been addressed.

When this work began in 1976, we were inclined to believe on physical grounds that the single determinantal assumption would turn out to be a serious restriction [8], omitting as it does all of the two-body correlations (except of anti-symmetry). Yet as we strove to specify that claim precisely, we came to realize that for some physical systems, single determinants might provide an excellent description. (For one example where determinants are exact, see reference [9].) Then we began to search for structural parallelism, even while still expecting quantitative divergences, for nuclei at least, between the Schroedinger and TDHF theories [7].

In this paper we review certain aspects of the $\mathcal{S}$-matrix approach to these questions [7], and report recent developments based on the nature of the periodic TDHF solutions to certain model problems [11]. The result is remarkable: a consistent description of quantum reaction amplitudes is obtained which is fully analogous structurally to the Schroedinger theory. It is built upon the (whole set of) self-consistent TDHF solutions, and requires that the asymptotic channel states involve gauge invariant periodic solutions as the analogs of Schroedinger eigenstates, and that the physical implications of the theory be interpreted on a time averaged basis.

The corollary implication for nuclear structure theory that gauge-invariant periodic TDHF solutions are the appropriate "TDHF-eigensolutions"

for describing bound states in the time dependent framerwork, is noted [11]. Nor need any restriction to small amplitudes be invoked.

2. COMMON VARIATIONAL ORIGINS OF TDHF AND SCHROEDINGER THEORIES

The Variational Principle,

$$\delta I = \delta \int_{t_1}^{t_2} \langle \Psi(\vec{x},t') | (H - i\hbar\partial/\partial t') | \Psi(\vec{x},t') \rangle dt' = 0 \qquad (1)$$

implies the exact non-relativistic time dependent Schroedinger equation [12]. If the wave function Ψ is required to be a single determinant, the same principle yields the unique "Constant-$\langle \mathcal{H} \rangle$" time-dependent Hartree-Fock equation [9]. Since the origins of the TDHF model and those of the Schroedinger theory lie so close, a close structural parallel between them is reasonably to be expected. It is that analogy upon which this paper is based.

3. TIME DEPENDENT $\mathcal{S}$-MATRIX HARTREE-FOCK REACTION THEORY

The T.D.-$\mathcal{S}$-H.F. approach to the single determinantal reaction theory [7] has been evolved by requiring the closest possible analogy between the self-consistent TDHF description and the exact Schroedinger theory. In particular, the general requirement has been imposed at every stage that the T.D.- $\mathcal{S}$ -H.F. must reduce identically to the Schroedinger description in case the exact solution happens to be a single determinant.

The S-matrix form of the Schroedinger reaction theory for localized wave packets has been chosen as the model. Thus, the symmetry in time which that theory displays is retained, together with the close parallel between initial and final reaction channel states.

Two conditions imposed rigidly upon the theory have been set as axioms. The first specifies the precise meaning of TDHF self-consistency, by requiring that every wave function allowed in the theory must be a single determinant and must propagate in time according to the self-consistent TDHF equation,

$$\text{Axiom (A):} \qquad \mathcal{H}[\Phi] \cdot \Phi = i\hbar\dot{\Phi} \qquad (2)$$

The second requires every wave function allowed in the theory to be subject to the statistical interpretation of quantum mechanics, in the sense that the spatial integral,

$$\text{Axiom (B):} \qquad a_{fi} = \langle \Phi_f(\vec{x},t) | \Phi_i(\vec{x},t) \rangle \qquad (3)$$

specifies the probability amplitude that a system described by Φ_i will under physical measurement exhibit the characteristics of the system described by Φ_f.

Without Axiom (A) the theory is not a self-consistent TDHF theory; lacking Axiom (B) the solutions are not Schroedinger wave functions, properly so called. It is hard to imagine any objection to either; the question is rather whether they can be sustained without preventing the construction of a theory reasonably analogous to the Schroedinger theory.

As its name implies, the T.D.-$\mathcal{S}$-H.F. reaction theory casts the Schroedinger S-matrix in a prominent role. Indeed, the S-matrix analog,

$$\mathcal{S}_{fi} = (T_2-T_1)^{-1} \int_{T_1}^{T_2} \langle \Phi_f(\vec{x},t') | \Phi_i(\vec{x},t') \rangle dt' \qquad (4)$$

describes the transition probability from an initial to a final self-consistent TDHF reaction channel. In reference [7] the form (4) for $\mathcal{S}$ is obtained heuristically by analogy with the exact Schroedinger theory in such a way that it reduces exactly to the S-matrix when the single determinantal solutions, Φ, is also the solution of the exact Schroedinger equation. In addition, the palpable physical error introduced by the spurious cross-channel correlations of the conventional Hartree-Fock description during the postbreakup phase, when the description of several channels is imposed upon the single determinant, is eliminated from the theory.

4. ASYMPTOTICITY IN SCHROEDINGER REACTION THEORY

In the exact Schroedinger theory, the wave function describing the system for times long after the collision process can be expanded in a complete mutually orthogonal basis of aymptotically stationary channel states, constructed from the eigenstates of every possible pair of fragments, and the functions describing their relative motion. It follows that the probability of measuring a certain value for any internal physical property of an ejected fragment is predicted not to depend upon the precise location of the measuring apparatus with respect to the collision volume, provided only that it is sufficiently distant to guarantee that the interactions between the fragments vanish. This independence of the predictive content of a reaction theory of the precise location of the measurement, we refer to as the "Asymptoticity" property of the theory. Clearly the Schroedinger theory exhibits this property.

5. INITIAL VALUE TDHF THEORY LACKS ASYMPTOTICITY

Asymptoticity is not a general property of the conventional initial-value TDHF theory, because the Hartee-Fock "Hamiltonian", $\mathcal{H}$, continues to be time-dependent even long after the collision. Indeed, this non-asymptoticity of TDHF lies at the root of the difficulties of precise interpretation of the physical implications of conventional initial-value TDHF descriptions of complex reactions. As a result, only a few "trajectory" characteristics, which remain constant once the fragments separate, can be unambiguously extracted from the numerical TDHF studies of nuclear systems.

Thus, although the expectation has frequently been expressed that some specific interpretation would be found in terms of an expansion on an appropriate basis for the late time wave functions of conventional initial-value TDHF theory, only one report of an explicit attempt is known to the present authors [13]. The result was that the expansion coefficients remained time dependent indefinitely.

6. ASYMPTOTICITY AND PERIODICITY

Under the ansatz (4) the single determinantal TDHF description need no longer be a machine which grinds inexorably the future out of the past. Rather it attributes physical content to matrix elements between solutions which have evolved from simple states in the past and other solutions which will evolve into simple states in the future. In the Schroedinger theory, of course, these viewpoints are equivalent. In the single determinantal case, they are not. Thus by choosing the S-matrix model, instead of the initial-value model, one finds new possibiliities. For example, there arises the freedom, and the need, to select reaction "channels" suitable for the physical description required. In initial-value TDHF one has, and can have, only the late time solution to interpret. In TD-$\mathcal{S}$-HF, the selection of channels is utilized to assure that the physical properties of the emergent droplets remain constant in time, the first step towards guaranteeing asymptoticity for the new theory.

This condition requires that a reaction channel wave function must describe stationary TDHF states of the emergent droplets. Or, if periodic TDHF states are allowed as channel states, then their physical properties can be considered as constant if interpreted on a time-averaged basis.

7. TIME AVERAGING IN THE TD-$\mathcal{S}$-HF THEORY

The use of periodic solutions to play the role of the exact eigenstates for the description of TDHF droplets in the asymptotic channel states, implies that their asymptotically constant physical characteristics must correspond to time averages (over the period) of physical operators. We note that also in the definition of $\mathcal{S}$, the time average defined by equation (4) was a consequence of the fact [7] that the overlap of two TDHF solutions, in contrast with the S-matrix overlap between exact solutions, is not constant in time. Thus (4) specifies that the reaction amplitude is to be obtained by time-averaging over the whole interaction interval.

8. TIME AVERAGING AND ASYMPTOTIC CHANNEL ORTHOGONALITY

Beside the definition of the $\bar{\mathcal{S}}$-matrix, and the constants of the periodic TDHF states, a third cause for a time averaged interpretation arises in connection with the non-orthogonality of the channel states built upon the periodic TDHF solutions. Here again we deal with a deviation of the TDHF from the exact theory which arises specifically from the self-consistency condition: the eigenstates of the exact linear Schroedinger Hamiltonian form a complete, orthogonal, linearly superposable set, while the TDHF "Hamiltonian" generates a set of stationary (and periodic) solutions which are not mutually orthogonal and which cannot be superposed to form arbitrary solutions, because of the nonlinearity of the (TDHF) equations they obey.

As a result of the non-orthogonality of the TDHF solutions, overlap amplitudes between distinct final channel functions, such as

$$a_{gf} = \langle \Phi_g(\vec{x},t) | \Phi_f(\vec{x},t) \rangle \tag{5}$$

do not automatically vanish. It follows that under the statistical interpretation of quantum mechanical amplitudes (Axiom B, equation (3), the statement that a system is described by the solution, Φ_f, must also assert with a probability amplitude, a_{gf}, that a measurement would show it to have the properties of channel $\{g\}$. Then the reaction amplitudes, $\bar{\mathscr{S}}_{fi}$, would not correspond one-to-one with the theoretical predictions for measured properties, $\{f\}$.

This difficulty also is resolved by the assumption that the amplitudes (5) must be interpreted not instantaneously, but on a time averaged basis. Then, not a_{gf} of (6), but its time average value,

$$\overline{a_{gf}} = (2\tau)^{-1} \int_{t-\tau}^{t+\tau} \langle \Phi_g(\vec{x},t') | \Phi_f(\vec{x},t') \rangle dt' \tag{6}$$

is to be interpreted as the amplitude that a system described by the solution, Φ_f, will be measured to have the physical properties of channel $\{g\}$. (In equation (7), the interval, τ, must be taken large enough for a to become independent of the interval; in the asymptotic region, this is always possible.) Then, as was shown in reference [7], the time averaged overlaps between distinct asymptotic channels all vanish,

$$\overline{a_{f'f}} = 0, \qquad \{f'\} \neq \{f\} \tag{7}$$

if only the energies of the periodic channel solutions are discrete and nondegenerate.

Thus, for channel states built upon a discrete nondegenerate set of periodic TDHF solutions, the time averaged channel orthogonality property (7) prevails. Then the one-to-one correspondence between the reaction amplitudes and the theoretically predicted values of the (now time-averaged) physical measurements which prevails in the exact reaction theory is retrieved for the TD-$\mathscr{S}$-HF theory.

9. REQUANTIZATION AND GAUGE INVARIANCE

Although it is not known whether the periodic TDHF solutions for isolated TDHF droplets occur always with a continuous range of energies, Kan, et al. [11] have recently studied special cases for which this situation prevails. Kan's work therefore forces one to deal with the requantization process discussed in reference [7], by which some set of solutions discrete in energy is selected from the continuous spectrum of periodic TDHF solutions to serve as reaction channel wave functions; or else to conclude that the single determinantal reaction theory, since it would then lack reaction channel orthogonality, and therefore could not consistently predict physical measurements in one-to-one correspondence with the reaction channel amplitudes characterizing the reaction process, was of an essentially different character, structurally, from the exact theory---an "intrinsically dissipative" trajectory theory, in the terminology of reference [7].

Remarkably, one finds, again arguing by analogy, that the requirement that the periodic TDHF channel solutions behave like the exact stationary eigenstates, and particularly that they be invariant under gauge transformation, leads to a unique and unambiguous selection of a discrete set of gauge-invariant periodic functions as suitable eigenstate analogs.

10. GAUGE TRANSFORMATION OF THE TIME DEPENDENT SCHROEDINGER THEORY

Consider the Schroedinger system characterized by the (time-independent) Hamiltonian, H, and the set of time-dependent descriptions specified by the gauge transformed time evolution operators, $\hat{H}$, of the form

$$H \rightarrow \hat{H} = H + \beta(t) \tag{8}$$

where $\beta(t)$ is an arbitrary space and momentum independent function of time.

Then the physical content of each of the transformed descriptions is exhausted by the matrices of all the possible physical observables, $\mathcal{O}(\vec{x},\vec{p})$, and is unaltered by the transformation (8) from H to $\hat{H}$.

11. GAUGE INVARIANCE OF EIGENSTATES

Then consider the time-dependent Schroedinger solution initiated at $t=t_0$ as an eigenfunction, $\psi_\lambda(\vec{x})$,

$$\Psi_\lambda(\vec{x},t) = \psi_\lambda(\vec{x})\{\exp - (i/\hbar)\langle H\rangle t\} \tag{9}$$

Under gauge transformation,(8) only the phase factor in (9) is altered, while the stationary state remains invariant. By analogy, then, we shall insist that the periodic TDHF channel solutions must also be invariant under arbitrary gauge transformations.

12. "TDHF EIGENSOLUTIONS": PERIODIC STATES AS GAUGE ANALOGS OF THE EXACT STATIONARY EIGENSTATES

In the Hartree-Fock case, consider the "Constant-$\langle\mathcal{H}\rangle$" solutions defined by the equation,

$$\mathcal{H}[\Phi]\cdot\Phi = \{\mathcal{H}^0 + \langle\Phi|H - \mathcal{H}^0|\Phi\rangle\}\Phi = i\hbar\dot{\Phi} \tag{10}$$

and a specified initial-value determinant. The TDHF "Hamiltonian", $\mathcal{H}$, of equation (14) is uniquely prescribed [9] by the variational principle (1). Then $\mathcal{H}^0$ may be the conventional self-consistent Hartree-Fock Hamiltonian, or that Hamiltonian augmented by any arbitrary additive function of time only. Now consider the effect upon a periodic solution, $\Phi_p(\vec{x},t)$, of a gauge transformation (8). Obviously, the gauge transformed function, $\hat{\Phi}$, need not be periodic even when Φ_p is periodic.

Since it is not possible for periodicity in general to be a gauge invariant property, the gauge analogy between the exact theory and TDHF

requires channel solutions in the form of a product of a periodic function and a phase factor determined by H alone; i.e.,

$$\Phi = \Phi_p(\vec{x},t)\{\exp - (i/\hbar)\langle H\rangle t\} \tag{11}$$

where Φ_p is a periodic function. A function of the form (11) transforms under the gauge transformation of H just as the exact solution (19) transforms, and the periodic solution, Φ_p, is precisely the analog of the stationary eigenstate, $\psi_\lambda(\vec{x})$.

13. GAUGE INVARIANT TDHF EQUATION

Of course the function (11) must satisfy the TDHF equation (10) implied by the variational principle (1). Then the periodic factor, Φ_p, of (11) satisfies the following gauge invariant TDHF equation,

$$\{\mathcal{H}^o - \langle\Phi|\mathcal{H}^o|\Phi\rangle\}\Phi = i\hbar\dot{\Phi} \tag{12}$$

so called since it is manifestly unaffected by any transformation of the form (18).

14. CONTINUA OF PERIODIC TDHF SOLUTIONS: GAUGE REQUANTIZATION

The equation (10) sometimes exhibits, for time-independent H, a continuous set of periodic solutions [11]. But among such a continuum, only those solutions whose energy is related to the period, T, by the equality,

$$\langle H\rangle = 2\pi N\hbar/T \tag{13}$$

are of the form (11) with a periodic factor which satisifies the gauge invariant TDHF equation (12). Then (13) selects a discrete subset of the periodic continuum, for which the space-dependent periodic factor Φ_p, is invariant under the gauge transformation (8), exactly as are the eigenstates of the exact Hamiltonian.

Thus, condition (13) offers a natural basis for the requantization of the continuum of periodic TDHF solutions into a discrete set of TDHF eigenfunctions. It selects those periodic states which remain periodic, just as the eigenstates remain stationary, under an arbitrary gauge transformation.

Alternatively, one could have sought in the first place as suitable analogs of the stationary eigenstates only those solutions whose periodity is a gauge invariant periodic function, like the stationarity of the eigenstates. Then one would at the outset have recognized only the discrete periodic spectrum of (12) as acceptable channel states, rather than the continuous spectrum of periodic solutions of $\mathcal{H}^o$. We note that Kan, et.al., [11], have also demonstrated the equivalence of the condition (13) with the Bohr-Sommerfeld quantization condition.

15. "TDHF-EIGENSTATES"

The gauge invariant periodic solutions offer a discrete spectrum of TDHF states which share the gauge transformation properties of exact time-dependent eigenstate solutions. These states are therefore natural objects to describe the large amplitude TDHF analogs of the Schroedinger eigenstates within the time dependent framework.

Indeed, by numerical calculation for certain model problems whose exact eigenstates are known, Kan et. al. [11] have shown excellent agreement between the energies of these gauge invariant periodic solutions (for which we therefore suggest the name "TDHF-eigenstates") and the exact energy eigenvalues. (Cf. also [14].)

16. CONCLUSIONS

The TDHF description of continuum reactions has been restructured from an initial-value problem into a form analogous to the S-matrix version of the Schroedinger theory. The resulting TD-$\mathcal{S}$-HF theory involves only self-consistent single determinantal solutions of the TDHF equations, and invokes time averaging to obtain a consistent interpretation of the TDHF analogs of quantities which are constant in the exact theory, such as the S-matrix and the asymptotic reaction channel properties.

Periodic TDHF solutions then play the role of stationary eigenstates, in the construction of suitable asymptotic reaction channel states. If these periodic channel states occur only at discrete energies, then the resulting channels are mutually orthogonal (on the time average) and the theory exhibits a structure fully analogous to the exact theory.

In certain special cases where the periodic solutions are known to occur as an energy continuum, the requirement that the periodicity of the channel solutions be a gauge invariant property provides a natural requantization condition, which turns our to be identical with the Bohr Sommerfeld quantization rule. Thus it emerges that the TD-$\mathcal{S}$-HF description can always exhibit a structure analogous to that of the Schroedinger reaction theory: the qualitative structural effect of the single determinantal assumption is to impose the requirement of time averaging upon the interpretation of the physical quantities of TD-$\mathcal{S}$-HF whose Schroedinger analogs are constant.

For nuclear structure physics, the "TDHF-eigensolutions" offer a time dependent description of stationary states which agrees well with the exact eigenstates for the model problems considered so far [11], and which invites comparison with the coprresponding stationary RPA states.

This research is supported by the U.S. Department of Energy.

REFERENCES

[1] DIRAC, P.A.M., Proc. Camb. Phil. Soc. 26(1930)376.
[2] BONCHE, P., KOONIN, S.E., and NEGELE, J.W., Phys. Rev C13(1976)227.
[3] See references [4,5], and other references cited therein.
[4] FLOCARD, H., KOONIN, S.E., and WEISS, M.S., Phys. Rev.C17(1978)1682.
[5] BONCHE, P., GRAMMATICOS, B., and KOONIN, S.E., Phys.Rev.C17(1978)1700.
[6] NEGELE,J.W., KOONIN,S.E., MØLLER, P., NIX,J.R., and SIERK,A.J., Phys. Rev.C17(1978)1098.
[7] GRIFFIN, J.J., LICHTNER, P.C., and DWORZECKA, M., U. of Maryland Tech. Report 79-045 (ORO#5126-56), to be published; "Nuclear Fermidynamics and TD- -HF", in AIP Conference Proceedings #47, Clustering Aspects of Nuclear Structure and Nuclear Reactions, AIP, New York(1978)114.
[8] GRIFFIN,J.J., and LICHTNER,P.C., Open Questions on Numerical TDHF Models, in Proc. IVth Int'l. Workshop on Gross Properties of Nuclei and Nuclear Excitations, IV(1976)21, Hirschegg, Austria, Jan.1976 (Inst. f.Kernphysik, Darmstadt, F.R.G. 1976).
[9] LICHTNER ,P.C.,GRIFFIN, J.J., SCHULTHEIS, H., SCHULTHEIS, R., and VOLKOV, A.B., U. of Maryland Tech. Report.79-010 (ORO#5126-49), to be published.
[10] LICHTNER,P.C., and GRIFFIN, J.J., Phys. Rev. Lett. 37(1976)1521.
[11] KAN, K., GRIFFIN, J.J., LICHTNER, P.C., and DWORZECKA, M., Bull. A.P.S. 24(1979)627, and U. of Maryland Tech. Report #79-114 (ORO-5126-66), to be published.
[12] MORSE, P.M., and FESHBACH, H., Methods of Theoretical Physics, McGrawHill, New York(1953)314.
[13] KAN, K.K., and TAMURA, T., private communication.
[14] PALTIEL, Z., LEVIT, S., and NEGELE, J., Bull. A.P.S. 24(1979)609, paper DK8 reports results identical with [11], obtained by what appears to be an entirely different method.

DISCUSSION

K.M. DIETRICH: I hope that my question is not an awkward one, but do you obtain stability with respect to changes in the time interval (T_1, T_2) that you used to calculate your $\mathscr{S}$ matrix?

J.J. GRIFFIN: In the figure I showed T_1 is defined as the latest time at which the backward-going solution $\Phi_f^{(-)}$ has no spurious cross-channel correlations, and T_2 as the latest time at which $\Phi_i^{(+)}$ has none either. Then - apart from small shifts arising from the finite nuclear skin thickness and the packet width - the interval (T_1, T_2) is the largest possible interval with no spurious cross-channel calculations in either wave function entering into $\mathscr{S}_{fi}$. So we feel that the interval is unique and that there is no physical reason for varying it.

K.M. DIETRICH: Thank you. I should also like to ask a more general question. Is it physically reasonable to expect a mean-field theory like HF to provide reliable information on the reaction cross-sections for specific microscopic channels? From the time-independent HF we know that a deformed Slater

determinant, after projection onto angular momentum eigenstates, can describe states of a rotational nature, but hardly a more complex excited state. So I wonder whether the TDHF solutions can be expected to provide all the information one would like.

J.J. GRIFFIN: Well, I know of no studies aimed at stationary HF descriptions of higher excited states, so I have no reason to expect them to be described, or not described, by higher HF states.

However, if one formulates a TDHF reaction theory, then that theory will describe TDHF droplets, whose dynamic behaviour is completely contained in the TDHF dynamic equation. These TDHF droplets may or may not describe nuclei; nevertheless, they alone can be described by a TDHF theory.

Our analysis deals with the *structure* of the reaction theory. Another question is whether such a theory, even though it has the correct structure, will describe nuclei. We have not dealt with this problem. But if TDHF droplets describing nuclear spectra reasonably well really exist, then TD-$\mathscr{S}$-HF may also be a quantitative success.

H.C. PAULI: We know that the cross-sections are proportional to $SS^{\dagger}$, and it is now taken, generally speaking, that $\overline{SS}^{\dagger} \neq \overline{S} \cdot \overline{S}^{\dagger}$, so how does this come out in your five-letter approach? Second, do you already know the relationships between your cross-sections and the classical cross-sections that the four-letter people give us? Ang third, do you believe it is possible to calculate the multiple cross-section $d^3\sigma/d\Omega\, dE\, dN$, which differs from the classical delta function?

J.J. GRIFFIN: In this approach the (multiple -) differential cross-section from {i}, a complete set of labels for the channel to {f}, another complete set, is proportional to $|\mathscr{S}_{fi}|^2$. An explicit expression for the cross-section is given in Ref.[7] of the paper. Note that since the TDHF solutions are (and must always be) localized wave packets, we are not free to assume an incident plane wave, as is usually done in scattering analyses. To obtain cross-sections like those yielded by initial-value TDHF, we have to integrate over most of the parameters which specify the channel, leaving only the velocity and angular variables unintegrated. Ref. [7] gives a complete account of the channel label parameters.

K.W. GOEKE: For your approach you need periodic solutions, which must be periodic on a macroscopic scale in order to ensure that your results are independent of the counter position. Are you sure that, besides simple stationary HF states moving at a certain velocity, there are such solutions?

J.J. GRIFFIN: Yes, these periodic solutions must obey the relationship $\psi(t+T)=\psi(t)$ for all t precisely. For two simple TDHF models which can be solved exactly in algebraic terms, it was shown that periodic solutions do exist, and even have a continuous energy spectrum. It is from these that the gauge-invariant periodic 'TDHF eigenstates' are selected by the re-quantization relationship of the Bohr-Sommerfeld form.

SUMMARY OF THE SYMPOSIUM

SUMMARY OF THE SYMPOSIUM

H.J. SPECHT
Physikalisches Institut der Universität Heidelberg,
Heidelberg, Federal Republic of Germany

At one of the last meetings, I had the privilege of being the first speaker. Now I am the last one. It is quite clear what I shall prefer next time. The usual task of a summary speaker – of coping with several years of very solid work, one week of solid lectures, and several hundred figures – is in some way really formidable. What should one do? First, one tries to remember how other summary speakers have solved the problem, and, in so doing, one finds that, in fact, there are all extremes. Some of the speakers really run through a hundred slides – others are found to be involved, instead, in ingenious exercises in poetry. Obviously, neither alternative really suited my purpose. What I did next, was to investigate how it had been done in this whole series of symposia. Going back first to the Salzburg Symposium of 1965, I found that it had been a theoretician who gave the summary. I also found that more than ninety percent of his time he spent on experiments. At that point, I was slightly horrified – do you expect me now to review more than ninety percent theory? So I went on to the next meeting in Vienna, 1969. The summary speaker there was an experimentalist, and fortunately that experimentalist was quite helpful. I learned from him that symbols are as important at these Symposia as everywhere else in life. Many of you will remember the story. The Salzburg symbol was that shown in Fig. 1a, and, in fact, with a few exceptions, it will probably continue to be a good symbol far into the 1980s. Vienna was, however, really very different. The symbol in Vienna was the one shown in Fig. 1b, and I think

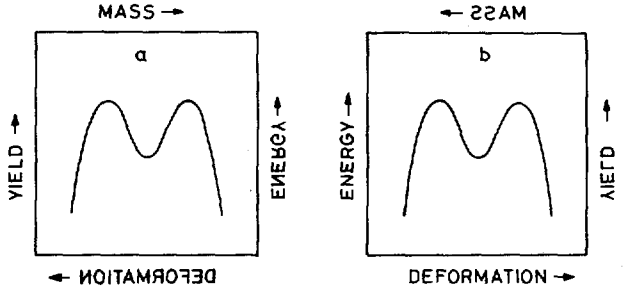

FIG. 1. The Vienna symbols.

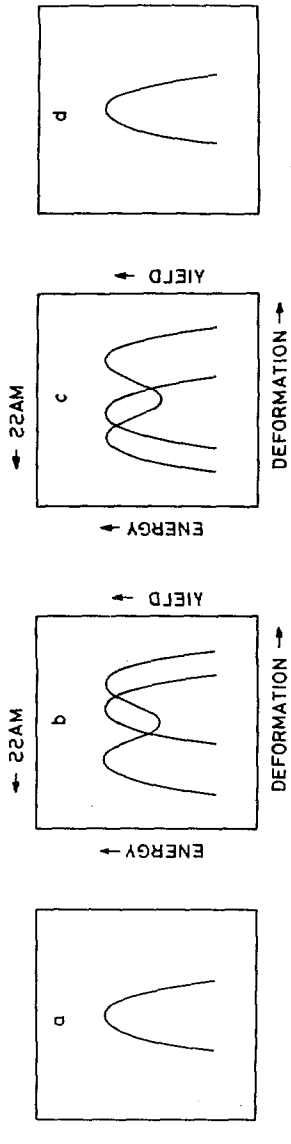

FIG. 2. The Jülich symbols.

TABLE I. OPEN PROBLEMS, TAKEN FROM SUMMARY, ROCHESTER 1973

'Detail':		
1)	Shell correction for magic numbers (Pb-anomaly)	+
2)	Shell correction at barriers (Th-anomaly)	−
3)	Odd-even effects in half-lives for spontaneous and isomeric fission	−
4)	Competition of symmetric and asymmetric fissions as a function of excitation energy	−
'Conceptual':		
1)	Viscosity	?
2)	Adiabatic approach or partial statistical equilibrium (collective degrees) or full statistical equilibrium	?
	weighted average	−

this also applied to the Rochester Symposium later on in 1973. In trying now to find what would be a good symbol for the Jülich Symposium of 1979, I decided it might be that given in Fig. 2a. I do admit that it would apply to many fields of physics, but you have to read it together with the old one, and then it becomes clear. For example, you use it like Fig. 2b to split the second barrier. There was a lot of heated discussion on this point, and we shall have to return to it later. One can also split the first barrier (Fig. 2c), and there was discussion about this, as well. But the nice thing about the symbol is that you cannot split both barriers at a time, and I don't think that Britt [1] claims that. These were different nuclei – the very light ones with a possibly split outer barrier, and the very heavy ones with a possibly split inner barrier. I don't know how this will develop until the next meeting; one finally may have to overlay two of the old symbols. Clearly, the new symbol can also be turned around and used in the traditional way (Fig. 2d). I should remind you in this connection of some very interesting contributions in terms of not-quite-so-traditional symmetrical mass distributions. You have just heard about the beautiful work on the Fm isotopes by Hoffman [2] and the strange behaviour reported by Hulet [3] if another proton is added. You also remember the missing Bussinaro-Gallone point [4] which, I think, might be quite an important feature of the dynamical liquid-drop model if it turns out to be true. You will finally recall some

TABLE II. POTENTIAL-ENERGY SURFACES (1)

Status (experimental):

1) Comprehensive systematics of barrier parameters
   - 'Reasonable' model independence
   - Indirect evidence for γ-deformed barriers
   - Collective saddle states

2) The 2:1 shape of fission isomers repeatedly verified

3) Beginning spectroscopy in the second well
   - Rotational excitations
   - Nilsson states

Open problems:

1) The true shape of the barrier in the actinides (2,3,4 peaks?)
   - Fine structure in Th (or other nuclides) from (n,f) or (d,p,f)
   - Systematics of isomeric shelves from (γ,f)
   - High-resolution (γ,f) experiments with tagged photons
   - Systematics of γ-decay back to the first minimum
   - Spectroscopy sensitive to 3-MeV barriers
   - β-delayed fission and the β-strength function
   - γ-spectra from the (n,f) reaction

2) Spectroscopy of highly deformed nuclei
   - Single-particle (Nilsson) states
   - Magnetic moments
   - Collective states (octupole vibrations, β- and γ-vibrations)

3) Γ_f/Γ_n-systematics
   - *Barriers of nuclei outside actinides and/or far-off stability*

remarkable news about how the width of the symmetrical mass distribution increases if one studies nuclei with a fission barrier vanishing either via high angular momentum [5] or via high Z^2/A [6]. Again, we shall have to return to this point later.

So then I went on to the last meeting in Rochester 1973. You all remember it, many of you were there. The general atmosphere, I think, was that a great optimism. Everything seemed to be solved. The double-humped barrier was firmly established. Many theoreticians had performed monstrous potential-energy

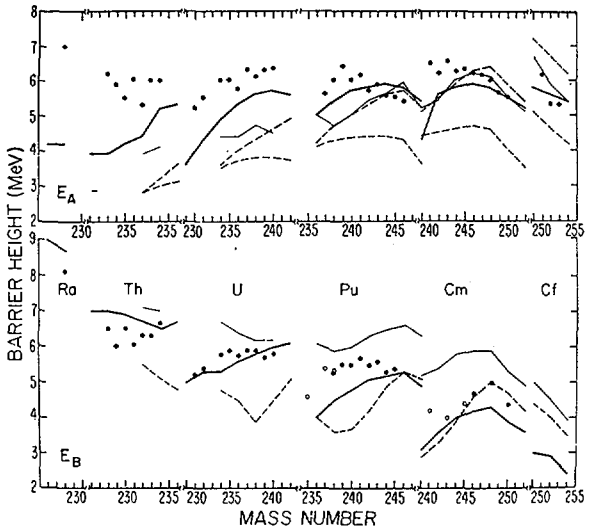

FIG. 3. Comparison of experimental fission barriers with various calculations [*1*].

calculations, yielding the heights of the first and second barriers. One of them did realize some small problems, but even the mass asymmetry fitted into the simple static picture: each theoretical group working in this field showed some correlation between the degree of mass asymmetry and the calculated size of the octupole deformation at the outer barrier. Actually, a number of prominent theoreticians as well as experimentalists (whose names you may have missed here in Jülich) left the field, turning into heavy-ion physics. The summary speaker of the Rochester meeting, was,however, very realistic. He was again a theoretician. He discussed a long list of unsolved problems, an excerpt of which (Table I) I shall inspect at this point just to check to what extent we have come up to his expectations over the last six years. Among the problems concerning details, we have, in fact, seen important progress in the understanding of the shell correction at magic numbers; this problem does seem to be solved (see below). The shell correction at the barriers continues, however, to be a matter of heavy dispute. The odd-even effects in the half-lives both for spontaneous fission from the ground state and for isomeric fission were very much discussed at Rochester; I do not think that there has been any progress at all. Nor has our knowledge of the competition between symmetric and asymmetric fissions as a function of the excitation energy reached the stage of real understanding. Then there were – and still are – the great conceptual problems: viscosity and the questions of whether the adiabatical or the statistical approach applies,

TABLE III. POTENTIAL-ENERGY SURFACES (2)

Status (theoretical);

1) Strutinsky procedure verified in Hartree-Fock
2) Pb-anomaly solved
3) Pairing-force constant independent of deformation (HFB)
4) Angular-momentum dependence of shell-corrected barriers

Open problems:

1) Statical and dynamical surfaces
2) Barriers too high from Hartree-Fock
   Force parameters?
3) Spin-orbit force

↳ 4) Improved detailed calculations of barriers
   Microscopic level density calculations including all influences of angular momentum
   Spectroscopical calculations for second minimum
   Single-particle (Nilsson) states
   Collective states (octupole vibrations, β- and γ-vibrations)

or, perhaps, something in between. In conclusion then, if I take the weighted average of all the progress since 1973 according to this list, it seems to be rather poor indeed.

Now, are things really that bad? I do, on the contrary, believe that there has been quite a bit of progress. It comes in little steps, and it comes in good solid numbers; the theoreticians will forgive me if I say that. But I think there definitely has been progress in that sense – not just cross-sections, but numbers that are important for our basic understanding. I hope to be able to make this statement a bit clearer if I now systematically go through the programme of the Symposium.

The first two days were more or less intensively concerned with the potential-energy surfaces. The status as far as the experimental situation goes is the following (Table II): We have this very remarkable systematics of barrier parameters mostly due to the Los Alamos group [1]. In this context, there have been very valid contributions from photofission by Tsipenyuk [7]. We should also mention the attempt by Just [8] to combine all these different data together with those on isomers to obtain a more consistent description. Still,

the resulting numbers are not all that different from group to group. Another result of these efforts, is an incipient spectroscopy of collective states at the barriers – something that should certainly be improved in the future. The systematics of the heights of the first and the second barriers as taken from Britt [1] is shown in Fig.3. The lines are calculations on the basis of Strutinsky's approach; they are actually five years old. There has not been anything basically new to this situation in the meantime. The great problem is obvious. The theoretical barriers agree among themselves within 1–2 MeV. The experimental numbers tend to support the outer-barrier values, but we have this discrepancy at the inner barrier which is already visible quite well in the U-isotopes, and very strong for Th. One remembers the alternatives for the solution of this problem – one is that the theoreticians are, at present, not clever enough to perform the correct calculations, the other one is that the experimentalists are not clever enough because what they really measure is the second and the third barriers instead of the first and the second ones, thus comparing the wrong quantities.

To put my personal judgement into proper perspective, let me first look at what theory *has* achieved in the meantime (Table III). The Strutinsky procedure is generally accepted. We have heard in the useful review undertaken by Brack [9] about how it can be understood in the framework of Hartree-Fock theory. We have learned from the very significant contribution by Werner et al. [10] and also from Strutinsky's paper [11] that the Pb-anomaly is finally solved: The methods are different, but the spirit appears to be similar, in the sense that basically the discrepancy with the experimental value has been due to an inconsistency between the shell-model part obtained after smoothing, and the liquid-drop part. We have, furthermore, obtained new insight into the behaviour of pairing from Hartree-Fock-Bogolyubov calculations [12]: The old question of whether the pairing-force constant depends on deformation seems to have been answered both from the theoretical (reported here) and the experimental side (work by Kneissl et al. [13] at Giessen, mentioned in some discussion remark). Finally, there has been an interesting theoretical contribution [14] pointing out the angular-momentum dependence of shell barriers. We have always lived with the expectation that if you put a lot of angular momentum into a nucleus, it decreases the fission barrier. But, in fact, from these calculations one can occasionally see the opposite.

The open problems on the theoretical side are nevertheless obvious: First of all, there is the philosophical question of what a static potential-energy surface really means in fission which is a time-dependent process after all. We have had some more contributions [15] to this problem. Then there is the general problem of Hartree-Fock theory that the results on barrier heights are just too high, and that does not seem to be understood at all. One of the questions is whether the force parameters used at present are really correct.

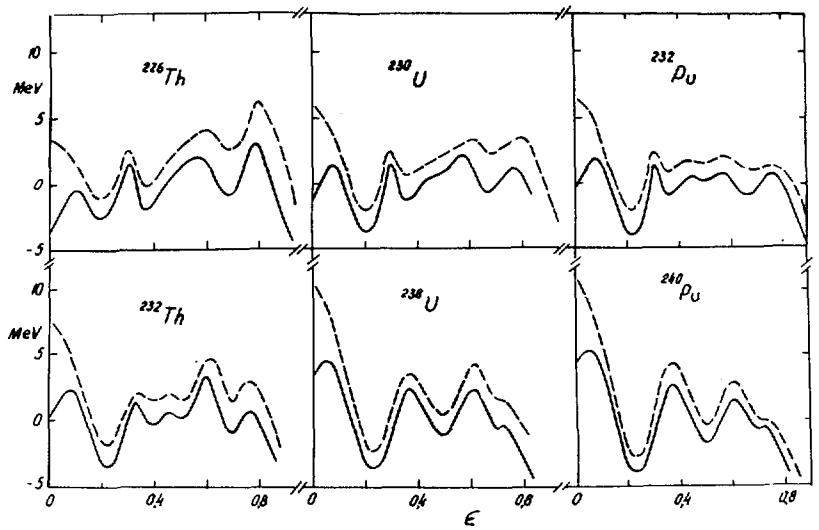

FIG. 4. Theoretical fission barrier shapes [11].

This has just to be studied in greater detail. Specifically, we have the problem of the spin-orbit force which, as Brack [9] has pointed out, really is a big unknown very strongly affecting the final result. If we take all these points together, we are tempted to conclude that the theoretical barriers at present may be insufficiently understood, to the extent that perhaps one should not worry too much about the discrepancies with the experimental values. This implies, of course, that both theoreticians *and* experimentalists should have to go back and work very seriously. The theoreticians should really try to solve these problems and get more accurate numbers on the barrier parameters, including the effects of the dynamical path. There should be improved microscopic-level-density calculations, including the effects of angular momentum on the shell correction. As can be seen from Britt's analysis [1], such calculations are vital for the extraction of barrier parameters from fission probability measurements.

The experimentalists, as I said, have to go back as well, and I think that I can present a large list in this context (now we are returning to Table II). What really is the true shape of the barrier? After all, this barrier might be very, very wiggly, and I should like to remind you of the latest work of Strutinsky (Fig.4). The traditional nuclei as ^{238}U or ^{240}Pu behave quite reasonably with just two pronounced barriers. But if one only goes to ^{232}Th, it is not clear from this calculation whether the first barrier is low and the outer higher barrier is

equally split, or whether the first and the third barriers are not of more or less equal height. And if we go down in neutron number (upper part of Fig.4), we see a landscape where three, and possibly four, wiggles are of equal height. This makes the situation very complicated. The question is, of course, as follows: Are the dips really as deep as to lead to spectroscopically observable consequences or are they so insignificant that all what this leads to are structures in cross-sections stemming from the penetration of barriers with a non-inverted-parabola shape? This has to be clarified by experiment, and I believe many things can actually be done in this connection. There has been the work by Paya et al. [16] trying to understand the fine structure in ^{230,232}Th (n,f). Personally, I very much enjoyed the heated discussion between Paya, Boldeman, Blons and others in this context. Nevertheless, I feel that we have an experimental problem here which has been open for many years, which is a very regrettable situation, to say the least. The problem of a possible third minimum causing the structure is really quite crucial and important, and it just has to be solved. We hope that all experimentalists involved will, at some point, shut themselves off in some lab and not come out again before they are able to give us an answer they all agree upon. I don't think that such fine-structure investigations should be restricted to (n,f) on the two thorium isotopes. There are several other methods of coping with the question of a third minimum, as well. Let us, for example, consider the systematics of the isomeric shelves in (γ,f). Whether the shelf in ^{232}Th [7] exists or not is completely unclear, at present, because of the error bars. This is again something that should be improved. I also sincerely hope that a lot of work will be done in the future with tagged photons using the new DC electron accelerators. We shall then have the unique possibility of studying fission just via 1^- and 2^+ states with an energy resolution comparable to what is now being used in direct reactions ($\sim$ keV). This will be extremely important because we would finally be able to determine the degree of the $K = 0^+/0^-$ degeneracy at the outer barrier (caused by the possible octupole shape) in a much less ambiguous way. Next, we have the open problem of the γ-decay back into the first well. I address myself to all experimentalists in this room if I call this a sad story. There are 35 shape isomers known to decay by fission, but just one example (^{238}U [17]) has been verified to also decay by gamma emission. One should study this phenomenon much more broadly than has been done up to now, since it may help to clarify the problems at the first barrier. There should be observalbe γ-decay in many nuclei, which would lead to a true systematics of the half-lives and, hopefully, the first barrier heights. Clearly, if the barriers become too low, the half-lives will become too short to be measurable, but there may be ways around this difficulty. The experiments are difficult, but can be done. There could possibly also be γ-spectroscopy, sensitive to these bumpy potential-energy surfaces in some more indirect way. Finally, one should look more closely into β-delayed fission. We had Wene's paper [18], who very

TABLE IV. FISSION AND HEAVY IONS

Status:

1) No real progress in compound-nucleus fusion-fission
2) Fission properties of nuclei with a vanishing fission barrier
3) Fission – deep-inelastic collisions?
4) Coulomb fission established

Open problems:

1) More accurate fragment angular distributions
   - Angular-momentum dependence of liquid-drop barriers
   - K-conservation at higher excitation energies
2) Time scales
3) Fission – deep-inelastic collisions
4) Simulation of fission (cold reactions, low ℓ)

validly pointed out what problems are involved at present. I am not convinced that he has solved them, but at least he gave us a lot to think about, and I hope the authors are going ahead both with further calculations and, still more important, with supporting experiments. This reaction is not just esoteric. I am aware of a lot of experimental information in Dubna from Gangerski et al. on a number of nuclei, where experimental information has been obtained for β-delayed fission which could never properly be analysed because of these problems with the strength function. Moreover, there is this relevance for the element synthesis along the r-process path.

Let us now quickly discuss the second point (Table II) – spectroscopy of highly deformed shapes. In terms of the present status, I should like to remind you of Metag's [18] paper, pointing out that there is at least one solid rock in this wiggly landscape: the measured quadrupole moments support a 2:1 deformation for the fission isomers, not 3:1 or anything else. He also reported on the first identification of a Nilsson state in the second well with its implications for a possible deformation dependence of the spin-orbit force. Nevertheless, there are still tremendous tasks to be solved. More single-particle states should be found. The magnetic moments constitute a completely unsolved problem. No single low-lying collective state like the octupole vibration, the γ-vibration or the β-vibration is known at present in the second well. Admittedly, gamma or conversion electron spectroscopies have to be pushed to their extreme limits. However, the experimentalists also need support from spectroscopical calculations (as

indicated in Table III). A remarkable amount of very detailed theoretical work has been done on 'normal' deformed nuclei in the rare-earth region or the actinides, but hardly anything for the second well. The phonon energies associated with the octupole or gamma degree of freedom are of particular interest in view of the possible instabilities of the barriers. I should finally mention the comprehensive Γ_f/Γ_n-systematics given by Schmitt [19] from GSI for nuclei far outside the valley of stability in the region of the N = 126 shell. Clearly, his interesting conclusions depend on the way one extracts the barriers although they may survive even improved level density calculations incorporating all the effects of angular momentum.

This then is the appropriate point to go quickly through the heavy-ion session. I must admit that I was not particularly happy with this field. Basically, there are two aspects of heavy ions (Table IV). Heavy ions can be used as a tool to study fission properties of nuclei following heavy ion reactions in several different ways. We can have compound-nucleus formation followed by fission. We have had speculations about non-compound nucleus fusion still followed by fission. Both of these types lead to binary events. We have also heavy-ion reactions where one partner survives and the other one fissions, or even both fission, leading then to three or even more particles in the exit channel. Coulomb fission belongs to this category as well. But there exists this other aspect of heavy-ion reactions: The dynamics of nuclei in heavy-ion reactions and in fission have so much to do with each other that one field should teach us about the other. Now, what is the state of the art? I don't think there was very much progress in the compound-nucleus type of fusion-fission. The question of whether the liquid-drop barriers for zero angular momentum have to be lowered to 0.6 or rather to 0.8 was discussed [21]. Although the latter value is a bit more comfortable, I still doubt as to whether this really is the final word. As long as one, in a way, just compares the physics coming out with the results from a standard computer code with a nice girl's name, I don't think the final problem will be solved. Again I should like to emphasize the need for better microscopic level density calculations with shell-corrected barriers including angular momentum (one encouraging attempt in this direction was actually contained in Andersen's talk [20], who, being asked about Jensen's computer program afterwards, answered that it did not have a name). As far as the second point is concerned, we have heard of the interesting contributions by Ngô et al. [5] and v. Harrach et al. [6], showing how nuclei with a fission barrier vanishing either via high angular momentum or high Z^2/A behave in terms of a rapid increase in the width of the fragment mass distribution, and in the latter case also in terms of peculiar fragment angular distributions. It appears to be completely unclear what that really means – whether fast processes are being observed or, rather, inherent properties of the liquid drop for nuclei unbound by a barrier. This will have to be evaluated in the future. Such experiments are, in any case, a very interesting development. Turning next to the third point – the

TABLE V. THE SADDLE-TO-SCISSION STAGE (1)

Status (theoretical):

1) The ultimate theory of fission is (nearly) as far away as ever
2) The struggle to understand TDHF
3) Elements of 'simple' approaches
   - Dynamical path to scission
   - Viscosity, coupling to gp-excitations
   - Results on odd-even effects and damping widths

Open problems:

1) The struggle to understand TDHF and what comes beyond
2) How to quantitatively describe all the experimental facts

relation between fission and deep-inelastic collisions – I have just made a big question mark. The time is probably not yet ripe for this problem to be solved. Fission has seen so many very detailed investigations over so many years, whereas heavy-ion physics is still very young and has first concentrated on the gross overall features rather than the important little detail. For example, just compare what we know of α-emission in fission with what we know of α-emission in deep-inelastic scattering, and we see a real qualitative and quantitative difference both in the data and in their interpretation. But I do think that the next fission meeting should have more fruitful interactions between the two fields. As a more successful last point, Wilhelmy's short post-deadline contribution [22][1] told us that Coulomb fission (in the reaction $^{184}W + ^{238}U$) finally seems to be established.

There are some more open problems. The angular distributions should actually be explored in more detail than has been done so far. It is not only that the angular-momentum dependence even of the liquid-drop barrier has not been completely verified as yet (a discussion remark made by W. Reisdorf). I also believe that the question of K-conservation, at least at high excitation energies, has not yet been solved. The important problem of the time scales will be discussed in more detail below. Finally, the true 'simulation of fission' in heavy-ion reactions has not yet really taken place. People have so far concentrated on reactions above the Coulomb barrier with a lot of angular momentum. This leads to phenomena like angular-momentum dissipation from the orbital motion which just does not exist in fission. If, however, one tried to study relatively cold systems, one might

[1] Not published in these Proceedings.

TABLE VI. THE SADDLE-TO-SCISSION STAGE (2)

Status (experimental):

1) Gross properties of fragment mass and energy distributions

   Still more shell effects

2) The 'little big detail' in dynamics

   Odd-even effects in yields and total kinetic energy

   ↳ Fission mode weakly coupled to qp-excitations

   Total kinetic energy E_K independent of excitation energy E_X

   ↳ Fission made strongly coupled to other collective modes

   Narrow width of α-angular distribution, varying with E_K

   ↳ Pre-scission kinetic energy $\leqslant 8$ MeV (2?)

   Compact scission configurations, the same for U and Cf

   Scission configuration fluctuations

   Together with variance of charge distribution independent of E_K

   ↳ Fission slow (10^{-20} s)

Open problems:

1) Gross behaviour of symmetric and asymmetric fission versus excitation energy and Z^2/A

2) The 'little big detail' in dynamics

   Systematics of odd-even effects versus Z^2/A and E_X

   Systematics of total kinetic energy E_K versus Z^2/A for sub-barrier fission and isomers (better tests of limits of strong-damping hypothesis)

3) Polar emission of light particles

be able to obtain results that are really relevant to the discussion of the different alternative models in fission (scission models, etc.).

This then brings us to the final chapter – the saddle-to-scission stage. Here, I should like to start with the theoretical aspects (Table V). It appears that the ultimate theory of fission is nearly as far away as ever. Solely from the number and weight of recent papers it is also fair to say that the present period is, in a way, characterized by the struggle to really understand these time-dependent Hartree-Fock calculations. Flocard's review [23] has been very illuminating in this context. Theoreticians have not yet reached the point where they could produce numbers which experimenters can use to compare with experiments. There are elements,

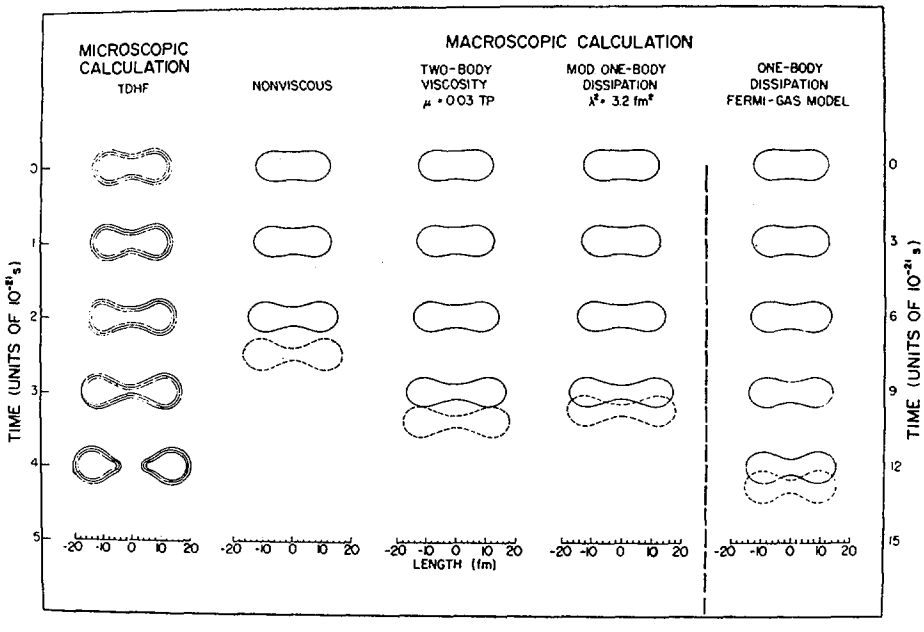

FIG. 5. Theoretical nuclear shapes and time scales [27].

of course, of much simpler approaches, very encouraging elements indeed. We have heard about them mostly in connection with the problem of viscosity in the widest sense. Some were quite specific: Schütte's [24] estimates for odd-even effects, for example, or Jensen's [25] calculations of the damping widths in the framework of linear response theory, one of the cases of a theoretical feedback of heavy-ion physics to fission. *The* big open problem in this field hardly needs any discussion – how should the vast amount of experimental data be described in a coherent way and more or less from 'first principles'?

Let me now pass to the experimental situation (Table VI). The first point, concerning the gross properties of fragment mass distributions with still more evidence for shell effects, was already commented on in the introduction. For completeness, I also mention Iyer's work [26] on the little shoulders of the fragment mass distribution (on the 10^{-6} level) which should make the theoretical group at Frankfurt happy. But I believe that even more important progress has actually been achieved in what I call the 'little big detail'. To make the implications quite clear, the final figure (Fig.5), taken from the paper of Negele et al. [27], demonstrates the present state of the art of calculations for the saddle-to-scission shapes and the relevant time scales. The results from TDHF are given on the left, those from the liquid drop with various assumptions on viscosity on the right.

Significant differences arise from the different approaches, more elongated shapes, for example, in the cases of two-body viscosity or modified one-body viscosity, more compact shapes in the other cases. Note also the saddle-to-scission times: 3×10^{-21} s for most of the cases, 12×10^{-21} s for the old one-body viscosity. Recall, finally, the high pre-scission kinetic energies of ~ 20 MeV (again, with the exception of the old one-body viscosity). This then is the appropriate point to comment on the paper of Niefenecker [28], who has really given a lot of strong points. I just repeat the main conclusions which he and also other contributors to this Symposium have arrived at (again Table VI). The odd-even effects both in yields and in total kinetic energy have been found now to occur rather universally. One also starts seeing their rapid decrease with increasing excitation energy and increasing Z^2/A. The general conclusion seems to be that the fission mode is relatively weakly coupled to the quasi-particle excitations, at least at low excitation fission close to the barrier or below. There is also this evidence about the average total kinetic energy to be rather independent of the excitation energy in the barrier region and above. This has been taken to imply that fission is strongly coupled to, at least, other collective degrees of freedom (in terms of the old Nörenberg model). A word of warning should be said here with regard to the much-discussed exception of ^{232}Th reported by David [29] (see below). The data on α-emission have historically developed in a remarkable way. The width of the angular correlation was first very large, and the trajectory calculations simulating it resulted in pre-scission kinetic energies of up to 40 MeV, apparently in accordance with the numbers from most of the theoretical approaches quoted in connection with Fig.5. With all these improved experimental techniques and efforts, however, the width has significantly decreased, and it now even varies with the total kinetic energy. Although the models used to extract numbers may still be a bit crude, the semi-quantitative conclusions can just not be discussed away. First, the pre-scission kinetic energy has to be < 8 MeV (according to Fong's discussion remark, it may even be < 2 MeV, i.e. very small in any case). The analysis also points to a rather compact scission configuration. Moreover, this configuration may hardly vary from U to Cf, which is also quite contrary to what the calculations would have pointed out. Clearly, there are shell effects present whose influence has to be investigated. Next, the variance of the total kinetic energy release seems to be accounted for mostly by scission configuration fluctuations, and not by fluctuations of the pre-scission kinetic energy. And, finally, including now the evidence for the charge distribution width being independent of the kinetic energy, there is even a number for the saddle-to-scission time: fission may be very slow, of the order of 10^{-20} s. Interestingly enough, we have this very first, rough analysis from the three-body heavy-ion reactions reported by v. Harrach [6], yielding more or less the same number for the lower limit of what he called the scission-to-scission time (which may not be quite the same, to be cautious). To conclude, this coherent analysis of a large amount of, at first sight, independent experimental material

really represents an important development, narrowing the freedom and the ambiguities associated with the various theoretical approaches.

Still, there are many open problems in this field, as well. I don't want to enlarge on the first point, but to me the understanding of the competition between symmetric and asymmetric fissions as a function of excitation energy is still rather poor. Let us just remember the inconsistencies in the level density description of this competition between ^{228}Ra and ^{236}U, as pointed out by Britt [1]. In terms of the 'little big detail' in dynamics, things have to be verified more reliably and in more detail to be on more solid grounds. This should not only cover the systematics of the odd-even effects both as a function of Z^2/A and of the excitation energy. Personally, I should not like to regard the hypothesis of strong damping to other collective degrees of freedom as completely established, because most of the data supporting it have been taken either at the barrier or above. The example of ^{232}Th [29] may actually present evidence for the contrary, up to some point in excitation energy. It is, at least, conceivable that this point in excitation energy (the pairing gap at the outer barrier?) slips down with increasing Z^2/A, thus hiding the initial rise of the total kinetic energy as long as the excitation is at or above the (outer) barrier. One should then still be able to detect it by going into the sub-barrier region. There are, after all, the experimental results of Lachkar et al. [30] on ^{240}Pu, which have never been verified by anybody else. Therefore, much more systematical work should be done in this field. The total kinetic energies of fission isomers may also present a very valid point in this context. Without going into any detail, I conclude the list with some more open topics, where the latter has been extensively discussed in Piasecki's review [31].

This brings me to my last open problem, that of superheavy elements. This meeting has been amazing in the sense that everybody tried to avoid even mentioning it (with one possible exception, namely Lund [32]). People were extremely careful even with indirect remarks. Werner [10], for example, pointed out how the Pb-anomaly was solved, but he did not draw any conclusions from this, leaving this to the audience. Whatever happens somewhere beyond $Z \sim 106$ appears to be completely unsolved, both theoretically and, of course, also experimentally. To my surprise, I also observed that after von Harrach's talk about ^{238}U + ^{248}Cm [6], discussing all these reaction aspects, nobody stood up and asked the question: Did you find any superheavy elements? or: What are your estimates for the possible production rates of superheavy elements? Imagine the situation just five years back – people would have stood up in masses to ask such questions. That, I think, signifies the present atmosphere of pessimism in this field. Since the question was not asked, I am of course not going to answer it either.

To summarize my summary, I should like to state that the meeting has been successful and useful. I am sure that I am speaking for everybody if I thank the IAEA for organizing the Symposium, and if, at the same time, I encourage the

IAEA to continue this tradition. Let me, however, strongly advocate that the arrangement should be changed in the future, so that, finally and fully, fission and heavy-ion physics could be united in one Symposium.

REFERENCES

[1] BRITT, H.C., Paper SM-241/A1, these Proceedings.
[2] HOFFMAN, D., Paper SM-241/F14, these Proceedings.
[3] HULET, E.K., WILD, J.F. LOUGHEED, R.W., BAISDEN, P.A., LANDRUM, J.H., DOUGAN, R.J., MUSTAFA, M., GHIORSO, A., NITSCHKE, J.M., Paper SM-241/F15, these Proceedings.
[4] ANDERSSON, G., ARESKOUG, M., GUSTAFSSON, H.-Å., HYLTEN, G., SCHRØDER, B., HAGEBØ, E., Paper SM-241/F17, these Proceedings.
[5] HANAPPE, F., PETER, J., TAMAIN, B., LEBRUN, C., LECOLLEY, J.F., LEFEBVRES, F., NGÔ, C., Paper SM-241/D3, these Proceedings.
[6] v. HARRACH, D., GLÄSSEL, P., CIVELEKOĞLU, Y., MÄNNER, R., SPECHT, H.J., WILHELMY, J.B., FREIESLEBEN, H., HILDENBRAND, K.D., Paper SM-241/D4, these Proceedings.
[7] SMIRENKIN, G.N., TSIPENYUK, Yu.M., Paper SM-241/A2, these Proceedings.
[8] JUST, M., GOERLACH, U., HABS, D., METAG, V., SPECHT, H.J., Paper SM-241/A4, these Proceedings.
[9] BRACK, M., Paper SM-241/C1, these Proceedings.
[10] WERNER, E., DIETRICH, K.M., MÖLLER, P., NIX, R., Paper SM-241/C26, these Proceedings.
[11] STRUTINSKY, V.M., Paper SM-241/C12, these Proceedings.
[12] BERGER, J.F., GIROD, M., Paper SM-241/C2, these Proceedings.
[13] GÜNTHER, W., HAAG, R., HUBER, K., KNEISSL, U., KRIEGER, H., MAIER, H.J., STRÖHER, H., in Nuclear Physics with Electromagnetic Interactions, Conference Mainz (1979), Contribution No. 4.10.
[14] FABER, M.E., FÄSSLER, A., PLOSZAJCZAK, M., Paper SM-241/C5, these Proceedings.
[15] REINHARD, P.G., GÖKE, K.W., Paper SM-241/H2, these Proceedings.
[16] PAYA, D., Paper SM-241/B6, these Proceedings.
[17] RUSSO, P.A., PEDERSEN, J., VANDENBOSCH, R., Nucl. Phys. **A240** (1975) 13.
[18] METAG, V., Paper SM-241/B3, these Proceedings.
[19] SCHMIDT, K.H., FAUST, W., MÜNZENBERG, G., REISDORF, W., CLERC, H.G., VERMEULEN, D., LANG, W., Paper SM-241/C8, these Proceedings.
[20] ANDERSEN, J.U., JENSEN, A.S., LAEGSGAARD, E., NIELSEN, K.O., Paper SM-241/C7, these Proceedings.
[21] PLASIL, F., FERGUSON, R.L., Paper SM-241/D1, these Proceedings.
[22] BACKE, H., WEIK, F., BUTLER, P., METAG, V., WILHELMY, J., HABS, D., HIMMELE, G., SPECHT, H.J., preprint (1979).
[23] FLOCARD, H., Paper SM-241/H1, these Proceedings.
[24] SCHÜTTE, G., Paper SM-241/G1, these Proceedings.
[25] JENSEN, A.S., REESE, K., SIEMENS, P.J., HOFMANN, H., Paper SM-241/H4, these Proceedings.

[26] IYER, R.H., BHARGAVA, V.K., RAO, V.K., MARATKE, S.G., SAHAKUNDU, S.M., Paper SM-241/F16, these Proceedings.
[27] NEGELE, J.W., KOONIN, S.E., MÖLLER, P., NIX, J.R., SIERK, A.J., Phys. Rev. C17 (1098) 1978.
[28] NIFENECKER, H.A., BLACHOT, J., BOCQUET, J.P., BRISSOT, R., CRANÇON, J., HAMELIN, C., MARIOLOPOULOS, G., RISTORI, C., Paper SM-241/F1, these Proceedings.
[29] DAVID, P., DEBRUS, J., SCHULZE, J., VAN DER PLICHT, J., HARAKEH, M.N., VAN DER WOUDE, A., Paper SM-241/C6, these Proceedings.
[30] LACHKAR, J., PATIN, J., SIGAUD, J., J. de Phys. 36 (1975) 79.
[31] PIASECKI, E., NOWICKI, L., Paper SM-241/F11, these Proceedings.
[32] ÅBERG, S., LARSSON, S.E., MÖLLER, P., NILSSON, S.G., LEANDER, G., RAGNARSSON, I., Paper SM-241/C4, these Proceedings.

CHAIRMEN OF SESSIONS

Session A	A.F. MICHAUDON	France
Session B	S.S. KAPOOR	India
Session C(1)	K.M. DIETRICH	FRG
Session C(2)	H.C. PAULI	FRG
Session D	E. CHEIFETZ	Israel
Session E	E. CHEIFETZ	Israel
Session F(1)	P. ARMBRUSTER	FRG
Session F(2)	B.G. YANKOV	USSR
Session F(3)	G.F. HERRMANN	FRG
Session G	B.G. YANKOV	USSR
Session H	P. FONG	USA

SECRETARIAT OF THE SYMPOSIUM

Scientific Secretary:	J. DOLNICAR	Division of Research and Laboratories, IAEA
Administrative Secretary:	Edith PILLER	Division of External Relations, IAEA
Editor:	J.W. WEIL	Division of Publications, IAEA
Records Officer:	J. RICHARDSON	Division of Languages, IAEA

LIST OF PARTICIPANTS

AUSTRALIA

Boldeman, J.W.	Service de physique nucléaire, Centre d'études de Bruyères-le-Châtel, B.P. 561, F-92542 Montrouge, France
Walsh, R.L.	Australian Atomic Energy Commission Research Establishment, Private Mail Bag, Sutherland, N.S.W. 2232

AUSTRIA

Cech, H.	Atominstitut of the Austrian Universities, Schüttelstrasse 115, A-1020 Vienna
Dorninger, C.	Atominstitut of the Austrian Universities, Schüttelstrasse 115, A-1020 Vienna
Jasicek, H.A.	Technical University of Vienna, Karlsplatz 13, A-1040 Vienna

BELGIUM

Berlanger, M.G.H.	Service de physique nucléaire expérimentale, Université libre de Bruxelles, CP 229, Campus de la Plaine, Boulevard du Triomphe, B-1050 Brussels
De Frenne, D.J.A.	Nuclear Physics Laboratory, Proeftuinstraat 86, B-9000 Gent
De Gelder, P.C.M.	Nuclear Physics Laboratory, Proeftuinstraat 86, B-9000 Gent
del Marmol, P.	Nuclear Energy Centre, S.C.K./C.E.N., Boeretang 200, B-2400 Mol
D'Hondt, P.J.C.	Nuclear Physics Laboratory, Proeftuinstraat 86, B-9000 Gent

BELGIUM (cont.)

Hanappe, F.	Service de physique nucléaire expérimentale, Campus de la Plaine, Université libre de Bruxelles, Boulevard du Triomphe, B-1050 Brussels
Jacobs, E.T.C.	Nuclear Physics Laboratory, Proeftuinstraat 86, B-9000 Gent
Neve de Mevergnies, M.	Nuclear Energy Centre, S.C.K./C.E.N., Boeretang 200, B-2400 Mol
Proot, B.M.J.	Nuclear Physics Laboratory, Proeftuinstraat 86, B-9000 Gent
Thierens, H.M.A.	Nuclear Physics Laboratory, Proeftuinstraat 86, B-9000 Gent
Wagemans, C.M.C.	Nuclear Energy Centre, S.C.K./C.E.N., Boeretang 200, B-2400 Mol

CANADA

Forster, J.S.	Chalk River Nuclear Laboratories, Atomic Energy of Canada Limited, Chalk River, Ontario K0J 1J0

DENMARK

Andersen, J.U.	Institute of Physics, University of Aarhus, My Munkegade, DK-8000 Aarhus
Jensen, A.S.	Institute of Physics, University of Aarhus, My Munkegade, DK-8000 Aarhus
Polikanov, S.	Niels Bohr Institute, Blegdamsvej 17, DK-2100 Copenhagen

FRANCE

Asghar, M.	Division physique, C.C.R. – Euratom, B.P. 44, I-21020 Ispra (Varese), Italie

Barreau, G.	Centre d'études nucléaires de Bordeaux-Gradignan, Le Haut Vigneau, F-33170 Gradignan
Bengtsson, B.R.	DRF/CPN, Centre d'études nucléaire de Grenoble, B.P. 85 X, F-38041 Grenoble Cedex
Berger, J.F.	Service de physique nucléaire, Centre d'études de Bruyères-le-Châtel, B.P. 561, F-92542 Montrouge Cedex
Blachot, J.	Département de recherche fondamentale, Laboratoire de chimie physique nucléaire, Centre d'études nucléaires de Grenoble, 85 X, F-38041 Grenoble Cedex
Blons, J.	Centre d'études nucléaires de Saclay, B.P. 2, F-91190 Gif-sur-Yvette
Bocquet, J.P.	U.S.M.G. – Centre de Tri, B.P. 53, F-38041 Grenoble Cedex
Brissot, R.	U.S.M.G. – Centre de Tri, B.P. 53, F-38041 Grenoble Cedex
Butaye, C.	Service R.C.P., Commissariat à l'énergie atomique, B.P. 516, F-92542 Montrouge Cedex
Caïtucoli, F.	Département de recherche fondamentale, Laboratoire de chimie physique nucléaire, Centre d'études nucléaires de Grenoble, 85 X, F-38041 Grenoble Cedex
Cârjan, N.	Centre d'études nucléaires de Bordeaux-Gradignan, Le Haut Vigneau, F-33170 Gradignan
Crançon, J.	Département de recherche fondamentale, Laboratoire de chimie physique nucléaire, Centre d'études nucléaires de Grenoble, 85 X, F-38041 Grenoble Cedex
Debeauvais, Monique	Centre de recherches nucléaires de Strasbourg, B.P. 20, F-67037 Strasbourg Cedex
Doan, T.P.	Centre d'études nucléaires de Bordeaux-Gradignan, Le Haut Vigneau, F-33170 Gradignan

FRANCE (cont.)

Flocard, H.	Institut de physique nucléaire, B.P. 1, F-91406 Orsay
Galin, J.R.P.	Institut de physique nucléaire, B.P. 1, F-91406 Orsay
Guet, C.R.	Institut Laue-Langevin, 156 X, Centre de Tri, F-38042 Grenoble Cedex
Hamelin, C.A.	U.S.M.G. – Centre de Tri, B.P. 53, F-38041 Grenoble Cedex
Joly, R.L.	Centre d'étude nucléaires de Saclay, B.P. 2, F-91190 Gif-sur-Yvette
Leroux, B.	Centre d'études nucléaires de Bordeaux-Gradignan, Le Haut Vigneau, F-33170 Gradignan
Mariolopoulos, G.	Département de recherche fondamentale, Laboratoire de chimie physique nucléaire, Centre d'études nucléaires de Grenoble, 85 X, F-38041 Grenoble Cedex
Michaudon, A.F.	Service de physique nucléaire, Centre d'études de Bruyères-le-Châtel, B.P. 561, F-92542 Montrouge Cedex
Montoya, M.	Centre d'études nucléaires de Saclay, B.P. 2, F-91190 Gif-sur-Yvette
Nifenecker, H.A.	Département de recherche fondamentale, Laboratoire de chimie physique nucléaire, Centre d'études nucléaires de Grenoble, 85 X, F-38041 Grenoble Cedex
Patin, Y.M.	Service physique nucléaire, Centre d'études nucléaires de Bruyères-le-Châtel, B.P. 561, F-92542 Montrouge Cedex
Paya, D.	Centre d'études nucléaires de Saclay, B.P. 2, F-91190 Gif-sur-Yvette
Perrin, P.E.J.	Département de recherche fondamentale, Laboratoire de chimie physique nucléaire, Centre d'études nucléaire de Grenoble, 85 X, F-38041 Grenoble Cedex

Péter, J.	Lawrence Berkeley Laboratory, Building 70 A, Berkeley, CA 94720, USA
Ristori, C.	Département de recherche fondamentale, Laboratoire de chimie physique nucléaire, Centre d'études nucléaires de Grenoble, 85 X, F-38041 Grenoble Cedex
Schrader, H.	Institut Laue-Langevin, 156 X, Centre de Tri, F-38042 Grenoble Cedex
Schuk, P.	Institut Laue-Langevin, 156 X, Centre de Tri, F-38042 Grenoble Cedex
Sicre, A.	Centre d'études nucléaires de Bordeaux-Gradignan, Le Haut Vigneau, F-33170 Gradignan
Signarbieux, C.	Centre d'études nucléaires de Saclay, B.P. 2, F-91190 Gif-sur-Yvette
Trochon, J.	Service de physique nucléaire, Centre d'études nucléaires de Bruyères-le-Châtel, B.P. 561, F-92542 Montrouge Cedex

GERMAN DEMOCRATIC REPUBLIC

Arlt, R.	Technical University Dresden, Section of Physics, Mommsenstrasse 13, DDR-8027 Dresden

GERMANY, FEDERAL REPUBLIC OF

Ansari, A.	Institut für Kernphysik, Kernforschungsanlage Jülich, Postfach 1913, D-5170 Jülich
Armbruster, P.	Gesellschaft für Schwerionenforschung, Postfach 110 541, Planckstrasse 1, D-6100 Darmstadt-Arheilgen
Bauhoff, W.	Institut für Theoretische Physik, Universität Tübingen, Auf der Morgenstelle 14, D-7400 Tübingen

GERMANY, F.R. (cont.)

Brack, M.	Institut für Theoretische Physik, Fachbereich Physik, Universität Regensburg, Universitätsstrasse 31, D-8400 Regensburg
Brandt, R.	Kernchemie, F.B. 14, Philipps Universität, D-3550 Marburg
Braun, H.	Institut für Kernchemie, Universität Mainz, Postfach 3980, D-6500 Mainz
Clerc, H.G.	Institut für Kernphysik, Technische Hochschule Darmstadt, Schlossgartenstrasse 9, D-6100 Darmstadt
David, P.	Institut für Strahlen- und Kernphysik, University of Bonn, Nussallee 14–16, D-5300 Bonn
Debrus, J.	Institut für Strahlen- und Kernphysik der Universität Bonn, Nussallee 14–16, D-5300 Bonn
Denschlag, H.O.	Institut für Kernchemie, Universität Mainz, Postfach 3980, D-6500 Mainz
Dickmann, F.	Institut für Angewandte Kernphysik, Kernforschungszentrum Karlsruhe, Postfach 3640, D-7500 Karlsruhe
Dietrich, K.M.	Department of Physics of the Technical University of Munich, James Franck Strasse, D-8046 Garching
Duhm, H.H.	I. Institute for Experimental Physics, University of Hamburg, Luruper Chaussee 149, D-2000 Hamburg
Esterlund, R.	Institut für Kernchemie, Universität Marburg, Lahnberge, D-3550 Marburg/Lahn
Faber, M.E.	Institut für Kernphysik, Kernforschungsanlage Jülich, Postfach 1913, D-5170 Jülich

Faessler, A.	Institut für Kernphysik, Kernforschungsanlage Jülich, Postfach 1913, D-5170 Jülich
Fiedler, G.	II. Physikalisches Institut der Justus-Liebig-Universität Giessen, Arndtstrasse 2, D-6300 Giessen 1
Fischbach, G.	Institut für Kernchemie, Universität Mainz, Postfach 3980, D-6500 Mainz
Freiesleben, H.	Gesellschaft für Schwerionenforschung, Postfach 110 541, Planckstrasse 1, D-6100 Darmstadt-Arheilgen
Glässel, P.	Physikalisches Institut, Universität Heidelberg, Philosophenweg 12, D-6900 Heidelberg
Goeke, K.W.	Institut für Kernphysik, Kernforschungsanlage Jülich, Postfach 1913, D-5170 Jülich
Goerlach, U.	Max-Planck-Institut für Kernphysik, Postfach 103 980, D-6900 Heidelberg
Gönnenwein, F.	Physikalisches Institut, Universität Tübingen, Auf der Morgenstelle 14, D-7400 Tübingen
Habs, D.R.	Universität Heidelberg, Philosophenweg 12, D-6900 Heidelberg
Hahn, J.	Institut für Theoretische Physik, J.W. Goethe Universität, Robert Mayer-Strasse 8–10, D-6000 Frankfurt
Hallfarth, G.	I. Institute for Experimental Physics, University of Hamburg, Luruper Chaussee 149, D-2000 Hamburg
Harrach, D.,von	Physikalisches Institut, Universität Heidelberg, Philosophenweg 12, D-6900 Heidelberg
Herrmann, G.F.	Instut für Kernchemie, Universität Mainz, Postfach 3980, D-6500 Mainz and Gesellschaft für Schwerionenforschung, Postfach 110 541, Planckstrasse 1, D-6100 Darmstadt

GERMANY, F.R. (cont.)

Iwamoto, A.	Institut für Theoretische Physik, J.W. Goethe Universität, Robert-Mayer Strasse 8–10, D-6000 Frankfurt
Jahn, H.	Kernforschungszentrum Karlsruhe GmbH., Postfach 3640, D-7500 Karlsruhe 1
Jahn, P.V.	Institut für Kernphysik, Kernforschungsanlage Jülich, Postfach 1913, D-5170 Jülich
Janssen, H.	Institut für Strahlen- und Kernphysik der Universität Bonn, Nussallee 14–16, D-5300 Bonn
Just, M.	Physikalisches Institut, Universität Heidelberg, Philosophenweg 12, D-6900 Heidelberg
Klapdor, H.V.	Max-Planck-Institut für Kernphysik, Postfach 103 980, D-6900 Heidelberg
Kneissl, U.	Institut für Kernphysik, Strahlenzentrum der Justus-Liebig-Universität Giessen, Leihgesterner Weg 217, D-6300 Lahn-Giessen
Koch, H.R.	Institut für Kernphysik, Kernforschungsanlage Jülich, Postfach 365, D-5170 Jülich
Koldobski, A.	Institut für Kernphysik, Technische Hochschule Darmstadt, Schlossgartenstrasse 9, D-6100 Darmstadt Permanent Address: Moscow Physical Engeneering Institute, Moscow, USSR
Krieger, H.	Institut für Kernphysik, Strahlenzentrum der Justus-Liebig-Universität Giessen, Leihgesterner Weg 217, D-6300 Lahn-Giessen
Lang, W.	Institut für Kernphysik, Technische Hochschule Darmstadt, Schlossgartenstrasse 9, D-6100 Darmstadt
Lauppe, W.D.	Institut für Kernphysik, Kernforschungsanlage Jülich, Postfach 1913, D-5170 Jülich

Machner, H.	Institut für Kernphysik, Kernforschungsanlage Jülich, Postfach 1913, D-5170 Jülich
Melkonian, A.	Gesellschaft für Kernenergieverwertung im Schiffbau und Schiffahrt m.b.H., Institut für Physik, D-2054 Geesthacht-Tesperhude
Metag, V.	Max-Planck-Institut für Kernphysik, Postfach 103 980, D-6900 Heidelberg
Morsch, H.P.	Institut für Kernphysik, Kernforschungsanlage Jülich, Postfach 1913, D-5170 Jülich
Mosler, E.	Max-Planck-Institut für Kernphysik, Postfach 103 980, D-6900 Heidelberg
Münzel, H.P.	Technische Hochschule Darmstadt, F.B. 8, Eduard Zintl-Institut, Hochschulstrasse 4, D-6100 Darmstadt
Mutterer, M.	Institut für Kernphysik, Technische Hochschule Darmstadt, Schlossgartenstrasse 9, D-6100 Darmstadt
Naqvi, A.A.	Institut für Angewandte Kernphysik II, Kernforschungszentrum Karlsruhe GmbH, Postfach 3640, D-7500 Karlsruhe 1
Pauli, H.C.	Max-Planck-Institut für Kernphysik, Postfach 103 980, D-6900 Heidelberg
Plischke, P.	I. Institut für Experimentalphysik Zyklotron, Universität Hamburg, Luruper Chaussee 149, D-2000 Hamburg 50
Quade, U.B.	Sektion Physik, Abteilung Kernphysik, Ludwig-Max Universität, Am Coulombwall 1, D-8046 Garching
Reinhard, P.G.	Institut für Kernphysik, Universität Mainz, J.J. Becher Weg 33, D-6500 Mainz
Reisdorf, W.	Gesellschaft für Schwerionenforschung, Postfach 110 541, Planckstrasse 1, D-6100 Darmstadt-Arheilgen

GERMANY, FEDERAL REPUBLIC OF (cont.)

Schmidt, K.H.	Gesellschaft für Schwerionenforschung, Postfach 110 541, Planckstrasse 1, D-6100 Darmstadt-Arheilgen
Schult, O.W.B.	Institut für Kernphysik, Kernforschungsanlage Jülich, Postfach 1913, D-5170 Jülich
Schultheis, H.	Institut für Theoretische Physik, Universität Tübingen, Auf der Morgenstelle 14 D7, D-7400 Tübingen
Schultheis, R.	Institut für Theoretische Physik, Universität Tübingen, Auf der Morgenstelle 14 D7, D-7400 Tübingen
Schulze, J.	Institut für Strahlen- und Kernphysik, Universität Bonn, Nussallee 14–16, D-5300 Bonn
Schütte, G.	Institut für Theoretische Physik, Universität Heidelberg, Philosophenweg 19, D-6900 Heidelberg
Sistemich, K.	Institut für Kernphysik, Kernforschungsanlage Jülich, Postfach 1913, D-5170 Jülich
Specht, H.J.	Physikalisches Institut, Universität Heidelberg, Philosophenweg 12, D-6900 Heidelberg
Speth, J.	Institut für Kernphysik, Kernforschungsanlage Jülich, Postfach 1913, D-5170 Jülich
Sükösd, C.	Institut für Kernphysik, Kernforschungsanlage Jülich, Postfach 1913, D-5170 Jülich
Tepel, J.W.	Fachinformationszentrum Energie, Physik, Mathematik GmbH., Kernforschungszentrum Eggenstein, D-7514 Eggenstein-Leopoldshafen 2

Theobald, J.P.	Institut für Kernphysik Technische Hochschule Darmstadt, Schlossgartenstrasse 9, D-6100 Darmstadt
Weber, J.	Sektion Physik, Universität München, Am Coulombwall 1, D-8046 Garching
Weismann, D.	Institut für Radiochemie, Technische Universität München, D-8046 Garching
Werner, E.	Institut für Theoretische Physik, Universität Hannover, D-3000 Hannover
Westmeier, W.	Institut für Kernchemie, Lahnberge, Geb. J., D-3550 Marburg/Lahn
Wilhelmy, J.B.	Max-Planck-Institut für Kernphysik, Postfach 103 980, D-6900 Heidelberg

HUNGARY

Jéki, L.	Central Research Institute for Physics, P.O. Box No. 49, H-1525 Budapest

INDIA

Iyer, R.H.	Radiochemistry Division, Bhabha Atomic Research Centre, Trombay, Bombay-400 085
Kapoor, S.S.	Fission Physics Section, Nuclear Physics Division, Bhabha Atomic Research Centre, Trombay, Bombay-400 085

ISRAEL

Cheifetz, E.	Weizmann Institute of Science, Rehovot
Gilat, J.	Soreq Nuclear Research Center, Yavne 70600

ISRAEL (cont.)

Selič, H.A.	Weizmann Institute of Science, Rehovot
Shmid, M.	Nuclear Chemistry Department, Soreq Nuclear Research Center, Yavne 70600
Wolf, A.	Nuclear Research Center Negev, P.O. B. 9001, Beer-Sheva

ITALY

Bellia, G.	Istituto Fisica, Universitá Catania, Corso Italia 57, I-95129 Catania
Del Zoppo, A	Istituto Fisica, Universitá Catania, Corso Italia 57, I-95129 Catania
Russo, G.	Istituto Fisica, Universitá Catania, Corso Italia 57, I-95129 Catania
Ventura, A.	Centro di Calcolo del Comitato Nazionale per l'Energia Nucleare, Via G. Mazzini 2, I-4038 Bologna

JAPAN

Igarasi, S.	Tokai Research Establishment, Japan Atomic Energy Research Institute, Tokai-mura, Naka-gun, Ibaraki-ken 319-11

NETHERLANDS

Harakeh, M.N.	Kernfysisch Versneller Instituut, Zernikelaan 25, NL-9747 AA Groningen
Van der Plicht, J.	Kernfysisch Versneller Instituut, Zernikelaan 25, NL-9747 AA Groningen
Van der Woude, A.	Kernfysisch Versneller Instituut, Zernikelaan 25, NL-9747 AA Groningen

POLAND

Dakowski, M.	Institute of Nuclear Research, PL-05-400 Świerk
Piasecki, E.	Institute of Nuclear Research, PL-05-400 Świerk
Sobiczewski, A.	Institute for Nuclear Research, Hoza 69, PL-00-681 Warsaw

SAUDI ARABIA

Al-Feaar, M.Z.	University of Petroleum and Minerals in Dhahran, Dhahran

SWEDEN

Åberg, S.	Department of Mathematical Physics, University of Lund, P.O. Box 725, S-220 07 Lund 7
Gustafsson, H.A.	Department of Physics, University of Lund, Sölvegatan 14, S-223 62 Lund
Möller, P.	Department of Mathematical Physics, P.O. Box 725, S-2207 Lund 7
Ragnarsson, A.I.	Theory Division, C.E.R.N., CH-1211 Geneva, Switzerland
Sandell, A.	Department of Physics, University of Lund, Sölvegatan 14, S-223 62 Lund
Schrøder, B.	Department of Physics, University of Lund, Sölvegatan 14, S-223 62 Lund
Wene, C.O.	Department of Nuclear Physics, Lund Institute of Technology, University of Lund, Sölvegatan 14, S-223 62 Lund

SWITZERLAND

Junker, K.	Eidgenössisches Institut für Reaktorforschung, CH-5303 Würenlingen
Reist, H.W.	Eidgenössisches Institut für Reaktorforschung, CH-5303 Würenlingen

TURKEY

Aras, N.K.	Department of Chemistry, Middle East Technical University and Ankara Nuclear Research and Training Centre, Beşevler, Ankara
Erten, H.N.	Institut für Kernchemie, Universität Mainz, Postfach 3980, D-6500 Mainz, Federal Republic of Germany

UNION OF SOVIET SOCIALIST REPUBLICS

Blinov, M.V.	Khlopin Radium Institute, Röntgen Street, Leningrad
Danilyan, G.V.	Institute for Theoretical and Experimental Physics, B. Cheremushkinskaya 25, 117259 Moscow
Okolovich, V.N.	Institute for Nuclear Physics of the Kazakh Academy of Sciences, Alma-Ata
Tsipenyuk, Yu.M.	Institute for Physical Problems, Academy of Sciences, Moscow
Yankov, G.B.	I.V. Kurchatov Institute of Atomic Energy, Moscow

UNITED KINGDOM

Bett, R.	Atomic Energy Research Establishment, Harwell, Didcot, Oxon OX11 0RA
Cuninghame, J.G.	Atomic Energy Research Establishment, Harwell, Didcot, Oxon OX11 0RA

Ferguson, A.T.G.	Atomic Energy Research Establishment, Harwell, Didcot, Oxon OX11 0RA
Grant, I.S.	Department of Physics, Schuster Laboratory, University of Manchester, Manchester M13 9P1
Hemingway, J.D.	Universities Research Reactor, Risley, Warrington WA3 6AT
James, G.D.	Atomic Energy Research Establishment, Harwell, Didcot, Oxon OX11 0RA
Reid, J.M.	Department of Natural Philosophy, University of Glasgow, Glasgow G12 8QG
Robinson, V.J.	Department of Chemistry, University of Manchester, Manchester M13 9P1
Scobie, J.	Scottish Universities, Research and Reactor Centre, East Kilbride, Glasgow
Vass, D.G.	Department of Physics, University of Edinburgh, The James Clerk Maxwell Building, The King's Buildings, Mayfield Road, Edinburgh EH9 3JZ
Walker, J.	Department of Physics, University of Birmingham, Birmingham B15 2TT
Zimmermann, C.H.	Department of Physics, The James Clerk Maxwell Building, University of Edinburgh, The King's Buildings, Mayfield Road, Edinburgh EH9 3JZ

UNITED STATES OF AMERICA

Bauer, R.W.	Lawrence Livermore Laboratory. University of California, Livermore, CA 94550
Britt, H.C.	Sektion Physik, Universität München, D-8046 Garching, Federal Republic of Germany

UNITED STATES OF AMERICA (cont.)

Clark, D.D.	Cornell University, Wald Laboratory, Ithaca, NY 14853
Ferguson, R.L.	Oak Ridge National Laboratory, Post Office Box X, Oak Ridge, TN 37830
Fong, P.	Physics Department, Emory University, Atlanta, GA 30322
Friedlander, G.	Brookhaven National Laboratory, Upton, NY
Gindler, J.E.	Argonne National Laboratory, 9700 South Cass Avenue, Argonne, IL 60439
Griffin, J.J.	Department of Physics and Astronomy, University of Maryland, College Park, MD 20742
Hoffman, Darleane C.	Los Alamos Scientific Laboratory, C.N.C. Division, MS-760, Los Alamos, NM 87545
Hulet, E.K.	Lawrence Livermore Laboratory, University of California, L-232, P.O. Box 808, Livermore, CA 94550
Warner, R.A.	Pacific Northwest Laboratory, Richland, WA

ORGANIZATIONS

CEC

Budtz-Jorgensen, C.	CBNM-EURATOM, Steenweg naar Retie, B-2440 Geel, Belgium
Knitter, H.H.	CBNM-EURATOM, Steenweg naar Retie, B-2440 Geel, Belgium

JINR

Penionzhkevich, Y.E.	Head Post Office, P.O. Box 79, 101000 Moscow, USSR
Sowinski, M.	Head Post Office, P.O. Box 79, 101000 Moscow, USSR
Ter-Akopyan, G.M.	Head Post Office, P.O. Box 79, 101000 Moscow, USSR

AUTHOR INDEX

Roman numerals are volume numbers.
Italic numerals refer to the first page of a paper by the author concerned.
Upright numerals denote comments and questions in discussions.

TRANSLITERATION INDEX

Батенков, О.И.	Batenkov, O.I.
Блинов, М.В.	Blinov, M.V.
Боровлев, С.П.	Borovlev, S.P.
Витенко, В.А.	Vitenko, V.A.
Воденников, Б.Д.	Vodennikov, B.D.
Данилян, Г.В.	Danilyan, G.V.
Дроняев, В.П.	Dronyaev, V.P.
Игнатюк, А.В.	Ignatyuk, A.V.
Истеков, К.К.	Istekov, K.K.
Музычка, Ю.А.	Muzychka, Yu.A.
Новицкий, В.В.	Novitskij, V.V.
Оганесян, Ю.Ц.	Oganesyan, Yu.Ts.
Околович, В.Н.	Okolovich, V.N.
Орлова, О.А.	Orlova, O.A.
Павлов, В.С.	Pavlov, V.S.
Плеве, А.А.	Pleve, A.A.
Пустыльник, Б.И.	Pustyl'nik, B.I.
Смиренкин, Г.Н.	Smirenkin, G.N.
Тер-Акопьян, Г.М.	Ter-Akopyan, G.M.
Флеров, Г.Н.	Flerov, G.N.
Ципенюк, Ю.М.	Tsipenyuk, Yu.M.
Чепигин, В.И.	Chepigin, V.I.

HOW TO ORDER IAEA PUBLICATIONS

An exclusive sales agent for IAEA publications, to whom all orders and inquiries should be addressed, has been appointed in the following country:

UNITED STATES OF AMERICA UNIPUB, 345 Park Avenue South, New York, NY 10010

In the following countries IAEA publications may be purchased from the sales agents or booksellers listed or through your major local booksellers. Payment can be made in local currency or with UNESCO coupons.

ARGENTINA	Comisión Nacional de Energía Atomica, Avenida del Libertâdor 8250, RA-1429 Buenos Aires
AUSTRALIA	Hunter Publications, 58 A Gipps Street, Collingwood, Victoria 3066
BELGIUM	Service Courrier UNESCO, 202, Avenue du Roi, B-1060 Brussels
CZECHOSLOVAKIA	S.N.T.L., Spálená 51, CS-113 02 Prague 1 Alfa, Publishers, Hurbanovo námestie 6, CS-893 31 Bratislava
FRANCE	Office International de Documentation et Librairie, 48, rue Gay-Lussac, F-75240 Paris Cedex 05
HUNGARY	Kultura, Hungarian Foreign Trading Company P.O. Box 149, H-1389 Budapest 62
INDIA	Oxford Book and Stationery Co., 17, Park Street, Calcutta-700 016 Oxford Book and Stationery Co., Scindia House, New Delhi-110 001
ISRAEL	Heiliger and Co., Ltd., Scientific and Medical Books, 3, Nathan Strauss Street, Jerusalem 94227
ITALY	Libreria Scientifica, Dott. Lucio de Biasio "aeiou", Via Meravigli 16, I-20123 Milan
JAPAN	Maruzen Company, Ltd., P.O. Box 5050, 100-31 Tokyo International
NETHERLANDS	Martinus Nijhoff B.V., Booksellers, Lange Voorhout 9-11, P.O. Box 269, NL-2501 The Hague
PAKISTAN	Mirza Book Agency, 65, Shahrah Quaid-e-Azam, P.O. Box 729, Lahore 3
POLAND	Ars Polona-Ruch, Centrala Handlu Zagranicznego, Krakowskie Przedmiescie 7, PL-00-068 Warsaw
ROMANIA	Ilexim, P.O. Box 136-137, Bucarest
SOUTH AFRICA	Van Schaik's Bookstore (Pty) Ltd., Libri Building, Church Street, P.O. Box 724, Pretoria 0001
SPAIN	Diaz de Santos, Lagasca 95, Madrid-6 Diaz de Santos, Balmes 417, Barcelona-6
SWEDEN	AB C.E. Fritzes Kungl. Hovbokhandel, Fredsgatan 2, P.O. Box 16356, S-103 27 Stockholm
UNITED KINGDOM	Her Majesty's Stationery Office, Agency Section PDIB, P.O. Box 569, London SE1 9NH
U.S.S.R.	Mezhdunarodnaya Kniga, Smolenskaya-Sennaya 32-34, Moscow G-200
YUGOSLAVIA	Jugoslovenska Knjiga, Terazije 27, P.O. Box 36, YU-11001 Belgrade

---

Orders from countries where sales agents have not yet been appointed and requests for information should be addressed directly to:

Division of Publications
International Atomic Energy Agency
Wagramerstrasse 5, P.O. Box 100, A-1400 Vienna, Austria

INTERNATIONAL
ATOMIC ENERGY AGENCY
VIENNA, 1980

SUBJECT GROUP: III
Physics/Nuclear Physics, Reactor Physics, Fission
PRICE: Austrian Schillings 725,–